COST Action TU1207

Next Generation Design Guidelines for Composites in Construction

STATE-OF-THE-ART

COST is supported by the EU Framework Programme

Preface

This State-of-the-Art report included 76 contributions on key areas of development, from material development to testing, design and application.

I would like to thank COST for enabling the development of an inclusive, strong community highly committed to enhancing the current state-of-the-art on the use of advanced composites in construction, thus enabling a faster uptake of new and emerging technologies in the construction industry.

A special thanks to all of the members who have actively contributed to the preparation of this report, your continuous support and dedication was much appreciated.

Maurizio Guadagnini
Chair of Action TU1207

Contents

Experimental results on FRP RC members exposed to fire
Antonio Bilotta& Emidio Nigro

Theoretical models for FRP RC members exposed to fire
Antonio Bilotta, Emidio Nigro

Thermo-mechanical response of GFRP reinforced concrete sandwich panels
A. Schmitt, M. Haffke, V. Carvelli, M. Pahn

2.6 Novel Structural Systems

Prefabricated thin-walled HPC structural elements prestressed with pultruded carbon tendons (collaboration with company SACAC from Switzerland)
G. P. Terrasi

New fiber-reinforced polymer thermal break for energy-efficient constructions –structural system performance
Kyriaki Goulouti, Julia de Castro, Thomas Keller

WG3 Strengthening Applications

3.1 Bond

Experimental characterisation of bond between flexural EB FRP and concrete
A. Serbescu, M. Guadagnini and K. Pilakoutas

Bond problems in NSM systems
Antonio Bilotta , Francesca Ceroni, Emidio Nigro

Discontinous bond in RC beam elements externally strengthened with CFRP
Trombeva-Gavriloska Ana, Lazarevska Marijana

Modeling of discontinous bond in RC beam elements externally strengthened with CFRP
A. T. Gavriloska, M. Lazarevska

3.2 Flexural strengthening

Near surface mounted reinforcement for flexural strengthening of RC columns
Dionysios A. Bournas

CFRP Laminate Strengthening of Concrete Beams with Corroded Steel
Garyfalia G. Triantafyllou, Theodoros C. Rousakis, Athanasios I. Karabinis

Fatigue Behavior and Design of Reinforced Concrete Beams Strengthened in Flexure with FRP
Barbara Charalambidi , Theodoros Rousakis, Athanasios Karabinis

3.3 Shear and Torsional Strengthening

The Use of FRP Jackets as Shear Reinforcement
C. Chalioris, and C. Karagiannis

FRP-EBR Repairs of RC Members in Torsion
C. Chalioris, and C. Karagiannis

Cyclic response of shear critical RC columns strengthened with CFRP strips
M. Del Zoppo, M. Di Ludovico, A. Balsamo, A. Prota, G. Manfredi

3.4 Confinement

Use of Composites in Strengthening Reinforced Concrete Structures
I. Balafas, S.P. Tastani, S.J. Pantazopoulou

Deterioration of FRP jacket effectiveness due to the compaction of low and medium strength concrete
S.P. Tastani, I.Balafas, S. J. Pantazopoulou

Deterioration of FRP jacket effectiveness due to reinforcement buckling
S.P. Tastani, I.Balafas, S. J. Pantazopoulou

Recovery of strength mechanisms in corrosion-damaged reinforced concrete through FRP jacketing
S.P. Tastani, I.Balafas, S. J. Pantazopoulou

About COST

Founded in 1971, COST – European Cooperation in Science and Technology – is the first and widest European framework for the transnational coordination of nationally funded research activities. It is based on an inter-governmental agreement between 35 European countries.

COST enables break-through scientific developments leading to new concepts and products and thereby contributes to strengthen Europe's research and innovation capacities.

It is a unique means for European researchers to jointly develop their own ideas and new initiatives across all scientific disciplines through trans-European networking of nationally funded research activities.

COST key features are:

- building capacity by connecting high-quality scientific communities throughout Europe and worldwide;
- providing networking opportunities for early career investigators
- increasing the impact of research on policy makers, regulatory bodies and national decision makers as well as the private sector.

Through its inclusiveness, COST supports integration of research communities, leverages national research investments and addresses issues of global relevance.

As a precursor of advanced multidisciplinary research, COST plays a very important role in building a European Research Area (ERA). It anticipates and complements the activities of the EU Framework Programmes, constituting a "bridge" towards the scientific communities of emerging countries. It also increases the mobility of researchers across Europe and fosters the establishment of scientific excellence in the nine key domains:

- Biomedicine and Molecular Biosciences
- Food and Agriculture
- Forests, their Products and Services
- Materials, Physics and Nanosciences
- Chemistry and Molecular Sciences and Technologies
- Earth System Science and Environmental Management
- Information and Communication Technologies
- Transport and Urban Development
- Individuals, Societies, Cultures and Health

In addition, Trans-Domain Proposals allow for broad, multidisciplinary proposals to strike across the nine scientific domains.

COST is funded through the EU RTD Framework Programmes.

About Transport and Urban Development (TUD)

TUD fosters research coordination in the fields of transport and the built environment, which play a strategic role in the modern society and economy.

The Domain is by definition cross-sectoral and multidisciplinary, encompassing a wide range of scientific expertise within the transport and land use planning, design, and management activities with a special emphasis on the strong interrelationships among the relevant policy fields as well on all aspects related to sustainable development.

The domain activities should be innovative and complementary to other European programmes in the relevant fields. The aim is to cover both basic and applied research activities including technical and technological developments and their changeovers that are relevant to policy and decision making processes.

A significant concern is devoted to activities exploring new research needs and developments.

About COST Action TU 1207

Construction is rapidly becoming the leading outlet for FRP composites. Although the use of composite materials in construction started in the 1980s, civil engineers only recently started gaining confidence in this technology for use in primary structural applications. Despite the considerable technological developments in this field, there are still key scientific and logistical issues that need to be addressed for the widespread acceptance in construction. For example, existing design recommendations are largely based on work carried out more than fifteen years ago on first generation reinforcing products and their conservativeness is hindering the development of innovative and more efficient products and design solutions.
This Action aims to:

- coordinate European research in the field
- develop and maintain a critical mass of researchers
- offer a link between academia and industry
- develop a new generation of design guidelines based on European Standards

This will facilitate the adoption of European products not only in Europe but also internationally and help Europe stay one step ahead of International competitors.

General information

Start of Action: 12/04/2013
End of Action: 11/04/2017

Chair of the Action: Dr Maurizio GUADAGNINI (UK)
Vice Chair of the Action: Prof Stijn MATTHYS (BE)

Scientific Officer: Dr Mickael PERO
Administrative Officer: Ms Carmencita MALIMBAN

Domain website: http://www.cost.eu/tud
Action website: http://www.tu1207.eu

Action TU1207 Working Groups

WG1 Material Development and Characterisation

Chair: Renata KOTYNIA (PL)
Co-Chair: Sandor SOLYOM (HU)

- Assessing the different tests so as to select candidates for standardisation
- Bond behaviour of FRPs to concrete, steel, timber and masonry
- Behaviour of FRPs at elevated temperatures
- Accelerated tests and development of models to assess durability of FRPs in typical environments, including embedment in cement mortars and concrete

WG2 New Reinforced Concrete (RC) Structures

Chair: Lluis TORRES (ES)
Co-Chair: Kypros PILAKOUTAS (UK)

- Serviceability requirements
- New products and prefabricated solutions
- Long-term behaviour
- Behaviour of FRP RC elements exposed to fire or elevated temperatures

WG3 Strengthening Applications

Chair: Thanasis TRIANTAFILLOU (EL)
Co-Chair: Francesca CERONI (IT)

- Behaviour of confined concrete using different types of fibres and bonding systems
- Behaviour of strengthened reinforced concrete, masonry, steel and timber elements, in flexure, shear and punching shear
- Models and techniques for the prestressing of strengthening systems to enhance the utilisation of composites at service conditions
- Novel seismic strengthening and rehabilitation solutions and development of design models to avoid shear, anchorage, splice and buckling failures

WG4 Whole-life-costing and life cycle assessments

Chair: Matthias PAHN (DE)
Co-Chair: Jose SENA CRUZ (PT)

- Whole-life cost assessment of new FRP reinforced concrete structures
- Whole-life cost assessment of rehabilitated structures
- Recycling and reuse of composite materials
- Innovative structural solutions using existing and future materials

WG5 Knowledge Transfer

Chair: Joaquim BARROS (PT)
Co-Chair: Christoph CZADERSKI (CH)

WG5 will coordinate and promote inter-sectorial collaboration and outreach activities, including the maintenance and management of the Action website, organisation of industry seminars, training schools, Short-Term Scientific Mission (STSMs), maintenance of online databases, preparation and dissemination of reports and publications.

WG1

Material Development and Characterisation

Creep behavior of cold-curing epoxy adhesives: analysis and predictive approach

K. Benzarti[1], N. Houhou[2], S. Chataigner[3] and M. Quiertant[1]

Abstract

This study investigates the creep behavior of two commercially available cold-curing epoxy adhesives, intended for the bonding of external composite reinforcements on concrete structures. In a preliminary stage, the characteristics of the mineral fillers (nature, content and size) contained in the two systems were determined, and the viscoelastic properties of the unfilled epoxy matrices extracted from these systems were analyzed. Short-term tensile creep experiments were then carried-out on cured samples of the two adhesives and their unfilled matrices, in order to evaluate the influence of the fillers and the polymer network characteristics on the instantaneous and delayed mechanical responses. Finally, two predictive approaches based on either the Time-Temperature Superposition Principle (TTSP) or the Time-Stress Superposition Principle (TSSP), were applied to evaluate the long-term creep behavior, and their suitability in the case of cold-curing adhesives was discussed.

Introduction

Cold-curing epoxy adhesives are commonly used to install external fiber reinforced polymer (FRP) composite systems for repairing or upgrading reinforced concrete (RC) infrastructures. These epoxies are usually bi-components systems that contain a certain amount of mineral fillers and additives to set

the rheological and mechanical properties. Their formulation is also adjusted according to the type of process intended for the installation of the FRP materials (wet lay-up, or bonding of pultruded FRP plates, for instance). For this reason, their mechanical behavior, can significantly vary from an epoxy system to another, which may affect the durability and performances of the bonded FRP reinforcement, especially under environmental ageing or sustained loads (Houhou, 2012; 2014)

In this study, it is first proposed to investigate the parameters related to the adhesive formulation (nature and content of the mineral fillers, characteristics of the polymer network) that govern the viscoelastic properties in general, and the creep behavior in particular. In this line, physicochemical characterizations are carried-out on two adhesive systems from the market, and on the unfilled epoxy binders extracted from these adhesives as well. The viscoelastic and tensile creep behaviors of the bulk adhesives cured at ambient temperature are then analyzed in the light of the previous results, in order to point out influential parameters. A second part explores two predictive approaches intended for evaluating the long-term creep behaviour, based on the Time-Temperature or Time-Stress Superposition Principles. Their suitability is examined in the case of cold-curing adhesives, which exhibit an incomplete crosslinking.

[1] Université Paris-Est, IFSTTAR, France, karim.benzarti@ifsttar.fr
[2] Chryso, France, noureddine.houhou@chryso.fr
[3] LUNAM Université, IFSTTAR, France, sylvain.chataigner@ifsttar.fr

Description of the selected epoxy adhesives

Two cold-curing and bi-component epoxy adhesives were selected among the various commercial products available on the French market. Both systems are used for the installation of pultruded carbon FRP (CFRP) plates on RC concrete structures. The names of the two products are not explicitly cited in this paper, and the two systems are noted *Adhesive 1* and *Adhesive 2*.

The main physical and mechanical characteristics of these products are gathered in Table 1. The two systems contain a substantial amount of mineral fillers in their components, but the content and nature of the fillers are not mentioned in the technical data sheets.

Table 1: Properties of the two epoxy adhesives under study, as provided by the manufacturers

	Adhesive 1	**Adhesive 2**
Organic components	Part A: diglycidylether Bisphenol A Part B : aliphatic amines hardener	Part A: diglycidylether Bisphenol A Part B : modified polyamines and cyclo-aliphatic amines
Density at +23°C	1.65 ± 0.1 kg/l (mix A+B)	Part A : 1.43 kg/l Part B : 1.52 kg/l
Pot life in mn	120 (+8°C), 90 (+20°C), 20 (+35°C)	120 (+10°C), 60 (+23°C), 30 (35°C)
Glass transition Temp. (Tg) (*ISO 11357-2*)	62°C (after 7 days at +45°C)	54 ± 2°C
Tensile strength (*ISO 527*)	24-27 MPa (after 7 days at +15°C) 26-31 MPa (after 7 days at +35°C)	29.5 ± 1 MPa
Tensile modulus (*ISO 527*)	11200 MPa (at +23°C)	4940 ± 170 MPa

Preliminary characterizations of the adhesives

In a first step, basic characterizations were carried-out in order to:

- assess precisely the nature and content of the mineral fillers in the 2 epoxies under study,
- determine the viscoelastic properties of the cured adhesives, and that of the organic binders (*i.e*, the epoxy matrices whose mineral fillers have been removed prior to cure). At this stage, the objective is to evaluate the influence of the fillers on the viscoelastic properties of the two commercial systems. In a further step, this will help us to understand possible differences in the experimental creep behaviors of the two products.

Observations by optical and scanning electron microscopy (SEM) techniques, coupled with energy dispersive X-ray (EDS) elemental analysis were first conducted to assess the size, the volume distribution and the nature of the mineral fillers. Fig. 1 shows polished sections of the two cured adhesives. In *Adhesive 1* (Figure 1.a), there is a uniform distribution of large smooth particles in the polymer matrix and the largest particle sizes are around 250μm. The elemental analysis reveals that these fillers are mainly composed of silica sand. As regards *Adhesive 2*, a large density of voids can be observed (air bubbles in black on Figure 1.b), and filler particles appear to be much smaller (size < 50 μm) and exhibit an elongated angular shape. In this case, EDS analyses show that these fillers consist of a mix of calcium carbonate, silica, alumina and titanium dioxide.

(a) 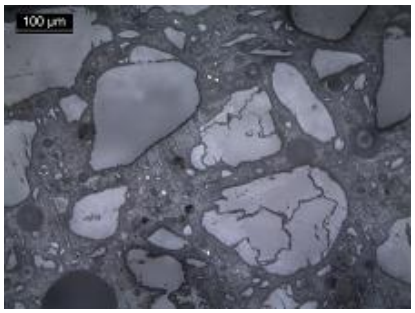

(b) 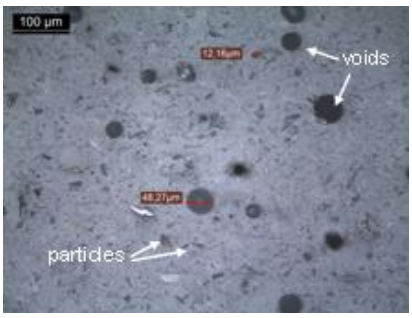

Figure 1: Micrographic observations of polished sections for *Adhesive 1* (a) and *Adhesive 2* (b)

The filler contents in the two pasty components (part A and B) of each adhesive were also assessed, and the global content in the mix as well (part A+ part B, according to the mix ratio recommended by the manufacturer). A centrifugation in a solution of methyl ethyl ketone (MEK) followed by a filtration made it possible to separate the organic binders from the fillers, hence to quantify their relative weight contents. Corresponding results are reported in Table 2. It was found that the filler content of *Adhesive 1* (mix A+B) is close to 80 wt.%, and much higher than that of *Adhesive 2* which is around 60 wt. %. This result is consistent with properties reported on the technical datasheet (Tab. 1), which indicate a higher density and a much higher tensile modulus for *Adhesive 1* compared to the other system.

Table 2: Relative weight contents of organic binders and fillers in the 2 epoxy adhesives

System	Components	Organic binder *(wt. %)*	Filler content *(wt. %)*
Adhesive 1	*A*	18.4 ± 0,8	79.7 ± 0,4
	B	15.4 ± 0,8	85.2 ± 0,9
	Mix A+B (ratio 3/1)	***17.7***	***81.1***
Adhesive 2	*A*	48 ± 2	52 ± 2
	B	31 ± 2	68 ± 2
	Mix A+B (ratio 1/1)	***39***	***60***

Following the centrifugation stage, the organic binders that were extracted from components A and B of the two systems, were recombined into a mix (binder A + binder B), which was used to mold parallelepiped samples (25mm x 4mm x 1 mm) of unfilled epoxy matrices. It is to note that the mix ratio (binder A/binder B) was recalculated, so that the stoichiometry is respected for the two systems, and the resulting samples were cured at ambient temperature for at least 1 month before further characterization. Similar specimens were produced with the filled (as received) adhesives, to serve as control samples.

Finally, the viscoelastic properties were determined by Dynamical Mechanical Analyses (DMA) for the cured samples of filled adhesives and unfilled extracted matrices. Tests were carried-out under traction/compression mode with an imposed dynamic displacement of amplitude 10 µm, at a frequency of 1 Hz. The test specimen was simultaneously subjected to a ramp of temperature between 20 and 140°C at a heating rate of 2°C/min. This made it possible to record the evolution of the storage modulus (E') and the loss factor (tanδ) over the temperature interval. Results are plotted in Figure 2.

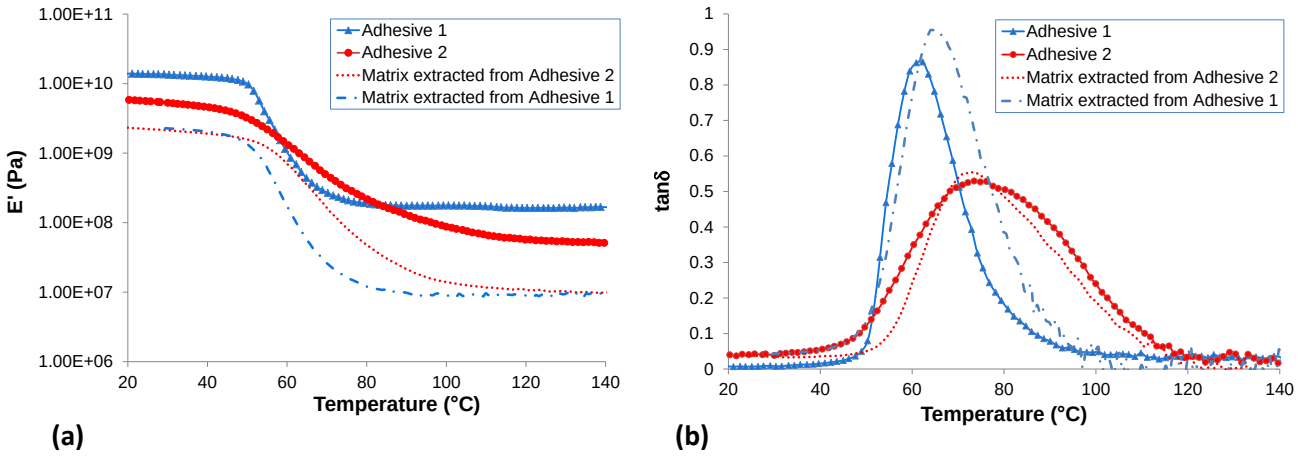

Figure 2: DMA experiments at 1 Hz: Evolutions of the storage Modulus E' (a) and the loss factor tan (b) versus temperature, for *Adhesive 1* and *Adhesive 2* and their unfilled extracted matrices

As regards the filled adhesives, a large drop of the storage modulus is observed through the glass transition (Figure 2.a.) for both systems. However, the moduli of *Adhesive 1* in the vitreous and rubbery domains remain much higher than that of *Adhesive 2,* due the higher filler content. On Figure 2.b., the temperature at the maximum of the tanδ peak, called Tα and closely connected to Tg, is found to be higher for *Adhesive 2* compared to *Adhesive 1* (deviation of 12°C). This feature is contradictory with the values of Tg mentioned in the technical datasheet; which may be due to the unrepresentative cure conditions chosen by the manufacturer of *Adhesive 1* (7 days at 45°C, as reported in Table 1).

In the case of the unfilled extracted matrices, a drop of E' is also observed through the glass transition region; however, differently from the filled epoxies, the unfilled matrices extracted from *Adhesive 1* and *Adhesive 2* exhibit very similar values of the vitreous and rubbery storage moduli. This confirms the major role played by fillers on the mechanical elastic properties of commercial adhesives. As regards the loss factor peak, the matrix extracted from *Adhesive 1* exhibits a lower value of Tα and a higher peak amplitude, as compared to the matrix extracted from *Adhesive 2*. This feature suggests a lower crosslink density, hence a higher molecular mobility of the epoxy network in *Adhesive 1*.

Finally, DMA characterizations have shown that the elastic characteristics (storage moduli in the vitreous and rubbery domains) of the two commercial adhesives are mainly dependent on the filler content, whereas the dispersive characteristics (Tα and amplitude of the loss factor peak) are rather related to the structure of the epoxy network (nature of the reactive components, crosslink-density).

Analysis of the short-term creep behavior

Short-term tensile creep experiments (25°C, applied stress of 5 MPa) were carried-out on samples of the two commercial adhesives and their unfilled extracted matrices. Creep curves are displayed in Figure 3.

The two extracted matrices exhibit a similar level of elastic strain (instantaneous strain) following the initial loading stage, which is consistent with their similar storage moduli in the vitreous state. Nevertheless, matrix extracted from *Adhesive 1* presents a higher creep rate (slope of the asymptote), which can be explained by a higher molecular mobility of the epoxy network, as shown previously by DMA analyses.

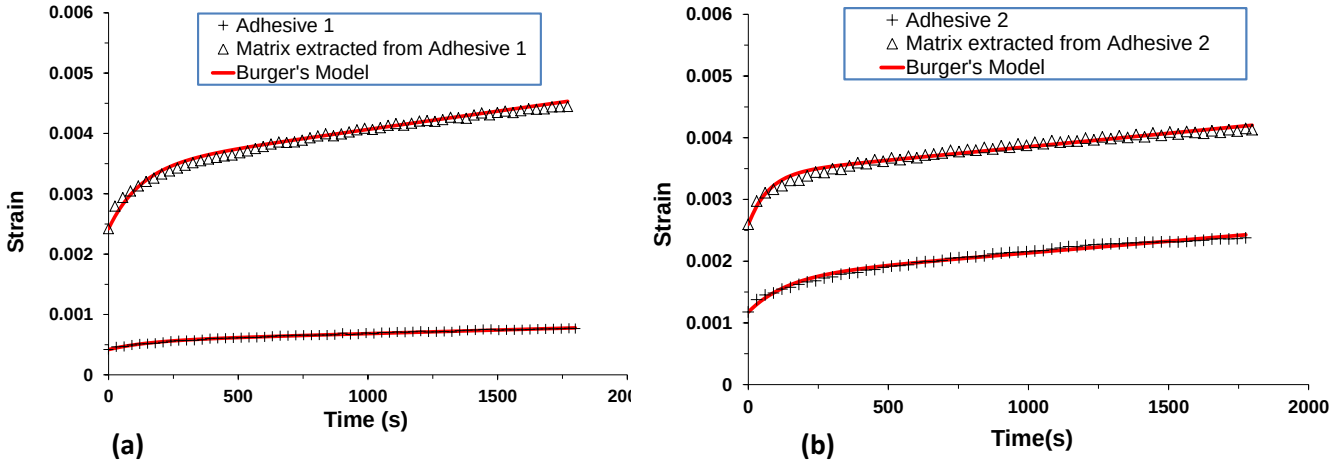

Figure 3: Short-term creep tests for *Adhesive 1* (a) and *Adhesive 2* (b) and their unfilled matrices, at 25°C for an applied stress of 5 MPa. Fitted curves of Burger's model are also displayed.

Filled adhesives show globally lower levels of deformation than their extracted matrices, due to the presence of mineral fillers. When comparing the 2 filled systems together, large differences are observed in terms of initial elastic strain (it is much lower for *Adhesive 1* which has the highest filler content and vitreous elastic modulus) and in terms of creep rate (which appears higher for *Adhesive 2*). This latter result contradicts the trend observed for the extracted matrices, as the matrix of *Adhesive 1* exhibits the highest creep rate. It is thus suggested that the creep rate of filled adhesives in the vitreous state is not only dependent on the molecular mobility of the polymer matrix, but also on other factors such as interactions between filler particles. It is likely that friction phenomena between sand particles hamper the creep process in *Adhesive 1*, due to the high filler content and the large size of the sand particles.

Finally, the well-known rheological Burger's model (Figure 4) was used to simulate the creep behaviors of both the filled adhesives and the extracted matrices. Parameters of the model were identified by fitting the experimental data, according to the method described in (Houhou et al, 2012; 2014). Values of these parameters are not reported in this paper, but it is obvious from Figure 3 that a fair agreement was obtained between experimental and modelled curves.

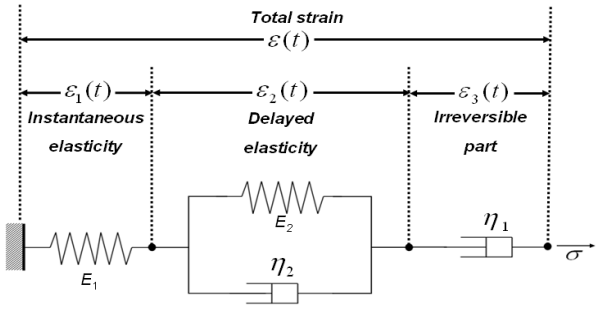

Figure 4 : Schematic description of Burger's rheological model

Predictive approaches

This last part aims at comparing two predictive methods for evaluating the long-term creep response of cold curing adhesives, based on the Time Temperature Superposition Principle (TTSP) and the Time Stress Superposition Principle (TSSP). Both approaches are applied to the case of *Adhesive 1.*

The TTSP method consists in conducting short-term creep experiments at various temperatures and build a creep compliance master curve by shifting the experimental compliance curves horizontally along the log-time scale axis, so that they fit the curve at a chosen reference temperature. Figures 5.a and 5.b display respectively the experimental compliance curves recorded at several temperatures between 25 and 57°C (for an applied stress level of 5 MPa), and the compliance mater-curve at the reference temperature of 25°C for *Adhesive 1*. From this master curve, it is then easy to determine the long-term evolution of the creep strain for the material under study, and to fit this curve with the Burger's model (Figure 5.c.).

In the case of adhesive systems that exhibit a highly non-linear creep behavior, Houhou et al. (2014) have demonstrated that the previous TTSP procedure can be reproduced for various levels of applied stress, and one can finally identify a non-linear Burger's model. However, a drawback of the TTSP method is that the polymer adhesive is heated during the multiple isothermal tests, and this may affect its microstructure and provide unrepresentative results. This is especially true for cold-curing epoxies, which present usually an incomplete crosslinking after curing at ambient temperature.

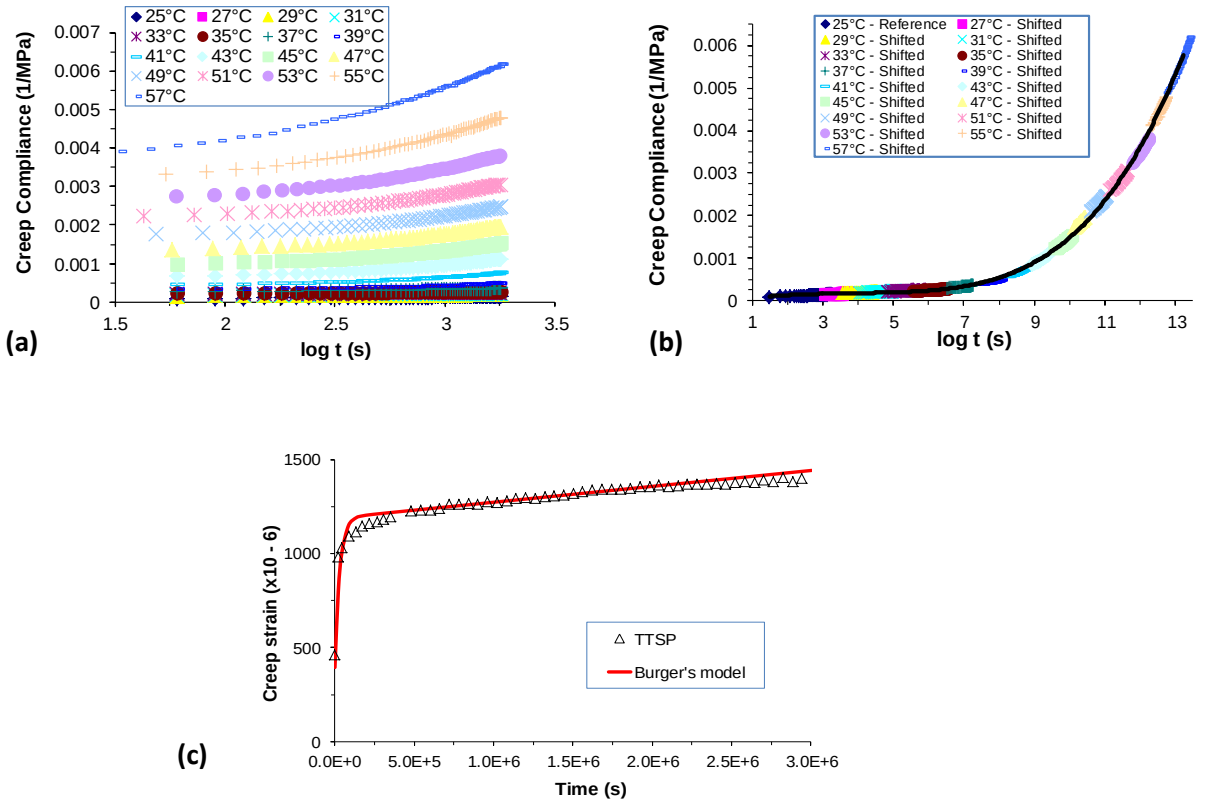

Figure 5: Creep compliance *vs.* time curves obtained from short-term creep tests under isothermal conditions for a stress of 5 MPa (a). Master curve for the reference temperature of 25 °C (b). Comparison of creep strain *vs* time curves obtained from TTSP approach and Burger's model (c)

An alternative predictive method based on the Time-Stress Superposition Principle (TSSP) might be more adapted for cold curing adhesive systems, as it doesn't require to heat the samples. It involves short term creep experiments at various loading levels, and the master-curve is again constructed by shifting the experimental compliance curves along the log-time scale axis. Figure 6. shows an example of application for *Adhesive 1*. Successive creep/recovery cycles (15 min creep/15 min recovery) were carried-out at several levels of applied stress in the range 3 - 25 MPa. Unfortunately, for the highest stress levels (above 20 MPa, which is lower than the expected tensile strength), a rapid failure of the samples was observed, due to the brittleness of *Adhesive 1*. For this reason, a master curve was built by

shifting only the available creep compliance curves, providing a prediction of the creep behavior limited to 5 decades (10^5 s). Nevertheless, several authors have reported successful predictions up to $10^{7.5}$ s (one year) for other polymer materials (Jazouli et al, 2007), using this TSSP approach which remains of high interest.

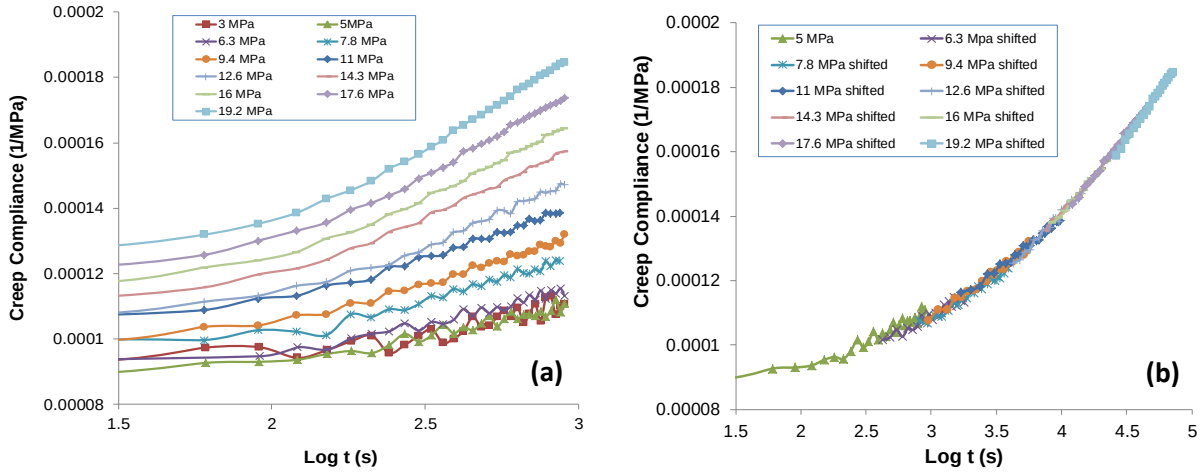

Figure 6: Creep compliance *vs.* time curves obtained from short-term creep tests at various load levels and at a temperature of 25°C (a). Master curve for a reference stress level of 5 MPa (b).

Conclusion

The present study has investigated the creep behavior of two selected cold curing epoxy adhesives, which are commercially available and commonly used in construction for the bonding of CFRP plates.

Preliminary physicochemical characterizations revealed significant differences in the composition and properties of the two systems, in terms of nature, content and size of the mineral fillers. Viscoelastic analyses performed on the unfilled matrices extracted from these two systems and cured at room temperature also demonstrated differences in terms of crosslink density of the epoxy networks.

Short-term tensile creep tests were then carried-out on cured samples of the two adhesives and their unfilled extracted matrices, showing that the level of the instantaneous elastic strain associated to the loading stage strongly depends on the filler content of the adhesive, while the creep rate depends upon both the molecular mobility of the epoxy network and the possible interactions between filler particles.

Finally, two predictive approaches were applied to evaluate the long-term creep behavior, based either on the Time-Temperature or the Time-Stress Superposition Principles. The first method appears to be very efficient but may provide unrepresentative results, as it requires heating the samples, which can alter their microstructure. The second method doesn't involve heating, but requires creep tests at high stress levels, which may be difficult, hence limiting the predictions to a few decades.

Key References

Houhou, N, Quiertant, M., Benzarti, K., Chataigner, S., Rabasse, M., Flety. A. (2012). Innovative experimental device for the creep characterization of the concrete/FRP adhesive bond, 6th Int. Conf. on FRP Composites in Civil Engineering –CICE 2012, Rome, Italy, 13-15 June, 8 p. on CD.

Houhou, N., Benzarti, K., Quiertant, M., Chataigner, S., Flety, A. and Marty, C. (2014). Analysis of the nonlinear creep behavior of concrete/FRP-bonded assemblies. *Journal of Adhesion Science and Technology*. Vol. 14-15, 1345-1366.

Jazouli, S., Luo, W., Bremand, F., Vu-Khan, T. (2005). Application of time-stress equivalence to non-linear creep of polycarbonate. *Polymer Testing*. Vol. 24, 463-467

Mechanical properties of resins: tensile strength and E-modulus since early ages

A. Benedetti[1], José Sena-Cruz[2], José Granja[3], Pedro Fernandes[4], Miguel Azenha[5]

Introduction

In Fibre-Reinforced Polymer (FRP) installations, the mechanical behaviour of the strengthening system is strongly influenced by the epoxy adhesive, particularly at early ages, while the mechanical properties of the adhesive are still enduring significant evolution (Borchert and Zilch, 2008). Various experimental research works have shown that the evolution of the tensile properties of epoxy resins is dependent on environmental curing conditions, especially temperature (Moussa et al., 2012). Therefore, it is clear that studying how the mechanical properties increase along time is of utmost importance. The present contribution summarizes the work described in the references (Fernandes et al., 2014; Granja et al., 2014); it aims to assess the early-age evolution of the mechanical properties of epoxy adhesives used in FRP strengthening applications, and better understand the relationship between distinct approaches for their assessment. The study involved adapting an existing technique devised for continuous monitoring of concrete stiffness since casting, called EMM-ARM (Elasticity Modulus Monitoring through Ambient Response Method) for evaluation of epoxy stiffness. Furthermore, monotonic tensile tests according to ISO standards (MTT) and cyclic tensile tests (CTT) were carried out at several ages on the same adhesive mixture. All experimental procedures (mixing and testing) took place under controlled environmental conditions (in climatic chamber), with temperature of 20±1ºC and relative humidity of 55±5%. A comparison between the obtained results was performed in order to assist clarifications about the applicability of several approaches/techniques in predicting the stiffness of epoxy resins.

Evaluation of E-modulus and tensile strength with tensile tests at several ages

An extensive set of thirty tensile tests were performed in order to determine the epoxy E-modulus and the ultimate tensile strength at several ages. The specimens for testing were manufactured according to "type 1A" defined in EN ISO 527-2:2012. The experimental program comprised the testing ages of 12, 18, 36 and 84 hours. For each age of testing, three monotonic tests and three cyclic tests were carried out using a universal testing machine (AG-X Shimadzu) with 50 kN capacity load cell and test force measurement precision of 1/1000 ±0.5%. The monotonic tensile tests were conducted under displacement control, at a rate of 1 mm/min, according to EN ISO 527-1:2012. In regard to the load configuration of cyclic tests, each CTT experiment was composed of six load/unload cycles between 10 N and the force corresponding to 1/3 of the average tensile strength of the specimen at the age of testing. Figure 1 presents the stress-strain curves obtained at various ages by monotonic and cyclic tensile tests. From this figure, it is possible to observe the increase on stiffness and strength along the curing process of epoxy adhesive. In addition, Figure 1(b) clearly shows the viscoelastic effect that occurred during the consecutive loading/unloading cycles, especially at the early ages of testing. The Young's modulus of epoxy adhesive was obtained by various methods. Concerning the monotonic tensile tests, two methods were contemplated: (i) the first tensile modulus, $E_{MTT\text{-}std}$, was calculated as the slope of the secant line between 0.05% and 0.25% strain on the stress-strain plot, according to ISO 527-1:2012; (ii) the second, $E_{MTT\text{-}inslop}$, represents the slope of the linear trend line of the experimental values gathered until 1/3 of the ultimate strength, according to the American Standard ASTM D638M-93. The schematic representation of these two methods are shown in Figure 2.

[1] ISISE, University of Minho, Portugal, andrea.benedetti@outlook.com
[2] ISISE, University of Minho, Portugal, jsena@civil.uminho.pt
[3] ISISE, University of Minho, Portugal, granja@civil.uminho.pt
[4] ISISE, University of Minho, Portugal, pfernandes@civil.uminho.pt
[5] ISISE, University of Minho, Portugal, Miguel.Azenha@civil.uminho.pt

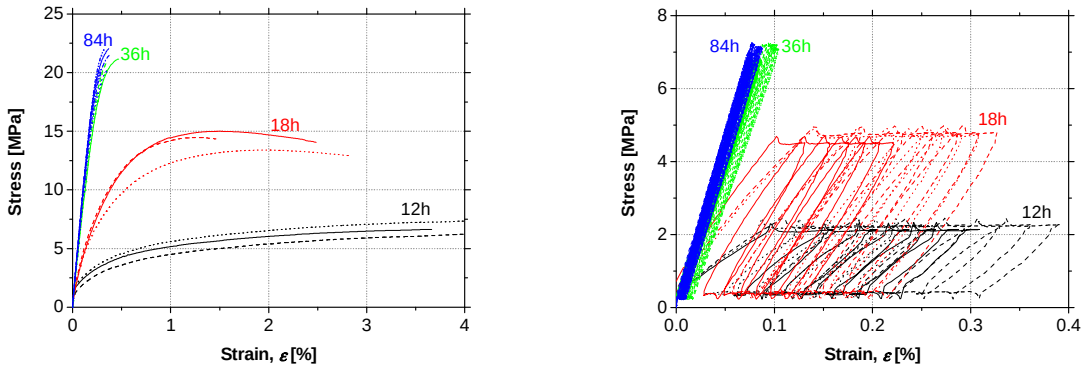

Figure 1 – Stress-strain curves obtained from (a) monotonic tensile tests and (b) cyclic tensile tests

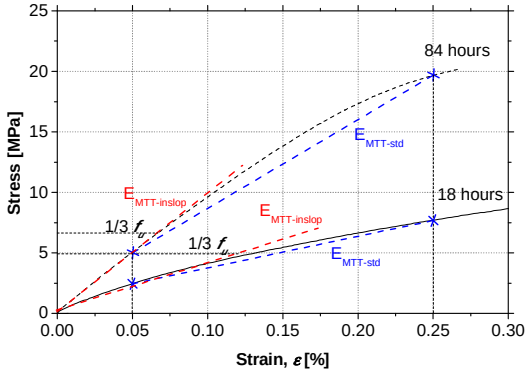

Figure 2 – Example of different methods of E-modulus calculation.

Concerning the cyclic tests, the first cycle of loading was neglected and the slope of the trend line calculated for each following loading and unloading stage was taken into account for determining E-modulus values. During the entire tensile cycling process, the slope of the elastic loading and unloading did not decrease, i.e. the calculated E-modulus values were very similar for all the cycles. Therefore, it is feasible to average all these slopes within each test to obtain a representative E-modulus of the cyclic test (E_{CTT}). The evolution of the average elasticity moduli evaluated according to the cyclic tensile test methodology (CTT) is shown in Figure 3, together with the previous two methodologies. It is interesting to observe that the coherence between CTT tests results (E_{CTT}) and those obtained through the trend line method on the MTT tests ($E_{MTT\text{-}inslop}$) is quite satisfactory, particularly for the ages 18 and 84 hours. However, for all the tested ages, the method for calculation of E-modulus provided by ISO 527:1:2012 led to lower values of the elasticity modulus for the tested epoxy resin, due to the fact that, in the considered strain interval (0.05-0.25%), the adhesive had a non-linear behaviour. Since the non-linear mechanical behaviour of epoxy adhesive is further marked at very early ages, it is clear that ISO method leads to even higher deviations (as compared to the other methods described here) for determining the epoxy resin E-modulus at the early stage of curing process. Therefore, a linear regression procedure applied on the initial part of the stress-strain curve corresponding to the values gathered until 1/3 of the ultimate strength is considered recommendable. In fact, at the indicated lower stress range, the stress-strain relationship can be considered linear. Figure 3, also shows the evolution of the ultimate tensile strength of the epoxy resins along the curing period. From this figure, it is possible to observe that, at 36 hours, the final strength was already reached (21 MPa), with no further significant increase in the following hours.

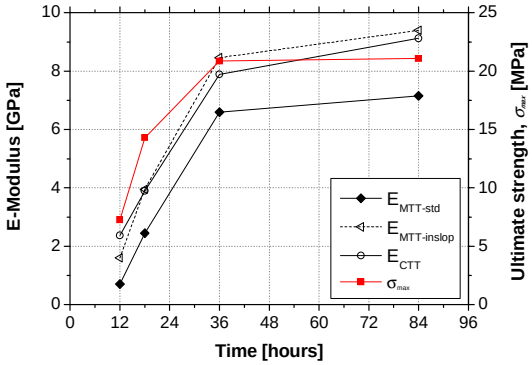

Figure 3 – Evolution of E-moduli and ultimate strength of epoxy obtained by tensile tests.

Evaluation of E-modulus and tensile strength with tensile tests at several ages

The EMM-ARM is a variant of the traditional resonant frequency methods, based on the identification of the first flexural resonant frequency of a composite beam formed by a self-supporting mould filled with the material under testing. The natural frequency of the composite beam at each instant of testing can be analytically related to the E-modulus of the tested material, which allows determining the evolution of this elastic property since very early ages. In the original implementation of EMM-ARM for evaluating the stiffness evolution of concrete, the tested material was put inside an acrylic cylinder which was placed in simply supported condition (Azenha et al., 2010). Thereafter the methodology was adapted to study cement pastes by means of a smaller composite cantilever beam (Azenha et al., 2012). The EMM-ARM experimental setup adopted for testing epoxy resin is reproduced in Figure 4. The specimen consists in a cantilever beam where the accelerations are monitored at its free end. The measured accelerations are converted to the frequency domain by applying Fast Fourier Transforms (FFT), allowing the determination of the resonant frequency of the system. Based on the dynamic equation of free vibration together with full information about the geometry and mass of the system, and knowledge of the stiffness properties of the acrylic tubes, the E-modulus of the epoxy adhesive could be determined along time.

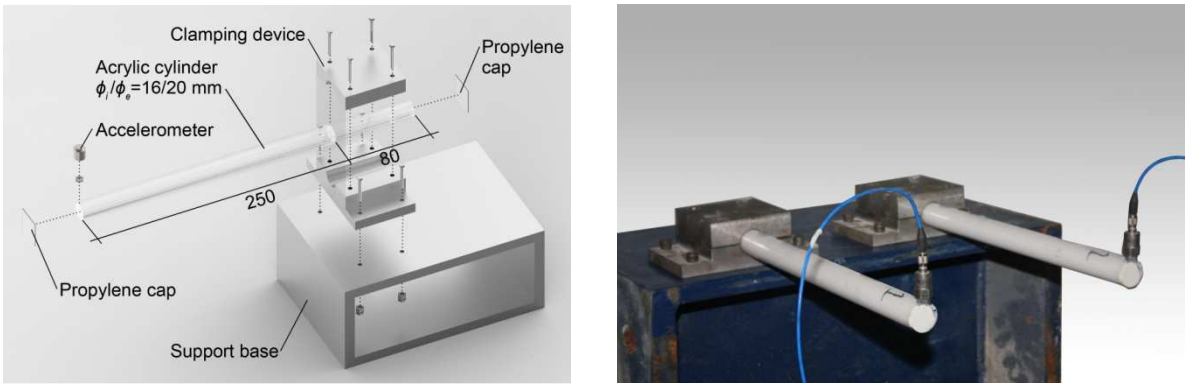

(a) (b)

Figure 4 – Experimental setup of EMM-ARM tests: (a) exploded view [units: mm]; (b) photo

The resulting E-modulus evolution for the two tested specimens (EMM1 and EMM2) is shown in Figure 5. Firstly, it is possible to verify the good agreement between the results of the two specimens, with absolute stiffness differences always remaining under 2.5%, revealing the good repeatability of the experimental setup and procedure. During the first 6.4 hours the epoxy stiffness was nearly null for both specimens, which is consistent with the fluid-like behaviour of the adhesive at the early stages of the cure. Then a drastic increase in the stiffness occurred, reaching an average value of ~9.4 GPa at the

age of 36 hours, instant after which the E-modulus evolution reached a plateau during the following 140 hours. In summary, EMM-ARM technique revealed its capability in clearly identifying the hardening kinetics of epoxy adhesives, measuring the material setting time and the stiffness growth since very early ages. This method allows measurements since the tested material still has 'fluid-like' behaviour, overcoming the main drawback of the traditional resonance methods.

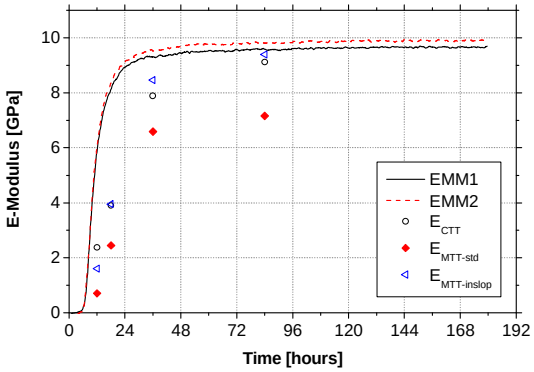

Figure 5 – E-modulus evolution obtained by EMM-ARM, MT and CT tests.

Comparison between EMM-ARM and tensile tests

Figure 5 also shows the comparison between the elastic modulus results obtained by EMM-ARM and by tensile test methods (monotonic and cyclic). At the age of 84 hours, there is a good agreement between the values obtained through the EMM-ARM (EMM1 and EMM2), those collected in cyclic tests (E_{CTT}) and those calculated from the initial slope of monotonic stress-strain curves ($E_{MTT\text{-}inslop}$). However, the results show relevant differences at the earlier ages of 12, 18 and 36 hours. At such ages, all the E-modulus values obtained from tensile tests are significantly lower than the ones acquired from EMM-ARM, particularly at 12 and 18 hours. This deviation may be explained by the fact that epoxy adhesive showed a visco-elastic behaviour. Therefore, the high visco-elasticity that epoxy exhibited at very early ages have influenced the measurement of elastic modulus through tensile tests, leading to lower values. EMM-ARM probably provided the actual stiffness evolution of the epoxy adhesive since the earliest ages after mixing. As the importance of creep strains decreased over curing time, the Young's modulus obtained by quasi-static tests got closer to the actual E-modulus.

Key references

Azenha, M., Faria, R., Magalhães, F., Ramos, L., and Cunha, Á. (2012). Measurement of the E-modulus of cement pastes and mortars since casting, using a vibration based technique. *Materials and Structures* 45(1-2), 81-92.

Azenha, M., Magalhães, F., Faria, R., and Cunha, Á. (2010). Measurement of concrete E-modulus evolution since casting: A novel method based on ambient vibration. *Cement and Concrete Research* 40(7), 1096-1105.

Borchert, K., and Zilch, K. (2008). Bond behaviour of NSM FRP strips in service. *Structural Concrete* 9127-142.

Fernandes, P., Granja, J., Benedetti, A., Sena-Cruz, J., and Azenha, M. (2014). (Submitted) Quality control and monitoring of NSM CFRP systems: E-modulus evolution of epoxy adhesive and its relation to the pull-out force. *Composites Part B: Engineering*.

Granja, J., Fernandes, P., Benedetti, A., Azenha, M., and Sena-Cruz, J. (2014). (Submitted) Monitoring the early stiffness development in epoxy adhesives for structural strengthening. *Int. J. Adhes. Adhes.*

Moussa, O., Vassilopoulos, A. P., de Castro, J., and Keller, T. (2012). Early-age tensile properties of structural epoxy adhesives subjected to low-temperature curing. *International Journal of Adhesion and Adhesives* 359-16.

Physical and mechanical properties during aging of a cold-curing structural epoxy adhesive for bridge construction

Maria Savvilotidou[1], Anastasios P. Vassilopoulos[2], Mariaenrica Frigione[3], Thomas Keller[4]

Introduction

Structural adhesives used in bridge construction are in most cases applied on the construction site and are thus mainly cold-curing systems based on thermosetting epoxy resins. Cold-curing adhesive joints, if properly designed and executed, are normally not exposed to humidity, high temperature and UV radiation. The main aging mechanisms that still occur in such dry environments, at low or moderate outdoor temperatures (well below T_g), are physical aging and continuation of curing. In this respect however, most of the works published on physical aging concern hot-cured epoxy resins, i.e. cured at elevated temperatures (often above 100°C) by artificial heating and works about cold- or outdoor-curing are rare [Moussa, 2012; Frigione, 2001].

Physical aging of epoxy adhesives occurs in the glassy state, i.e. after vitrification and at aging temperatures (T_a) lower than T_g, and is driven by a thermodynamic disequilibrium in this state [Montserrat, 1991]. During aging, i.e. approaching the thermodynamic equilibrium, an increase in mass density (densification), and thus a decrease in specific volume (volumetric relaxation) (v), and a decrease in molecular configurational energy are observed [Frigione, 2001; Montserrat, 1991; Moosburger-Will, 2014; Odegard, 2011; Struik, 1977]. Physical aging effects may be erased however, i.e. the adhesive is de-aged, if heating occurs at temperatures above T_g, i.e. in the rubbery state, and subsequently cooled down into the glassy state, where physical aging begins [Frigione, 2001; Odegard, 2011; Struik, 1977].To quantify physical aging, the specific enthalpy (h) is an appropriate physical metric [Odegard, 2011], which decreases with physical aging time. This results in an increase of the endothermic peak (ΔH_{rel}) [Frigione, 2001; Montserrat, 1991; Cook, 1999] which appears in the specific heat capacity vs temperature curves obtained by Differential Scanning Calorimetry (DSC), and an increase in T_g.

Concerning the mechanical properties, since physical aging decreases the specific volume, the E-modulus increases accordingly [Frigione, 2001; Moosburger-Will, 2014], while the tensile strength normally decreases as a result of the embrittlement and potential microcracking [Kong, 1986]. The continuation of curing, i.e. increasing of the curing degree, in contrast to physical aging, decreases the mass density (and thus increases the specific volume) but increases the cross-link density, defined as the number of chemical cross-links per unit volume. In accordance with the increase of the specific volume the E-modulus decreases during curing [Moosburger-Will, 2014; Gupta, 1985; Wang, 1992]. The glass transition temperature and strength, however, increase with increasing cross-link density, i.e. curing degree [Moussa, 2012].

In this work, the physical and mechanical behaviors of cold-curing epoxy adhesive specimens are investigated during an aging period of up to 12 months in a dry environment. Post-cured epoxy specimens, i.e. heated for short times at temperatures not much higher than their T_g, are used as reference in order to derive the different behaviors at cold curing, compared to hot-cured conditions concerning which the knowledge is much broader. The physical and mechanical property changes are discussed on the basis of the sequence or concurrence of the above-described aging mechanisms, i.e.

[1] Ecole Polytechnique Fédérale de Lausanne, Switzerland, maria.savvilotidou@epfl.ch
[2] Ecole Polytechnique Fédérale de Lausanne, Switzerland, anastasios.vasilopoulos@epfl.ch
[3] University of Salento, Italy, mariaenrica.frigione@unisalento.it
[4] Ecole Polytechnique Fédérale de Lausanne, Switzerland, thomas.keller@epfl.ch

physical aging and continuation of curing. The current work is a continuity of a previous study [Moussa, 2012; Moussa, 2013], where cold-curing structural epoxies were physically and mechanically investigated during the first ten days of isothermal curing at low temperatures (5-20°C). Post-curing treatments had also served as reference.

Experimental program

Materials and conditioning

The epoxy adhesive used in this study was Sikadur-330, supplied by SIKA Schweiz AG. The primary commercial use of this cold-curing adhesive or resin is manual application to surfaces in order to bond FRP strips and impregnate FRP fabrics employed to strengthen existing concrete or steel structures. Sikadur-330 is a thixotropic bi-component adhesive comprising a bisphenol-A-based epoxy base resin and a hardener consisting of aliphatic amines. Its viscosity is approximately 6000 mPa·s (at 23 °C), according to the product data sheet. A small quantity, less than 20% per weight, of silica-based fillers has been identified by burn-off tests and optical microscopy observations [Moussa, 2013]. The adhesive was produced with a 4:1 resin-to-hardener mixing ratio, suggested by the manufacturer. After the mixture, it was poured into aluminum molds or applied using a spatula onto a Teflon work surface to form thin sheets. The glass transition temperature of specimens cured for two weeks under laboratory conditions was 43.7°C (based on DSC) [Moussa, 2013].

Both cold-curing and post-cured specimens were manufactured according to the different conditioning processes shown in Table 1. Specimens C13 and C21, directly after pouring, were conditioned at a low 13°C and moderate 21°C temperature. The post-cured P21 reference specimens, after curing for five or seven days at 21°C, were post-cured for three days at 60°C and then allowed to cool in the air and age at 21°C. A total of 172 specimens were subjected to the above conditions, 112 for the mechanical and 60 for the physical characterization, for a period of up to 350 days. For all specimens, the aging time zero ($t_a = 0$) corresponds to their fabrication day.

Table 1: Designation, characterization and conditioning of epoxy specimens

Specimen	Characterization	Conditioning Ta *(°C)*	Aging time ta *(days)*
C13	Mechanical	13 ± 0.5	338
C21	Physical (DSC)	21 ± 3	327
	Mechanical	21 ± 3	350
P21	Physical (DSC)	21 ± 3	5
		60 ± 0.5	8
		21 ± 3	331
	Mechanical	21 ± 3	7
		60 ± 0.5	10
		21 ± 3	316

Methods of characterization and specimen types

Physical characterization was performed using Differential Scanning Calorimeter analyses (DSC), while for the mechanical characterization standard tensile experiments were carried out, both at irregular frequencies, following the development of the properties. An overview of the experimental program is shown in Table 1.

DSC was selected to derive the thermo-physical characteristics, such as the glass transition temperature ($T_{g,DSC}$), enthalpy relaxation (ΔH_{rel}), residual heat (ΔH_{res}), and curing degree (α) (calculated as the ratio between ΔH_{res} and the total residual heat ($\Delta H_{res,tot} \approx 315$ J/g) measured for the uncured/fresh resin) for both cold-curing (C21) and post-cured epoxy conditions (P21). The experiments were performed using a Netzsch 204 F1 Phoenix thermoanalyzer. The samples, weighing between 10-20 mg, were cut from appropriately conditioned epoxy sheets of 1-mm thickness. Each DSC experiment was composed of two subsequent scans from -25°C to 250°C at a heating rate of 10 °C/min under a nitrogen atmosphere, and an intermediate cooling at 20°C/min. Properties from two DSC experiments on two different samples of each condition and time have been obtained.

Quasi-static tensile experiments were performed under laboratory conditions (i.e. at T = 21 ± 3°C and RH = 38 ± 10%) according to ASTM D638, using an MTS Landmark servo-hydraulic loading machine, calibrated at a maximum load capacity of 5 kN. The dog-bone-shaped specimens used for the mechanical experiments were fabricated in aluminum molds with geometry according to ASTM D638, as shown in Fig. 1. The specimens were clamped by flat-faced pneumatic metal grips and loaded under displacement control at a rate of 3.5 mm/min. For determining the E-modulus, the longitudinal strain was measured by using an MTS clip-on extensometer, with a gage length of 25 ± 0.05 mm and a minimum accuracy of ± 0.5% of the calculated strain, as shown in Fig. 1. Nominal strengths, derived after dividing the maximum load by the initial cross section of each specimen, were used. Furthermore, the tensile E-modulus was calculated as the slope of the stress vs strain curve in the initial linear part, between 0.05% and 0.15% strain. Four specimens were considered for the mechanical characterization at each condition and time.

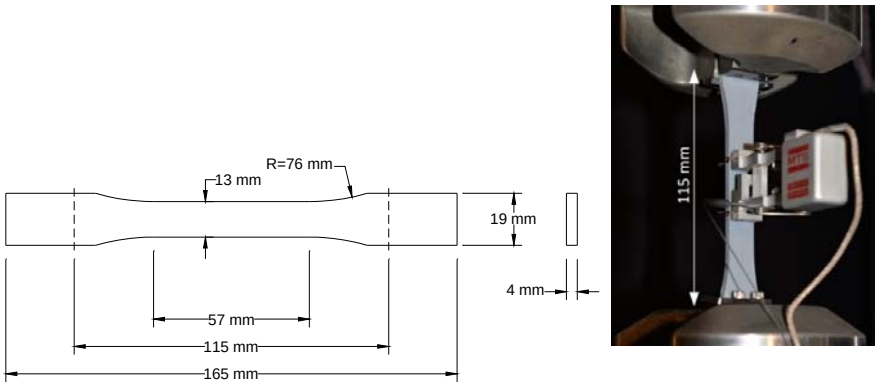

Figure 1: Tensile experiments, specimen dimensions and experimental set-up according to ASTM D638

Discussion of experimental results

Physical characterization

A high curing degree (α) of approximately 94% was achieved by all C21 and P21 samples at five days of curing. At nine days, after post-curing, the P21 samples appeared fully cured ($\alpha = 1$). After 327 days, the C21 samples also achieved an almost complete curing of 99% -100%.

After five days, the $T_{g,DSC}$ of the two conditions ranged around 40°C. The values for the cold-curing specimens C21 then slowly developed, while a jump to values above 70°C occurred after post-curing in the P21 specimens (at nine days). After almost one year, the C21 specimens reached values of around 60°C.

The variations of the relaxation enthalpy (ΔH_{rel}) over time of the C21 and P21 samples are shown in Fig. 2. The values of the cold-curing C21 increased up to a maximum after around 17 days and then started decreasing. At five days, the post-cured P21 started at the same values as those of the C21, but the former then decreased by 50% after post-curing (at nine days). Subsequently, similarly to C21 but on a lower level, a peak appeared at around 17 days, followed by a decrease and then a slight increase again after 121 days.

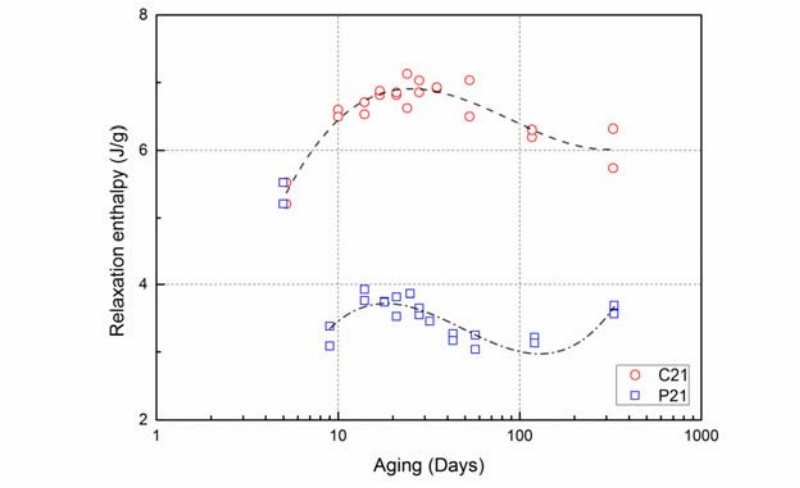

Fig. 2: Development of relaxation enthalpy with aging time.

Mechanical characterization

The tensile modulus, strength and failure strain of all specimens C13, C21 and P21 are shown in Figs. 3 to 5 respectively; average values and standard deviations are indicated. The peak in the E-modulus curves shown in Fig. 3 for all specimens almost coincided with the peak in the ΔH_{rel} responses shown in Fig. 2 for the C21 and P21 conditions. This confirmed the dependence of the epoxy stiffness on the specific volume, the former varied according to the latter due to physical aging and continuation of cure. In the earlier age, physical aging was the predominant mechanism that led to the E-modulus increase, while after the peak, continuation of curing became predominant, decreasing the E-modulus. The new E-modulus increase after the minimum at 180 days could be an indication of the reactivation of physical aging. A similar increasing trend could be seen in the last measurements of the relaxation enthalpy of the P21 condition in Fig. 2.

In contrast to the E-modulus development, the similar strength and failure strain of the cold-curing specimens C13 and C21 were significantly different from those of the P21 post-cured specimens, see Figs. 4 and 5 respectively. This could be attributed to their primary dependency on the cross-link density and not the mass density (on which the E-modulus mainly depended). Up to 180 days, the strength and failure strain, for both cold-curing conditions C13 and C21, followed a behavior inversely proportional to the E-modulus (compare Figs. 3, 4 and 5), i.e. the modulus peaks coincided with strength and failure strain valleys, evidencing the embrittlement induced by physical aging. Between 180 and 260 days, the values deviated from the inversely proportional behavior, i.e. strength and failure strain continued increasing and approached the P21 values, confirming that they were driven by the increasing cross-link density due to the continuation of curing, and not by the newly increasing mass density due to physical aging. Up to 200 days, the strength and failure strain of the P21 were almost constant (on average) and high, as a result of their high level of cross-linking directly after post curing. After 200 days, a new increase of the E-modulus of the P21 (see Fig .3), possibly due to a new physical aging cycle, may explain the slight strength and strain decrease of the already fully cross-linked material.

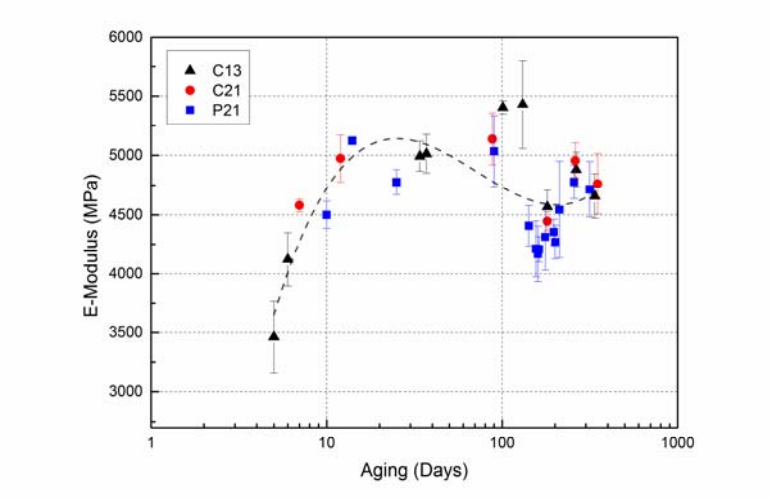

Fig. 3: Tensile E-modulus vs aging time relationship.

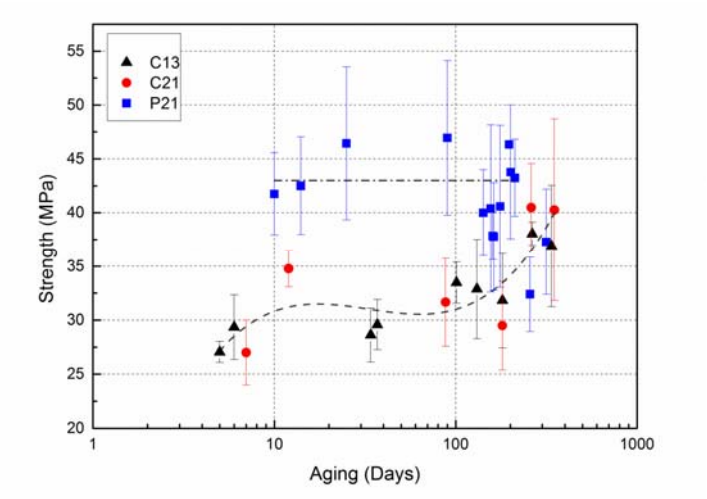

Fig. 4: Tensile strength vs aging time relationship.

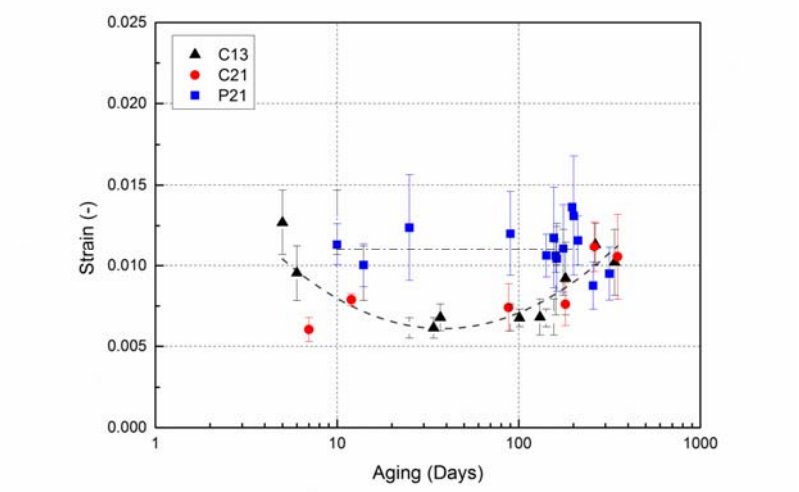

Fig. 5: Tensile failure strain vs aging time relationship.

Conclusions

The effect of physical aging and continuation of curing on the physical and mechanical properties of a cold-curing structural epoxy adhesive in a dry environment was investigated during the first year. The following conclusions have been drawn:

- The physical and mechanical properties are driven by predominant physical aging in the earlier age and predominant curing in the later age during the first year.
- The E-modulus mainly depends on the mass density and reaches a maximum in the earlier age due to physical aging. At the later age curing becomes predominant and the decreasing mass density decreases the E-modulus. After the first week, the E-modulus development becomes independent of the curing conditions, i.e. cold or hot/post-cured.
- Tensile strength and failure strain change mainly with the cross-link density and their development is thus dependent on the curing treatment, i.e. cold or hot/post cured. With regard to the cold-curing conditions, the strength and failure strain development is delayed in the earlier age due to physical aging.
- Eventually, all curing conditions (cold, or hot/post-cured) result in similar tensile properties, i.e. maximum strength and failure strain and a reduced E-modulus after a maximum, after less than nine months of aging.

In view of the long service life of bridges, up to 100 years, it can however not be excluded that, sooner or later, an initially sealed joints may start leaking and the adhesive may thus be exposed to moisture or even stagnant water. Investigations are thus ongoing, related to the development of the adhesive's properties in wet environments.

Key references

Cook, W. D., Mehrabi, M., Edward, G. H. (1999), Aging and yielding in model epoxy thermosets. Polymer, 40: 1209–1218.

Frigione, M., Naddeo, C., Acierno, D. (2001), Cold-Curing Epoxy Resins: Aging and Environmental Effects. I & II- Thermal & Mechanical Properties. J. Polym. Eng., 21: 23–51 & 349–368.

Gupta, V. B., Drzal, L. T., Lee, C. Y.-C., Rich, M. J. (1985), The temperature-dependence of some mechanical properties of a cured epoxy resin system. Polym. Eng. Sci., 25: 812–823.

Kong, E. S. W. (1986), Physical aging in epoxy matrices and composites. Adv. Polym. Sci., 80: 125–171.

Montserrat, S. (1991), Vitrification and physical aging on isothermal curing of an epoxy resin. J. Therm. Anal, 37: 1751–1758.

Moussa, O., Vassilopoulos, A. P., de Castro J., Keller, T. (2012), Early-age tensile properties of structural epoxy adhesives subjected to low-temperature curing. Int. J. Adhes. Adhes, 35: 9–16.

Moussa, O., Vassilopoulos, A. P., de Castro, J., Keller, T. (2013), Long-term development of thermophysical and mechanical properties of cold-curing structural adhesives due to post-curing. J. Appl. Polym. Sci., 127: 2490–2496.

Odegard, G. M., Bandyopadhyay, A. (2011), Physical aging of epoxy polymers and their composites. J. Polym. Sci. B Polym. Phys., 49: 1695–1716.

Struik, L. C. E. (1977), Physical aging in plastics and other glassy materials. Polym. Eng. Sci., 17: 165–173.

Wang X., Gillham, J. K. (1992), Tg - temperature property (TgTP) diagram for thermosetting systems: anomalous behavior of physical properties vs extent of cure. J. Coat. Technol., 64: 37–45.

CFRP ground anchors with strap ends

Haifeng Fan[1], Anastasios P. Vassilopoulos[2], Thomas Keller[3]

Introduction

Fiber reinforced polymer (FRP) tendons are increasingly used to replace conventional steel tendons in ground anchors, taking advantage of their high strength-to-weight ratio and good corrosion resistance. The applications of AFRP and CFRP tendons, especially in permanent prestressed cases, have been reported since 1990 (Tokyo Rope Co. Ltd 2016). Conceptually similar to steel strands, FRP strands were also developed by twisting a certain number of small-diameter wires. A high load-bearing capacity could be achieved by forming a FRP cable assembled from several strands, for example in the Carbon Fiber Composite (CFCC) system commercialized by Tokyo Rope in Japan (Benmokrane et al. 1997, Tokyo Rope Co. Ltd 2016). FRP Cables with a similar concept, assembled from rods with nominal diameters of 4.0 mm (Wang et al. 2015) or 12.6 mm (Zhang et al. 2014), were also developed and studied.

To anchor the tendon on the air and ground sides, mechanical or bonded anchors are commonly used (Schmidt et al. 2012). However, two problems exist in these types of CFRP anchors, which could lead to a premature failure in the anchor and thus not allow to exploit the full tendon capacity: 1) high shear and through-thickness stress concentrations existing at the anchorage are critical due to the anisotropic properties of CFRP fibers; 2) uneven load distributions among the assembled strands or rods occur, i.e. some of them were obviously less loaded compared to others (Wang et al. 2015).

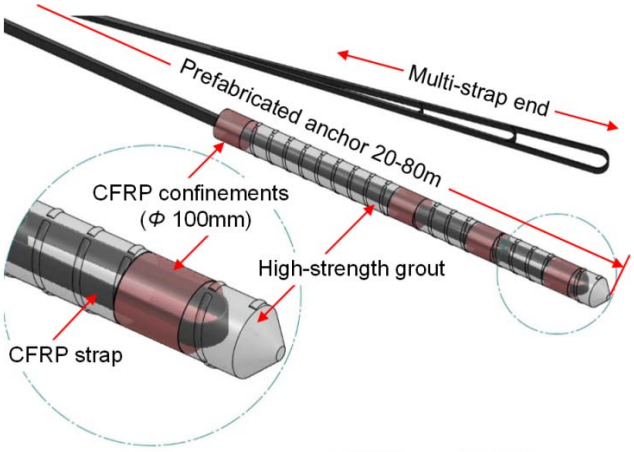

Figure 1: Permanent prestressed CFRP ground anchor with multi-strap end

A simpler and much more material-tailored anchorage method, based on strap ends, was thus developed (Winistoerfer 1999). In this project, a new application of this strap anchorage method for permanent prestressed CFRP ground anchors was proposed, which consists of a CFRP tendon with a multi-strap end on the ground side, embedded in a prefabricated high-strength grout cylinder confined with CFRP rings, as shown Figure 1. The main purpose of the rings is to deviate the spreading forces at the embedded strap ends into the cylinder's axial direction and not to increase the grout strength. The grout cylinder is thus stepwise axially loaded by the axial components of the spreading forces. The ground anchor with the prefabricated anchor body can be 20–80 m long and coiled, then transported to the construction site, inserted into the borehole, anchored by injecting fresh standard (normal-strength) grout and finally prestressed to 60% of the design load.

[1] Ecole Polytechnique Fédérale de Lausanne, Switzerland, haifeng.fan@epfl.ch
[2] Ecole Polytechnique Fédérale de Lausanne, Switzerland, anastasios.vasilopoulos@epfl.ch
[3] Ecole Polytechnique Fédérale de Lausanne, Switzerland, thomas.keller@epfl.ch

In a first stage, a CFRP ground anchor with a single-strap end on the ground side was developed. The anchor capacity was determined in pull-out experiments. The influence of different confinement levels and CFRP ring arrangements on the load-bearing behavior of the anchor was investigated. In a second development stage, a two-strap end was conceived on the ground side to increase the load-bearing capacity to a load of more than 1000 kN, which normally needs a rock media to be anchored. Anchor specimens were pulled out from mortar cylinders confined by steel tubes of different thicknesses, which simulated different confinement levels of the rock mass.

Experimental Program

CFRP ground anchor specimens

Both the single-strap and two-strap CFRP tendons were composed of unidirectional UTS50 F24 24k 1600tex D carbon fibers impregnated with XB 3515 epoxy resin; the fiber volume fraction was 60 ± 2%. In the single-strap anchors, four anchor specimens with different configurations of the grouted part on the ground side, simulating applications in both rock and soil, were investigated, as shown in Figure 2. In experiment S605, a 7- mm-thick and 605-mm-long steel tube with an inner diameter of 100 mm was used to simulate the stiffness and confining pressure of a surrounding rock mass, as shown in Figure 2 (a). For applications in soil, a 2-mm-thick CFRP confinement ring with an inner diameter of 100 mm was installed around the grout-embedded strap end to deviate the spreading forces, as shown in Figure 2 (b) and (c).

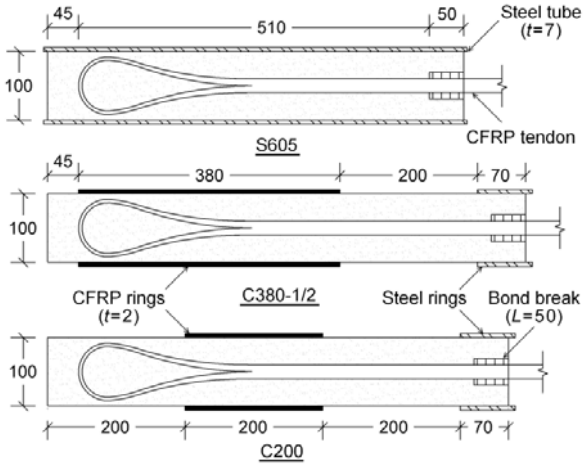

Figure 2: Configuration of CFRP anchors with single-strap end (dimensions in [mm])

In the two-strap anchors, the end of the CFRP tendon was embedded in a 1060-mm-long high-strength grout body with inclined and corrugated surface on the ground side. Three 150-mm-long and 2-mm-thick identical CFRP confinement rings, consisting of the same materials as the tendon, were installed around the two strap ends and the division point. The prefabricated anchor body was inserted into a 1200-mm-long steel tube, simulating a rock mass as shown in Figure 3. Pull-out experiments were conducted on three anchor specimens with two different tube thicknesses to study the influence of the rock stiffness on the load-bearing capacity of the anchor.

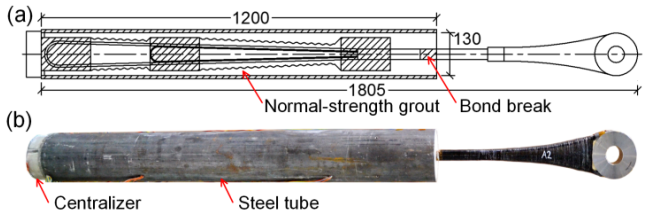

Figure 3: CFRP two-strap anchor specimen: (a) schematic (dimensions in [mm]); (b) photo

Experimental setup and instrumentation

In the single-strap anchors, a self-balanced experimental set-up was designed for the pull-out experiments, as shown in Figure 4 (a). The load was transferred from two identical hollow-plunger hydraulic cylinders of 576-kN capacity to the upper strap end through a steel frame, while the vertical movement of the anchor body was blocked by steel plates under the cylinders. Five load cycles up to 25, 50, 100, 150 and 200 kN respectively were applied to anchors C380-1/2 before the failure cycle. Only the first three were applied in S605 and the first two in C200 due to the lower expected capacity. The instrumentation layout is shown in Figure 4 (b). Three types of instruments were used: Linear Variable Differential Transformer (LVDT) transducers, strain gages and video extensometers.

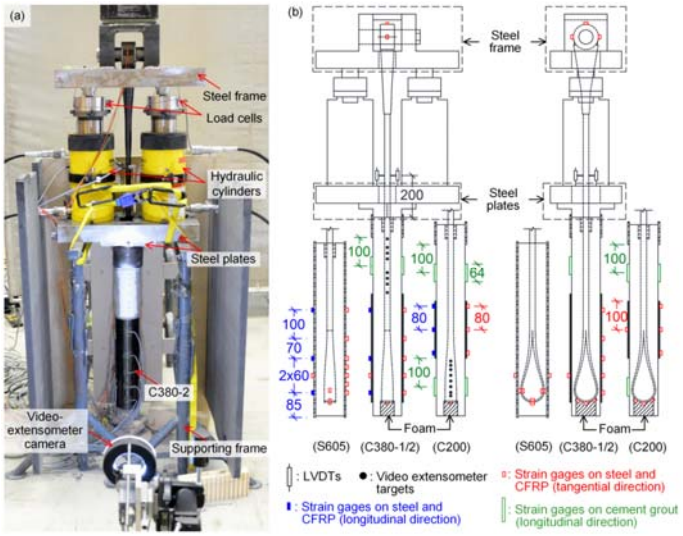

Figure 4: Experimental set-up and instrumentation layout of single-strap anchors(dimensions in [mm])

In two-strap anchors, the pull-out experiments were conducted on a Trebel 10MN machine, as shown in Figure 5. The anchor was suspended at the air side through a steel pin to the top fixed beam of the machine.

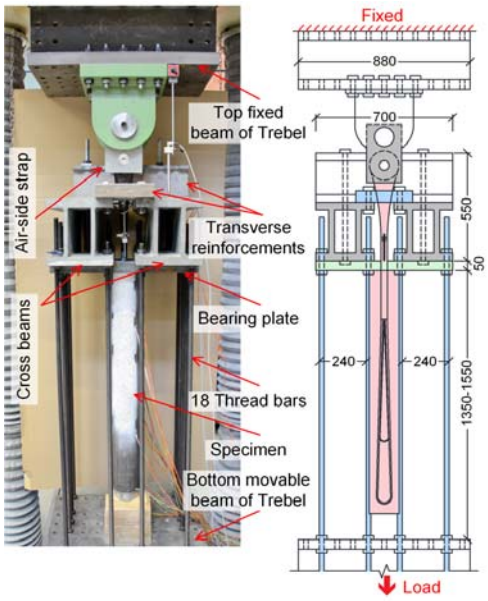

Figure 5: Experimental set-up of two-strap anchors (dimensions in [mm])

The pulling load was applied to the top surface of the anchor body through a loading frame consisting of a bearing plate, two cross beams, two transverse reinforcements and 18 thread bars; the bars were fixed

to the cross beams on one side and to the bottom movable beam of the machine on the other side. The loading was applied to the bottom movable beam in displacement-control mode at a rate of 1 mm/min. After four load cycles up to 100, 300, 500 and 700 kN respectively, the anchor was loaded up to failure. The instrumentation layout is shown in Figure 6. Three types of instruments were used: Linear Variable Differential Transformer (LVDT) transducers, strain gages and Digital Image Correlation (DIC).

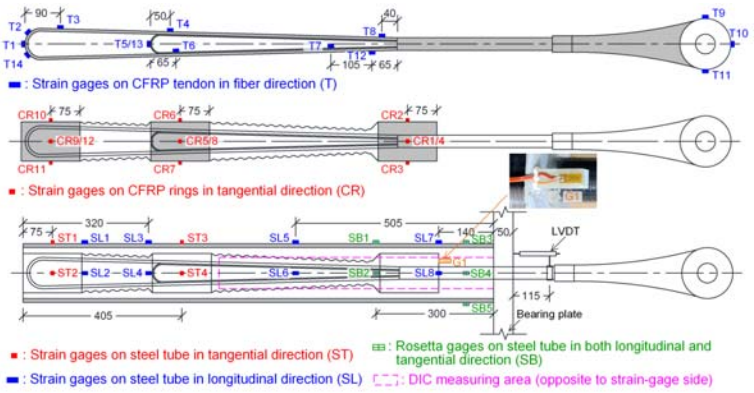

Figure 6: Instrumentation layout of two-strap anchors

Results and Discussions

Single-strap CFRP anchors

All anchors exhibited similar load pull-out displacement responses in the failure cycle, as shown in Figure 7; the load cycles of anchor C380-1 are shown in the window of Figure 7. A linear response was mainly observed, except the minor nonlinear behaviors at the beginning in all the specimens and at the end close to the ultimate load in the partially confined anchors. No stiffness degradation was observed between the cycles, but slight residual displacements were seen after unloading to 5 kN, resulting from the friction at the CFRP/grout interface. Anchor S605 exhibited strap rupture, while compression failure (C380-1/2) and splitting failure (C200) of the unconfined grout occurred in the partially confined cases. In anchors C380-1/2, a double-cone grout failure mode was observed in the unconfined part, which resembled the one in the uniaxial compression experiments on cylinder specimens.

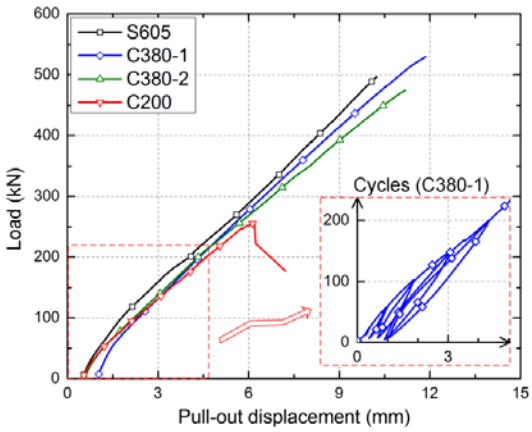

Figure 7: Load vs pull-out displacement responses of single-strap anchors (failure cycle)

The embedded straps remained undamaged. In contrast, anchor C200, where the strap was only partially confined, exhibited a 46.0 and 51.6% lower ultimate load compared to C380-1 and C380-2 respectively. It could be concluded that the length and position of the CFRP ring had a significant influence on the load-bearing capacity of the partially confined anchors. The load-bearing capacity of these anchors mainly

depended on the uniaxial compressive strength of the unconfined grout outside the strap region, if the CFRP confinement ring was installed at an optimized position to balance the spreading forces from the strap.

Two-strap CFRP anchors

All specimens exhibited similar load vs pull-out displacement responses in the failure cycle up to a first peak, as shown in Figure 8. An almost linear response was observed, except a slight nonlinear behavior at the beginning; the latter was attributed to a progressive debonding at the CFRP/grout interface, which also caused a small residual displacement after the four initial load cycles up to 700 kN, as shown in Figure 8 for anchor ST5. The stiffness in the linear range, Kexp, assumed as being the slope of the linear segment between 500 and 1200 kN, was similar, as shown in Table 1; anchor ST5 exhibited only 6.3% lower stiffness than the ST10-1/2, which could be attributed to a slightly larger deformation due to the weaker confinement.

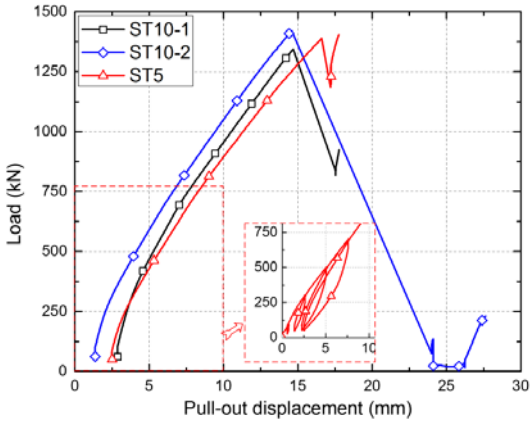

Figure 8: Load vs pull-out displacement responses of two-strap anchors

The three anchors reached similar loads at the first peak, indicating that the confinement level had low influence on the load-bearing capacity of the anchor. At this first peak, delamination was observed in the visible air-side straps in anchors ST10-1/2, while no damage was recognizable in ST5. After the first peak, the load dropped and increased again to a second peak in all specimens where partial or complete rupture of the air-side strap occurred in anchors ST10-2 and ST5 respectively, see Figure 9.

After failure, the specimens were cut into two halves in the strap plane, see Figure 9. All anchors exhibited rupture in the embedded CFRP tendons; no compression failure in the grout parts was observed, except small cracks located in the normal-strength grout at the end of the CFRP rings, see Figure 9 (a). In anchor ST10-1, the large and small straps were completely separated from the rod at the division point on one side, while partial rupture or delamination occurred in the semicircles of the small or large straps, see Figure 9 (b). In anchor ST10-2, complete rupture was visible at the division point of the large strap and in the semicircle of the small strap. Furthermore, partial rupture or delamination occurred in the semicircle of the large strap and the division point of the small strap, see Figure 9 (c). In anchor ST5, complete rupture occurred in the semicircle of the large strap and partial rupture in one straight part of the large and at the end of the small strap; no damage was visible at the division point.

Conclusions and Points for Discussions

Pull-out experiments were performed on four CFRP ground anchors with single-strap ends and three CFRP ground anchors with two-strap ends. The results showed that:

- For single-strap anchors: in rock applications, the anchor can be applied directly without additional confinement, while in the case of soil, an additional CFRP confinement ring is needed to prevent premature grout failure in the strap region.

- For two-strap anchors: 1) the targeted 1000-kN anchor capacity was reached. 2) failure occurred in the CFRP tendons at different positions on the embedded air- and ground- sides which proved an almost uniform use of the capacities of the different strap components. 3) the conceptual elements to prevent grout failure, i.e. selection of high-strength grout in the anchor body, CFRP confinement rings to balance and deviate spreading forces and the complex conical anchor body shape to introduce the forces into the normal grout proved to be effective and well-tailored, grout failure did not occur.

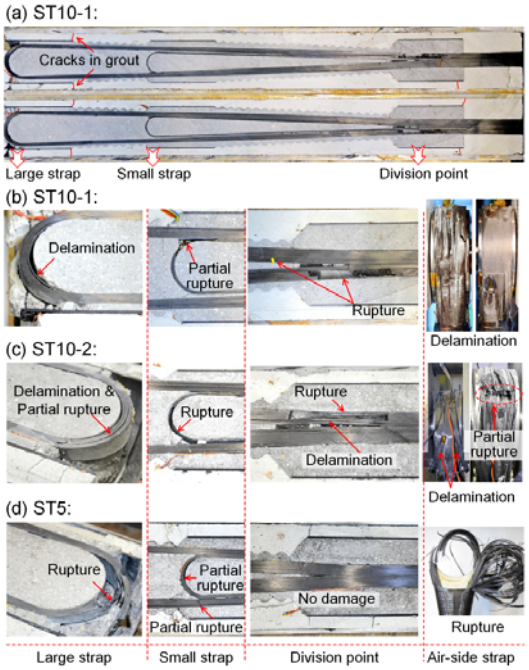

Figure 9: Failure modes of two-strap anchors: (a) cut view of anchor ST10-1; details in (b) ST10-1, (c) ST10-2, (d) ST5

Key references

B. Benmokrane, H. Xu, I. Nishizaki (1997). Aramid and carbon fibre-reinforced plastic prestressed ground anchors and their field applications, *Can. J. Civ. Eng.* 24; 968-85.

J.W. Schmidt, A. Bennitz, B. Täljsten, P. Goltermann, H. Pedersen (2012). Mechanical anchorage of FRP tendons–A literature review. *Constr. Build. Mater.*;32:110-21.

Tokyo Rope Co. Ltd. (2016). "Summary of application projects." <https://isabou.net/sponsor/nm-anchor/sekou.asp> (May 02, 2016).

X. Wang, P. Xu, Z Wu, J. Shi (2015). A novel anchor method for multitendon FRP cable: manufacturing and experimental study. *J. Compos. Constr.* 19:04015010.

A.U. Winistoerfer (1999). Development of non-laminated advanced composite straps for civil engineering applications. Coventry, UK: University of Warwick.

K. Zhang, Z. Fang, A. Nanni, J. Hu, G. Chen (2014). Experimental Study of a Large-Scale Ground Anchor System with FRP Tendon and RPC Grout Medium. *J. Compos. Constr.* 19:04014073.

Numerical examples for calculation of laminated composite plates with delamination

Marina Rakočević[1], Svetislav Popović[2]

Introduction

Inter-laminar cracking of laminated composite plates can occur due to a defect in the production, transport, storage or during exploitation load. Instability in the production process, imperfections of various nature and thermal or chemical components of the laminate components, may also be the cause of the initial delaminations.

Depending on the position of the structural element, there are two basic types of delaminations. The first type represents a delamination located deep inside the section, corresponding to the cracks that are usually studied in the classical fracture mechanics. The second type, delaminations placed near the surface of the structural element, are a specific type of defect because their behaviour is almost always associated with a buckling of the surface layers. The study of this form of delamination requires, in addition to other factors, to take into account the stability of the lamina from the standpoint of the theory of elastic stability, which is of a particular importance for the elements in pressure. Not only the full delamination, but also a phenomenon of multiple cracks without separation of layers, characterizes the laminate composite materials, and significantly affect the overall bearing capacity and safety of the structure.

This paper presents a model for calculating the realistic stress-strain state of a simply supported laminated composite plates with delamination by using a layerwise theory. Internal delamination which is stable under exploitation transverse load, with the assumption of no further growth or propagation, is considered. It will be shown that it is possible to obtain stresses and displacements in the cross-section of the plate with delamination. Presented model is based on the mathematical model of Reddy's layerwise theory for laminated composite plates. Stresses and displacements are calculated by using the double trigonometric series with discretization through the thickness of the plate.

Theoretical background

We consider the simply supported laminated composite plate with the thickness *h* and dimensions *axb* which consists N orthotropic layers, Figure 1. Each layer has the orientation of layer in the direction of x or y axis. Through the thickness of the plate, cross-section contains one internal delamination whose position is known in advance.

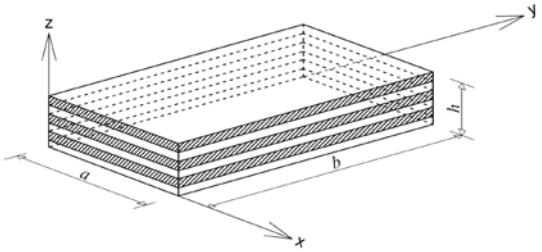

Figure 1: Composite plate

The displacement field is assumed in a following form:

$$\begin{aligned} u(x,y,z) &= u(x,y)+U(x,y,z) \\ v(x,y,z) &= v(x,y)+V(x,y,z) \\ w(x,y,z) &= w(x,y) \end{aligned} \tag{1}$$

[1]University of Montenegro, Faculty of Civil Engineering, Montenegro, marinara@ac.me
[2]Europoles GmbH & Co. KG, Neumarkt in der Oberpfalz, Germany, svetislav.popovic@europoles.com

where $u(x,y)$, $v(x,y)$ and $w(x,y)$ are the displacements of the points in the middle plane of the plate, and $U(x,y,z)$ and $V(x,y,z)$ are additional displacements which are assumed to be a sum of multiplication of unknown nodal displacements $u^J(x,y)$ and $v^J(x,y)$ ($J=1,..,n$, n-total number of the nodes through the thickness of the plate), and the one-dimensional linear interpolation functions $\psi^j(z)$ along the independent layers:

$$U(x,y,z)=\sum_{J=1}^{n}u^J(x,y)\psi^J(z)$$
$$V(x,y,z)=\sum_{J=1}^{n}v^J(x,y)\psi^J(z) \qquad (2)$$

For the cross-section without delamination, the total number of nodes is one greater than the number of the layers N, $n=N+1$, Fig. 2(a). For the cross-section with m_d delaminations, the number of nodes increases because the position of the crack introduces two nodes, thus allowing a different displacement of the point in which a delamination is defined. The total number of nodes in which it is necessary to calculate displacements and stresses is defined with an expression:

$$n_d = N + m_d + 1 \qquad (3)$$

Number of nodes through the thickness of the for the cross-section with one delamination is $n_d = N+2$, Fig.2(b). Figure 2(c) shows the linear interpolation function which is adopted for five-layer plate with delamination between the second and the third layer.

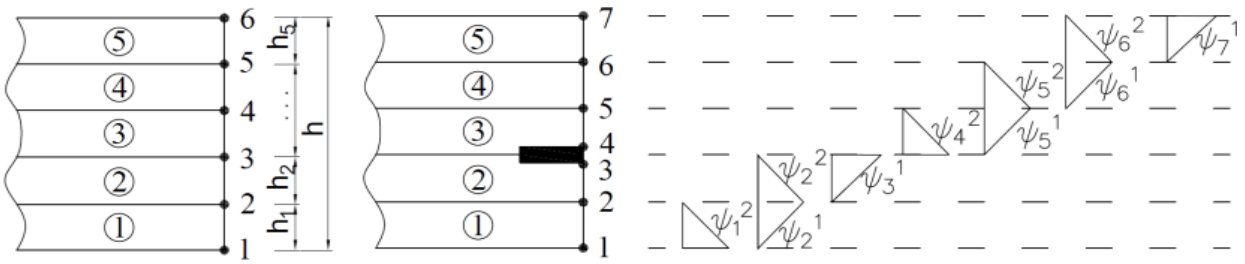

(a) (b) (c)

Figure 2: Discretization through the thickness of the plate

When the relations (1) and (2) are substituted into the known relations of the displacements and deformations, and after that into the known relations between the strains and the stresses, it is possible to finally obtain relations between the stresses and displacements of layer j:

$$\begin{Bmatrix}\sigma_{xx}\\ \sigma_{yy}\\ \sigma_{xy}\\ \sigma_{yz}\\ \sigma_{xz}\end{Bmatrix}^{(j)} = \begin{bmatrix}\overline{Q}_{11} & \overline{Q}_{12} & \overline{Q}_{16} & 0 & 0\\ \overline{Q}_{12} & \overline{Q}_{22} & \overline{Q}_{16} & 0 & 0\\ \overline{Q}_{16} & \overline{Q}_{26} & \overline{Q}_{66} & 0 & 0\\ 0 & 0 & 0 & \overline{Q}_{44} & \overline{Q}_{45}\\ 0 & 0 & 0 & \overline{Q}_{45} & \overline{Q}_{55}\end{bmatrix}^{(j)} \begin{Bmatrix}\dfrac{\partial u}{\partial x}+\sum_{J=1}^{n}\dfrac{\partial U^J}{\partial x}\phi^J\\ \dfrac{\partial v}{\partial y}+\sum_{J=1}^{n}\dfrac{\partial V^J}{\partial y}\phi^I\\ \dfrac{\partial u}{\partial y}+\dfrac{\partial v}{\partial x}+\sum_{J=1}^{n}\left(\dfrac{\partial U^J}{\partial y}+\dfrac{\partial V^J}{\partial x}\right)\phi^J\\ \sum_{J=1}^{n}V^J\dfrac{\partial\phi^J}{\partial z}\\ \sum_{J=1}^{n}U^J\dfrac{\partial\phi^J}{\partial z}\end{Bmatrix} \qquad (3)$$

where $\overline{Q}_{ij}$ are the transformed stiffnesses of j-th orthotropic layer which depend on material characteristics of the layer and the orientation angle of the fibers in the layer.

Cross-section forces are calculated with the following expressions:

$$\begin{Bmatrix} N_x \\ N_y \\ N_{xy} \\ Q_x \\ Q_y \end{Bmatrix} = \begin{bmatrix} A_{11} & A_{12} & A_{16} & 0 & 0 \\ A_{12} & A_{22} & A_{16} & 0 & 0 \\ A_{16} & A_{26} & A_{66} & 0 & 0 \\ 0 & 0 & 0 & A_{44} & A_{45} \\ 0 & 0 & 0 & A_{45} & A_{55} \end{bmatrix} x \begin{Bmatrix} \frac{\partial u}{\partial x} \\ \frac{\partial v}{\partial y} \\ \frac{\partial u}{\partial y} + \frac{\partial v}{\partial x} \\ \frac{\partial w}{\partial x} \\ \frac{\partial w}{\partial y} \end{Bmatrix} + \sum_{J=1}^{N} \begin{bmatrix} B_{11}^J & B_{12}^J & B_{16}^J & 0 & 0 \\ B_{12}^J & B_{22}^J & B_{26}^J & 0 & 0 \\ B_{16}^J & B_{16}^J & B_{66}^J & 0 & 0 \\ 0 & 0 & 0 & B_{44}^J & B_{45}^J \\ 0 & 0 & 0 & B_{45}^J & B_{55}^J \end{bmatrix} x \begin{Bmatrix} \frac{\partial U^J}{\partial x} \\ \frac{\partial V^J}{\partial y} \\ \frac{\partial U^J}{\partial y} + \frac{\partial V^J}{\partial x} \\ U^J \\ V^J \end{Bmatrix} \tag{4}$$

$$\begin{Bmatrix} N_x^J \\ N_y^J \\ N_{xy}^J \\ Q_x^J \\ Q_y^J \end{Bmatrix} = \begin{bmatrix} B_{11}^J & B_{12}^J & B_{16}^J & 0 & 0 \\ B_{12}^J & B_{22}^J & B_{26}^J & 0 & 0 \\ B_{16}^J & B_{26}^J & B_{66}^J & 0 & 0 \\ 0 & 0 & 0 & B_{44}^J & B_{45}^J \\ 0 & 0 & 0 & B_{45}^J & B_{44}^J \end{bmatrix} x \begin{Bmatrix} \frac{\partial u}{\partial x} \\ \frac{\partial v}{\partial y} \\ \frac{\partial u}{\partial y} + \frac{\partial v}{\partial x} \\ \frac{\partial w}{\partial x} \\ \frac{\partial w}{\partial y} \end{Bmatrix} + \sum_{I=1}^{N} \begin{bmatrix} D_{11}^{JI} & D_{12}^{JI} & D_{16}^{JI} & 0 & 0 \\ D_{12}^{JI} & D_{22}^{JI} & D_{26}^{JI} & 0 & 0 \\ D_{16}^{JI} & D_{16}^{JI} & D_{66}^{JI} & 0 & 0 \\ 0 & 0 & 0 & D_{44}^{JI} & D_{45}^{JI} \\ 0 & 0 & 0 & D_{45}^{JI} & D_{55}^{JI} \end{bmatrix} x \begin{Bmatrix} \frac{\partial U^I}{\partial x} \\ \frac{\partial V^I}{\partial y} \\ \frac{\partial U^I}{\partial y} + \frac{\partial V^I}{\partial x} \\ U^I \\ V^I \end{Bmatrix} \tag{5}$$

The occurrence of delamination at the connection between the two layers results in a significant change in the calculation process of stiffnesses of laminated plate, A_{ij}, B_{ij} and D_{ij}. Stiffnesses of laminated composite plate depend on the geometric and material characteristics of the plate, as well as on the adopted interpolation function through the thickness:

$$A_{ij} = \sum_{k=1}^{N} \int_{z_j}^{z_{k+1}} \bar{Q}_{ij}^{(k)} dz \qquad (i, j = 1,2,6,4,5)$$

$$B_{ij}^J = \sum_{k=1}^{N} \int_{z_k}^{z_{k+1}} \bar{Q}_{ij}^{(k)} \psi^J dz \qquad (i, j = 1,2,6) \qquad B_{ij}^J = \sum_{k=1}^{N} \int_{z_k}^{z_{k+1}} \bar{Q}_{ij}^{(k)} \psi,_z^J dz \qquad (i, j = 4,5) \tag{6}$$

$$D_{ij}^{JI} = \sum_{k=1}^{N} \int_{z_k}^{z_{k+1}} \bar{Q}_{ij}^{(k)} \psi^I \psi^J dz \quad (i, j = 1,2,6) \qquad D_{ij}^{JI} = \sum_{k=1}^{N} \int_{z_k}^{z_{k+1}} \bar{Q}_{ij}^{(k)} \psi,_z^I \psi,_z^J dz \qquad (i, j = 4,5)$$

The static equilibrium equations are derived from the general principle of virtual displacements. In the case when the angles of layers' orientation are parallel to the x and y-axes, zero values for the stifnesses $A_{16}=A_{26}=A_{45}=B_{16}^J=B_{26}^J=B_{45}^J=D_{16}^{JI}=D_{26}^{JI}=D_{45}^{JI}$ are obtained. In this case, the system of equations is determined by:

$$\begin{aligned}
&A_{11} u,_{xx} + A_{12} v,_{yx} + A_{66}\left(u,_{yy} + v,_{xy}\right) + \sum_{J=1}^{n}\left[B_{11}^J U,_{xx}^J + B_{12}^J V,_{yx}^J + B_{66}^J\left(U,_{yy}^J + V,_{xy}^J\right)\right] = 0 \\
&A_{12} u,_{xy} + A_{22} v,_{yy} + A_{66}\left(u,_{yx} + v,_{xx}\right) + \sum_{J=1}^{n}\left[B_{12}^J U,_{xy}^J + B_{22}^J V,_{yy}^J + B_{66}^J\left(U,_{yx}^J + V,_{xx}^J\right)\right] = 0 \\
&A_{55} w,_{xx} + A_{44} w,_{yy} + \sum_{J=1}^{n}\left[B_{55}^J U,_{x}^J + B_{44}^J V,_{y}^J\right] + q = 0 \\
&B_{11}^J u,_{xx} + B_{12}^J v,_{yx} + B_{66}^J\left(u,_{yy} + v,_{xy}\right) - B_{55}^J w,_{x} + \sum_{I=1}^{n}\left[D_{11}^{JI} U,_{xx}^I + D_{12}^{JI} V,_{yx}^I + D_{66}^{JI}\left(U,_{yy}^I + V,_{xy}^I\right) - D_{55}^{JI} U^I\right] = 0 \\
&B_{11}^J u,_{xy} + B_{21}^J v,_{yy} + B_{66}^J\left(u,_{yx} + v,_{xx}\right) - B_{44}^J w,_{y} + \sum_{I=1}^{n}\left[D_{12}^{JI} U,_{xy}^I + D_{22}^{JI} V,_{yy}^I + D_{66}^{JI}\left(U,_{yx}^I + V,_{xy}^I\right) - D_{44}^{JI} V^I\right] = 0
\end{aligned} \tag{7}$$

System of equations (7) consists of $(3+2n_d)$ equations for the section with delamination, or $3+2(N+2)$ equations, with the same number of unknown componental displacements.

Analytical solution

Displacement (1) and (2) are sought in the form of double trigonometric series, wherein the boundary conditions for a simply supported plate are met:

$$u=\sum_{m,n}^{\infty}X_{mn}\cos\frac{m\pi x}{a}\sin\frac{n\pi y}{b}\qquad v=\sum_{m,n}^{\infty}Y_{mn}\sin\frac{m\pi x}{a}\cos\frac{n\pi y}{b}\qquad w=\sum_{m,n}^{\infty}W_{mn}\sin\frac{m\pi x}{a}\sin\frac{n\pi y}{b}$$
$$U^{J}=\sum_{m,n}^{\infty}R_{mn}^{J}\cos\frac{m\pi x}{a}\sin\frac{n\pi y}{b}\qquad V^{J}=\sum_{m,n}^{\infty}S_{mn}^{J}\sin\frac{m\pi x}{a}\cos\frac{n\pi y}{b} \tag{8}$$

When the relations (8) are substituted in equation (7), the system of *3+2(N+2)* equations with unknown coefficients X_{mn}, Y_{mn}, W_{mn}, R_{mn} *and* S_{mn} is obtained. The system of equations is presented in an abbreviated form (9) :

$$\begin{bmatrix}[K] & [K^{j}]\\ [K^{j}]^{T} & [K^{ji}]\end{bmatrix}\begin{Bmatrix}X_{mn}\\ Y_{mn}\\ W_{mn}\\ R_{mn}^{J}\\ S_{mn}^{J}\end{Bmatrix}=\begin{Bmatrix}0\\ 0\\ Q_{mn}\\ 0\\ 0\end{Bmatrix} \tag{9}$$

After the determination of the unknown coefficients (9), by applying (1) and (2), the displacements of the arbitrary point with the coordinates (x, y, z) are obtained, and thus the corresponding stresses (3).

Numerical examples

The simply supported four-layer square laminated composite plate *axa,* with the thickness *h=0.1a* and loaded by uniformly distributed load of intensity q, is considered. Material characteristics of the layers are: $E_1/E_2=25$, $E_2=1$, $G_{12}=G_{13}=0.5$, $G_{23}=0.2$, $\nu_{12}=\nu_{13}=0.25$. The anti-symmetric arrangement of layers $0^0/90^0/0^0/90^0$ is adopted. Delamination is located between the second and the third layer.

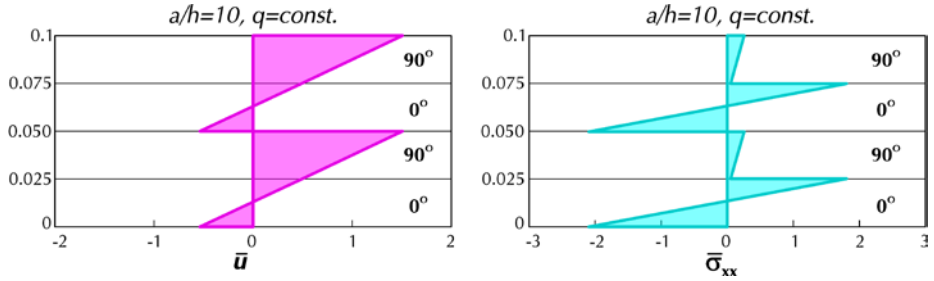

Figure 3: Displacements $\bar{u}(A,A,z)$ and stresses $\bar{\sigma}_{xx}(A,A,z)$, *h=0.1a*

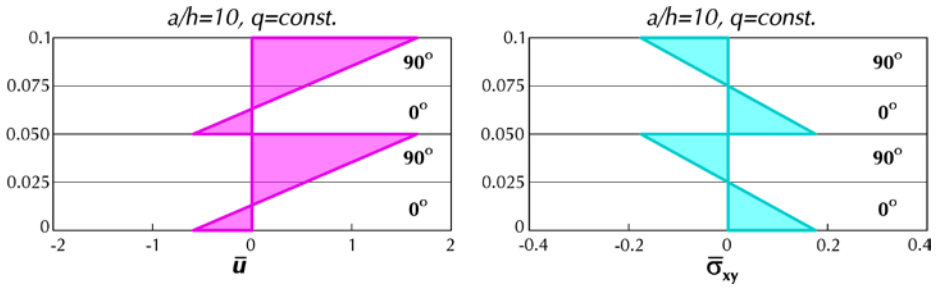

Figure 4: Displacements $\bar{u}(B,B,z)$ and stresses $\bar{\sigma}_{xy}(B,B,z)$, *h=0.1a*

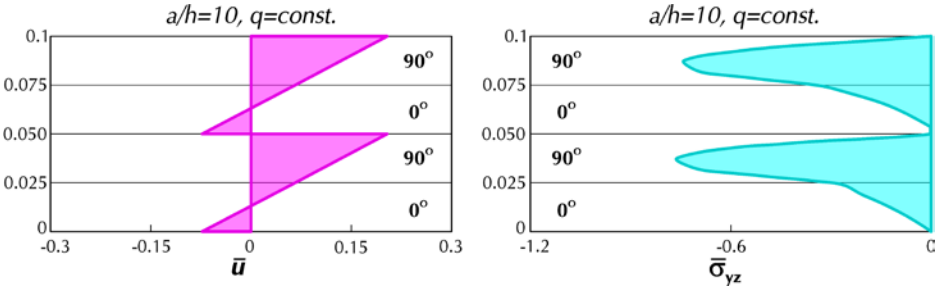

Figure 5: Displacements $\bar{u}(A,B,z)$ and stresses $\bar{\sigma}_{yz}(A,B,z)$, *h=0.1a*

The stresses and displacements are presented in dimensionless form, where *s=a/h*:

$$\bar{\sigma}_{xx} = \frac{1}{s^2 q}\sigma_{xx}, \bar{\sigma}_{xz} = \frac{1}{sq}\sigma_{xz}, \bar{\sigma}_{yz} = \frac{1}{sq}\sigma_{yz}, \bar{u} = \frac{100E_2}{hs^3 q}u \qquad (10)$$

in nodes with the coordinates *A=1.105662 (a/2)* and *B=1.894338 (a/2)*. Figures 3 to 6 show the displacement in the direction of x-axis and the normal and the transverse shear stresses through the thickness of the plate for *a/h=10* and q=const.

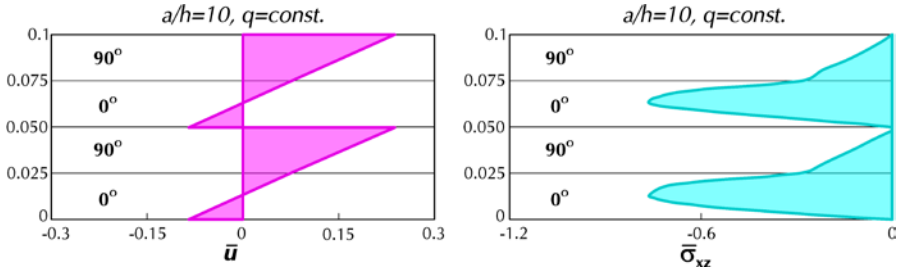

Figure 6: Displacements $\bar{u}(B,A,z)$ and stresses $\bar{\sigma}_{xz}(B,A,z)$, *h=0.1a*

Conclusions and Points for Discussions

Delamination between the layers can be included in the calculation by considering the problem at the level of layer. This paper presents the semi analytical method for the definition of the stress-strain state of laminated composite plate subjected to bending, by comprising inner delamination between two layers, wherein the anisotropy of the plate is included. Differential equations, obtained by applying Reddy's layerwise theory were solved analytically, whereby the discretization through the thickness of the plate is conducted by use of the 1D element.

For the characteristic points of the four-layer simply supported square laminated plate h=0,1 with anti-symmetric arrangement of orthogonal layers, and with delamination between the second and third layer, the results of calculated stresses and displacements are graphically displayed through the thickness of the plate.

It can be concluded that the maximum values of the stresses and displacement can be significantly changed by taking into account delamination. The plate thickness and the number of layers are influenced to the size of sliding at the node with delamination.

Key references

Bolotin, V.V. Delaminations in composite structures: its origin, buckling, growth and stability. Composite: Part B. 27(B), 129-145.

Reddy, J.N., Barbero, E.J., Teply, J.L.(1989). A plate bending element based on a generalized laminated plate theory. Int J Numer Meth Eng. 28, 2275-2292.

Reddy, J.N., Robbins, D.H. (1994). Theories and computational models for comp. lam. Appl Mech Rev 1994;47(6),147-65.

Rakočević, M., Vuksanović, Đ.(2002). Analytical solution of laminated rectangular composite plates - Monograph "Researches". Podgorica: Faculty of Civil Engineering, 253-266.

WG2

New Reinforced Concrete (RC) Structures

2.1 Serviceability Limit States

Serviceability limit states

Antonio Bilotta [1], Emidio Nigro [2]

The term Fiber Reinforced Polymers (FRP) indicates a wide range of composite materials, consisting of a polymeric organic matrix, which is impregnated with continuous fiber reinforcement. The technology can be used to produce bars with high mechanical properties.

In the fields of civil engineering, the use of FRP bars to reinforce the concrete was demonstrated particularly advantageous for the construction of civil or industrial buildings as well as bridge decks (Rizkalla and Nanni, 2003) mainly because FRP can ensure adequate durability of the structures. Moreover, a further specific property of fiber-reinforced composites, such as magnetic transparency, can be particularly useful when magnetic disturbance is required to be avoided: for instance in the construction of hospital rooms where advanced diagnostic equipment for Magnetic Resonance Imaging (MRI) is used (fib bulletin no. 40, 2007). Other possible applications, which appear as very promising and attractive, are related to provisional structures and tunnel coatings (M. Schürch and P. Jost, 2006). In particular, for tunneling projects the main purpose of a ground containment wall in concrete (namely soft eye walls) is allowing both the entrance and removal of the Tunnel Boring Machine (TBM). By using concrete reinforced with GFRP bars in the soft-eye region, the cutting operations are simplified due to the low transversal resistance of GFRP materials compared to steel.

It is clear that the use of these materials to replace steel, significantly increases the initial cost of the structure, but this increase may be acceptable if the total cost is considered (i.e. by incorporating maintenance costs) in a lifetime-oriented design. However, the use of FRP should be considered when tradition reinforcement is shown inadequate.

Despite FRP are a relatively new class of materials, thanks to several research studies over the last thirty years, they were quickly accepted as a valid structural materials for a variety of applications in civil engineering. In fact, high mechanical properties of FRP can ensure very high flexural strength to the concrete member, even if the elastic-fragile constitutive law is more suitable for statically determined structures in which bending redistribution is not required (Bakis et al., 2002). In addition, the vulnerability of FRP to high temperatures, typical of fire events, was shown to be mitigated when using to reinforce concrete members (Bisby et al., 2005).

For these reasons in the last decade several codes have been developed and also revised for the design of FRP reinforced concrete (RC) structures (CNR DT-203/2006, 2006; ACI 440.1 R-06 2006, CAN/CSA-S6-02, 2002) by extending with suitable modifications design criteria adopted for steel reinforced concrete structures.

However, the use of FRP bars shows a critical aspect for the serviceability checks due to different bond and mechanical properties of FRP bars with respect to steel bars. As concern the bond properties the bond mechanisms depends on the surface treatment very diversified among the industrial products. Similarly, the mechanical properties strongly depend on fiber type (Glass, Carbon, and Basalt) and percentage used for FRP bar manufacturing; in particular, the Young modulus of Glass and Basalt, less expensive than Carbon, is significantly lower than steel bars one. Taking this in mind, it is clear that design of FRP-RC members can be more governed by serviceability limit state (SLS) than ultimate limit state (ULS) (Pecce et al., 2000).

[1] DIST – Department of Structures for Engineering and Architecture, University of Naples Federico II, Italy
antonio.bilotta@unina.it
[2] DIST – Department of Structures for Engineering and Architecture, University of Naples Federico II, Italy
emidio.nigro@unina.it

In this regard, both research studies and the above codes provide check procedures obtained by design formulations for steel RC members refined, for FRP RC members, on experimental results of flexural test. Often suggestions provided by international codes for the assessment of the limit deflection do not lead to the same result (fib bulletin no. 40, 2007). Hence, a validation of theoretical predictions on further experimental results seemed suitable (Pecce et al 2001; Fico et al., 2008).

Nigro et al 2012, showed and discussed the results of flexural tests carried out in a four-point bending scheme on concrete slabs reinforced with GFRP bars in order to provide additional experimental data. Deflection prediction provided by Italian, American and Canadian codes for design of FRP reinforced concrete structures were in a good agreement with the experimental results at the serviceability limit state, and some times more conservative than prediction provided by more sophisticated procedure, such as integration of curvature along the member. However, a more depth investigation on the prediction provided by relationships suggested in Italian code pointed out that deflection predicting relationships should be better calibrated, being design of FRP- RC members more governed by serviceability limit state (SLS) than ultimate one (ULS).

Experimental results were also simulated by a FEM model analysis. Numerical analyses were performed by relying the FEM model used by Ellobody & Bailey (2008) to study the behavior of unbonded post-tensioned one-way concrete slabs and the uniaxial tension stress-strain law suggested by Belarbi & Hsu (1994), suitably modified to properly modeling the effect of tension stiffening in FRP reinforced concrete members.

Barris et al (2013) presents the results of an experimental programme on the cracking and deflections of 14 Glass-FRP RC beams. The adequacy of the most representative prediction models for the serviceability limit states of cracking and deflections of FRP RC beams was investigated. The influence of the most relevant parameters was analysed, and the suitability of different prediction models, as well as the adjustment of empirical coefficients, was analysed and discussed.

Gribniak et al (2013) showed test results of eight beams reinforced with glass fiber reinforced polymer (GFRP) or steel bars, combined with steel fibers. Experimental curvatures were checked against the predictions by design codes and recommendations to study capability of different code techniques to predict deformations of beams with varying reinforcement characteristics. It was shown that distribution of reinforcement had a significant influence on the prediction accuracy. In a more elaborate analysis, the tension-stiffening effect was investigated using an inverse technique earlier developed by the authors. Stress–strain tension-stiffening relationships were obtained for each of the beams using the test moment–curvature diagrams. Unlike the common practice, the analysis took into account the shrinkage effect which was different for steel and GFRP reinforced elements. To verify adequacy of the obtained results of constitutive modeling, the derived tension- stiffening relationships were implemented into finite element simulation as material laws for tensile concrete. It was shown that the above inverse approach offers an alternative and versatile tool for constitutive modeling.

Key references

ACI 440.1R-04 (2004). “Guide for the Design and Construction of Concrete Reinforced with FRP Bars”. American Concrete Institute, Farmington Hills, MI, USA.

Bakis C.E., Bank L.C., Brown V.L., Cosenza E., Davalos J.F., Lesko J.J., Machida A., Rizkalla S.H. and Triantafillou T.C. (2002) Fiber-Reinforced Polymer Composites for Construction - State-of-the-Art Review. Journal of Composites for Construction, Vol. 6, No. 2, May 1, 2002, ASCE. ISSN 1090-0268/2002/2-73-87

Barris C., L. Torres, J. Comas, C. Miàs (2013) Cracking and deflections in GFRP RC beams: An experimental study. Composites Part B: Engineering Volume 55, December 2013, Pages 580–590

Belarbi A. and Hsu T.T.C. (1994). “Constitutive Laws of Concrete in Tension and Reinforcing Bars Stiffened by Concrete”. Structural Journal - American Concrete Institute, Vol 91, pp. 465-474.

Bisby L.A., Green M.F., Kodur V.K.R. (2005) “Response to fire of concrete structures that incorporate FRP”. Prog Struct Eng Mater 2005, John Wiley & Sons Ltd, 7(3):136–49.

CAN/CSA-S6-02 (2002). “Design and Construction of Building Components with Fiber Reinforced Polymers”. Canadian Standards Association, Rexdale, Canada.

CNR-DT203/2006 (2006). “Guide for the Design and Constructions of Concrete Structures Reinforced with Fiber Reinforced Polymer Bar”. National Research Council, Rome, Italy.

Ellobody E. and Bailey C.G. (2008). “Behaviour of Unbonded Post-Tensioned One-way Concrete Slabs” Advances in Structural Engineering Vol. 11 No. 1 2008.

fib Bulletin No. 40 (2007). “FRP reinforcement in RC structures” pp. 160. September 2007. ISBN: 978-2-88394-080-2 Fico R., Prota A., G. Manfredi (2008). “Calibration of Bond Coefficient for Deflection Control of FRP RC Members”

Fourth International Conference on FRP Composites in Civil Engineering (CICE2008) 22-24 July 2008, Zurich, Switzerland

Gribniak V., G. Kaklauskas, L. Torres, A. Daniunas, E. Timinskas,E. Gudonis (2013). Comparative analysis of deformations and tension-stiffening in concrete beams reinforced with GFRP or steel bars and fibers Composites Part B: Engineering Volume 50, July 2013, Pages 158–170

Nigro E., A. Bilotta, G. Cefarelli, G. Manfredi, E. Cosenza (2012). Flexural tests on GFRP RC slabs: experimental results and numerical simulations. In: F. Biondini, D. Frangopol. Bridge, Maintenance, Safety, Management, Resilience and Sustainability. Stresa (VB), 8-12 July 2012, p. 3576-3585, London:CRC Press, ISBN: 9780415621243

Pecce, M., Manfredi, G., and Cosenza, E. (2000). "Experimental response and code models of GFRP RC beams in bending." Journal of Composites for Construction, 4(4), 182-190.

Pecce, M., Manfredi, G., and Cosenza, E. (2001). "A probabilistic assessment of deflections in FRP RC beams." 5th International Symposium on Fibre-Reinforced Polymer Reinforcement for Concrete Structures, 2 887-896.

Rizkalla S. and Nanni A., (2003). “Field applications of FRP reinforcement: case studies”. ACI SP-215, Farmington Hills Michigan, USA.

Schürch M. and Jost P. (2006). “GFRP Soft-Eye for TBM Breakthrough: Possibilities with a Modern Construction Material” International Symposium on Underground Excavation and Tunnelling. 2-4 February 2006, Bangkok, Thailand.

Cracking behaviour of GFRP RC flexural elements: an experimental study

C. Barris[1], L. Torres[2]

Introduction

Due to the mechanical properties of FRP, basically their lower modulus of elasticity and different bond behaviour, FRP reinforced concrete (RC) flexural members usually undergo large crack widths. Although crack width of FRP RC members can be relaxed because of the non-corrosive properties of FRP bars, it does need to be controlled to ensure other important serviceability aspects, such as appearance or being watertight.

Different theories to calculate crack width for steel RC elements state that it is mainly affected by the tensile strain of the rebar, the bond behaviour between the concrete and the rebar, the concrete cover and the distance between bars. Some of these theories have been adapted to FRP RC elements by introducing a bond coefficient, which should be provided, but at present very few studies show particular values according to their experimental data.

On the other hand, crack width has been traditionally measured in experiments with optical magnifiers or microscopes, although such techniques have shown to be subjected to a lack of homogeneity. Other methods, such as the placement of transducers once the crack has appeared, provide greater accuracy in the results, but imply that the test has to be stopped, and only the data at the position where the transducer is placed are registered. Deriving the crack width from the elongation of the layer where the reinforcement lies is another means of capturing the mean crack width, but with this technique the test needs also to be stopped and few data are recorded. Digital Image Correlation (DIC) is an optical and contactless measurement technique based on the acquisition and treatment of pictures of a previously defined field of interest to obtain full-field displacements and deformations during the test.

This contribution summarises the work presented in Barris et al. (2016), giving the results of the effect of different parameters affecting the cracking patterns of flexural elements reinforced with different types of Glass-FRP (GFRP) and steel bars, in order to assess the influence of these parameters on the cracking behaviour.

Experimental programme

The experimental programme aimed at evaluating the influence of the type of reinforcement, the reinforcement ratio, the concrete cover and the stirrup distance on the crack spacing and crack width of flexural RC elements. For this reason, 15 beam specimens internally reinforced with different types of GFRP or steel bars were tested under a four-point bending configuration (Figure 1).

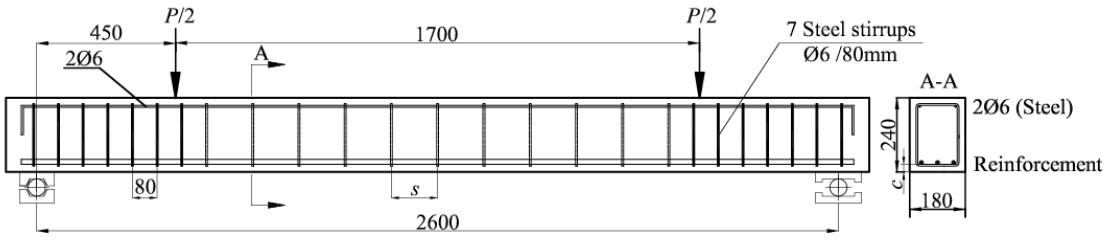

Figure 1: Geometric details of the tested beams (in mm).

The specimens were designated as Mat-Reinf-Cov-Sep (Table 1), where Mat denotes the material of the reinforcement (G1 or G2, for FRP type G1 or G2, respectively), Reinf the number and diameter of the

[1] AMADE, University of Girona, Spain, cristina.barris@udg.edu
[2] AMADE, University of Girona, Spain, lluis.torrres@udg.edu

reinforcement (i.e. 212 for 2 bars of 12 mm of diameter), Cov the concrete clear cover, and Sep the distance between the stirrups. In the case where FRP-G2 stirrups were provided this was indicated by the letter G at the end of the specimen designation. The load was applied in a displacement control mode at a displacement rate of 0.5 mm/min.

Table 1: Test specimens.

	Reinforcement		Cover (mm)	Stirrups in the flexural zone		ϕ/ρ_{eff}
Specimen	N. bars	Bar type		Type	Sep	
G1-216-25-150	2f16	FRP-G1	25	Steel	150	429
G1-216-25-250	2f16	FRP-G1	25	Steel	250	429
G1-216-25-000	2f16	FRP-G1	25	Steel	---	429
G1-212-25-150	2f12	FRP-G1	25	Steel	150	597
G1-212-40-150	2f12	FRP-G1	40	Steel	150	601
G1-212-55-150	2f12	FRP-G1	55	Steel	150	605
G2-213-25-150	2f13	FRP-G2	25	Steel	150	596
G2-213-25-000	2f13	FRP-G2	25	Steel	---	596
G2-310-25-000	3f10	FRP-G2	25	Steel	---	525
G2-213-25-150G	2f13	FRP-G2	25	FRP-G2	150	596
G2-213-25-250G	2f13	FRP-G2	25	FRP-G2	250	596
G2-216-25-150	2f16	FRP-G2	25	Steel	150	468
G2-313-25-150	3f13	FRP-G2	25	Steel	150	386
S-212-25-150	2f23	Steel	25	Steel	150	577
S-212-25-000	2f12	Steel	25	Steel	---	577

The concrete compressive strength ranged between 33.1 and 34.3 MPa and the modulus of elasticity varied between 24.8 and 27.9 GPa. As previously mentioned, two different types of GFRP bars were used as internal flexural reinforcement The modulus of elasticity of bars FRP-G1 ranged between 64.4 and 69.1 GPa, wilst for FRP-G2 bars ranged between 45.7 and 48.8 GPa.

Figure 2: Geometric details of the tested beams (in mm).

Crack width and spacing were consistently acquired by Digital Image Correlation (DIC) technique. The 2D setup was chosen for acquiring the vertical and horizontal displacements of the front face of the beam

specimens. The test setup comprised 4 high-resolution digital cameras with a resolution of 2452x2056 pixels that recorded pictures at regular time intervals of 2 pictures/second during each test. The central flexural zone was acquired and between 8 to 11 cracks were analysed per specimen.

Results on crack spacing

Maximum crack spacing was found to be 1.32 times the mean crack spacing and 2.14 times the minimum crack spacing. These values are in accordance with those found previously in the literature (Borosnyói and Balázs 2005).

The ϕ/ρ_{eff} ratio, which is generally attributed to influence on the transfer length and to internal cracks in the vicinity of the crack, influences crack spacing: the bigger the ϕ/ρ_{eff} ratio, the larger the crack spacing. This was observed for both maximum and mean values.

The effect of concrete cover on crack spacing in steel RC has been widely discussed in the literature. The experimental crack patterns obtained in Barris et al. (2016) highlight the influence of cover on crack spacing at the surface of the specimen. In general, it was observed that higher covers provided higher values of crack spacing, although the dispersion of values also increased.

Bond behaviour between concrete and bar was assessed through adjusting the bond coefficients in expressions of Eurocode 2 to the experimental results. Results show that FRP-G1 bar provides lower values of the bond coefficient and FRP-G2 bar provides higher values, compared to that obtained for steel reinforcement. This is attributed to the different types of coating of the FRP bars that give different distribution of strains along the reinforcement.

Results on crack width

Crack width was obtained by the difference between the displacement values of two points, each one at one side of the crack and at the same height. On average, the maximum crack width at the height of the reinforcement is 1.36 times the mean value, and it is 0.87 times the maximum crack width at the bottom of the beam. These values are in agreement with those previously found in Barris et al. (2013).

The effect of the reinforcement ratio, as expected is that higher reinforcement ratios provide lower crack widths due to the higher stiffness of the section. Specimens having similar reinforcement ratios provide close values of the crack width and with slightly higher values for larger bar diameter and bar spacing. On the other hand, changing the cover implies modifying the stiffness of the section by changing the effective depth. Barris et al. (2016) found that higher values of cover derived to higher values of reinforcement strain for the same load and consequently higher values of crack width.

The influence of bond between concrete and reinforcement on crack width is one aspect that needs to be further studied for FRP RC members. Barris et al. (2016) present an adjustment of the bond coefficient k_b to the experimental maximum crack width for the three types of reinforcing bars by using different formulations presented in design codes and guidelines. The bond coefficient is calculated following the least squares methodology at different load levels between the stabilised cracking load and the service load, and is shown in Table 2. The results show that FRP-G1 bars provide bond coefficient values lower than those for FRP-G2 and steel reinforcement. This difference is attributed to the type of bar and surface configuration.

Table 2: Bond coefficient k_b for the maximum crack width.

Standard	Expression	FRP-G1	FRP-G2	Steel
CAN/CSA-S806	$w = 2 \cdot \frac{f_f}{E_f} \cdot \beta \cdot k_b \cdot \sqrt{d_c^2 + \left(\frac{s}{2}\right)^2}$	1.20	1.35	1.21
ISIS Canada	$w = 2.2 \cdot \frac{f_f}{E_f} \cdot \beta \cdot k_b \cdot \sqrt[3]{d_c A}$	1.21	1.31	1.33
JSCE	$w = k_b \cdot \left(4c + 0{,}7 \cdot (s - \phi)\right) \cdot \frac{f_f}{E_f}$	0.94	1.00	0.98

Conclusions and Points for Discussions

The cracking behaviour of FRP RC elements is revised in Barris et al. (2016) trough an experimental programme. In this case, DIC technique is used to assess crack spacing and crack width. The main parameters that are studied are the type of reinforcing bar, the reinforcement ratio, the concrete cover, and the influence of stirrups. The study concludes with the following outcomes:

- DIC technique is proven to be a powerful tool to consistently acquire the field of displacements of a given field of view.
- In general terms, crack spacing increases with cover and ϕ/ρ_{eff} ratio.
- The experimental mean crack width value, calculated as the mean of 8-11 cracks created in the central zone, increases with the decrease of $n\rho$ and the increase of the cover.
- Bond coefficients have been adjusted for different formulations regarding crack width and spacing. The obtained coefficients show that FRP-G1 bars present lower values of bond coefficients than FRP-G2 bars.

Points for discussion that need further research can be:

- The influence of concrete cover on crack width independently of the stiffness of the section.
- The bond coefficients presented in this communication are only calibrated for the data presented in Barris et al. (2016). Further data is needed to better assess bond coefficients on the present empirical equations .

Key references

Barris, C., Torres, L., Vilanova, I., Miàs, C., Llorens, M. (2016). Experimental study on crack width and crack spacing for Glass-FRP reinforced concrete beams. *Engineering structures*, under publication. Doi: 10.1016/j.engstruct.2016.11.007.

Borosnyói, A., Balázs, G. (2005). Models for flexural cracking in concrete: The state of the art. *Structural Concrete* 6, 53-62.

Barris, C., Torres, L., Comas, J., Miàs, C. (2013). Cracking and deflections in GFRP RC beams: An experimental study. *Composites Part B: Engineering* 55, 580-490.

Deflections in FRP RC elements

C. Barris[1], L. Torres[2]

Introduction

When FRP bars are used as internal reinforcement of concrete members, different structural behaviour is expected due to their different mechanical and bond properties compared to those of steel rebars, in particular, their relatively low modulus of elasticity and their linear stress-strain behaviour until failure. The lower stiffness of FRP bars can yield to large strains being mobilized in the bars at low levels of external loads and lead to large crack widths and deflections. As a result, the design of concrete elements reinforced with FRP materials is often governed by the serviceability limit states (SLS), especially in the case of GFRP.

In the last decades, a number of studies were carried out to investigate the flexural response of FRP reinforced concrete (RC) beams. Most of them show a limited number of experimental results and comparisons that often arrive at proposals for modifications of existing design procedures. In the case of serviceability, and specifically for deflections of FRP RC elements, several authors propose coefficients to modify Branson's equation used in steel design codes, whereas other researchers suggest a modified equivalent moment of inertia derived from the integration of curvatures along the beam. These different approaches have been adopted in the various design guideline proposals for FRP RC.

This contribution aims at collecting different design equations regarding the calculation of deflections of FRP RC flexural elements, and compares their predictions with the experimental results obtained in the experimental programme of Barris and Torres (2011).

Existing approaches for the calculation of deflections for FRP RC flexural elements

In the literature, some theoretical approaches to estimate the deflection for a FRP RC flexural element are based on Branson equation (Branson 1977), which is an empirical relationship that provides a gradual transition of a transformed moment of inertia, from the uncracked to the fully cracked state. Although Branson equation gives an adequate estimate for the deflection of steel RC elements, it clearly underestimates the deflection of FRP RC elements (Faza and GangaRao 1992, Benmokrane et al. 1996, Pecce et al. 2000, Razaqpur et al. 2000, Toutanji and Saafi 2000, Yost et al. 2003, Mota et al. 2006, Saikia et al. 2007, Rafi et al. 2008, Vogel and Svecova 2009, Barris et al. 2009, Al-Sunna et al. 2012). Bischoff (2005) attributes this difference to the different relationship between the uncracted and the cracked moment of inertia of a FRP RC member compared to that of usual steel RC elements. In Table 1, a summary of the available prediction models to calculate deflections of FRP RC flexural members is shown. They can be classified in those derived from Branson equation (Benmokrane et al. 1996, Toutanji and Saafi 2000, Yost et al. 2003), and those where deflection is calculated as an interpolation between a cracked and an uncracked state of a deformation parameter, curvature or deflection (Faza and GangaRao 1992, CEN 2004, Bischoff 2005). Some of the existing design guidelines for FRP RC have adopted these approaches in their methodology to calculate deflections (ISIS Canada 2007, ACI Committee 440 2006).

Comparison with the experimental programme in Barris and Torres (2011)

An experimental programme on 26 GFRP RC beams was performed in Barris and Torres (2011), and it is summarised below. The beams were designated with an adequate amount of longitudinal and shear reinforcement to fail by crushing of the concrete in the central zone. Their dimensions and test setup is shown in Figure 1.

[1] Universitat de Girona, Spain, cristina.barris@udg.edu
[2] Universitat de Girona, Spain, lluis.torres@udg.edu

Table 1: Available formulations to calculate deflections of FRP RC flexural elements

Approach	Expresion
Benmokrane et al. (1996)	$I_e = \alpha I_{cr} + \left(\frac{I_g}{\beta} - \alpha I_{cr}\right)\left(\frac{M_{cr}}{M_a}\right)^3$ $\alpha = 0.84$ $\beta = 7$
Faza and GangaRao (1992)	$\delta_{\max} = \frac{23PL^3}{648E_cI_m}$ $I_m = \frac{23I_{cr}I_e}{8I_{cr}+15I_e}$
Yost et al. (2003)	$I_e = \left(\frac{M_{cr}}{M_a}\right)^3 \beta_d I_g + \left(1-\left(\frac{M_{cr}}{M_a}\right)^3\right) I_{cr} \le I_g$ $\beta_d = \alpha_b\left(\frac{E_f}{E_s}+1\right)$ $\alpha_b = 0.064\left(\frac{\rho}{\rho_{fb}}\right)+0.13$
ACI 440.1R-03	$I_e = \left(\frac{M_{cr}}{M_a}\right)^3 \beta_d I_g + \left(1-\left(\frac{M_{cr}}{M_a}\right)^3\right) I_{cr} \le I_g$ $\beta_d = \alpha_b\left(\frac{E_f}{E_s}+1\right)$ $\alpha_b = 0.5$
ACI 440.1R-06	$I_e = \left(\frac{M_{cr}}{M_a}\right)^3 \beta_d I_g + \left(1-\left(\frac{M_{cr}}{M_a}\right)^3\right) I_{cr} \le I_g$ $\beta_d = \frac{1}{5}\left(\frac{\rho}{\rho_{fb}}\right)$
Alsayed et al. (2000)	$I_e = \left(\frac{M_{cr}}{M_a}\right)^{5,5} I_g + \left(1-\left(\frac{M_{cr}}{M_a}\right)^{5,5}\right) I_{cr} \le I_g$
Toutanji and Saafi (2000)	$I_e = \left(\frac{M_{cr}}{M_a}\right)^m I_g + \left(1-\left(\frac{M_{cr}}{M_a}\right)^m\right) I_{cr} \le I_g$ $m = 6 - 10\left(E_f/E_s\right)\rho$ if $\left(E_f/E_s\right)\rho < 0.3$ $m = 3$ if $\left(E_f/E_s\right)\rho \ge 0.3$
CAN/CSA-S806 (2012)	$\delta_{\max} = \frac{PL^3}{24E_cI_{cr}}\left[3\left(\frac{a}{L}\right) - 4\left(\frac{a}{L}\right)^3 - 8\left(1-\frac{I_{cr}}{I_g}\right)\left(\frac{L_g}{L}\right)^3\right]$
ISIS Canada (2007)	$I_e = \frac{I_g I_{cr}}{I_{cr} + \left(1 - 0.5\left(M_{cr}/M_a\right)^2\right)\left(I_g - I_{cr}\right)}$
Bischoff (2005)	$I_e = \frac{I_{cr}}{1-\eta\left(M_{cr}/M_{\max}\right)^2} \le I_g; \eta = 1 - \frac{I_{cr}}{I_g}$
CNR-DT203 (2006)	$\delta = \zeta\delta_{II} + \left(1-\zeta\right)\delta_I$ $\zeta = 1 - \beta_1\beta_2\left(\frac{M_{cr}}{M_{\max}}\right)^2$ $\beta_1 = 0.5$
Eurocode 2 (1992)	$\delta = \zeta\delta_{II} + \left(1-\zeta\right)\delta_I$ $\zeta = 1 - \beta_1\beta_2\left(\frac{\sigma_{sr}}{\sigma_s}\right)^2$

Eurocode 2 (2004)	$\delta = \zeta\delta_{II} + (1-\zeta)\delta_I \qquad \zeta = 1-\beta\left(\frac{\sigma_{sr}}{\sigma_s}\right)^2$

Notation:
I_e: effective moment of inertia; I_{cr}: cracked moment of inertia; I_g: gross moment of inertia; M_{cr}: cracking moment; M_a: applied moment; M_{max}: maximum applied moment; E_f, E_s: modulus of elasticity of the reinforcement (subscript *s* for steel, *f* for FRP); ρ: reinforcement ratio; ρ_{fb}: balanced reinforcement ratio; δ: deflection; δ_I: uncracked-state deflection; δ_{II}: cracked-state deflection; β_1: 1.0 for high-bond or 0.5 for plain rebars; β_2, β (EC2): 1.0 for short-term loading or 0.5 for sustained; *P*: applied load; *L*: beam length; L_g: distance of the uncracked beam; *a*: length of the shear span E_c: concrete modulus of elasticity.

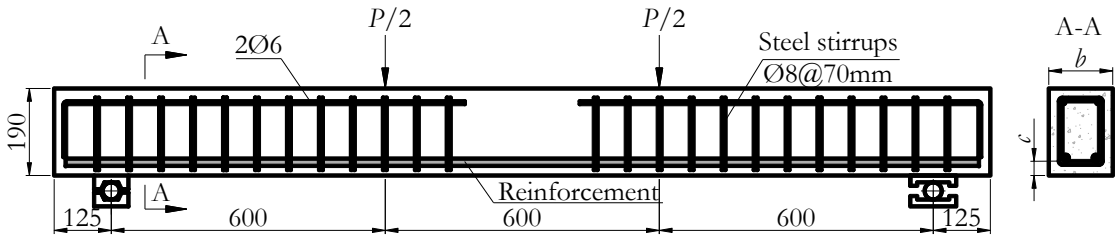

Figure 1: Geometric and reinforcement details (dimensions in mm)

Three different amounts of longitudinal reinforcement, two different effective depth-to-total depth ratios and two different concrete grades were used to obtain a wide range of cracked stiffness response. Further information regarding the test setup and parameters is found in Barris and Torres (2011).

In this section, the experimental load-midspan deflection is compared to the prediction models shown in Table 1. The evolution of the deflection, both theoretical and experimental, is shown up to a load level of 35% the ultimate load, which is considered in this work an upper bound value for the service load. The experimental cracking load has been considered independently of the approach used for the deflection calculation. Hence, the possible influence of the environmental factors has been inherently incorporated.

Figure 2 shows the comparison between experimental and theoretical midspan deflection for those models derived from Branson equation. As it was previously reported in the literature, those expressions which propose a reduction on the gross and/or cracked moment of inertia generally overestimate the deflection response. This result may be a consequence of the different values of the reinforcement ratio considered in this study compared to the values at which those equations were calibrated. On the contrary, Toutanji and Saafi (2000) approach, which suggests a modification on the power factor *m* of Branson equation depending on the reinforcement ratio, results to fit correctly the experimental data response.

Figure 3 shows the comparison between experimental and theoretical midspan deflection for those models based on a rational interpolation of a deformational parameter. Results show that these approaches compare relatively well with the experimental data in the range of the serviceability loads; however, a trend to underestimate deflections when the load increases is observed. To evaluate the deflection according to Eurocode 2 (2004) provisions, the interpolation of curvatures and an integration of the curvature along the beam has been performed, with a β_2 coefficient equal to 1. Bischoff (2005)

equation, which was adopted by ACI 440.1R-15 uses a tension stiffening approach that allows deriving an effective moment of inertia for the member. The deflection resultant from its application is practically coincident with that obtained from integration of curvatures using Eurocode 2 approach. ISIS Canada (2007) suggests a similar approach to Bischoff (2005); however, the equation includes a factor $\gamma = 0.5$ that shifts horizontally the deflection response just after the cracking load is attained. Finally, models neglecting the tension stiffening effect such as CAN/CSA-S806 (2012) or Faza and GangaRao (1992) are proven to overestimate the deflection response, especially at load levels close to the cracking load.

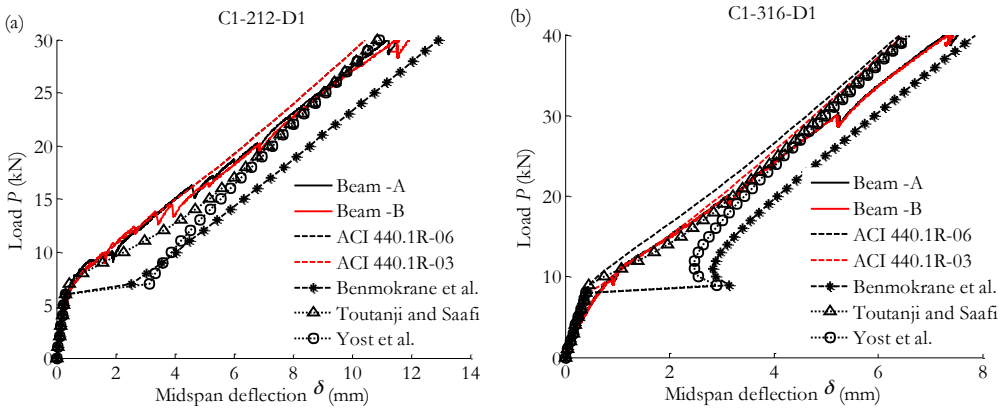

Figure 2: Experimental vs. theoretical midspan deflection for models derived from Branson equation. Comparison for beam with (a) ρ=1%, (b) ρ=2.7%

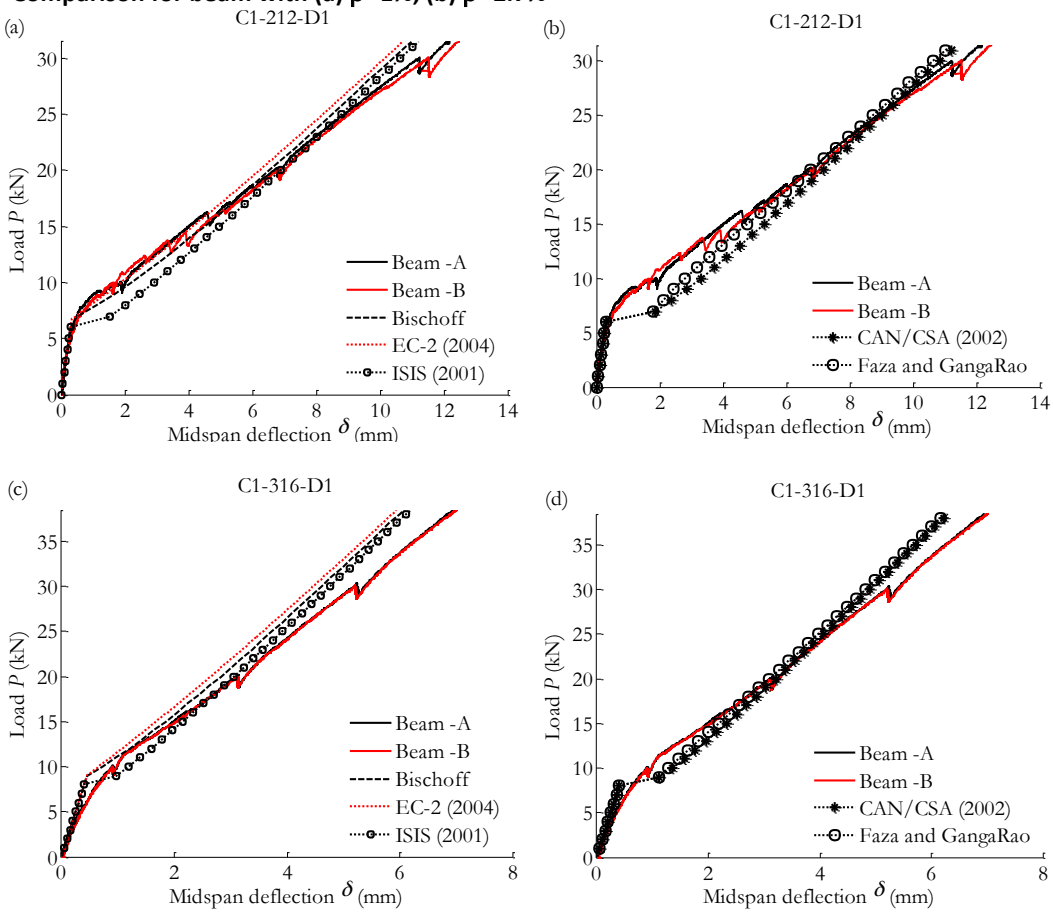

Figure 3: Experimental vs. theoretical midspan deflection for models derived from integration of a deformational parameter. Comparison for beam with (a) ρ=1%, (b) ρ=2.7%

Comparison between experimental results and theoretical models

In this section, a measure of the relative fit between the experimental and the theoretical deflections is presented through the ratio δ_{th}/δ_{exp}, evaluated at a moment ratio M/M_{cr} of 1.5, 3 and 4.5. In Table 2, the mean value and standard deviation of the ratio δ_{th}/δ_{exp} are shown. As observed, the most scattered results, with σ_δ = 0.17-1.03, are obtained for M_a/M_{cr} = 1.5.

At M_a/M_{cr} = 1.5, Benmokrane et al. (1996), CAN/CSA-S806 (2012), Faza and GangaRao (1992), ISIS Canada (2007) and Yost et al. (2003) prediction models propose a theoretical deflection that is about twice or more the experimentally obtained. On the contrary, Eurocode 2, which is a design code though for steel RC, presents the best estimate to the experimental deflection, together with ACI 440.1R-06 and ACI 440.1R-03. None of the studied approaches underestimates the experimental deflection.

At M_a/M_{cr} = 3.0, all of the approaches get closer to the experimental data. Evidence of that statement is that all the mean values and standard deviations of the ratio δ_{th}/δ_{exp} are closer to 1.0 and 0.0 respectively. Benmokrane et al. (1996), however, provides a theoretical deflection that is 45% higher than the experimental.

Finally, at M_a/M_{cr} = 4.5, the approaches converge even more to the experimental data, except Eurocode 2, who slightly underestimates deflections at this loading ratio.

Table 2: Statistical parameters for deflection provisions

Approach	M_s/M_{cr} = 1.5		M_s/M_{cr} = 3.0		M_s/M_{cr} = 4.5	
	$\bar{\delta}$	σ_δ	$\bar{\delta}$	σ_δ	$\bar{\delta}$	σ_δ
ACI 440.1R-03	1.29	0.20	1.09	0.09	1.00	0.06
ACI 440.1R-06	1.27	0.26	1.09	0.09	1.00	0.07
Benmokrane et al. (1996)	1.98	1.03	1.45	0.14	1.23	0.07
Bischoff (2005)	1.51	0.28	1.10	0.10	0.99	0.06
CAN/CSA-S806 (2012)	2.23	0.45	1.20	0.12	1.03	0.06
Eurocode 2 (2004)	1.14	0.33	1.03	0.15	0.96	0.12
Faza and GangaRao (1992)	1.94	0.34	1.15	0.10	1.01	0.06
ISIS Canada (2007)	1.98	0.39	1.16	0.11	1.01	0.06
Toutanji and Saafi (2000)	1.62	0.26	1.21	0.18	1.03	0.06
Yost et al. (2003)	2.72	0.46	1.23	0.13	1.03	0.06

Conclusions and Points for Discussions

Due to the lower modulus of elasticity of FRP reinforcement compared to that of steel, FRP RC flexural elements usually undergo larger deflections. This communication presents a summary of different design equations to calculate the instantaneous deflection of FRP RC elements. Formulation is compared to an experimental programme on 26 GFPR RC beams described in Barris and Torres (2011). It is found that formulations based on rational procedures of interpolation between a cracked and an uncracked deformational parameter reproduce adequately the deformational behaviour of GFRP RC flexural elements. Other approaches that underestimate tension-stiffening effect or suggest a large

increase in deflections after reaching the cracking load result in overestimating the experimental response at the first stages of loading. Nevertheless, further studies are needed to expand these conclusions to actual structures such as statically indeterminate beams or prestressed members. Moreover, the effect of repeated loading and the influence of shear deformations on the overall deflection response should be also further analysed.

Key references

ACI Committee 440. (2001). ACI 440.1R-01. Guide for the design and construction of concrete reinforced with FRP bars. American Concrete Institute (ACI), Farmington Hills, Mich., USA, 41pp.

ACI Committee 440. (2003). ACI 440.1R-03. Guide for the design and construction of concrete reinforced with FRP bars. American Concrete Institute (ACI), Farmington Hills, Mich., USA, 42pp.

ACI Committee 440. (2006). ACI 440.1R-06. Guide for the design and construction of concrete reinforced with FRP bars. American Concrete Institute (ACI), Farmington Hills, Mich., USA, 45pp.

ACI Committee 440. (2015). ACI 440.1R-15. Guide for the design and construction of concrete reinforced with FRP bars. American Concrete Institute (ACI), Farmington Hills, Mich., USA, 83pp.

Alsayed, S. H., Al-Salloum, Y. A., and Almusallam, T. H. (2000). Performance of glass fiber reinforced plastic bars as a reinforcing material for concrete structures. *Composites Part B: Engineering*, 31(6-7), 555-567.

Al-Sunna, R., Pilakoutas, K., Hajirasouliha, I., Guadagnini, M. (2012). Deflection behaviour of FRP reinforced concrete beams and slabs: An experimental investigation. *Composites Part B: Engineering*, 43(5), 2125-2134.

Barris, C. Torres, L., Turon, A., Baena, M., Catalan, A. (2009). An experimental study of the flexural behaviour of GFRP RC beams and comparison with prediction models. *Composite Structures* 91(3), 286-295.

Barris, C., and Torres, L. (2011). Fibre reinforced polymer reinforced concrete beams. Serviceability behaviour: testing and analysis. PhD Thesis, Universitat de Girona (Spain), LAP LAMBERT Academic Publishing GmbH & Co. KG, 321 pp.

Benmokrane, B., Chaallal, O., and Masmoudi, R. (1996). Flexural response of concrete beams reinforced with FRP reinforcing bars. *ACI Structural Journal*, 93(1), 46-55.

Bischoff, P. H. (2005). Reevaluation of deflection prediction for concrete beams reinforced with steel and fiber reinforced polymer bars. *Journal of Structural Engineering*, 131(5), 752-762.

Branson, D. (1977) Deformation of concrete structures. McGraw-Hill, New York.

CAN/CSA. (2002). CAN/CSA-S806. Design and construction of building components with fibre-reinforced polymers. Canadian Standards Association, Ontario, Canada, 177pp.

CEN. (1992). Eurocode 2: Design of concrete structures - Part 1.1: General rules and rules for buildings (EN 1992-1-1:1992). Comité Europeen De Normalisation, Brussels, 195 pp.

CEN. (2004). Eurocode 2: Design of concrete structures - Part 1.1: General rules and rules for buildings (EN 1992-1-1:2004). Comité Europeen De Normalisation, Brussels, 225 pp.

CNR-DT 203. (2006). Guide for the Design and Construction of Concrete Structures Reinforced with Fiber-Reinforced Polymer Bars. Advisory Committee on Technical Recommendations for Construction, 39pp.

Faza, S. S., and GangaRao, H. V. S. (1992). Pre- and post-cracking deflection behaviour of concrete beams reinforced with fibre-reinforced plastic rebars. *Proceedings of The First International Conference on the Use of Advanced Composite Materials in Bridges and Structures,* K.W. Neale and P. Labossière, Editors; Canadian Society for Civil Engineering, 1992, 151-160.

ISIS Canada. (2007). Reinforcing concrete structures with fibre reinforced polymers - Design manual No. 3. ISIS Canada Corporation. University of Manitoba, Manitoba, Canada, 150pp.

Mota, C., Alminar, S., Svecova, D. (2006). Critical review of deflection formulas for FRP-RC members. *Journal of Composites for Construction* 10(3), 183-194.

Pecce, M., Manfredi, G., Cosenza, E. (2000). Experimental response and code models of GFRP RC beams in bending. *Journal of Composites for Construction*, 4(4), 182-190.

Rafi, M.M., Nadjai, A., Ali, F., Talamona, D. (2008). Aspects of behaviour of CFRP reinforced concrete beams in bending. Construction and Building Materials 22, 277-285.

Saikia, B., Kumar, P., Thomas, J., Rao, K. S. N., and Ramaswamy, A. (2007). Strength and serviceability performance of beams reinforced with GFRP bars in flexure. Construction and Building Materials 21(8), 1709-1719.

Toutanji, H. A., and Saafi, M. (2000). Flexural behavior of concrete beams reinforced with glass fiber-reinforced polymer (GFRP) bars. *ACI Structural Journal*, 97(5), 712-719.

Razaqpur, A., Svecova, D., Cheung, M. (2000). Rational method for calculating deflection of fiber-reinforced polymer reinforced beams. *ACI Structural Journal*, 97(1), 175-184.

Vogel, H., Svecova, D. (2009). Effective moment of inertia expression for concrete beams reinforced with Fiber-Reinforced Polymer (FRP). *ACI Special Publication* 264, 77-93.

Yost, J. R., Gross, S. P., and Dinehart, D. W. (2003). Effective Moment of Inertia for Glass Fiber-Reinforced Polymer-Reinforced Concrete Beams. *ACI Structural Journal*, 100(6), 732-739.

2.2 Ultimate Limit States

Shear Strength and Size Effect in FRP RC beams

S. Cholostiakow[1], M. Di Benedetti[2], M. Guadagnini[3]

Introduction

The shear performance of reinforced concrete (RC) members is governed by the development of a complex set of mechanisms. Shear stresses can, in fact, be transferred through a section of an element by the portion of concrete in compression, aggregate interlock, friction along a diagonal shear crack, dowel action of the longitudinal reinforcement and, when provided, the transverse shear reinforcement. Various studies have examined the shear behaviour of steel RC beams and have shown that member size directly affects the magnitude of the shear resisting mechanisms. Kani (1967) examined the performance of a series of beams with varying depth and constant steel reinforcement ratio and observed that lower normalised shear strength can be developed in beams with higher effective depth. Work by various researchers (Shioya et al. 1990, Frosch 2000, Lubell et al. 2004) proved that size effect may be attributed mainly to the reduction of aggregate interlock as a result of the larger cracks that develop in larger elements. Although shear in FRP RC beams is transferred through the development of the same resisting mechanisms as for steel RC, their magnitude and individual contributions to overall shear capacity needs to be carefully reassessed. In fact, under similar loading conditions FRP RC elements can develop much higher deformations, thus exhibiting wider cracks than their equivalent steel RC counterparts. In turn, these larger deformations result in a reduced portion of concrete in compression resisting shear and in a weakened aggregate interlock along the cracks. In addition, due to the low transverse shear resistance of the FRP bars, the contribution of dowel action is significantly lower (Razaqpur et al. 2004).
While the overall shear behaviour of FRP RC is well documented (e.g, Guadagnini et al. 2006), research on the effect of element size on shear strength is still limited (Bentz 2010, Alam and Hussein 2013, Ashour and Kara 2014). This paper discusses the results of an extensive experimental programme carried out on geometrically similar FRP RC beams (with and without FRP shear reinforcement), with varying overall depth. The results will help to understand better shear behaviour of FRP RC beams and will assist in developing more reliable predictive design models for large FRP RC members.

Experimental programme

The experimental programme was designed primarily to investigate the size effect on shear behaviour of FRP RC beams with and without FRP shear reinforcement. A total of 12 tests were carried out on 6 FRP reinforced RC beams similar in geometry and mechanical parameters, otherwise varying in the overall depth. The specimens were divided in two groups, where the first contained beams without shear reinforcement (GB54-GB59) and the second beams reinforced with closed external FRP links (GB60-GB65) in an amount to satisfy the minimum shear stress demand according to ACI440. The primary variables were overall depth of the member, concrete compressive strength and the presence of shear reinforcement. All other parameters, including reinforcement ratio, shear-span-to-depth ratio and modulus of elasticity of the longitudinal reinforcement were kept constant for all specimens. The beams were cast using two concrete batches of ready mix concrete and the average concrete strength,

[1] University of Sheffield, UK, s.cholostiakow@sheffield.ac.uk
[2] University of Sheffield, UK, m.dibenedetti@sheffield.ac.uk
[3] University of Sheffield, UK, m.guadagnini@sheffield.ac.uk

f_{cy}, for each beam is also reported in Table 1 as measured on the day of testing. The longitudinal reinforcement ratio, ρ_{lf}, and shear span to depth ratio, a/d, were similar for all specimens (Table 1), while the overall depth, d, varied from 260 mm to 460 mm (Fig. 1b). The longitudinal reinforcement consisted of 12.7 mm GFRP bars in tension, while 6 mm basalt FRP (BFRP) bars were used as compression and lateral reinforcement.

Two tests were performed on each of the specimen examining each shear span separately (example of the test setup for beams GB54 and GB64 and their retests are shown on Fig. 1a). During the first phase (specimens with the even numbers) the position of the load was selected so as to induce shear failure along the shorter of the shear spans, (a) in Figure 1a, while maintaining relatively low average shear stress levels along the adjoining shear span (b+c) to ensure that this would remain relatively undamaged. Before the second phase of the test (specimens with the odd numbers), the damaged portion of each beam (shear span a) was cut, and post-tensioned metal straps (PTMS) were wrapped along span b to provide the required additional shear strength and avoid failure in this zone. Given that the two shear spans of the beams of 460mm overall depth were similar, PTMS were used in each phase of testing to strengthen one of the shear spans and ensure failure of the investigated shear span.

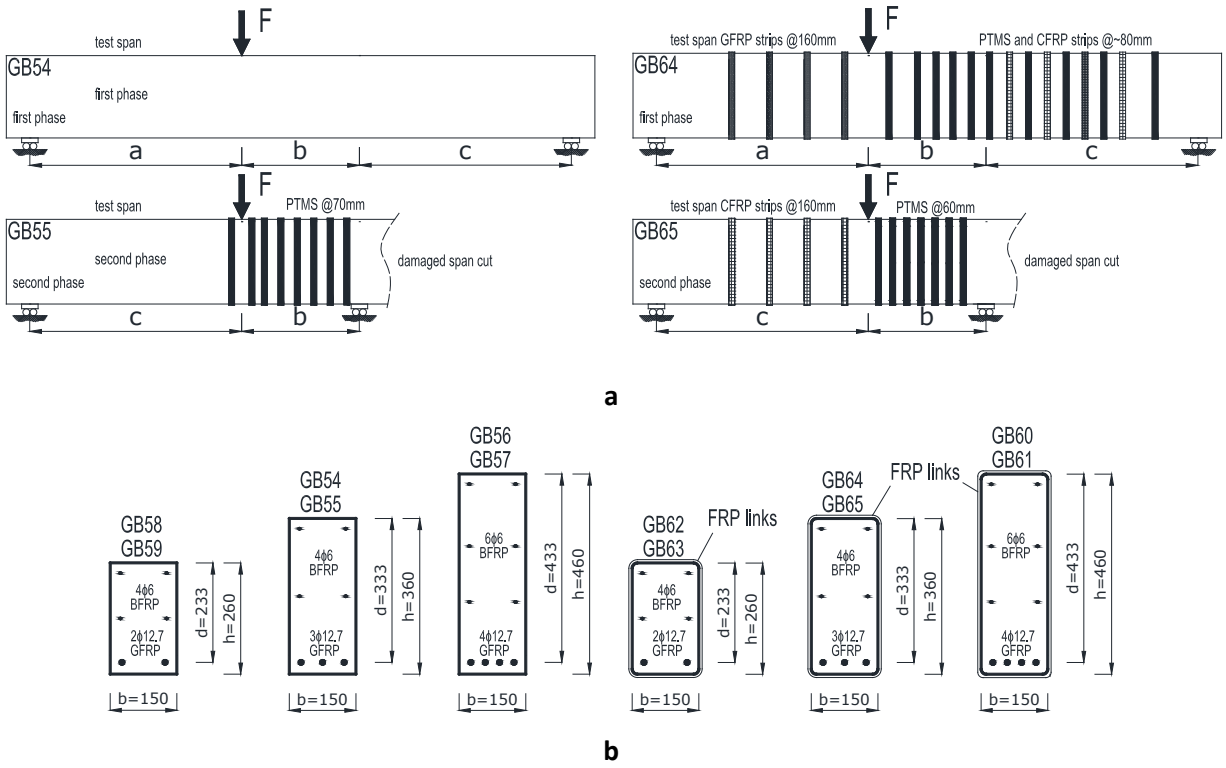

Figure 1: a – test phases of the beams GB54 and GB64 and their retests; b – cross sections of the beams

Instrumentation and test setup

A three-point bending test was carried out on simply supported specimens in displacement control at a rate of 0.25 mm/min. Quasi-static incremental loading cycles were performed at load levels inducing predefined levels of strain in the tensile reinforcement (i.e. about 3000 με and 4500 με), before the specimens were loaded to failure. The instrumentation was designed to measure the load, vertical displacement of the beam and strains in the FRP reinforcement. The deflections of the beam were measured by 3 LVDTs placed under the load point and in the mid shear spans. The rigid motion of the supports was monitored by 2 transducers placed on the top of the beam and at the end extracted from the total deflection of the beam.

A DIC was employed to obtain the full field deformations within the shear span of the beams, and in particular, a three dimensional (3D) configuration was used to eliminate the effects of possible out of plane displacement of the specimens during testing (i.e., generation of apparent strains) (Di Benedetti et al. 2015). Images were acquired with two CMOS digital cameras having a 4272×2848 pixel resolution (Canon EOS 1100D) and equipped with zoom lenses with F-number and focal length of 3.5-5.6 and 18-55 mm, respectively (Canon EF S 18 55mm f/3.5 5.6 IS II). The two cameras were rigidly connected 430 mm apart and mounted on a tripod. A light-emitting diode (LED) lamp was used to illuminate the measurement surface. The stereo vision system was calibrated by taking images of a known pattern with different positions and orientations. During the load test, the shutter was remotely triggered three times every 10 seconds by the DAQ recording the point wise sensors in order to synchronize all data.

Experimental results

The main experimental results are summarized in the table 1 where a, b and c correspond to the dimensions of the beams according to Fig. 1a, V_{exp} is the experimental shear capacity of the beams, $V_{Rd,c}$ is the predicted shear capacity of the element and v_{norm} is the shear strength normalised by the concrete strength.

Table 1: Main test results and material properties of the beams

Beam	a, b, c *(mm)*	a/d *(-)*	f_{cy} *(MPa)*	ρ_f *(%)*	V_{exp} (kN)	$V_{Rd,c}$ (kN)	$V_{Rd,c}$ / V_{exp} (-)	v_{norm} (MPa)	links spacing (mm)
GB58	620,1060,620	2.66	36.64	0.72	37.3	26.9	0.72	0.18	-
GB59			37.53		57.6	27.1	0.47	0.27	-
GB62			52.70		48.2	42.7	0.89	0.19	120
GB63			50.91		54.2	43.4	0.80	0.22	
GB54	900,500,900	2.70	30.16	0.76	31.3	33.8	1.08	0.11	-
GB55			30.16		47.3	33.8	0.71	0.17	-
GB64			47.54		61.7	55.9	0.91	0.18	160
GB65			47.54		63.4	58.3	0.92	0.18	
GB56	1120, 1180	2.59	38.04	0.78	43.9	45.3	1.03	0.11	-
GB57			36.64		50.0	44.7	0.89	0.13	-
GB60			38.40		77.2	65.1	0.84	0.19	260
GB61			38.40		85.4	64.4	0.75	0.21	

All the specimens failed in shear exhibiting a brittle diagonal tension failure caused by a propagation of the leading diagonal crack towards the compression zone of the beam, which initiated from a tip of the flexural crack, close to the support (see Fig. 2a). The diagonal shear failure of the members strapped with the vertical links was abrupt and followed by sequent rupture of the links, thus creating wider crack openings and overall more damage in shear spans of the tested beams (Fig. 2b).

In general, an increase of the member stiffness and the ultimate shear capacity were observed with an increase in the overall depth of the members, d (Fig3a,c). The retest on each beam (Fig3b,d) resulted in overall higher capacity, which can be attributed to the fact that shortening the clear span of the beams to remove the damaged portion of the specimen after the first test (GB54, GB58, GB62, GB64), partially changed the internal resisting mechanisms affecting both stiffness and ultimate behaviour. For example,

in the test of GB55, the short span (green curve on Fig.3b) contributed to the overall shear capacity by engaging a strut-and-tie action, resulting in a much higher shear resistance than that provided by GB54 (first test).Beam GB54 and GB56 failed at a load level close to the theoretical value predicted according to Eq. 1 (Guadagnini et al. 2006).

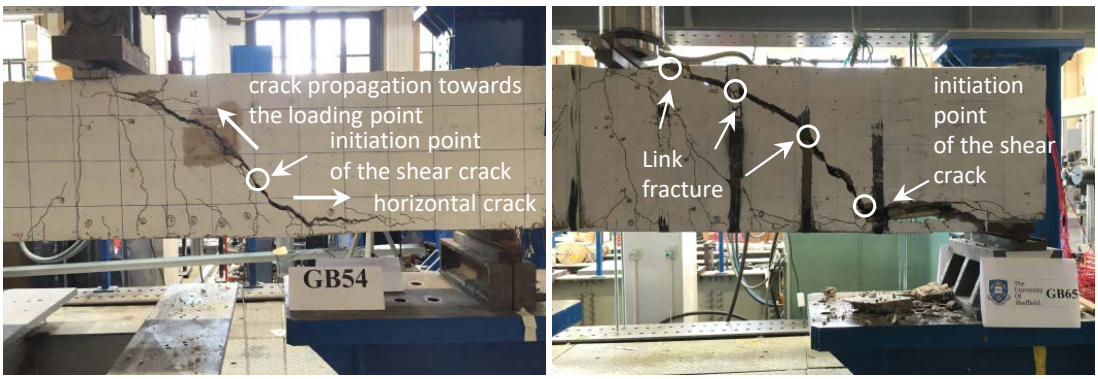

a **b**

Figure 2: Shear failure mode of the beams; a – test GB54; b – test GB65

The maximum level of strain developed along the flexural reinforcement of these two beams was close to the limiting allowable strain used in Eq. 1 (4500με) and failure developed rapidly upon the development of critical diagonal cracking, indicating a rapid degradation of the contributing shear resisting mechanisms.

$$V_{Rd,c} = \left[\frac{0.18}{\gamma_c} \cdot \left(1 + \sqrt{\frac{200}{d}} \right) \cdot (100 \cdot \frac{A_{fl}}{b_w \cdot d} \cdot \frac{E_{fl}}{E_s} \cdot \frac{0.0045}{0.0025} \cdot f_{ck})^{\frac{1}{3}} \right] \cdot b_w \cdot d \qquad (1)$$

Beam GB58, which was expected to develop the lowest shear resistance, exhibited a shear capacity almost 30% higher than that predicted according to Eq. 1. It should be noted, however, that a significant degradation in the stiffness of the shear load-deflection response is observed at a shear load below 30kN, which is closer to the theoretical estimate and can give an indication of the load at which the critical shear crack initiates (Fig. 3a). Upon the development of the critical shear crack, however, GB58 did not fail abruptly and continued to carry load, albeit this was accompanied by a gradual degradation of the shear resisting mechanisms as a result of the high strains developed in the FRP reinforcement (up to 7000με) and the large crack widths. This residual strength does not appear to be adequately captured by the theoretical model.

The capacity of the beams reinforced in shear was calculated as a sum of concrete shear capacity (Eq.1) and the capacity provided by the links (using ACI440 code approach) to account for the overall shear resistance of these components. However, the predictions were conservative and presented values around 10% lower than from the experiments. In addition, the allowable strain limits in the main reinforcement largely exceeded the design limits reaching values up to 11000με at failure of the specimen.

The experimental shear strength $V_{exp}/b_w d$, was normalized by the concrete strength, $\sqrt{f_{ck}}$, and was plotted against the members' effective depth, d (Fig. 4a). The results show that the normalized shear strength decreases with an increase in d, which is in good agreement with available literature (Ashour and Kara 2014). In particular, a drop in shear strength of about 60% was observed between tests GB59 and GB56, when overall depth increases from 260 mm to 460 mm, respectively. The size effect observed

in the tested GFRP RC beams seems to be more significant and visible than in steel RC beams of same dimensions (Alam and Hussein 2012). This could be explained by the higher deformations and larger diagonal shear cracks that developed in the tested beams, which caused a reduction in the shear resistance offered by aggregate interlock along the cracks. When minimum shear reinforcement was provided by applying external FRP links, size effect was significantly mitigated and the reduction of shear strength was only about 10%.

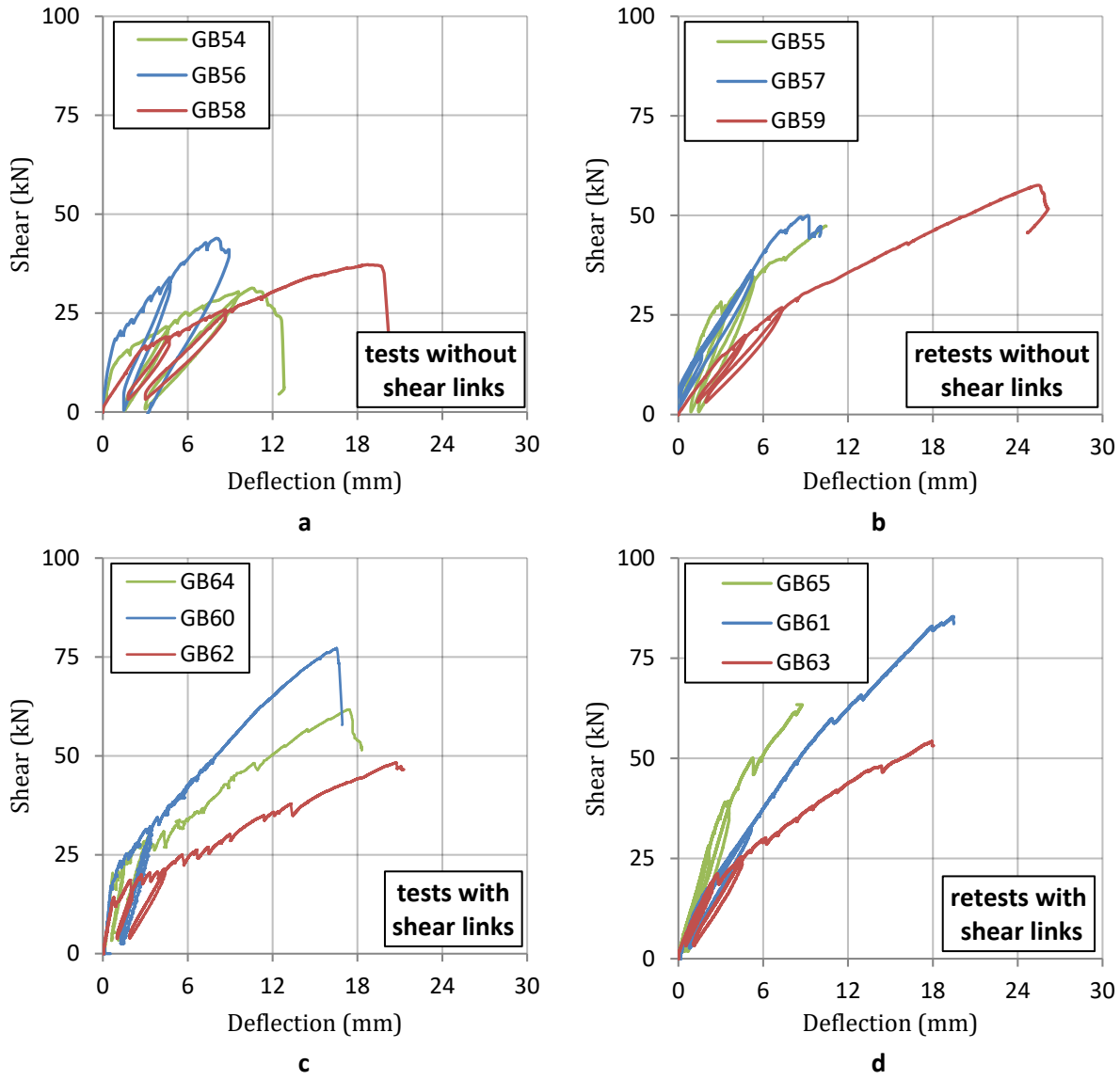

Figure 3: Shear load-deflection responses for the all specimens; a – no shear reinforcement; b – no shear reinforcement (retest); c – with shear links; d – with shear links (retest)

Figure 4b shows the vertical strains along the shear span of the largest beam with GFRP shear links (GB60). The map shows the contribution of the links in resisting diagonal shear failure. The average vertical strain measured by DIC in the shear reinforcement crossing the inclined cracks was around 15000με, which was in good agreement with the strain values measured by the strain gauge installed on the surface of the link (16800με). It can be observed that shear links were not stressed uniformly across the height of the specimen and were utilised to a higher degree close to the bottom of the shear crack rather than the tip. The high level of damage and high strains led to the failure of link 2 (see figure 4b) and subsequent failure of the specimen. It is worth noting, that no strains were recorded in the links in the regions free of cracks, indicating good bond between the links and the concrete.

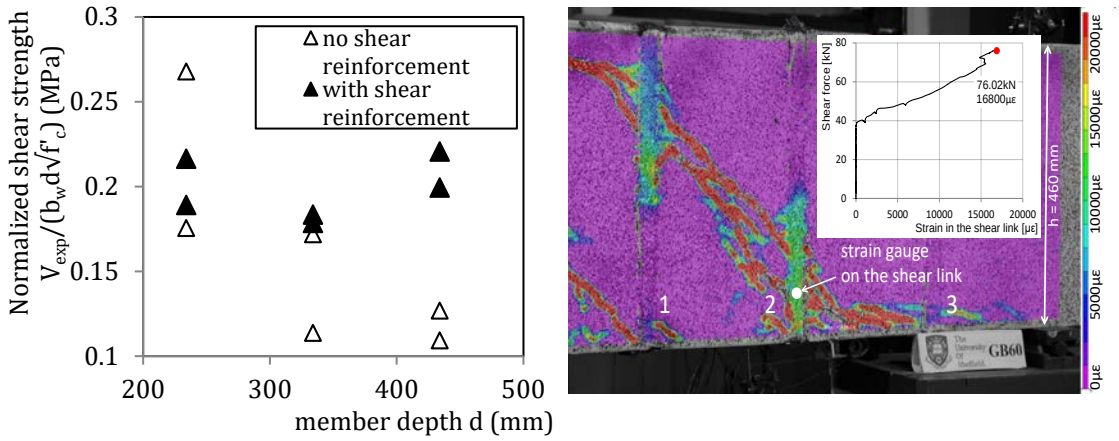

a b

Figure 4: a – size effect in tested elements; b – vertical strain distribution in the beam GB60

Conclusions

The experimental tests confirmed that beam depth plays an important role in determining the shear behaviour of FRP RC beams without shear reinforcement, which can already be significant for a change in overall depth from 260 mm to 460 mm (typical of most laboratory tests). The addition of shear links, however, seems to mitigate effectively size effect.

Although only preliminary results were presented for the analysis of strain distribution using DIC, this promising measuring technique can enable a better understanding of local deformation phenomena of the shear links and could be used to obtain critical damage parameters to inform the development of more reliable numerical models, which still to date cannot simulate the complex behaviour of concrete elements subjected to brittle failure modes.

Key references

ACI Committee 440. Guide for the design and construction of concrete reinforced with FRP bars. *ACI 440.1R-15. American Concrete Institute*, Farmington Hills, Michigan; 2015.

Ashour, A. and Kara I. (2014). Size effect on shear strength of FRP reinforced concrete beams. *Composites: Part B.* 60, 612–620.

Alam, M. and Hussein A. (2013). Size Effect on Shear Strength of FRP Reinforced Concrete Beams without Stirrups. *J. Compos. Constr.* 2013.17:507-516.

Bentz, E. et al. (2010). Shear Strength of Large Concrete Members with FRP Reinforcement. *J. Compos. Constr.* ASCE, v14, No. 6, 2010, pp. 637-646.

Di Benedetti, M. et al. (2015). 3D-DIC for strain measurement in small scale GFRP RC specimens. *The proceedings of the SMAR2015 conference*. 7-9 Sep 2015, Antalya, Turkey.

Guadagnini, M. et al. (2006). Shear Resistance of FRP RC Beams: Experimental Study. *J. Compos. Constr.* 2006.10:464-473.

Frosch, R.J. (2000). Behavior of Large-Scale Reinforced Concrete Beams with Minimum Shear Reinforcement. A*CI Structural Journal*, 97(6), 814-820.

Kani, G.N.J. (1967). How Safe Are Our Large Reinforced Concrete Beams. *ACI Journal*, 64(12), 128–141.

Lubell, A., et al. (2004). Safe Shear Design of Large Wide Beams. *Concrete International*, 26(1), 66–78.

Razaqpur, A.G. et al. (2004). "Concrete Contribution to the Shear Resistance of Fiber Reinforced Polymer Reinforced Concrete Members", *J. Compos. Constr.*, ASCE, 8(5): 452–460.

Shioya, T., et al. (1990). Shear Strength of Large Reinforced Concrete Beams. *ACI Structural Journal*, SP-118, V.C. Li and and Z.B. Bazant, eds, ACI, Farmington Hills, 259-279.

Experimental and numerical investigation of concrete columns reinforced with FRP bars

Zijadin GURI[1], Gjorgi Kokalanov[2], Danilo Ristic[3]

Introduction

The use of FRP materials is of particular importance because of durability aspects, especially at elements of reinforced concrete bridges in and the elements of structures that are subject to aggressive environmental conditions. Other reasons for using of FRP bars instead of ordinary steel bars are low weight to strength ratio, electromagnetic neutrality, high cut ability in temporary applications, lightweight and flexibility of FRP bars. Almost all types of FRP bars present in market are made from aramid (AFRP), glass (GFRP) and carbon (CFRP).

As a numerical and experimental task six concrete columns with different percentage of steel rebar and FRP bar are tested under combined constant axial load and increasing cyclic lateral load. All columns are RC columns of diameter 29.7cm, and height 150cm. Two columns are reinforced with ordinary reinforcement, and other four columns are reinforced with FRP reinforcement with different diameters. Stirrups are steel reinforcement (B500C) for all models but in different steps (15 cm and 7.5 cm) to provide different confinement conditions.

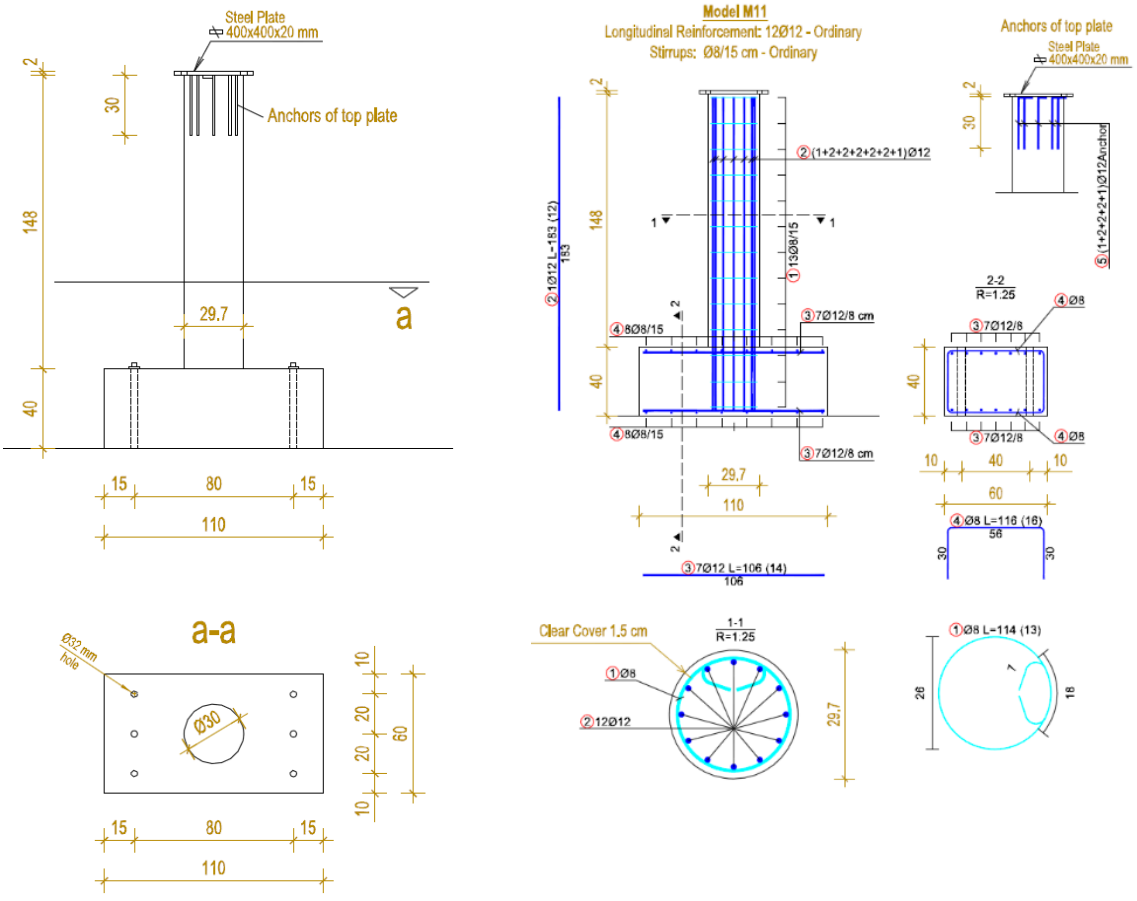

Figure 1 - Geometry, dimensions and reinforcement details for Experimental Models

[1] Ass, PhD Can. University of Prishtina - Faculty of Civil Engineering, Kosovo, zijadin.guri@uni-pr.edu
[2] Prof. Dr, University of Skopje – Faculty of Civil Engineering, Macedonia, kokalanov@gf.ukim.edu.mk
[3] Prof. Dr. Institute of Earthquake Engineering and Engineering Seismology (IZIIS), Macedonia, danilo@pluto.iziis.ukim.edu.mk

Model M11 longitudinal reinforcement 12Φ12 – Ordinary reinforcement. Stirrup spacing 15 cm

Model M12 longitudinal reinforcement 12Φ12 – Ordinary reinforcement. Stirrup spacing 7.5 cm

Model M21 longitudinal reinforcement 12Φ10 – FRP reinforcement. Stirrup spacing 15 cm

Model M22 longitudinal reinforcement 12Φ10 – FRP reinforcement. Stirrup spacing 7.5 cm

Model M31 longitudinal reinforcement 12Φ 8 – FRP reinforcement. Stirrup spacing 15 cm

Model M32 longitudinal reinforcement 12Φ 8 – FRP reinforcement. Stirrup spacing 7.5 cm

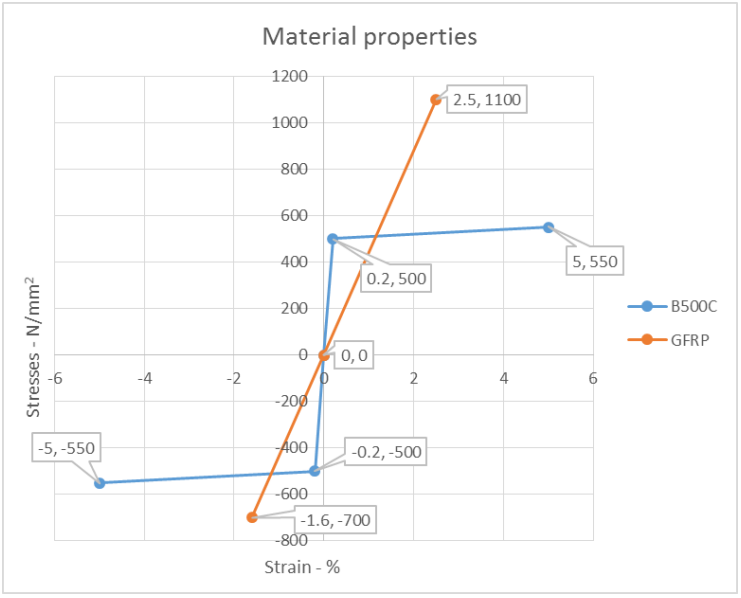

Figure 2 – Properties of GFRP and Steel used

Analytical Modelling

Detailed nonlinear finite element models is analysed using 3D solid finite elements using SOFiSTiK software and Fibre Section approach using SEISMOSTRUCT. For concrete modelling, brick element (volume elements) of concrete as confined and unconfined is used. For modelling of reinforcement, truss model with nonlinear properties of ordinary reinforcement and FRP reinforcement is used. Full bond assumption between reinforcement and concrete is accepted.

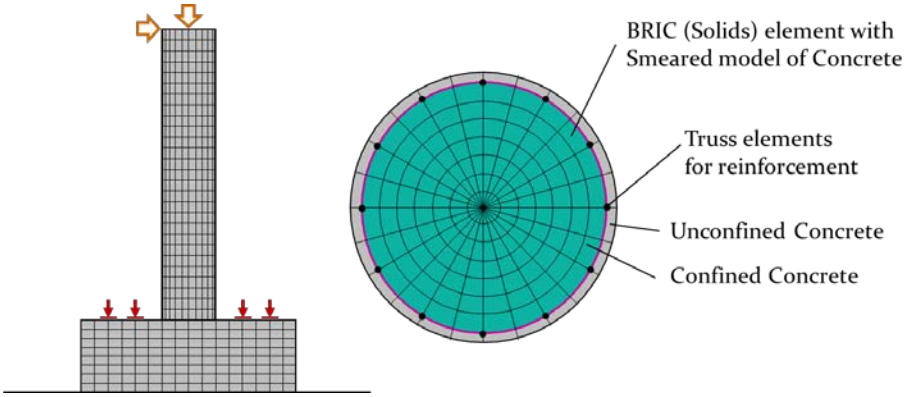

Figure 3 - Analytical FEM Model of Column

Bond between concrete and FRP reinforcing bars is important aspect for developing the composite behaviour between concrete and FRP bar. To reach composite behaviour, sufficient bond must be mobilized between FRP bar and concrete to be able for transferring of forces between them. Bond interaction of FRP bar with concrete is different from bond of concrete with profiled steel bar. At the profiled (deformed) steel bar the interaction with concrete arises primarily from the mechanical action of the bar lugs against concrete. When the tensile stress in concrete is exceeded this mechanical bond

action leads to primary cracking extending to the surface. At the FRP bars, with lower elastic modulus and small surface of undulations, bond interactions has more frictional character. Bond failure in steel bars is mainly archived by crushing of concrete from lugs. Bond failure in FRP bars is mainly caused from partial failure in concrete and some surface damage on the FRP.
Analytical models of bond-slip are essential for the determination of structural performance of FRP reinforced concrete structures by means of numerical analysis. Rosetti, Galeota & Giammatteo (1995) and Cosenza, Manfredi & Realfonzo (1995) have successfully applied the well-known model for deformed steel rebars by Eligehausen, Popov & Bertero (1983) (B.P.E. model) to FRP rebars. The ascending branch of this bond-slip (s ≤sm) relationship is given by:

$$\frac{\tau}{\tau_m} = \left(\frac{s}{s_m}\right)^{\alpha} \qquad (1)$$

Where α is an experimental parameter less than 1 (α = 0.40 in case of steel reinforcements).

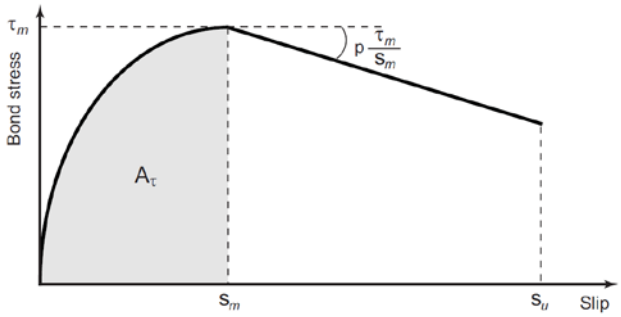

Figure 4 - Modified B.E.P. constitutive law for Bond – Slip

The bond behaviour of FRP bars depends on the characteristics of the surface and for the same type of surface, depends on the manufacturing process. It is generally possible to obtain bond strengths for FRP bars of similar or greater magnitude than for steel. Indented and grain covered bars seem to provide the best results in terms of bond strength.
Pull out is performed experimentally for testing of bond features of FRP bars. For modelling of bond in FEM model theoretical models from literature and measured data from experiments are used.

Preliminary analytical results

In this paper preliminary analytical results are extracted in terms of force-displacement capacity, Moment Curvature or Rotation and Interactions surfaces N-M for models. Vertical load N=250kN is applied during all time and horizontal loads are increased gradually during failure of column.

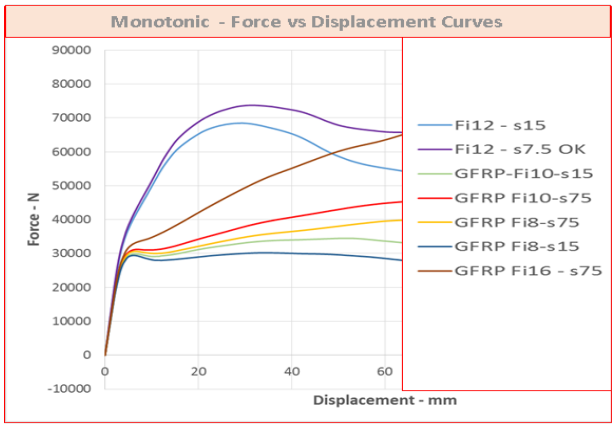

Figure 5 – Force – Displacement curve

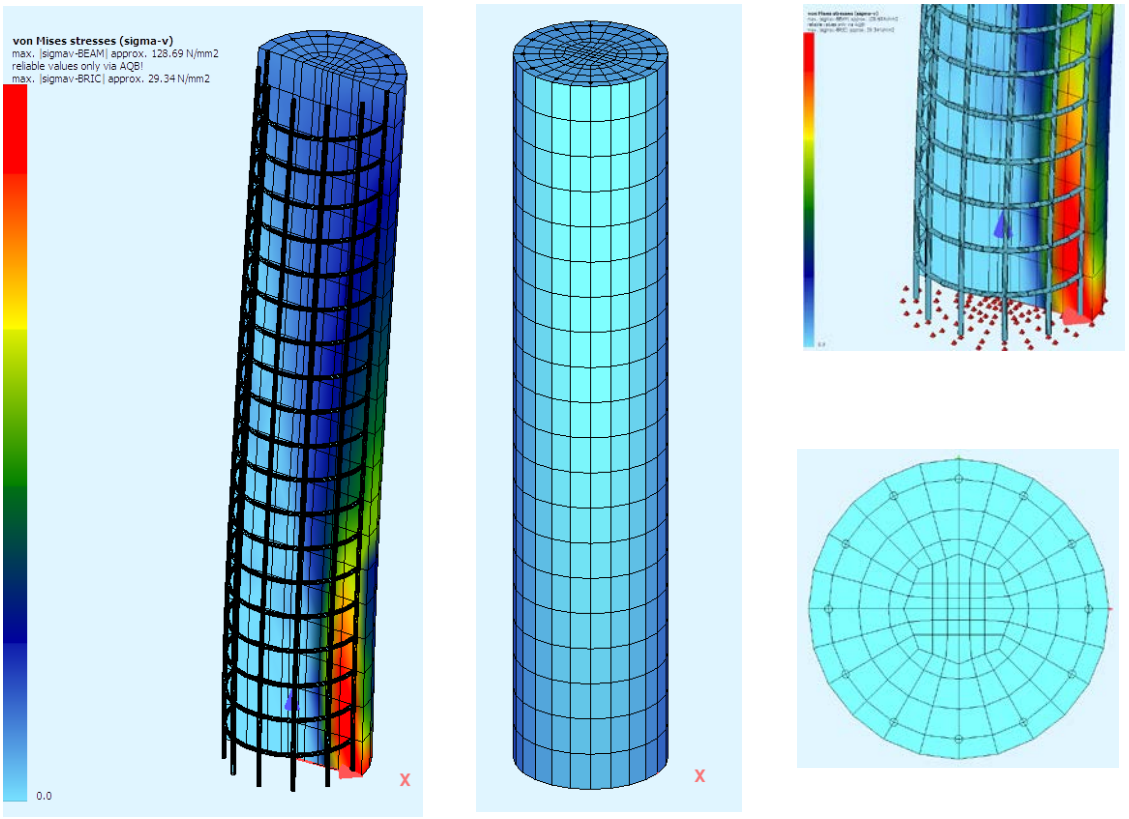

Figure 6 – FEM model for column. Iteration factor of ultimate loads

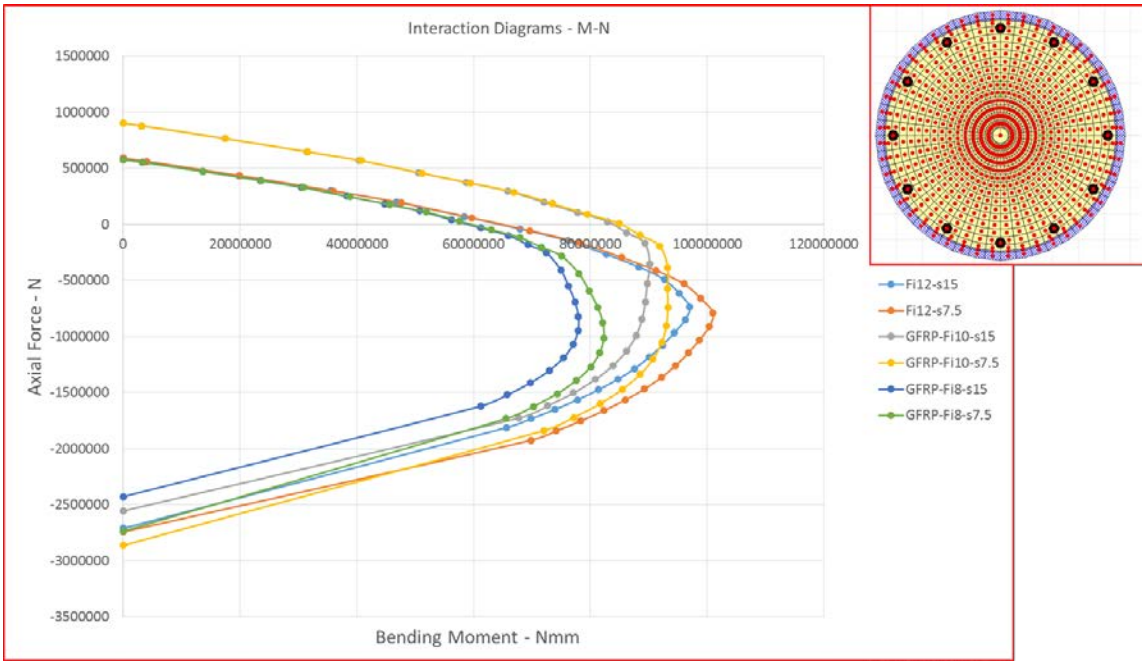

Figure 7 - Fibre model for calculations and Interaction Surface for M11 Model

Models are loaded with constant vertical load and cyclic horizontal load. Main goal will be study of behaviour of columns from cyclic horizontal loads. Their hysteresis behaviour including ductility will be investigated experimentally and numerically. Mathematical models are calibrated based on measured experimental data.

Experimental Program – Bond behaviour and materials

For the purpose of understanding of behaviour of concrete columns reinforced with GFRP and steel, 6six columns with different percentage of reinforcement are constructed and tested. This chapters describes the material properties, bond testing of GFRP and Steel rebar from cube (pull out testing), specimen details and test setup.

Concrete with specified 28-day compressive strength of 35 MPa is used. After concreting of six columns a three specimens (cubes with dimensions 150x150x150 mm) are tested and results of compressive stresses are presented below. Fc = 35 N/mm2

For the definition of mechanical properties of GFRP bars used in constructed columns, a tensile test is performed. Results and pictures of testing are given below.

$Ft_1 = 1108.52\ N/mm^2$

$Ft_2 = 1110.65\ N/mm^2$

$Ft_3 = 1101.22\ N/mm^2$

$Ft_4 = 1117.20\ N/mm^2$

$Ft_5 = 1104.32\ N/mm^2$

$Ft_6 = 1107.72\ N/mm^2$

$\mathbf{Ft_{mes} = 1100.00\ N/mm^2}$

Figure 8 - Testing of GFRP Bars and Results

For determination of bond behaviour of Steel rebars and GFRP rebars a pull out test is performed.

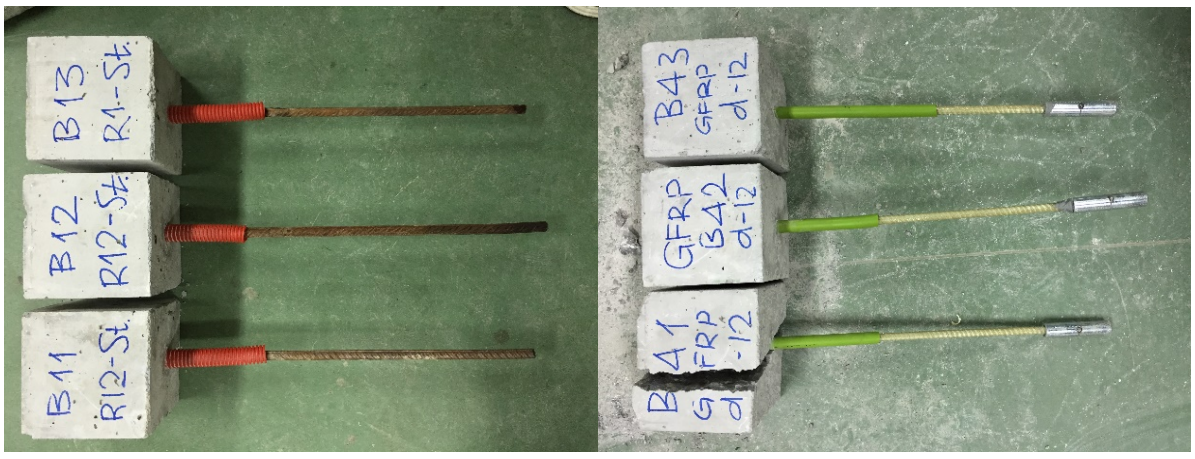

Figure 9 - Specimens for testing of GFRP and Steel rebars – Pull-Out test

Tension force is registered and sliding displacement, and Force – Sliding displacement is plotted.

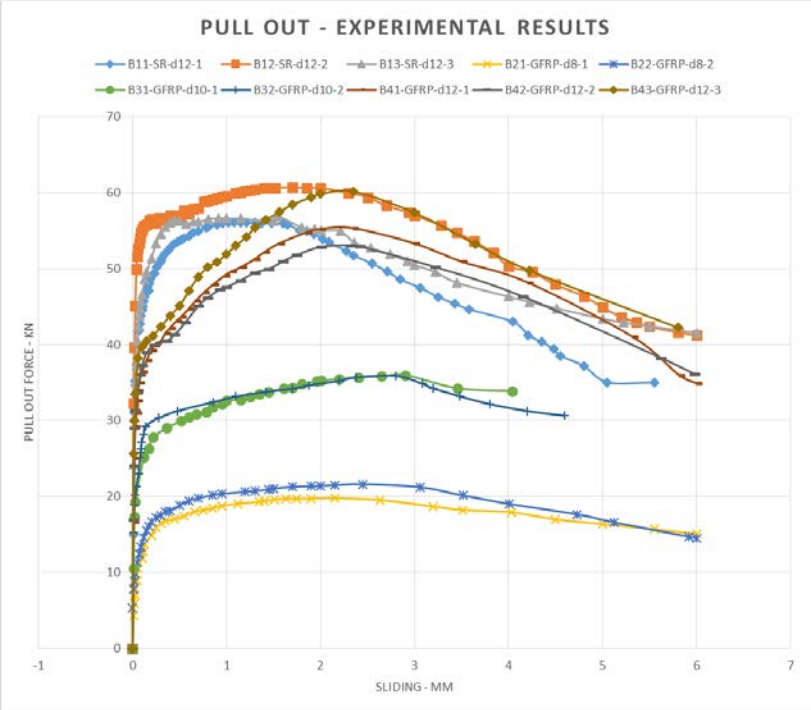

Figure 10 - Pull Out experimental results – Force – Sliding

Experimental Program – Experimental testing of columns

Experimental testing of six columns is performed under constant axial load 250 kN and gradually increasing horizontal displacement by 5mm up to 80 mm. Experimental results in terms of hysteresis and other sequences of damage of columns during testing are given below.

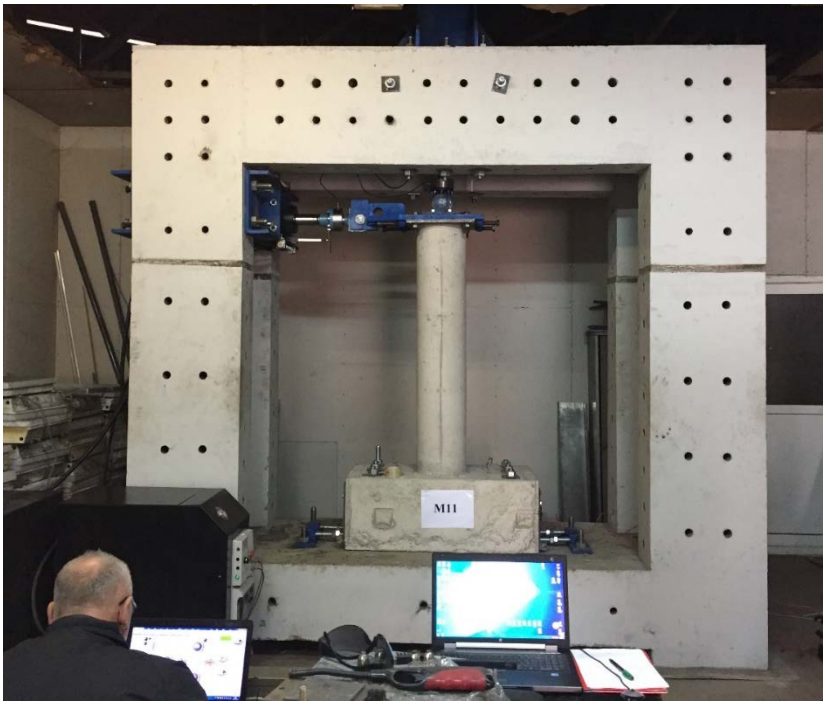

Figure 11 - Testing Frame and Testing of Columns

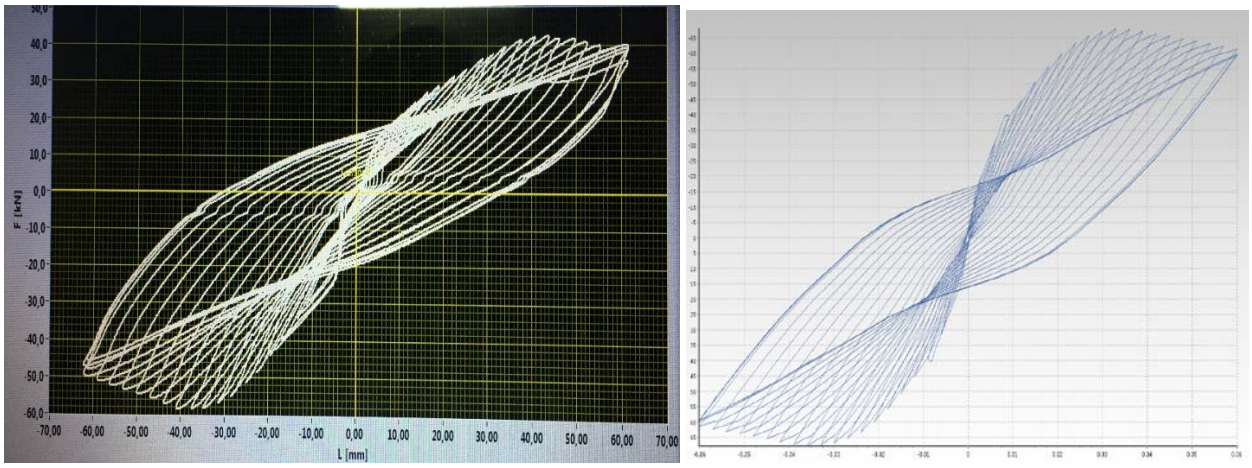

Figure 12 - Experimental and Theoretical Hysteresis – Column M12

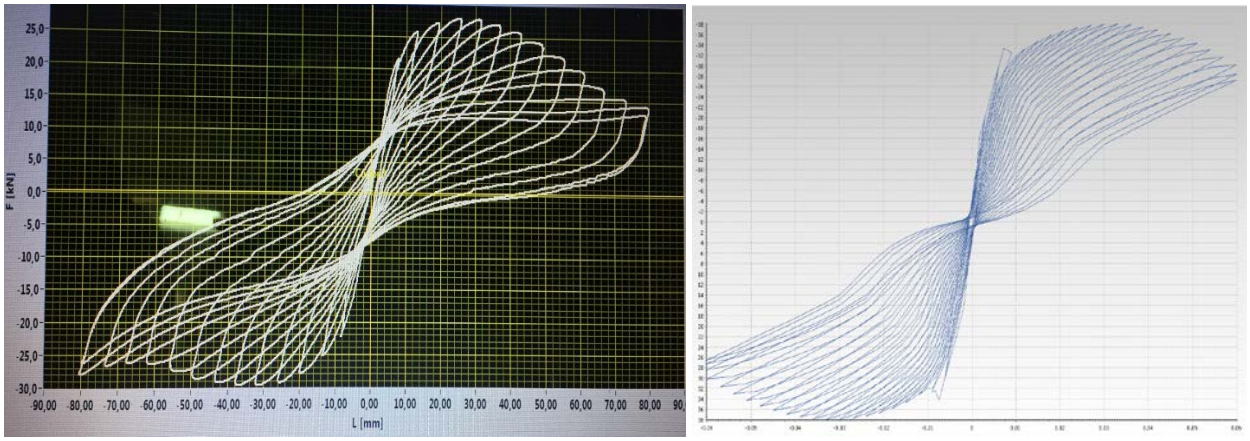

Figure 13 - Experimental and Theoretical Hysteresis – Column M22

Conclusions

The conclusions obtained from experimental testing observations and analysis can concluded as follows:

- Using of FRP reinforcement in concrete columns is possible in any case of loading because the can reach large displacement without significant reducing of element stiffness.
- Durability of element reinforced with FRP bar is increased, because of its resistance from corroding.
- GFRP rebar have good behaviour in compression and buckling of those bars can occur when they are in good confined conditions by stirrups.
- Bond between concrete and FRP reinforcing bars is important aspect for developing the composite behaviour between concrete and FRP bar. Bond failure in FRP bars is mainly caused from partial failure in concrete and some surface damage on the FRP. They have shown very good bond behaviour from pull out tests in terms of bond stresses.

Key references

[1] ACI (2006), ACI 440.1R-06 - Guide for the design and construction of concrete reinforced with FRP bars, ACI Committee 440, American Concrete Institute (ACI).

[2] Byars, E.A., Waldron, P.W., Dejke, V. and Demis, S. (2001), Durability of FRP in Concrete, Current Specifications and a New Approach, Proceedings of FRP Composites in Civil Engineering, Vol. II, Elsevier, Hong Kong, December, 1497-1507.

[3] CAN/CSA-S806-02 (2002), Design and Construction of Building Components with Fibre Reinforced Polymers, Canadian Standards Association, Toronto, Ontario, Canada.

[4] Cosenza, E., Manfredi, G., Pecce, M. and Realfonzo, R. (1999), Bond between GFRP Rebars and Concrete: an Experimental Analysis, Proceedings of the 4th International Symposium on Fiber Reinforced Polymer for Reinforced Concrete Structures, American Concrete Institute, Detroit,

[5] Duranovic, N., Pilakoutas, K. and Waldron, P. (1997a), FRP reinforcement for concrete structures: Design Considerations, Proceedings of Third International Symposium on Non-metallic (FRP) Reinforcement for Concrete Structures, Japan Concrete Institute, Sapporo, Japan, Vol. 2, 527-534.

[6] Fib - 40, FRP reinforcement in RC structures, State-of-art Report, Bulletin 40, fib - International Federation for Structural Concrete, Lausanne

[7] JSCE (1997), Recommendation for design and construction of concrete structures using continuous Fibre reinforcing materials, Research Committee on Continuous Fiber Reinforcing Materials, Japan Society of Civil Engineers, Tokyo, Japan.

[8] Kotsovos, M. D., and Pavlovic, M. N. (1999), Ultimate Limit State Design of Concrete Structures - A New Approach, Thomas Telford, Ltd., London, UK.

[9] Weber, A. (2006), advanced reinforcement technology with GFRP Rebar, Proceedings of the 2nd International fib Congress, Naples, Italy.

2.3. Long Term Behaviour and Durability

Long-term deflections

C.Miàs[1], Ll. Torres[2], M.Guadagnini[3]

State-of-art

The long-term increase in deflection is a function of member geometry, load characteristics (magnitude and duration of sustained load, and age of concrete at the time of loading), and material properties (elastic modulus of concrete and FRP reinforcement, creep and shrinkage of concrete) (ACI 440.1R-06). Therefore, properties of the FRP bars have a significant influence on the long-term deflections of FRP reinforced concrete (RC) beams.

Due to lower stiffness of FRP bars compared to steel, under the same conditions (concrete class, dimensions and area of reinforcement), the neutral axis depth of FRP RC cracked sections are lower than those of steel RC. Consequently, the sectional curvature and the tensioned area are larger, while the compressed area is smaller, and therefore, larger deformations are expected. However, in terms of time-dependent behaviour, the relative curvature increment associated with creep and shrinkage is lower than for conventional steel RC due to the smaller compressed area of concrete, and therefore lower time-dependent deflections are expected in FRP RC.

Up to now, few published studies have examined the time-dependent deflection of FRP RC beams (Brown&Bartholomeu 1996, Brown 1997, Arockiasamy 2000, Hall&Ghali 2000, Gross et al. 2003, Gross et al. 2006, Laoubi et al. 2006, Al-Salloum&Almusallam 2007, Miàs et al. 2013). The reported results have generally concluded that total mid-span deflection versus time since loading of FRP and steel RC beams follow a similar trend. However, deflection increase, as a multiplier of the initial deflection, is significantly lower for FRP RC members than that observed for steel (Brown 1997, Hall&Ghali 2000, Gross et al. 2006, Miàs et al. 2013b). Likewise, experimental data (Gross et al. 2003 , Miàs et al. 2013b) reported that concrete strength has a considerable influence in time-dependent behaviour. In general, the beams cast with higher concrete strength lead to lower time-dependent deflection multipliers.

In addition, experimental results carried out by Al-Salloum and Almusallam (2007) has shown the possible influence of environmental conditions on the creep behaviour of GFRP RC structures exposed to hot and wet environments such as arid coastal areas, by means of an experimental campaign with beams, which were completely or partially immersed in different environments (tap-water and sea-water) at elevated temperature, and subjected to a sustained load. On the other hand, in reported results from Laoubi et al. 2007, no significant effect of the single or coupled action of freeze/thaw cycles and sustained bending stresses has observed on the behaviour of the tested beams in terms of deflections, strains, and ultimate capacity.

Methodologies to predict long-term deflections

Proposed formulations for calculating immediate deflections of FRP RC structures are based on the same principles already established for steel RC structures. Nevertheless, the equations have been modified to be adapted to the particular behaviour of FRP RC members. Similarly, to compute long-term deflections in FRP RC, ACI 440.1R-06 and CSA S806-08 guidelines have been adopted Branson (1971) equation, where the long-term deflection can be obtained from the immediate deflection due to sustained load and a corresponding factor, which depends on time since loading. In addition ACI 440.1R-06, based on tests carried out by Brown and Bartholomew (1996) and Brown (1997), proposes multiplying the factor used for steel RC by 0.6.

[1] AMADE – University of Girona, Spain, cristina.mias@udg.edu
[2] AMADE – University of Girona, Spain, lluis.torres@udg.edu
[3] University of Sheffield, United Kingdom, m.guadagnini@sheffield.ac.uk

According to that, the long-term the total deflection, $\delta_{T(ACI440)}$, can be obtained from the following equation:

$$\delta_{T(ACI440)} = (1 + 0.6\lambda)\delta_{t_0} \quad (1)$$

where λ is the coefficient proposed by Branson(1971) and adopted in ACI 318, which is given as:

$$\lambda = \frac{\xi}{1 + 50\rho'} \quad (2)$$

ρ' is the compression reinforcement ratio and ξ is a time-dependent factor for sustained loads, which includes the effects of creep and shrinkage and equals 1.0, 1.2 and 1.4, for 3, 6 and 12 months, respectively. For 5 years or more ξ is set to 2.

Likewise, Arockiasamy *et al.* (2000), proposed a modified factor ξ, specific for CFRP RC. The values of the coefficient were adjusted to their experiments on CFRP reinforced concrete beams.

However, the Canadian standard CSA S806-02 proposes a more conservative approach, adopting the same coefficients as for steel (with no correction factors):

$$\delta_{T(CSA)} = (1 + \xi)\delta_{t_0} \quad (3)$$

On the other hand, ISIS recommends the use of general CEB-FIP procedure (CEB 1985) together with creep and shrinkage curvature coefficients found in Ghali and Favre (1994) , which can be obtained from the age-adjusted transformed section properties calculated using the age-adjusted elastic modulus of concrete, $\overline{E_e}(t,t_0)$:

$$\overline{E_e}(t,t_0) = \frac{E_c}{1 + \chi(t,t_0)\varphi(t,t_0)} \quad (4)$$

E_c is the elastic modulus of concrete at t_0. $\chi(t,t_0)$ and $\varphi(t,t_0)$ are the ageing coefficient and creep coefficient at time t, respectively.

It is worth mentioning that the methodology accounts for the effects of member geometry, load characteristics (age of concrete at the time of loading, magnitude and duration of sustained load) and material properties (elastic moduli of concrete and FRP reinforcement, creep and shrinkage of concrete).

Experimental results presented in Hall and Ghali (2000), Arockiasamy et al.(2000) and Miàs et al.(2013b) have shown that the procedure described above give also accurate predictions when FRP materials are used.

Recently, straightforward method, based on multiplicative coefficients, to calculate long-term deflections in FRP RC members due to creep and shrinkage, has been presented in Miàs et al. (2010) and Torres et al. (2012). The multiplicative coefficients are based on general principles of structural mechanics and have been deduced using the *Effective Modulus Method (*CEN 2004*)*. After mathematical manipulation they have been reduced to be simple, but allowing to account for variations in the environmental conditions and mechanical properties of materials.

According to that, the total deflections due to creep and shrinkage can be computed as follows:

$$\delta_{T,proposed} = \delta_{sus}\left(1 + k_{creep}\right) + \frac{\varepsilon_{sh}(t,t_0)l^2}{8d}k_{sh} \quad (5)$$

where δ_{sus} is the immediate deflections due to sustained load ,which can be computed according to Eurocode 2 (CEN 2004) formulation or using the effective moment of inertia calculated using Bischoff

(2005)'s equation, with β=0.5 . ε_{sh} is the free shrinkage strain, *d* is the effective depth and *l* is the span length. The multiplicative coefficients, k_{creep} and k_{sh}, are reduced to:

$$k_{creep} = 0.73\varphi\sqrt{n\rho_f} \qquad k_{sh} = 1+\sqrt{n\rho_f} \qquad (6)$$

where *n* is the modular ratio and ρ_f is the FRP tensile reinforcement ratio.

Comparision between methodologies

Predictions of total deflection using the ACI 440.1R-06, CSA-S806-02 equations, as well as, ISIS recommendations and Torres et al.(2012) methodology are analysed and compared by varying different parameters that can influence the results to highlight their influence on the different approaches. The comparison is made for a simply supported beam with rectangular section and uniformly distributed load. Typical values of reinforcement ratio ρ ranging between 0 and 0.03, and elastic modulus of FRP, E_f, ranging between 40 and 120 GPa are considered (which cover typical values for GFRP, AFRP, and CFRP). *d/h*=0.9, f_c=30MPa, M=1.5M_{cr}. Two different values for free shrinkage strain, ε_{sh}, equal to 200 and 500με and for creep coefficient, φ, equal to 2 and 3 have been considered. A typical value of 0.8 has been taken for the aging coefficient $\chi(t,t_0)$.

As observed in Figure 1, the ISIS and Torres et al. (2012) predictions present the same trend, with little differences between them, showing a clear dependence on $n\rho$, φ and ε_{sh}. It is shown that increasing $n\rho$ leads to higher total-to initial deflection prediction ratio due to the increase in the height of the compressive concrete block, which implies an increment of curvature caused by creep and shrinkage of concrete. An influence of environmental conditions (affecting creep and shrinkage) can also be observed. The total-to-initial deflection prediction ratio increases as the values of creep and shrinkage increase. Nevertheless, the ratio is constant when using ACI 440.1R-06 and CSA-S806-02 methods, since their time-dependent factors do not depend either on sectional properties or values of creep and shrinkage of concrete.

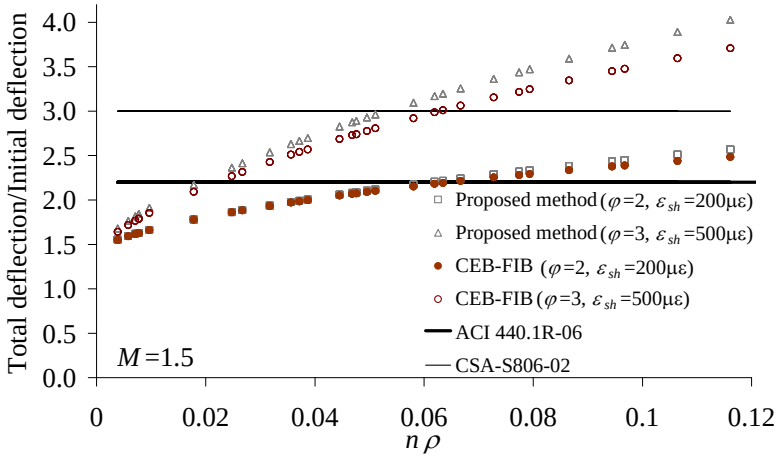

Figure 1: Effect of the free shrinkage strain and creep coefficient on the total-to-initial deflection prediction ratio

Conclusions and Points for Discussions

Regarding the state-of-the-art in long-term deflections, further experimental data is needed to study the effect of material properties (concrete strength, elastic modulus of FRP, creep of FRP and concrete), environmental conditions (freeze/taw, humidity, temperature), as well as, bond in the long-term behaviour of FRP RC elements. In addition, an analytical study of the effect of loading history on long-term deflections, supported by experiments, should be performed to check the generalization of the available methodologies.

Key references

American Concrete Institute Committee, ACI, 440 (2006). Guide for the design and construction of structural concrete reinforced with FRP bars (ACI 440.1R-06). Farmington Hills. Michigan, USA.

Al-Salloum, YA. and Almusallam, TH. (2007). Creep effect on the behavior of concrete beams reinforced with GFRP bars subjected to different environments. Constrution and Building Materials. 21(7):1510-19.

Arockiasamy, M., Chidambaram, S., Amer, A., Shahawy, M. (2000). Time-dependent deformations of concrete beams reinforced with CFRP bars. Composites Part B: Engineering. 31(6-7):577-92.

Bischoff, PH. (2005). Reevaluation of Deflection Prediction for Concrete Beams Reinforced with Steel and Fiber Reinforced Polymer Bars. Journal of Structural Engineering, ASCE. 131(5):752-67.

Branson, D.E. (1971) . Compression steel effect on long-time deflections. ACI Journal Proceedings. 68(8):555-59.

Brown, V. and Bartholomeu, C. (1996). Long-term deflections of GFRP-reinforced concrete beams. First International Conference on Composites in Infra-Structure. Tucson, Arizona, USA. pp. 389-00.

Brown, V. (1997). Sustained load deflections in GFRP-reinforced concrete beams. 3rd International RILEM Symposium on Non-Metallic (FRP) Reinforcement for Concrete Structures (FRPRCS-3). Sapporo, Japan. pp. 495-02.

(CEB) Comité Euro-International du Béton (1985).Manual on Cracking and Deformations.Bulletin d'Information 158-E.

CEN 2004. Eurocode 2: Design of Concrete Structures. Part 1.1: General rules and rules for buildings (EN 1992-1-1:2004). Comité Européen de Normalisation, Brussels, 2004.

CSA Standard CAN/CSA-S806-02 (2002). Design and construction of building components with fibre-reinforced polymers. Canadian Standards Association, Mississauga, Ontario, Canada; 2002.

Ghali, A. and Favre, R. (1994). Concrete Structures: Stresses and Deformations. Ed. Chapman and Hall, London.

Gross, SP., Yost, JR., Kevgas, G. (2003). Time-dependent behavior of normal and high strength concrete beams reinforced with GFRP bars under sustained loads. High Performance Materials in Bridges 2003; pp.451-62.

Gross, S.P., Yost Y.R., Crawford, J.V. (2006). Serviceability of high strength concrete beams with internal FRP reinforcement under sustained load. In: 3rd International Conference on FRP Composites in Civil Engineering (CICE 2006). Miami, Florida, USA; 2006.

Hall, T. and Ghali, A. (2000). Long-term deflection prediction of concrete members reinforced with glass fibre reinforced polymer bars. Canadian Journal of Civil Engineering . 27(5):890-98.

Laoubi, K., El-Salakawy, E., Benmokrane, B (2006). Creep and durability of sand-coated glass FRP bars in concrete elements under freeze/thaw cycling and sustained loads. Cement and Concrete Composites. 28(10):869-878.

Miàs, C., Torres, L., Turon, A., Baena, M., Barris, C. (2010). A simplified method to obtain time-dependent curvatures and deflections of concrete members reinforced with FRP bars. Composite Structures . 92(8):1833-38.

Miàs, C., Torres, L., Turon, A., Barris, C. (2013). “Experimental study of immediate and time-dependent deflections of GFRP reinforced concrete beams”, *Composite Structures*. 96 : 279-285.

Miàs, C., Torres, L., Turon, A., Sharaky, I.A. (2013b). "Effect of Material Properties on Long-term Deflections of GFRP Reinforced Concrete Beams." Construction and Building Materials. 41 : 99-108.

Torres, L., Miàs, C., Turon, A., Baena, M. (2012). A rational method to predict long-term deflections of FRP reinforced concrete members. Engineering Structures 2012; 40:230-39.

Durability of GRFP reinforcing bars and their bond in concrete

A. Rolland[1], S. Chataigner[2], M. Quiertant[3], K. Benzarti[3], P. Argoul[3]

Introduction

The use of composite reinforcing bars (rebars) for the reinforcement of concrete appears as an attractive solution to prevent corrosion, which is the main pathology encountered on concrete structures. Although such rebars are being used for more than ten years, there is a clear lack of knowledge regarding their durability, especially under alkaline environment.
This paper aims at investigating the evolutions of tensile properties and bond in concrete of GFRP (Glass Fiber Reinforced Polymer) bars under accelerated laboratory environmental conditions. Both plain rebars and rebars embedded in concrete specimens were exposed to these conditions, in order to assess the influence of the alkaline environment. GFRP rebars were chosen for this study, as this type of bars is considered as the most economically competitive solution in comparison with classical steel rebar.

Description of the ageing procedure

GFRP rebars under study are processed by pultrusion, using a vinylester (VE) polymer matrix. The surface of the rebar is sand coated before the end of the polymerization process, in order to improve adhesion with concrete.
Several samples were prepared simultaneously for the experimental program: 1.2 meter-long straight rebars for the tensile investigations, pull-out samples, and 32 cm-long straight rebars either alone or embedded in concrete to perform short-beam tests and assess the interlaminar shear strength. These samples were exposed to five different ageing environments: immersion in alkaline solutions (AKS) at 20, 40 and 60°C, or exposure in air at 40 or 60°C to be able to discriminate between the influence of the alkalinity or a pure thermal effect on the evolutions of the mechanical properties. The alkaline solution was composed of 0.1 mol/L of NaOH, and 0.5 mol/L of KOH.
Samples were stored for a total period of 240 days, and three test campaigns were carried out (initial state, and after 120 and 240 days). In the meantime, both temperature and pH were monitored continuously to check the stability of the ageing environments.

Description of the experimental investigations

For each test period, different characterizations were carried out to investigate the ageing mechanisms and their effect on mechanical properties. These experimental procedures were very similar to those specified by ASTM standards:

- Microscopic observations using scanning electron microscopy (SEM) associated with an Energy Dispersive X-ray (EDX) device to identify the chemical elements.
- Differential Scanning Calorimetry (DSC) analyses to determine the glass transition temperature of the VE matrix, and infrared spectroscopy (FTIR) to get an insight of the main chemical links present in the matrix.

[1] CEREMA, Direction Territoriale Nord-Picardie, France, arnaud.rolland@cerema.fr
[2] LUNAM Université, IFSTTAR, France, sylvain.chataigner@ifsttar.fr
[3] Université Paris-Est, IFSTTAR, France, karim.benzarti@ifsttar.fr

- Tensile tests on the GFRP rebar, to assess the evolution of the ultimate strength and the elastic modulus.
- 3 point bending tests (short-beam test) to measure the interlaminar shear strength (ILSS)
- Pull-out tests to follow the evolution of the GFRP to concrete bond behavior after ageing.

Experimental results

Microscopic observations revealed an embrittlement of the rebar close to the surface due to accelerated ageing (Figure 1). This phenomenon was more pronounced in the case of GFRP bars immersed directly in the alkaline solution than for bars embedded in concrete and immersed in the solution. In addition, EDX analyses detected the presence of a limited amount of potassium in the peripheral ring of the aged rebars.

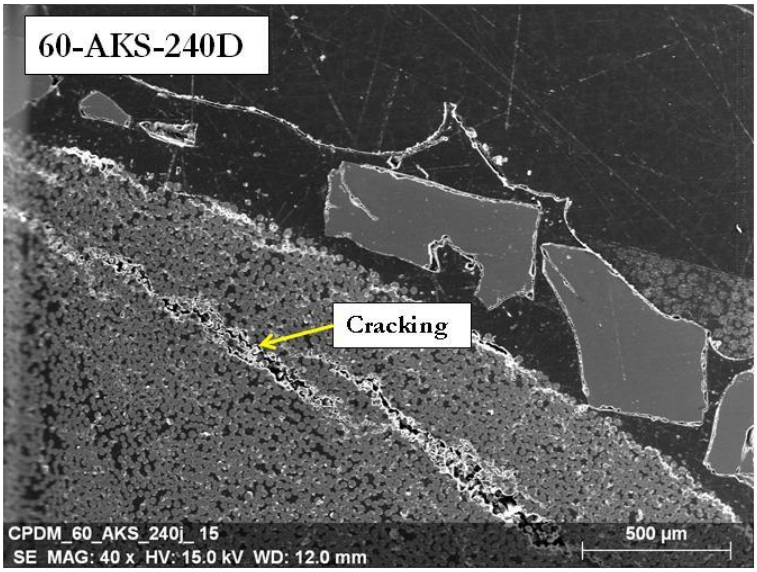

Figure 1: SEM observation of a GFRP rebar cross-section after 240 days immersion in the alkaline solution at 60 °C

Investigations by DSC and FTIR did not reveal any particular evolution of the VE matrix in terms of glass transition temperature and chemical structure, suggesting a good chemical resistance of the polymer.
As far as the tensile test investigations are concerned, only limited evolutions of the Young's modulus were observed (up to 7% loss), while a significant drop of the tensile strength was obtained over ageing time (Figure 2). This latter effect can be ascribed to the alkaline attack of the glass fibers by hydroxyl ions. For all tests, a brittle failure was observed in the middle part of the bars.. In addition, the damage rate was clearly accelerated by temperature. A maximum drop of strength was around 40% for specimens immersed 240 days at 60°C. Yet, the ageing procedure (direct immersion in the alkaline solution) is considered as too severe compared with on-site ageing.

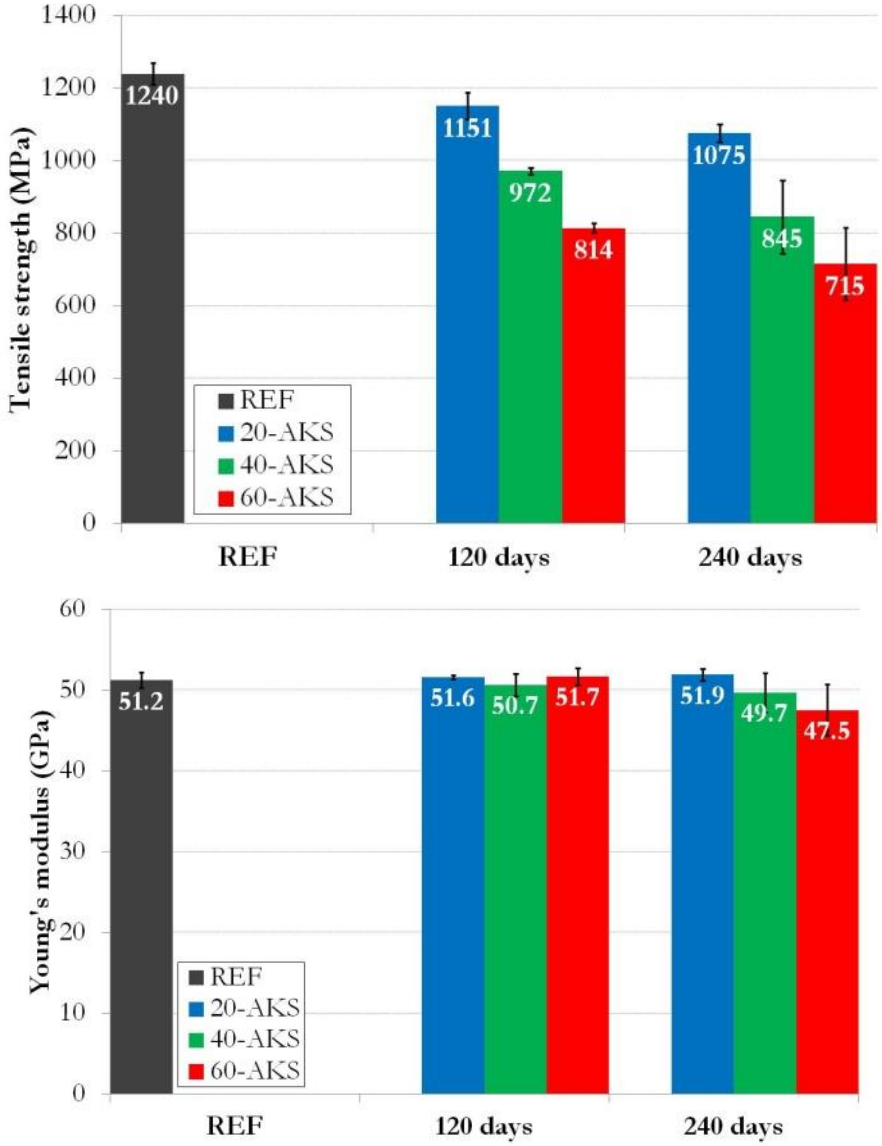

Figure 2: Evolution of the tensile strength and Young's modulus of GFRP rebars after immersion in alkaline solution at different temperatures

Differently, the short beam tests did not reveal any significant evolution of the ILSS or the failure mode, regardless the environment and temperature. This trend seems contrary to that reported in the literature (Chen, 2007), but it may account for the good resistance of the VE matrix and the fiber/matrix interface.

Results of the pull-out test in terms of average bond strength (maximum force/embedded surface) are given in Figure 3. A global increase in the bond capacity is observed after 120 days ageing, which may result from concrete curing / shrinkage over time. Then, after 240 days, the ultimate properties decreased slightly (but remained above the initial values). This may be due to the actual damage of the bar/concrete interface that becomes predominant over the other effects. Unfortunately, this durability study has not been conducted over a sufficiently long period to check these hypotheses in the long term. No evolution of the failure mode was observed on pull-out specimens. For all samples, failure occurred at the interface between concrete and the sand coating at the surface of the bars.

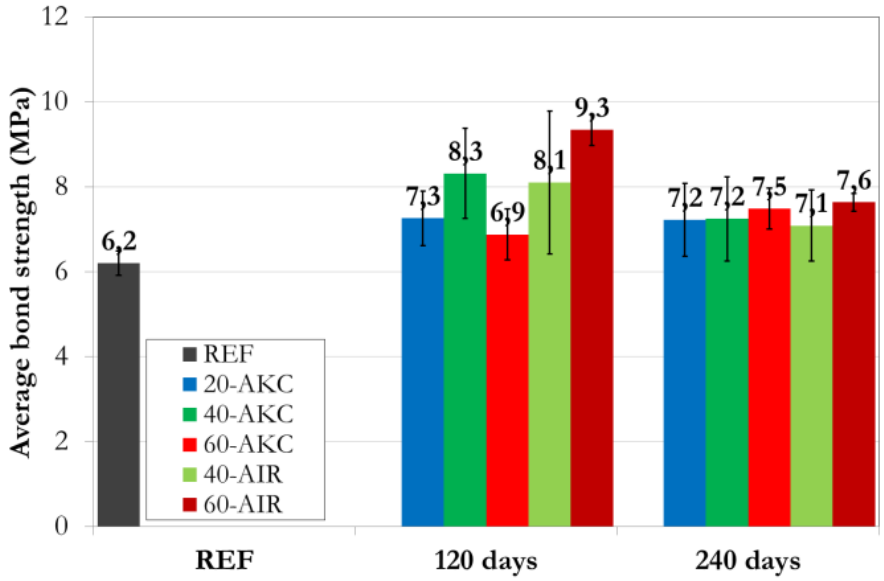

Figure 3: Evolution of the average bond strength, after indirect immersion in the alkaline solution (AKC) and exposure in the air at different temperatures

Conclusion

This study investigated the accelerated ageing behavior of GFRP rebars and their bond with concrete. Specimens were exposed to various environments and the evolutions of both their microstructure and mechanical properties were assessed after different period of time.

The main degradation was observed for the tensile strength of specimens directly immersed in the alkaline solution, with more than 40% loss after 240 days at 60°C, ascribed to the alkaline attack of glass fibers. Thanks to the different temperatures studied in this experimental campaign, it will be possible to set up a prediction method based on Arrhenius law. However,, direct immersion in the alkaline solution proved to be much more severe than actual site conditions.

No significant evolution has been found regarding the matrix microstructure, ILSS and the bond of the rebar in concrete. The 240 days ageing period may have been two short to detect damage on these issues. Yet, a deeper analysis of the pull-out results is currently being developed using an analytical interface model in which the parameters are identified from experimental data, as described in (Rolland, 2014; 2015).

Acknowledgement

The authors wish to acknowledge Pultrall Inc. (Canada) for their contribution to this study.

Key References

Chen, Y., Davalos, J.F., Ray, I., Kim, H.Y. (2007). Accelerated aging tests for evaluations of durability performance of FRP reinforcing bars for concrete structures. *Composite structures*, 78(1):101-111.

Rolland, A., Chataigner, S, Benzarti, K., Quiertant, M., Argoul, P., Paul, J.M. (2014). Mechanical-behavior of aramid fiber reinforced polymer (AFRP) rebar/concrete interfaces. *TRA- Trans.port Research Arena 2014*, April 2014, Paris La Défense (France).

Rolland, A. (2015). Comportement mécanique et durabilité de structures en béton renforcées par des armatures composites internes, PhD thesis, University Paris-Est (in French). https://tel.archives-ouvertes.fr/tel-01223307

2.4. Bond and Tension Stiffening

Bond of GFRP bar and concrete under static and cyclic loading

Ana Veljkovic[1], Marcin Michal Haffke[2], Valter Carvelli[3], Matthias Pahn[4]

Introduction

Being one of the main aspects in design of reinforced concrete structures, bond of rebar to concrete is extensively investigated in last decades [1]. In this light, great effort is spent as well in research and manufacturing in order to explain and to increase bond properties of FRP (fibre reinforced polymer) rebar to concrete. Rilem [2] recommended standard pull-out test as simple, but still effective method, for experimental assessing of bond properties. With the aim of simulating better real conditions in structure, but also for estimating concrete splitting tendency, pull-out test with eccentric placement of the bar is recommended by fib Bulletin 10 [1]. Due to excellent behaviour in aggressive environments and low cover splitting tendency, FRP rebar can be used in combination with very thin concrete cover, still ensuring the proper bond condition to concrete.

Delay in cover splitting along FRP bars is the consequence of its softer surface comparing to steel bars, which results in avoiding high local stress concentrations in bond contact points to concrete [3]. GFRP (glass fibre reinforced polymer) bars with trapezoidal ribs showed that cracking caused by splitting forces is delayed in specimens reinforced with GFRP rebars, comparing to ones reinforced with classical steel rebars [4]. GFRP bars with sand coating and spiral wrap demonstrated earlier cover cracking for higher concrete mechanical properties [3]. The concrete cover value can change the bond failure mechanism. Helically wrapped bars, cover of one bar diameter, generate splitting failure, while higher covers, two or more diameters, generate pull out or fracture of the bar [5].

The fatigue behaviour of FRP bars embedded in concrete depends on the bond strength mechanisms and therefore bar surface treatment is playing a great role and must be included when cyclic bond behaviour is described. Fatigue causes more serious effects in steel/concrete than in FRP/concrete bond, mainly because more stiff steel rebar develops bond mechanism with higher damage effects on interface during cyclic loads [6]. Helical wrapping and sand coating of FRP rods considerably reduced the resistance of the bond to cyclic loading, even for small loading levels in case of helical wrapping [7], [8]. Standard pull-out specimens showed that the best bond under cyclic loading was demonstrated by GFRP rods having stiff external layer of polymer, with large deformation of the external surface to increase the adhesion [7]. Post-cyclic bond behaviour is still not well-understood, due to different results from different studies, showing increased, decreased or same bond strength before and after cyclic loading [6], [9], [10], [11].

Eccentric pull-out tests, in below presented experimental campaign, investigated possibilities of application of low concrete cover in combination with GFRP reinforcement. This is particularly important for application in thin plate elements that are usually prefabricated and used as façade panels, pavement or layers in sandwich composite plates. The pull-out test set-up with eccentrically positioned GFRP bar was adopted to measure the effect of: external surface of the bar, thickness of the concrete cover and concrete mechanical properties. In addition, for cyclic loaded specimens, the maximum load in cycle is added as fourth parameter, in order to estimate the fatigue bond behaviour. This research gives an overview on best FRP/concrete bond performances considering all mentioned input parameters.

[1] Politecnico di Milano, Italy, ana.veljkovic@polimi.it
[2] Fachgebiet Massivbau und Baukonstruktion, Technische Universität Kaiserslautern, Germany, marcin.haffke@bauing.uni-kl.de
[3] Politecnico di Milano, Italy, valter.carvelli@polimi.it
[4] Fachgebiet Massivbau und Baukonstruktion, Technische Universität Kaiserslautern, Germany, matthias.pahn@bauing.uni-kl.de

Experimental setup and materials

The pull-out setup with eccentrically positioned bar was adopted (Figure 1a, b) together with standard Rilem centric pull-out test for comparison. Position of bars in tests was centric or with cover of 10, 15 and 20 mm. The length of bonded zone between bar and concrete was 5Ø, provided by an aluminium pipe that prevent forming of bond on the remaining part of the bar.

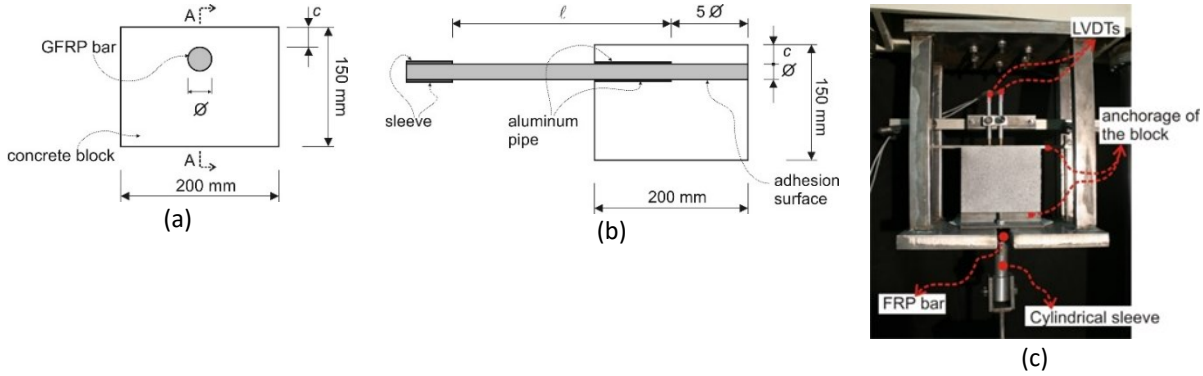

Figure 1: Eccentric pull-out specimen geometry: (a) top view; (b) longitudinal section A-A; and (c) experimental setup.

Figure 1c shows photo of test setup with two displacement transducers (LVDT) that were placed on the top of the cube to continuously measure displacement: one of the bar and another of the concrete surface next to the bar. The quasi-static pull-out tests were performed setting a cross-head displacement rate of 1 mm/min.

In case of cyclic tests, loading levels were selected according to the average static strength assuming R = 60 and 70%, where R represents ratio of the maximum load in the cycle and the static bond strength ($R=\tau max/\tau u$). The ratio of maximum and minimum loads in the cycle was set to 0.1. The tension-tension cyclic loading was applied with a frequency of 5 Hz. Tests were considered valid after the complete bond failure or after one million cycles. In the latter case, bar was pulled out statically to estimate the residual bond strength.

Two types of unidirectional E-glass FRP rebars were adopted, namely, ASLAN 100 rebars [12] of nominal diameter 6 mm and ComBAR® [13] rebar of nominal diameter 8 mm. The GFRP rebars of both types were produced by pultrusion technique with vinyl-ester resin. Those of diameter 6 mm have surface deformed with helical wrap and coated with coarse sand, while 8 mm rebars have external ribbed surface cut into the bar after curing (Figure 2). Table 1 contains the mechanical properties of the rebars in the direction of the bar axis, according to the data sheet of the producers. For the sake of comparison, tests were carried out with conventional steel ribbed bars (grade B500B, Table 1) of the same nominal diameters (6 and 8 mm).

Table 1: Mechanical properties of bars (*yield strength of steel bars).

Material	Nominal diameter [mm]	External surface	Tensile strength [MPa]	Tensile modulus of elasticity [GPa]
GFRP (ASLAN 100)	6	Wrapped, sanded	896	46
GFRP (ComBAR®)	8	Ribbed	1500	60
Steel (B500B)	6 and 8	Ribbed	500*	210

Figure 2: Surface of the GFRP rebars: (top) ASLAN 100, Ø 6mm; (bottom) ComBAR, Ø 8mm.

In total, four different concrete classes were used, named in the following C1, C2, C3 and C4. Average compressive cubic strengths, tensile strengths and moduli of concretes are listed in Table 2.

Table 2: Mechanical characteristics of the considered concretes.

Concrete ID	Average compressive cubic strength [MPa]	Average tensile strength [MPa]	Average compressive modulus of elasticity [GPa]
C1 (C20/25)	23.3	2.29	19.71
C2 (C30/37)	38.9	3.32	22.45
C3 (C45/55)	56.3	3.96	27.88
C4 (C50/60)	62.3	n.a.	n.a.

Results and Comparisons

Assuming the average shear stress (τ) on the contact surface between bar and concrete, estimated as $\tau = F/(\pi \varnothing * 5l)$, the average shear strengths are compared in Figure 3 [14]. The bond strength of ComBAR GFRP bars of diameter 8 mm are quite similar to the one of steel bars (values are in the same experimental scatter (Figure 3b)), while Aslan GFRP bars of diameter 6 mm had lower shear strength comparing to steel bars of same diameter (Figure 3a).

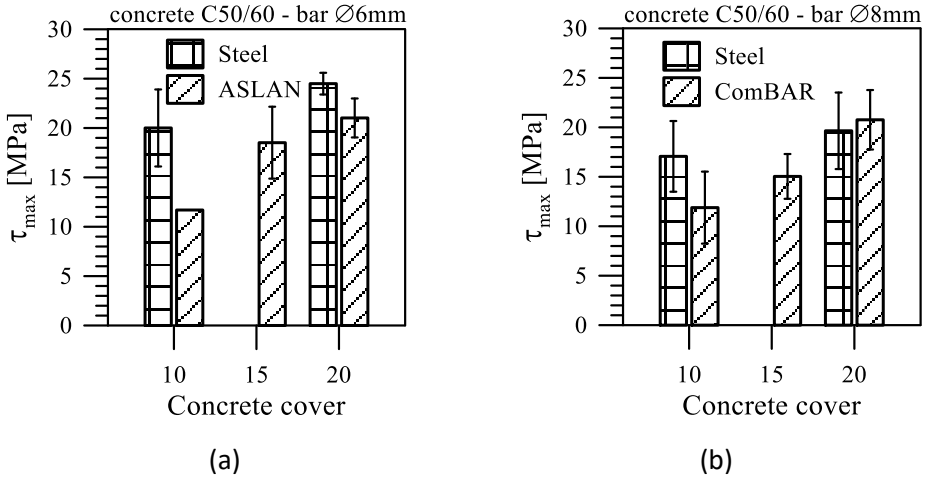

Figure 3: Comparison of the average shear strength for the concrete C4 (C50/60) and considered concrete covers (10, 15 and 20mm): (a) Steel and ASLAN rebars of diameter 6 mm; (b) Steel and ComBAR rebars of diameter 8 mm. Error bars indicate standard deviation of three tests.

One of the main reasons for the different behaviour of these two GFRP bars is clear observing their external surface after pull-out process. Sanded and wrapped Aslan 100 bars had external layer completely detached from the bar core, including the helical wrap and coarse sand (Figure 6a), while on the other hand, the ribbed ComBAR bars showed undamaged ribs and concrete still attached to the bar between its ribs [14].

(a) (b)

Figure 4: External surface of the GFRP rebars after pull-out: (a) ASLAN 100 with concrete cover 20 mm; (b) ComBAR with concrete cover 15 mm.

More tests were performed with steel and GFRP ribbed bars of diameter 8 mm, in order to get more precise information about debonding behaviour and damage modes. Figure 5a demonstrate that ribbed GFRP bars and steel bars showed even more comparable values of bond strength for 10 and 20 mm concrete cover [15] than in previous research [14]. The main difference between shear stress vs. slip curves of mentioned bars is the highest area underneath the curves of GFRP, meaning a higher energy to have a complete separation of the bar and concrete (Figure 5b) [15].

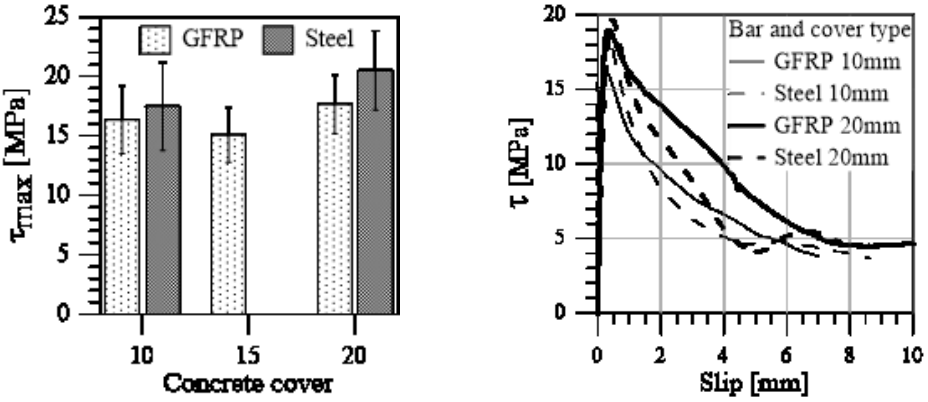

(a) (b)

Figure 5: GFRP and steel bars of diameter 8, in concrete C4, with covers of 10, 15 and 20 mm (a) Comparison of the bond strength (b) Representative shear stress vs. slip curves.

The influence of concrete class and thickness of concrete cover on bond with GFRP ribbed bar of diameter 8 mm is analysed on Figure 6.

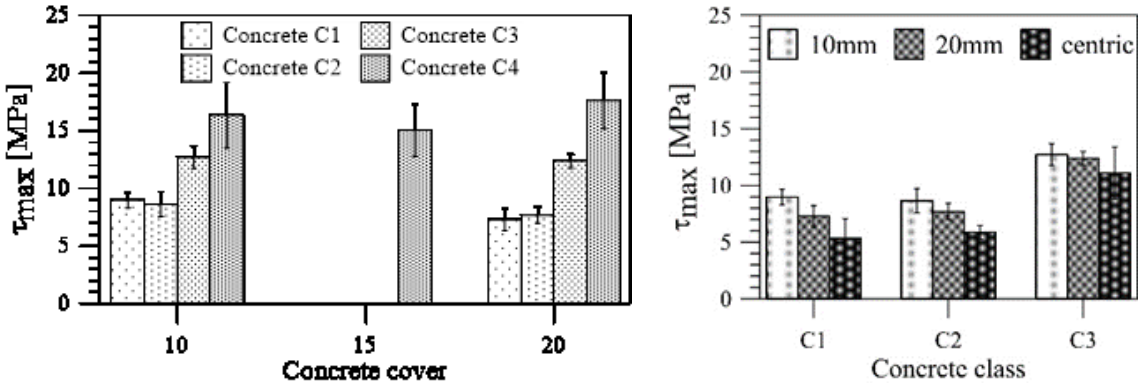

(a) (b)

Figure 6: Comparison of the bond strength for: (a) GFRP ribbed bar in concrete C1-C4 and three covers; (b) GFRP ribbed bar in concrete C1-C3 and three positions of the bar.

Concrete class improves significantly bond characteristics (Figure 6a), while concrete confinement increase had negative influence on bond strength (Figure 6b). Namely, comparison of the eccentric and centric pull-out tests showed tendency of the bond strength to decrease with increasing the confinement

for the lower concrete qualities, while this effect becomes less pronounced as concrete class increases (Figure 6b) [15]. Figure 7 shows typical bond shear stress vs. bar slip curves, for covers 10 and 20 mm and centrically positioned bars, and concrete classes C1 – C3. Presented curves demonstrate a typical bonding behaviour with almost no slip up to the maximum shear stress (shear strength) and similar non-linear post peak branches. However, different post peak behaviour was observed for different concrete classes. The higher concrete cover showed a higher fracture energy, i.e. higher area underneath the τ-slip curves [15].

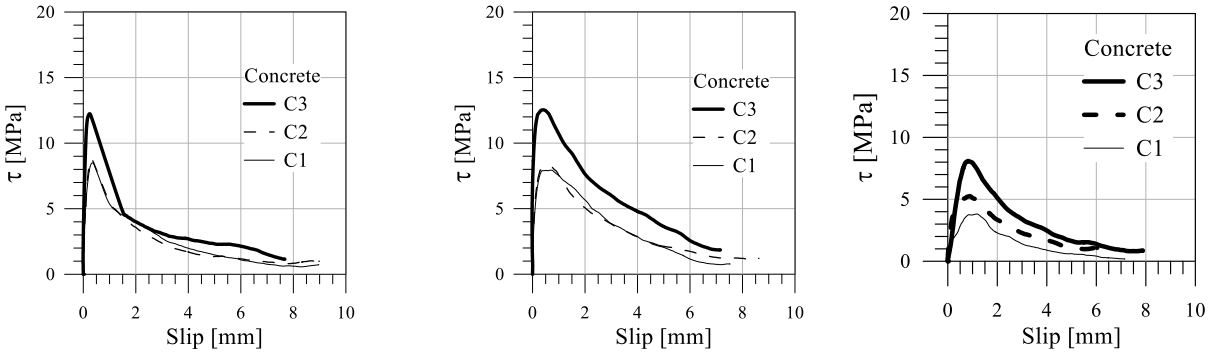

Figure 7: Representative shear stress vs. slip curves for ∅8mm: (a) GFRP ribbed bar cover 10 mm; (b) GFRP ribbed bar cover 20 mm; (c) GFRP ribbed bar centric specimen.

Visual inspection showed that in case of ribbed GFRP bars of diameter 8 mm, for concrete cover 10 mm splitting of the concrete cover occurred and for all other cases pull-out of the bar was recorded [15]. The bond surfaces (GFRP and concrete one) after failure were observed locally in details after sawing the specimen along the plane passing through the bar centre, orthogonally to the cover side [16].

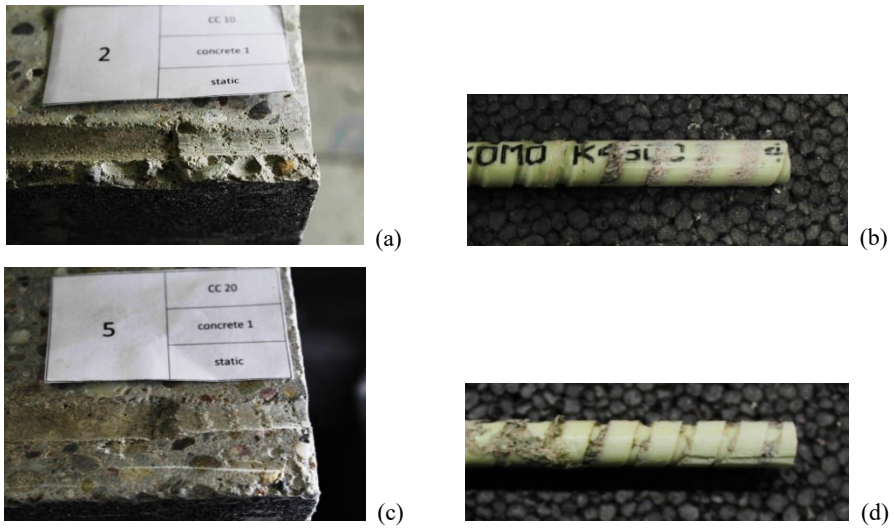

Figure 8: Failure surfaces after static loading of specimens of concrete C2 (C30/37) and ribbed GFRP bar of diameter 8 mm: (a, b) cover 10 mm; (c, d) cover 20 mm. (a, c) surface of the concrete, (b, d) surface of the rebar.

In case of 10 mm cover, the bar ribs pattern is clearly visible on the concrete side (Figure 8a), while the bar has still concrete attached between ribs as well as longitudinal grooves on the bar contact portion (Figure 8b). This reveals a failure mechanism involving both the concrete and the external layer of the bar. Specimens of 20 mm cover have less distinguishable imprint of the bar on the concrete (Figure 8c) and reduced quantities of concrete in between the bar ribs (Figure 8d) [16].

The fatigue tests performed for the lowest stress level (R=60%) did not generate complete failure of the specimens after one million cycles for all combinations of concrete qualities and bar covers (GFRP ribbed bar of diameter 8 mm, concretes C2 and C3, and concrete covers of 10, 20 mm and 100 mm) [15]. The second load level for fatigue test was selected as R = 70%. In this case, bond failure of almost all specimens was obtained before one million cycles. Different fatigue life occurred for different specimen types, as presented in Figure 9 [15].

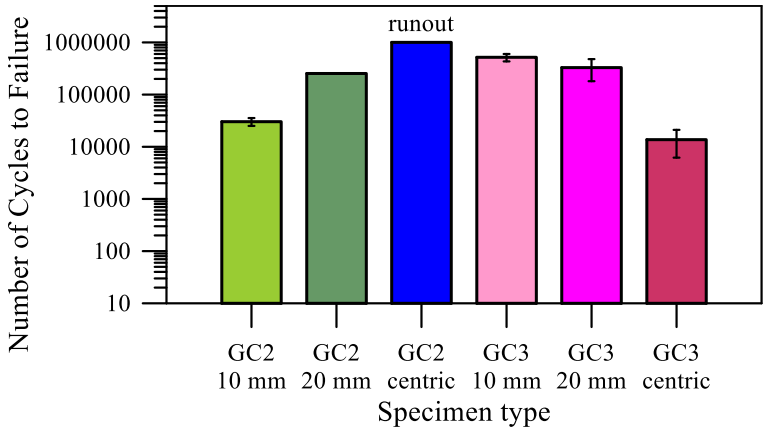

Figure 9: Fatigue life for bond of concrete and ribbed GFRP bar of diameter 8 mm, load level R = 70%.

For 10 mm concrete cover, significantly longer fatigue life is achieved by specimens of higher concrete class (concrete C3), one order of magnitude longer comparing to lower class concrete C2 (Figure 9). For cover of 20 mm, more similar values of the average fatigue lives were obtained for both concrete classes, C2 and C3. Centric specimens of concrete C2 exhibited very good fatigue behaviour at loading level R=70%. These specimens showed tendency to survive one million cycles even with such high value of cyclic load. However, due to insufficient data for this specimen type, it still remains issue to be checked in next investigations. In case of higher concrete class (C3), specimens with centrically positioned bar showed a reduction of fatigue life, that is consistent with the quasi-static behaviour (Figure 9) [15].

The local observation of the bond surfaces after fatigue failure showed more damaged bar surfaces comparing to quasi-static tests of same characteristics. Failure mechanism involved deeper grooves in the bar surface, while thin layer of fibres from the external surface of the bar was observed still bonded to the concrete [16].

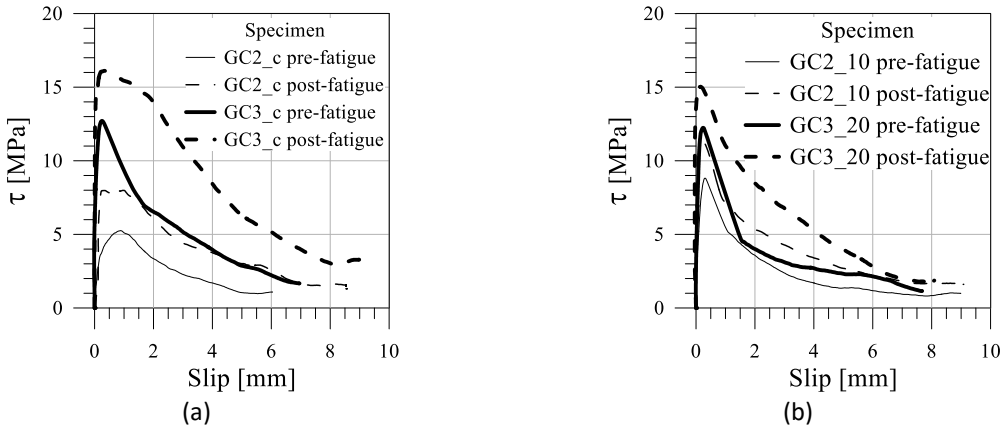

Figure 10: Comparison of the pre- and post-fatigue representative shear stress vs. slip curves of bond between concrete (C2 and C3) and ribbed GFRP bar of diameter 8 mm, for: (a) centric specimens; (b) eccentric specimens.

In case of no failure after one million cycles, for the load level R=60%, post-fatigue quasi-static pull-out was performed. Resulting bond strength did not have a reduction, in some cases result even showed an increase in bond strength (Figure 10), but in the experimental scatter band of the pre-fatigue quasi-static bond strength [15].

Conclusions

Quasi-static and fatigue behaviour of the bond between GFRP (glass fibre reinforced polymer) rebars and concrete was investigated considering the influence of bar surface, concrete cover and concrete mechanical properties.

The main conclusions of the experimental investigation are as follow.

For static loading:

- The bond strength of ComBAR GFRP bar of diameter 8 mm are quite similar to the one of steel bar, while ASLAN bar of diameter 6 mm has lower bond strength comparing to steel.
- The different external surface of the GFRP bars lead to different damage modes: the ASLAN 100 had complete delamination of the external layer; the ComBAR showed mainly undamaged ribs and concrete still attached in between them after pull-out.
- Reducing the confinement of concrete from 100 mm to 10 mm, for this type of ribbed GFRP bar of diameter 8 mm, affects bonding conditions in different manner: it lowers bond fracture energy, but it does not lower the value of the bond strength. Moreover, the concrete compressive strength influence on bond properties is much more pronounced than that of the concrete cover.

For cyclic loading:

- Specimens of all combinations of ribbed GFRP bar of diameter 8 mm, concretes C2 and C3 and cover of 10, 20 and 100 mm, did not fail after one million cycles of cyclic loading at R = 60%. Moreover, they showed an unchanged post-fatigue bond strength compared to the pre-fatigue quasi-static one.
- For cyclic loading with R = 70%, the higher concrete quality demonstrated a longer fatigue life with the lower concrete cover, that is consistent with the results of the quasi static pull out tests. Fatigue life does not depend on the considered bar cover for concrete C3 (C45/55), while the mechanical properties of the concrete have a considerable influence on the fatigue life of the bonding with the lower concrete cover (10 mm).

Key references

[1] Fib Task Group Bond Models, "fib Bulletin 10 “Bond of reinforcement in concrete”," International Federation for Structural Concrete (fib)/Sprint-Druck, Lausanne, Switzerland/Stuttgart, Germany, 2000.

[2] RILEM TC9-RC, "RC6 - Bond Test for Reinforcement Steel. 2. Pull-out test, 1983.," in RILEM Recommendations for the Testing and Use of Constructions Materials, London, E & FN SPON, 1994, p. 218–220.

[3] R. Tepfers and L. De Lorenzis, "Bond of FRP Reinforcement in Concrete — A Challenge," vol. 39, no. 4, pp. 477-496, 2003.

[4] A. Weber, "Bond Properties of a Newly Developed Composite Rebar," in Proceedings of the International Symposium on Bond Behaviour of FRP in Structures, Hong Kong, China, 2005, December 7 – 9.

[5] M. R. Ehsani, H. Saadatmanesh and S. Tao, "Design Recommendations for Bond of GFRP Rebars to Concrete," Journal of Structural Engineering, vol. 122, pp. 247-254, 1996.

[6] C. Shield, C. French and A. Retika, "Thermal and Mechanical Fatigue Effects on GFRP Rebar–Concrete Bond," in Third international symposium on Non-Metallic (FRP) Reinforcement for Concrete Structures, Sapporo, Japan, 1997, October 14 – 16.

[7] A. Katz, "Bond to Concrete of FRP Rebars after Cyclic Loading," Journal of Composites for Construction, vol. 4, pp. 137-144, 2000.

[8] J.-Y. Lee, C.-K. Yi and Y.-G. Cheong, "Experimental Study on the FRP-Concrete Bond Behaviour under Repeated Loadings," Mechanics of Composite Materials, vol. 45, no. 6, pp. 879-892, 2009.

[9] F. Ceroni, E. Cosenza, G. Manfredi and M. Pecce, "Durability Issues of FRP Rebars in Reinforced Concrete Members," Cement & Concrete Composites, vol. 28, p. 857–868, 2006.

[10] H. Wang and A. Belarbi, "Static and Fatigue Bond Characteristics of FRP Rebars Embedded in Fiber-reinforced Concrete," Journal of Composite Materials, vol. 44, no. 13, pp. 1605-1622, 2010.

[11] J. Alves, A. El-Ragaby and E. El-Salakawy, “Durability of GFRP Bars’ Bond to Concrete under Different Loading and Environmental Conditions,” Journal of Composites for Construction, vol. 15, pp. 249-262, 2011.

[12] Hughes Brothers, "Glass Fiber Reinforced Polymer (GFRP) Rebar - Aslan™ 100 series," November 2011. [Online]. Available: http://www.aslanfrp.com/.

[13] ComBAR® Schöck, "Schöck ComBAR Glass Fibre Reinforcement - Technical Information," August 2013. [Online]. Available: http://www.schoeck-combar.com/.

[14] M. M. Haffke, A. Veljkovic, V. Carvelli and M. Pahn, "Experimental investigation of the static bond of GFRP rebar and concrete," in Proceedings of Third Conference on Smart Monitoring, Assessment and Rehabilitation of Civil Structures - SMAR 2015, Antalya, Turkey, 2015.

[15] A. Veljkovic, M. M. Haffke, V. Carvelli and M. Pahn, "Static and Fatigue Bond Behaviour of GFRP Bars and Concrete," in Proceedings of the 8th International Conference on Fibre-Reinforced Polymer (FRP) Composites in Civil Engineering - CICE 2016, Hong Kong, China, 2016.

[16] A. Veljkovic, M. M. Haffke, V. Carvelli and M. Pahn, "Experimental investigation of the static and fatigue bond behaviour of GFRP bars and concrete," in Proceedings of the 11th fib International PhD Symposium in Civil Engineering, Tokyo, Japan, 2016.

Tension stiffening effect in FRP RC tensile members

M. Baena[1], L. Torres[2], A. Turon[3]

Introduction

Suitable modelling of reinforced concrete (RC) cracking and, particularly, post-cracking behaviour, is the most important and difficult task of the deformation analysis. Due to the interaction between reinforcement and concrete, the intact tensioned concrete between adjacent cracks is able to sustain certain level of tensile stresses and contributes to the stiffness of the RC element. This tension stiffening (TS) effect is of high importance in deformation analysis (crack formation, crack spacing and crack widths) and should be accounted for in design practice, especially at service loads.

Strategies in modelling TS in RC

The cracking behaviour of RC structures has been widely studied for traditional steel reinforced concrete (SRC) structures. Several methods have been used to implement the stiffening effect by the concrete between cracks. However, the extension of these methods to FRP RC structures is not always straightforward.

Effective cross sectional area

Some models evaluate the deformability of the whole element by an elastic analysis, where an effective cross-sectional area (or effective moment of inertia for flexural elements) is introduced (ACI 224.2R-92 (1992) (see Eq. 1), ACI-318.11 (2011)). This effective cross-sectional area (A_e) varies gradually from the gross sectional area (A_g) to the cracked cross sectional area (A_{cr}), as loading of the member increases beyond the cracking load (P_{cr}):

$$A_e = \left(\frac{P_{cr}}{P}\right)^3 A_g + \left[1 - \left(\frac{P_{cr}}{P}\right)^3\right] A_{cr} \quad (1)$$

No adaptation of this equation to FRP reinforcement has been proposed in the code for tensile elements. However, a reduction coefficient (see Eq. 2) was introduced in ACI 440.1R-03 (2003) to modify the equation for SRC flexural elements and adapt it to the FRP characteristics.

$$\beta_d = 0.5\left[\frac{E_{FRP}}{E_s} + 1\right] \leq 1 \quad (2)$$

Smeared crack methods

As an alternative, other models propose the use of average stress-strain approaches for characterizing material properties, where an effective tensile stress-strain relationship is developed with the displacements at cracks distributed over the length between cracks. Following this strategy, some models have been presented where the TS effect is coupled in the constitutive equation of embedded reinforcement, thus giving an expression for the average strain in the reinforcement after cracking. This is for instance the case of Eurocode 2 (1992), where the TS effect is simulated by multiplying the strain in the reinforcement at a crack by a factor less than 1 (see Eq. 3 where σ_s is the stress in reinforcement at crack due to applied load, σ_{sr} is the stress in reinforcement calculated on assumption of cracked section at load corresponding to cracking load, β_1 is a factor accounting for bond characteristics of

[1] University of Girona, Spain, marta.baena@udg.edu
[2] University of Girona, Spain, lluis.torres@udg.edu
[3] University of Girona, Spain, albert.turon@udg.edu

reinforcement (reading 1 for deformed bars and 0.5 for plain bars), and β_2 is a factor accounting for loading type (reading 1 for short term loading and 0.5 for sustained/repeated loading).

$$\epsilon_{sm} = \frac{\sigma_s}{E_s}\left[1 - \beta_1\beta_2\left(\frac{\sigma_{sr}}{\sigma_s}\right)^2\right] \leq \frac{\sigma_s}{E_s} \quad (3)$$

Model Code 90 (1993) proposes a similar expression for the average strain in the reinforcement after cracking (ε_m). In this case, the code makes a differentiation between being at the cracking stage or at the post-cracking stage:

$$\epsilon_m = \epsilon_2 - \frac{\beta_t\,(\sigma_s - \sigma_{sr1}) + (\sigma_{srn} - \sigma_s)}{(\sigma_{srn} - \sigma_{sr1})}\,(\varepsilon_{sr2} - \varepsilon_{sr1}) \quad \text{cracking stage} \quad (4)$$

$$\epsilon_m = \epsilon_2 - \beta_t(\varepsilon_{sr2} - \varepsilon_{sr1}) \quad \text{post-cracking stage} \quad (5)$$

where ε_2 is the strain in reinforcement for a fully cracked section, ε_{sr1} and ε_{sr2} are the strains for the uncracked and the fully cracked section, when first crack forms, σ_{sr1} and σ_{srn} are the reinforcement stress at crack when first and last crack are formed, and β_t is a coefficient for transmission length (reading 0.4 for pure tension). It has to be noticed that Eqs. 3-5 are no longer included in the latest versions of both codes (Eurocode 2 (2004) and Mode Code 90 (2010)). Besides, no mention to FRP reinforcement can be found.

Alternatively to this two code models, coupling of the TS effect in the reinforcement constitutive equation has also been proposed by Gilbert and Warner (1978) and Lee and Kim (2009). The latter modified β_t coefficient in Eq. 5 to include the effect of concrete strength and cover thickness. As an alternative to the TS coupling in the constitutive equation of embedded reinforcement, TS has also been coupled in the constitutive equation of cracked concrete (Vecchio and Collins (1986), Torres et al. (2004), Kaklauskas and Ghaboussi (2001), Stramandinoli and La Rovere (2008)). These models are usually dependent on geometrical and mechanical parameters such as reinforcement ratio and modular ratio, among others. Besides, most of these models have been developed for SRC and cannot be directly extended to FRP RC structures, particularly in the serviceability analysis where FRP material's higher deformability may condition the RC mechanical properties. However, most of these models have been obtained from experimental data where shrinkage effects have not been analysed, and only a few shrinkage-free models have been proposed. This is the case of Bischoff and Paixao (2004), who proposed a shrinkage-free tension stiffening factor applicable to concrete reinforced with bars of different stiffness. This tension stiffening factor represents the tensile response of cracked concrete relative to the initial cracking strength, and is presented to be independent of reinforcing ratio and concrete strength. In this same line, Kaklauskas and Gribniak (2011) propose a method for the removal of shrinkage from moment-curvature and tension-stiffening relations.

Bond-slip based models

TS effect heavily relies on the bond between concrete and reinforcement to transfer stresses. Therefore, a third possible strategy to model TS effect is to evaluate the member deformability by an analysis that takes into account both the effective behaviour of materials (concrete and reinforcement) and their interaction (by means of a bond-slip law). The assumption of a member block between two consecutive cracks, appropriate constitutive models (for concrete, reinforcement and interaction) and the application of equilibrium and compatibility conditions, allows one to evaluate the state of strain and stress at every cross section of the block.

Although being more accurate, these models involve either the solution of the system of differential equations that arise from the analytical study of the problem (Gupta and Maestrini (1990), Russo and Romano (1992), Yankelevsky et al. (2008)) or the use of numerical procedures, such as finite difference method and/or finite element method (Ferracuti and Savoia (2005), Vollum et al. (2008), Wu and Gilbert (2009)).

However, although these models include the bond phenomenon, most of the existing works use a linear or bilinear bond-slip law to model the interaction between the reinforcing bar and the concrete. In addition, although stress and strain distributions caused by cracking can be predicted, no comparison to experimental results is usually reported. In a recent work presented by Baena et al. (2013), non-linear bond-slip law obtained from experimental pull-out tests were used in the validation of the numerical model, and numerical results for strains distribution were compared to experimental data.

Experimental database on FRP RC tensile elements

Being tension stiffening effect occurring in RC subjected to tensile loads, the direct tension test seems to be the more appropriate o study the influence of the different parameters on the tension stiffening effect. However, most of the existing work is based on flexural elements, and limited database on tensile members is available.

First results of an experimental program on FRP RC tensile members can be found in Aiello et al. (2004). Ordinary concrete ($f_c^{'}$=47 MPa) was used, and CFRP rebars (E_{CFRP}=110 GPa and f_{fu}=2400 MPa, d_b=8mm) were considered as internal reinforcement. The experimental investigation was carried out on cylindrical specimens varying the concrete cover thickness. According to presented results, there exists a threshold value of concrete cover over reinforcement diameter (c/d_b=3) over which little further benefit from the bond interaction between reinforcement and concrete is obtained.

An experimental program on FRP RC ties was presented in Bischoff and Paixao (2004). The average concrete compressive strength was 48.8 MPa and GFRP bars with E_{GFRP}=41 GPa were considered. One reinforcing bar was centered at the square concrete cross section (100mm x 100mm) of each tie and three different reinforcement ratios were obtained (ρ=1.3, 2, 2.9%). According to experimental results, given any member strain, GFRP RC exhibited greater TS than SRC.

A parallel in time investigation was conducted by Sooriyaarachchi (2006), where the influence of reinforcement ratio (ρ), concrete compressive strength ($f_c^{'}$), and bar diameter (d_b) was studied. According to experimental results, the reduction of reinforcement ratio and the increase of concrete grade derived in an increase of the additional stiffness observed at the post-cracking stage of RC tensile elements, and no influence on the rebar diameter was found when results for equal reinforcement ratio were considered.

More recently, an experimental programme on the cracking behaviour of GFRP RC tensile elements was presented in Baena et al. (2011). The programme consisted on 6 RC tensile elements with reinforcement ratios ranging from 0.44% to 1.63% (combining two section sizes and three diameters). Experimental results showed the dependence of load-deformation response and crack spacing on the reinforcement ratio. Besides, crack spacing was found to be dependent on the ratio d_b/ρ_{eff}, and the role of concrete cover on crack spacing was found to differ from that of flexural members, where smaller covers are usually found.

Conclusions and Points for Discussions

The controversy in experimental results of limited published works depicts that there is a need on the development of a numerical model, capable to account for the singularities of the interaction between FRP reinforcement and concrete.

Besides, the limited amount of experimental programs centered on the behaviour of FRP RC tensile elements is partially understood if one considers that there are some aspects on the behaviour of SRC tensile elements that have not been yet accurately studied (concrete cover influence on splitting crack and crack with predictions at the concrete surface, among others).

Key references

ACI 224.2R-92 (1992). Cracking of concrete members in direct tension. Michigan (USA): Farmington Hills.

ACI 318-11 (2011). Building code requirements for structural concrete and commentary. Michigan (USA): Farmington Hills.

ACI 440.1R-03 (2003). Guide for the design and construction of concrete reinforced with FP bars. Michigan (USA): Farmington Hills.

Aiello, M; Leone, M; Ombres, L. (2004). Cracking analysis of fibre-reinforced polymer-reinforced concrete tension members. *Proceedings of the ICE - Structures and Buildings*. 157(1), 53-62.

Baena, M; Turon, A; Torres, L; Miàs, C. (2011). Experimental study and code predictions of fibre reinforced polymer reinforced concrete (FRP RC) tensile members. *Composite Structures*. 93 (10), 2511-20.

Baena, M; Torres, L; Turon, A; Miàs, C. (2013). Analysis of cracking behaviour and tension stiffening in FRP reinforced concrete tensile elements. *Composites Part B - Engineering*. 45 (1), 1360-67.

Bischoff, PH; Paixao, R. (2004). Tension stiffening and cracking of concrete reinforced with glass fiber reinforced polymer GFRP bars. *Canadian Journal of Civil Engineering*. 31 (4), 579-88.

CEB-FIP Model Code 90 (1993). Design Code. Comité euro international du béton-fédération international de la précontraint. London: Thomas Telford Services Ltd. 437p

Model Code for Concrete Structures 2010 (2013). Berlin: Ernst & Sohn. 402p.

CEN 1992. Eurocode 2 (1992). Design of Concrete Structures. Part 1-1: General rules and rules for buildings. Brussesls: Europeen committee for Standardisation.

Eurocode 2 (2004). Design of Concrete Structures. Part 1-1: General rules and rules for buildings. Brussesls: Europeen committee for Standardisation.

Ferracuti, B.; Savoia, M. (2005). Tension-stiffening law for FRP-reinforced concrete elements under service loadings. *International Symposium on Bond Behaviour of FRP in Structures*. Hong Kong, 7-9 December: Chen and Teng Ed.

Gilbert, RI; Warner, RF. (1978). Tension stiffening in reinforced concrete slabs. *Journal of the Structural Division - ASCE*. 104 (12), 1885-900.

Gupta, AK; Maestrini, SR. (1990). Tension-stiffness model for reinforced-concrete bars. *Journal of Structural Engineering - ASCE*. 116 (3), 769-90.

Kaklauskas, G; Ghaboussi, J. (2001). Stress-strain relations for cracked tensile concrete from RC beam tests. *Journal of Structural Engineering – ASCE*. 127 (1), 64-73.

Kaklauskas, G; Gribniak, V. (2011). Eliminating shrinkage effect from moment-curvature and tension-stiffening relationships of reinforced concrete members. *Journal of Structural Engineering - ASCE*. 137(12), 1460-69.

Lee, GY; Kim, W. (2009). Cracking and tension stiffening behaviour of high strength concrete tension members subjected to axial load. *Advances in Structural Engineering*. 12 (2), 127-37.

Russo, G; Romano, F. (1992). Cracking response of RC members subjected to uniaxial tension. *Journal of Structural Engineering - ASCE*. 118 (5), 1172-90.

Sooriyaarachchi, H. (2006). Tension stiffening effect in GFRP reinforced concrete elements. PhD Thesis, University of Sheffield.

Stramandinoli, RSB; La Rovere, HL. (2008). An efficient tension-stiffening model for nonlinear analysis of reinforced concrete members. *Engineering Structures*. 30 (7), 2069-80.

Torres, L; López-Almansa, F; Bozzo, LM. (2004). Tension-stiffening model for cracked flexural concrete members. *Journal of Structural Engineering – ASCE*. 130 (8), 1242-51.

Vecchio and Collins (1986). The modified compression-field theory for reinforced concrete elements subjected to shear. *Journal of the ACI*. 83(2), 219-31.

Vollum, RL; Afshar, N; Izzuddin, BA. (2008). Modelling short-term tension stiffening in tension members. *Magazine of Concrete Research*. 60 (4), 291-300.

Wu, HQ; Gilbert, RI. (2009). Modelling short-term tension stiffening in reinforced concrete prisms using a continuum-based finite element model. *Engineering Structures*. 31 (10), 2380-91.

Yankelevsky, DZ; Jabareen, M; Abutbul, AD. (2008). One-dimensional analysis of tension stiffening in reinforced concrete with discrete cracks. *Engineering Structures*. 30 (1), 206-17.

Removing the shrinkage effect from short-term moment-curvature and tension-stiffening relations

V. Gribniak[1], G. Kaklauskas[2]

Introduction

Shrinkage is important, although most frequently neglected, effect related to the constitutive modelling of reinforced concrete (RC). In the general practice, shrinkage along with creep is taken into account in pre-stress loss and/or long-term deformation analysis. However, even at the first loading, free shrinkage strain of concrete may be of magnitude that exceeds the cracking strain. Due to restraining action of a stiff reinforcement, shrinkage induces tension stresses in the concrete that might significantly reduce the crack resistance and, consequently, increase deformations of RC members. *Kaklauskas et al.* (2009), *Kaklauskas & Gribniak* (2011) and *Gribniak et al.* (2013a, 2013b) indicated that the short-term test data of shrunk RC elements might be essentially distorted ignoring the shrinkage effect.

Gribniak et al. (2013a) revealed that correct assessment of the shrinkage effect might be important in correct numerical modelling of deformations of RC members. In numerical simulation, shrinkage can be taken into account in two ways: *implicitly* or *explicitly*. In the implicit approach, common for engineering practice, a numerical analysis is performed using the tension-stiffening laws coupled with shrinkage. In the explicit approach, shrinkage is introduced as a prescribed deformation or as a fictitious force (Kaklauskas *et al*. 2009). *Gribniak et al.* (2013a) reported that, in the cases of high demands on accuracy, shrinkage should be accounted explicitly. Such analysis has to employ material (tension-stiffening) models with the removed shrinkage effect. These models can be obtained from the modified experimental data (by removing shrinkage). Until nowadays, only a few such (i.e., *shrinkage-free*) models were proposed.

Current paper presents a numerical procedure for removing shrinkage from moment-curvature and tension-stiffening relations. Based on this procedure, the *shrinkage-free* relations are derived using the test data of two RC beams reported by *Gribniak et al*. (2013c).

Removing the shrinkage effect

The presented procedure is based on the *Layer* section model (Kaklauskas 2004). Tension-stiffening is modelled by equivalent constitutive law of tensile concrete using next approaches and assumptions.

Approaches and assumptions

- Concrete is considered to be a homogeneous material.
- The smeared crack approach is adopted.
- Linear strain distribution within the section depth.
- The same stress-strain law is used for each layer of concrete in tension.

Direct technique: Moment-curvature analysis

Let us consider RC section subjected to an external bending moment M_{ext} shown in Figure 1a. It is divided into n longitudinal layers corresponding to either concrete or reinforcement (Figure 1b). The centroid of tensile reinforcement layer corresponds to the effective depth of section. Height of this layer t_s is taken from the condition of the equivalent area, i.e. $t_s = A_s / b$ (Figure 1b), where A_s is the area of reinforcement; b is the width of section.

[1] Vilnius Gediminas Technical University, Lithuania, Viktor.Gribniak@vgtu.lt
[2] Vilnius Gediminas Technical University, Lithuania, Gintaris.Kaklauskas@vgtu.lt

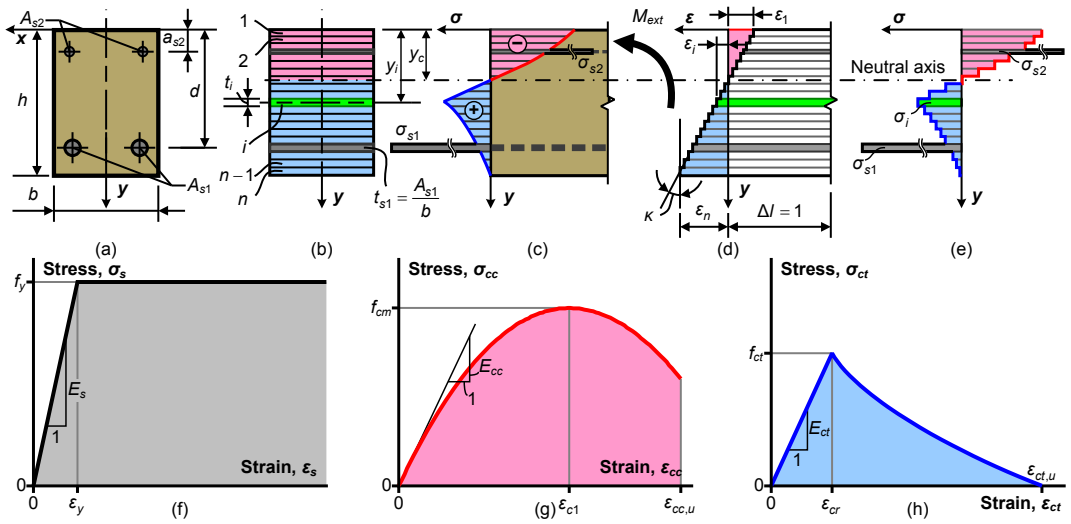

Figure 1: *Layer* section model (a)–(e) and constitutive laws for reinforcement (f) and concrete in compression (g) and in tension (h)

The technique is based on the secant deformation modulus conception (Kaklauskas *et al*. 2009). It needs to assume material laws for the reinforcement (Figure 1f) as well as for the concrete in compression (Figure 1g) and in tension (Figure 1h). The traditional approach of deformation analysis of RC structures is based on section transformation in relation to reference modulus of elasticity. Present technique uses a slightly different formulation applicable for the analysis of composites having different properties of layers that contribute to integral stiffness of the section. Curvature κ and strain ε_i at any layer i (Figure 1d) are calculated by the formulae:

$$\kappa = \frac{M_{ext}}{EI};\quad \varepsilon_i = \kappa\left(y_i - y_c\right);\quad y_c = \frac{SE}{AE};\quad AE = b\sum_{i=1}^{n} t_i E_{i,sec};$$
$$AE = b\sum_{i=1}^{n} t_i y_i E_{i,sec};\quad IE = b\sum_{i=1}^{n}\left[t_i^3/12 + t_i\left(y_i - y_c\right)^2\right]E_{i,sec}. \qquad (1)$$

Here *AE*, *SE* and *IE* are the area, the first and the second moments of inertia multiplied by the secant modulus $E_{i,sec}$, respectively. Other notations are evident from Figure 1b.

The analysis starts by using the linear elastic properties of materials. For the given strain ε_i and the constitutive law (see Figure 1f, 1g and 1h), stress σ_i is obtained. The secant deformation modulus $E_{i,sec} = \sigma_i / \varepsilon_i$ is determined for each of the layers ($i = 1…n$). Once this is done, the new curvature and strains ε_i are calculated by Equation (1) and the whole process repeated until there is no change (within the assumed tolerance Δ) in the computed values of secant modulus at each of layers. Figure 1d and 1e illustrate strain and stress distributions within the *Layer* section model. The calculation is terminated when the ultimate load step is reached.

Inverse technique: Deriving tension-stiffening relationships

The inverse analysis has an objective to determine parameters of the model based on the response of the structure. It is based on the concept of a progressive calculation of the stress-strain relationship for the extreme tension layer of the section. Figure 2 presents a flow chart of the inverse technique. Based on geometrical parameters of the cross-section, the *Layer* section is composed. Stress-strain material laws for steel and compressive concrete are assumed. Computations are performed iteratively for an incrementally increasing bending moment. At each moment increment *i*, an initial value of the secant deformation modulus of stress-strain relationship under derivation is assumed equal to zero ($E_{i,0} = 0$). Curvature $\kappa_{th,i}$ is calculated by the direct analysis. If the agreement between the calculated and the original curvature $\kappa_{obs,i}$ is not within the assumed tolerance Δ, i.e. Condition **1** is not fulfilled (Figure 2), the analysis is repeated using the hybrid *Newton-Raphson & Bisection* procedure (Gribniak *et al*. 2012) until Condition **2** is satisfied. At each iteration *k*, a secant deformation modulus $E_{i,k}$ is calculated. If the

solution is found (i.e. Condition **1** is satisfied), the obtained value of $E_{i,k}$ is fixed and used for next load increments. If the limit iteration number is exceeded ($k > N = 30$), the calculated $E_{i,N}$ is rejected, meaning that the secant deformation modulus E_i is not defined at the moment increment i, and the analysis moves to the next load step. The calculation is terminated when the ultimate loading step is reached (Condition **3**).

Shrinkage-free moment-curvature and tension-stiffening relationships

The shrinkage removing procedure combines direct and inverse techniques described above. The procedure is performed in the following steps sketched in Figure 3.

Step 1. Using the moment-curvature diagram schematically shown in Figure 3a, the stress-strain relationship is derived (Figure 3b) by the inverse technique.

Step 2. Using the stress-strain relationship, obtained in Step 1, the moment-curvature diagram is calculated by the direct technique. In this analysis, in order to remove shrinkage, the shrinkage strain of concrete is taken positive, i.e. as the expansion strain. The calculated *shrinkage-free* moment-curvature diagrams are shown in Figure 3c along with the initially assumed curve. It should be noted that due to the expansion of concrete, initial negative curvature was obtained. In absolute value, it is equal to the initial curvature (the positive one) due to shrinkage.

Step 3. As unloaded non-shrunk beam has no curvature, the obtained *shrinkage-free* moment-curvature diagram is shifted to the zero point (see dashed line in Figure 3c). Using this diagram, the *shrinkage-free* stress-strain relationship is obtained by the inverse analysis. This relationship is shown in Figure 3d along the one obtained from the "test" of shrunk member.

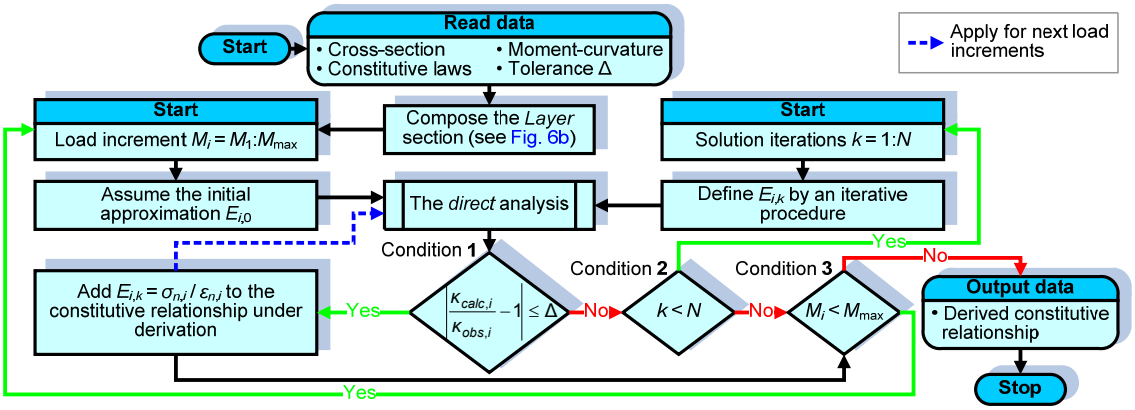

Figure 2: Flow chart of the inverse problem

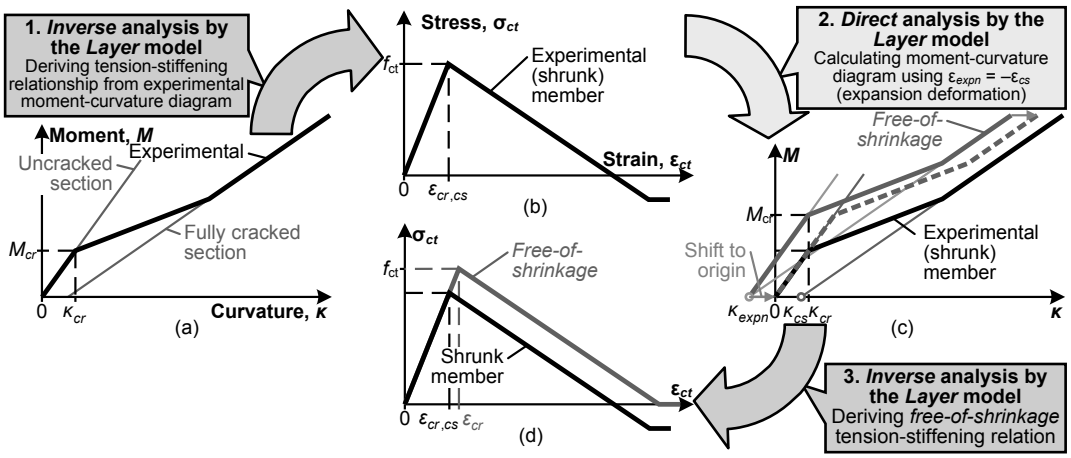

Figure 3: Deriving *shrinkage-free* moment-curvature and tension-stiffening relationships

Analysis of experimental data

For illustration purpose, present analysis uses experimental results of two beams reported by *Gribniak et al*. (2013c). The beams had a rectangular section reinforced with GFRP or steel bars having similar area of reinforcement. The beams were tested under a four-point-bending scheme with the concentrated forces dividing 3000 mm span into three equal parts. Main characteristics of the beams are given in Table 1, where *b*, *h*, and *d* are the width, height and effective depth of the section; A_f (or A_s) and E_f (or E_s) are area and deformation modulus of the tensile GFRP (or steel) reinforcement; E_c, f'_c and ε_{cs} are the deformation modulus, compressive ∅150×300 mm cylinder strength and shrinkage strain of concrete at age of testing.

Figure 4a gives the experimental and *shrinkage-free* moment-curvature diagrams. The black lines represent diagrams coupled with shrinkage, whereas stress-strain relations after removing the shrinkage effect are shown by the grey lines. Tangible differences between the transformed and the original curvature diagrams can be noted for the beam S2-3 having steel reinforcement.

The derived tension-stiffening relationships are shown in Figure 4b. It can be noted that shrinkage-induced stresses cause additional tension in the concrete surface near maximum concentration of reinforcing bars and, thus, reduction of the cracking resistance (reflected by the peak stress at the derived tension-stiffening diagrams). After the removal of this effect, the peak stresses increase.

Although the beams reinforced with GFRP and steel bars exhibited similar tension-stiffening stresses at strains prior to yielding of steel reinforcement, the limit strains (corresponding to zero tension-stiffening stress) of the derived diagrams were quite different. The ultimate strain for steel reinforcement did not exceed 2500 micro-strains, whereas for GFRP bars it was almost twice as big. This occurs due to very high tensile strength of GFRP in respect to steel bar that is not able to carry tensile stresses in the crack where yielding was reached. In other words, the tension-stiffening effect disappears after the yielding of steel.

It should be pointed out that the considered beams were reinforced using bars with different deformational moduli (Table 1). Due to differences in the restraining stiffness and, consequently, magnitude of shrinkage-induced stresses, the shrinkage effect has to be accounted for the comparative analysis of different reinforcement materials as well as for constitutive modelling purposes.

Table 1: Mechanical properties of the reinforcement

Beam	*b* (mm)	*h* (mm)	*d* (mm)	A_f or A_s (mm^2)	E_f or E_s (GPa)	E_c (GPa)	f'_c (MPa)	ε_{cs} (μm/m)	*t* (days)
S2-4-1nm	273	304	275	452.4	64.4	35.0	47.2	–318	31

S2-3	282	300	272	466.1	210.5	35.0	48.1	–268	66

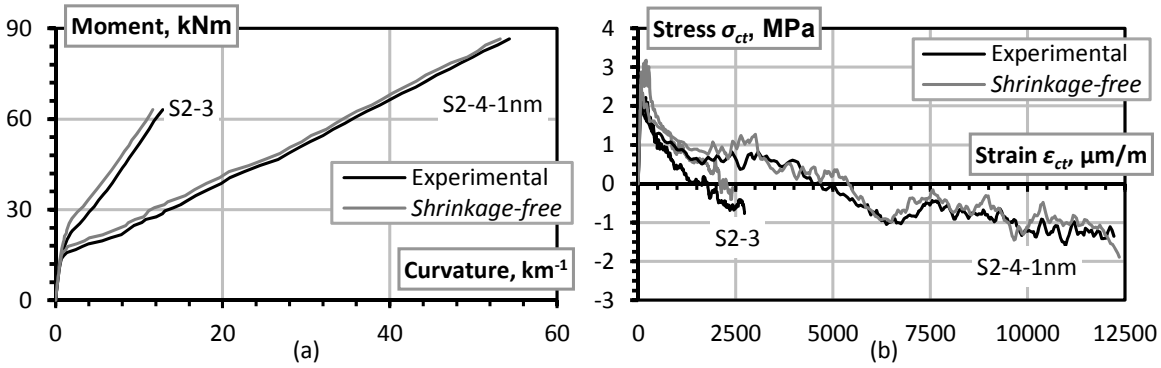

Figure 4: Deriving *shrinkage-free* moment-curvature and tension-stiffening relationships

Conclusions and Points for Discussions

- Shrinkage-induced stresses cause additional tension in the concrete surface near maximum concentration of stiff reinforcement and consequent reduction of the cracking resistance. The shrinkage effect significantly varies due to differences in the restraining stiffness related to the deformation modulus and area of reinforcement.
- The beams reinforced with GFRP and steel bars exhibited similar tension-stiffening stresses with the difference that these stresses in the steel reinforced elements practically disappeared after the yielding of steel.

Acknowledgments

The authors wish to express their sincere gratitude to Dr.-Ing. *André Weber* (Head of Research and Development, Division of Glass Fibre Reinforcement at *Schöck Bauteile* GmbH) for the kindly supplied samples of GFRP bars. The authors gratefully acknowledge the financial support provided by the *Research Council of Lithuania* (Research Project No MIP–050/2014).

Key references

Gribniak, V., Kaklauskas, G., Kacianauskas, R., Kliukas, R. (2012). Improving efficiency of inverse constitutive analysis of reinforced concrete flexural members. *Scientific Research and Essays*. 7 (8), 923-938.

Gribniak, V., Cervenka, V., Kaklauskas, G. (2013a). Deflection prediction of reinforced concrete beams by design codes and computer simulation. *Engineering Structures*. 56, 2175-2186.

Gribniak, V., Kaklauskas, G., Kliukas, R., Jakubovskis, R. (2013b). Shrinkage effect on short-term deformation behavior of reinforced concrete – When it should not be neglected. *Materials and Design*. 51, 1060-1070.

Gribniak, V., Kaklauskas, G., Torres, L., Daniunas, A., Timinskas, E., Gudonis, E. (2013c). Comparative analysis of deformations and tension-stiffening in concrete beams reinforced with GFRP or steel bars and fibers. *Composites Part B: Engineering*. 50, 158-170.

Kaklauskas, G. (2004). Flexural layered deformational model of reinforced concrete members. *Magazine of Concrete Research*. 56 (10), 575-584.

Kaklauskas, G., Gribniak, V. (2011). Eliminating shrinkage effect from moment-curvature and tension-stiffening relationships of reinforced concrete members. ASCE Journal of Structural Engineering. 137 (12), 1460-1469.

Kaklauskas, G., Gribniak, V., Bacinskas, D., Vainiūnas, P. (2009). Shrinkage influence on tension stiffening in concrete members. *Engineering Structures*. 31 (6), 1305-1312.

Experimental investigation and modeling of the bond between Aramid Fiber Reinforced Polymer bars and concrete

A. Rolland[1], S. Chataigner[2], K. Benzarti[3], M. Quiertant[3], P. Argoul[3], J-M. Paul[2]

Abstract

Aramid Fiber Reinforced Polymer (AFRP) bars are being used as internal reinforcement of concrete structures for more than twenty years. Their main advantages over common reinforcing steel bars rely on their lightness, durability performances, mechanical properties, and electromagnetic neutrality. For this application, interfacial properties between the reinforcing bar (rebar) and surrounding concrete play a major role on the mechanical performances of the reinforced concrete structure. In this context, this research aims at investigating the bond behaviour of commercially available AFRP reinforcing bars (rebars) embedded in concrete. The first part of the paper is devoted to the assessment of mechanical and physical properties of the selected rebars. A second part is then dedicated to the study of interfacial properties between the rebars and concrete: the interfacial bond strength is first assessed using a specifically designed pull-out test, and a novel modelling of the interface behaviour is then developed, based on an analytic bond-slip law. The method used for identifying the key theoretical parameters of the model is also discussed.

Introduction

Corrosion of steel reinforcing bars (rebars) is the main cause of deterioration of concrete structures. Consequently, some researchers investigated the use of alternative reinforcing materials such as advanced fiber reinforced polymers. This technology is being used for almost twenty years in some countries such as Canada or the USA (Benmokrane *et al.*, 2012), and specific design guidelines and test procedures have been developed to characterize this type of material and promote its introduction in new structures (JSCE, 1995) (ACI, 2004) (ISIS, 2006) (FIB, 2007) (CNR-DT, 2007) (ACI, 2008). A wider use of such a technology would have a beneficial effect on durability, and may thus lead to decrease the total cost of a structure as shown in (Eamon *et al.*, 2012).

The present work is concerned with braided Aramid Fiber Reinforced Polymer (AFRP) rebars that are produced in Japan by Fibex® Company (Figure 1). Both plain and sand-coated AFRP rebars are studied. This research is part of an ongoing investigation program focusing on this material (Rolland *et al.*, 2013) (Chataigner *et al.,* 2013). The first part of the paper presents the experimental characterizations that were conducted on AFRP rebars, including microscopic observations, tensile tests, determination of the glass transition temperature (T_g) of the polymer matrix, and measurement of the thermal expansion coefficient. Considering that the bond properties between the rebars and surrounding concrete is a key point regarding the performance of AFRP reinforced structures, the second part of the paper focuses on pull-out tests that were performed to characterize the bond behaviour. Finally, the last part is devoted to the modelling of the interfacial behaviour using a bond-slip analytical model.

[1] CEREMA, Direction Territoriale Nord-Picardie, France, arnaud.rolland@cerema.fr
[2] LUNAM Université, IFSTTAR, France, sylvain.chataigner@ifsttar.fr
[3] Université Paris-Est, IFSTTAR, France, karim.benzarti@ifsttar.fr

Figure 1: Pictures of the studied reinforcing bars.

Material properties at ambient temperature

Braided AFRP rebars are produced by a specific manufacturing process: braided aramid ropes are first impregnated in an epoxy bath before being stretched and cured in a continuous production line. Produced rebars are non-corrosive, non-magnetic and non-conductive.

Microscopic observations

Some microscopic observations were carried out in order to get a thorough understanding of the structure of the rebar and to investigate the presence of defects such as voids for instance. Some pictures showing the fiber arrangement are presented in Figure 2. The rebar is composed of four braided bundles of aramid fibers having diameters ranging from 15 to 18 micrometers, and twisted around a central nylon wire. No inclusions and no voids could be detected, suggesting a good quality of the manufactured products. For the reinforcement of concrete structures, Fibex® Company produces also sand-coated AFRP rebars specially designed to offer efficient bond performances with the surrounding concrete.

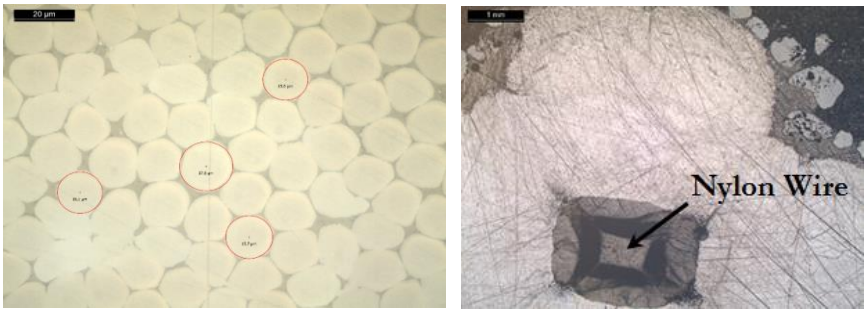

Figure 2: Microscopic observations of the cross-section of the studied rebar.

Tensile tests

For the purpose of tensile testing, a specific anchorage system was developed in accordance with (ACI, 2004). 20 cm long steel tubes were sealed with cement based grouting mortar at the gripping ends of the rebars (see Figure 3). This anchorage made it possible to systematically obtain tensile failures in the middle part of the tested rebars, as depicted in Figure 3. Tests were performed on AFRP rebars of diameter 11 mm, with a free length of 600 mm between the 2 anchorages. A mean tensile capacity of 106 kN was found, based on a series of three tests, corresponding to a mean tensile strength of 1120 MPa. The rebars exhibited an elastic and brittle behaviour, with a mean elastic modulus of 72 GPa.

Figure 3: Failure mode after a tensile test.

Glass transition temperature

Analyses were carried out by Differential Scanning Calorimetry (DSC), in order to assess the glass transition temperature (T_g) of the epoxy matrix according to (ASTM, 2008). Moreover, for security purpose it is important to check that T_g is much higher than the expected ultimate service temperature of the rebar embedded in the reinforced structure. Three determinations were done on small samples of plain rebars weighing 4-5 mg, placed in aluminium pans and analyzed using a TA Instruments® DSC Q100 calorimeter. Specimens were heated using a modulated ramp of temperature from 0 to 200 °C, at a heating rate of 1.5 °C/min, with a modulation period of 60 s and an amplitude of 0.239°C. A T_g value of 71.6 °C ± 2.1 °C was obtained by this method. An example of thermogram is illustrated in Figure 4. It is important to note that the T_g may vary depending on the curing cycle adopted for the rebar.

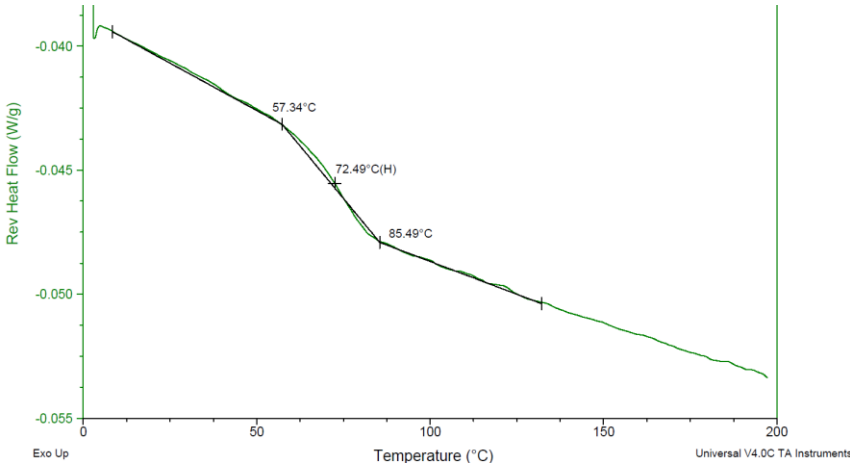

Figure 4: Example of thermogram provided by DSC experiments.

Thermal expansion

A major advantage of steel in the framework of civil engineering applications is certainly the fact that it has a thermal expansion close to that of concrete. This is not always the case for alternative materials, and especially for composite rebars as shown by (Ceroni *et al.*, 2006). Evaluation of the thermal expansion of studied rebars was carried-out according to two different methods, in order to evaluate the Coefficients of Thermal Expansion (CTE) in the longitudinal and transversal directions (with respect to the fiber axis), as composite rebars are known to be orthotropic. Thermo Mechanical Analyses (TMA) were first performed to assess the longitudinal CTE between 20 °C and 60 °C. The second method involves the use of strain gages and of a climatic chamber. One gauge was bonded in the longitudinal direction and another in the transverse direction. An additional strain gage was used to compensate the expansion of the measurement system itself. A picture of the experimental setup is given in Figure 5.

Results of measurements are summarized in Table 1. A large dispersion is observed for the longitudinal CTE values derived from TMA experiments. Moreover, the 2 methods provide very different values for

this longitudinal CTE. Nevertheless, results from the strain gage measurements are in agreement with literature data for AFRP composite bars (Erki and Rizkalla, 1993; Ceroni *et al.*, 2006). Additional investigations are currently in progress to check the previous results, especially for the transversal CTE.

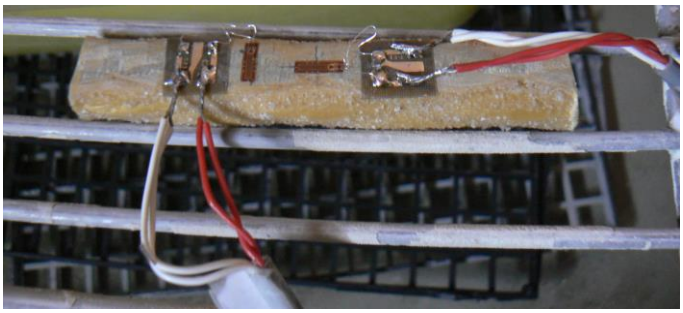

Figure. 5: AFRP rod sample monitored with strain gages for CTE measurements

Table 1: Experimental evaluation of the coefficients of thermal expansion.

Direction	Longitudinal CTE ($.10^{-6}$ °C^{-1})	Transverse CTE ($.10^{-6}$ °C^{-1})
Using TMA (3 tests)	-17; -25; -42	ND
Using strain gages (1 test)	-9	84

Bond tests

In order to investigate the bond behaviour between the AFRP rebars and surrounding concrete, pull-out tests were carried out.

Geometry and preparation of the pull-out specimens

The geometry of the test specimens is described in Figure 6. Two batches of concrete, named B1 and B2, were used for the preparation of the pull-out samples. The compressive strength of concrete was assessed on cylindrical specimens of diameter 160 mm and height 320 mm, providing values of R_{c1} = 36.1 MPa and R_{c2} = 34.1 MPa for the 2 batches, respectively. Different series of pull-out specimens were prepared, using steel bars (for control samples), plain and sand-coated AFRP rebars of various diameters. The adopted embedded length was six times the rebar diameter *d* for all test series (see Fig. 6). The objective was to investigate the effects of the diameter and the sand-coating on the bond properties between AFRP rods and concrete, and to make a comparison with traditional steel rebars.

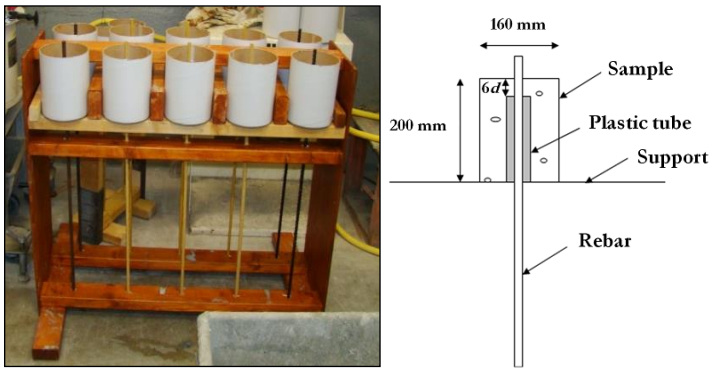

Figure 6: Picture of the preparation procedure and scheme of the pull-out specimens.

Test procedure

Tests were carried-out on a 350kN tensile testing machine. A tendon and specific grips allowed the application of the force to the rebar. The concrete block is supported by a steel beam drilled in the middle, so that the rebar can pass through it. The displacement at the free end of the sample is measured during the test (Figure 7) and the displacement rate is set constant at 1.3 mm/min, as recommended in (ACI, 2004).

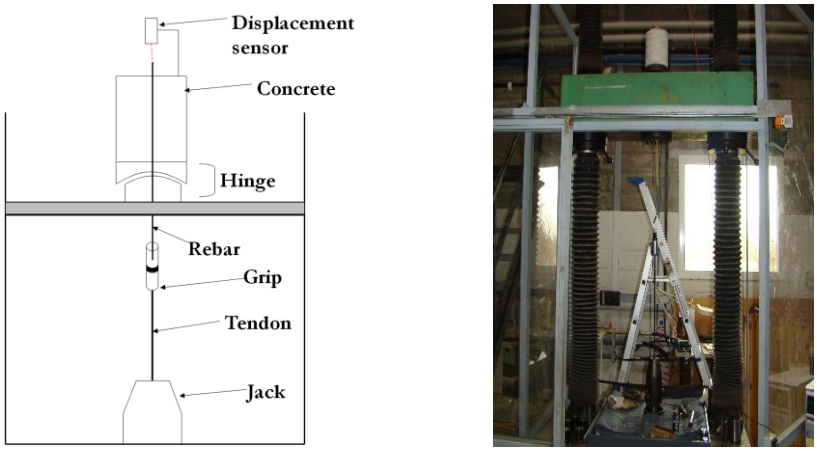

Figure 7: Scheme of the pull-out test and picture of the testing machine.

Results

The measured ultimate capacities are listed in Table 2. Average shear stress *versus* displacement curves are illustrated in Figure 9 for tests performed on specimens with steel, plain and sand-coated AFRP bars of various diameters. Three samples were tested for each diameter of AFRP rebars and two for steel rebars. In Table 2, the bond strength refers to the maximum value of the average bond stress, where the failure occurs. The bond stress is calculated as the ratio between the applied force and the embedded area of the bar.

It is interesting to note that only a small difference is found between specimens with steel and AFRP rebars, as far as the two smaller rebar diameters are considered. However, a large difference is noticed for the larger diameter. Besides, the sand-coating does not notably modify the ultimate pull-out capacity but alters the initial interfacial stiffness in the elastic domain. In the case of composite rebars, it can be observed that the bond strength decreases as the rebar diameter increases. Some pictures of the failure modes are given in Figure 8. In the case of the steel rebars, failure occurs within concrete, thus creating a sliding plane around the bar. In the case of AFRP rebars, it seems to occur in the rebar close to the interface for both sand-coated and plain samples. Similar results were found in the literature, suggesting that the pull out test is suitable and reproducible for bond characterization of composite rebars in concrete (Okamoto *et al.,* 1988).

Figure 8: Typical failure modes observed after pull-out tests.

Table 2: Results of the pull-out tests.

Type of rebar	Diameter *(mm)*	Concrete batch	Average ultimate capacity *(kN)*	Standard deviation *(kN)*	Average ultimate shear stress *(MPa)*
Steel	8	B1	18.50	1.43	15.33
	12	B2	38.35	4.35	14.13
	16	B2	93.10	4.77	19.29
Aramid	9	B1	20.31	0.39	13.30
	11	B1	38.95	1.58	17.08
	15	B2	49.53	0.47	11.68
Sand-coated aramid	9	B1	20.90	0.21	13.69
	11	B1	24.55	3.14	10.76
	15	B2	53.71	2.35	12.66

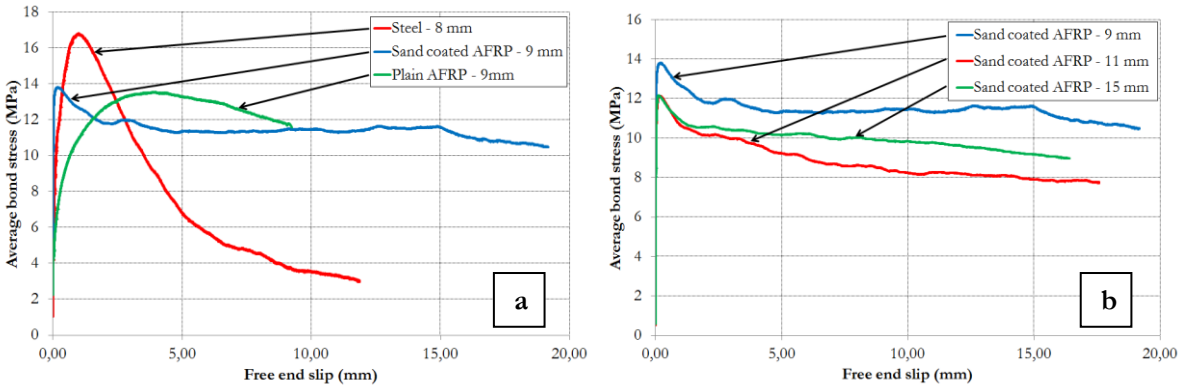

Figure 9: Examples of average bond stress *versus* displacement curves for : (a) Steel rebar of diameter 8mm, plain and sand-coated AFRP rebar of diameter 9mm, and (b) sand-coated AFRP rebars of various diameters (9 mm, 11 mm, and 15 mm).

Modeling

This part deals with the presentation of a novel analytical modelling of the bond behaviour between AFRP rebars and concrete. The model is formulated as a bond-slip law $\tau(s)$, with τ the interfacial shear stress (in MPa) and s the relative slip (in mm), and can be further implemented in finite element codes, using cohesive zone models, to simulate the behavior of reinforced concrete structures.

Analytical law

Some analytical models have already been proposed in literature, and the most cited are BEP (Eligehausen et *al.,* 1982) and CMR (Cosenza *et al.,* 1997) models. Typical responses associated to these models are presented in Figure 10. The response for a monotonic pull-out loading consists in a first nonlinear ascending branch until the ultimate shear stress τ_1, followed by a linear decreasing branch (an

additional plateau is proposed in BEP model), until a residual constant shear stress τ_3. The expression of the ascending branch proposed by BEP is $\tau = \tau_1 \left(\frac{s}{s_1} \right)^{\alpha}$, whereas CMR expression is $\tau = \tau_1 \left(1 - e^{-\frac{s}{s_r}} \right)^{\beta}$.

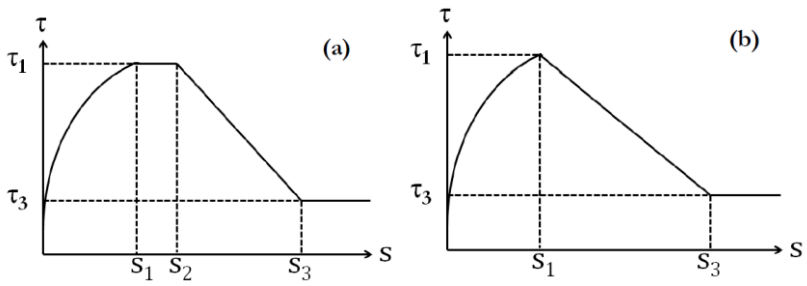

Figure 10: Typical responses of (a) the BEP model and (b) the CMR model.

Both expressions lead to an infinite slope at the origin point (s = 0). For this reason, their implementation into a finite element model is not recommended (infinite initial stiffness). Thus, we propose the following expression of the analytical bond-slip law $\tau_{model}(s)$:

$$\tau_{model}(s) = \begin{cases} \tau_0 \dfrac{s}{s_0} & \forall 0 \le s \le s_0 \\ \tau_0 + (\tau_1 - \tau_0)\left(1 + \dfrac{1}{\alpha}\right)\left(1 - \dfrac{1}{1 + \alpha\left(\dfrac{s - s_0}{s_1 - s_0}\right)}\right) & \forall s_0 < s \le s_1 \\ \tau_\infty + (\tau_1 - \tau_\infty)\dfrac{1}{1 + \beta\left(\dfrac{s - s_1}{s_1}\right)} & \forall s > s_1 \end{cases} \quad (1)$$

The typical bond-slip response associated with the proposed model is represented in Figure 11. The response for a monotonic pull-out loading consists of a first linear ascending branch of finite slope $K_T = \tau_0 / s_0$, followed for slip values above s_0 by a nonlinear branch (hyperbolic type) up to the value τ_1 when the slip is equal to s_1, and finally a third descending branch (also of the hyperbolic type), with a horizontal asymptote of value τ_∞. The two parameters α and β respectively govern the curvatures of the two hyperbolic ascending and descending branches.

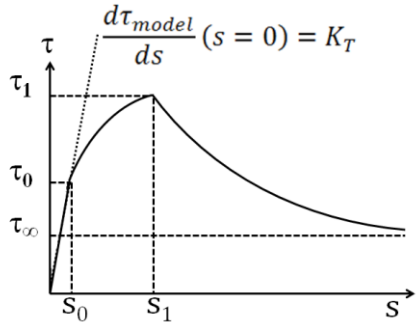

Figure 11: Bond-slip law $\tau_{model}(s)$ of the proposed model.

Parameter identification method

The proposed model (Eq. 1) is governed by seven parameters s_0, τ_0, s_1, τ_1, τ_∞, α, and β. The objective of this part is to identify all these parameters from experimental pull-out data (s_i , τ_i) for $1 \le i \le n$, n being the number of measurement points.

The identification procedure is divided into three successive steps:

(1) For each experimental curve, the value of τ_1 is determined by the value of the maximum shear strength obtained during the test, and the value s_1 is set as the corresponding slip value.

(2) The five other parameters are combined in a vector $\underline{\vartheta}$: $\underline{\vartheta} = [s_0\ \tau_0\ \tau_0\ \tau_\infty\ \alpha\ \beta]^T$. The optimum value of $\underline{\vartheta}$ is determined according to the least squares method, by minimizing the following discrepancy $\Lambda(\underline{\vartheta})$:

$$\Lambda(\underline{\theta}) = \sum_{i=1}^{n} (\tau_i - \tau_{\text{model}}(s_i, \underline{\theta}))^2. \qquad (2)$$

(3) The minimization of $\Lambda(\underline{\vartheta})$ is performed using the BFGS Quasi-Newton iterative method (Broyden, 1970), using the *Leastsq*® algorithm in the Scilab® environment. Initial values of the parameters to be optimized were set to $s_{0,0} = s_1/2$, $\tau_{0,0} = \tau_{\infty,0} = \tau_1$, and $\alpha = \beta = 1$. The iterations stop when the norm of the gradient of $\Lambda(\underline{\vartheta})$ becomes less than 10^{-6}.

Results

The method has been computed, based on experimental results obtained from tests performed on two sand-coated AFRP rebars of diameter 9 mm and two steel rebars of diameter 8 mm, due to their good representativeness.

Results of the parameter identification procedure are summarized in Table 3. Both experimental and theoretical bond-slip curves are drawn in Figure 12 for the steel rebars and in Figure 13 for the sand-coated AFRP ones. A good agreement can be noticed between the analytical and experimental curves.

In a further study, the next step will consist in identifying the parameters on a larger set of experimental results. The identified bond-slip law will then be implemented in a finite element code, using cohesive zone models elements, to simulate the behavior of reinforced concrete structures, taking into account the interfacial phenomenon. This has been done in the framework of a PhD study (Rolland, 2015).

Table 3. Identified parameters of the model

Rebar	Diameter (mm)	s_0 (mm)	τ_0 (MPa)	s_1 (mm)	τ_1 (MPa)	τ_∞ (MPa)	α	β
Sand-coated aramid rebar 1	9	0.015	7.96	0.19	13.81	11.00	15.50	0.19
Sand-coated aramid rebar 2	9	0.011	6.21	0.36	13.53	11.83	25.12	0.39
Steel rebar 1	8	0.037	6.17	1.01	16.78	-6.31	3.71	0.17
Steel rebar 2	8	0.016	7.02	1.12	16.50	-0.39	5.35	0.36

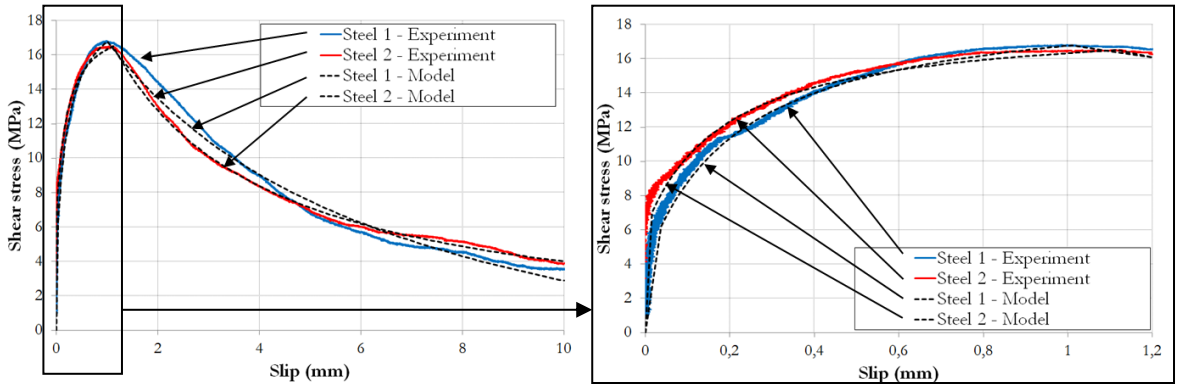

Figure 12: Experimental and identified bond-slip behaviour laws for pull-out specimens with 8 mm steel rebars

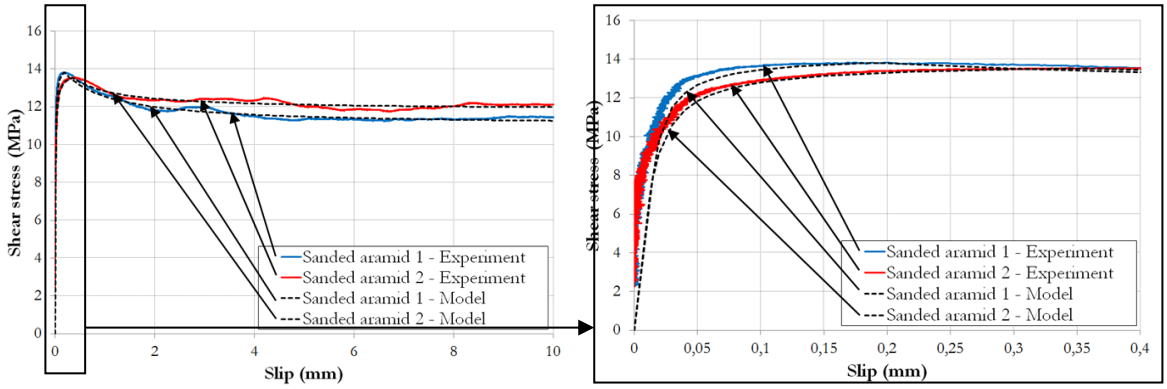

Figure 13: Experimental and identified bond-slip behaviour laws for pull-out specimens with 9 mm sand-coated aramid rebars.

Conclusions

The proposed investigations aimed at studying AFRP composite rebars used as internal reinforcement in concrete structures, with an emphasis on the bond behavior between these bars and concrete. Tests were first conducted on the rebars alone in order to characterize their microstructure and their mechanical properties, and to check the quality of the manufacturing process as well. It made it possible to assess the maximum service temperature of such rebars in concrete, which is directly related the glass transition temperature of the epoxy matrix. Preliminary investigations were also made regarding the determination of the coefficient of thermal expansion, but further work is needed since large dispersions were observed on experimental results.

Pull-out tests were conducted to check the adequacy of the experimental method. Results were found consistent with those of previous studies from the literature, suggesting an adequate preparation of the test specimens and a proper implementation of the test characterizations. Then, a modeling approach of the pull-out test has been presented. The experimental bond-slip behavior was satisfactorily simulated by an analytical bond-slip law model, whose parameters where identified using the least squares method. Besides, this identified bond-slip law could be implemented in a finite element code, taking into account the interfacial phenomenon between rebars and concrete. Such a code will be helpful to improve the design of concrete structures reinforced by AFRP rebars.

Acknowledgements

The authors express a strong acknowledgement to Fibex Company for providing the AFRP composite rebars, and to Cerema (DL Autun, France) for their participation in the experimental investigations.

Key references

ACI. (2004). Guide test methods for Fiber-Reinforced Polymers (FRPs) for reinforcing or strengthening concrete structures. ACI 440.3R-04.

ACI. (2008). Specification for construction with Fiber-Reinforced Polymer reinforcing bar. ACI 440.5-08.

AFGC (Association Française du Génie Civil). (2011). Réparation et renforcement des structures en béton au moyen des matériaux composites – Recommandations provisoires.

ASTM D 3418. (2008). Standard Test Method for Transition Temperatures and Enthalpies of Fusion and Crystallization of Polymers by Differential Scanning Calorimetry. ASTM.

Benmokrane, B., Ahmed, E., Dulude, C., & Boucher E. (2012). Design, construction and monitoring of the first worldwide two-way flat slab parking garage reinforced with GFRP bars. *Proceedings of the International conference on Composites In Civil Engineering CICE*, Rome.

Broyden, C., G. (1970). The convergence of a class of double-rank minimization algorithms. *Journal of the Mathematics and its Applications*, Vol. 16 (1), 76-90.

Ceroni, F., Cosenza, E., Gaetano, E., Pecce, M. (1988). Durability issues of FRP rebars in reinforced concrete members. *Cement and concrete composites*, Vol. 28 (10), 857-868.

Chataigner, S., Rolland, A., Benzarti, K., Dieng, L., Bouidarene, O., Paul, J. M., Quiertant, M., Argoul, P., Collet, P. (2013). Caractérisation d'armatures en PRF d'aramide utilisées dans les structures en béton armé. *18èmes Journées Nationales sur les Composites (JNC 18)*, Nantes, France, 10 p.

CNR-DT. (2007). Guide for the design and construction of concrete structures reinforced with fibre-reinforced polymer bars. National Research Council, Rome.

Cosenza, E., Manfredi, G., Realfonzo, R. (1997). Behaviour and modeling of bond of FRP rebars to concrete. *Journal of Composites for Construction*, May 1997, 40-51.

Eamon, C.D., Jensen, E.A., Grace, N.F., Shi, X. (2012). Life cycle cost analysis of alternative reinforcement materials for bridge superstructures considering cost and maintenance uncertainties. *Journal of composites for construction, and concrete composites*, Vol. 24 (4), 373-380.

Eligehausen, R., Bertero, V., Popov, E. (1982). Analytical model for deformed bar bond under generalized excitations. *Report No. UCB/ERC 82/23*, University of California, Berkeley, USA.

Erki, M. A., Rizkalla, S. H. (1993) FRP Reinforcement for Concrete Structures. Concrete International. Vol. 15 (6), 48-53.

Fib. (2007). FRP reinforcement in RC Structures, bulletin 40. Technical report.

ISIS Canada. (2006). Exigences pour l'homologation de barres d'armature en polymères renforcés de fibres pour les structures en béton. Canada.

JSCE. (1995). Quality specifications for continuous fiber reinforcing materials. JSCE-E 131-1995.

Okamoto, T., Endo, K., Matsubara, S., Tanigaki, M. (1988). Study on braided aramid fiber rods – Part 3. Bond characteristics I – Results of pull-out tests. Summaries of technical papers of annual meeting, architectural institute of Japan.

Rolland, A., Chataigner, S., Benzarti, K., Dieng, L., Bouidarene, O., Paul, J. M., Quiertant, M., Collet, P. (2013). Low temperature bond behavior of concrete with braided aramid fiber bars. *Proceedings of the 11th International Symposium On Fiber Reinforced Polymers For Reinforced Concrete Structures (FRPRCS 11)*, Guimarães, Portugal, Abstract pp.65-66 (10 pages. on CD proceedings).

Rolland, A. (2015). Comportement mécanique et durabilité de structures en béton renforcées par des armatures composites internes, PhD thesis, University Paris-Est (in French). https://tel.archives-ouvertes.fr/tel-01223307

2.5 Fire and Elevated Temperatures

Thermo-mechanical behaviour of GFRP reinforced thin concrete panels

Andreas Schmitt[1], Valter Carvelli[2], Matthias Pahn[3]

Introduction

The possibility in replacing steel rebars with GFRP (Glass Fibre Reinforced Polymer) rebars in reinforced concrete is increasingly investigated in the last decades [1]. Researches available in the literature are dedicated mainly to FRP reinforced concrete members with bearing function ([2], [3]). But in construction engineering several low bearing function concrete components have a relevant importance. In particular, very thin concrete elements are adopted like façade panels or slabs for pavements [4]. In spite of the interest in constructions industry on low bearing function FRP reinforced concrete members, their durability and in particular their thermo-mechanical behaviour is not deeply known and investigated. The latter is very important in external cladding of buildings or in pavements exposed to irradiation in very warm climates.

The present experimental investigation deals with the behaviour of thin concrete panels reinforced with GFRP rebars exposed to increasing temperature and bending loading [5]. The considered thin panels (thickness of 4 cm) are typical for low bearing function concrete layers in façade claddings. The influence of two aspects is studied: the concrete cover and the external surface of rebars. The adopted heating condition allows to have the temperature of the internal GFRP rebars almost at the level of the transition temperature of the resin. This does not match to a real fire exposure, but represents an extreme heating condition of low bearing panels.

Materials and GFRP reinforced thin concrete panels

Reinforced concrete thin panels of 170 x 40 x 4 cm are considered (Figure 1) fitting the available heating device [5]. Two concrete covers (5 and 10 mm) are considered and two GFRP unidirectional E-glass rebars (Schöck ComBAR® and FiReP® Rebar P), in the following B1 and B2, respectively. The panels do not have shear reinforcement. The pultruded GFRP rebars ComBAR® has external ribbed surface, cut into the bar after curing (Figure 2a), while the external surface of FiReP® Rebar P has a wave shaped thread profile (Figure 2b). For both rebars, vinyl ester resins are adopted with glass transition temperature of about 180°C, according to the producers. The nominal diameter of the rebars is 8 mm.

The mix for concrete has compressive cubic strength of 61.89 MPa and compressive elastic modulus of 28 GPa. The tensile strength is 3.5 MPa.

[1] Fachgebiet Massivbau und Baukonstruktion, Technische Universität Kaiserslautern, Germany, andreas.schmitt@bauing.uni-kl.de
[2] Politecnico di Milano, Italy, valter.carvelli@polimi.it
[3] Fachgebiet Massivbau und Baukonstruktion, Technische Universität Kaiserslautern, Germany, matthias.pahn@bauing.uni-kl.de

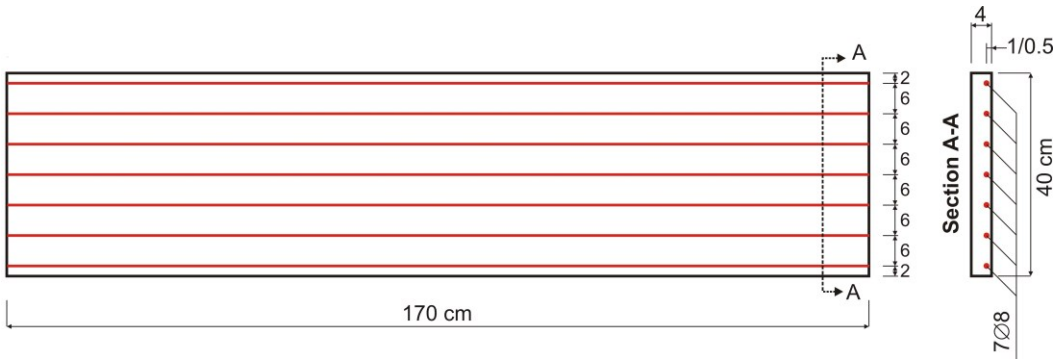

Figure 1. Reinforcement layout.

Figure 2. Rebars external surface: (a) Schöck ComBAR®; (b) FiReP® Rebar P.

Experimental procedure

The response of GFRP reinforced concrete panels is investigated with two consecutive experimental phases [5]: the first consists of the application of a bending constant load and then heating, while in the second the post-heating mechanical response under bending loading was measured up to failure at room temperature.

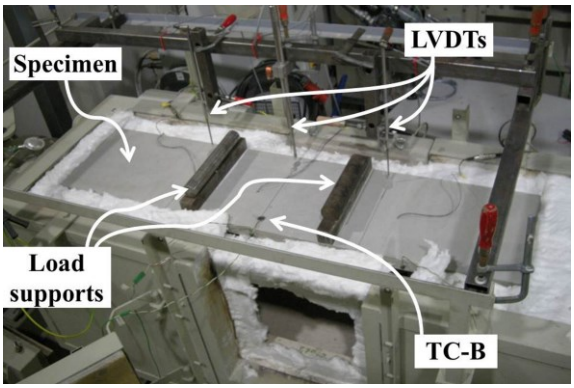

Figure 3. Test set-up of the first experimental phase.

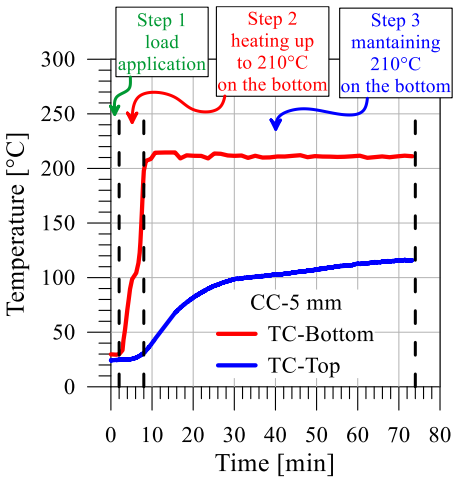

Figure 4. Representative diagram temperature vs. time of specimen reinforced with Schöck ComBAR, 5 mm concrete cover.

In the first phase, initially a quasi-static four-points bending loading with supports span of L=140 cm and loads span of 50 cm is imposed and then heating with increasing temperature on the full bottom surface. The loading is applied quasi-statically up to the maximum resultant of 3.6 kN, estimated, by ACI-440, in the range of the theoretical concrete first cracking, supposed to start at about 2.6 kN. Once the maximum load is reached, it remained constant for the heating time. The heating on the bottom surface of the sample is applied by the device in Figure 3. The temperature on the bottom and top surface of the specimen is continuously measured by two thermocouples (TC-B and TC-T) in the mid span at 5 cm from one longitudinal side. After the application of the load, the temperature on the bottom surface of the specimen is increased from the room temperature (25 °C) to the maximum considered of 210 °C and maintained nearly constant for about 65 min (Figure 4). The maximum imposed temperature is not as in some real applications of thin concrete panels (e.g. on façade panels the temperature could be below 100°C in very warm latitudes). It was considered to investigate the thermo-mechanic behaviour under an extreme condition. Moreover, the maximum temperature of 210 °C was imposed to have at the rebars level a temperature close to the glass transition temperature of the adopted resins (Tg ≈ 180 °C). The diagrams in Figure 4 show two representative evolutions in time of the temperature recorded on the bottom and top surface of specimen. The maximum recorded temperature on the top surface was about 120 °C, after 65 min of exposition. Assuming a linear distribution of the temperature in the thickness (this is reasonable for the considered small thickness) at the bar level the temperature should be about 189°C and 178°C for 5 and 10 mm cover, respectively. During loading and heating, the deflection of the specimen is measured by three transducers (LVDT), one in the mid span and two 35 cm beside both supports (see Figure 3). They are placed on the top surface, 5 cm from the opposite longitudinal side of the thermocouples.

In the second experimental phase, the samples were quasi-statically loaded using the same four-points bending scheme at room temperature. This allowed to estimate the mechanical behaviour of the panels after the thermo-mechanical conditioning.

Results

The first experimental phase provides the evolution of the displacement in Figure 5. The measurements of the three LVDTs, on specimens reinforced with ComBAR (see Figure 5), show the contribution of three steps (Figure 4) on the global deformation, namely: mechanical loading up to the considered maximum load; heating up to the maximum considered temperature (210 °C); maintaining the temperature constant on the bottom surface for 65 min. The contributions on the mid span displacement of the three thermo-mechanical steps are compared in Figure 6. On one hand, the smaller concrete cover gives the lower maximum deflection for both rebars. On the other, the influence of the rebar external surface is

visible, the reinforcement with ComBAR rebars shows a lower mid span displacement for both concrete covers in each step.

The thermo-mechanical loading of the first phase develops the cracks pattern on the bottom surface of the panels detailed in Figure 7, where the longer cracks are highlighted. The main distribution of the cracks is, as expected, in the central part of the panels between the two positions of the load application where the constant maximum bending moment is generated. The panels with different rebars and the same concrete cover do not have considerable differences in the crack patterns.

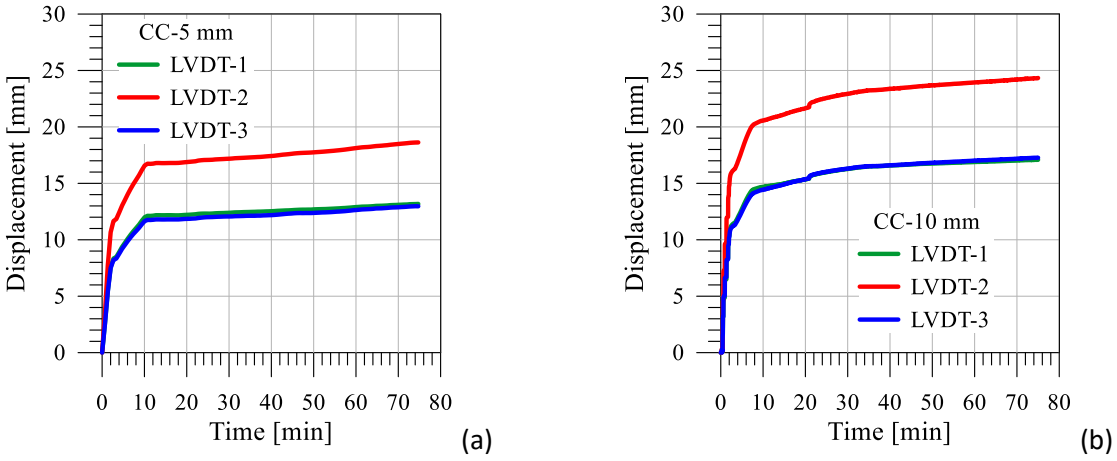

Figure 5. Representative diagrams LVDTs displacement vs. time of specimens reinforced with Schöck ComBAR for (a) 5 mm and (b) 10 mm concrete cover. 'cc' means concrete cover.

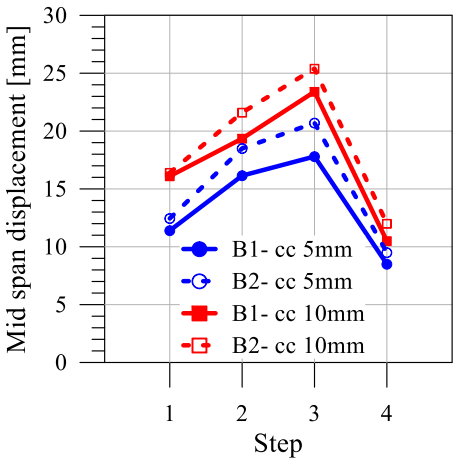

Figure 6. Average LVDT mid span displacement at different steps: '1' at the maximum load before heating; '2' after heating up; '3' after 65 min of maintaining the maximum temperature; '4' after unloading and complete cooling. B1 and B2 indicate Schöck ComBAR and FiReP Rebar P, respectively. 'cc' means concrete cover.

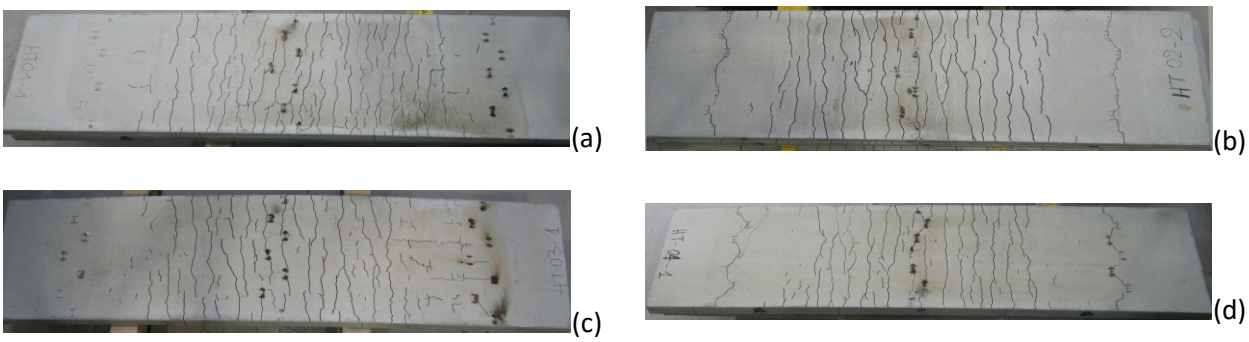

Figure 7. Cracks pattern after unloading and cooling. Specimens reinforced with: (a, b) Schöck ComBAR; (c, d) FiReP Rebar P. (a, c) 5 mm and (b, d) 10 mm concrete cover.

The influence of combining mechanical load and elevated temperature on the mechanical response of the panels is measured in the second experimental phase with four points bending tests at room temperature up to failure (Figure 8). The global response of the panels is detailed in Figure 9a. The post-heating load vs. mid span deflection curves show a similar behaviour of the panels with the same concrete cover. The only relevant difference is on the failure load of the panels with 5 mm cover. The panels with ComBAR have a maximum load almost 30% higher than those with FiReP rebars. This is probably connected to their external surfaces leading to different adhesion failure mechanisms, more evident with the lower concrete cover.

The variation of the pre- and post-heating mechanical behaviour is detailed comparing the stiffness of the panel. The initial stiffness is defined as the slope of the segment passing through load 0 and 3.6 kN (Figure 9a). The degradation of the initial stiffness (Figure 9b), due to loading and heating, is higher for concrete cover 10 mm than 5 mm for both rebars. Moreover, the panels reinforced with FiReP rebars have a lower initial stiffness with concrete cover of 5 mm, while those with concrete cover of 10 mm have almost the same stiffness. The latter depends on the position of the bars and the involvement of the concrete on the bottom of the panel in sustaining the tensile stress.

All specimens have failure of the concrete in compression (see the typical failure mode in Figure 10). The bars are not extensively damaged and not broken. Extracting some rebars from the specimens after failure, they show still a good adhesion with concrete and an external surface not apparently modified by the elevated temperature (see Figure 11 for rebars in panels with 5 mm concrete cover).

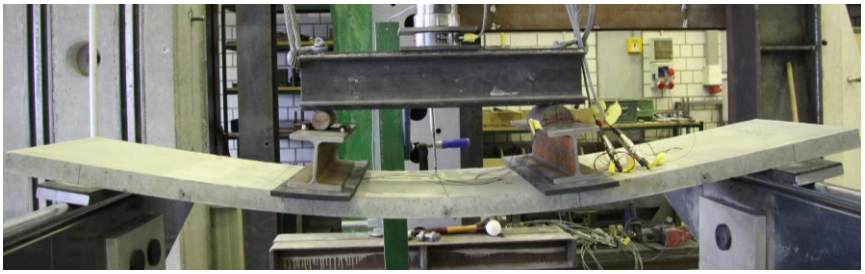

Figure 8. Post-heating four points bending test at room temperature.

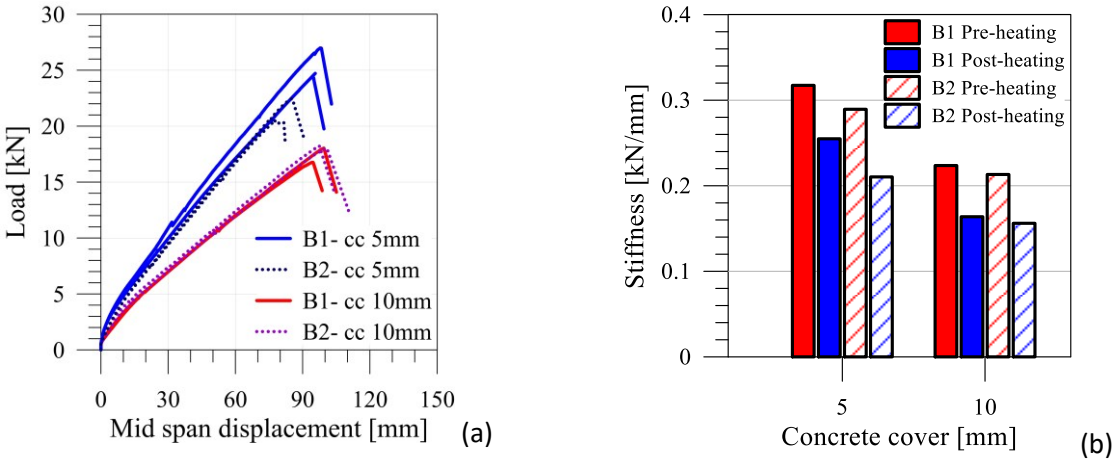

Figure 9. Post-heating bending. (a) Load vs. LVDT mid span displacement. (b) Average initial stiffness of the panels. B1 and B2 indicate Schöck ComBAR and FiReP Rebar P, respectively. 'cc' means concrete cover.

Figure 10. Post-heating bending. Typical failure mode of the panels.

Figure 11. Post-heating bending. Rebars after failure of the panels with 5 cm concrete cover: (a) Schöck ComBAR and (b) FiReP Rebar P.

Conclusions

The experimental research is focused on understanding the thermo-mechanical response of thin concrete panels reinforced with GFRP rebars. The considered panels have 4 cm thickness and are typically adopted as low bearing function concrete components (e.g. façade panels or slabs for pavements). The main results of the research (extensively discussed in [5]) highlight, as consequence of the loading and heating with maximum temperature of 210 °C: the influence of the external surface of the GFRP rebars on the bending response of the panels; the considerable residual deflection of the panels after heating and complete cooling; the reduction of the initial global stiffness; the negligible degradation of the GFRP reinforcement and of its adhesion to concrete.

Acknowledgements

The research was partially developed during the 'Short Term Scientific Mission' of the second Author financed by COST Action TU1207. Schöck Bauteile GmbH and FiReP Inc. are gratefully acknowledged for supplying the GFRP rebars.

Key references

[1] Bakis C., Bank L., Brown V., Cosenza E., Davalos J., Lesko J., Machida A., Rizkalla S., Triantafillou T. (2002). Fiber-Reinforced Polymer Composites for Construction — State-of-the-Art Review. Journal of Composites for Construction - ASCE, 6, 73-87.

[2] Nigro E., Bilotta A., Cefarelli G., Manfredi G., Cosenza E. (2012). Performance under Fire Situations of Concrete Members Reinforced with FRP Rods: Bond Models and Design Nomograms. Journal of Composites for Construction - ASCE, 16, 395-406.

[3] Carvelli V., Pisani M. A., Poggi C. (2013). High temperature effects on concrete members reinforced with GFRP rebars. Composites: Part B, 54, 125-132.

[4] Schmitt A., Pahn M. (2014). Examination of the structural behaviour of filigree GFRP-reinforced concrete slabs under bending. In Improving Performance of Concrete Structures - The Fourth International fib Congress, Mumbai. Universities Press, 761-763.

[5] Schmitt A., Carvelli V., Pahn M. (2015). Thermo-mechanical loading of GFRP reinforced thin concrete panels. Composites Part B, 81, 35-43.

Experimental results on FRP RC members exposed to fire

Antonio Bilotta [1], Emidio Nigro [2]

Fiber-reinforced polymer (FRP) materials have several important characteristics, such as high strength-to-weight ratios and resistance to corrosion, which are advantageous in the construction field. Recent progress in research and technology of FRPs have led to reduced material costs and increased confidence in the use of polymers for a variety of civil engineering applications, as testified by many examples worldwide.

Recent studies carried out at by Keller et al. (2005,2006) and Correia et al. (2010) on the fire response of GFRP pultruded profiles showed that FRP profiles can be used also in fire situation. On the other hand, several building codes (CAN/CSA 806-02, 2002; ACI 440.1R-04, 2003; CNR- DT203, 2006) are now available for the design of concrete structures reinforced with fiber reinforced polymer (FRP) bars in place of traditional steel reinforcement, even if few provisionsand no calculation model have been suggested that take account of fire conditions. Only the Canadian code (CAN/CSA 806-02, 2002) provides a design procedure in fire situations based onthe results of a parametric study conducted by Kodur and Baingo (1998). They found that the fire resistance of FRP-reinforced concrete slabs mainly depends on (a) the critical temperature of FRP reinforcement, (b) the thickness of the concrete cover, and (c) the type of aggregate in the concrete mix. They then provided different design abacuses which allow evaluation of the minimum concrete cover required to maintain the bars' temperatures within acceptable limits depending on the critical temperatures of the FRP reinforcement. Nevertheless, the critical temperature of FRP bars remains unknown for most currently available FRP-reinforcing products. Consequently, employment of FRP-reinforced concrete (FRP-RC) is limited mainly to applications where fire resistance aspects are not particularly relevant. Thus performance of these materials in fire situations must be evaluated in order to improve confidence in the use of FRP-RC members in multi-story buildings, parking garages, and industrial structures.

On this point, the literature provides a broad state of the art on the behavior in fire events of concrete structures reinforced or strengthened with FRPs (Bisby et al., 2005) and some results of failure tests performed on FRP-reinforced concrete members working in flexure that were exposed to conventional fire conditions (Blontrock et al., 1999; Sakashita, 2007; Saafi, 2001; Tanano et al., 1999; Weber, 2008).

Kodur et al. (2005) showed that higher fire resistance for FRP–RC slabs can be obtained by using larger concrete cover thickness and through the use of carbonate aggregate concrete. Moreover, they pointed out that it is necessary to consider the effects of two important factors on the fire endurance of RC slabs, namely the applied load and the reinforcement bond degradation.

Weber (2008) pointed out the importance of distinguishing between two different limit temperatures: one related to the deterioration of the bond strength and one related to the decrease of the tensile strength in the bars. Indeed, bond test results showed that bond strength between FRP and concrete decreases substantially when the glass transition temperature (Tg ≅ 180°C) was attained. Moreover, the results of tensile tests at 400°C - 500°C showed a bar strength reduction ranging between 30% and 80%.

Finally, a full-scale test, performed according to DIN EN 1363 (2001) on a concrete slab reinforced with the same GFRP bars, highlighted that failure after 90 minutes of fire exposure was not attained due to the rupture of the bars. Indeed, the longitudinal bars were all lap spliced in the middle of the slab and failure was attained due to the loss of bonding between bars and concrete in the midspan of the slab.

[1] DIST – Department of Structures for Engineering and Architecture, University of Naples Federico II, Italy
antonio.bilotta@unina.it
[2] DIST – Department of Structures for Engineering and Architecture, University of Naples Federico II, Italy
emidio.nigro@unina.it

Abassi et al. (2006) performed fire tests on concrete beams reinforced with GFRP bars with a concrete cover of about 70mm; the tests showed that beams can attain fire endurance for longer than 90 min. Therefore a minimum concrete cover of 70mm was recommended for design of GFRP RC beams under fire conditions. The value suggested is non-standard and particularly high with respect to both those required for corrosion control of steel-RC beams and those adopted for FRP-RC members. Such a suggestion does not seem to be suitable from a practical and economic point of view, even if encouraging results seem to depend on the large value of the concrete cover. Therefore, further experimental tests are required to improve knowledge of the structural response of FRP-reinforced concrete members in fire conditions.

In Nigro et al. (2011a,b,c,) fire tests on nine concrete slabs are showed. The slabs are reinforced with glass fiber reinforced polymer (GFRP) bars characterized by different values of concrete cover and anchorage length. They were exposed to heat in a furnace according to the time-temperature curve of ISO834 provided in (EN 1363-1, 2001). Tests were performed to evaluate their resistance and deformability in fire situations by varying (a) external loads in the range of the service loads,

(b) concrete cover in the range of usual values and (c) bar anchorage lengths and shape at the end of the concrete members, namely in the zone not directly exposed to fire. It is worth noting that that in concrete structures zones of this type, not directly exposed to fire, are often represented by mutual connections between members.

Experimental results showed that the use of FRP as internal reinforcement of concrete members seems possible also for constructions in which safety in case of fire is a key requirement.

It was pointed out that:

- higher fire resistance can be obtained by using larger concrete cover thickness; bar temperatures largely depend on the concrete cover, whereas fire endurance depends on fiberstrength at high temperatures and hence may depend on fiber type;
- the type of aggregate used for concrete can modify fire strength, both due to different conductivities and sensitivity to spalling;
- the stress level in FRP particularly affects fire endurance whatever the failure mechanism is (namely the loss of bonding or attainment of the limit strength of the bars);
- the use of overlapping bars in the zone exposed to fire can lead to premature failure of the concrete member. Indeed, deterioration of bond strength (i.e. when FRP bars temperature exceed glass transition temperature, Tg) in the fire-exposed zone can be attained before the decrease in the tensile strength in the bars. Therefore, in order to avoid this premature failure, continuous reinforcement should be used in the zone of the concrete element directly exposed to fire, except if particular reinforcement profiling are adopted (Carvelli et al. 2013);
- failure due to rupture of the fibers (i.e. in the middle of the member), for simply supported members, is attained only when continuous bottom reinforcement is used in the zone of concrete element directly exposed to fire and the FRP bars are well anchored at the end zones not directly exposed; these zones allow suitable anchorage of bars at the ends once Tg has been reached in the fire-exposed zone of the slab and resin softening reduces adhesion at the FRP-concrete interface;
- the length of this zone not directly exposed to fire required for anchoring straight bars can be reduced if the bars are bent at the end.

Key references

Abbasi A, Hogg PJ. Fire testing of concrete beams with fibre reinforced plastic rebar. Composites Part A, Elsevier 2006; Vol. 37, pp. 1142-1150.

ACI. Guide for the Design and Construction of Concrete Reinforced with FRP Bars. ACI 440.1R-04, American Concrete Institute, Farmington Hills, MI; 2003. 42pp.

Bisby LA, Green MF, Kodur VKR. Response to fire of concrete structures that incorporate FRP. Prog Struct Eng Mater 2005, John Wiley & Sons Ltd, 7(3):136–49.

Blontrock H, Taerwe L, Matthys S. Properties of Fiber Reinforced Plastics at Elevated Temperatures with Regard to Fire Resistance of Reinforced Concrete Members. In: Proceedings of IV International Symposium on Fiber Reinforced Concrete Structures, Baltimore, 1999.

Carvelli, V., Pisani, M.A., Poggi, C. (2013). "High temperature effects on concrete members reinforced with GFRP rebars" Composites Part B, 54, pp. 125–132

Correia JR, Branco FA, Ferreira JG, Bai Y, Keller T. Fire protection systems for floors of buildings made of GFRP pultruded profiles Part 1: Experimental investigations. Composites Part B: Volume 41, Issue 8, December 2010, Pages 617-629

CNR. Guide for the design and constructions of concrete structures reinforced with Fiber Reinforced Polymer bars. CNR-DT203/2006, Italian National Research Council, 2006.

CSA. Design and construction of building components with fiber reinforced polymers. CAN/CSA S806-02, Canadian Standards Association, Ottawa, ON; 2002. 210pp.

European committee for standardization. EN 1363-1:2001. Fire resistance tests - General requirements. 2001.

Keller T., A. Zhou, C. Tracy, E. Hugi and P. Schnewlin, Experimental study on the concept of liquid cooling for improving fire resistance of FRP structures for construction, Compos Part A: Appl Sci Manuf 36 (11) (2005), pp. 1569–1580.

Keller T., C. Tracy and E. Hugi, Fire endurance of loaded and liquid-cooled GFRP slabs for construction, Composites: Part A 37 (7) (2006), pp. 1055–1067.

Kodur VKR and Baingo D. Fire Resistance of FRP-Reinforced Concrete Slabs. Internal Report No. 178. Institute for Research in Construction, National Research Council Canada, 1998.

Kodur VKR, Bisby LA, Foo S. Thermal behaviour of fire-exposed concrete slabs reinforced with fibre reinforced polymer bars. ACI Struct J 2005; 102(6):799–808.

Nigro, E., Cefarelli, G., Bilotta, A., Manfredi, G. and Cosenza, E. (2011a). "Fire resistance of concrete slabs reinforced with FRP bars. Part I: experimental investigations on the mechanical behavior". Composites: Part B, 42 (2011), 1739–1750.

Nigro, E., Cefarelli, G., Bilotta, A., Manfredi, G. and Cosenza, E. (2011b). "Fire resistance of concrete slabs reinforced with FRP bars. Part II: experimental results and numerical simulations on the thermal field". Composites: Part B, 42 (2011), 1751–1763.

Nigro, E., Cefarelli, G., Bilotta, A., Manfredi, G. and Cosenza, E. (2011c). "Tests at high temperatures on concreteslabs reinforced with bent FRP bars". Proc., 10th International Symp. on Fiber Reinforced Polymer Reinforcement for Reinforced Concrete Structures, ACI SP-275, Farmington Hills Michigan, USA, April.

Sakashita M. Deflection of continuous fiber reinforced concrete beams subjected to loaded heating. Proceedings of non- metallic (FRP) reinforcement for concrete structures, vol. 58. Japan Concrete Institute; 1997, pp. 51–8.

Saafi M. Design of FRP Reinforced Concrete Beams under Fire Conditions. FRP Composites in Civil Engineering – Vol.II, Elsevier, Alabama, USA, pp. 1235-1244, 2001.

Tanano H, Masuda Y, Tomosawa F. Characteristics and Performances Evaluation Methods of Continuous Fiber Bars – State-of–the-Art Studies on Fire Properties and Durability of Continuous Fiber Reinforced Concrete in Japan. In: Proceedings of IV International Symposium on Fiber Reinforced Concrete Structures, Baltimore, 1999.

Weber A, Fire-resistance tests on composite rebars. In: Proceedings of CICE2008, Zurich, Switzerland, 2008.

Theoretical models for FRP RC members exposed to fire

Antonio Bilotta [1], Emidio Nigro [2]

The vulnerability of organic polymers to high temperatures is probably the biggest drawback for the fiber-reinforced polymer (FRP) bars. Although many examples of FRP reinforced concrete (RC) structures are available worldwide, they are often structures for which fire is not a significant design condition. Though fire is an event that cannot be ignored for many civil structures, as well as parking lots and industrial structures, many international codes generally provide suggestions for design in normal temperature conditions of concrete structures reinforced with (FRP) bars in place of traditional steel reinforcement (CNR-DT 203/2006, 2006; CSA S806-02, 2002; ACI 440.1R-06, 2006; fib Task Group 9.3, 2007) However, few provisions and no calculation models are suggested that take account of fire conditions.

Among the standards listed above, the ACI Technical Guide (ACI 440.1R-04) directly recommends that FRP reinforcement should not be used in cases where fire resistance is an essential requirement. On the other hand, the Canadian guide (CAN/CSA-S806-02, 2002) provides specific design requirements with regard to the effects of high temperatures on concrete slabs reinforced with FRP bars. A series of nomograms are provided to estimate the concrete cover necessary to maintain the temperature in the FRP bars within an acceptable limit defined as “critical temperature” (i.e. the temperature of FRP reinforcement at which slab collapse under service loads in fire conditions is expected). However, the method can be applied only if the critical temperature is known.

Abundance of codes on FRP, yet insufficient guidance on FRP under fire conditions, clearly reflects that FRP is a high-performance material but shows complicated behavior in case of fire and that, due to the diversity of the application opportunities in civil engineering, no simple code can be written although considerable research has been performed in recent years. Indeed, better understanding about thermo-chemical, thermo-physical and thermo-mechanical processes is undoubtedly available (Bai et al. 2007). Hence the models show an increasing degree of complexity which may be desirable and appropriate for many FRP applications (e.g. railway applications or usage in the nautical and aeronautical field). Nevertheless, the models are not comprehensive enough to examine reliably effects like spalling, crack formation, debonding, etc., that are typical of RC structures.

Therefore, fire safety engineers active in the field of structural design have called for easy-to-use calculation procedures, which are reliable within defined application areas, including FRP-RC structures design. Indeed, there is no doubt that the designer is more confident in the design of structures with FRP if there are clear guidelines.

Deterioration of the mechanical properties of FRP (especially strength and Young’s modulus), as well as the bond properties, starts when temperatures close to the glass transition temperature, Tg, are reached (Palmieri et al. 2012). The value of Tg for the products provided by major FRP manufacturers currently ranges between 70°C and 175°C (Bootle et al. 2001), depending on the type of resin. Only a very substantial increase in Tg (more than 500°C) is compatible with temperatures that can be reached during a fire. On the other hand, it is worth noting that deterioration of mechanical and bond properties depends on fiber type, surface treatment type and, above all, the temperature attained in FRP (Palmieri et al. 2013).

It is clear that temperatures in FRP can be greatly reduced when bars embedded in concrete are used, thanks to low thermal conductivity of the latter. Therefore, performance of FRP-RC members in fire can be much better than other FRP structural members (namely pultruded structural profiles), even if no particular fire protection system is used (e.g. passive protection systems, consisting of normal coatings or

[1] DIST – Department of Structures for Engineering and Architecture, University of Naples Federico II, Italy
antonio.bilotta@unina.it
[2] DIST – Department of Structures for Engineering and Architecture, University of Naples Federico II, Italy
emidio.nigro@unina.it

special insulating materials or active protection systems, Correia et al. 2010), because concrete intrinsically provides reliable protection for the bar.

On FRP-RC structures, the literature provides a wide-ranging state of the art on the fire-exposed behavior of concrete structures reinforced or strengthened with FRP (Bisby et al., 2005) and some results of flexure tests performed on FRP-RC members exposed to conventional fire conditions (Blontrock et al., 1999; Sakashita, 1997; Saafi, 2001; Tanano et al., 1999; Weber, 2008; Kodur et al., 2005, Nigro et al. 2011a,b,c). Although further theoretical and experimental studies are required, experimental results to date show that the use of FRP as internal reinforcement of concrete members seems possible also for constructions in which safety in case of fire is a key requirement. Key aspects of on-going research entailed experimental work and theoretical analysis to develop empirical mechanical models and simplified methods for the evaluation of load-bearing capacity in case of fire. Suggestions for guidelines are showed in (Nigro et al., 2014). Even if some simplifications were assumed with respect to more advanced check procedures developing in fire safety engineering, experimental and theoretical results comply with the fire analysis conducted for single members, currently available in the major design codes.

Based on these results, technical suggestions for the drafting of guidelines regarding the design of concrete members reinforced with FRP bars subject to fire were provided. The design methodology takes into account the possibility of decoupling thermal and mechanical analyses, in compliance with the provisions of Eurocodes. This holds for members subject to sagging and hogging bending, namely both beams and slabs. Moreover, for slabs simplified methods validated on experimental test results recalled in the paper were proposed for thermal and mechanical analyses.

Clearly, further research developments should be devoted to determining (a) the effects of structural continuity, with membrane effect and possible bending moment redistribution during fire exposure, and (b) shear strength of concrete members reinforced with FRP bars in fire situations.

Key references

ACI 440.1R-04 (2004). “Guide for the Design and Construction of Concrete Reinforced with FRP Bars”. American Concrete Institute, Farmington Hills, MI, USA.

Bai Y, Vallée T, Keller T. (2007). “Modeling of thermo-physical properties for FRP composites under elevated and high temperature”, Composites Science and Technology, Vol. 67, pp. 3098–3109.

Bisby, L.A., Green, M.F., Kodur, V.K.R. (2005). “Response to fire of concrete structures that incorporate FRP”. Prog Struct Eng Mater 2005, John Wiley & Sons Ltd, 7(3):136–49.

Blontrock, H., Taerwe, L., Matthys S. (1999). “Properties of Fiber Reinforced Plastics at Elevated Temperatures with Regard to Fire Resistance of Reinforced Concrete Members”. Proceedings of IV International Symposium on Fiber Reinforced Concrete Structures, American Concrete Institute, Baltimore, MD.

Bootle, J., Burzesi, F., and Fiorini, L. (2001). “Design Guidelines”. ASM Handbook, V. 21, Composites, ASM International, Material Park, Ohio, pp. 388-395.

CAN/CSA-S6-02 (2002). “Design and Construction of Building Components with Fiber Reinforced Polymers”. Canadian Standards Association, Rexdale, Canada.

CNR-DT203/2006 (2006). “Guide for the Design and Constructions of Concrete Structures Reinforced with Fiber Reinforced Polymer Bar”. National Research Council, Rome, Italy.

Correia, J.R., Branco, F.A, Ferreira, J.G., Bai Y., Keller, T. (2010). “Fire protection systems for building floors made of pultruded GFRP profiles: Part 1: Experimental investigations”. Composites: Part B, 41 (2010), pp. 617-629.

fib Bulletin No. 40 (2007). “FRP reinforcement in RC structures”. ISBN: 978-2-88394-080-2.

Kodur, V.K.R., Bisby, L.A., Foo, S. (2005). “Thermal behaviour of fire-exposed concrete slabs reinforced with fibre reinforced polymer bars”. ACI Struct. J., 102(6), 799–807.

Nigro, E., Cefarelli, G., Bilotta, A., Manfredi, G. and Cosenza, E. (2011a). “Fire resistance of concrete slabs reinforced with FRP bars. Part I: experimental investigations on the mechanical behavior”. Composites: Part B, 42 (2011), 1739–1750.

Nigro, E., Cefarelli, G., Bilotta, A., Manfredi, G. and Cosenza, E. (2011b). “Fire resistance of concrete slabs reinforced with FRP bars. Part II: experimental results and numerical simulations on the thermal field”. Composites: Part B, 42 (2011), 1751–1763.

Nigro, E., Cefarelli, G., Bilotta, A., Manfredi, G. and Cosenza, E. (2011c). “Tests at high temperatures on concrete slabs reinforced with bent FRP bars”. Proc., 10th International Symp. on Fiber Reinforced Polymer Reinforcement for Reinforced Concrete Structures, ACI SP-275, Farmington Hills Michigan, USA, April.

Nigro, E., Cefarelli, G., Bilotta, A., Manfredi, G., Cosenza, E. (2014). Guidelines for flexural resistance of FRP reinforced concrete slabs and beams in fire. Composites Part B: Engineering 58 PP. 103 - 112 doi: 10.1016/j.compositesb.2013.10.007

Palmieri A., Matthys S. and Taerwe L. (2012). " Experimental investigation on fire endurance of insulated concrete beams strengthened with near surface mounted FRP bar reinforcement". Composites PART B-Engineering, 43(3), p. 885-895

Palmieri A., Matthys S. and Taerwe L. (2013) Fire endurance and residual strength of insulated concrete beams strengthened with near surface mounted reinforcement" Journal of Composites for Construction 17(4). P 454-462.

Sakashita, M. (1997). “Deflection of continuous fiber reinforced concrete beams subjected to loaded heating”. Proceedings of non-metallic (FRP) reinforcement for concrete structures. vol. 58. Japan Concrete Institute, pp. 51–8.

Saafi, M. (2001). “Design of FRP Reinforced Concrete Beams under Fire Conditions”. FRP Composites in Civil Engineering - Vol.II, Elsevier, Alabama, USA, pp. 1235-1244.

Tanano, H, Masuda, Y, Tomosawa, F. (1999). “Characteristics and Performances Evaluation Methods of Continuous Fiber Bars – State-of–the-Art Studies on Fire Properties and Durability of Continuous Fiber Reinforced Concrete in Japan”. Proceedings of IV International Symposium on Fiber Reinforced Concrete Structures, American Concrete Institute, Baltimore, MD,.

Weber, A (2008). “Fire-resistance tests on composite rebars”. Proceedings of Fourth International Conference on FRP Composites in Civil Engineering, M. Motavalli, ed., EMPA-Akademie, Zurich, Switzerland.

Thermo-mechanical response of GFRP reinforced concrete sandwich panels

A. Schmitt[1], M. Haffke[2], V. Carvelli[3], M. Pahn[4]

Introduction

The present experimental investigation aims to give a contribution focused on the examination of the residual mechanical performance of steel free sandwich panels. It continues the investigation of the authors detailed in Schmitt et al. (2015), in which the attention was focused on the thermo-mechanical behaviour of thin panels reinforced with GFRP bars, considering the influence of the concrete cover and the external surface of rebars. In the present paper, sandwich panels with two thin GFRP reinforced concrete layers were exposed to increasing temperature and bending loading. The heating condition allowed to reach on the bottom internal GFRP rebars temperatures higher than the glass transition temperature. This does not simulate a real fire exposure, but it is an extreme heating condition for low bearing sandwich panels. The consequences of the thermo-mechanical loading were assessed measuring the variation of the deformability and of the load carrying capacity of the panels with pre- and post-heating bending tests.

Materials and Samples

The geometry of the sandwich panels is detailed in Figure 1. The two concrete layers of thickness 4 cm were reinforced with E-glass fibres reinforced polymer (GFRP) bars. Concrete cover of 10 mm was adopted for the GFRP rebars, named commercially Schöck ComBAR®. The configuration of the reinforcement consists of longitudinal and transverse rebars of nominal diameter 8 mm. In between the two concrete layers, a 6 cm expanded polystyrene insulation layer (typical for façades, named commercially Joma EPS 040 WDV) was placed to reproduce a sandwich panel adopted as external cladding. Point-shaped GFRP connectors of diameter 12 mm were used to link the three layers. They had the same shape of the external surface of the reinforcement, as in Figure 1.

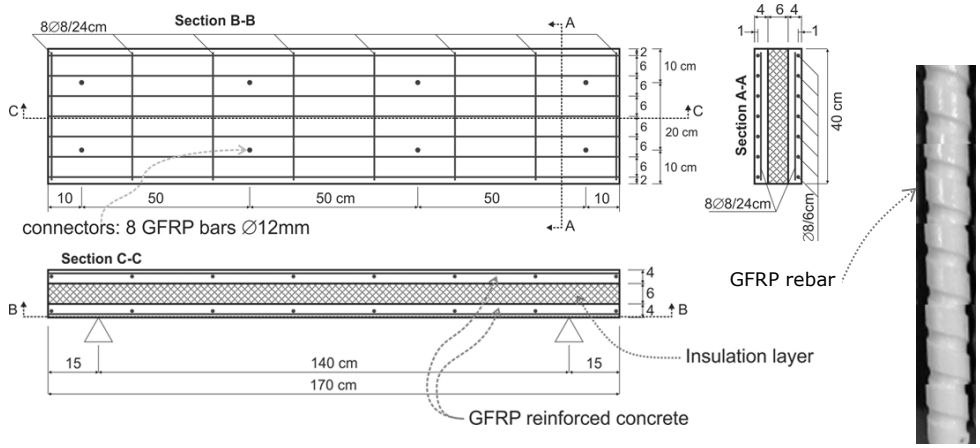

Figure 1: Specimen geometry and reinforcement

The number of tests is summarized in Table 1. The GFRP rebars were produced by pultrusion technique using vinyl ester resin with glass transition temperature (T_g) of about 180 °C, according to the producer. The main mechanical properties in the longitudinal direction of the rebars are the tensile strength of ≈ 1000 MPa and the elastic modulus of ≈ 60 GPa. During casting, some specimens were prepared to

[1] Fachgebiet Massivbau und Baukonstruktion, Technische Universität Kaiserslautern, Germany, andreas.schmitt@bauing.uni-kl.de
[2] Fachgebiet Massivbau und Baukonstruktion, Technische Universität Kaiserslautern, Germany, marcin.haffke@bauing.uni-kl.de
[3] Politecnico di Milano, Italy, valter.carvelli@polimi.it
[4] Fachgebiet Massivbau und Baukonstruktion, Technische Universität Kaiserslautern, Germany, matthias.pahn@bauing.uni-kl.de

measure the average mechanical properties of concrete: compressive cubic strength 49.9 MPa, compressive elastic modulus 23.4 GPa and tensile strength 3.1 MPa.

Experimental Set-up

First phase: pre-heating mechanical response

Two panels were loaded to have the reference mechanical behaviour before heating. During loading, the deflection of the specimen was measured by five transducers (LVDT), one in the mid span, two 35 cm beside both supports and two at the supports position (see Figure 2).

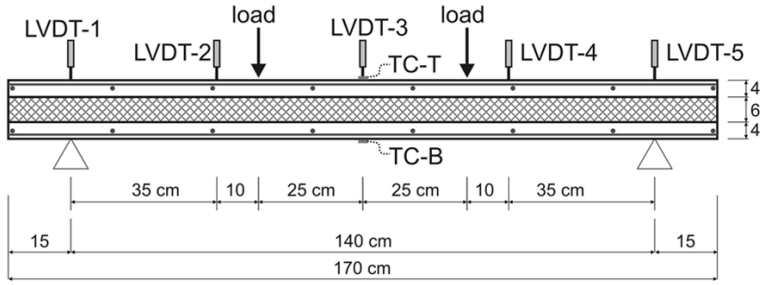

Figure 2 Test set-up and external instruments position of first and third phase

Second phase: thermo-mechanical loading

In the second phase, quasi-static four-points bending loading was first imposed with same scheme as in the first phase. At the maximum imposed load, the heating device started increasing the temperature on the full bottom surface of the specimen, which was exposed for the time listed in Table 1. The heating on the bottom surface of the samples was applied by the device in Figure 3a. The temperature was controlled by a thermocouple in the centre of the device.

Table 1 Numbering of samples and some heating features

	Panel ID	Heating rate [°C/min]	Heating time [min]	Exposition time [min]
Pre-heating loading	1 and 2	-		-
Heating and Post-heating loading	3	20	16	60
	4	50	6.4	60
	5	20	20	80

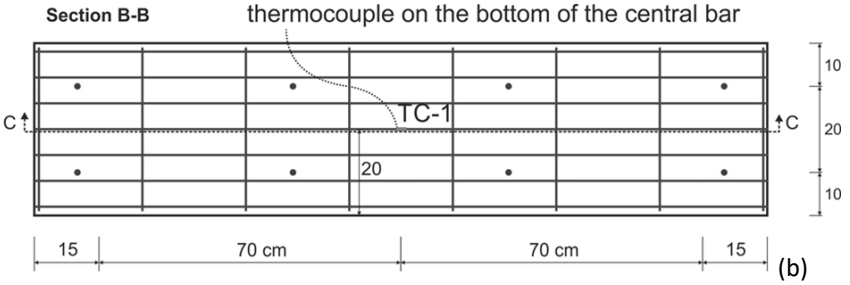

Figure 3 Heating device (a); Test set-up and external instruments position of second phase (b)

The temperature on the bottom and top surface of the specimen was measured by two thermocouples TC-B and TC-T. Moreover, one thermocouple (TC-1) was placed mid-span on the central rebar to monitor the internal temperature at the bar level (see Figure 3b). After the application of the loading, the temperature inside the device was increased to the maximum of almost 320 °C for panel 3 and 4 and almost 400 °C for panel 5, with different heating rates. When the temperature in the centre of the device reached the desired maximum, it was maintained constant until the end of the heating phase. The heating phase was about 60 min for panels 3 and 4 and 80 min for panel 5. The maximum temperature was imposed to reach at the rebars level a temperature higher than the glass transition temperature.

Third phase: post-heating mechanical response

In the third experimental phase, after complete cooling, the specimens were quasi-statically loaded using the same four-points bending setup and procedure of the pre-heating tests (see Figure 2) at room temperature. This allowed comparing the pre and post mechanical behaviour of the panels.

Results and discussion

First phase: pre-heating mechanical response

The load vs. mid span deflection curves (Figure 4a) show a very similar behaviour of panel 1 and 2. The two branches shape is quite similar to those recorded for the same load condition of sandwich panels with different reinforcements (Schmitt et al. 2014). An initial branch with the maximum stiffness of the panel up to a load level (19 kN), for which the propagation and diffusion of cracking generate a high decrease of stiffness, in the second branch, leading to failure. Looking more in detail the first branch of the two curves in the low range of load, they can be considered linear up to a load level of almost 4 kN (Figure 4b), then the curves had a variation of slope meaning initiation of cracks. This was considered as reference level for loading in the second phase. Both panels failed under compression of concrete (see Figure 4c).

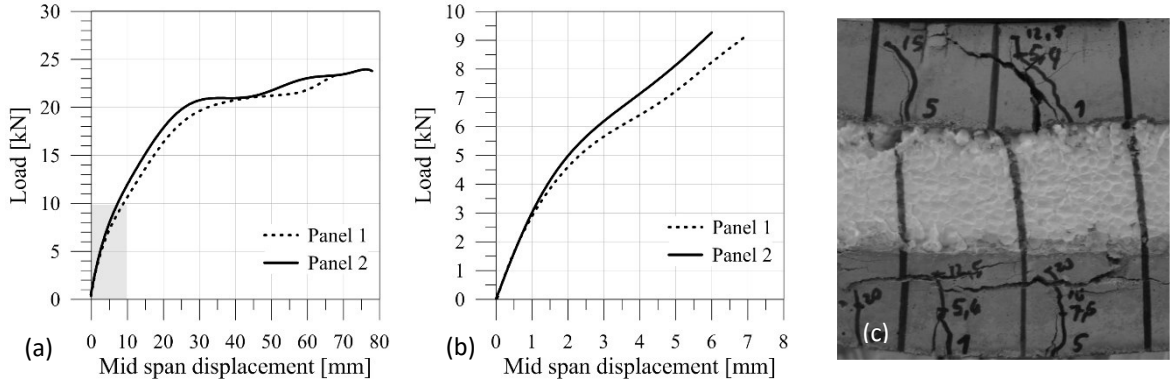

Figure 4 Load vs. displacement: complete curves (a); curves in low range load (b); Failure mode (c)

Second phase: thermo-mechanical loading

In the second experimental phase, the bending loading was applied quasi-statically increasing the load in almost 2 minutes up to the maximum resultant of 5 kN to impart an initial cracking before heating. The maximum load was estimated assuming the results of the room temperature bending tests in the first phase (see Figure 4b).

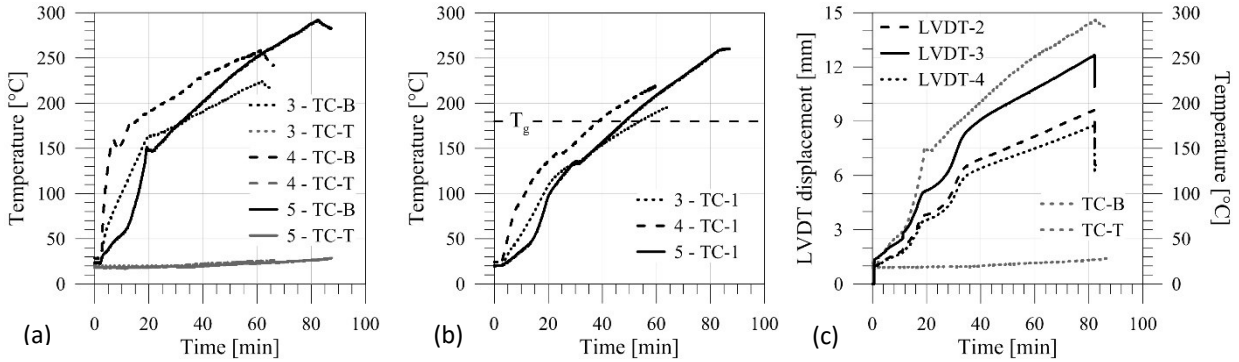

Figure 5 Temperature vs. time of panels 3, 4 and 5 on the centre of top (TC-T) and bottom (TC-B) (a) and at mid span on central bar (TC-1) (b); LVDTs displacement vs. time during heating of panel 5 (c)

The temperature on the bottom and top surface of the specimen was measured in the mid span (see Figure 5a). During the exposition time, the temperature on the top was below 30°C, while on the bottom had differences: panel 3 with the lowest heating rate and heating time had a maximum temperature of 225 C, panel 4 with the highest heating rate and the lowest heating time had a maximum temperature of 260 C and panel 5 with the lowest heating rate and the highest heating time a maximum temperature of 292 C was recorded. The diagram in Figure 5b shows the evolution in time of the temperature recorded on the bottom rebar (TC-1). The protection of 1 cm concrete cover allowed to enable maximum temperatures of the rebars in the range of 195÷260 C. The temperature of the rebars after 40 to 50 min

was higher than the T_g for almost 10, 20 and 30 min in panel 3, 4 and 5, respectively. When the temperature at the bottom side of the insulation reached 90 C, the material underwent a continuous degradation until the evaporation of a large portion of the insulation. The continuous recording of the LVDTs provided the evolution of the displacement as illustrated in Figure 5c. In particular, the considered heating rates and exposition times imparted different deformation of the panels. The global deformation measured after the exposition phase does not seem dependent on the considered heating rates and times, but is proportional to the maximum temperature imposed on the bottom surface. The mid-span displacement after heating of panel 5 is 30 % higher than that of panel 3. The thermo-mechanical loading imparted a crack pattern on the bottom surface of the panels. The main distribution of the cracks is located in the central part of the panels with the constant maximum bending moment. Few longitudinal cracks were observed, mainly in the external portions close to the supports.

Third phase: post-heating mechanical response

The global response of the panels is detailed in Figure 6a comparing the pre- and post-heating load vs. mid span deflection curves. Panel 3, subjected to the lowest temperature, had a reduction of the maximum load of about 8 %, while panel 4 and 5, which were heated with higher temperatures, had a failure load 27 % and 30 % lower than the reference panels. This highlights that the reduction of the failure load is not dependent on the considered heating rates and times, but mainly on the maximum temperature recorded on the bottom surface. The influence of the thermo-mechanical exposition is also measurable comparing the initial stiffness of the panels (see Figure 6b). The stiffness of the panel had a reduction of 22 %, 52 % and 59 % for panel 3, 4 and 5, respectively. The comparison shows, that the higher the applied maximum temperature, the higher is the reduction of the stiffness.

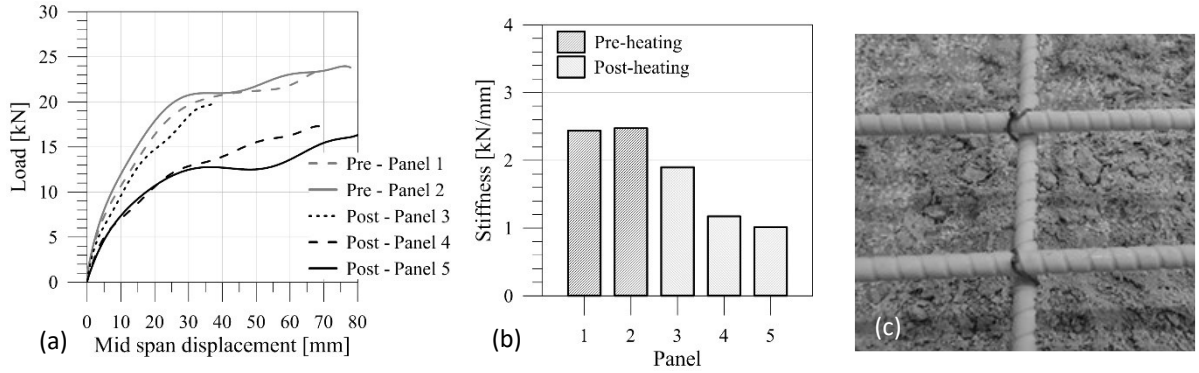

Figure 6 Comparison of the pre- and post-heating bending load vs. mid span displacement (a); initial stiffness of the panels (b); rebars in the mid span of the bottom concrete layer after failure in third phase (c)

Two reasons can be attributed to the discussed reduction of the mechanical properties. The first is the damage imparted in the concrete layers during the thermo-mechanical loading. In fact, the rebars had, after removing of concrete, the shape in Figure 6c. They had still a good adhesion with concrete and their external surface was not apparently modified by the elevated temperature. Therefore, the observed level of the damage imparted could have only a marginal influence on the reduction of the mechanical features of the panels. The second reason is the degradation and lack of large portion of the insulation after heating. This is the main responsible of the significant reduction of the mechanical response of the panels. Therefore, the structural role of the insulation (Schmitt *et al.* 2014; Müller *et al.* 2012) in transferring the shear forces between the concrete layers was completely lost.

Conclusions

The thermo-mechanical response of the considered concrete sandwich panels reinforced with GFRP rebars provides the following understandings.

- The imposed thermo-mechanical exposition created some transversal and longitudinal cracks on the bottom surface of the panels. The GFRP bars were not damaged, had still a good adhesion with concrete and their external surface was not apparently modified.

- When the temperature of the expanded polystyrene was about 90 C, the insulation started melting and the material had a continuous degradation until the evaporation of a large portion of the layer.
- The significant reduction of the mechanical properties (in terms of failure load and stiffness) was mainly related to the degradation and lack of large portion of the insulation after heating. The absence of insulation layer reduces the load transfer capacity from the top to the bottom concrete layer.

Acknowledgements

The research was partially developed during the 'Short Term Scientific Mission' of the first Author financed by COST Action TU1207. Schöck Bauteile GmbH is gratefully acknowledged for supplying the GFRP rebars.

Key references

Carvelli, V., Pisani, M. A. and Poggi, C. (2013). "High temperature effects on concrete members reinforced with GFRP rebars", Composites: Part B, vol. 54, 125–132.

Müller, F., Kohlmeyer, C. and Schnell, J. (2012). "Load-Bearing Behaviour of Sandwich Strips with XPS-Core and Reinforced HPC-Facings", in Ultra-High Performance Concrete and Nanotechnology in Construction, Kassel University Press.

Schmitt, A., Carvelli, V. and Pahn, M. (2015). "Thermo-mechanical loading of GFRP reinforced thin concrete panels", Composites Part B, vol. 81, 35-43.

Schmitt, A. and Pahn, M. (2014). "Investigation on flexural stressed sandwich panels with GFRP-reinforcement", in Proceedings of the 7th International Conference on FRP Composites in Civil Engineering - CICE, Vancouver (Canada), 164-169.

2.6 Novel Structural Systems

Prefabricated thin-walled HPC structural elements prestressed with pultruded carbon tendons (collaboration with company SACAC from Switzerland

G. P. Terrasi, head of laboratory for Mechanical Systems Engineering, Empa Switzerland

Why should the new combination of materials 'CFRP prestressed HPC' be beneficial for the prefabrication of concrete elements? The following short paper will deal with slender beams which are primarily subjected to bending and are manufactured in an adapted pre-tensioning method. In this context it should be noted that an eminent reference (Burgoyne, 1997) discussing the fundamental issue of making rational use of advanced composite reinforcements in concrete comes to the conclusion that to be economic, advanced composites will have to be used for prestressing tendons (pre-tensioning resin matrix bar or wire systems are a viable option), but not for passive reinforcement.

The CFRP prestressing reinforcement used in this work consists of fine, unidirectional carbon fibre-reinforced wires with a diameter of 3 to 6 mm, typically produced using the pultrusion method with an epoxy resin matrix. Unidirectional reinforced CFRP wires have high design tensile strengths around 2000 - 2500 MPa. The density of CFRP is 1.6 kg/m^3 which is just short of one fifth of the density of prestressing steel. The wires are coated with quartz sand particles (mean diameter 0.5 mm) in order to control bond to the high performance concrete. The quartz sand coating is bonded in-line following pultrusion using the same epoxy resin used to impregnate the carbon fibres of the wire. Perhaps the biggest advantage of CFRP wires as a prestressing reinforcement is their total immunity to corrosion in practically all relevant media, even if subjected to high mechanical stresses. The complete absence of any tendon stress-corrosion allows the concrete cover to be reduced to well below that necessary for the protection of prestressing steel wires. The actual Swiss civil engineering standard SIA 262 (SIA, 2003), e.g., requires tendon covers between 40-55 mm depending on the environmental exposure class defined when designing the structure. Hence the 5 mm diameter CFRP prestressing wires used in the first high-voltage transmission pylons manufactured in 2000 (Figure1 and Terrasi et al., 2001) have a concrete cover of just 18 mm. The concrete cover size is determined on the basis of static considerations (reception of the compressive stresses due to bending and of the bursting tensile stresses in the anchorage zone of prestressing reinforcements) and of the mismatch in thermal expansion coefficient between CFRP (transverse to fibre direction) and high-performance concrete (Terrasi, 1998).

The extremely favourable fatigue properties and the absence of time-dependent mechanical prestress losses (creep and relaxation) should not be underestimated (Terrasi, 1998). On top of the high tensile strengths, the last mentioned properties lend this material outstanding properties for prestressing of concrete elements.

It should be mentioned as well that the modest mechanical properties of unidirectional carbon-fibre reinforced wires transverse to the fibre direction (in the range of 10% of the corresponding longitudinal properties) must also be given careful consideration, e.g. in view of the anchorage of the prestressing wires.

The high quality of quartz sand-coated CFRP wires and hence the cost which is still high (specific prices around 0.05 € per kN tensile capacity) require high quality for the concrete matrix. HPC with a strength in the range of class C100 is the appropriate matrix material for the carbon fibre reinforced polymer prestressing reinforcement. HPC can be produced today in the prefabrication element plant with suitable mixing equipment with a consistently high quality providing the production process is mastered well and the personnel are suitably qualified. Typically, a very precisely batched fine-grain concrete (mortar) is used with high strength aggregates. The cement content is around 450 kg/m^3, micro silica and high-performance plasticizer are essential components of these concretes which have a water/cement factor of 0.32-0.4 for optimum workability. C90 to C100 high-performance concretes are relatively inexpensive (with material costs around 125 €/m^3) but have high durability, high tensile

bending strength (with fractiles over 5 MPa), a relatively high modulus of elasticity (around 40 GPa depending on the aggregates) as well as the high compressive cube strength over 90 MPa. The compaction of HPC can be achieved by centrifugal casting, vibration or following a more advanced mix design by the self compacting method (High Performance Self Compacting Concrete [HPSCC]). The treatment after casting often corresponds to a simple covering of the moulds in order to keep the young HPC humid for typically 36 hours before prestress release and demoulding.

Taking advantage of the properties of the two components CFRP and HPC, it is possible to minimise the weight of the bending element by reducing the wall thickness while guaranteeing excellent service characteristics (no susceptibility to corrosion, high bending stiffness and high fatigue strength.

The outstanding durability of HPC prestressed with pultruded CFRP wires has been confirmed by several full-scale field tests and by up to 15 years of service for CFRP pretensioned precast HPC plyons and façade elements (Figures 1 and 2)

Figure 1: CFRP prestressed pylon made from high performance spun concrete

Figure 2: College building Zurich Falletsche: filigree vertical CFRP prestressed HPSCC façade columns

Discussion and Conclusions

The prefabrication of CFRP prestressed high performance concrete (HPC) elements permits the realisation of thin-walled, light-weight and durable structural elements with excellent service characteristics (no susceptibility to corrosion or ageing, high bending stiffness and high fatigue strength). Lower cost for maintenance, transportation and installation with respect to conventional reinforced concrete elements make CFRP prestressed HPC economically interesting. The new shaping possibilities in conjunction with advanced concrete compaction techniques (self compacting HPC) make these novel concrete elements fascinating from the aesthetic/architectural point of view.

A first full-scale structural element made from HPC prestressed with pultruded CFRP wires was realised in the year 2000 by the Swiss prefabrication element plant SACAC Schleuderbetonwerk AG in the form of a thin-walled overhead power line pylon. This 27 metres high tubular pylon for high voltage transmission lines was produced by a centrifugally casting technique with a concrete wall-thickness of merely 48 mm. It was therefore 40% lighter than a conventional steel-reinforced concrete pylon used for the same purpose. The transport and erection costs were reduced which, with an expected maintenance-free service life of 50 years, should result in lower life-cycle costs than those of tubular steel or steel lattice pylons which need a new coat of corrosion protection paint after approximately 20 years. Using CFRP prestressed HPC has also proved beneficial in other applications: For example, in 2005-2008 aesthetics, installation and structural considerations lead to the realisation of three large building façades in Zurich, Switzerland using slender and thin-walled CFRP prestressed self compacting HPC profiles (Figure 2). All these applications have shown outstanding durability up to the current service time of 15 years, with no cracks arising or relevant deflection increases under service loads in outdoors mid-European climatic conditions.

The thin-walled HPC elements prestressed with CFRP wires described are designed as members subjected primarily to flexure. In terms of design criteria, the following has to be considered:

• The total bending safety factor for these elements is typically in the range of 1.8, meant as the ratio between design failure moment to maximum service moment according to (SIA, 2003). No preference is made between the two possible bending failure modes, i.e., “crushing of the concrete” or “tensile failure of the CFRP wires”, since both of them are brittle failures. The controlling failure mode depends on the section's geometry, the concrete's strength, the configuration of the prestressing reinforcement (at present the cost determining factor) and the prestressing level. The latter is determined by the serviceability issue of fully prestressing the element for service loads. Furthermore, the anchorage of the highly prestressed CFRP wires must be carefully verified (Terrasi, 2001).

• In most cases, the design is controlled by the fulfillment of the serviceability criteria. In particular, deflections under service loads can be limited by fully prestressing: The formation of bending cracks is avoided so that the moment of inertia of the entire cross section is available for the service moment reception. The maximum service moment defines the minimum cracking moment that has to be guaranteed at the critical cross section of the element. This can be calculated under consideration of a part of the tensile strength of the concrete (f_{ct} = 5 MPa for the HPC studied) and is principally controlled by the height of the total prestressing force (Terrasi, 1998). In order to make rational use of the still expensive CFRP wires and considering the space limitations in the slender elements, the wires should be prestressed at an initial prestressing degree of 60%-70% of their guaranteed tensile strength of 2000 - 2500 MPa (Table 1). It is advisable to use small diameter CFRP wires (typically 3–6 mm) in order to obtain a smooth transfer of the prestressing forces, to prevent bond failures through longitudinal cracks of the low HPC covers (in the range of 20 mm) and to elude thermal compatibility cracks. A complete loss of prestress would be the consequence of these cracks and has clearly to be avoided (Terrasi, 1998).

• One additional requirement to be fulfilled by the chosen design of the flexural element is the attainment of a high deflection at failure (i.e. in the cracking stage, see (Terrasi, 1998)), which can be interpreted as a warning by the system when loaded at an unforeseen high level.

The fulfilment of the design criteria listed above allows a weight reduction of up to 40% over traditional steel reinforced and prestressed concrete flexural elements.

Acknowledgements

The author would like to thank SACAC Schleuderbetonwerk AG and in particular its former managing director, Mr. Georges Bättig, for their collaboration in the fruitful development work over the last 15 years. The valuable advice regarding design matters by Dr. Janet M. Lees of Cambridge University UK and the continuous support with discussions by Prof. U. Meier and Dr. A.J. Brunner of Empa are also greatly appreciated.

Key references

Burgoyne, C. (1997). Rational Use of Advanced Composites in Concrete. *Proc., FRPRCS-3: Non-Metallic (FRP) Reinforcement for Concrete Structures*. edited by Japan Concrete Institute, Sapporo, Japan, 75-88.

SIA (Swiss engineers and architects association) (2003). Swiss Standard SIA 262.

Terrasi, G.P. (1998). *Mit Kohlenstoffasern vorgespannte Schleuderbetonrohre* (PhD thesis No. 12‘454). ETH Zurich, Switzerland.

Terrasi, G. P., Bättig, G., & Brönnimann, R. (2001). Pylons made of High-Strength Spun Concrete and prestressed with CFRP for high power transmission lines. In C. J., Burgoyne (Eds.), Proc., FRPRCS 5: Non-Metallic Reinforcement for Concrete Structures, University of Cambridge, England, 1103-111.

New fiber-reinforced polymer thermal break for energy-efficient constructions – structural system performance

Kyriaki Goulouti[1], Julia de Castro[2], Thomas Keller[3]

Introduction

In the context of sustainable development, the reduction of the energy consumption of the overall building stock represents a major challenge. Developments towards construction designs with high thermal insulation capacity are increased and new standards are set, e.g. the European Directive 2010/31/EU (EPBD recast)[1], which prescribes that all new buildings must be conceived as 'nearly zero-energy buildings' by the end of 2020. One construction detail that can cause up to 30% of the heat losses of a building is the thermal insulation-penetrating connection of building exterior balconies to interior concrete slabs[2]. Thermal break elements are used for these connections that partially interrupt the heat flow towards the external environment. However, they still comprise insulation-penetrating stainless steel bars with high thermal conductivity. On the other hand, fiber-reinforced polymer materials (FRPs) – composed of glass (GFRP) or, even much more insulating, aramid fibers (AFRPs) – have an up to 170 times lower thermal conductivity than stainless steel and are therefore much more appropriate for this specific application. Several attempts had already been made to replace the stainless steel bars by GFRP components[3,4] but none of them was successful on the market for various reasons[5].

A new concept for a highly insulating, combined AFRP/GFRP thermal break was recently developed and its excellent thermal insulation capacity has been proven[5]. The new thermal break is shown in Fig. 1a and is able to transfer negative bending moments and shear forces from the exterior balcony to the interior concrete slab. The concrete slab is interrupted in the envelope's insulation layer by a 55-mm- wide PVC box, which is filled with a highly insulating aerogel granulate material and can be adapted to slab height. The upper tension forces, caused by the balcony's negative bending moments, are transferred through the PVC box and anchored in the adjacent concrete slabs by 720-mm-long AFRP loops, spaced at 150 mm. The lower compression forces, also resulting from the bending moment, are transferred by 55.9-mm-long GFRP compression bars. Glass fibers had to be chosen in this case due to the relatively low compression strength of the (thermally much better) aramid fibers. The GFRP bars are integrated into a hexagonal sandwich component, which provides a compression diagonal through the PVC box to transfer the shear forces, see Fig. 1b. The three directions of the hexagon are either wrapped with AFRP or GFRP laminates and polyurethane (PU)-foams of different densities are used as core materials.

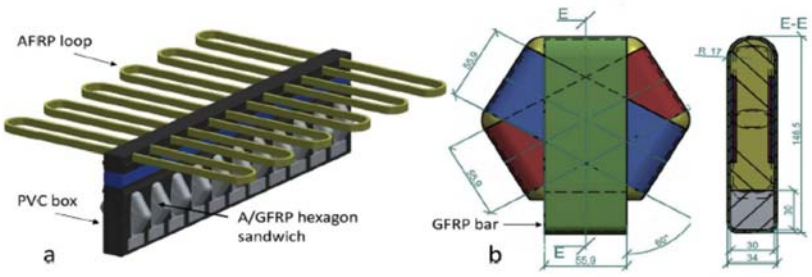

Figure 1. New A/GFRP thermal break: a) components assembled, b) A/GFRP hexagon sandwich component with integrated compression bar, (dimensions in (mm).

[1] Ecole Polytechnique Fédérale de Lausanne, Switzerland, Kyriaki.goulouti@epfl.ch
[2] Ecole Polytechnique Fédérale de Lausanne, Switzerland, julia.decastro@epfl.ch
[3] Ecole Polytechnique Fédérale de Lausanne, Switzerland, thomas.keller@epfl.ch

The structural behavior of the individual AFRP/GFRP components has already been experimentally investigated and characterized. The corresponding results were presented in Chapter 3 and form the basis for this work. In the following, the behavior of the whole system, the new thermal break embedded in the adjacent concrete slabs, is investigated. The behavior in the serviceability and ultimate limit states is analyzed and the maximum balcony span derived.

Experimental

The dimensions and mechanical properties of the thermal break components (AFRP tension loop, A/GFRP hexagon diagonal, GFRP compression bar), which are relevant for describing the system behavior, i.e. the interaction between the thermal break components and the surrounding concrete, are summarized in Table 1.

Table 1: Cross sections and mechanical properties of components (average experimental values[7]).

Component	Length L (m)	Area A (mm^2))	Stiffness S (kN/mm)	E-modulus E (GPa)	Ult. Load Fu (kN)	Strength fu (MPa)
AFRP tension loop	720	300[1] 1500[2]	18	47	274	913
A/GFRP hexagon compression diagonal, PU 98kg/m^3	125	224[3] 1677[4]	65	36	59	264
A/GFRP hexagon compression diagonal, PU 131kg/m^3	125	224[3] 1677[4]	76	42	69	309
GFRP compression bar	55	900[5]	792	44	315	350

[1] AFRP (2·15·10 mm^2), [2]concrete contact (projection, 15·100 mm^2)

[3] A/GFRP (2·2·55.9 mm^2), [4]concrete contact (projection, 30·55.9 mm^2)

[5] GFRP (30·30 mm^2) = concrete contact (30·30 mm^2)

Since balconies are normally subjected to uniformly distributed loads and thus represent one-way cantilevering slab structures, their structural behavior can be experimentally simulated using a beam configuration. Accordingly, six experimental beams of full-scale dimensions, comprising, with one exception, one thermal break unit each – i.e. one loop combined with two hexagons with integrated compression bars[5]– were investigated. In one beam, however, one loop was combined with only one hexagon/bar component. Hexagons with higher foam density (and thus wrinkling resistance) were selected in the cases where higher shear loads were expected.

The slab inside the building was represented by a beam of 1000-mm length, 220-mm height and 300-mm width (denominated 'interior' beam in the following), to which a 700-mm-long cantilevering ('exterior') beam of the same cross section, representing the balcony, was connected through the thermal break unit, see Figs. 2 and 3. The gap of 55-mm length between the two beams, normally containing the PVC box filled with aerogel insulation, was kept open in order to observe the components' behavior. The 100-mm-long steel plate of the cantilever support was moved 110 mm back from the gap edge in order to simulate the most unfavorable case[3] and not create a favorable confinement of the concrete at the support of the

GFRP compression bars. The beams were reinforced with two longitudinal steel bars B5009 of ϕ 14 mm on the top and two bars of ϕ 10 mm on the bottom side and stirrups of ϕ 10 mm spaced at 150 mm.

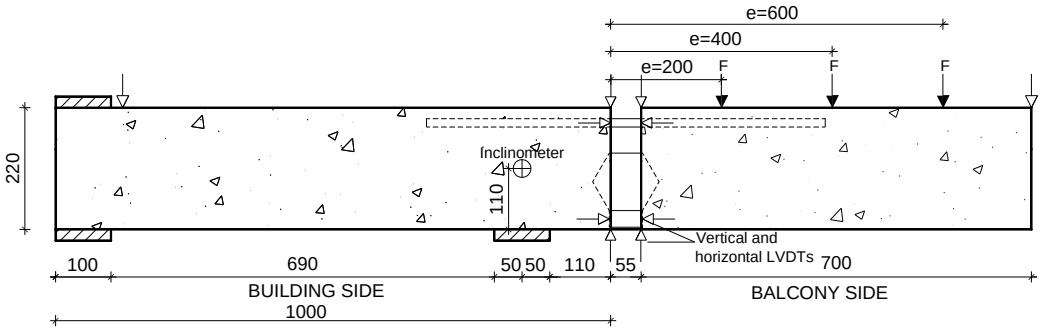

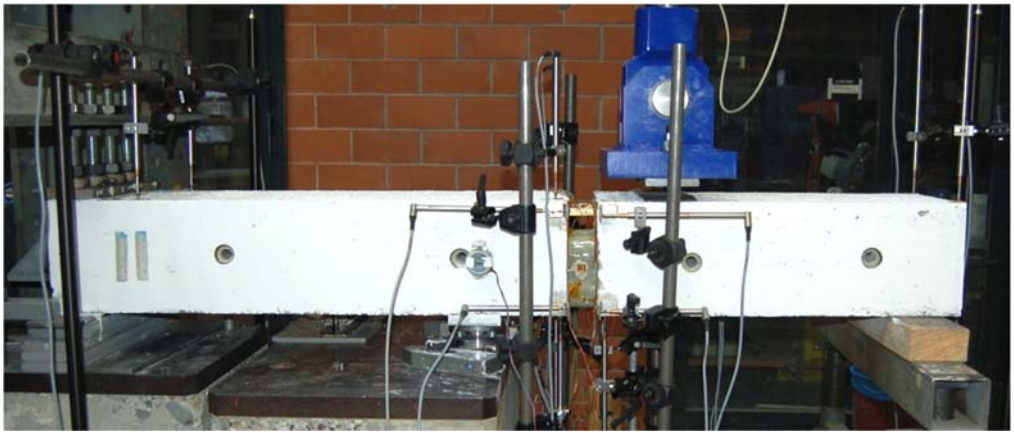

Figure 2. Experimental set-up with instrumentation and loading positions, dimensions in (mm), (timber block removed prior to loading).

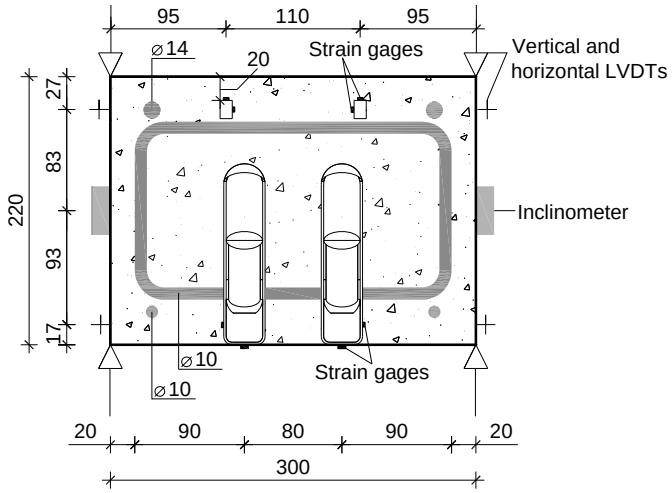

Figure 3. Cross section of experimental beam with one thermal break unit, concrete reinforcement and instrumentation, dimensions in (mm).

More details about configuration, material properties and results analysis can be found in [6].

Load deflection curves and failure modes

All six beams exhibited a nonlinear load-deflection response, the latter indicating the average value of the two LVDTs at the cantilever end, see Fig. 4 (only the failure cycles are shown). With decreasing load distance, e, the initial stiffness and ultimate load increased, while the ultimate displacement decreased. As the ultimate load was approached, the stiffness of all beams further decreased and the load then gradually decreased (in half of the cases) with increasing displacement. The two beams with the same lever arm exhibited a similar response; the different wrapping of the hexagons (AFRP or GFRP) thus did not significantly influence the behavior – in particular not at the serviceability load, FSLS, which was determined at a cantilever end deformation of 2L/350=4.9mm, with L= 700+55+110 = 865mm.The ultimate load of the beam with only one hexagon (G400-1) was significantly lower than that of the same beam with two hexagons (G400). Their ratio Fu/FSLS varied according to the lever arm length between 1.9 (shortest lever arm) and 4.6 (longest lever arm).

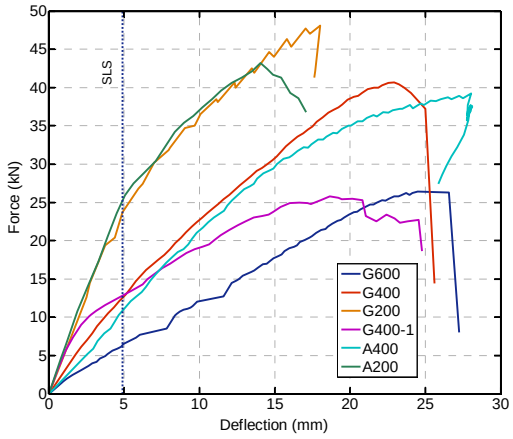

Figure 4. Load-deflection responses of all beams (deflections at cantilever end of failure cycle).

The load-displacement responses of beams G200 and G600, during all the cycles, are compared in Fig. 4. Some permanent deformations were obviously accumulated during concrete cracking, which occurred on top of the interior span due to the negative bending moments. However, concrete cracking was limited to only one to three cracks, see Fig. 5. The curves also show significant load decreases while displacements were maintained before unloading from the top of the individual cycles. These decreases were much more pronounced in the case of shorter lever arms, i.e. higher loads in the hexagons' compression diagonal, and thus could be attributed to the viscoelastic behavior of this component.

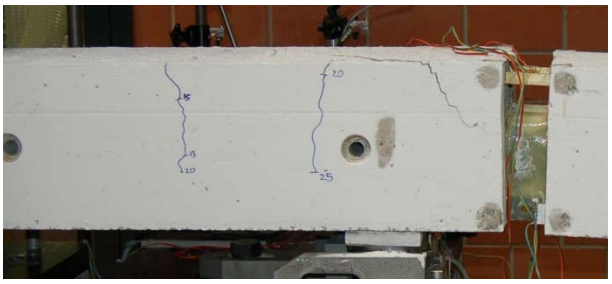

Figure 5. Crack formation and propagation in beam G600 during 15-, 20-, 25-kN cycles.

The failure modes depended primarily on the lever arm length and fiber type of the hexagon wrapping. With longer lever arms, the concrete in the AFRP loop anchorage zone of the interior span failed through crushing and a diagonal crack plane formed through the whole beam width from the upper loop

anchorage zone down to the two hexagon compression diagonal supports, see Fig. 6a. Small cracks formed at the supports of the GFRP bars, but this zone did not fail, see Fig. 6b. The hexagons with GFRP wrapping remained undamaged, while those with AFRP wrapping exhibited wrinkling in the compression diagonal. The beams exhibited a clear rotation in the gap; the two adjacent concrete planes remained not parallel, as shown in Fig. 7.

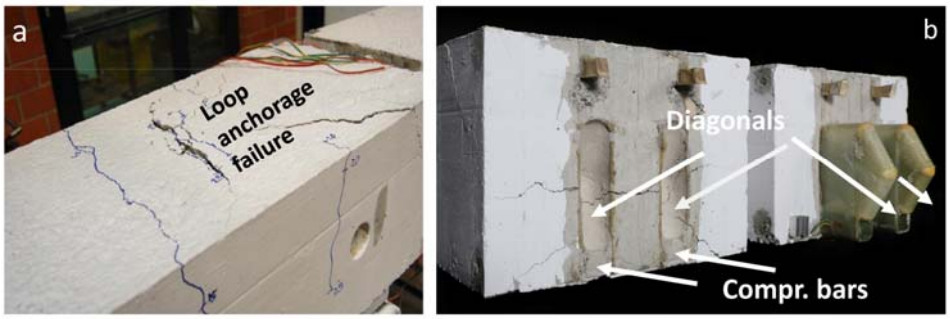

Figure 6. Failure mode of beam G600: a) top concrete failure in loop anchorage zone, b) cracks through the hexagon diagonals' support area of interior (left) beam, undamaged hexagons in cantilever (right) beam.

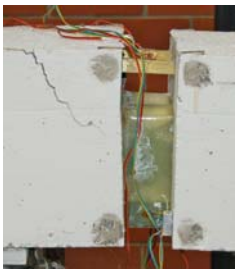

Figure 7. Beam G600 at ultimate load: concentrated rotation in insulation gap.

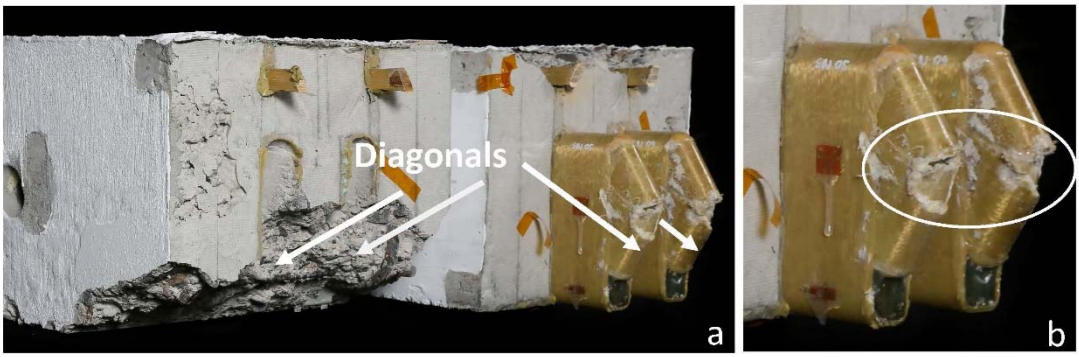

Figure 8. Failure mode of beam A200: a) bottom concrete spalling in interior (left) beam, b) wrinkling/crushing of AFRP hexagon diagonal.

The beams with the shortest lever arm failed differently. The bottom part of the concrete on the supported part failed, i.e. the part below the prolongation of the hexagon compression diagonals spalled, see Fig. 8a. The loop deformed into an S-shape, see Fig. 9, and was thus torn off from the concrete on the loading side. The hexagons with GFRP wrapping remained undamaged (with the exception of minor crushing at one edge in one of them) while those with AFRP wrapping were crushed in the upper part of

the compression diagonal, see Fig. 8b. In addition to the rotation in the gap, a clear vertical offset was visible, see Fig. 9 (and compare to Fig. 7). Beam G400-1, which had only one hexagon with GFRP wrapping, again failed differently. No significant damage could be observed in the concrete, see Fig. 10a, while the hexagon's GFRP diagonals failed through wrinkling on one side, see Fig. 10b. Overall, all beams exhibited a ductile failure mode caused, in all cases but one, by progressive concrete failure and in one case by GFRP wrinkling.

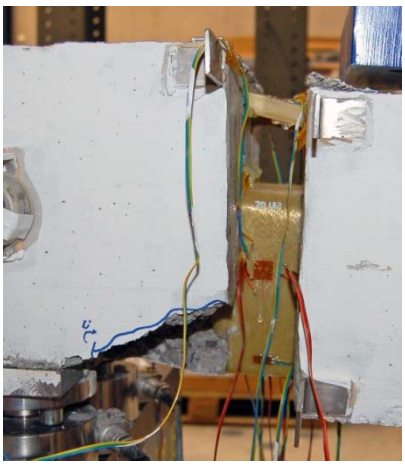

Figure 9. Beam A200 at ultimate load: rotation and vertical offset in insulation gap.

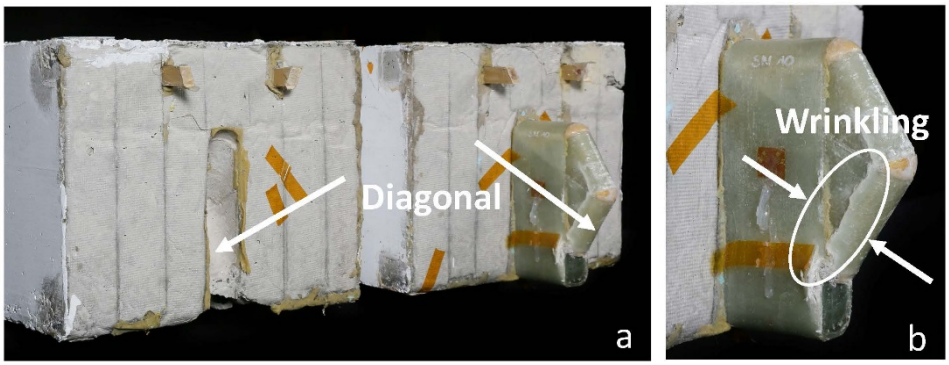

Figure 10. Failure mode of beam G400-1: a) undamaged concrete in interior (left) beam, b) wrinkling of GFRP hexagon diagonal.

Conclusions and Points for Discussions

A new highly insulating balcony thermal break has been developed which consists of combined AFRP/GFRP loop and sandwich components. In a previous work, the excellent thermal performance has been demonstrated and the load-bearing behavior of the components characterized. In the current work, the system behavior, i.e. the behavior of the thermal break embedded at the interface between a building interior and an exterior balcony concrete slab, has been investigated.

The failure modes are ductile due to prevailing concrete failures and, in the cases of AFRP hexagons, simultaneous wrinkling of the sandwich faces. However, the ultimate loads using GFRP hexagons (which did not wrinkle) were not significantly higher than those using AFRP hexagons. The much better thermal performance of AFRP hexagons can thus be exploited.

The maximum balcony span of the current system is approximately 2.50 m and is limited by the anchoring resistance of the AFRP loops in the concrete cover. To further increase the balcony span, the loop ends could be slightly bent downwards to activate more concrete resistance. A further improvement might be a covering of the curved hexagon diagonal ends by small Teflon sheets in order to eliminate friction and thus better assure that the compression forces do not deviate from the diagonal direction

Key references

1. EPBD:2010. Directive 2010/31/EU of the European Parliament and of the Council of 19 May 2010 on the energy performance of buildings (recast).
2. Goulouti K, de Castro J, Vassilopoulos AP, Keller T. Thermal performance evaluation of fiber-reinforced polymer thermal breaks for balcony connections. Energy and Buildings 2014; 70: 365-371.
3. Keller T, Riebel F, Zhou A. Multifunctional hybrid GFRP/steel joint for concrete slab structures. Journal of Composites for Construction 2006; 10/6: 550-560.
4. Keller T, Riebel F, Zhou A. Multifunctional all-GFRP joint for concrete slab structures. Journal of Composites for Construction 2007; 21: 1206-1217.
5. Goulouti K, de Castro J, Keller T. Aramid/glass fiber-reinforced thermal break – thermal and structural performance. Composite Structures 2016; 136: 113-123.
6. Goulouti, K (2016). Thermal and structural performance of a new fiber-reinforced polymer thermal break for energy-efficient constructions, THÈSE NO 7097, Ecole Polytechnique Fédérale de Lausanne, 2016.

WG3

Strengthening Applications

3.1 Bond

Experimental characterisation of bond between flexural EB FRP and concrete

A. Serbescu[1], M. Guadagnini[2] and K. Pilakoutas[3]

Introduction

The strengthening potential of externally bonded FRP reinforcement (EBR) is already well established. However, the efficiency of FRP plate bonding systems is limited due to premature debonding, especially at the plate ends. Despite the large amount of research efforts, improving the accuracy of predictive models for debonding capacity continues to be a research challenge. The prediction ability of most of the available models relies on the accuracy of the bond-stress characteristics considered. These characteristics are normally determined by using experimental data from small-scale bond tests.

Simplified bond tests

Bond characteristics cannot be obtained from simple material tests, whilst the more realistic full-scale element tests (Fig. 1a) are time consuming and expensive. Thus, simplified bond tests (Fig. 1b), which are more economic, are generally preferred for parametric investigations.

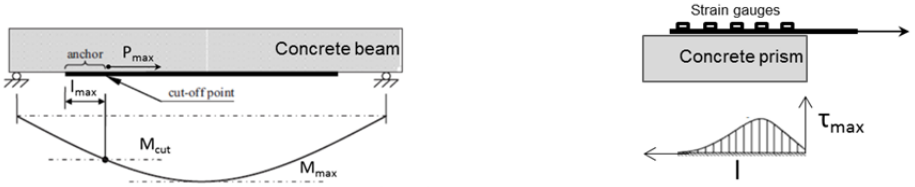

Figure 1: a) Anchorage zone in beams and b) simulation of anchorage zone with small scale specimens

The common test-set ups used to determine the bond characteristics are shown in figure 2: a) single shear pull (far end) test, b) single shear push test (near end), c) double shear push tests (near end), d) double shear pull test (far end), e) hinge bending test, f) steel block bending test and g) saw cut bending test.

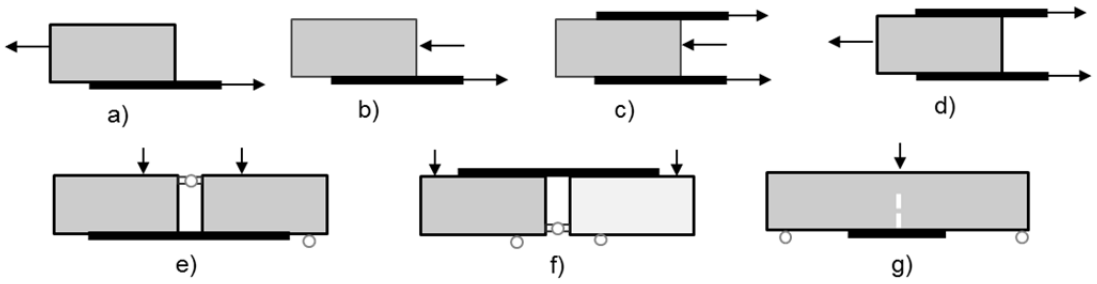

Figure 2: Common test set-ups

In the absence of a standardised procedure, these tests are very often further modified or adapted to suit individual laboratory conditions (Gartner et al., 2011). The bending test specimens may be T-shaped (Miller and Nanni, 1999) and include internal steel reinforcement/FRP bars or external FRP shear reinforcement (Gartner, 2011).

The interfacial stress state in FRP strengthened RC beams is best reproduced by bending (e.g. Pellegrino et al., 2008; Gartner et al., 2011; Kotynia, 2011) but such tests may appear cumbersome to setup. The force transfer between FRP plate and concrete substrate takes place primarily through shear stresses and thus, shear tests, which are more convenient for laboratory investigations, are most commonly

[1] The University of Sheffield, UK, a.serbescu@sheffield.ac.uk
[2] The University of Sheffield, UK, m.guadagnini@sheffield.ac.uk
[3] The University of Sheffield, UK, k.pilakoutas@sheffield.ac.uk

adopted (Chen et al. 2001; Yao et al. 2005a). Nevertheless, comparisons of different set-ups have shown that, in general, shear tests offer lower bond strength than bending tests (Horiguchi and Saeki 1997; Brosens cited in Mazzotti et al., 2009). Due to symmetry and for better control of induced normal stresses, the double-shear test (e.g. Nakaba, 2001; Leone et al., 2006; Serbescu et. al., 2013) may be preferred over the single shear test. However, specimens for a single shear tests are simpler to manufacture and mount and thus single shear tests appear the most commonly performed bond tests (e.g. Ceroni and Pecce, 2010; Bilotta et al., 2011; Yao, et al., 2005; Pellegrino et al., 2008).

Bond characteristics

Irrespective of the test set-up, the results of bond tests enable the determination of key interfacial characteristics such as local bond stress, slip at maximum local bond stress, maximum transferable force and corresponding maximum bond length. The maximum transferable load is directly recorded whilst the maximum bond length can be determined by regression analysis (minimum length to transfer the maximum force). The local bond law parameters, such as bond stress and slip, are determined by derivation (Eq. 1) and integration (Eq. 2) of measurements taken by discrete strain gauges mounted along the bonded length (Nakaba, 2001; En-Core, 2008)

$$\tau_{i,i+1} = \frac{E_f A_f (\varepsilon_{i+1} - \varepsilon_i)}{b_f (x_{i+1} - x_i)} \quad (1)$$

$$s_{i,i+1} = s_i + \frac{(\varepsilon_{i+1} - \varepsilon_i)}{(x_{i+1} - x_i)} \frac{x^2}{2} + \varepsilon_i x \quad (2)$$

A_f, b_f, E_f - FRP area, width and elastic modulus
ε_i, ε_{i+1} - strains at locations “i” and “i+1”
x_i, x_{i+1} - distance from the free end to the strain gauges located at “i” and “i+1”

Apart from the different set-ups, there is a lack of test specifications such as loading rate, instrumentation location, surface preparation, FRP/concrete width ratio, adhesive thickness. This, alongside the wide range of available material characteristics (e.g. FRP stiffness, concrete strength) can only lead to substantial variability of τ-s relationships (bond law or bond model). Figure 3 (not to scale) show some of the bond models available in the literature. A more review can be found in studies such as Toutanji et al., (2012) or Wu and Jiang (2013). The most often used model implements a bilinear law, which was initially developed by Holzenkampfer (1994).

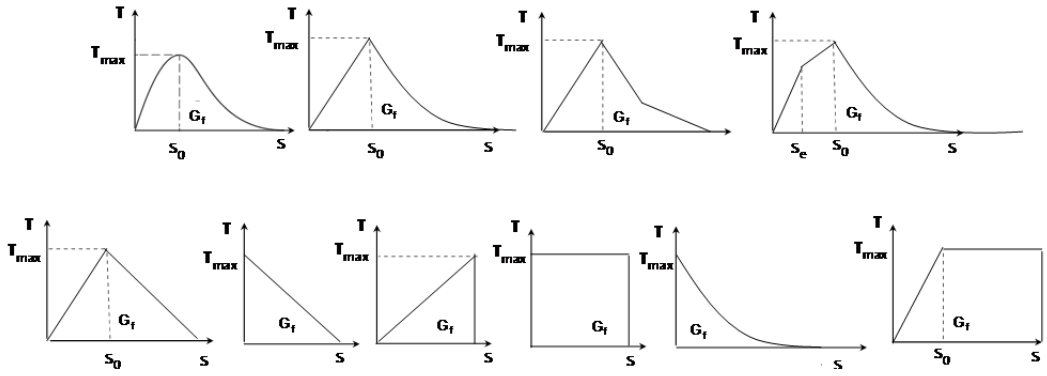

Figure 3: Common test set-ups

Another important aspect of these tests is the instrumentation type. The measurement of the relative displacement between the FRP and the concrete block (slip) at the loaded end using conventional methods such as linear variable differential transformers (LVDT) may appear simple but accurate measurements are difficult to obtain as the readings often contain contributions from other sources such as support movements and deformation of concrete (Cao et al., 2007; Serbescu et al., 2013). Strain

gauges, micrometers and various contact displacement devices are generally used to measure the deformation in the FRP plates but alternative full-field techniques such as electronic speckle pattern interferometry (Murukeshan et al., 1999; Gonzalez-Pena et al., 2000; Tripi et al. 2000 referenced in Cao et al., 2007) or 2D/3D digital image correlation (Czaderski et al., 2010, Ghiassi et al., 2013) can be used to obtain more detailed information. However, such techniques are not yet widely available.

Performance of existing bond-models

The high discrepancy between the large amount of bond models available in the literature is well documented. This can be partially attributed to the different test set-ups adopted by the various researchers to calibrate the analytical models, as well as the different parameters examined in each study. The performance (predicted maximum force in the plate P_{th}) of a selection of models proposed by most common design guidelines is shown in figure 4, based on 278 single and double shear tests collected from the literature (Serbescu et al., 2013).

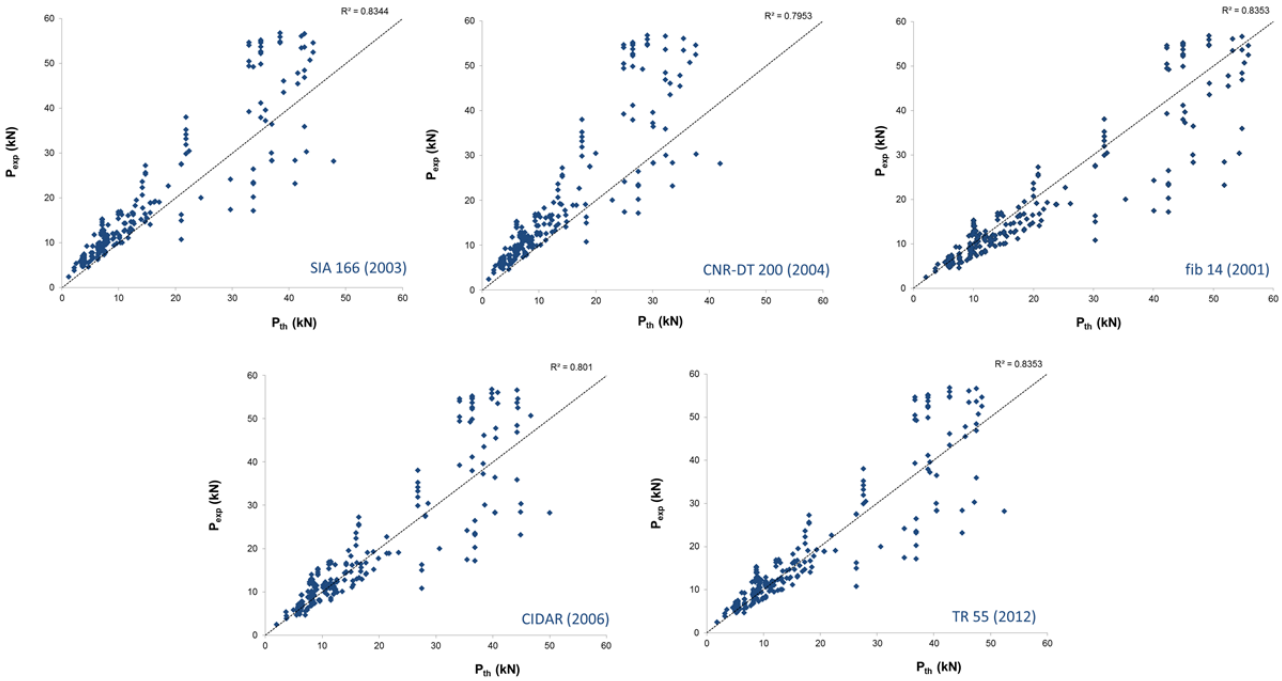

Figure 4: Predicted debonding load according to various design models (Serbescu et al., 2013)

Round Robin Testing (RRT)

In an attempt to identify a potential candidate for a standardised bond test, 6 international laboratories engaged into a RRT exercise and more than 108 specimens, both single and double pull shear, were tested (En-Core, 2008). The exercise was initiated by EU network EN-CORE and completed with the support of fib Task Group 9.3. As can be seen in figure 5, the variability of the results was relatively high.

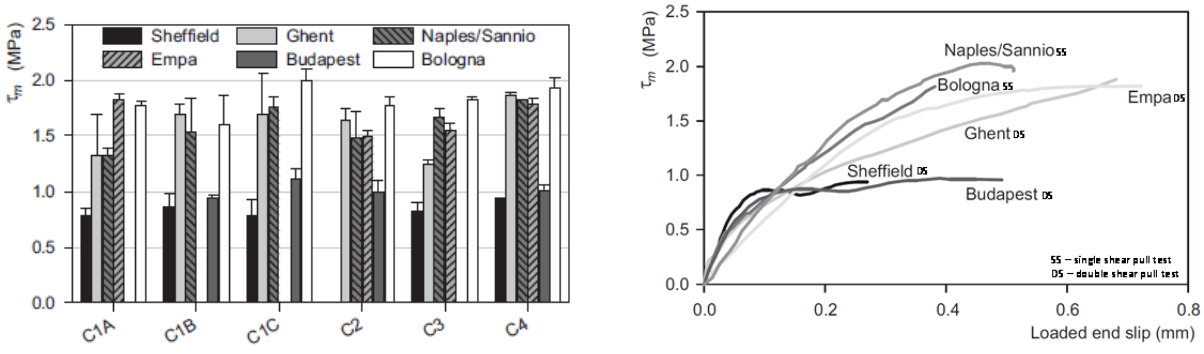

Figure 5: Average bond strength (left) and bond –slip behaviour (right)

The results confirmed that the quality of the concrete substrate, primarily in terms of surface finish, affects the bond behaviour of EBR systems to a large extent. The preparation and mounting of specimens for double-shear tests has proven to be problematic and concerns have been raised at various of the participating laboratories regarding the ability of effectively ensure alignment of the various components and avoid the development of undesired bending effects. The number of specimens exhibiting concrete splitting related failures, however, was comparatively higher for single shear tests than for double shear tests. This could be attributed to the possible effects of load eccentricity, but also to the lower concrete strength used for the specimens tested in the single-shear configuration.

Conclusions and Points for Discussions

The research community is yet to agree on a unified experimental set-up and testing procedure for these tests. The lack of standard tests leads to high variability in published results and hinders the development of reliable design models. Undoubtedly there is a need for a standardised bond test that is reliable, repeatable, easy to perform and able to represent the stress state that is observed in real field applications in the best possible way.

Key references

Ceroni, F. and Pecce, M. (2010). Evaluation of Bond Strength in Concrete Elements Externally Reinforced with CFRP Sheets and Anchoring Devices. J. Compos. Constr., 14(5), 521–530.

Chen, J.F. and Teng, J.G. (2001). Anchorage strength models for FRP and steel plates bonded to concrete. Journal of Structural Engineering 2001; 127(7):784-791.

CIDAR (2006). Design Guideline for RC structures retrofitted with FRP and metal plates: beams and slabs DRAFT 3. Centre for Infrastructure Diagnosis, Assessment and Rehabilitation, Standards Australia

CNR-DT 200 (2004). Guidelines for design, execution and control of strengthening interventions by means of fibre-reinforced composites materials, reinforced concrete and prestressed concrete structures, masonry structures. National Research Council, Advisory Committee on Technical Regulations for Constructions, Rome

Czaderski, C., Soudki, K. and Motavalli, M. (2010). Front and Side View Image Correlation Measurements on FRP to Concrete Pull-Off Bond Tests. Journal of Composites for Construction, ASCE 14(4): 451-463.

En-Core (2008) - En-Core European Network for Composite Reinforcement - RRT Methodology, available at: http://encore.shef.ac.uk/irrt/, access date: 02/02/2013.

fib 14. Externally bonded FRP reinforcement for RC structures, International Federation for Structural Concrete - Technical report, Lausanne, 2001.

Guadagnini, M., Serbescu, A., Palmieri, A., Matthys, S., Bilotta, A., Nigro, E., Ceroni, F., Czaderski, C., Olia, S., Szabo, Z., Balazs, G., Mazzotti, C. (2012). Round Robin Test on the Bond Behaviour of Externally Bonded FRP Systems to Concrete. In: Proceedings of CICE - 6, Rome (Electronic Proceedings).

Holzenkampfer, P. (1994). Ingenieurmodelle des verbunds geklebter bewehrung fur betonbauteile. Ph.D. thesis, TUBraunschweig, Braunschweig, Germany.

Horiguchi, T. and Saeki, N. (1997). Effect of test methods and quality of concrete on bond strength, In: Proceedings of the 3rd International Symposium on Non-metallic Reinforcement for Concrete Structures, JCI. Sapporo 1997; 1:265-70.

Mazzotti, C., Savoia, M. and Ferracuti, B. (2009). A new single-shear set-up for stable debonding of FRP–concrete joints. Journal of Construction and Building Materials 2009; 23(4):1529-1537.

to be completed

Bond problems in NSM systems

Antonio Bilotta[1], *Francesca Ceroni* [2], *Emidio Nigro* [3]

In general, the bond behavior between the concrete and any external Fiber Reinforced Polymer (FRP) reinforcement influences the transfer of stresses between the reinforced member and strengthening. Then it affects the ultimate load carrying capacity of the FRP strengthened concrete members, as well as some serviceability aspects, such as crack width and crack spacing. In particular, the bond strength of a Near Surface Mounted (NSM) system made of FRP materials is directly related to the type of failure (at the bar-adhesive interface, at the adhesive-concrete interface, within the concrete, cohesive at the adhesive and in the FRP material). The overall bond strength is dependent on local bond strength and, thus, on the distribution of bond shear stresses along the interface. The local bond-slip behavior is affected by the following main parameters: materials' mechanical properties, FRP reinforcement and grooves surface treatment, geometry of the strengthening system (bars or strips), grooves' dimensions and depth of the FRP reinforcement in the groove. The shape ratio, *k*, namely the ratio between groove and FRP dimensions, also affects the failure mode of the strengthening system (Sena Cruz and Barros, 2004; De Lorenzis and Teng, 2007; Seracino et al., 2007). In general, the local bond-slip behaviour and the bond strength are experimentally assessed by bond tests.

Failure modes of NSM systems

Based on the experimental results of bond tests carried out by several researchers, the possible failure modes can be defined as:

1) *Debonding at FRP bar/strip - adhesive interface*

This type of failure is identified by the virtual absence of adhesive attached to the bar surface after failure.

2) *Cohesive shear failure within the adhesive*

Such a failure is identified by the presence of adhesive on both FRP bar or strip and concrete after failure and occurs when the tensile strength of the adhesive is exceeded. Since surrounding concrete is much stiffer than the adhesives, it introduces some confinement at the concrete-adhesive interface.

3) *Debonding at adhesive - concrete interface*

Bond failure at the adhesive-concrete interface may occur as pure interfacial failure or as cohesive shear failure in the concrete. The pure interfacial failure mode was found to be critical for pre-cast grooves (De Lorenzis et al., 2002) and, in general, for grooves with smooth surfaces. In general, the failure at the adhesive-concrete interface was experimentally observed for values of the shape factor k > 1.5-2 (De Lorenzis and Teng, 2007); these limits, indeed, warrant a sufficient adhesive thickness around the FRP bar/strip in order to avoid the adhesive cover

[1] DIST – Department of Structures for Engineering and Architecture, University of Naples Federico II, Italy antonio.bilotta@unina.it
[2] DING - Structural Engineering, University of Sannio, Italy ceroni@unisannio.it
[3] DIST – Department of Structures for Engineering and Architecture, University of Naples Federico II, Italy emidio.nigro@unina.it

splitting.

4) Adhesive cover splitting

Longitudinal cracking of the adhesive is generally identified as cover splitting. This was observed to be the critical failure mode for deformed (i.e. ribbed and spirally wound) round bars in moderate strength concrete (De Lorenzis and Nanni, 2002; De Lorenzis et al., 2004). Specimens with low values of groove size (k≈1) and very brittle adhesive can show its splitting without significant damage in the surrounding concrete. A minimum value of k = 1.5 is suggested to avoid splitting (De Lorenzis and Nanni, 2002).

5) Concrete splitting

When an NSM bar/strip is close to the edge of a concrete member, failure can involve the splitting of the edge concrete (Galati and De Lorenzis 2009). This kind of failure mode can be easily eliminated by keeping a minimum distance from the edge. Moreover this kind of failure can be quite common mainly in elements of relatively low strength class.

Bond tests

Experimental bond tests on concrete elements strengthened with NSM FRP bars or strips have been performed by several researchers during the last decade.

In (De Lorenzis et al., 2004), GFRP and CFRP ribbed bars with 9.5 mm diameter and spirally wounded CFRP bars with 7.5 mm diameter were tested in concrete elements with mean compressive strength of 22 MPa. Most of the specimens failed by adhesive splitting. In De Lorenzis and Nanni (2002), GFRP deformed bars (13 mm diameter) and CFRP deformed bars (9.5 mm diameter) were tested in concrete elements (27.5 MPa). All specimens failed by adhesive splitting. Moreover, sand blasted CFRP bars (9.5 and 13 mm diameter) were tested too and a FRP-adhesive interface failure occurred.

In De Lorenzis et al. (2002) spirally wounded CFRP bars (7.5 mm diameter) were tested in concrete elements (22 MPa). All specimens attained an adhesive-concrete interface failure.

In Sena Cruz and Barros (2004) and Sena Cruz et al. (2006) smooth carbon strips with dimensions 10 mm x 1.4 mm were tested in specimens characterized by three values of concrete strength (35, 45, and 70 MPa). Failure always occurred at the FRP-adhesive interface.

In Seracino et al. (2007), smooth carbon strips with thickness of 1.2 mm and width of 10, 15 and 20 mm were tested. Concrete strength varied in the range 30-60 MPa. For the specimens with concrete strength equal or higher than 50 MPa a tensile failure of the FRP occurred, except for two cases which showed a FRP-adhesive interface failure. For lower values of strength, an adhesive- concrete interface failure was observed.

In Teng et al. (2006), smooth carbon strips (16 mm □ 2 mm) were tested in concrete specimens (44 MPa) and a FRP-adhesive interface failure occurred.

In Novidis and Pantazopoulou (2008), sand blasted deformed CFRP bars (12 mm diameter) were tested in concrete specimens (30 MPa) and an adhesive-concrete interface failure was observed.

Regarding the setup, both numerical and experimental studies (Novidis and Pantazopoulou, 2008) showed that different test setups can significantly change the experimental results. Nevertheless, at present, no consensus on a standard test procedure has been still reached. For this reason, a Round Robin initiative was recently carried out involving several research laboratories (Palmieri et al. 2012; En-Core & fib TG 9.3, 2010) and aimed at testing the bond strength of the same FRP materials according to different setups in different laboratories. In

particular, the laboratories of the Universities of Naples, Ghent, Minho and Budapest tested various NSM systems. All laboratories adopted a double shear test (DST), where two concrete blocks were connected by the NSM reinforcements on two opposite sides. The only exception was the laboratory of Naples (Bilotta et al. 2011), which used a single shear test (SST) setup (see figure 1). Nevertheless, all the laboratories tested the same NSM systems, failure modes were quite different; in particular in the tests carried out by the University of Minho an adhesive-concrete interface failure occurred in most cases. In the tests performed at the University of Ghent, the failure happened at the FRP-adhesive interface for the smooth carbon bars and strips . Adhesive splitting occurred for sand coated basalt bars and for ribbed glass bars. In the other cases, an adhesive-concrete interface failure occurred. In

most of the tests carried out by the University of Budapest, failure occurred in the concrete block and only in some cases it was due to adhesive splitting. Finally, a concrete-adhesive interface failure occurred in most specimens strengthened with NSM systems at the University of Naples. Even if the DST setup led, in some cases, to the failure of the concrete due to an incorrect alignment of the two blocks, it is worth noting that the concrete strength could more affect the failure mode. Indeed concrete strength varied in the range 27-32 MPa for the tests at University of Ghent, was 43 MPa at University of Budapest and 35 MPa at University of Minho. At the University of Naples, a lower concrete strength (about 19 MPa) was used in order to replicate the conditions of existing RC buildings. For low strength, a concrete-adhesive interface failure is more probable than adhesive splitting. Moreover, it is worth to note that, nevertheless the different concrete strength, the different experimental set-up and measurement systems, the variability of the failure loads was quite limited since the values of the Coefficient of Variation (CoV) ranged between 6% and 15% referring to the average loads obtained by the four laboratories. This results is also significant because it might evidence that the SST set-up is referable since it is more simple to be realized and less affected by alignment problems of the blocks before and during the tests in comparisons with the DST set-up.

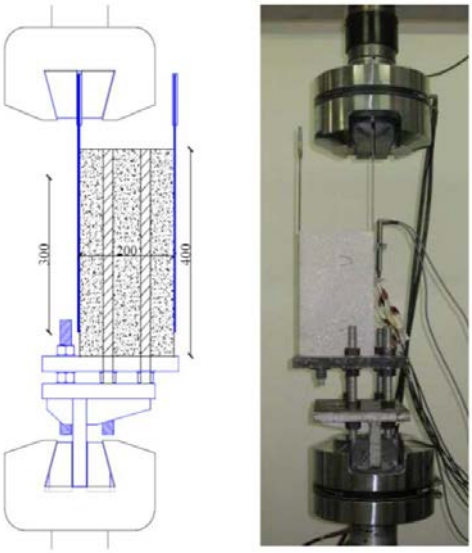

Figure 1 – Example of bond test setup

Debonding predicting formulae

Despite of failure modes, experimental results of bond tests clearly showed that the NSM technique could represent a sound alternative to Externally Bonded Reinforcement (EBR) systems since it allows the FRP tensile strength to be better exploited. The results of bond tests on different types of NSM reinforcement carried out by the authors and other test results available in literature will be collected and analyzed in terms of maximum bond shear stress and maximum strain at failure, in order to provide an experimentally calibrated relationship aimed to predict both average and characteristic values of the maximum strain of the FRP NSM reinforcement in case of bond failure at the anchorage.

References

Bilotta A., Ceroni F., Di Ludovico M., Nigro E., Pecce M., Manfredi G. (2011). Bond efficiency of EBR and NSM FRP systems for strengthening of concrete members. Journal of Composites for Construction - ASCE, vol. 15, p. 757-772. ISSN: 1090-0268. doi: 10.1061/(ASCE)CC.1943-5614.0000204

Bilotta A., Ceroni F., Di Ludovico M., Nigro E., Pecce M., Manfredi G (2012). Experimental Bond Tests on Concrete Members Strengthened with NSM FRP Systems: Influence of Groove Dimensions and Surface Treatment. 6th International Conference on FRP Composites in Civil Engineering (CICE2012), Rome, ITALY, June 13–15, 2012, Paper ID: 01-079, 8 pp.

Costa, I.G., Barros, J.A.O. Assessment of the bond behavior of NSM FRP materials by pullout tests. In: Proc. of First Middle East Conference on Smart Monitoring, Assessment and Rehabilitation of Civil Structures, Dubai, 8-10 February 2011.

De Lorenzis L., Nanni A. (2002), Bond between NSM fiber-reinforced polymer rods and concrete in structural strengthening. ACI Structural Journal, 99 (2), 123-132.

De Lorenzis, L., Rizzo, A., La Tegola, A. (2002), A modified pull-out test for bond of near-surface mounted FRP rods in concrete. Composites Part B: Engineering, Elsevier, 33 (8),589-603.

De Lorenzis L., Ludgren K., Rizzo A., (2004), Anchorage length of near surface mounted FRP bars for concrete strengthening –experimental investigation and numerical modelling, ACI Structural Journal, 101(2), 269-278.

De Lorenzis L., Teng J.G. (2007), Near-surface mounted FRP reinforcement: an emerging technique for structural strengthening. Composites: Part B, Elsevier, 38, 119–143.

En-Core & fib TG 9.3. Internal reports: Round robin testing exercise – Universities of Gent, Minho and Budapest; 2010. <http://cigroup.shef.ac.uk/encore/rrt/index.php>.

Galati D., De Lorenzis L. (2009) Effect of Construction Details on the Bond Performance of NSM FRP Bars in Concrete ADVANCES IN STRUCTURAL ENGINEERING Volume: 12 Issue: 5 Pages: 683-700 Published: OCT 2009

Novidis D.G., Pantazopoulou S.J. (2008), Beam pull out tests of NSM – FRP and steel bars in concrete. Proc. of CICE 2008, 22-24 July 2008, Zurich, Switzerland, CD-ROM.

Palmieri A., S. Matthys, J. Barros, I. Costa, A. Bilotta, E. Nigro, F. Ceroni, Z. Szambo, G. Balazs (2012). Bond of NSM FRP Strengthened Concrete: Round Robin Test Initiative. In: 6th International Conference on FRP Composites in Civil Engineering. Roma, 13–15 June 2012, p. 03-228-1-03-228-8pp.

Sena-Cruz J.M., Barros J.A.O. (2004), Bond between near-surface mounted CFRP laminate strips and concrete in structural strengthening. J. of Composites for Construction, ASCE, 8 (6), 519-527.

Sena-Cruz JM, Barros JAO, Gettu R, Azevedo AFM. (2006). Bond behavior of nearsurface mounted CFRP laminate strips under monotonic and cyclic loading. ASCE J Compos Constr 2006;10(4):295–303

Seracino R., Jones N.M., Page M.W., Ali M.S.S., Oehlers D.J. (2007), Bond strength of near-surface mounted FRP-to-concrete joints. J. of Composites for Construction, ASCE, 11 (4), 401-409.

Teng J. G., De Lorenzis L., Wang Bo, Li Rong, Wong T. N., Lam L., (2006). Debonding failures of RC beams strengthened with Near Surface Mounted CFRP strips, ASCE J. of Composites for Construction, 10(2), 92-105.

DISCONTINOUS BOND IN RC BEAM ELEMENTS EXTERNALLY STRENGTHENED WITH CFRP

Trombeva-Gavriloska Ana [1], Lazarevska Marijana [2]

Contemporary structures are typically designed for a service life of 50 or more years. Over this time period, it can be observed that loading, as well as the environmental conditions, may significantly change. As a consequence, numerous reinforced concrete structures exhibit non-adequate performance and are therefore in need of poststrengthening during their service life. Nowadays steel plates that have been traditionally used for this purpose are often replaced by lighter, stronger and more durable FRP strips.
It is obvious that the bond between the concrete substrate and the FRP plate plays a crucial role in the occurrence of failure mode with loss of composite action. One of the problems that could be encountered during the strengthening of reinforced concrete structures in the practice is inadequate execution of the bonding process. This may lead to weakening of the bond layer in some positions along the length of the plate, and to creation of discontinuities within the bond layer. Significant changes of the bearing capacity, which were not taken into the account during the design stage, may be observed in such case. It is extremely difficult to evaluate the influence of these weak zones within the bond layer upon structural response of the strengthened beam.
For a proper determination of the bearing capacity of the RC structure strengthened with externally added FRP reinforcement, a model has to be used, which can accurately describe the stresses in the bond layer [1]. To evaluate the influence of the presence of such discontinuous zone upon overall response of the beam, a numerical assessment was proposed, where the bond between reinforced concrete beam and CFRP plate was modeled by a numerical displacement- based fibber model [1].
In order to model the weak spot in the bond, a modification was introduced to the bond law, incorporated in the existing model [2], [4]. The magnitude of the maximum shear stress remains unchanged while the displacement at slip is significantly increased. A much more flexible bond (compared to the perfectly bonded area) is achieved by this modification. The significance of numerical modelling of such discontinuous zones and evaluation of the influence that they have upon overall response of the strengthened beam are highlighted and evaluated by a sensitivity analysis [3].
Parametric analyses were carried out for selected values of increasing displacement at slip. The obtained results showed that the values of the calculated bearing capacity are approaching an asymptotic value when the displacement at slip is increasing, while corresponding bond stresses in the region of discontinuity are approaching zero values, which is in accordance with the actual situation [2], [3], [4], [5]. Based on the parametric analysis it can be concluded that proposed modification of the bond law is appropriate and correct modelling values for the weak zone can be selected.
Furthermore, for verification of the implemented modification in the bond constitutive law, bond stress distribution and tensile plate force distribution along the externally strengthened reinforced concrete beam with discontinuous zone in the bond layer under equal load were analyzed.[6], [7], [8]. The obtained results show that the displacement at slip used in the process of modeling has no influence on the ultimate tensile force in CFRP strip. By increasing the value of the displacement at slip used in the modeling process tensile force in the CFRP strip in the weak zone approaches the constant value [6], [7], [8].
Influence of the length and place of the discontinuity was evaluated from the global response of the strengthened beam, bond stress distribution and tensile force distribution in the CFRP sheet [3], [4]. From the analysis could be concluded that the weak zone in the bond layer may decrease the tensile force in the CFRP plate, which means that its bearing capacity is not completely used. Results show that local bond stress concentrations, which appear where cross- section is changed, have negative influence on the quality of the bond between concrete substrate and CFRP plate.
Artificial neural networks were applied for prognostic modeling of the distribution of tensile force in CFRP

[1] Ss. Cyril and Methodius University, Skopje, Macedonia
[2] Ss. Cyril and Methodius University, Skopje, Macedonia

strip along the beam, for the selected values of the displacement at slip that were used in the modeling process of the weak bond zone. Numerically generated data from the proposed modeling of the weak zone were used for creation of the prognostic neural network's model. The results obtained by the neural network's model for the analyzed case show excellent accuracy for quality prognoses of the output data [9].

Key References

[1] Monti, G., Spacone, E., Reinforced concrete fiber beam element with bond- slip, *Journal of Structural Engineering*, V. 126, No. 6, 2000.

[2] Šelih, J., Trombeva, A., Žarnić, R., Behaviour of FRP Strengthened Beams having Discontinuous Bond, *Durability and Maintance of Concrete Structures: Proceedings of the International Symposium organized by Croatian Society of Structural Engineers (CSSE) and Austrian Society for Concrete and Construction Technology (ASCCT),* Dubrovnik, R. Croatia, 2004.

[3] Trombeva, A., Šelih, J., Žarnić, R., Influence of the Position of Discontinuous Bond upon Response of Reinforced Concrete Beams Strengthened with CFRP Sheets, *Proc. 11th International Symposium of Macedonian Association of Structural Engineers,* Ohrid , R. Macedonia, 2005.

[4] Trombeva-Gavriloska, A., Šelih, J., Žarnić, R., Role of Discontinuous Bond in RC Beams Strengthened with CFRP Plates, *Proceeding of the International Conference on Civil Engineering Design and Construction,* Varna, R. Bulgaria, 2006.

[5] Trombeva-Gavriloska, A., Šelih, J., Žarnić, R., Modelling and Role of Discontinuous Bond in RC Beams Strengthened with CFRP Plates, *Proc. 8th International Symposium on Fiber-Reinforced Polymer Reinforcement for Concrete Structures*, Patras, R. Greece, 2007.

[6] Trombeva-Gavriloska, A., Gavriloski, V., Modelling of Discontinous Bond between Reinforced Concrete Beam Strengthened with CFRP Sheet under Same Loading, *Proc. 13th International Symposium of Macedonian Association of Structural Engineers ,* Ohrid, R. Macedonia, 2009.

[7] Gavriloska, T., A., Šelih, J., Cvetkovska, M., Samardzioska, T., Behaviour Analysis of Modelled Discontinous Bond in RC Beam Strengthened with CFRP Plate Under the Equal Load, Proceeding of 7th International Conference of Analytical Models and New Concepts in Concrete and Masonry Structures, Krakow, Poland, 2011.

[8] Gavriloska-Trombeva, A., Šelih, J., Cvetkovska, M., Samardzioska, T., Modeling of Discontinous Bond under the Equal Load in RC Beam Strengthened with CFRP Plate, Journal of Architecture, Civil Engineering, Environment, No. 4, The Silesian University of Technology, 2011.

[9] Lazarevska, M., Gavriloska-Trombeva, A., Knežević, M., Samardzioska, T., Cvetkovska, M., Neural Network Prognostic Model for RC Beams Strengthened with CFRP Strips, Journal of Applied Engineering Science, Serbia, Vol. 10, 2012.

MODELING OF DISCONTINOUS BOND IN RC BEAM ELEMENTS EXTERNALLY STRENGTHENED WITH CFRP

A. T. Gavriloska[1], M. Lazarevska[2]

Introduction

The effects of change in the environmental conditions, the increasing of the loads and the design of older structures, which may have been adequately compared with contemporary codes but are inadequate against the current codes, are all factors which contribute either for decreasing of the bearing capacity or structural safety of the construction. Non adequate performance of the reinforced concrete construction imposes the need for their repair and strengthening. In the recent years, typical retrofitting technique involves use of external bonded fibber reinforced polymer (FRP) plates.

Failure behaviour of a plated beam can be very strongly influenced by the integrity of the bond between the plate and the concrete. One of the problems that can be encountered during the strengthening of reinforced concrete structures in the practice is inadequate execution of the bonding process. This may lead to weakening of the bond layer in some positions along the length of the plate, and to creating discontinuities within the bond layer.

Numerical model formulation

For a proper determination of the bearing capacity of the RC structure strengthened with externally added FRP reinforcement, a model has to be used, which can accurately describe the stresses in the bond layer. Numerical model, which is used for the analysis of the strengthened beam element, is based on a fibber model [1]. Two-node displacement based beam element has been used. It has two components: a two-node concrete beam and a strengthening plate. The nodal degrees of freedom of the concrete beam and of the strengthening plate are different to permit slip. The reinforced concrete section is discretized into fibbers layers as is shown on Fig. 1.

Cubic transverse and linear axial displacement fields are assumed for the beam, and linear axial displacement for the strengthening plate. The distribution of the bond slip is quadratic. The element is implemented in the finite element program FEAP [2].

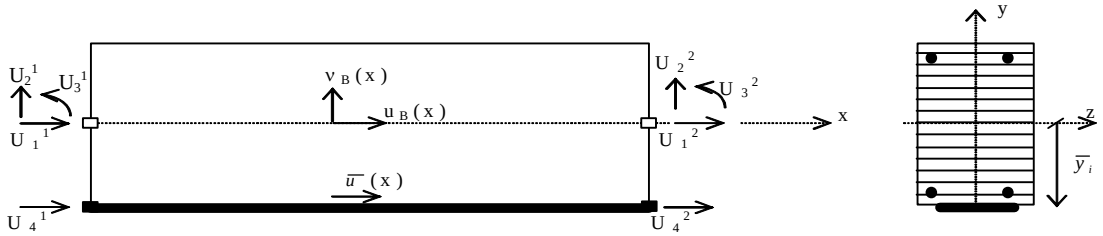

$$U = \{U_1^1 \quad U_2^1 \quad U_3^1 \quad U_4^1 \quad | \quad U_1^2 \quad U_2^2 \quad U_3^2 \quad U_4^2\}^T \quad u(x) = \{u_B(x) \quad v_B(x) \quad | \quad \bar{u}(x)\}^T$$

Figure 1: Node and field displacements of the reinforced concrete beam element with bond slip

[1] Faculty of Architecture, Republic of Macedonia, agavriloska@arh.ukim.edu.mk
[2] Faculty of Civil engineering, Republic of Macedonia, marijuana@gf.ukim.edu.mk

Analyzed case

The analyzed case is presented in Figure 2. A 3200 long reinforced concrete beam strengthened with CFRP (carbon fibber reinforced polymer) strip is subjected to four-point bending condition. Due to the symmetry of the case, only a half of the beam is being analyzed. The discontinuous part of the bond layer is defined by its position and length, i.e., by x_{ini}, x_{fin} and Δ.

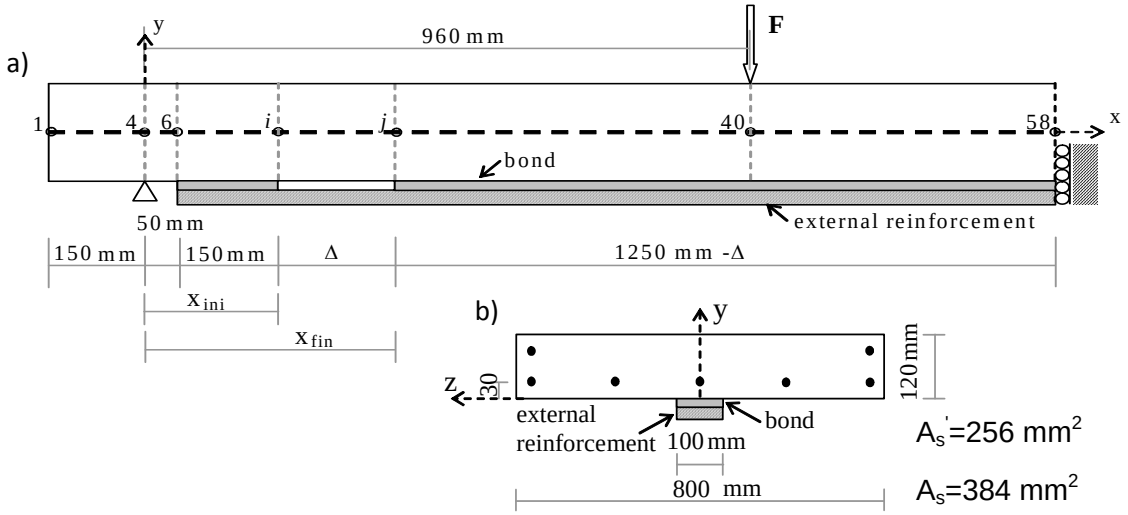

Figure 2: Beam element strengthened with CFRP strip: a) geometry of half beam; b) cross section of the strengthened beam

Dimensions of the transverse section of the reinforced beam are b/h=800/120 mm. Width of the external CFRP reinforcement is 100 mm. Young's modulus and the yielding strength of the CFRP strip taken in the analysis are 150 GPa and 2400 MPa, respectively. The corresponding values for the reinforcing steel are 210 GPa and 460 MPa, respectively.

Modelling of the bond layer between concrete and external CFRP reinforcement

The original constitutive bond law is described by a linear relation between displacement and shear stresses in the bond layer up to the maximal bond strength. When this value of bond shear stresses is reached, slip occurs, which means that displacement is increasing while the corresponding shear stress is zero.

In order to model weak zone in the bond layer, a modification was introduced in the bond law. Maximal shear stress, τ_1, remains unchanged, while displacement at slip is significantly increased. By this modification a much more flexible bond is achieved compared to the perfectly bond area. The perfect bond is described by values $u_{1,cont}$=0.0013 mm and τ_1=3.1 MPa. The original and modified bond law are presented in Figure 3.

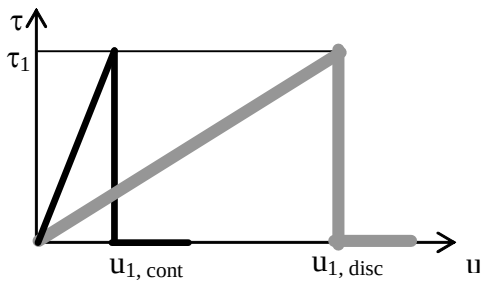

Figure 3: Original and modified constitutive bond law

Results and discussion

Introduced modification in the bond law was confirmed by sensitivity analysis of the numerical model for selected values of increasing $u_{1,disc}$. In Figure 4 is presented influence of the selected value for parametar $u_{1,disc}$, used in the process of modelling for discontinous bond presented in Figure 3, upon its bearing capacity. The values of the calculated bearing capacity are decreasing and approaching an asymptotic value when $u_{1,disc}$ is increasing. The results of the analysis show that the modification introduced to the model is appropriate.

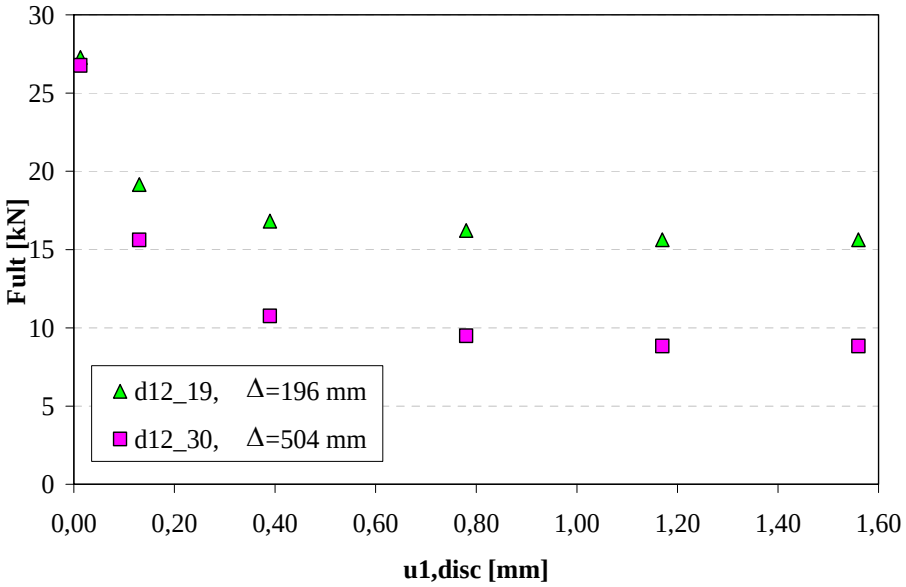

Figure 4: Modelling of discontinuous bond: influence of selected value for $u_{1,disc}$ upon bearing capacity, F_{ult} ; discontinuity starts at x_{ini} =200 mm and has a length of Δ=196 and 504 mm

Figure 5 indicates that the corresponding bond stresses in the region of discontinuity decrease and approach zero values as the $u_{1,disc}$ increase, which is in accordance with the actual situation. This meets our expectations and confirms that the modification of the bond-slip behaviour for the weak part was appropriate.

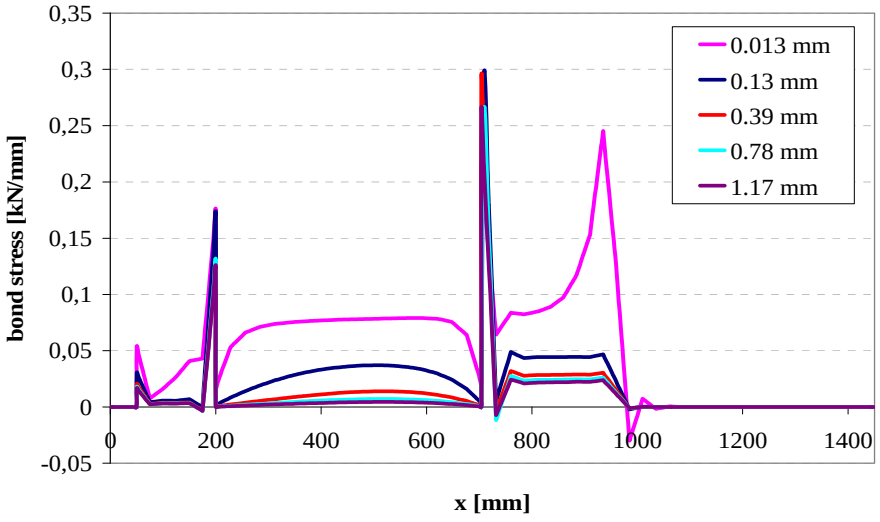

Figure 5: Influence of the weakened bond presence upon bond stress distribution (discontinuity starts at x_{ini} =200 mm and has a length of Δ =504 mm); $u_{1,disc}$=0,013; 0,13;0,39; 0,78; 1,17 mm

Figure 6 shows the tensile force in the CFRP plate along the beam, which corresponds to the bond stresses depicted in Figure 5. It can be observed that in the section of the weak bond, the tensile force rate is smaller when a larger value of $u_{1,disc}$ is employed in the analysis. This is in accordance with the obtained bond stress distribution, as bond stresses are proportional to the tensile plate force derivative.

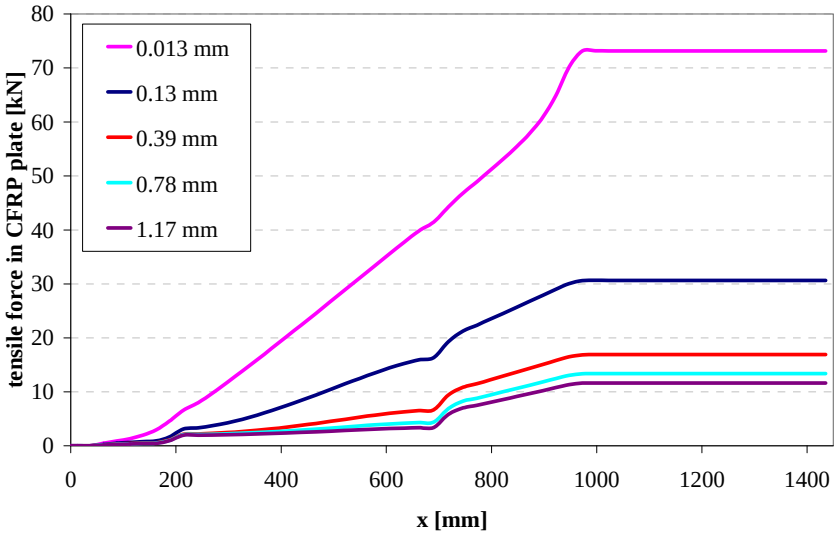

Figure 6: Influence of the weakened bond presence upon tensile plate force distribution (discontinuity starts at x_{ini} =200 mm and has a length of Δ =504 mm); $u_{1,disc}$=0,013; 0,13; 0,39; 0,78; 1,17 mm

Conclusions and Points for Discussions

The results obtained show that the proposed modification of the bond law is appropriate. Based on the parametric analysis, appropriate modelling values for the weak zone can be selected.

The analysis leads to a conclusion that the weak zone in the bond layer may decrease the tensile force in the CFRP plate, which means that its bearing capacity is not completely used. Results show that local bond stress concentrations, which appear where cross-section is changed, have negative influence on the quality of the bond between concrete substrate and CFRP plate.

Further validation of the proposed model and results obtained by parametric analysis using this model, has to be carried out by the experimental researches.

Key references

[1] Monti, G., Spacone, E. (2000). Reinforced concrete fiber beam element with bond- slip, *Journal of Structural Engineering*, 126 (6), 654-661.

[2] Taylor, R.L. (2002). FEAP: A Finite Element Analysis Program. Users Manual: Version 7.4, Department of Civil Engineering, University of California, Berkeley, http://www.ce.berkeley.edu/~rlt/feap/

3.2 Flexural strengthening

Near surface mounted reinforcement for flexural strengthening of RC columns

Dionysios A. Bournas [1]

Introduction

Bournas and Triantafillou (2009) and Perrone et al. (2009) presented the results of full-scale experimental programmes which were aiming to provide a fundamental understanding of the behavior of reinforced concrete (RC) columns under simulated seismic loading, strengthened in flexure (of crucial importance in capacity design) with different types and configurations of near-surface mounted (NSM) reinforcing materials.

Experimental programme

The experimental programme of Bournas and Triantafillou (2009) aimed to study the flexural strengthening of old-type non-seismically detailed RC columns with NSM reinforcement and to compare the effectiveness of different flexural strengthening schemes. A total of eleven full-scale RC column specimens with the same geometry were constructed and tested under cyclic uniaxial flexure with constant axial load as shown in Fig. 1.

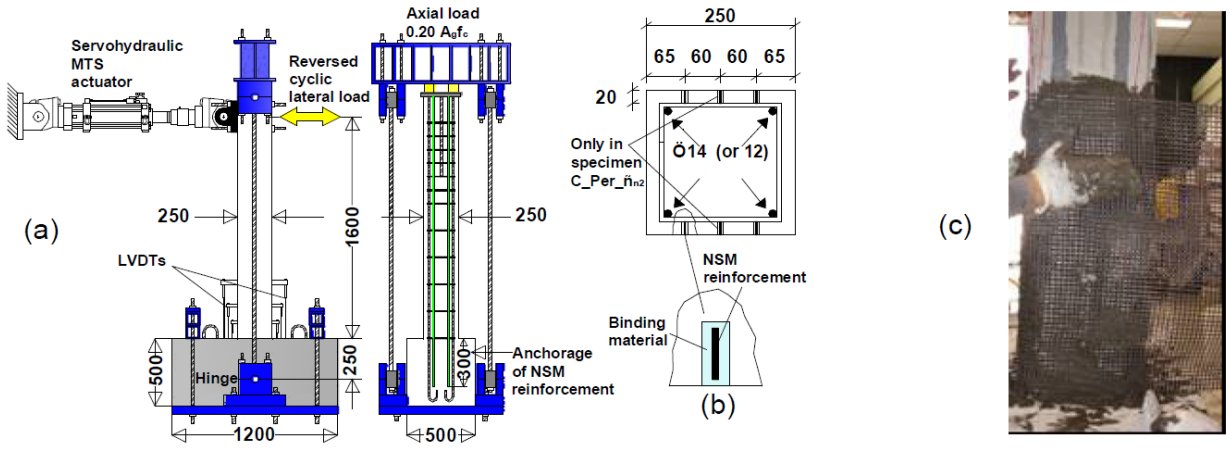

Figure 1: (a) Schematic of test setup. (b) Cross section of columns. (c) NSM reinforcement and application of TRM jacket.

The specimens were designed such that the effect of a series of parameters on the flexural capacity of RC columns could be investigated. These parameters comprised: type of NSM reinforcement (CFRP strips, GFRP bars, stainless steel rebars), configuration of NSM reinforcement (CFRP strips placed with their large cross section side perpendicular or parallel to the column sides, depending on whether a proper concrete cover is available or not), geometrical reinforcing ratio of NSM or internal reinforcement, type of bonding agent for the NSM reinforcement (epoxy resin versus cement-based mortar) and NSM reinforcement with or without local jacketing at the member ends.

[1] Faculty of Engineering, The University of Nottingham Nottingham, NG7 2RD, UK, Dionysios.bournas@nottingham.ac.uk

Experimental results and conclusions

The response of all columns tested in Bournas and Triantafillou (2009) is given in Fig. 2 in the form of load-drift ratio curves. All columns responded as designed and failed by flexural yielding of the internal steel, followed by failure of the NSM reinforcement. With only one exception (column C_Par), all strengthened specimens displayed higher (up to about 100%) flexural resistance compared to the control specimen.

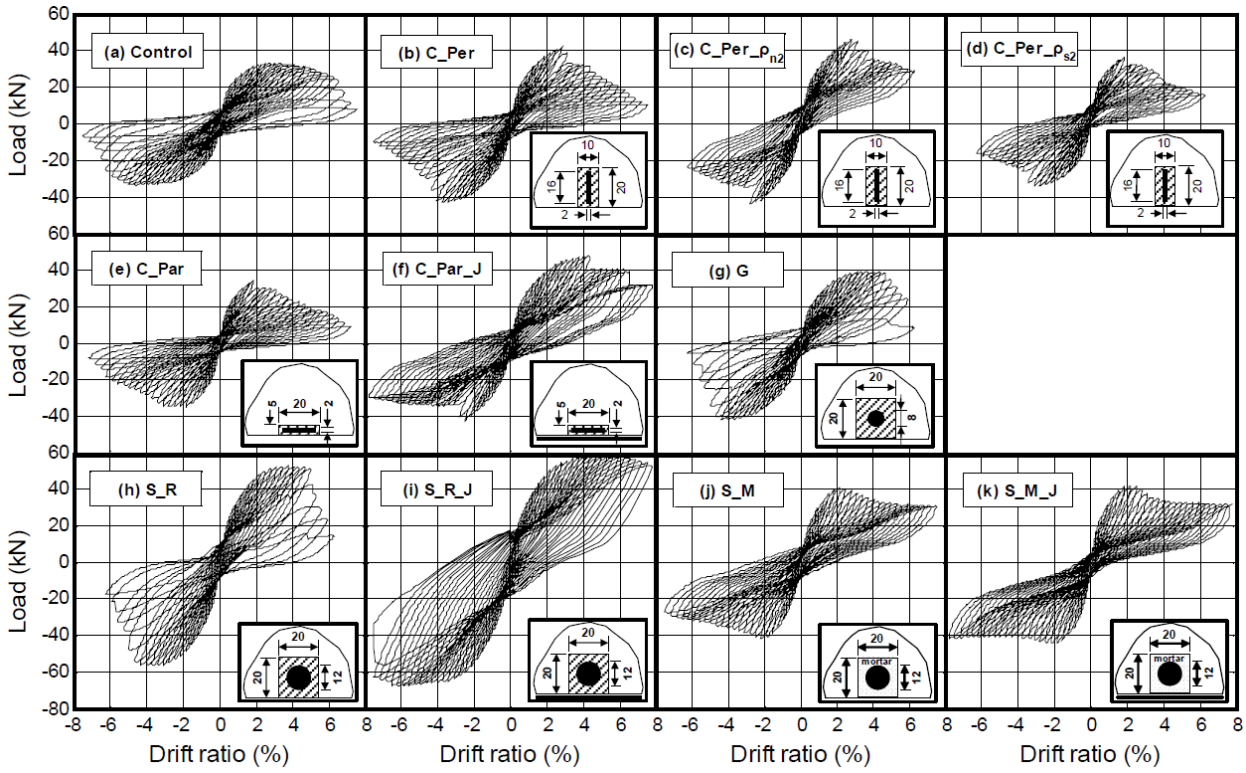

Figure 2: Load versus drift ratio curves for tested specimens (the inserts illustrate NSM reinforcement configurations).

The results demonstrated that NSM FRP or stainless steel reinforcement is a viable solution towards enhancing the flexural resistance of reinforced concrete columns subjected to seismic loads, especially when the retrofitting scheme combines epoxy-bonded NSM bars with local confining jackets (provided in this study with textile-reinforced mortars – TRM). Following up the very promising experimental results, Bournas and Triantafillou (2013) developed an analytical model for the design of NSM strengthened columns subjected to uniaxial or biaxial bending. The agreement between analysis and test results was very satisfactory.

Key references

Bournas, D.A., and Triantafillou, T.C. (2009). “Flexural Strengthening of RC Columns with NSM FRP or Stainless Steel”, ACI Structural Journal, 106(5), 495-505.

Bournas, D.A., and Triantafillou, T.C., (2013), "Biaxial Bending of RC Columns Strengthened with Externally Applied Reinforcement Combined with Confinement", ACI Structural Journal, 110(2), 193-204.

Perrone M., Barros J.A.O., and Aprile A. (2009). “A CFRP-Based Strengthening Technique to Increase the Flexural and Energy Dissipation Capacities of RC Column”, ASCE Journal of Composites for Construction, 13(5), 372-383.

CFRP Laminate Strengthening of Concrete Beams with Corroded Steel

Garyfalia G. Triantafyllou[1], Theodoros C. Rousakis[2], Athanasios I. Karabinis[3]

Introduction

Corrosion of steel reinforcement is one of the major causes that limit durability and serviceability performance of reinforced concrete (RC) structures. Damage and residual capacity assessment as well as suitable repair and strengthening of deficient reinforced concrete members are urgent for most existing structures. Externally bonded reinforcements (EBR) in the form of fabrics and FRP laminates for flexure in corroded RC beams increase the ultimate strength but significantly reduce the deflection capacity compared to unrepaired beams (El Maaddawy and Soudki 2005, Al-Saidy et al. 2010). The behavior of corroded beams in need of cracked concrete removal and application of additional repair mortar before FRP strengthening lacks adequate experimental evidence. The effects of concrete patching before bonding carbon FRP were investigated by Xie and Hu (2012) and Al-Saidy and Al-Jabri (2011), who found replacing the damaged concrete cover with a new concrete layer prior to strengthening with FRP, to be more effective in the load transfer mechanism between FRP and concrete. Retrofit with Near Surface Mounted (NSM) reinforcement has been developed in order to treat the bond failure at the interface between the EBR and the concrete surface by inserting the FRP reinforcement into concrete cover grooves filled with epoxy adhesives. Very few researchers studied corroded RC members repaired and strengthened with NSM systems. Kreit et al. (2011) and Almassri et al. (2014) strengthened naturally corroded RC beams with one 6 mm diameter NSM CFRP rod without repaired the damaged concrete cover. They concluded that the efficiency of the NSM technique could be limited by the separation of the concrete cover due to longitudinal corrosion induced cracks on the corroded substrate.

Thus, there are unidentified gaps that concern the understanding of steel corrosion process combined with the force transfer at old concrete-new mortar patch and new mortar patch-FRP strengthening interfaces. The objective of the current research is to study the behavior of RC beams with corroded steel reinforcement to a low mass loss (around 7.5%). Also demonstrates the need for removal of cracked concrete cover, treatment of steel bars, application of cement-based repair patch and of externally bonded EBR or NSM FRP laminates at the characteristic limit state of initiation of concrete cover separation. Test results have demonstrated that the beam strengthened with two NSM FRP strips of equivalent axial rigidity with EBR FRP laminate presented 18.2% higher load and 41.6% higher deflection than the latter.

Experimental Program

Specimens configuration

A total of 4 RC beams with a width of 150 mm, a height of 300 mm and a length of 2300 mm were tested in the Reinforced Concrete Laboratory of D.U.Th. Beam RC-N was a reference beam with no corrosion, while the remaining three beams were subjected to an accelerated corrosion technique. Beam RC-COR1 was the control corroded beam, while RC-COR1S1 and RC-COR1S2 were corroded beams repaired and strengthened with EBR and NSM carbon FRP systems respectively. All beams had three tensile ribbed rebars of 12 mm diameter, two 10 mm diameter ribbed bars in compression, 8 mm stirrups of 8 mm diameter spaced at 150 mm (with 50 mm spacing at the support) and 20 mm clear concrete cover. The specimen details appear in figure 1.

[1] Democritus University of Thrace (D.U.Th.), Greece, gtriant@civil.duth.gr
[2] Democritus University of Thrace (D.U.Th.), Greece, trousak@civil.duth.gr
[3] Democritus University of Thrace (D.U.Th.), Greece, karabin@civil.duth.gr

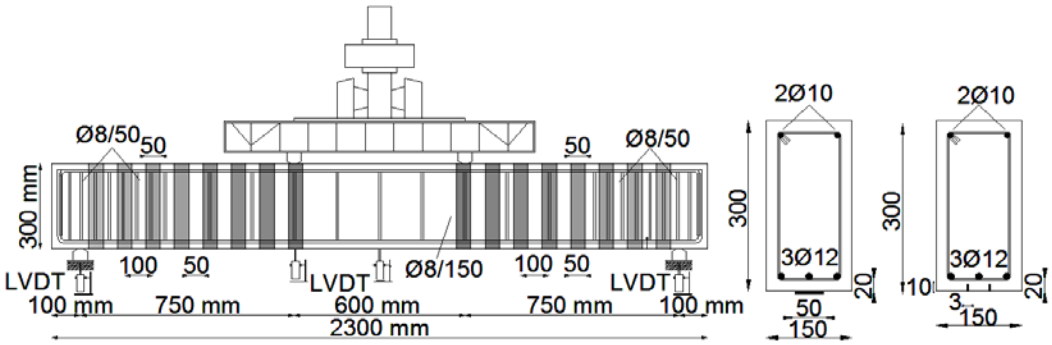

Figure 1: Experimental setup and layout of the reinforcement.

Materials

The average compression stress on cylindrical concrete specimens was 34.6 MPa, the elastic modulus 32300 MPa and the tensile strength was 2.2 MPa after 28 days. The tensile strength, measured using the splitting test, was 2.2 MPa. The reinforcing bars and stirrups had nominal yield strength of 500 MPa. Tensile tests on steel bars with or without corrosion were also executed and the tensile stress-strain curves for both non corroded and corroded rebars are shown in figure 2.

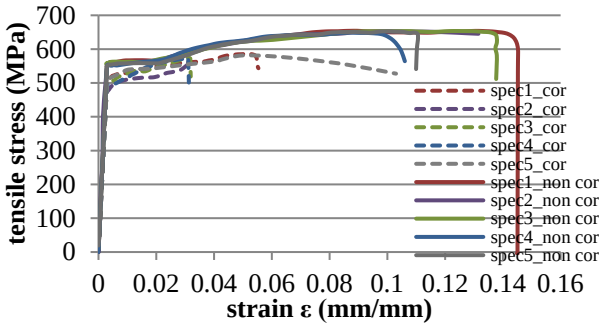

Figure 2: Tensile stress-strain curves of non corroded and corroded steel reinforcement bars.

After removal of cracked concrete, corroded rebars were treated with corrosion inhibitor for reinforced concrete and an epoxy-cement and anti-corrosive bonding primer. Substrate repair was realized with polymer modified cementitious repair mortar having compressive strength of 50 MPa at 28 days. Table 1 shows the mechanical characteristics of CFRP laminate, CFRP plates used for the NSM technique and U-CFRP sheets for shear strengthening. Epoxy resin was used for the bonding of CFRP laminate having flexural strength of 90 MPa, tensile strength of 30 MPa and elastic modulus of 11200 MPa. The epoxy resin was used for the bonding of CFRP plates into slits, for UCFRP sheets and for filling the grooves in NSM technique. It had tensile strength of 30 MPa and elastic modulus of 4500 MPa.

Table 1: Mechanical characteristics of CFRP materials.

Type of composite	Width *(mm)*	Thickness (mm)	Young's Modulus *(GPa)*	Ultimate stress *(MPa)*	Ultimate strain *(%)*
CFRP laminate	50	1.2	165	3100	1.7
CFRP NSM plates	10	3	165	3100	1.7
U-CFRP sheets	50	0.167	230	4000	1.7

Accelerated corrosion

The accelerated corrosion process included beams placed inside a tank which contained industrial salt solution NaCl of 3% concentration and then subjected to wet-dry cycles (4 weeks wet and 4 weeks dry alternately in total). The beams were also subjected to constant electric current. The current was only applied during the wetting period. Wet-dry cycles allowed for better physical representation of the natural corrosion process (taking place in most cases of practice). Detailed mapping of corrosion induced crack patterns and of their widths were also recorded at the end of each corrosion cycle. The corrosion process was terminated for measured maximum concrete crack width higher than 0.3 mm (SLS limit).

Patch repair and FRP strengthening

The damaged concrete cover could be easily removed to the level of the tensile steel reinforcement, on the whole length of the beams. Pull-off tests according to European Standard on the tensile-cracked bottom face confirmed extremely low tensile concrete strength, between 0.8-1.9 MPa (average 1.1 MPa). In-situ direct pull-off tests may serve as an efficient assessment tool in order to proceed with mortar patch repair. The exposed corroded steel bars were cleaned and corrosion products were removed by mechanical means. The corrosion inhibitor was applied with a brush onto the revealed bar and substrate and penetrated into the concrete, protecting the reinforcement by forming a protective film all around the steel surface. The application of the epoxy-cementitious bond agent layer to the repair zones followed. Then, the polymer modified cementitious mortar was applied by patching technique to form 20 mm cover.

The surface of the mortar patch was ground to expose the aggregates and then it was cleaned with a high-pressure air jet. The bottom edges of the beams' sections were rounded to a radius of about 17 mm for the application of U-CFRP wraps for shear strengthening. Beam RC-COR1S1 was strengthened in flexure with CFRP laminate on the tensile face and beam RC-COR1S2 with two CFRP NSM plates inserted into the mortar cover grooves at the tension side. The grooves had a depth of 15 mm (1.5 times the plate width) and width of 9 mm (3 times the plate thickness). The axial rigidity of FRP reinforcement was equivalent for both strengthened beams (EBR or NSM). In order to prevent shear failure caused by an increase in the beam load capacity and CFRP end debonding, each shear span was wrapped with eight U-shaped CFRP strips of 50 mm width and in two layers spaced at 50 mm (figure 1).

Test setup

The specimens were subjected to four- point monotonic loading up to failure. The load was applied using a 500 kN actuator through a spreader steel beam to the specimen (Figure 1). Four linear variable displacement transducers (LVDTs) were used to measure the load line and mid-span deflections of the beam during testing. Strain gauges were installed on the main longitudinal steel bar to measure the axial strain. For strengthened beams, three more strain gauges were installed on the CFRP laminate and the CFRP plates to measure the axial strain.

Test results and discussion

Cracking maps and corrosion crack widths

Crack patterns and widths were recorded at each cycle by visual screening and crack width detectors. One longitudinal crack was formed at the tensile bottom running parallel mainly to the middle tensile rebar and on the front and back sides of each corroded beam. Rust staining was also noted along these cracks. As corrosion proceeded, longitudinal cracks increased their width and at the end of the last corrosion cycle the maximum width of the bottom face was measured equal to 0.35 mm. On side faces the longitudinal cracks were smaller in extent and thinner in width and their maximum width was

measured equal to 0.20 mm. The cracking maps of corroded beam RC-COR1 were shown in figure 3 before testing to failure. It is also mentioned that all corroded beams presented similar crack patterns.

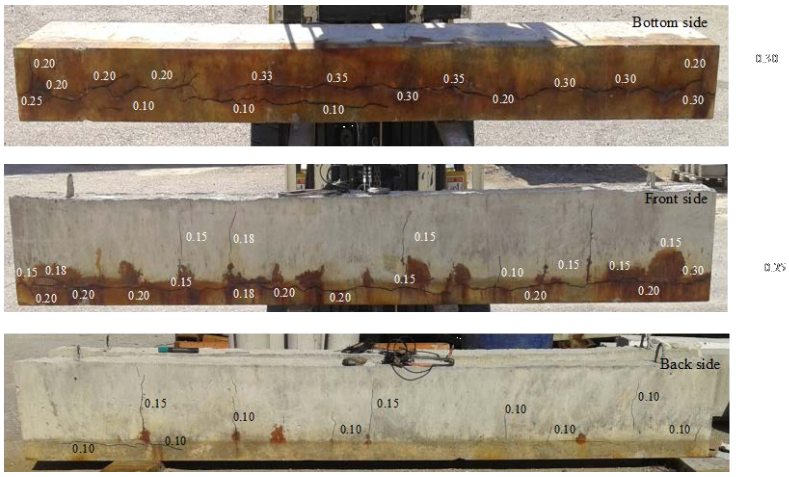

Figure 3: Crack pattern of corroded beam RC COR1 after the end of the accelerated corrosion.

Structural performance of non corroded and corroded beams

The failure mode for both non corroded RC-N and corroded RC-COR1 beams was flexural by yielding of tensile steel bars, followed by crashing of concrete in the compression zone. The load at tensile steel yielding of the corroded beam RC-COR1 (136.8 kN) was about 5.55% lower than that of the uncorroded beam (144.4 kN). The maximum bearing load of the corrode beam was 150.9 kN compared with 156.9 kN for non corroded (around 4 % lower). A slight increase in the deflection capacity of 2.45% for the corroded beam RC-COR1 was noted. The beam with the corroded steel rebars had 78.1 mm deflection at failure, while the uncorroded beam failed at a lower deflection of 76.3 mm. Figure 4a depicts the load versus midspan deflection relationship of all beams, while figure 4b shows the midspan strains on the steel versus load. Steel strains were recorded up to 0.5% strains.

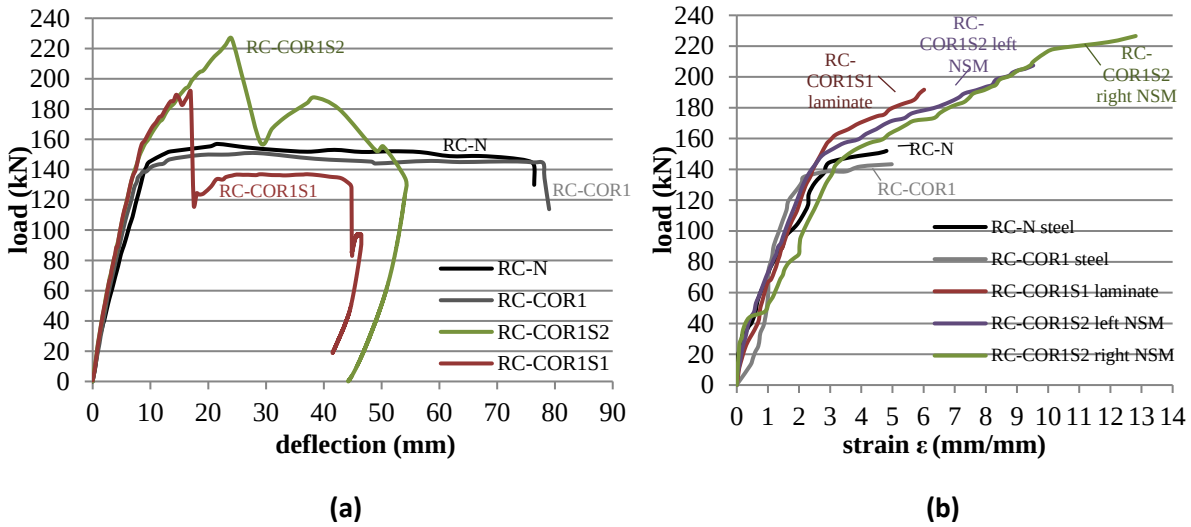

Figure 4: (a) Load-deflection curves of all beams. (b) Load-steel/carbon FRP strain curve.

For the corroded beam existing longitudinal cracks due to corrosion did not increase their width during loading. When RC-COR1 reached maximum load, a part of the concrete cover was detached from the bottom middle region of the beam as shown in figure 5. The maximum longitudinal crack due to corrosion opened from 0.35 mm to 0.40 mm. For higher beam deflections, longitudinal cracks and

flexural-shear cracks did not increase in range, while more concrete cover parts failed and the corroded reinforcement was exposed.

Figure 5: Flexural crack pattern of corroded beam RC-COR1 after testing to failure.

Structural performance of patch-repaired and FRP strengthened corroded beams

The failure mode of the patch repaired and strengthened corroded beam with EBR CFRP laminate RC-COR1S1was debonding of the flexural CFRP laminate after yielding of the tensile steel reinforcement. As presented in figure 6, CFRP laminate was detached in the middle area of the bottom face after the beam reached the maximum load. Then, intermediate debonding between the old concrete and repaired mortar layer followed and finally the compressive concrete zone crushed. The yield load (156.6 kN) presented a slight increase of about 8.4% compared to that of the uncorroded beam and 14.4% more than the corroded unstrengthened one. The maximum load of the repaired beam was 22.1% higher (191.7 kN) than that of the reference beam and 27.1% than the corroded unstrengthened beam at 17 mm deflection. The residual post debonding bearing load was limited to 130 kN up to the corresponding post debonding deflection of 44.5 mm. At post debonding failure the maximum interface longitudinal crack between old and repaired concrete was equal to 0.60. Figure 4b shows the midspan strains on FRP laminate versus load. The maximum FRP strain was equal to 0.6% at the maximum load, which corresponds to the $0.35\varepsilon_{fu}$ of the ultimate strain of the CFRP laminate. This value agrees well with the EBR FRP debonding strain calculated according to ACI 440-2R08 recommendations equal to 0.7% ($0.41\ \varepsilon_{fu}$) for high mortar strength.

Figure 6: RC-COR1S1 beam after testing to failure.

The corroded beam strengthened with 2 NSM CFRP plates (RC-COR1S2) exhibited debonding in the form of concrete cover separation, after yielding of the tensile steel bars. Intermediate debonding between the old and the new concrete substrate took place and finally concrete crushing (figure 7). Debonding at the epoxy-CFRP strips interface and localized splitting of the epoxy cover were detected after failure. The beam yielded at a load 153.3kN, 6.2% higher compared to the uncorroded beam and 12% higher compared to the corroded unstrengthened beam. When the load reached 183.6kN, a longitudinal crack in the interface between the old and the new repair mortar opened in a parallel direction, equal to 0.40 mm. This crack opened further at width of 0.60 mm when the load was equal to 198.4kN. A significant increase in the load carrying capacity and deflection when compared to the EBR strengthened beam was observed. The ultimate load at debonding was 226.6 kN, that is 18.2% higher compared to the EBR strengthened beam, 44.4% higher than the uncorroded beam and 50.2% higher than the corroded beam without FRP strengthening at 24.1 mm deflection. The new mortar cover layer enhanced the load transfer between the NSM FRP plates and the existing beam. After sudden bond loss of NSM FRP

strengthening, the residual post debonding bearing load was limited to 157.6 kN at 29.1 mm and then increased to 183.9 kN at 37.1mm deflection. However, the failure load at extensive concrete crushing was 134 kN at 54.1 mm deflection. Carbon FRP strains were also measured on the midspan of the two NSM plates (figure 4b). The strain gauge of the NSM plate placed on the left side stopped recording at a value of 0.95% which corresponds to the $0.56\varepsilon_{fu}$ of the ultimate strain of the CFRP NSM strip. The other NSM plate on the right side of the beam continued to deform and reached strain equal to 1.28% at the maximum load, which corresponds to the $0.75\varepsilon_{fu}$ of the ultimate strain of the CFRP NSM strip, which agrees well with the debonding strains according to ACI 1.19% ($0.7\varepsilon_{fu.}$). The contribution of the NSM technique in the utilization of the ultimate strain of the CFRP element is double the corresponding of the EBR technique.

Figure 7: RC-COR1S2 beam after testing to failure.

Measurements of steel mass loss on extracted bars

The tensile steel reinforcement was revealed after the testing of beam RC-COR1. Corrosion was uniform along the entire length of steel rebars, while some pitting was observed in a few parts, essentially at the flexural region of the beam. Six coupons of tensile corroded steel bars were taken out at least 150 mm long and cleaned of rust according to ASTM G1-90 standard (figure 8). The average gravimetric mass loss of coupons of the tensile bars was measured equal to $m_{grav} = 7.56\%$.

Figure 8: Corroded steel rebar.

Conclusions

The mass loss level that corresponds to maximum corrosion induced longitudinal crack width of 0.35 mm is investigated in the current paper, just failing to fulfil SLS value of 0.3 mm. This study suggests that even low mass loss levels may require removal of cracked concrete, treatment of corroded steel bars and application of repair patches in order to enable FRP strengthening and reliable and significant extension of beam residual life. Mass loss of reinforcement up to 7.5% led to marginal decrease of the flexural capacity of the beam around 4%. The force contribution at failure of 2 NSM plates was double that of the EBR with identical axial rigidity, as the measured strains at failure were 0.6% and 1.28% respectively. The EBR FRP strengthened beam exhibited 22.1% higher maximum load than the reference beam and 27.1% than the corroded one. The NSM FRP strengthened beam exhibited 44.4% higher maximum load than the reference beam and 50.2% than the corroded one. The beam strengthened with two NSM FRP strips of equivalent axial rigidity with EBR FRP laminate presented 18.2% higher load and 41.6% higher deflection than the latter.

Acknowledgements

This research was supported by the IKY (Greek State Scholarships Foundation) RESEARCH PROJECTS FOR EXCELLENCE IKY/SIEMENS. The authors wish to acknowledge the support by Sika Hellas for providing the CFRP reinforcement, filling materials (adhesive epoxy), materials for corrosion protection and mortar for the repair technique.

Key References

El Maaddawy T. and Soudki K. (2005). Carbon-Fiber-Reinforced Polymer Repair to Extend Service Life of Corroded Reinforced Concrete Beams. Journal of Composites for Construction, 9(2), 187-194.

Al-Saidy A., Al-Harthy A., Al-Jabri K., Abdul-Halim M., Al-Shidi N. (2010). Structural performance of corroded RC beams repaired with CFRP sheets. Composite Structures, 92, 1931-1938.

Xie J. and Hu R. (2012). Experimental study on rehabilitation of corrosion-damaged reinforced concrete beams with carbon fiber reinforced polymer. Construction and Building Materials, 38, 708-716.

Al-Saidy A., and Al-Jabri K..(2011). Effect of damaged concrete cover on the behavior of corroded concrete beams repaired with CFRP sheets. Composite Structures, 93, 1775-1786.

Kreit A., Al Mahmoud F., Castel A., Francois R. (2011). Repairing corroded RC beam with near-surface mounted CFRP rods. Materials and Structures, 44, 1205-1217.

Almassri B., Kreit A., Al Mahmoud F., Francois R. (2014). Mechanical behavior of corroded RC beams strengthened by NSM CFRP rods. Composites:Part B, 64, 97-107.

American Concrete Institute (ACI) (2008). Guide for the Design and Construction of Externally Bonded FRP Systems for Strengthening Concrete Structures. *ACI 440.2R-08.*

ASTM G1-90 (2002), Standard Practice for Preparing, Cleaning and Evaluating Corrosion Test Specimens. *ASTM International,* West Conshohocken, Pa., 2002, 8pp.

European Standard EN 1542: Products and systems for the protection and repair of concrete structures- Test methods- Measurement of bond strength by pull-off; English version of DIN EN 1542:1999

Fatigue Behavior and Design of Reinforced Concrete Beams Strengthened in Flexure with FRP

Barbara Charalambidi [1], Theodoros Rousakis[2], Athanasios Karabinis[3]

Introduction

The aim of the present research is the experimental and analytical investigation of the response of CFRP strengthened large scale RC beams under fatigue loading. For this purpose, beams were cast with web dimensions of 200 mm x 500 mm and 3050 mm in length. The beams were strengthened in flexure with externally bonded CFRP laminate or with NSM CFRP laminates. Two different amplitudes of cycles were investigated, simulating the service loads of a bridge beam and the maximum steel stress limit for the SLS. The available fatigue prediction models in literature provide the number of cycles to failure with respect to the steel stress range assuming indirectly a sustained load between a minimum and maximum level. The present research also aims to introduce a new analytical model for predicting the fatigue life of FRP strengthened RC beams. The parameters used are the maximum stress of tensile steel (σ_{max}) to the yielding strength (f_y) ratio, as well as the axial rigidity of longitudinal steel (k_s) and FRP (k_f) reinforcement. The predictions of the proposed model are compared against the experimental results as well as against the predictions of fatigue models in the literature.

Experimental Program

The experimental program concerned the fatigue investigation of seven reinforced concrete beams, measuring 200 mm wide x 500 mm deep x 3050 mm in length (Charalambidi et al. 2016a). Normal strength, ready-mixed concrete was used of 24.8 MPa average compressive and steel of 500 MPa nominal yield stress. The beams had internal steel reinforcement consisted of three bottom bars of 16 mm diameter and two top bars of 12 mm diameter. Stirrups of 8 mm diameter were placed in the beam as shear reinforcement, at a spacing of 290 mm. At the support regions, and for a length of 450 mm, stirrups were spaced at a distance of 50 mm (Fig. 1).

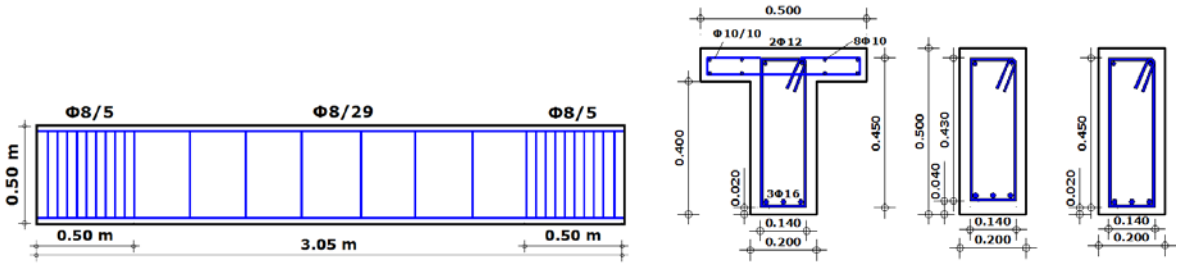

Figure 1. Concrete beam geometry, detailing of reinforcements

The specimens were strengthened for both shear and flexure. The shear strengthening was accomplished with U shaped CFRP sheets with unidirectional fibers, wrapped at the shear spans of the beams. The sheets had a reported mean tensile strength of 3500 MPa, mean modulus of elasticity of 225 GPa and 0.129 mm thickness. The flexural strengthening included two different strengthening schemes. Four beams were externally bonded with one carbon fiber laminate of 3100 MPa mean tensile strength, 165 GPa mean modulus of elasticity, 100 mm width and 1.2 mm thickness. The remaining beams were strengthened with 2 NSM CFRP laminates of 3100 MPa mean tensile strength, 165 GPa mean modulus of elasticity, 10 mm height and 3.0 mm thickness. The beams were tested under four-

[1] Democritus University of Thrace, Greece, vcharal@civil.duth.gr
[2] Democritus University of Thrace, Greece, trousak@civil.duth.gr
[3] Democritus University of Thrace, Greece, karabin@civil.duth.gr

point bending, at a constant loading frequency of 2 Hz. Two different loading amplitudes were performed. The low amplitude loading, denoted as series L (low), ranged from 20% to 60% of the design ultimate strength of the beams. This amplitude represents the ratio of live to dead design loads of a common bridge girder. The high load amplitude, denoted as series H (high), ranged from 20% of the design ultimate strength of the beam to 80% of the strength corresponding to the nominal yield stress of the longitudinal reinforcement simulating the maximum stress limit for the SLS.

Test Results

The L series beams, REX20-L and TEX20-L, successfully sustained fatigue loading reaching 2 million cycles and 1.3 million cycles and then the testing was stopped. Flexural cracks were observed at the midspan of the beams of width up to 0.20 mm. The specimens of the H series failed at less than 1.5 million cycles. The beams of H series exhibited a similar primary mode of failure due to tensile fracture of the steel reinforcement. No prior fatigue failure of the concrete cover in between the steel bar and the FRP strengthening was recorded (Charalambidi et al. 2016a). In all cases, a main crack was formed at the midspan region of the specimen. As the number of fatigue loading cycles increased, an increase of the number of cracks and of their width was observed. During the last cycles, one particular crack was much wider than the rest of the recorded cracks. This main crack indicated the region where the steel fracture occurred. Debonding of the externally bonded FRP laminate was a secondary failure mechanism of the strengthened beams in the H series, that occurred after the fatigue failure of the bar reinforcement. The debonding of the laminate initiated at the place where the wider crack occurred and expanded towards almost the whole midspan of the beam. In the cases of beams strengthened with NSMs, there was no laminate debonding observed and the laminates were kept in place, even after the fracture of the steel bars.

Figure 2. Steel failure of beam REX20-H at 990,147 fatigue cycles

Figure 3. Debonding of EBR CFRP laminate after fatigue loading (REX20-H)

The maximum and minimum applied loads, the number of the fatigue cycles, the maximum recorded load and the corresponding deflection of the beams during the fatigue tests are presented in Table 1. Beams' load – deflection response may be divided in three different phases. At the first cycles of the fatigue loading, an increase of the deflections was recorded (Curves A to B, Fig. 5a). Then, the deflections remained relatively constant (Curves B to D, Fig. 5a). At the end of the fatigue loading, during the last hundreds of cycles, beam REX20-H exhibited an abrupt increase of deflections (curve at points D-E1-E2 in Fig. 5a) and failed.

Figure 4. No debonding occurred in the case of NSM strengthened beams after fatigue loading (RNSM40-H)

Table 1: Test results, fatigue lives

Test series	Specimen	Fmax (kN)	Fmin (kN)	Cycles	Pmax (kN)	δPmax (mm)
Series L	REX20-L	126	41	2,000,000	126	5.75
	TEX20-L	128	44	1,300,000	127	9.01
Series H	REX20-H	161	41	990,147	153	21.65
	REX40-H	161	41	1,450,105	159	21.18
	RNSM20-H	150	40	807,437	147	26.79
	RNSM40-H	150	37	696,500	148	22.46
	TNSM20-H	153	44	774,411	153	22.75

The described response is typical for all the specimens in this study. The curves of midspan deflections versus number of cycles (Fig. 5b) suggest that in all cases, there was an initial increase of the midspan deflection proportional to the increase in cycles, followed by a stable region where the deflection remained relatively constant for many cycles. Then, an abrupt increase of deflection occurred decades of thousands of cycles just before failure.

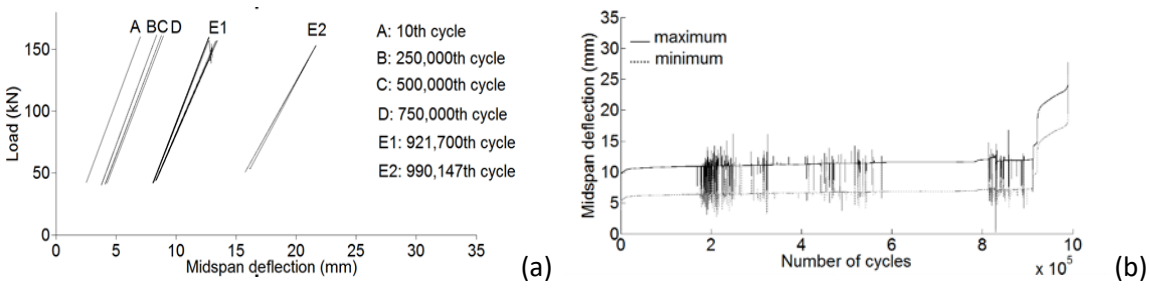

Figure 5. Load – deflection (a) and deflection – number of fatigue cycles curves of beam REX20-H

The mechanical behavior of beams is assessed through their load – deflection diagrams and diagrams of deflection vs number of cycles. The specimens of the H series achieved an ultimate deflection almost three times higher than the specimens of the L series (Fig. 6 and Table 1).

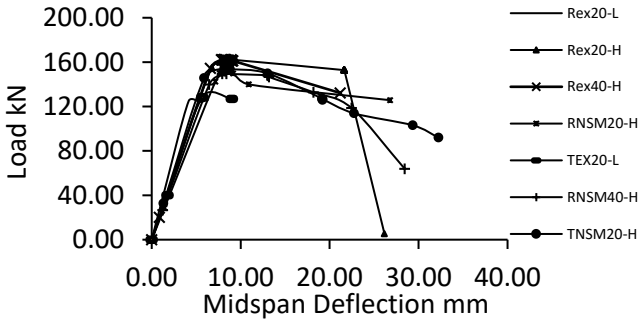

Figure 6. Load vs deflection envelops for all specimens under fatigue loading

Analytical Model

The effect of the maximum stress and the stress range of the steel reinforcement to the fatigue behavior of the reinforced concrete beams, has already been investigated by several authors (Papakonstantinou et al. 2001, Kim and Heffernan 2008 among others). ACI Committee 440.2R-08 guide, recommends stress limits for FRP strengthening under tension and concrete under compression as well as a peak reinforcing bar stress of 80% of yield strength to estimate the upper limit of fatigue loading in Serviceability Limit State (SLS). It is acknowledged by the existing literature that the critical material vulnerable to fatigue failure is steel and that stresses on steel about 60% of its yielding strength practically do not lead to fatigue failure (Papakonstantinou et al. 2001, Heffernan and Erki 2004, Gussenhoven et al. 2005, Gheorgiu et al. 2007). The available fatigue prediction models provide the number of cycles to failure with respect to the steel stress range (Helgason and Hanson 1974, Moss 1982, CEB 1990, Mallet 1991, Papakonstantinou et al. 2001, Diab and Wu 2008 among others) assuming indirectly a sustained load between a minimum and maximum level. Given the SLS design approach for steel stress limitation, the present research aims to introduce directly the ratio of maximum steel stress to the yielding strength of steel σ_{max}/f_y into the fatigue design. There is a beneficial effect from the restrictive action of the elastic strengthening material (FRP laminate) while other critical parameters remain that are not adequately addressed. In general, strengthening of the tension zone with an elastic material that does not yield, such as the FRP materials, may enhance the restrictive mechanism through constant FRP stiffness that may delay fatigue failure in steel. Therefore, besides σ_{max}/f_y, a second variable that should be taken into consideration, is the ratio of axial rigidity of the steel bars to that of the FRP reinforcement k_s / k_f, as it affects the fatigue life of RC beams. The present analytical study proposes a fatigue model that includes the effect of the yielding strength of steel as well as the effect of FRP strengthening restrictive mechanism (Charalambidi et al. 2016b). The proposed model is a $y=a \cdot x^b$ equation type. Two sets of parameters a, b are proposed to account for the effectiveness of maximum stress and yielding strength. For the determination of parameters a and b regression analysis was carried out, taking into account the yielding stress of specimens in literature. A detailed review of the analysis can be found in Charalambidi et al. (2016b). The proposed model has the following expression:

$$\frac{\sigma_{\max}}{f_y} = (0.00336 \cdot f_y + 2.383) \cdot N_{an}^{'\,(-0.00019 \cdot f_y - 0.04967)} \quad (1)$$

where σ_{max} is the maximum stress of steel, f_y is the yielding stress of steel and N is the number of cycles.

In order to include the effect of the FRP strengthening to the proposed fatigue model, a new regression analysis was designed and further improved equations are proposed that involve the ratio of axial rigidity of steel to FRP reinforcement and depend on the value of σ_{max}/f_y ratio. The model requires the calculation of the analytical number of cycles N'_{an}, of Equation 1. Then the k_s/k_f effect is included according to the different σ_{max}/f_y and the final theoretical number of cycles Ntheor is estimated. The model is modified for various σ_{max}/f_y ratios according to regression analysis of the experimental data of literature that correspond to different σ_{max}/f_y values. The final model for the estimation of N cycles to fatigue failure is cited below ($N=N_{theor}$). The proposed model is a $y=a\cdot x^b$ equation type. Two sets of parameters a, b are proposed to account for the effectiveness of maximum stress and yielding strength. For the determination of parameters a and b regression analysis was carried out, taking into account the yielding stress of specimens in literature.

$$N_{theor} = [(\frac{\sigma_{\max} / f_y}{(0.00336 \cdot f_y + 2.383)})^{(1/(-0.00019 \cdot f_y - 0.04967))}] / (0.1192 \frac{k_s}{k_f} + 0.4798) \quad (2)$$

for $0.60 \le \sigma_{max}/f_y < 0.68$,

$$N_{theor} = [(\frac{\sigma_{\max} / f_y}{(0.00336 \cdot f_y + 2.383)})^{(1/(-0.00019 \cdot f_y - 0.04967))}] / (0.00259 \frac{k_s}{k_f} + 0.91157) \quad (3)$$

for $0.68 \le \sigma_{max}/f_y < 0.78$,

$$N_{theor} = [(\frac{\sigma_{\max} / f_y}{(0.00336 \cdot f_y + 2.383)})^{(1/(-0.00019 \cdot f_y - 0.04967))}] / (0.0125 \frac{k_s}{k_f} + 1.2983) \quad (4)$$

for $\sigma_{max}/f_y \ge 0.78$

For the evaluation of the theoretical models available in the literature and of the model proposed in this paper, the criterion of the average absolute errors of the predictions for each model of the experimental data of the literature were used (Eq. 5).

$$AAE = \frac{\sum_{i=1}^{N} E_i}{N} \quad (5)$$

where the error of each theoretical prediction Ntheor over the experimental values Nexp is calculated as E as follows:

$$E(N)\% = \frac{N_{theor} - N_{\exp}}{N_{\exp}} \cdot 100 \quad (6)$$

The proposed model shows an average absolute error equal to 23.82% and an average ratio of 0.88 compared to the models provided in the literature. The performance of the proposed analytical model is presented in Table 2 and Figure 7.

Table 2: Assessment of the proposed model

	Proposed model	CEB 1990	Helgason & Hanson	Moss	Diab & Wu
AAE (%)	23.82	58.10	43.38	229.8	50.19
Average	0.88	1.02	0.90	2.74	1.12

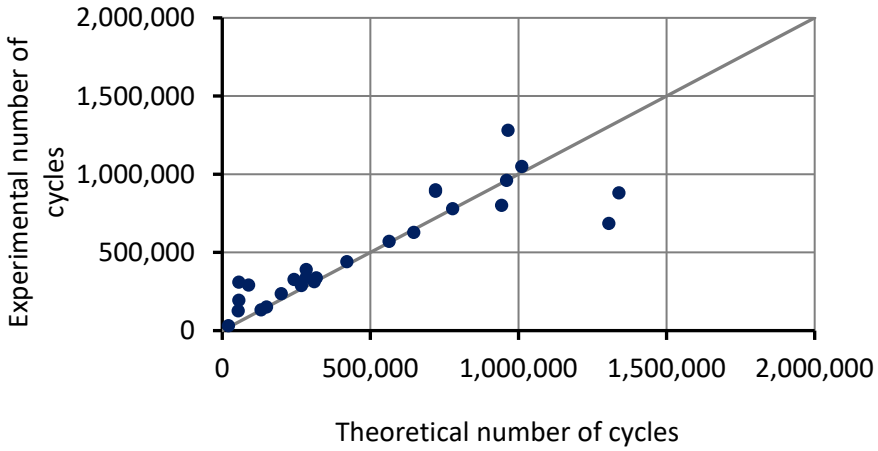

Figure 7. Performance of the proposed analytical model

Conclusions and Points for Discussions

The present study concerns the experimental and analytical investigation of reinforced concrete beams strengthened through FRP configurations. For that purpose, seven reinforced concrete beams were tested both of rectangular and T cross-section, strengthened with two different FRP techniques: externally bonded CFRP laminates and NSM CFRP laminates. The specimens were subjected to fatigue loading up to failure. In all cases of fatigue loading:

- The failure of the beams was due to tensile fracture of the steel bar reinforcement under fatigue loading.
- In the case of the externally strengthened beams with FRP laminates, the steel fracture was followed by the FRP laminate debonding.
- No debonding occurred in the cases of NSM laminate strengthening.
- An increase in deflections with the number of cycles was recorded. All specimens experienced an abrupt increase of the deflections during the last decades of thousands cycles before failure.

A fatigue design model is proposed in this study. The model estimates the number of cycles with respect to the maximum stress of the tensile steel reinforcement, the steel yielding strength and the axial rigidity of steel and FRP. The proposed model provides improved predictions compared to other existing models in the literature. It provides an absolute average error prediction equal to 23.82% and an average ratio of 0.88. Beams of steel reinforcement alone, show a variably and gradually weakened restrictive mechanism in the tension zone, under cyclic loading. Strengthening with an elastic material

that does not yield, such as the FRP, may enhance the combined restrictive mechanism through constant stiffness and suppress fatigue failure of steel under service loading. Incorporation of fy as a significant parameter for fatigue design should be further refined to better address the different post-yielding restrictive action of the steel, depending on the characteristics of its yielding plateau and of its hardening modulus. Also, previous static and fatigue loading history of the beams should be properly assessed and considered in the design.

Acknowledgements

The authors wish to thank Sika Hellas S.A. for providing the FRP materials and resins, DUTh RC Laboratory staff for the assistance in the construction, casting and preparation of the specimens and DUTh RC Laboratory and Sika Hellas S.A. staff for the assistance in the FRP implementation

Key references

American Concrete Institute (ACI) Committee 440.2R-08 (2008). “Guide for the Design and Construction of Externally Bonded FRP Systems for Strengthening Concrete Structures.” American Concrete Institute, Michigan.

Aidoo, J., Harries, K. a., & Petrou, M. F. (2004). Fatigue Behavior of Carbon Fiber Reinforced Polymer-Strengthened Reinforced Concrete Bridge Girders. Journal of Composites for Construction, 8(6), 501–509

Charalambidi B., Rousakis T., Karabinis A. (2016). Fatigue behavior of large scale reinforced concrete beams strengthened in flexure with fiber reinforced polymer laminates. Journal of Composites for Construction 2016; DOI: 10.1061/(ASCE)CC.1943-5614.0000689

Charalambidi B., Rousakis T., Karabinis A. (2016). Analysis of the fatigue behavior of reinforced concrete beams strengthened in flexure with fiber reinforced polymer laminates. Composites Part B 2016; paper accepted for publication

De Lorenzis L., Nanni A. (2002). Bond between Near-Surface Mounted FRP rods and concrete in structural strengthening. ACI Structures Journal, 99(2), 123-133

Diab H.M., Wu Z. (2008). Review of existing fatigue results of beams externally strengthened with FRP laminates. Fourth International Conference on FRP Composites in Civil Engineering (CICE2008), 22-24July 2008, Zurich, Switzerland

Ferrier E., Bigaud D., Clément J.C., Hamelin P. (2011). Fatigue-loading effect on RC beams strengthened with externally bonded FRP. Construction and Building Materials 25, 539-546

Gheorgiu C., Labossiere P., Proulx J. (2007). Response of CFRP strengthened beams under fatigue with different load amplitudes. Construction and Building Materials 21, 756-763

Gussenhoven R., Brena S.F. (2005). Fatigue Behavior of Reinforced Concrete Beams Strengthened with Different FRP Laminate Configurations. Proceedings of the Seventh Fiber Reinforced Polymers for Reinforced Concrete Structures (FRPRCS7) Conference, New Orleans, November 2005

Heffernan P.J., Erki M.A. (2004). Fatigue Behavior of Reinforced Concrete Beams Strengthened with Carbon Fiber reinforced plastic laminates. Journal of Composites for Construction. Vol.8, No 2, 132-140

Kim Y., Heffernan P. (2008). Fatigue Behavior of Externally Strengthened Concrete Beams with Fiber-Reinforced Polymers: State of the Art. Journal of Composites for Construction. Vol.12, No 3, 246-256

NCRP Report 679 (2011). Design of Concrete Structures using High-Strength Steel Reinforcement. Transportation Research Board

Papakonstantinou C.G., Petrou M.F., Harries K.A. (2001). Fatigue behavior of RC beams strengthened with GFRP sheets. Journal of Composites for Construction. 5(4), 246-253

Sena Cruz J., Barros J.A.O. (2004). Modeling of bond between near surface mounted CFRP laminate strips and concrete. Computers and Structures 82, 1513–1521

Wahab N., Soudki K.A., Topper T. (2011). Mechanics of bond fatigue behavior of concrete beams strengthened with NSM CFRP rods. . Journal of Composites for Construction. 15(6), 934-942

Wang Y.C., Lee M.G., Chen B.C. (2007). Experimental study of FRP-strengthened RC bridge girders subjected to fatigue loading. Composite Structures 81, 491-498

Williams G., Higgins C. (2008). Fatigue of diagonally cracked RC girders repaired with CFRP. Journal of Bridge Engineering. 13(1), 24-33.

3.3 Shear and Torsional Strengthening

Research on FRP at Democritus University of Thrace, Greece

C. Chalioris[1], and C. Karagiannis

The Use of FRP Jackets as Shear Reinforcement

The effectiveness of the use of externally epoxy-bonded carbon FRP sheets as external transverse reinforcement to shear critical reinforced concrete beams with rectangular and T-shaped cross-section has been investigated in the experimental works of Karayannis & Chalioris (2003) and Chalioris (2003). The following FRP retrofits were examined: FRP sheets that (i) fully wrapped around the cross-section of rectangular beams along the entire shear span, (ii) fully wrapped around the cross-section and covered only a part of the shear span, (iii) U-jacketed T-beams along the entire shear span and (iv) U-jacketed T-beams along the entire shear span with FRP anchorage using bolted steel laminates. From the experimental results it is deduced that:

- The fully wrapped rectangular beam with bonded FRP sheets at the entire length of the shear spans exhibited flexural and rather ductile response since shear diagonal cracks finally appeared at a high level of loading and deformation along with FRP rupture. On the contrary, all the other beams exhibited brittle shear failure.
- Beams strengthened with FRP sheets that cover part of the shear span exhibited significantly improved shear performance since the presence of FRP sheets inhibited the propagation of shear diagonal cracks. The effect of the FRP sheets on the increase of the shear strength is greater when the sheets were applied at the half middle parts of the shear spans of the beam, than in the case that FRP sheets were added at the end parts of the shear spans. Thus, the proposed alternative technique of shear strengthening with bonded FRP sheets that cover only a part of the shear span can be used successfully in cases that constructional problems prevent the application of FRP sheets along the entire length of the shear span of the beam.
- Epoxy-bonded carbon FRP sheets can be used to enhance the shear capacity of T- beams as externally applied shear reinforcement. However, all retrofitted T-beams exhibited shear diagonal cracks and brittle shear failure whereas premature debonding failures at the concrete – FRP sheets adhesive interface were observed. Thus, substantial reductions of the potential capabilities in shear strength were reported. The use of special anchorage of the FRP sheet using bolted steel laminates was a potential improvement to the observed premature debonding.

References

Karayannis C.G., Chalioris C.E., "*Experimental Investigation of the Contribution of Bonded C-FRP jackets to Shear Capacity of RC Beams*", Proceedings of the International Symposia "Celebrating Concrete: People and Practice", University of Dundee, Scotland, UK, Vol. Role of Concrete in Sustainable Development, pp. 689-696, Sept. 2003.

Karayannis C.G., Chalioris C.E., "*Strengthening of Shear T-beams using Carbon FRP*", Proceedings of the 1st International Conference on Concrete Repair, St- Malo, Brittany, France, Vol. 2, pp. 775-782, July 2003.

Chalioris C.E., "*Shear Performance of RC Beams using FRP Sheets Covering Part of the Shear Span*", Proceedings of the 1st International Conference on Concrete Repair, St-Malo, Brittany, France, Vol. 2, pp. 809-816, July 2003.

[1] Democritus University of Thrace, chaliori@civil.duth.gr

FRP-EBR Repairs of RC Members in Torsion

The effectiveness of the use of externally epoxy-bonded carbon FRPs as external transverse reinforcement to under-reinforced concrete beams with rectangular and flanged cross-section under torsion has been experimentally evaluated in the work of Chalioris (2008). Three different FRP configurations were examined: (i) Fully and completely wrapped rectangular beams with continuous FRP sheets along the entire length and around the cross-section of the beam (full wrapping with sheets). (ii) Completely wrapped rectangular beams with discrete FRP strips around the cross- section of the beam (wrapping with strips). (iii) U-jacketed flanged beams with FRP sheets along the entire length of the beam that were bonded on the width and on both vertical sides of the web of the T-beam (U-jacketing with sheets). Based on the test results of this research, the following concluding remarks were drawn:

- Retrofitting with epoxy-bonded carbon FRP fabrics is a feasible strengthening technique for existing under-reinforced beams under torsion. Strengthened beams using FRP sheets and strips as the only transverse reinforcement exhibited better overall torsional performance than the non-strengthened control beams.
- Full wrapping with continuous FRP sheets caused a significant increase on the ultimate torsional strength and torsional failure occurred at high levels of strength and twist along with tensile rupture of the sheets. This retrofitted scheme is far more efficient for torsional upgrading than the use of wrapping with the same volume of discrete strips.
- Failure of wrapped beams with FRP strips was partially delayed in respect to the failure of the control specimens and fibres initially prevented cracking. However, torsional diagonal cracks eventually appeared and widened in the unwrapped concrete of the beams, while fibre rupture has not been observed.
- U-jacketed flanged beams exhibited premature debonding failure at the concrete and the FRP sheet adhesive interface. Substantial reductions of the potential capability in torsional strength are reported. Despite this fact, the post-ultimate responses of the U-jacketed beams were rather smooth regarding to the steep post-cracking response of the control non-strengthened T-beam.

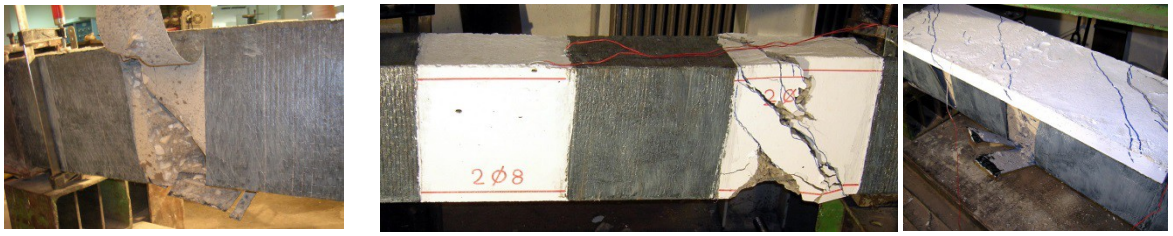

(i) Full wrapping with continuous FRP sheets

(ii) Wrapping with FRP strips

(iii) U-jacketing with FRP sheets

Figure. Crack patterns of typical beams tested under pure torsion

An analytical approach for the prediction of the torsional response of reinforced concrete beams strengthened with externally bonded FRP has been proposed by Chalioris (2007). The analysis method employs the combination of two different theoretical models; a smeared crack model for plain concrete in torsion for the elastic till the first cracking response and a properly modified truss model for the post-cracking response. The proposed method addresses the contribution of the externally bonded FRP materials to the torsional capacity of RC beams using specially developed equations in the well-known truss theory and utilizes softened and FRP-confined concrete stress-strain relationships. Verification of this model has been achieved through comparisons between analytically predicted behaviour curves and experimentally obtained ones. Further, application of this method allows for a realistic modelling of the elastic and the post-cracking response of FRP strengthened beams under torsion.

References

Chalioris C.E., "*Analytical Model for the Torsional Behaviour of Reinforced Concrete Beams Retrofitted with FRP Materials*", **Engineering Structures**, Vol. 29, No. 12, pp. 3263-3276, 2007.

Chalioris C.E., "*Torsional Strengthening of Rectangular and Flanged Beams using Carbon Fibre-Reinforced-Polymers – Experimental Study*", **Construction and Building Materials**, Vol. 22, No. 1, pp. 21-29, 2008.

Experimental Report on FRP Repairs of Beam-Column Joints

A repair and strengthening technique of beam-column joints was examined in the experimental work of Karayannis & Sirkelis (2008). Epoxy resin injections were used to repair the damaged specimens in combination with externally bonded carbon FRP sheets that were used to wrap the joint body of external beam-column connections as a confining jacketing system. Carbon FRP sheets were also used to wrap the critical regions of the beam member of the examined subassemblages providing this way for confining of these regions and ensuring a good anchorage of the FRP sheets used for the jacketing of the joint body. Further, carbon FRP sheets were also used for the confining of the critical regions of the column member of the specimens. From the observed responses and the comparisons of the initially tested specimens and the rehabilitated ones it can be deduced that the use of epoxy resin even in cases of large scale damage can restore the response of the specimens. The combination of this repair technique with the application of bonded carbon FRP sheets leads to a significant improvement of the loading capacity, the energy absorption and the ductility and finally it leads to improved type of damages comparing to the damage modes of the specimens during the initial loading. It is emphasized that the observed damages in FRP retrofitted specimens concentrated away from the joint area near the end of the FRP strengthened region.

Reference

Karayannis C.G., Sirkelis G.M., "*Strengthening and Rehabilitation of RC Beam- Column Joints Using Carbon-FRP Jacketing and Epoxy Resin Injection*", Earthquake Engineering and Structural Dynamics, Vol. 37, No. 5, pp. 769-790, 2008.

Cyclic response of shear critical RC columns strengthened with CFRP strips

M. Del Zoppo[1], M. Di Ludovico[2], A. Balsamo[3], A. Prota3[4], G. Manfredi[5]

[1] Department of Engineering, University of Naples "Parthenope", ITALY.

[2,3,4,5] *Department of Structures for Engineering and Architecture, University of Naples "Federico II", ITALY.*

Abstract

To reduce the vulnerability of substandard RC members to shear failures, the use of carbon fibres (CFRP) discontinuous strips has been recognized as a reliable method for increasing the member's capacity. However, the experimental studies on RC columns subjected to compressive axial load and cyclic horizontal displacements are still lacking.
The present experimental research aims at investigating the effectiveness of CFRP strengthening system on shear critical short RC columns (i.e. Ls/h = 3). In particular, three RC columns with square cross-section and governed by shear mode were analysed: one reference column, termed "as built" in the following, and two columns externally reinforced with one and two plies of CFRP strips, respectively. The columns have been strengthened using a discontinuous wrapping along their entire length. The specimens were cantilevers loaded with a low compressive axial load and subjected to cyclic horizontal displacements. The responses of the columns have been analysed in terms of failure modes and increased strength and deformation capacity in case of one and two layers of external CFRP wrapping.

Introduction

The high vulnerability of existing RC structures even to moderate seismic events has been confirmed from recent post-earthquake surveys. Indeed, the lack of a proper seismic detailing typical of such members could lead to brittle failures due to shear before the flexural yielding, especially in case of short members. After L'Aquila earthquake (Italy - 2009, magnitude 6.3), thousands of RC buildings resulted heavily damaged, with significant damage at both structural and non-structural components (Di Ludovico et al. 2016a,b). In many of those heavy damaged RC buildings, the columns showed brittle failures due to the shear actions (Del Zoppo et al. 2016,a), see Figure 1. However, a few experimental studies have been developed on RC columns subjected to compressive axial load and cyclic horizontal displacements (Priestley et al. 1997, Ye et al. 2002, Colomb et al. 2007). Thus an experimental research has been carried out to investigate the effectiveness of CFRP strengthening system on shear critical short RC columns (i.e. Ls/h = 3).

[1] Department of Engineering, University of Naples "Parthenope", ITALY. (E-mail: <marta.delzoppo@uniparthenope.it>)
[2] Department of Structures for Engineering and Architecture, University of Naples "Federico II", ITALY. (E-mail: diludovi@unina.it)
[3] Department of Structures for Engineering and Architecture, University of Naples "Federico II", ITALY. (E-mail: albalsam@unina.it)
[4] Department of Structures for Engineering and Architecture, University of Naples "Federico II", ITALY. (E-mail: <aprota@unina.it>)
[5] Department of Structures for Engineering and Architecture, University of Naples "Federico II", ITALY. (E-mail: <gamanfre@unina.it>)

Figure 1: Damaged columns from L'Aquila earthquake (Del Zoppo et al. 2016,a)

Experimental program

Four short RC columns were designed with geometric properties and reinforcement detailing as depicted in Figure 2. Each specimen had a square cross-section 300 x 300 mm reinforced with ten 22 mm diameter deformed bars (longitudinal geometrical reinforcement ratio, ρ_l = 4.2%).

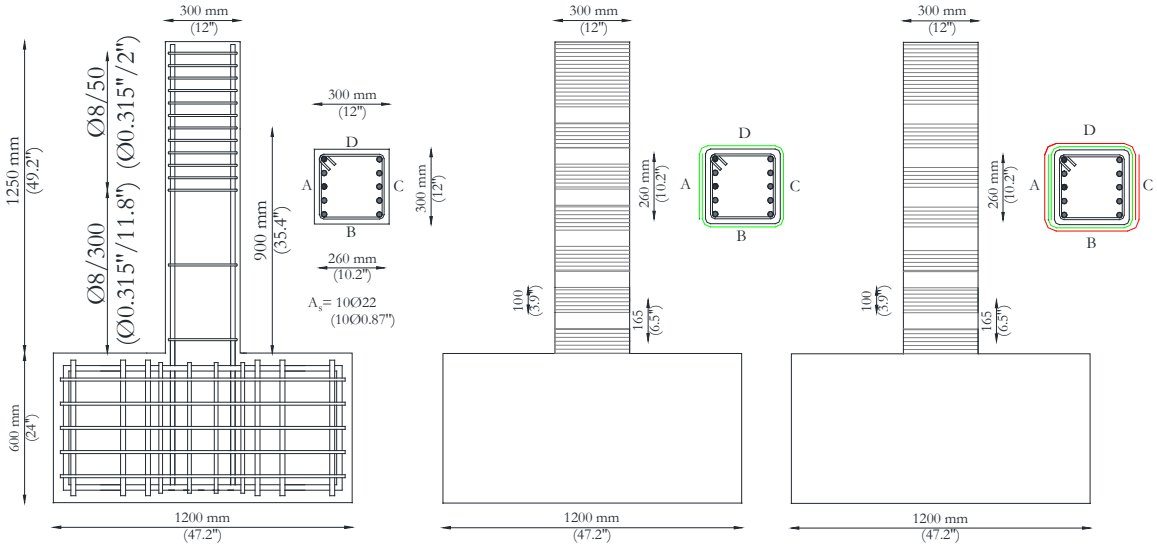

Figure 2: Experimental program

Transverse reinforcement was made of 8 mm diameter ties, spaced at 300 mm apart (transverse geometrical reinforcement ratio, ρ_w = 0.11%) and with hooked ends. A reduced spacing has been adopted in the zone of load application to avoid localized damages.
The lateral load is applied at a distance of 900 mm from the foundation block, in order to simulate the behavior of short columns [i.e. Ls/h = 3 with shear length Ls = 900 mm (35.43 in.)]. The four columns were over-designed for flexure, in order to achieve a brittle failure governed by the shear.
Two specimens were used as control (specimens A1 and B1) and the other two were strengthened with one (specimen A2) or two plies (specimen B2) of discontinuous uniaxial CFRP strips with fibres perpendicular to the column longitudinal axis. The CFRP strips, width w_f = 100 mm, were spaced at s_f = 165 mm. The external reinforcement was extended for the total height of the column. The radius of rounded corners is R = 20 mm.
The specimens were subjected to normalized compressive axial load ($v = N / A_c f_{cm}$, where N is the compressive axial load, Ac is the concrete gross area) equal to 0.1 and horizontal cyclic displacements.

Table 1: Description of the experimental program

Specimen	f_{cm} *(MPa)*	f_{yw} *(MPa)*	N° of CFRP plies	CFRP Young Modulus *(GPa)*	CFRP Ultimate strain *(%)*	CFRP Ultimate strength (MPa)	Thickness of composite system (mm)
A1	14.3	525	-	-	-	-	-
A2	16.2		1	85.4	1.23	1050	0.864
B1	23.9		-	-	-	-	-
B2	32.3		2	85.4	1.23	1050	0.864

Mechanical properties of materials

Two classes of concrete have been adopted: low compressive strength for specimens A1 and A2 and medium compressive strength for specimens B1 and B2. The average compressive strength were f_{cm} = 14.3 MPa and f_{cm} = 16.2 MPa for columns A1 and A2, and f_{cm} = 23.9 MPa and f_{cm} = 32.3 MPa for columns B1 and B2, respectively. The same class of steel has been used for all the columns: average yielding strength f_{ym} = 525 MPa. The tensile modulus and strain corresponding to minimum ultimate strength of the composite system provided by the manufacturer were E_f = 85.4 GPa and ε_{fu} = 1.23%, respectively. The CFRP sheet unit weight was 600 g/m^2. The mechanical properties are summarized in Table 1.

Test results

The force-drift relationships are reported in Figure 3 for all specimens. The main test results, in terms of observed failure mode, peak force and ultimate drift (assumed at a strength degradation of 20%) are summarized in Table 2. A further description of the experimental results can be found in Balsamo et al. 2016 and Del Zoppo et al. 2016,b.

Table 2: Main test results

Specimen	Failure mode	Peak force *(kN)*	Ultimate drift *(%)*
A1	shear	159.6	2.9
		-151.8	-2.8
A2	shear	249.9	6.2
		-253.0	-6.0
B1	shear	188.9	2.7
		-191.0	-2.5
B2	Flexure-shear	308.3	8.5
		-300.6	-8.0

Specimens A1 and A2:

The control specimen A1 reached a peak force F_{max} = +159.6 kN (-151.8 kN) in the positive (and negative) direction. The ultimate drift has been assumed equal to $\Delta_{0.8Fmax}$ = + 2.9% (-2.8%), corresponding to a strength degradation of 20% (i.e. a lateral force lower than 80% of the maximum one). The specimen exhibited a shear failure, with crushing of the concrete strut.
Both strength and drift capacity have been increased for the specimen strengthened with one ply of CFRP strips (A2). Indeed, the experimental peak force was F_{max} = +249.9 kN (-253.0 kN) in the positive (and negative) direction. The ultimate conventional drift, corresponding to a strength degradation of 20%, was significantly greater than in the case of A1 test and equal to $\Delta_{0.8Fmax}$ = + 6.2% (-6.0%). If compared with the "as built" specimen, the external reinforcement provided a strength enhancement of 56% and a drift enhancement of 114%. In this case, the concrete governed the brittle failure mode, since no failure or debonding were observed in the CFRP strips.

Specimens B1 and B2:

The control specimen with a medium compressive strength B1 achieved a peak force F_{max} = +188.9 kN (-191.0 kN) in the positive (and negative) direction. The conventional ultimate drift was $\Delta_{0.8Fmax}$ = + 2.7% (-2.5%), corresponding to a strength degradation of 20% (i.e. a lateral force lower than 80% of the maximum one). As expected, specimen B1 exhibited a shear failure, governed by the crushing of the concrete strut.

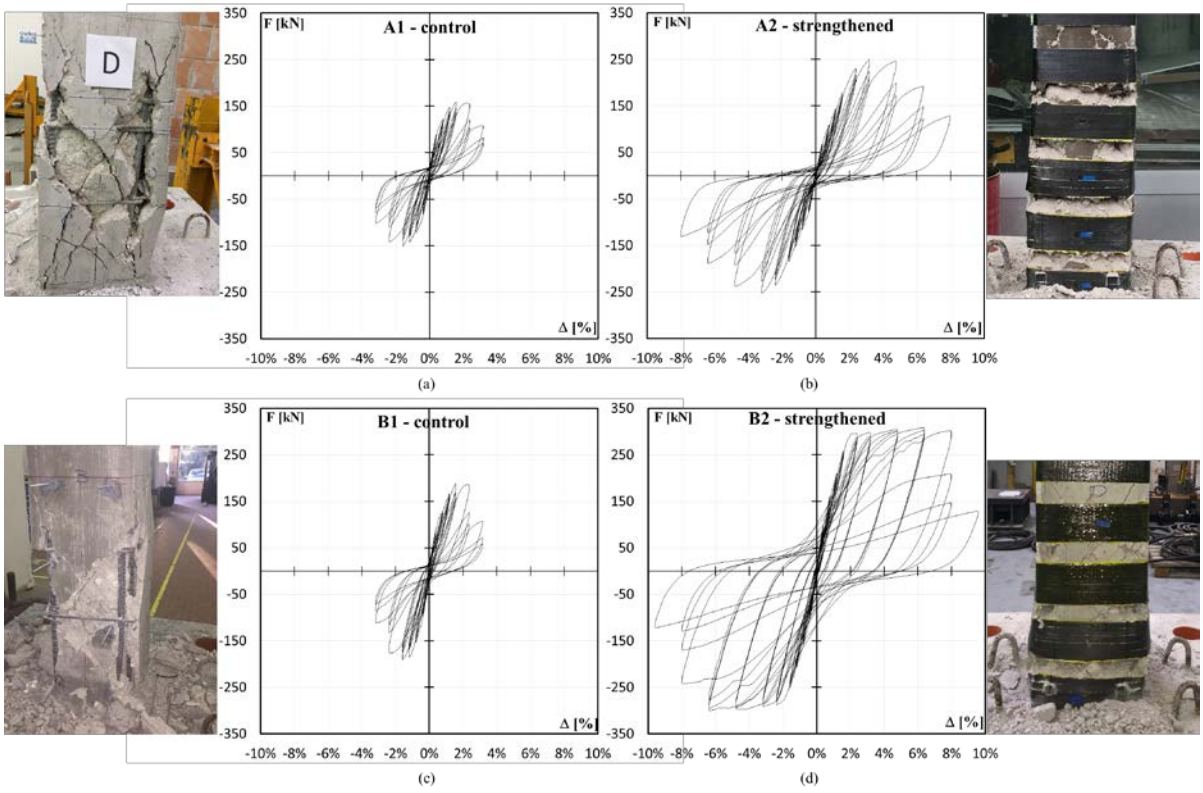

Figure 2: Force-drift relationships for specimen A1 (a), A2 (b), B1 (c) and B2 (d).

The recorded peak forces for specimen B2, strengthened with two plies of CFRP, was F_{max} = +308.3 kN (-300.6 kN) in the positive (and negative) direction, whereas the conventional ultimate drift achieved values

of $\Delta_{0.8Fmax}$ = + 8.5% (-8.0%). The specimen B2 attained large plastic deformations, probably due to the better concrete quality and to the confinement effect given by a higher amount of fibres, before the failure governed by the concrete. Indeed, no failure or debonding were observed in the CFRP strips. It should be noted that the external wrapping with two plies of CFRP changed the failure mode of the specimen from brittle to quasi-ductile (i.e. flexure-shear failure).

CFRP strain profiles

The effective strain on the CFRP strips due to combined shear action and concrete lateral dilatation has been investigated. The CFRP strains were measured by means of strain gauges located at mid-span and mid-height of each side of the first four strips for both specimens A2 and B2. The layout of strain gauges on CFRP strips is shown in Figure 4. The ratio between CFRP effective strain, ε_f, and nominal ultimate strain, ε_{fu}, is presented as a function of the column height, H, for different levels of drift Δ in Figure 4 for specimen A2. The CFRP strains were plotted at each peak drift imposed by the load protocol up to the drift after the column conventional failure.

The carbon fibers effective strain recorded on the four sides of the specimen A2 resulted quite uniformly distributed. Indeed, the fibers axial strains achieved 40% of the nominal strain at failure ε_{fu} along each side of the column. A singular peak strain of 75% was observed on the second CFRP strip of one side parallel to the shear action, probably due to a stress concentration near a concrete crack. Nonetheless, it should be noted that the strain profiles related to the second and third strips achieved greater axial strains with respect to the first and forth strips.

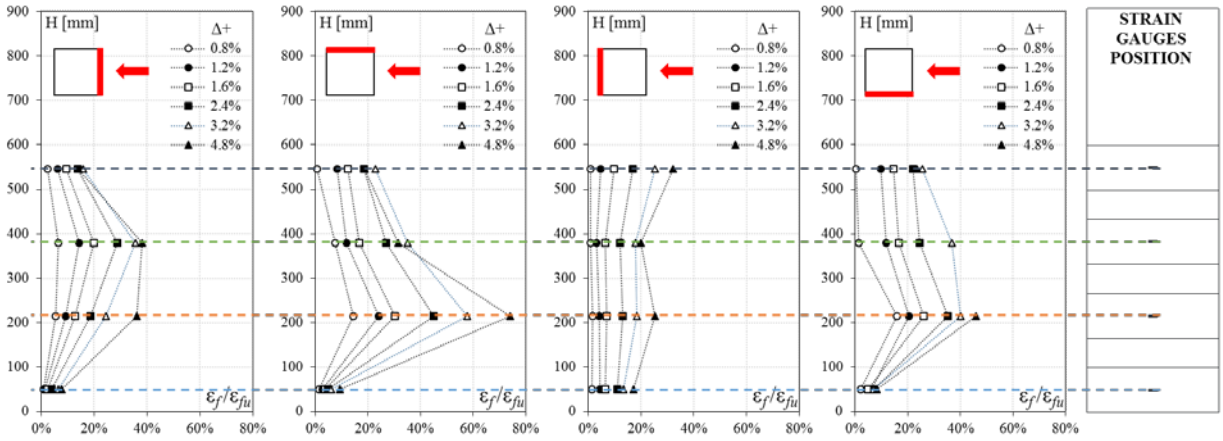

Figure 4: Strain profiles for specimen A2.

Conclusions

The results of the experimental program carried out on four short columns (Ls/h = 3), two control specimens and two strengthened with discontinuous CFRP strips, subjected to load reversal have been presented and discussed. The external reinforcement increased significantly both strength and deformation capacity of tested members. In particular, the specimen A2 characterized by low concrete compressive strength and strengthened with one ply of CFRP strips increased its strength capacity of +56% and its deformation capacity of 114%. Conversely, the specimen B2 characterized by medium concrete compressive strength and strengthened with two plies of CFRP strips increased its strength capacity of +63% and its deformation capacity of 215%. Moreover, for specimen B2 the external wrapping modified the failure mode from brittle to a quasi-ductile one, with large inelastic deformations attained before the failure.

Analysing the distribution of CFRP axial strains along the cross-section perimeters, recorded by means of strain gauges, a uniform distribution of stress/strain along the four sides has been recognized in both

specimens tested in the strengthened configuration. CFRP strain peaks were achieved when the fibres cross the concrete diagonal cracks developed on the sides parallel to the shear action.

Acknowledgements

This study was performed in the Framework of PE 2014-2016; joint program DPC-Reluis Task 1.2: Seismic capacity of r.c. structural members: beams, columns, beam-column joints and shear walls.

References

Colomb, F., Tobbi, H., Ferrier, E., Hamelin, P. (2008). Seismic retrofit of reinforced concrete short columns by CFRP materials. *Composite Structures*, 82(4), 475-487.

Balsamo A., Del Zoppo M., Pisapia D., Di Ludovico M., Morandini G., Prota A., (2016) “Experimental behavior of FRP strengthened RC columns governed by flexure or shear failure”, International Workshop on RC FRP seismic retrofitting, 19-20 September 2016, Lyon (France).
Del Zoppo M., Di Ludovico M., Prota A., Manfredi, G., (2016). Shear failure of existing r.c. columns under seismic actions. Italian Concrete Days (Rome – Italy - Oct. 27th – 28th 016).

Del Zoppo M., Di Ludovico M., Balsamo A., Prota A., (2016). Experimental response of CFRP strengthened short RC columns governed by shear failure”, IV Edition of the Workshop on the New Boundaries of Structural Concrete (Capri – Italy - Sept. 29th – Oct. 1st2016), code E3, pp. 263-270.

Di Ludovico, M., Prota, A., Moroni, C., Manfredi, G., Dolce, M., (2016). Reconstruction process of damaged residential buildings outside historical centres after the L’Aquila earthquake: part I—"light damage" reconstruction. *Bulletin of Earthquake Engineering*, 44 (10): 1539-1557, DOI 10.1007/s10518-016-9877-8

Di Ludovico M., Prota A., Moroni C., Manfredi G., Dolce M., (2016), “Reconstruction process of damaged residential buildings outside historical centres after the L'aquila earthquake - part II: "heavy damage" reconstruction ", *Bulletin of Earthquake Engineering*, DOI 10.1007/s10518-016-9979-3..

Seible, F., Priestley, M. N., Hegemier, G. A., Innamorato, D. (1997). Seismic retrofit of RC columns with continuous carbon fiber jackets. *Journal of composites for construction*, 1(2), 52-62.

Ye, L., Yue, Q., Zhao, S., Li, Q. (2002). Shear strength of reinforced concrete columns strengthened with carbon-fiber-reinforcebd plastic sheet. *Journal of Structural Engineering*, 128(12), 1527-1534.

3.4 Confinement

Use of Composites in Strengthening Reinforced Concrete Structures

I. Balafas, Instructor, Dept. Civil & Env. Eng., University of Cyprus, Cyprus, ibalafas@ucy.ac.cy
S.P. Tastani, Lecturer, Civil Eng. Dept., Democritus Univ. of Thrace, Greece, stastani@civil.duth.gr
S.J. Pantazopoulou, Dept. Civil & Env. Eng., University of Cyprus, Cyprus, pantazopoulou.stavroula@ucy.ac.cy

General Aspects

Concrete in compression cannot fail unless the material volume is free to expand laterally. When concrete is restraint laterally then failure is postponed and consequently strength and strain capacities are enhanced. This enhancement is a function of stiffness and strength and strain capacity of the restraint.

The adequacy of FRPs as a lateral restraint material has been proved through experiments from early eighties. FRPs in the forms of jackets are wrapped laterally on the surface of concrete elements, restraining the natural tendency of concrete to expand and damage can be accumulated in the form of internal cracking. Initially, unreinforced cylindrical or prismatic specimens either wrapped with FRP jackets, or encased in FRP-tubes were studied in compression. Variables such as: the type of the composite, the orientation of fibers, the number of layers, the arrangement of wraps in strips, the cross sectional geometry of the specimen, the chamfering radius at the corners od specimens with orthogonal cross sections, the concrete quality and the mode of loading (monotonic or cyclic) were investigated. Later, the research was extended to include the confinement effectiveness in reinforced concrete members due to the need to retrofit existing brittle construction after the occurrence of significant earthquakes worldwide. For this reason, most of the experimental studies in this area focused into lightly reinforced columns with widely spaced stirrups.

Most of the confinement models published in the literature have been derived and calibrated with data obtained from tests of cylinders and prisms under uniaxial compression. Tested specimens have relatively small aspect ratios (height to section size around 2), dictated as a rule by the test space of compression frames. But, even if the aspect ratios of the specimens could resemble those of actual columns, it has to be emphasized that all published tests of this type correspond to single point on the axial load/bending moment interaction diagram, that of concentric compression, marked by the red circle on Fig. 1, whereas the region of design interest in marked by the green line on the Figure. This is an important disclaimer to be recalled of, when confinement models are used in order to analyze usual columns, where the axial load / flexural moment combinations lie below the point of balanced failure (axial load ratio $N/A_g f_{co}<0.4$).

The research has exposed that the lateral presence of FRPs on concrete exhibits:

(a) a relatively mild increase of confined concrete strength over that of unconfined concrete owing to the passive nature of the confining action,

(b) an impressive increase of axial strain capacity (i.e. the range of deformation that may be developed without significant loss of strength).

(c) Significant shear strength increase, and clamping action that effectively confines jacketed lap splices of column longitudinal reinforcement in tension, as well as lateral restraint against buckling of embedded longitudinal reinforcement in compression, enhanced bond in confined

anchorages, significant enhancement of displacement and rotational ductility, and postponement of undesirable brittle modes of failure.

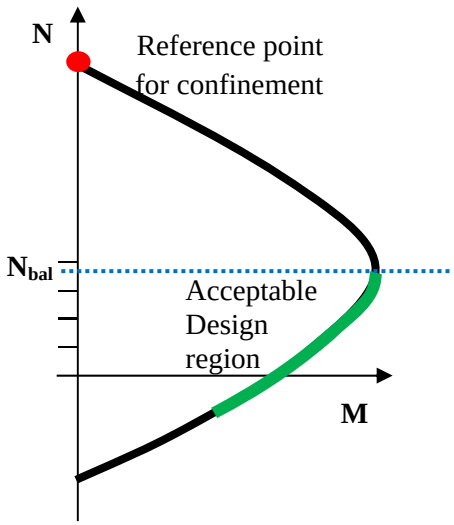

Figure 1: Axial Load – Flexural Moment Interaction Diagram of typical column

The jackets are also proved to be most effective in circular plain concrete specimens. Jacket effectiveness is progressively lower in specimens with: (i) Square sections, where strain concentrations at the corners induce local jacket rupture thereby limiting the axial strain capacity of encased concrete; (ii) Orthogonal sections, as in these cases, the confinement effectiveness is reduced with increasing aspect ratio of the cross section, tending to a negligible contribution in terms of enhancement of concrete compressive strength in wall-like cross sections. (iii) Hollow sections; in these sections, the interior opening enables some degree of radial dilation thereby partly relieving the restraint to volumetric expansion that gives rise to passive lateral confining stress.

FRP confinement effectiveness is reduced on specimens already reinforced longitudinally and transversely; particularly when transverse stirrup details are non-conforming with modern standards or are corroded. Jacket failure by rupture in compressed wrapped reinforced concrete members is often attributed to longitudinal bar buckling that occurs over the unsupported length between one or more stirrup spacings. Failure is then caused by disintegration of the encased concrete column. However, there are reported occasions where jacketed reinforced concrete columns have attained similar levels of strain capacity as identical unreinforced jacketed specimens. Hence, there are cases where the presence of FRP jacketing suppresses bar buckling, whereas in others it prevails, thereby threatening the safety of the rehabilitation scheme. It is therefore essential, within the framework of performance-based strengthening, that FRP jacketing design details (number of layers, arrangement and material chosen) be linked explicitly to the targeted deformation capacity of the strengthened member, by consistently sorting through all the possible modes of failure of the application. The passive confining pressure imparted by FRP jackets is a continuous phenomenon, linearly increasing with the axial stiffness of the jacket (quantified as the product of the jacket thickness and its modulus of Elasticity) and inversely proportional to the dimensions of the confined member's cross section. Thus, a feasible design objective would be to define a critical value for the FRP confining pressure such that the retrofit scheme may fundamentally alter the structural response of lightly reinforced concrete members from brittle to ductile by suppressing or postponing undesirable modes of failure.

Chapter outline

This chapter will review the issues of confinement in plain and reinforced concrete under concentric compression. It will also summarize the state of the art regarding the available confinement models for strength and the stress-strain behavior of encased confined concrete, and the corresponding magnitude of dependable strain capacity. Table 1 gives a sample of strength and strain prediction models available in the literature.

Table 1: A sample of models for FRP confined concrete strength and strain capacity.

Source	Strength capacity	Strain capacity
Fardis & Kahalili (1982)	$\bar{f}_{cc} = 1 + 4.1 \cdot \bar{f}_{lat}$ and $\bar{f}_{cc} = 1 + 3.7 \cdot \bar{f}_{lat}^{0.86}$; $f_{lat}=2f_{fu}nt_f/D$	$\varepsilon_{cc} = \varepsilon_{co} + 0.001 \frac{E_f n t_f}{f_{co} D}$
Mirmiran & Shahawy (1997)	$\bar{f}_{cc} = 1 + 4.269 \cdot (f_{lat}^{0.59} / f_{c,o})$	N.A.
Karbhari & Gao (1997)	$\bar{f}_{cc} = 1 + 2.1 \cdot \bar{f}_{lat}^{0.87}$	$\varepsilon_{cc} = \varepsilon_{co} + 0.01 \bar{f}_{lat}$
Kono et al. (1998)	$\bar{f}_{cc} = 1 + 0.0572 \cdot f_{lat}$	$\varepsilon_{cc} = \varepsilon_{co}\left(1 + 0.14 \frac{4t_f \cdot f_f}{D}\right)$
Spoelstra & Monti (1999)	$\bar{f}_{cc} = 0.2 + 3 \cdot \bar{f}_{lat}^{0.5}$	$\varepsilon_{cu} = 0.004 + 1.4 \frac{\rho_f f_{fu} \varepsilon_{fu}}{f_{cc}}$ $\varepsilon_{cu} = \varepsilon_{co}(2 + 1.25 \frac{E_c}{f_{cc}} \varepsilon_{fu} \bar{f}_{lat}^{0.5})$
Toutanji (1999)	$\bar{f}_{cc} = 1 + 3.5 \cdot \bar{f}_{lat}^{0.85}$ $E_1 = 10200 f_{co}^{1/3}$; $E_2 = 0.272\left(\frac{f_{co}}{\varepsilon_{co}}\right)$	$\varepsilon_{cu} = \varepsilon_{co} \cdot \left[1 + k_2 \cdot \left(\frac{f_{cc}}{f_{co}} - 1\right)\right]$; $k_2 = 310.57 \varepsilon_{fu} + 1.9$
Xiao & Wu (2010)	$\bar{f}_{cc} = 1 + 3.24 \cdot \bar{f}_{lat}^{0.8}$;	$\varepsilon_{cc} = \varepsilon_{co}\left[1 + 17.4 \bar{f}_{lat}^{1.05}\right]$
Campione & Miraglia (2003)	$\bar{f}_{cc} = 1 + 2 \cdot \bar{f}_{lat}$	
Ilki & Kumbasar (2003)	$\bar{f}_{cc} = \alpha\left[1 + 2.23 \cdot \bar{f}_{lat}\right]$; $a=8$ for circular. Also, $\bar{f}_{cc} = \alpha\left[1 + 2.29 \cdot \bar{f}_{lat}^{0.87}\right]$, $f_{lat} = 0.5 k_\alpha \rho_f f_f$	$\varepsilon_{cc} = \varepsilon_{co}\left[1 + 15 \bar{f}_{lat}^{0.75}\right]$
Matthys et al. (2005)	$\bar{f}_{cc} = 1 + 2.3 \cdot \bar{f}_{lat}^{0.85}$; $\varepsilon_f^{eff} \approx 0.6 \varepsilon_{fu}$	$\varepsilon_{cu} = \varepsilon_{co} \cdot \left[1 + k_2 \cdot \left(\bar{f}_{cc} - 1\right)\right]$; $k_2 = 310.57 \varepsilon_{fu} + 1.9$
Kumutha et al. (2007)	$\bar{f}_{cc} = 1 + 0.93 \cdot \bar{f}_{lat}$	
Tastani et al. (2006)	$\bar{f}_{cc} = 1 + 3.1 \cdot \bar{f}_{lat}$	$\varepsilon_{cc} = \varepsilon_{co} \cdot \left(1 + 15 \bar{f}_{lat}\right)$ $\varepsilon_{cc,\mu} = \varepsilon_{cu} + 0.15 \cdot \left(\bar{f}_{lat} - 0.05\right)$
Vintzileou & Panagiotidou (2008)	$\bar{f}_{cc} = 1 + 2.8 \cdot \bar{f}_{lat}$; $\bar{f}_{lat} = 0.5 k_f \omega_w$ $\omega_w = (4t_j / d) \cdot (f_{je} / f_{co})$; $f_{je} = f_j n^{-1/4}$ (n: number of FRP layers)	$\varepsilon_{cc,\mu} = \gamma_f \cdot \left(0.003 \cdot \left(\bar{f}_{cc}\right)^2\right)$; $\gamma_{f-GFRP} = 1.15$; $\gamma_{f-CFRP} = 1.95$
Wu et al. (2009)	$\bar{f}_{cc} = 1 + 2.2 \cdot \bar{f}_{lat}^{0.94}$ / $\bar{f}_{cc} = 1 + 3.2 \cdot \bar{f}_{lat}$ (AFRP)	N.A./ $\varepsilon_{cu} = \varepsilon_{co} \cdot \left(1 + 9.5 \bar{f}_{lat}\right)$ (AFRP)
Lam & Teng (2003)	$\bar{f}_{cc} = 1 + 3.3 \cdot \bar{f}_{lat}$ for $\bar{f}_{lat} \geq 0.07$; $\bar{f}_{cc} = 1$ for $\bar{f}_{lat} < 0.07$; $\varepsilon_f^{eff} = k_e \cdot \varepsilon_{fu}$ $k_{e-CFRP}=0.586$, $k_{e-GFRP}=0.624$, & $k_{e-AFRP}=0.85$	$\varepsilon_{cc} = \varepsilon_{co}\left[1.75 + 6.5 \cdot \left(\frac{E_f}{f_{co}/\varepsilon_{co}}\right)^{0.8} \left(\frac{\varepsilon_{f,rupt}}{\varepsilon_{co}}\right)^{1.45}\right]$
Teng et al. (2009)	$\bar{f}_{cc} = 1 + 3.5 \cdot (\rho_k - 0.01) \cdot \rho_\varepsilon \geq 1$; $\varepsilon_{je} = 0.586 \varepsilon_{fu}$ $\rho_k = 2E_j t_j \varepsilon_{co} / (d \cdot f_{co})$; $\rho_\varepsilon = \varepsilon_{je} / \varepsilon_{co}$;	$\varepsilon_{cu} = \left[0.0033 + 0.6 \left(\frac{E_f}{f_{co}}\right)^{0.8} \cdot \left(\varepsilon_{f,rupt}\right)^{1.45}\right]$
Albanesi et al. (2007) Jiang and Teng (2007)	$\bar{f}_{cc} = 1 + 3.609 \bar{f}_{lat}$	$\varepsilon_{cu} = \varepsilon_{co} \cdot \left(1 + 18 \bar{f}_{lat}\right)$

Source	Strength capacity	Strain capacity
	$\bar{f}_{cc} = 1 + 3.5\bar{f}_{lat}$	$\varepsilon_{cc} = \varepsilon_{co} \cdot \left(1 + 17.5\bar{f}_{lat}^{1.2}\right)$
Girgin (2009)	$\bar{f}_{cc} = \bar{f}_{lat} + \sqrt{s + m\bar{f}_{lat}}$; $s = 1;\ m = \begin{cases} 2.9 \text{ for } f_{co} < 20MPa \\ 6.34 - 0.076 f_{co} \text{ for } 20 < f_{co} < 82MPa \\ 0.1 \text{ for } 82 < f_{co} < 108MPa \end{cases}$	N.A.
Wu & Zhou (2010)	$\bar{f}_{cc} = \bar{f}_{lat} + \sqrt{\left(\frac{16.7}{f_{co}^{0.42}} - \frac{f_{co}^{0.42}}{16.7}\right) \cdot \bar{f}_{lat} + 1}$	N.A.
Fahmy & Wu (2010)	$E_2 = m_2 \cdot \left(245.61 f_{co}^{m1} + 0.6728 E_f\right)$ $f_{cc} = f_{co} + k_1 f_{lat};\ \ k_1 = a f_{lat}^{-0.3};$ $a = 4.5, m_1 = 0.5, m_2 = 0.83 \text{ if } f_{co} \le 40MPa,$ $a = 3.75, m_1 = 0.2, m_2 = 1.73 \text{ otherwise}$	$\varepsilon_{cu} = \frac{f_{cc} - f_{co}}{E_2}$

The mechanisms of confinement failure will be debated. The evolution of Poissons's effects under low and high confinement (Figure 2) and the ensuing material compaction at high confining pressures (plastification) will be presented.

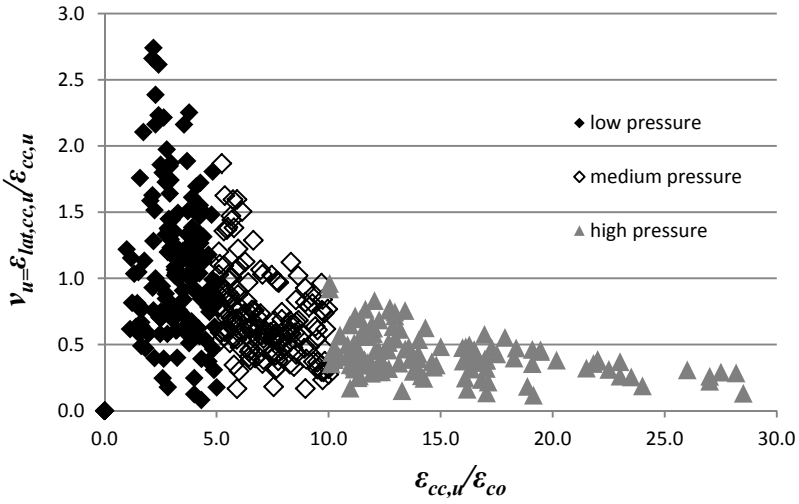

Figure 2: Apparent Poisson ratio versus axial strain ductility at failure.

The effects of stress concentrations near corners (Figure 3a), the effectiveness of layers and influence of adhesive, other scale effects and the influence of specimen morphology on mechanical behavior will also be outlined. The strain at the initiation of layer detachment from its substrate as a result of bond failure is controlled by the bond characteristics of the substrate, that is the shear strength of the adhesive and the associated slip value. Thickness and the mechanical properties of the resin layers are crucial parameters (Figure 3b). The details of the resin adopted in tests will be collected in an already built database.

Next, the chapter concentrates on the effects of embedded reinforcement both longitudinal and transverse. Experimental data shows reduced efficiency of FRPs on plain rather than reinforced members; this is due to bar buckling that occurs in the unsupported length between successive stirrups. This failure pattern is characterized by disintegration of cover and core concrete with abrupt reduction of the strength load (Figure 4). However, there are contradictive experimental observations published in the literature. In some studies failure is

reported due to FRP jacket rupture induced by the buckled compression bars. However in others the premature buckling is averted because the passive pressure exerted by the composite offer supports the bars against buckling (Pantazopoulou 2001).

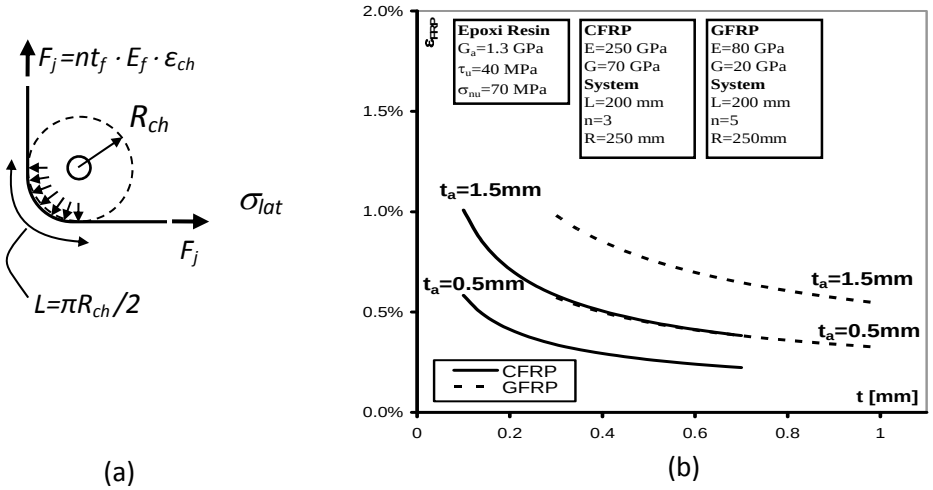

Figure 3: (a) Influence of FRP thickness on FRP hoop strain. (a) Stress concentration on FRP along the chamfered corner of specimen.

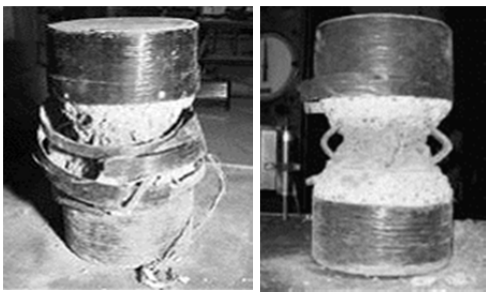

Figure 4: Bar buckling at specimens confined with CFRP jackets.

Confinement effectiveness in the presence of combined flexure and shear (in plastic hinge regions) and local effects due to rotation capacity increase and the effects of FRP confinement on overall member behavior will be discussed.

References

Fardis, M.N., Khalili, H., 1981. Concrete encased in fibreglass-reinforced-plastic. Journal of the American Concrete Institute. Proceedings, 78(6), 440-446.

Tastani S.P., Balafas I., Dervisis A. and Pantazopoulou S.J. (2013). “Effect of core compaction on deformation capacity of FRP-jacketed concrete columns”, Elsevier Construction and Building Materials, Vol. 47, October, pp. 1078-1092.

Pantazopoulou S., Bonacci J.F., Sheikh S., Thomas M.D.A., Hearn N. (2001). Repair of corrosion-damaged columns with FRP wraps. ASCE J. of Comp. for Constr., V.5, No.1: 3-11.

Mirmiran, A., Shahawy, M., Samaan, M., El Echary, H., Mastrapa, J.C., Pico, O., 1998. Effect of column parameters on FRP-confined concrete. Journal of Composites for Construction. 2(4), 175-185.

Kono, S., Inazumi, M., Kaku, T., 1998. Evaluation of confining effects of CFRP sheets on reinforced concrete members. Proceedings of the 2nd International Conference on Composites in Infrastructure ICCI'98, 5-7 January, Tucson, Arizona, 343-355.

Spoelstra MR, Monti G. (1999) FRP-confined concrete model. J Compos Constr 3(3):143–50.

Toutanji, H., 1999. Stress-strain characteristics of concrete columns externally confined with advanced fiber composite sheets. ACI Materials Journal, 96(3), 397-404.

Campione, G., 2006. Influence of FRP wrapping techniques on the compressive behaviour of concrete prisms. Cement and Concrete Composites, 28, 497-505.

Ilki, A., Kumbasar, N., 2003. Compressive behaviour of carbon fibre composite jacketed concrete with circular and non circular cross-section. Journal of Earthquake Engineering, 7(3), 381-406.

Matthys S., Toutanji H., Taerwe L., 2006. Stress-strain behaviour of large-scale circular columns confined with FRP composites. Journal of Structural Engineering, 132(1), 123-133.

Tastani, S.P., Pantazopoulou, S.J., Zdoumba, D., Plakantaras, V., Akritidis, E., 2006. Limitations of FRP jacketing in confining old-type reinforced concrete members in axial compression. Journal of Composites for Construction, 10(1), 13-25.

Wu YF, Wang LM. Unified Strength Model for Square and Circular Concrete Columns Confined by External Jacket. J Struct Eng 2009; 135(3):253-261.

Lam, L., Teng, J.G., 2003. Design-Oriented Stress-Strain Model for FRP-Confined Concrete. Construction and Building Materials, 17, 471-489.

Teng JG, Jiang T, Lam L, Luo YZ. Refinement of a Design-Oriented Stress–Strain Model for FRP-Confined Concrete. J. of Composites for Construction 2009; 13(4): 269–278.

Wu YF, Wang LM. Unified Strength Model for Square and Circular Concrete Columns Confined by External Jacket. J Struct Eng 2009; 135(3):253-261.

Deterioration of FRP jacket effectiveness due to the compaction of low and medium strength concrete

S.P. Tastani, Lecturer, Civil Eng. Dept., Democritus Univ. of Thrace, Greece, stastani@civil.duth.gr
I.Balafas, Instructor, Dept. Civil & Env. Eng., University of Cyprus, Cyprus, ibalafas@ucy.ac.cy
S. J. Pantazopoulou, Dept. Civil & Env. Eng., University of Cyprus, Cyprus, pantaz@ucy.ac.cy

When the FRP jackets are wrapped transversely on the lateral surface of a retrofitted concrete member they are able to develop passive confinement in response to lateral dilation of the encased concrete core. This dilation is owing to the longitudinal cracking that occurs in direction parallel to the compressive stresses (in axially loaded members or in the compression zone of structural members, Fig. 1a,b), as well as due to longitudinal cover splitting induced by rebar bond failure (Fig. 1c). For the definition of the FRP confining pressure (but also of included stirrups), by applying force equilibrium in a reinforced concrete section just upon longitudinal cracking (i.e. at ε_{lat}≥0.00015, thus the tensile stress undertaken by concrete is released) it may be shown that:

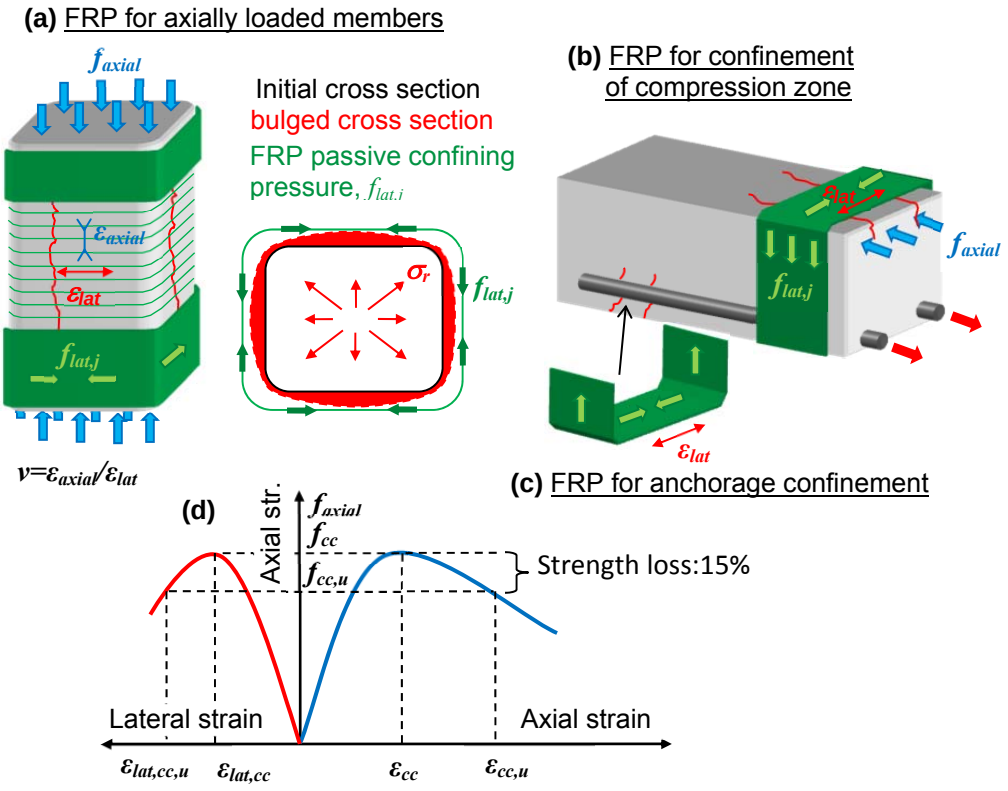

Figure 1. FRP confining devises applied a) in axially loaded members, b) in the compression zone of structural members, c) along the longitudinal cover to prevent splitting induced by rebar bond failure. d) Definition of stress and strain indices of a FRP confined element.

$$\sigma_{lat} = 0.5 \cdot \left(\underbrace{k_f \rho_{fv} E_f \varepsilon_f^{eff}}_{FRP\ jacket} + \underbrace{k_{st} \rho_{sv} f_{yst}}_{stirrups} \right) \quad (1a)$$

$$k_f = 1 - \frac{b_s^2 + d_s^2}{3A_g(1-\rho_s)} \quad ; \quad \rho_{fv} = 2nt_f \frac{b+h}{bh} \quad (1b)$$

where k_i is the confinement effectiveness and ρ_{iv} the volumetric ratio of the confining device (i=f for FRP or st for stirrups, the latter is defined in EC8-I, 2004). Also b, h and b_s, h_s are the cross section lengths before and after corner chamfering, A_g is the cross section area of the specimen and ρ_s the longitudinal reinforcement ratio). A conservative threshold of the axial strain capacity of confined concrete $\varepsilon_{cc,u}$ (as defined in Fig. 1c) can be estimated as a function of the available confining pressure σ_{lat} through Eq. (2).

$$\varepsilon_{cc,u} = \varepsilon_{cu} + 0.075 \cdot \left(\frac{k_f \rho_{fv} E_f \varepsilon_f^{eff} + k_{st} \rho_{sv} f_{yst}}{f_c} - 0.1 \right) \geq \varepsilon_{cu} \quad (2)$$

Correlation between the model above with test data show that with regards the effectiveness of confinement, calculated estimates often exceed the experimental measurements in the range of high FRP pressure to uniaxial concrete strength ratios (σ_{lat}/f_{co}), particularly so with regards the axial and lateral strain capacity (Tastani et al. 2013, 2010). This divergence arise in two categories of FRP-confined columns:

(i) with normal concrete strength and jacket with high axial stiffness (that means high number of plies) and,
(ii) comprising low-strength concrete confined with a conventional jacket.

The explanation is based on the pore compaction of the concrete material structure under high pressure, which causes a partial relief of lateral dilation of the concrete core and compromising the jacket effectiveness on strain capacity enhancement. Thus, referring to Fig. 2, if no pore compaction occurs then the confined specimen is able to develop higher lateral strain under a certain axial strain, but if internal pores collapse then a partial relief is attended as per the volume dilation of the element. To account this phenomenon, the above proposed equations are reformed through a pertinent reduction of the effectiveness coefficient of the FRP, k_f^{red}.

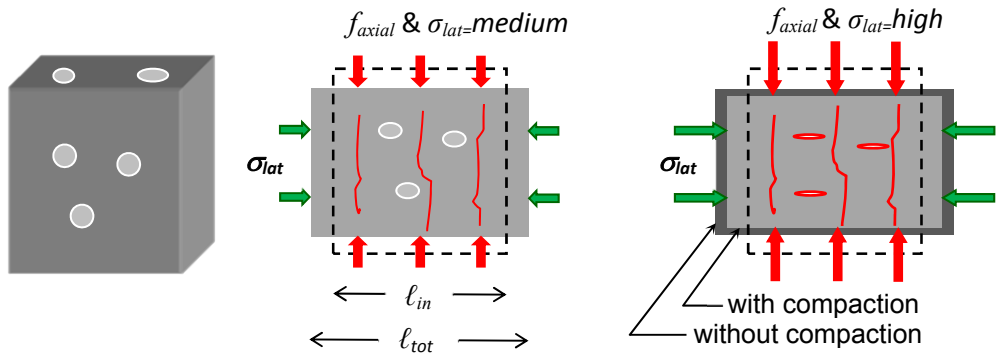

Dilation due to σ_{lat}: $\varepsilon_{lat}=(\ell_{tot}-\ell_{in})/\ell_{in}$ and *confinement effectiveness:* $k_f=f(\sigma_{lat}, V_p)$

Figure 2. Concrete core compaction: reduction of volume dilation due to pores collapse.

The occurrence of concrete compaction and collapse of the pore structure is identified based on any of the three conditions, developed below:

i) Limit of lateral confining pressure: $\sigma_{lat} \geq \left(\frac{f_{co}}{100MPa} \right) \cdot f_{co}$ for f_{co} up to 40MPa (3a)

ii) Limit value of hydrostatic pressure σ_{hydr}: $\sigma_{hydr} = \frac{f_{cc} + 2\sigma_{lat}}{3} \geq 1.1 f_{co}$ (3b)

where, f_{cc} is the compressive strength of the confined specimen (i.e. $f_{cc}=f_{co}+3.1\sigma_{lat}$). Thus, when the hydrostatic pressure exceeds $1.1f_{co}$ then concrete compaction occurs.

iii) Limit of volumetric compaction

$$\varepsilon_v = -\varepsilon_{cc,u} + 2 \cdot \varepsilon_{lat,ccu} \leq -0.004 \quad (3c)$$

where, ε_v is the volumetric strain, $\varepsilon_{cc,u}$ and $\varepsilon_{lat,ccu}$ are respectively the targeted though the FRP jacketing axial and lateral strains at failure (input values without a sign, see also Fig. 1d). Based on Tastani et al. (2013, 2010) when the volumetric strain ε_V (in absolute) is higher than 0.004 the response is altered from brittle to ductile under the condition of high pressure whereas the microstructure of the concrete solid material is compacted due to progressive collapse of the internal pores. This condition illustrates that the axially loaded member laterally restrained with passive confinement is under compaction (a volume reduction $\varepsilon_v=\Delta V/V$ *of* 0.4%) rather than dilation.

The validity of any of the three conditions stated (Eqs.3) activates calculation of a plastic component of lateral strain $\varepsilon_{lat}{}^{p}$ that corresponds to the state of porous collapse. This term is then deducted from the corresponding targeted strain variable of Eq. (2) (i.e. $\varepsilon_f^{eff}=\varepsilon_{lat,ccu}{}^{eff}=\varepsilon_{lat,ccu}-\varepsilon_{lat}{}^{p}$).

Definition of plastic strain

The plastic component of ultimate axial and lateral strains is connected to the porous collapse and as such is an irrecoverable amount of deformation. These components $\varepsilon_{axial}{}^{p}$ and $\varepsilon_{lat}{}^{p}$ are calculated as:

$$\varepsilon_{axial}^{p} = -\frac{0.004}{1+2\nu_{pl}} \cdot \left[\frac{\sigma_{hydr}}{1.1 f_{co}} \right]^{3/2} \quad ; \quad \nu_{pl} = abs\left| \frac{\sigma_{lat} - \sigma_{hydr}}{f_{cc} - \sigma_{hydr}} \right| \quad (4a)$$

$$\varepsilon_{lat}^{p} = \nu_{pl} \cdot \varepsilon_{axial}^{p} \quad (4b)$$

where ν_{pl} is the plastic apparent Poisson's ratio. Subtraction of the lateral plastic strain component from the initially targeted ultimate lateral strain at failure leads to strains $\varepsilon_{lat,ccu}{}^{eff}$ which is free from the plastic components that represent concrete pulverization:

$$\varepsilon_{lat,ccu}^{eff} = \varepsilon_{lat,ccu} - \varepsilon_{lat}^{p} \quad (5)$$

When an r.c. member is under low to moderate confinement it develops considerable expansion due to core cracking and the confinement effectiveness is maximized. On the contrary, at high confinements close to failure the specimen experiences volumetric compaction (the axial compression strain is greater than the tensile area strain) and thus the transverse reinforcement does not exhaust its available confining effectiveness. Note that the later depends on cross sectional geometry. For the class of highly confined specimens where Eq. (3c) is valid the coefficients of confining effectiveness k_i of Eq. (2) need be reduced to take this phenomenon under consideration, as:

$$k_i^{eff} = k_i \Big/ \left(1 + \frac{2\varepsilon_{lat}^{p}}{\varepsilon_{co}} \right), \quad i = f, st \tag{6a}$$

And thus Eq. (2) is reformed as:

$$\varepsilon_{cc,u}^{eff} = \varepsilon_{cu} + 0.075 \cdot \left(\frac{k_f^{eff} \rho_{fv} E_f \varepsilon_{lat,ccu}^{eff} + k_{st}^{eff} \rho_{sv} f_{yst}}{f_{co}} - 0.1 \right) \geq \varepsilon_{cu} \tag{6b}$$

Practical design example

Assume a reinforced concrete column of cross section h=400mm (h_s=350mm), b=250mm (b_s=*200mm*), internally reinforced with longitudinal reinforcement ρ_s=1.64% (8Φ16 at the perimeter of the section) and stirrups of ρ_{sv}=0.64% (Φ8/150, thus k_{st}=0.32) of $f_{st,y}$=400MPa and concrete with f_{ck}=15MPa (ε_{co}=0.002). Aiming to increase the concrete compressive strength to 30MPa the required lateral pressure is σ_{lat}=(f_{cc}-f_{co})/3.1=4.84MPa. (Note that any of the variables σ_{lat}, f_{cc}, ε_f^{eff} or $\varepsilon_{cc,u}$ can be the leader design parameter.) By choosing as confining device a 3-plies Carbon FRP with E_f=230GPa and t_f=3·0.15mm=0.45mm (thus ρ_{fv}=0.6% and k_f=0.61) the effective strain of the jacket is (Eq. 1) ε_f^{eff}= $\varepsilon_{lat,ccu}$=0.011. The strain capacity through Eq. (2) is $\varepsilon_{cc,u}$=0.0444 (thus compression strain ductility is as high as $\mu\varepsilon_c$=0.0444/0.002=22!). The first and the third condition (Eqs. 3a and c respectively) detect concrete compaction which aims to reduce the FRP jacket effectiveness with implications on the attainable ultimate strain and strength. By applying Eqs. (4) they result to ε_{axial}^{p}=-0.0014, ε_{lat}^{p}=0.00072 whereas the effective strain of the FRP is re-arranged through Eq. (5) to $\varepsilon_{lat,ccu}^{eff}$=0.0101 (93% of the initial estimation ε_f^{eff}= $\varepsilon_{lat,ccu}$=0.011). But, concrete compaction also reduces the effectiveness coefficients of the transverse reinforcement (steel and FRP); implementation if Eq.6a results k_f^{eff}=0.36 (for k_f=0.61) and k_{st}^{eff}=0.19 (for k_{st}=0.32). Now, the attainable axial strain capacity of the confined column is expected as (Eq. 6b) $\varepsilon_{cc,u}^{eff}$=0.022 resulting to a compression strain ductility half of the initial estimation.

Application on test results

Concrete compaction occurrence on highly confined specimens was checked on existing published test-data found in the literature. Those formed a database of 496 datasets, which consist of:

- 323 points on plain concrete,
- 169 points on reinforced with longitudinal steel bars and transverse stirrups,
- 334 points on circular sections,
- 158 points on prismatic sections,

The database is at the moment still under construction and its extended version will be presented in the form of a two-page abstract to the TU1207 COST-action.

The inclusion of compaction shows a definite correction of the analytical results to the recorded test-data. Equation 2 give higher lateral strains at high confinement pressures which were not observed during tests due to concrete pore-collapse.

This lateral strain reduction can also be observed on Poisson ratio plots similar to that shown on Figure 4. As pressure increase Poisson ratios reduce consistently to values well below the zero volume value of 0.5. Except from lateral strain reduction, compaction triggers a substantial increase to the axial strains which holds the Poisson ratios at negative volume values at failure. This reduction is more pronounced at plain and circular specimens rather than reinforced and prismatic sections.

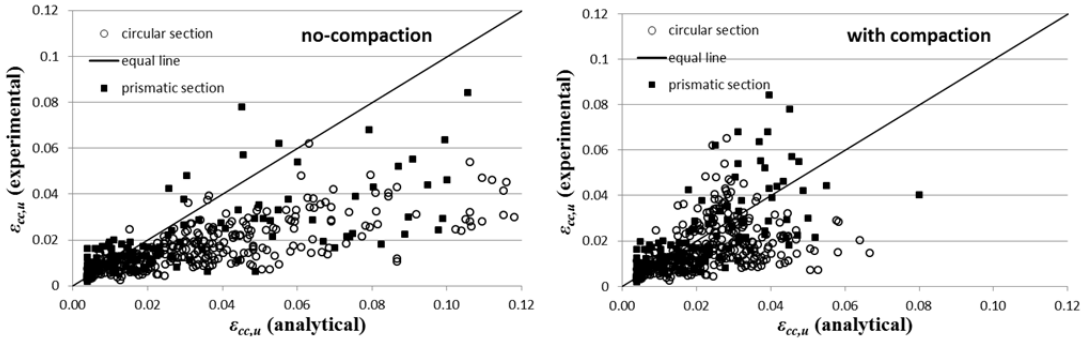

Figure 3. Experimental vs analytical data when: a. compaction is ignored (eq. 2), b. compaction is included (eq. 6b).

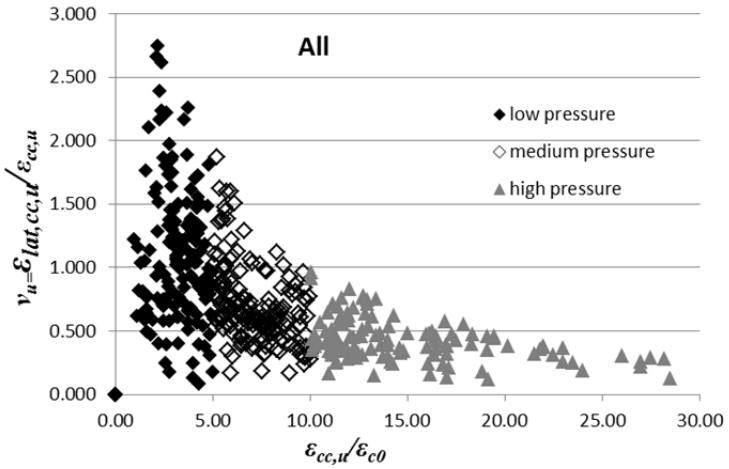

Figure 4. Poisson ratios at various levels of confining pressures

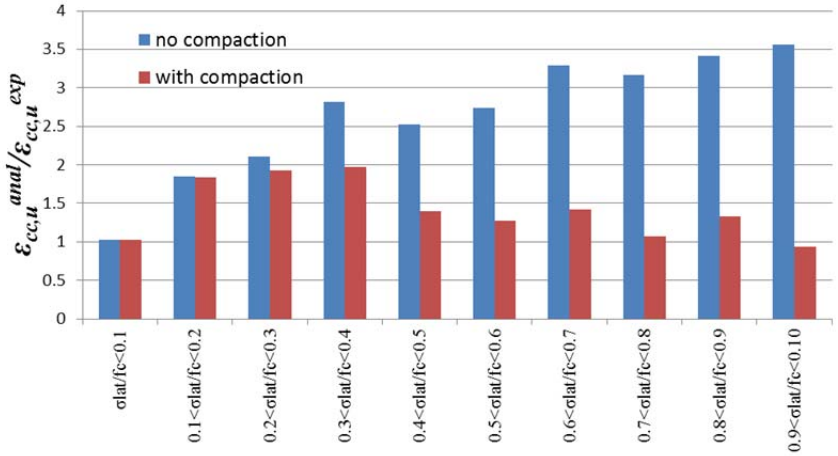

Figure 5. Ratios of analytical to experimental strain capacities at failure for various confinement ratios

The presence of compaction at high confinement levels is also demonstrated on Figure 5, which shows that as pressures increase the analytical to experimental strain capacities ratios are suppressed to equal values of 1.00. This drop is also accompanied by a substantial reduction to its prediction scatter. Figure 6 show ratios of standard-deviations-with-compaction/standard-deviations-without-compaction for analytical to experimental strain capacities predictions. The predictions scatters are reduced linearly from being equal at confined pressures (σ_{lat}) of ≈30% of unconfined concrete strength, f_c, to 5-times lower, in comparison to those performed by ignoring compaction, at σ_{lat}≈90%-100% of f_c.

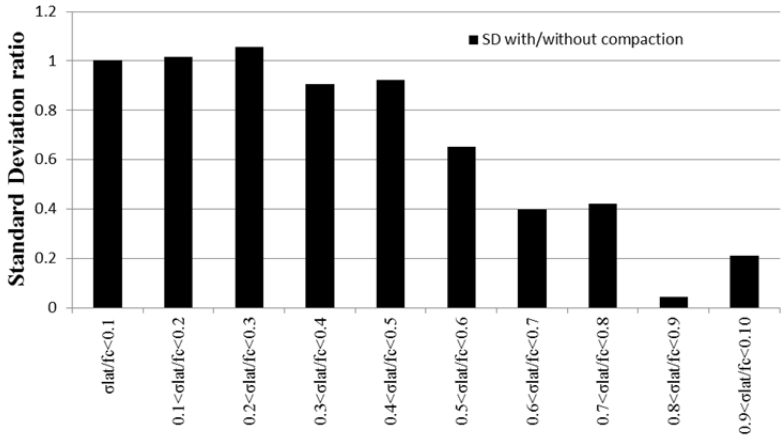

Figure 6. Standard deviation ratios - with/without compaction - for analytical to experimental strain capacities predictions.

References

Tastani S.P., Balafas I., Dervisis A. and Pantazopoulou S.J. (2013). “Effect of core compaction on deformation capacity of FRP-jacketed concrete columns”, Elsevier Construction and Building Materials, Vol. 47, October, pp. 1078-1092.

Tastani S.P, Dervisis A., and Pantazopoulou S.J. (2010). “FRP Jacketed Reinforced Concrete under Compression: Analysis of Concrete Compaction and bar Buckling”. Tech. Chron. Sci. J. TCG, No 3, pp. 61-76 (in greek).

EC8-I (2004). Eurocode 8: Design of structures for earthquake resistance - Part 1: General rules, seismic actions and rules for buildings (Ref. No. EN 1998-1:2004: E), Brussels.

Deterioration of FRP jacket effectiveness due to reinforcement buckling

S.P. Tastani, I.Balafas, S. J. Pantazopoulou

The efficacy of FRPs as confining reinforcement on r.c. members with longitudinal and insufficiently arranged transverse reinforcement (sparse and poor anchored) is compromised by the bar buckling that occurs in the unsupported length between successive stirrups. Bar buckling has serious consequences on the design for seismic upgrading: (i) If, confinement provided through FRP jacketing can totally prevent buckling of longitudinal bars regardless of magnitude of confining pressure then strengthening through FRP jackets of old-type r.c. members with sparse stirrups are totally safe regarding at least the developing strain ductility. (ii) If, on the contrary, the FRP jacket just postpones buckling to higher levels of axial deformation without eventually precluding it, then the several provisions for strengthening should be formulated so as the magnitude of the target compression strain plasticity be related with the design indices of the jacket (number of layers and material).

In most experimental studies buckling of compression reinforcement leads to brittle failure of the r.c. specimens accompanied with abrupt release of strain energy. Because this phenomenon is instantaneous there are two, equally contradictory scenarios of the failure mechanisms order that have been proposed based on visual observation:

- The FRP jacket fails owing to the exhaustion of its tensile strain capacity; in this case the confinement of concrete is released followed by buckling of the bars. Ductile behavior of the r.c. member is expected as the jacket is gradually activated under transverse tension until the exhaustion of its deformation capacity. The transverse strain of the member due to the dilation experienced by the encased concrete under axial loading approximates similar levers of the FRP fracture strain (i.e., 1-2%).
- As the compression bars are attaining instability conditions and start to bend outwards corrupt the FRP jacket; thus the strengthening device fails and concrete disintegration occurs. The developed ductility is limited because the average transverse strain of the FRP is much lower than its fracture strain. The associated compressive strain of the member at failure is determined by the capacity curve of the longitudinal reinforcement taking under consideration second order phenomena (i.e. buckling developing between successive stirrups).

From the above it is concluded that target is the definition of the critical FRP confining pressure which is capable to alter the structural response of the r.c. member under compression from that developed by only accounting the sparse stirrups. To this point, critical is the calculation of the undertaken from the compressive bars axial load before and after the attainment of the critical instability conditions. For this purpose the envelope curve of the dependable axial strain ductility ($\mu_{\varepsilon s}=\varepsilon_{s,crit}/\varepsilon_{sy}$) versus the compressive bar unsupported length (i.e. the s/D_b ratio) is necessary. An indicative diagram is shown in Fig. 1 and it basically depends on the hardening properties of the steel stress-strain law that follows the zero stiffness yielding branch. Its production could be based on the procedure proposed by Mau (1990). The following options are identified as per the attainable axial strain ductility (Fig. 1b):

- if the point is under the curve and $\mu_{\varepsilon s} \leq 1$ then the confined member prematurely fails due to elastic bar buckling,
- if the point is under the curve and $\mu_{\varepsilon s} > 1$ then the member fails due to inelastic buckling whereas the steel is in the horizontal branch of the stress – strain law,
- if the point coincides with the curve then the member fails due to bar buckling without any

potential of partial redistribution of bar load to the concrete core; the steel in this case has entered in the hardening branch, and

- if the point is over the curve then failure due to buckling has been shifted to higher strain level because the confined concrete core is able to undertake additional axial load.

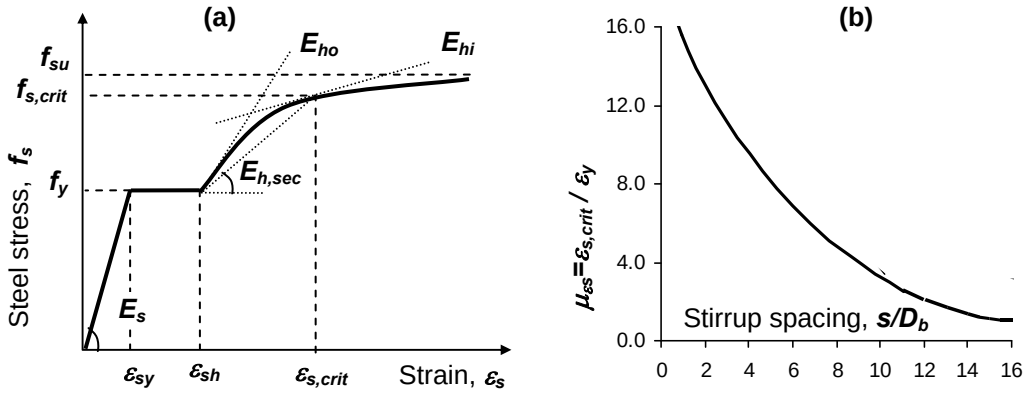

Figure 1 – (a) Constitutive law of compression steel. (b) Envelope curve of the dependable axial strain ductility ($\mu_{\varepsilon s}=\varepsilon_{s,crit}/\varepsilon_{sy}$) versus the bar unsupported length (s/D_b).

The definition of bar axial strain upon bar buckling, $\varepsilon_{s,crit}$, through the plot of Fig. 1b is used for the estimation of the average lateral strain of the FRP jacket ε_f^{buckl} as well as the local strain at corners $\varepsilon_{f,ch}$ (Fig. 2) by considering also the familiar relation for axial strain capacity, which in this case is related to the strain ε_f^{buckl} (Eq. (1)).

$$\varepsilon_{cc,\mu} = \varepsilon_{cu} + 0.075\left(\frac{k_f \rho_{fv} E_f \cdot \varepsilon_f^{buckl} + k_{st}\rho_{sv} f_{yst}}{f_{co}} - 0.1\right) \tag{1}$$

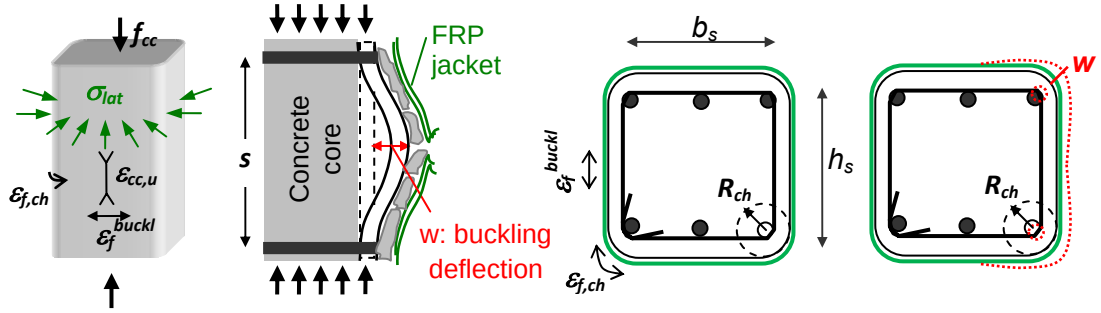

Figure 2 – Definition of strain indices and schematic representation of bar buckling.

Note that the FRP strain distribution is not uniform along the perimeter of the specimen: the maximum value occurs at the corners where the fibers change direction; this local strain $\varepsilon_{f,ch}$ is associated with local patterns of failure as the concrete cover crushing is due to stress concentration $\sigma_{lat,ch}$ originated by concrete cover to the FRP jacket and vs. versa (Fig. 3). This stress is defined by establishing force equilibrium and is given by Eq. (2).

$$\int_0^{\pi/2} \left(\sigma_{lat,ch} \cdot R_{ch}\right) \cdot d\theta = \sqrt{2 \cdot \left(n t_f E_f \varepsilon_{f,ch}\right)^2} \quad \Rightarrow \quad \sigma_{lat,ch} = 0.9 \frac{n t_f E_f}{R_{ch}} \cdot \varepsilon_{f,ch} \tag{2}$$

This pressure is proportional to the jacket stiffness (nt_fE_f), and to the lateral local FRP strain $\varepsilon_{f,ch}$ (lower than the fracture value, ε_{fu}); the increase of the jacket stiffness increases the local stress concentration, which is relieved by increasing variable R_{ch}. The potential scenarios of local failure at corners are:

- The pressure $\sigma_{lat,ch}$ exceeds the confined concrete compressive strength f_{cc} (i.e. $f_{cc} = f_{co} + 3.1\sigma_{lat}$ where σ_{lat} is the average confining pressure, $\sigma_{lat} = 0.5 \cdot (k_f \rho_{fv} E_f \varepsilon_f^{buckl} + k_{st} \rho_{sv} f_{y,st})$. In this case two alternatives are possible: either the jacket has the strain reserve and thus concrete cover crushing will occur, or concrete crushing and fiber fracture will occur simultaneously.
- The FRP strain demand $\varepsilon_{f,ch}$ exceeds the strain capacity ε_{fu}; thus fiber fracture will happen before concrete crushing.

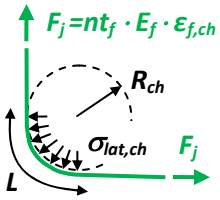

Figure 3 – Stress concentration $\sigma_{lat,ch}$ along the chamfered corner of the confined member.

The mean effective strain of the jacket ε_f^{buckl} as a result of buckling failure is calculated in the following section.

Definition of average FRP failure strain due to bar buckling, ε_f^{buckl}

Upon attainment of unstable conditions of the compression reinforcement the mean lateral strain of the FRP jacket due to concrete core dilation, ε_f^{buckl}, that corresponds to the critical axial strain $\varepsilon_{s,crit}$, is calculated through the apparent Poisson ratio v_u, as,

$$\varepsilon_f^{buckl} = v_u \varepsilon_{s,crit} \tag{3}$$

For low to moderate confinement the noted dilation corresponds to a range of values of the apparent Poisson ratio v_u in between 0.5 and 1 for circular and rectangular cross sections respectively.

Criterion for instantaneous failure due to bar buckling

Upon attainment of buckling conditions the bars gradually transfer part of their total load Δf_{ax} on concrete; this is given by Eq. (4) as:

$$\Delta f_{ax} = (f_{s,crit} - f_{s,res}) \cdot A_s / (A_{gross} - A_s) \tag{4}$$

where A_{gross} is the cross section area of the structural member, A_s the area of longitudinal reinforcement, $f_{s,res}$ the residual strength of the buckled bars for strain level $\varepsilon_s > \varepsilon_{s,crit}$ and $f_{s,crit}$ the bar stress associated to the strain $\varepsilon_{s,crit}$ (defined from the stress-strain law of the steel material). The residual strength in the case of symmetric buckling is given as,

$$f_{s,res} = 6 f_y / (s / D_b) \tag{5}$$

This load transfer on concrete core may occur if only it has the strength reserve Δf_{cc} due to confinement to undertake the additional load; this deposit is given by Eq. (6).

$$\Delta f_{cc} = 3.1 \cdot k_f \rho_{fv} E_f (\varepsilon_{fu} - v_u \varepsilon_{s,crit}) \frac{R_{ch} + 0.5 D_b}{b_s - 2R_{ch}} \geq 0 \tag{6}$$

If the strength reserve of the concrete core exceeds the overload (i.e. $\Delta f_{cc} > \Delta f_{ax}$) then the risk of failure due to buckling is suppressed to occur at higher strain levels, thereby enabling the concrete core to develop its full strain capacity before failure. On the other hand if the overload exceeds the strength reserve of the core (i.e. $\Delta f_{cc} < \Delta f_{ax}$) buckling will be instantaneous.

Design example

- Assume an axially loaded column of square cross section with $h_s = b_s = 350mm$ and

R_{ch}=50mm, made of concrete f_{co}=20MPa, reinforced with 8 bars of D_b=16mm and stirrups of $D_{b,st}$=8mm spaced at s=130mm (for both reinforcements steel has f_{sy}=400MPa and $\varepsilon_{sy}=\varepsilon_{sy,st}$=0.002). According to Fig. 1b and considering that $s/D_b \approx 8$ the bar axial strain upon bar buckling is $\varepsilon_{s,crit}$=0.01 whereas the associated stress is $f_{s,crit}$ =510MPa (assuming steel with f_{su}=600MPa, ε_{sh}=0.005, ε_{su}=0.01 and E_h=30GPa, see Fig. 1a). Also through Eq. (5) the bar residual strength after buckling is $f_{s,res}$ =295MPa. This column is chosen to be confined with an FRP jacket of parameters: fracture strain ε_{fu}=0.018, modulus of elasticity E_f=230GPa and total thickness $n \cdot t_f$=0.6mm. Implementing Eq. (3) the mean lateral strain of the FRP jacketed member due to the concrete core dilation is ε_f^{buckl}=0.01 (ν_u=1). The overload as well as the strength reserve are (through the Eqs. (4) and (6) respectively): Δf_{ax}=2.2MPa and Δf_{cc}=3.5MPa denoting that the risk of failure due to buckling is suppressed to occur at higher strain levels, thereby enabling the concrete core to develop its full strength and strain capacity before failure. Conservatively the strength capacity of the confined concrete is: $f_{cc} = f_{co} + 3.1 \cdot [0.5 \cdot (k_f \rho_{fv} E_f \varepsilon_f^{buckl} + k_{st} \rho_{sv} f_{y,st})]$ =34.7MPa whereas the strain capacity by implementing Eq. (1) is $\varepsilon_{cc,u}$=0.03, thus the axial strain capacity is increase by an amount of 0.02. Assuming that at corners the FRP jacket exhausts its fracture strain thus $\varepsilon_{f,ch} = \varepsilon_{fu}$ the local confining stress is (Eq. (2)) $\sigma_{lat,ch}$=44.7MPa exceeding the confined concrete compressive strength f_{cc}=34.7MPa and thus concrete crushing and fiber fracture will occur simultaneously because the jacket hasn't any strain reserve.

References

Tastani S.P., Balafas I., Dervisis A. and Pantazopoulou S.J. (2013). "Effect of core compaction on deformation capacity of FRP-jacketed concrete columns." Elsevier Construction and Building Materials, 47: 1078-1092.

Tastani S.P, Dervisis A., and Pantazopoulou S.J. (2010). "FRP Jacketed Reinforced Concrete under Compression: Analysis of Concrete Compaction and bar Buckling.". TCG Technika Chronika (Sc. J.), 3: 61-76 (in greek).

EC8-I (2004). Eurocode 8: Design of structures for earthquake resistance - Part 1: General rules, seismic actions and rules for buildings (Ref. No. EN 1998-1:2004: E), Brussels.

Mau, S. (1990). "Effect of tie spacing on inelastic buckling of reinforcing bars." ACI Structural J., 87(6): 671-677.

Recovery of strength mechanisms in corrosion-damaged reinforced concrete through FRP jacketing

S.P. Tastani, I.Balafas, S. J. Pantazopoulou

Corrosion of the reinforcement cage in concrete structures has manifold effects on strength, deformation capacity, and in the prevailing mode of failure through the following mechanisms:

- Reduction of the available steel area,
- Spalling of the concrete cover,
- Break-down of chemical adhesion between concrete and steel along the lateral bar surface,
- Reduced resistance to bar slip, owing to the cohesionless nature of rust and to attenuation of bar ribs, and
- Embrittlement of reinforcement.

Whether it occurs in stirrup reinforcement or in the longitudinal bars, bar section loss and cover spalling have direct consequences on all strength mechanisms (flexure, shear, bond resistance and development capacity) as well as in the associated deformation capacities. A second level implication is the change in the relative magnitudes of available strengths in the individual response mechanisms, a factor that controls the hierarchy of failure that eventually limits seismic resistance.

The mechanical implications of corrosion damage may be assessed from first principles if the extent of metal depletion and strain embrittlement are known: a commonly used measure for the former is the depth of corrosion penetration, X, defined as, $X=\Delta D_b/D_b$, i.e. it is the percent change of bar diameter (Fig. 1). The percentage of depleted mass, $\gamma=\Delta M_s/M_s$, is related to X from: $\gamma \approx 2X$ (valid for $X<15\%$). The volume of deposited rust, ΔV_r, is related to the volume of depleted metal ΔV_s, and therefore to the depth of penetration X, through: $\Delta V_r=\alpha_{rs}\cdot\Delta V_s$. The volume ratio α_{rs} ranges between 2 and 4 for hydrated red rust (Pantazopoulou and Papoulia 2001). Assuming uniform corrosion on the bar surface, deposition of the rust volume ΔV_r around the bar perimeter requires a free (unrestrained) radial displacement of the internal concrete boundary by,

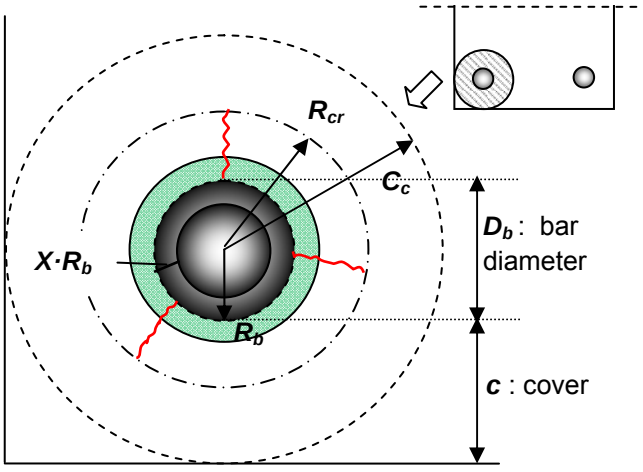

Figure 1. Thick cylinder idealization of cover concrete. The crack front is defined by R_{cr}.

$$\frac{u_{r,o}}{D_b} = 0.5\,\varepsilon_{cr}\left(\frac{\sqrt{0.25+(\alpha_{rs}-1)X(2-X)}}{\varepsilon_{cr}} - 0.5\right) \quad (1)$$

Embrittlement refers to a reduction in the deformation capacity of reinforcement, and occurs most severely in the case of pitting corrosion. Here, the reinforcement fracture strain ε_{su}^{cor} is reduced from its reference uncorroded value, ε_{su}, using a linear attenuation model (Corronelli and Gambarova 2004) in terms of α_{pit}, which is defined as the section area loss due to pitting. Different values of α_{pit}^{max} have been measured (ranging from 0.5 to 0.1, Cairns and Millard 1999, Castel et al 2000). Complete loss of ductility corresponds to $\alpha_{pit} = \alpha_{pit}^{max}$.

$$\varepsilon_{su}^{cor} = \varepsilon_{sy} + (\varepsilon_{su} - \varepsilon_{sy})(1 - r_{pit}), \quad \mathrm{r_{pit}} = \frac{a_{pit}}{a_{pit}^{max}} < 1 \quad (2)$$

FRPs in Rehabilitation of Corroded Structures

It is now established that apart from its efficacy as a confining means, FRP jacketing also slow down markedly the chemical process of iron depletion under conditions of continued post-repair exposure. Apparently, the hardened resin matrix acts as a diffusion barrier to further ingress of the agents necessary to sustain corrosion, i.e. oxygen, chlorides and water. Furthermore, the passive restraint provided by the jacket to the expansive tendency of the corrosion products has a subtle but important effect on the rate of steel consumption: all relevant tests conducted were carried out in simulated accelerated corrosion conditions. If unrestrained, the process of rust production follows a Faraday model, which is linear in time, i.e., the depleted mass of metal is in linear relation to impressed current density and time of exposure. However, when deposited in confined volume around the corroding bar the rust layer inhibits diffusion of Ferrous ions from the bar core to the surface where the chemical reaction takes place. Thus, as time proceeds the process of mass depletion follows a Boltzman-type law, with the rate of depletion decaying exponentially with time (Pantazopoulou and Papoulia 2001). Lee et al. (2000) described this rate reduction in the presence of confinement as a requirement for increased energy to sustain the reaction. Pantazopoulou et al. (2001) report a 47% reduction of corrosion rate in repair schemes with GFRP jacketing (providing no moisture would be trapped behind the jacket as a result of cover replacement). Tastani and Pantazopoulou (2004) reported even higher levels of rate reduction (up to 85%) when low permeability mortar was used for the patch repair under the FRP jacket (again, the need of drying prior to wrapping cannot be overstressed). Similar are the results reported by Debaiky et al. (2002): 95% decrease of corrosion current density resulting from the application of a single ply of FRP material. Soudki and Sherwood (2000) reported a reduction of corrosion activity owing to FRP jacketing, upon accelerated chloride exposure: for mass loss up to 10% they noticed reduced crack widths from 1mm (without jackets) to 0.3mm (in jacketed specimens).

Regarding seismic resistance, experiments on severely corroded column specimens under lateral sway (cyclic loading in double curvature) have illustrated intense loss of stiffness due to bond degradation, marked by increased pinching in the hysteresis loops as loading progressed (Lee et al 2003, Bousias et al 2004). In both studies, failure of corroded unrepaired specimens occurred by hoop fracture, buckling of compression reinforcement and brittle shear disintegration. Repair with FRP jacket acting as confining and shear reinforcement was successful in prolonging ductility and deformation capacity, as well as recovery of energy absorption to the levels attained by identical specimens in pristine (uncorroded) condition.

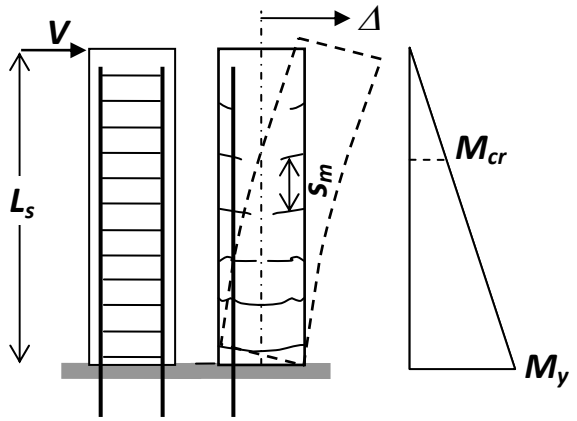

Figure 2. Response of a corroded column to lateral sway

In redesigning a corroded r.c. element for seismic resistance the most obvious performance objective is mitigation of all other failure modes except for flexural, which is the least undesirable. With reference to the simple cantilever model depicted in Figure 2, which represents half the span of a continuous member in a frame structure under lateral sway, forces used in redesign must satisfy the following qualitative relationship:

$$V_{u,lim}=min[V_{shear}, V_{anchor}, V_{iflex}] \quad (3)$$

where, V_{shear} the nominal shear strength, V_{anchor} the shear force acting in the span when the anchorage / lap-splice reach its development capacity and $V_{flex} = M_u/L_s$ is the seismic shear force required to develop the flexural strength of the member; L_s is the shear span. Implementation of Eq. 3 need be carried out at two stages: (a) in assessing available capacity, and (b) in detailing and dimensioning the upgrading scheme. In the following sections tools for assessment and redesign with FRP jacketing are developed from first principles with reference to the terms of Eq. (3).

1. Shear Strength

1.1 Deteriorated Shear Strength due to corrosion

The nominal shear resistance of r.c. members (V_{shear}) comprises contributions from concrete (V_c) and web reinforcement (V_s). Under cyclic displacement reversals both terms are known to degrade with increasing number of cycles and intensity of displacement ductility (Martin-Perez and Pantazopoulou 2001, Moehle et al. 2002). This reduction is a symptom of the susceptibility of concrete's mechanical resistance to cracking. Upon reversed seismic loading bi-diagonal cracks in the web limit the strength of the compression struts that sustain the V_s term, whereas aggregate interlock and dowel action (the V_c term) break down quickly with increasing width of cracks. A simple model is adopted (Moehle et al. 2002) so as to qualitatively describe the relationship between important variables while maintaining the familiar code format for V_{shear}:

$$\begin{aligned} V_{shear}(\mu_\Delta) &= \lambda \cdot (V_s + V_c) \\ V_s &= \sigma_{lat,st} \cdot bd = k_{st} \frac{A_{st}}{s \cdot b} f_{y,st} \cdot bd \\ V_c &= \left[0.25 f_{ct} K(1.2 + 40\rho_{sl}) + 0.15P/A_g\right] bd \\ \lambda &= 1.15 - 0.075\mu_\Delta, \quad 0.7 \le \lambda \le 1 \end{aligned} \quad (4)$$

Term $40\rho_{s1}$ in Eq. 4 represents dowel action of well anchored tension reinforcement (ρ_{s1} < 2%), whereas μ_Δ is the imposed displacement ductility. K is a size effect coefficient, A_g the cross sectional area and P the design axial compressive load. Transverse pressure $\sigma_{lat,st}$ contributed by any available embedded stirrups is calculated from: $\sigma_{lat,st} = k_{st} \cdot (A_{st}/(s \cdot b)) \cdot f_{y,st}$, where s and $f_{y,st}$ is the spacing and the yield stress of embedded stirrups, b the cross-section width (orthogonal to the applied shear force), A_{st} the total cross sectional area of stirrup legs in the direction of interest provided by a single stirrup layer and k_{st}^{v}=1 for closed stirrups. Clearly, stirrups, and thus the V_s term, are the first to be affected by corrosion owing to their proximity to the exposed surface, whereas the section loss is more dramatic for the transverse reinforcement as it is usually fabricated from small diameter bars. Thus, V_s is lowered by the apparent reduction of cross section area of stirrups since $A_{st}^{cor} = A_{st}\cdot(1-X)^2$. In assessing residual shear strength it is assumed that for general corrosion, in the presence of stirrups the effects on dowel action are negligible, but the corresponding contribution (i.e., $40\cdot\rho_{s1}$) in V_c shall be omitted in cases of pitting corrosion.

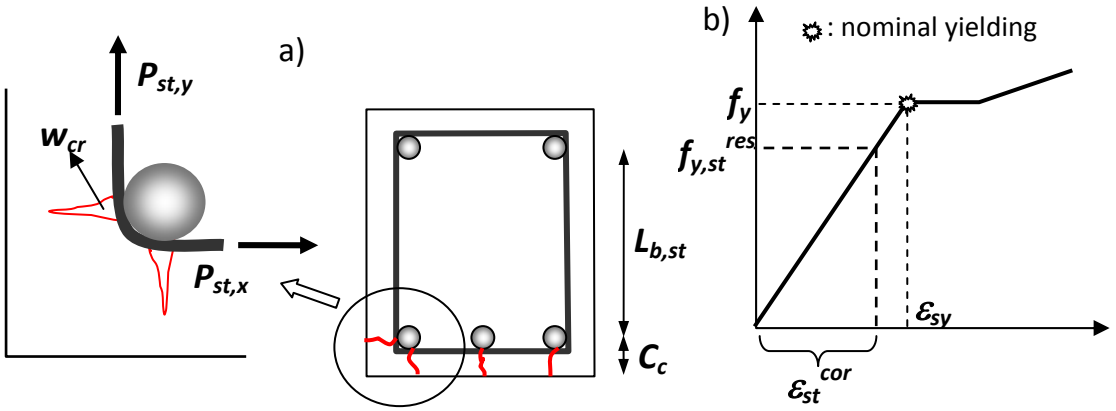

Figure 3. a) Stretching of stirrup leg due to splitting cracking along the longitudinal reinforcement and b) effect of corrosion on yielding of transverse reinforcement

Furthermore, opening of splitting cracks ($w_{cr}=\pi D_b\cdot(\alpha_{rs}-1)\cdot X$ – Coronelli and Gambarova 2004) due to corrosion along the longitudinal reinforcement results to stretching of the stirrup legs (Fig. 3a) consuming part of the available pre-yield deformation capacity of the metal (Fig. 3b):

$$\varepsilon_{st}^{cor} = \frac{1}{\beta}\cdot\frac{w_{cr}}{L_{b,st}} = \frac{1}{\beta}\cdot\frac{\pi\cdot D_b}{L_{b,st}}(\alpha_{rs}-1)\cdot X \qquad (5)$$

In Eq. 5 factor β accounts the number of radial cracks that develop around the perimeter of bar (i.e. for two cracks β=2) and $L_{b,st}$ is the anchorage length of the stirrup leg. For this reason, the available shear stress supported by stirrups, need be reevaluated using the reduced rather than the nominal yield strength ($f_{y,st}^{red}$) as (Tastani and Pantazopoulou 2005, 2007a),

$$\sigma_{lat,st}^{cor} = k_{st}\frac{A_{st}^{cor}}{s\cdot b}f_{y,st}^{res} \quad \text{where} \quad f_{y,st}^{res} = \begin{cases} f_{y,st} - E_s\cdot\varepsilon_{st}^{cor} & 0 \le \varepsilon_{st}^{cor} \le \varepsilon_{sy} \\ 0, & \varepsilon_{st}^{cor} > \varepsilon_{sy} \end{cases} \qquad (6)$$

In applying Eq. 4 to old-type construction with sparse stirrups maximum available displacement ductility, μ_Δ is taken as 1 (it is assumed that before rehabilitation with FRPs the structure can't sustain displacement greater than what corresponds to first yielding). Note that for widely spaced stirrups the contribution of web reinforcement to shear strength is

$V_s = n_{st} \cdot A_{st} \cdot f_{y,st}$ where n_{st} the number of stirrups crossing a 45^o possible crack path. For stirrup spacing equal to the depth d of the member (common in old-type members) $n_{st}=0$, and hence upon load reversal beyond cracking the shear strength of the member would be diminished.

1.2 Recovered Shear Strength

In redesigning FRP-jacketed r.c. members with corrosion-affected stirrups the objective is to recover the initial shear strength and to secure sufficient displacement ductility that would exceed the design demands. Here the jacket is taken to comprise n plies, having a thickness t_f per ply. Considering degradation of shear strength with ductility demand the repaired shear strength (after jacketing) is,

$$V_{shear}^{enh}(q) = min\{\lambda(q_{\Delta old}), \lambda(q_{\Delta new})\} \cdot V_{shear}^{res} + V_{w,f}$$
$$V_{w,f} = \sigma_{lat,f} \cdot b \cdot h\,, \quad \sigma_{lat,f} = 2k_f n t_f E_f \varepsilon_{eff} / b \qquad (7)$$
$$\lambda = 1.15 - 0.075\mu_\Delta\,, \quad 0.7 \le \lambda \le 1$$

where q is the behavior index, k_f^v depends on the strength of anchorage of the wrap (if the jacket is adequately closed, then $k_f^v=1$) and ε_f^{eff} is the effective design strain: in case of U-shape jackets it is taken as 0.004, whereas for closed jackets $\varepsilon_f^{eff}=0.5\varepsilon_{fu,d}$ (ACI 440.2R-02). The above equation can be used for determining the required number of jacket layers as shear reinforcement in the upgrading scheme. In Eq. 7 it has been implicitly assumed that the target displacement ductility, μ_Δ used in the redesign of the member is equal to the behavior index, q_{new}. This should not exceed the value of 3.5 ÷ 4 that is currently recommended for new designs. The proposed equation is a lower bound expression where shear resistance is taken to degrade with ductility demand even in the presence of jacketing because of the ongoing degradation of contributing mechanisms such as bond, dowel action and aggregate interlock. Usually, because of the high strength/stiffness of the composite material, the number of required layers for shear recovery is limited to 2 or 3 and so the application of reduction coefficient λ on FRP contribution is on the side of safety.

2. Anchorage / lap-splice development capacity

The shear force acting in the span when the anchorage / lap-splice reach its development capacity, V_{anchor}, is defined through the Eq. (8).

$$V_{anch} = [\pi D_b L_b f_b N_b jd + P(d - 0.5h)] / L_s \qquad (8)$$

where L_s the shear span, jd the internal lever arm in the cross section upon bar yielding, N_b the number of primary tension bars with diameter D_b whereas f_b is the bond strength. The latter is linearly-related to the normal pressure σ_n mobilized over the anchorage length through the frictional coefficient μ: $f_b=2\mu/\pi\sigma_n$. The normal confining pressure, σ_n, may be provided either by the cover concrete ($\sigma_{cover}=p_{cr}/D_b \cdot \zeta \cdot f_{ct}$, where p_{cr} is the potential path of the crack originated by the tip of the ribs up to the free surface, see Fig. 4, ζ account for the tensile response of the cover, 1 for elastic and 2 for plastic), by transverse reinforcement crossing the splitting crack path ($\sigma_{lat,st}=0.33A_{st}f_{y,st}/(SN_bD_b)$ where 0.33 is a coefficient that uniformly distributes the stirrup stress along the spacing S), and the dry shrinkage of concrete (it is usually taken as $\sigma_{shr}=3 \cdot f_{ct}$. At the ultimate limit state frictional coefficient μ ranges between 0.9 to 1.2 whereas the tensile concrete strength is taken as $f_{ct}=0.5(f_{co})^{0.5}$, thus the Eq. (9) gives an expression for the calculation of bond strength.

$$f_b = \mu \cdot \left(0.32 \cdot \zeta \frac{p_{cr}}{D_b} \sqrt{f_{co}} + 0.96 \sqrt{f_{co}} + 0.21 \frac{A_{st} f_{y,st}}{s N_b D_b} \right) \quad (9)$$

2.1 Deterioration of bond strength

It is evident that rust accumulation being an expansive process, generates radial stress over the lateral bar surface that compete for the tensile resistance of the concrete cover for equilibrium in the hoop direction. This accelerates splitting of the cover in corroded, stressed bars as compared to identical anchorages with no corrosion. On the other hand, the coefficient of friction μ degrades as rust proceeds: studies (Lundgren 2002) have illustrated that the rust layer accumulating around the corroding bar behaves as a cohesionless frictional material. Being rather loose and incompressible, under zero or negligible normal pressure there is no friction and the rust provides little or no resistance to sliding of the reinforcement. This is compounded by the fact that ribs are the first point of corrosion attack, and therefore, by the time a substantial layer of corrosion product has accumulated, the rib height may be dramatically attenuated or even eliminated completely**.** Loss of bond due to corrosion has many consequent implications: in the absence of bond, no stress gradient can develop on the reinforcement, as required by the statics (e.g. moment gradient over the member). Thus: (a) tension stiffening cannot be mobilized, leading to a dramatic loss of stiffness in the member even under serviceability conditions. (b) The flexural component of behavior is suppressed, whereas the "tied-arch" mechanism prevails, leading to excessive deflections. Bar anchorage is pushed further out towards the supports where the bar may happen to cross a diagonal field of compression. In that event, bars with cutoff points within the span cannot function as tension reinforcement.

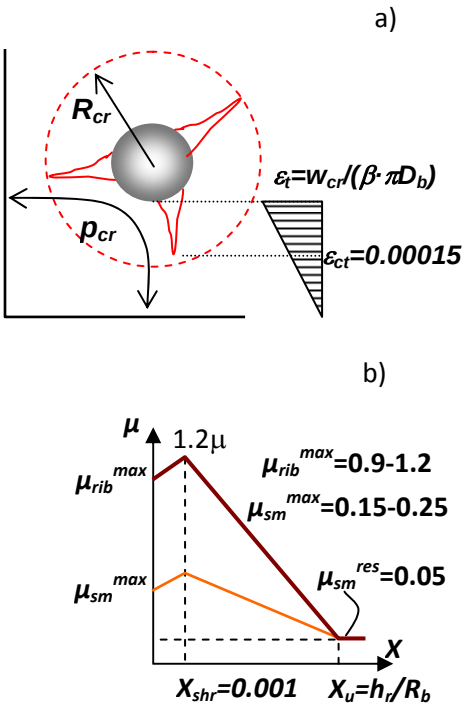

Figure 4. a) Definition of crack width and path in the concrete cover. b) Frictional coefficient as a function of the depth of corrosion penetration *X*

From the preceding it is evident that all terms in Eq. 9a are susceptible to corrosion leading to bond degradation: normal pressure, σ_n is affected by cover splitting (thus the available cover resistance is related to cracking front R_{cr}, Fig. 4) and stirrup attenuation owing to steel section loss and embrittlement as per the Eq. (6). Fictional coefficient μ depends on the volume of rust deposited over the bar as well as on the state of loading (strength plateau or descending branch of the bond –slip law); for this reason μ would have to be taken as a function rather than a constant value Tastani and Pantazopoulou, 2005, 2007a,b). Thus the affected by corrosion bond strength may be given by Eq. ((10).

$$f_b^{cor} = \mu(X) \cdot \left(0.32 \frac{p_{cr} - R_{cr}}{D_b} \zeta \sqrt{f_{co}} + 0.96 \frac{p_{cr} - R_{cr}}{c} \sqrt{f_{co}} + 0.21 \frac{A_{st}^{cor} f_{y,st}^{red}}{D_b N_b s} \right) \quad (10a)$$

The cracking front R_{cr} depends on the radial displacement $u_{r,o}$ (Eq. (1) and is calculated as:

$$R_{cr} = \frac{u_{r,o}\left(c + D_b\right)}{u_{r,o} + \varepsilon_{cr} \cdot c} \tag{10b}$$

The reduction of the coefficient of friction with increasing level of corrosion $\mu(X)$ may be follow a linear relation to the depth of corrosion penetration, X as per the Fig. 4b where the ultimate value for X is the total depletion of the ribs of height h_r.

2.2 Recover of Bond strength

Equation 10 for assessment of the residual bond strength recognizes two discrete mechanisms through which corrosion causes bond degradation, namely loss of frictional resistance and loss of confining pressure by the cover due to cracking. Because of the inevitable flattening of the ribs the coefficient of friction cannot be recovered, however, removal of cracked cover and replacement with healthy grout in combination with stirrups or FRP jacketing has been proven very effective in rehabilitating development capacity of corroded bar anchorages. To be effective, FRP sheets are bonded externally with the fiber weave oriented orthogonal to the bar or lap splice, so as to arrest propagation and opening of splitting cracks (Figure 8). To quantify this function of the jacket the frictional concept for bond is extended to include a jacket contribution to the confining term. Thus, the average bond strength f_b^{enh} after jacketing over the development length of a bar or lap splice equals:

$$f_b^{enh} = \mu(X) \cdot \left[\underbrace{0.32\frac{p_{cr}}{D_b}\zeta\sqrt{f_{co}} + 0.96\frac{p_{cr}}{c}\sqrt{f_{co}}}_{new\ cover} + \underbrace{0.21\frac{A_{st}^{cor} f_{y,st}^{red}}{D_b N_b s}}_{corroded\ stirrups} + \underbrace{1.27 \cdot \frac{n_f t_f E_f \varepsilon_f^{eff}}{D_b N_b}}_{FRP\ jacket} \right] \tag{11}$$

where the effective FRP strain ε_f^{eff} is in the order of 0.002.

3. Flexural Strength

3.1 Deterioration of Flexural Strength

The residual flexural strength of corroded r.c. members is controlled by the yield capacity of the tension reinforcement with residual area $A_s^{cor}=A_s(1-X)^2$ (In is neglecting the possible effect corrosion has on yield strain due to embrittlement). General equilibrium equations of a typical cross section discretized in i layers for flexural analysis result to the Eq. (12) regarding the flexural moment M^{res} and the associated lateral force V_{flex}^{res}.

$$M^{res} = \sum\left(f_{ci} A_{c,i}\left(\frac{h}{2} - y_i\right) + f_{si} A_{si}^{cor}\left(\frac{h}{2} - y_{si}\right)\right)$$
$$V_{flex}^{res} = \frac{M^{res}}{L_s}, \quad P^{res} = \sum\left(f_{ci} A_{c,i} + f_{si}^{cor} A_{si}^{cor}\right) \tag{12}$$

Residual capacity is calculated at a limiting compressive concrete strain ε_{cu}=0.004 that corresponds to cover spalling. Terms f_{ci} and f_{si} are the average normal stresses of the *i-th* layer (concrete or steel, respectively). $A_{c,i}$ and A_{si}^{cor} are the corresponding concrete and residual steel areas (after area loss due to corrosion) of the *i-th* layer. Using the plane-section kinematic assumption for flexure, layer stress is evaluated from layer strain assuming a Hognestad–type parabolic stress-strain relationship up to peak (at a strain of ε_{co}=0.002) and constant thereon till failure (at a strain of 0.004). Peak stress depends on confinement: the part of each concrete layer that belongs to cover concrete attains a residual concrete strength f_c^{res} which is reduced from the nominal strength value of f_{co}. Coronelli and Gambarova 2004 proposed a reduction coefficient to account for the transverse splitting strain, ε_1, on cover

concrete compressive strength. Their proposal is a modification of the original tension-softening model of Vecchio and Collins 1986:

$$f_c^{res} = f_{co} \cdot \frac{1}{1+0.1\varepsilon_1/\varepsilon_{co}}, \quad \varepsilon_1 = \frac{b^{cor}-b}{b} = \frac{N_{cb}\cdot w_{cr}}{b} = \frac{N_{cb}\cdot\left[\pi D_b\cdot(\alpha_{rs}-1)\cdot X\right]}{b} \tag{13}$$

Strain ε_1 is orthogonal to the direction of applied compression and is caused by corrosion of longitudinal compression reinforcement; it represents a smeared measure of splitting crack widths of the cover. Where N_{cb} in Eq. (13) is the number of bars in the compression zone of the cross section, w_{cr} is the crack width as a function of corrosion penetration and α_{rs} is the volume ratio of oxides with respect to the parent metal.

Concrete strength of layers confined by stirrups is increased owing to the exerted confining pressure, $\sigma_{lat,st}^{cor}$, which is also reduced from its nominal value due to corrosion (Pantazopoulou and Tastani 2004) as,

$$f_{cc}^{'} = f_c^{'} + 3.1\cdot\left(\frac{\sigma_{lat,st-y}^{cor}+\sigma_{lat,st-x}^{cor}}{2}\right) = f_c^{'} + 1.5\cdot k_{st}^{conf}\cdot\rho_{sv}^{cor}\cdot f_{y,st}^{red} \tag{14}$$

where, k_{st}^{conf} is the confinement effectiveness related with the arrangement of stirrups, ρ_{sv}^{cor} is the volumetric ratio of corroded stirrups (considering sectional area to be reduced by corrosion, $A_{st}^{cor}=A_{st}(1-X)^2$ and $f_{y,st}^{red}$ the reduced available stirrup stress (from Eq. 6).

3.2 Enhancement of Flexural Strength through FRP Jacketing

Flexural resistance is influenced only indirectly by jacket placement, through the strength increase of concrete in the compression zone owing to confinement. Flexural strength also benefits by containment of the cracked corrosion-contaminated cover that would otherwise have spalled-off at ultimate. In calculating V_{flex}^{enh} of the encased member from first principles, the enhanced axial strength and deformation capacity of concrete in the compression zone of the cross section is calculated from the modified classical confinement model of Richart et al 1928 (Pantazopoulou and Tastani 2004) as,

Confined Concrete Strength: $$f_{cc}^{'} = f_c^{'} + 1.5\left(k_{st}^{conf}\cdot\rho_{sv}^{cor}\cdot f_{y,st}^{red} + k_f^{conf}\cdot\rho_{fv}\cdot E_f\varepsilon_f^{eff}\right) \tag{15a}$$

Strain at Peak Stress: $$\varepsilon_{cc} = 0.002 + 0.015\frac{k_{st}^{conf}\cdot\rho_{sv}^{cor}\cdot f_{y,st}^{red} + k_f^{conf}\cdot\rho_{fv}\cdot E_f\varepsilon_f^{eff}}{f_c^{'}} \tag{15b}$$

Strain Capacity: $$\varepsilon_{cc,u} = \varepsilon_{c,u} + 0.075\cdot\left(\frac{k_{st}\cdot\rho_{sv}^{cor}\cdot f_{y,st}^{red} + k_f^{conf}\cdot\rho_{fv}\cdot E_f\cdot\varepsilon_f^{eff}}{f_c^{'}} - 0.1\right) \geq \varepsilon_{c,u} \tag{15c}$$

Strain $\varepsilon_{c,u}$ is in the range of 0.003 to 0.004. The effective strain, ε_f^{eff} is taken as $0.5\varepsilon_{fu,d}$ for closed jackets ($\varepsilon_{fu,d}$ is the nominal rupture strain of the jacket material). Coefficients k_f^{conf}, ρ_{fv} and E_f are the confinement effectiveness, the volumetric ratio of jacket and the modulus of elasticity of the composite material ($k_f^{conf}=1-((b'^2+d'^2)/3A_g(1-\rho_s)$), where b' and d' the straight sides of the rectangular cross section encased by the jacket after chamfering the corners, FIB 14, 2001).

Bousias et al. (2004) reported that the primary benefit by FRP jacketing on corrosion-damaged old-type members was an increase of deformation capacity from the initial condition (uncorroded, no jackets) up to full exploitation of the available strain ductility of corroded tension reinforcement (ε_{su}^{cor}). Based on this result, an upper limit to practicable increase of $\varepsilon_{cc,u}$ is obtained considering the associated strain profile in the critical section of the member: $\varepsilon_{cc,u} \leq \varepsilon_{su}^{cor}\cdot\xi/(1-\xi)$ where ξ the normalized depth of the compression zone.

References

ACI 440.2R-02 (2002). “Guide for the design and construction of externally bonded FRP systems for strengthening concrete structures”. American Concrete Institute, Detroit, Michigan.

Bousias N., Trianatafillou T., Fardis M., Spathis L. and O’Regan B. (2004). Fiber-reinforced polymer retrofitting of rectangular RC columns with or without corrosion. “ACI Structural Journal”, Vol. 101, No. 4, pp. 512-520.

Cairns, J., Millard, S. (1999). Reinforcement Corrosion and its Effect on Residual Strength of C. Strs. *Proc. of 8th Int. Conf. on Structure Faults & Repair*, M. Forde, ed., Eng. Technics Press, Edinburgh, U.K.

Castel, A., Francois, R., Arliguie, G. (2000). Mechanical Behavior of Corroded R.C. Beams. II: Bond and Notch Effects. *RILEM, Materials and Structures*, 33, pp. 545–551.

Coronelli D. and Gambarova P.G. (2004). Structural assessment of corroded r.c. beams: modeling guidelines. “ASCE J. of Structural Engineering”, Vol. 130, No. (8, pp. 1214–1224.

Debaiky A., Green M., Hope B. (2002). Carbon Fiber-Reinforced Polymer Wraps for Corrosion Control and Rehabilitation or R.C. Columns. *ACI Material J.*, 99 (2), pp. 129-137.

FIB Bulletin No. 14 (2001). Externally Bonded FRP Reinforcement for R.C. Structures. Technical report prepared by T.G. 9.3, *International Federation for Structural Concrete (fib)*

Lee. H., Kage T., Noguchi T. and Tomosawa F. (2003). An experimental study on the retrofitting effects of reinforced concrete columns damaged by rebar corrosion strengthened with carbon fiber sheets. “Cement and Concrete Research”, Vol. 33, No. 4, pp.563–570.

Lundgren K. (2002). Modelling the effect of corrosion on bond in r.c. “Magazine of Concrete Research”, Vol. 54, No. 3, pp. 165-173.

Martin-Perez B. and Pantazopoulou S. (2001). Effect of bond, aggregate interlock and dowel action on the shear-strength degradation of r.c. “Elsevier Engineering Structures”, Vol. 23, pp. 214-227.

Moehle J., Elwood K. and Sezen H. (2002). Gravity load collapse of building frames during earthquakes. “Proceedings of S. Uzumeri Symposium on Behavior and design of concrete structures for seismic performance”, ACI SP-197, pp. 215-238.

Pantazopoulou S.J. and Papoulia K.D. (2001). Modelling of cover-cracking due to reinforcement corrosion in RC structures. “ASCE Journal of Engineering Mechanics”, Vol. 127, No. 4, pp. 342-351.

Pantazopoulou S.J., Bonacci J.F., Sheikh S., Thomas M.D.A., and Hearn N. (2001). Repair of corrosion-damaged columns with FRP wraps. “ASCE J. of Composites for Construction”, Vol. 5, No. 1, pp. 3-11.

Soudki K., Sherwood T. (2000). Behavior of R.C. Beams Strengthened with Carbon Fibre Reinforced Polymer Laminates Subjected to Corrosion Damage. *Canadian J. of Civil Engineering, NRC, Special Issue on ISIS-Canada*, 27 (5), pp. 1005-1010.

Tastani S. and Pantazopoulou S. (2004). Experimental evaluation of FRP jackets in upgrading r.c. corroded columns with substandard detailing. “Elsevier Engineering Structures”, Vol. 26, No. 6, pp. 817-829.

Tastani S.P. and Pantazopoulou S.J (2005). “Recovery of seismic resistance in corrosion-damaged reinforced concrete through FRP Jacketing”, invited paper, *International Journal of Materials and Product Technology,* Vol. 23, Nos. 3/4, pp. 389 -415.

Tastani S.P. and Pantazopoulou S.J (2007a). “Seismic Assessment and Upgrading of corrosion-damaged R.C. members through FRP jacketing.” Tech. Chron. Sci. J. TCG, I, No 1-2

Tastani S.P. and Pantazopoulou S.J. (2007b). "Behavior of corroded bar anchorages”, *ACI Structural Journal*, Vol. 104, No. 6, pp. 756-766.

Vecchio, F., Collins, M. (1986). The Modified Compression Field Theory for R.C. Elements Subjected to Shear. *ACI Journal* 83(2), pp. 219–231.

Implications of anchorage bar yield penetration on the FRP jacketing effectiveness before and after repair

S. Tastani, Dept. of Civil Engrg., Democritus University of Thrace, stastani@civil.duth.gr
G. Thermou, Dept. of Civil Engrg., Aristotle University of Thessaloniki, gthermou@civil.auth.gr
and S. J. Pantazopoulou, Dept. Civil & Env. Engrg., University of Cyprus, pantaz@ucy.ac.cy

In lightly-reinforced columns repaired through FRP-jacketing (i.e., jacketed after some extent of initial damage had been induced), the level of damage attained during the first loading –the latter is quantified by the attained longitudinal bar tensile axial strain, see Fig. 1a- appears to be critical for the post repair structural response and the associated FRP effectiveness. Irreversible damage of the bar-concrete interface and the associated loss of bond strength owing to extensive yield penetration into the anchorage during initial loading seems to limit the FRP-jacketing effectiveness as compared with the case where the element had attained an initial premature mode of failure, usually by shear, or by lap-splice splitting (Thermou and

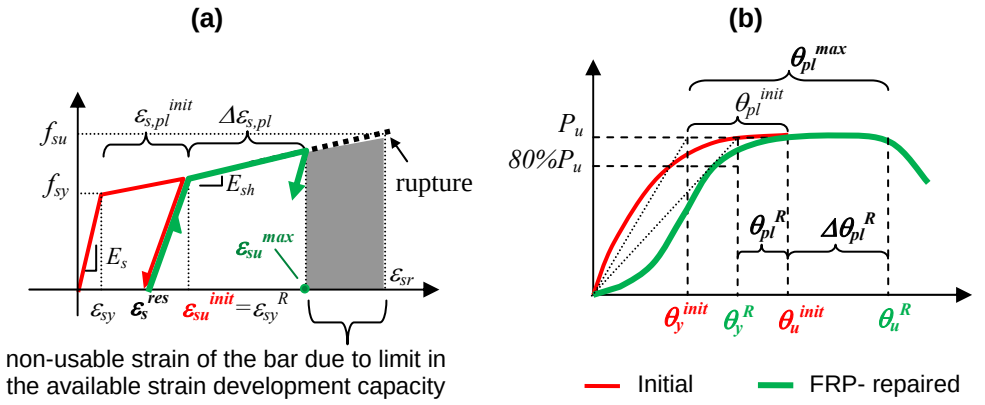

Figure 1. a) Stress–strain law of tension steel (definition of strain indices). b) Comparative representation between the initial and the FRP repaired response of a lightly reinforced column (definition of drift indices).

Pantazopoulou 2009, Syntzirma and Pantazopoulou 2006, Syntzirma et al. 2006). In this case damage is effectively suppressed in the wrapped region at the expense of increased contribution owing to pullout either from the reinforcement anchorage in the footing or from the lap-splice developed in the plastic hinge zone. The fraction of drift capacity due to pullout is greater when reinforcement has undergone large inelastic strains at the critical section during the pre-repair phase of loading. Actually, the increase of the inelastic strain at the critical section has a dually negative impact on the deformability of the post-repair response even if the interfacial bond is fully recovered prior to jacketing; firstly the available inelastic strain decreases by the amount of residual strain ε_s^{res} consumed in the initial phase of loading, with a consequent result being the limitation of the dependable post-repair flexural drift capacity. Furthermore, if no interventions are implemented within the anchorage, the available anchorage length is shortened by an amount equal to the yield penetration segment ℓ_r^{init} (Fig. 2a) which corresponds to a reduction in the effective development capacity. Note that for an anchorage to be fully retrofitted, before the application of the FRP jackets on the member length, it would be necessary to replace the concrete cover with a new cementitious

grout combined with epoxy injection wherever it is suspected that even fine cracks might have been formed in the concrete mass.

Comparing the pre- and post-repair resistance curve of load versus lateral drift (see Fig. 1b), it is noted that the initial stiffness of the repaired column is significantly lower than the slope of the ascending branch of a lightly reinforced column having the same details but loaded in pristine condition (stiffness is defined by the secant slope to the point of initial yielding θ_y^{init} -this corresponds to yielding strain ε_{sy}- or apparent yielding θ_y^{R}, the latter corresponds to the attained strain ε_{su}^{init} , Fig. 1a). Actually, the resistance curve of a repaired column that had initially developed some ductility, often presents a concave rather than an arched shape, due to the initial travel of the bar required in order to lock the ribs and mobilize the anchorage. This phenomenon is attributed to the plastic strains experienced by the longitudinal reinforcement during the first loading phase ($\varepsilon_{s,pl}^{init}$) inside the anchorage, which results in a residual inelastic strain ε_s^{res} after complete unloading. (From the stress – strain steel law depicted in Fig. 1a, it follows that $\varepsilon_s^{res}=\varepsilon_{s,pl}^{init}-E_{sh}/E_s(\varepsilon_{so}^{init}-\varepsilon_{sy})$.) This inelastic strain ε_s^{res} integrated over the initial yield penetration length ℓ_r^{init} (see Fig. 2a) in the anchorage produces a significant slip that remains in the critical cross section after unloading and also increases the initial drift rendering the post repair response more compliant; thus the chord drift at apparent yielding θ_y^{R} is greater than the initial θ_y^{init}. Note that the drift at apparent yielding θ_y^{R} is attained when strain reaches the apparent yield threshold at the post repair loading phase, $\varepsilon_{sy}^{R}=\varepsilon_{s,pl}^{init}$ (Figs. 1a, 2a). The residual inelastic strain ε_s^{res} is represented by the dashed area depicted in Fig. 2a and it is the result of the difference between the strain distribution at apparent yielding (post repair) and the strain distribution at yielding (prior-to-repair loading when the element is in pristine condition).

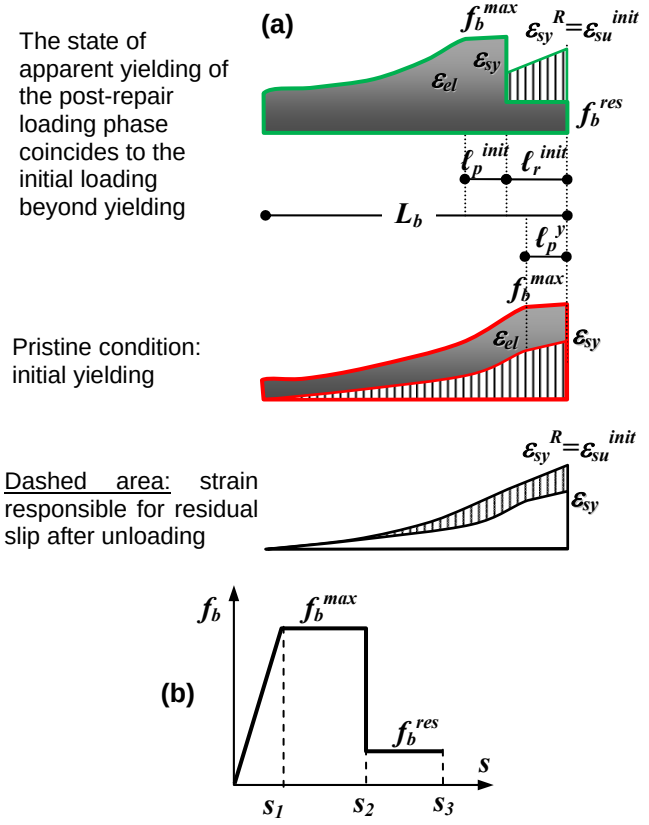

Figure 2. (a) Distribution of strain and bond along the anchorage length upon initial yielding and apparent yielding. (b) A simplified bond – slip law.

Initial loading phase (prior repair)

For the initial loading phase and for inelastic strain ε_{su}^{init} greater than the yield strain ε_{sy} at the loaded end of an intact anchorage the solution of the field equations of bond mechanism results in the following expressions that define the slip at the critical cross section (loaded end of anchorage where $f_b=f_b^{res}$) as well as the yield penetration length ℓ_r^{init} (Fig. 2a):

$$\varepsilon_{su}^{init}=\varepsilon_{sy}+\frac{4f_b^{res}}{D_bE_{sh}}\cdot\ell_r^{init}\quad\Rightarrow\quad\ell_r^{init}=\frac{\left(\varepsilon_{su}^{init}-\varepsilon_{sy}\right)\cdot D_bE_{sh}}{4f_b^{res}} \tag{1a}$$

$$s_o = s_1 + \left(\ell_p^{init} + 0.5\ell_r^{init} - \frac{(\ell_p^{init})^2}{2L_{b,min}} \right) \cdot \varepsilon_{sy} + \frac{1}{2}\ell_r^{init} \cdot \varepsilon_{su}^{init} \quad ; \quad L_{b,min} = \frac{D_b}{4}\frac{f_{sy}}{f_b^{max}} \tag{1b}$$

$$\ell_p^{init} = \frac{D_b E_s \left(\varepsilon_{sy} - \sqrt{\varepsilon_{sy}^{\,2} - 8 f_b^{max} (s_r - s_1)/(D_b E_s)} \right)}{4 f_b^{max}} \tag{1c}$$

For the definition of the unknown length ℓ_p^{init} where bond is plastified, the set of Eqs. (1d) should be solved (variables are s_r, ε_{el}, and ℓ_p^{init}).

$$\left.\begin{aligned} s_r &= s_1 + 0.5(\varepsilon_{sy} + \varepsilon_{el}) \cdot \ell_p^{init} \\ \varepsilon_{el} &= \varepsilon_{sy} - \frac{4 f_b^{max}}{E_s D_b} \cdot \ell_p^{init} \\ \varepsilon_{el} &= s_1 \omega \cdot \left(1 - e^{-2\omega(L_b - \ell_r^{init} - \ell_p^{init})} \right) / \left(1 + e^{-2\omega(L_b - \ell_r^{init} - \ell_p^{init})} \right) \quad ; \quad \omega = \sqrt{\frac{4 f_b^{max}}{E_s D_b s_1}} \end{aligned}\right\} \tag{1d}$$

Parameter E_s is the elastic modulus of steel. The strain ε_{el} corresponds to the initiation of the elastic response of bond along the remaining length, L_b-(ℓ_r^{init}+ℓ_p^{init}).

The associated total chord rotation θ_u^{init} is then:

$$\theta_u^{init} = \left(\frac{H_s}{6} + \ell_p^{init} + \ell_r^{init} - \frac{(\ell_p^{init})^2}{2L_{b,min}} \right) \varphi_y + \left(\ell_p^{span} + \frac{\ell_r^{init}}{2} \right) (\varphi_u - \varphi_y) \tag{1e}$$

where H_s the members total height, curvature φ_i=ε_{si}/(d-c) (index i=*y* for yield and *u* for ultimate) and *c* the depth of the compression zone (it can be defined through the diagram of Fig. 3).

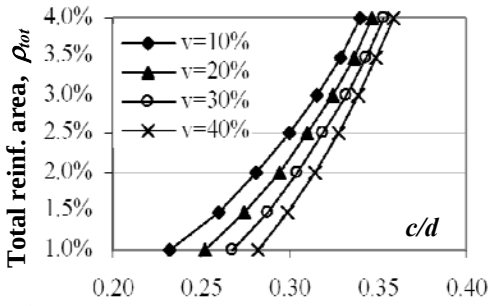

Figure 3. Compression zone depth as a function of reinforcement ratio and axial load.

Post repair loading phase associated to the anchorage strain capacity

When the bar axial strain attains its peak value ε_{su}^{max} at the critical section of the column an imminent failure of the bar by pullout occurs, where yielding has penetrated deep enough into the anchorage so that the remaining bonded length $L_{b,min}$ barely suffices to support the bar force. The strain capacity of the bar ε_{su}^{max} and the corresponding slip designated at the anchorage entrance s_o^{max} are given from Eqs. (2a, b). The region of maximum sustainable yield penetration is denoted as ℓ_r^R=L_b-$L_{b,min}$.

$$\varepsilon_{su}^{max} = \varepsilon_{sy} + 4 \cdot (L_b - L_{b,min}) f_b^{res} / (D_b E_{sh}) \tag{2a}$$

$$s_o^{max} = s_1 + 0.5 L_{b,min} \varepsilon_{sy} + \left(\varepsilon_{sy} + 2 \cdot (L_b - L_{b,min}) f_b^{res} / (D_b E_{sh}) \right) \cdot (L_b - L_{b,min}) \tag{2b}$$

The associated total chord rotation θ_u^{max} to this strain state ε_{su}^{max} is given by Eq. (2c):

$$\theta_u^{max} = \overbrace{H_s / 6 \cdot \varphi_y + \ell_p^{span} (\varphi_u^{max} - \varphi_y)}^{flexural} + \overbrace{0.5 L_b \varphi_y + 0.5 (L_b - L_{b,min}) \varphi_u^{max}}^{slip} \quad ; \quad \varphi_u^{max} = \frac{\varepsilon_{su}^{max}}{d - c} \tag{2c}$$

In this post repair loading phase critical is the definition of bond strength f_b^{max} (and its residual value f_b^{res}) used in Eqs. (2). Whereas bond strength is enhanced through the passive confining pressure exerted by the FRP jacket, its value depends also on the intervention measures within the anchorage: for an anchorage to be fully retrofitted, before the application of the FRP jackets on the member length, it would be necessary to replace the concrete cover with a new cementitious grout combined with epoxy injection wherever it is suspected that even fine cracks might have been formed in the concrete mass. This magnitude is given by Eq. (2d).

$$f_b^{max} = \frac{2\mu}{\pi} \cdot \left(\zeta \frac{C}{D_b} f_{ct} + 0.33 \frac{A_{st}\, f_{st,y}}{D_b\, N_b\, S} + \frac{2 t_j\, E_f\, \varepsilon_{f,eff}}{D_b N_b} \right) \quad \text{(2d)}$$

where μ is the coefficient of friction along the splitting plane (0.9-1.2 for ribbed, and 0.3 for smooth reinforcement), ζ accounts for the tensile behavior of the concrete cover (1 for fully elastic and 2 for fully plastic), C is the cover thickness, f_{ct} is concrete's tensile strength (0.35~0.5$\sqrt{f_{co}}$), N_b is the number of tension bars restrained by the stirrup legs included in A_{st} (A_{st} is the cross sectional area of stirrups crossing the splitting plane), s is the stirrup spacing, $f_{st,y}$ the stirrup yield stress, t_j, E_f and $\varepsilon_{f,eff}$ are the FRP jacket thickness the material modulus of elasticity and its effective strain as a mechanism of confinement for laps (in the range of 0.0015~0.002). The FRP contribution is omitted in the pre-repair loading phase. In anchorages that have been split lengthwise prior to FRP jacketing, the development capacity after the addition of the FRP is only marginally improved unless cover replacement has preceded the FRP jacketing. Thus, prior cover longitudinal cracking eliminates the first term in Eq. (2d), with commensurate implications on the strain development capacity of the anchorage. The residual bond strength f_b^{res} that is developed over the yield length of the anchorage may be taken equal to 0.4 f_b^{max} as a result of the clamping force exerted by transverse reinforcement at the discrete locations of contact between stirrups and the main bars.

References

Tastani S.P, Thermou G.E., Pantazopoulou S.J. (2012). "Deformation analysis of reinforced concrete columns after repair with FRP jacketing." 15th World Conference on Earthquake Engineering, September 24-28, Lisbon, Portugal (paper no. 3164).

Syntzirma D., Thermou G., Pantazopoulou S., Halkitis G. (2006). Experimental research of r.c. elements with substandard details. 1st European Conf. on Earthquake Eng. and Seismology, Geneva, Switzerland, 2006, (paper # 819).

Syntzirma, D.V., Pantazopoulou, S.J. (2006). Assessment of deformability of r.c. members with substandard details. 2nd International fib Congress, Naples, Italy, 2006 (paper number 446).

Thermou G., Pantazopoulou S. (2009). Fiber reinforced polymer retrofitting of substandard r.c. prismatic members. ASCE J. Composites for Construction 13:6, 535-546.

Tastani S.P. and Pantazopoulou S.J. (2013). "Reinforcement-Concrete Bond: State Determination along the Development Length." ASCE J. of Structural Engineering, 139(9); 1567-1581.

Lower Adequate FRP Confinement Limits for RC Columns

T.C. Rousakis[1], A.I. Karabinis[2]

Introduction

The contribution deals with columns of non-circular section having internal steel reinforcement according to modern design codes or old-type inadequate detailing. Columns with longitudinal bars which are critical to premature buckling are also included. The effect of slender bars on lower limit cases of strengthening through FRP confinement is examined. Plain concrete FRP confined columns and columns with bars adequately supported by transverse steel reinforcement are investigated for comparison. The columns under consideration were subjected to monotonic or cyclic axial compression.

A significant variation in the behavior of FRP confined concrete comes up when bars are unstable, for a light external strengthening scheme as well as for monotonic or cyclic loading. The lower limits proposed by existing recommendations for adequate FRP confinement strengthening of columns are examined.

Criteria for adequate confinement

Mirmiran et al. (1998) performed an elaboration of experimental data and proposed a Modified Confinement Ratio (MCR) as a measure of confinement effectiveness:

$$MCR = (2r/b)*(f_{le,FRP}/f_{co}) \quad (1)$$

where, b is the external dimension of a square concrete section (or diameter of cylinder), r is the corner radius, and $f_{le,FRP}$ is the maximum effective confining pressure provided by FRP for use on circular and rectangular reinforced concrete confined with FRP. Above researchers concluded that specimens with MCR <0.15 display inelastic softening stress-strain behavior (with degrading branch). Thus, these specimens represent inadequate external strengthening cases. Consequently, they proposed an extra relation to predict the failure stress ($f_{cu,FRP}$) for those cases. Spoelstra & Monti (1999), in their study performed a parametric analysis using their proposed model to produce rough relations for calculating the strength and failure strain of uniformly confined concrete (of circular sections). They noted that, for $f_{le,FRP}/f_{co}$ <0.07 a softening inelastic behavior occurs as the failure stress is lower than plain concrete strength $f_{cu,FRP} < f_{co}$. That is, their proposed limit expressed as MCR is less than half (for circular intersections where 2r=b, MCR= $f_{le,FRP}/f_{co}$ =0.15) of that by Mirmiran et al (1998). Lam & Teng (2003) found out after comparison with experimental data, the value 0.07 could serve as the threshold for identifying specimens where $f_{cu,FRP} < f_{co}$, if it pertains to the actual confining pressure at failure. That is, the effective strain at failure ($\varepsilon_{je,FRP}$ or $\varepsilon_{h,rup}$) as a percentage of the strain calculated from FRP jacket specimens subjected to direct tension (ε_{fu} or ε_{frp}), or taken as $\varepsilon_{je,FRP} = 0.586*\varepsilon_{fu}$. The American design recommendations (ACI 440.2R-08) consider the studies by Lam & Teng (2003) and those by Harries and Carey (2003) and Carey and Harries (2005). Thus, they adopt a coefficient 0.55 (instead of 0.586) and a limit ratio $f_{le,FRP}/f_{co}$ = 0.08, to ensure an ever-increasing behavior of the inelastic branch.

For rectangular sections, the ACI 440.2R-08 adopts the approach by Lam & Teng (2003) to calculate the confinement pressure considering a cross-section (dimensions b_{min} X b_{max}) of equivalent diameter d = $\sqrt{(b_{min}^2 + b_{max}^2)}$ or $\sqrt{(2b^2)}$ for square sections. Also, the ratio of the cross-sectional area where the concrete is under triaxial compressive stress state (A_e / A_c) is necessary, to get the suitably reduced confining force for rectangular sections.

[1] Democritus University of Thrace, Xanthi, Greece, trousak@civil.duth.gr
[2] Democritus University of Thrace, Xanthi, Greece, karabin@civil.duth.gr

The Italian guide CNR-DT 200/2004 adopts a similar approach with a limit ratio of $f_{le,FRP}/f_{cd} < 0.05$. By considering that, the design concrete strength includes a design material coefficient ($f_{cd} = f_{ck} / 1.5$). The limit is almost similar to that of the ACI. However, the ultimate confining pressure $f_{le,FRP}$ requires that $\varepsilon_{je,FRP} = 0.004$ or lower, while the effectiveness of confinement relations is different. Thus, the results differ from ACI's.

Pellegrino and Modena (2010) propose an FRP efficiency coefficient k_ε for rc columns, that provides the effective hoop strain of the FRP and is also related to bars' buckling effect. Coefficient k_ε is higher for higher axial rigidity of the FRP confinement. On the other hand they found out that higher mechanical percentage of steel bars requires higher rigidity of the jacket to contrast premature buckling. Otherwise, k_ε reduces considering that significant stress concentrations on the FRP cause premature fracture. The coefficient is lower for carbon than glass material.

As reported in Rousakis et al. 2012a, existing strength models need further modification to predict the concrete maximum bearing stress f_{cc} (and stress at failure f_{cu}) for very low external FRP confinement resulting in a softening stress-strain behaviour. Teng et al. 2009 proposed an advanced criterion for sufficient confinement of circular columns. They suggested that for $\rho_\kappa<0.01$ no strength enhancement takes place ($f_{cc}=f_{co}$) and that a degrading post-peak stress response follows. On the other hand, the model by Rousakis et al. 2012 could predict with high accuracy the ultimate load of columns with very low confinement (inadequate confinement with $\rho_\kappa<0.01$ or cases where $f_{cc}/f_{co}<1.15$).

Noncircular reinforced concrete columns

The main criteria of adequate confinement in recommendations concern only failure load approaches and mainly plain concrete sections. The experimental investigation by Rousakis and Karabinis 2012 on reinforced concrete columns under monotonic or cyclic compression revealed a varying behaviour of lightly FRP confined columns. The lower bound value for adequately FRP confined columns with softening inelastic branch was for MCR=0.184 (or 0.153 per ACI 440). It was valid for plain concrete square columns, as well as for columns with slender bars of the research. The value of MCR=0.153 is around the limit proposed by Mirmiran et al 1998 and close to the provisions by CNR for glass. Yet, inadequate behavior resulted for columns having slender bars, or marginal adequacy with softening branch for columns with close stirrups.

According to the ACI 440.2R-08, the upper limit of usable axial strain, considered for design of confined concrete is 10‰ to preserve its structural integrity. This limit strain could serve as the best objective in terms of succeeded strains. Though, it is not always more effective than strength enhancement, when a specific curvature ductility is of concern. In columns with slender bars, a softening branch resulted and inadequate load response for MCR=0.153 or lower. Also, the loading history of gradually increasing load-unload cycles resulted in further degraded response of those columns.

FRP Strengthened columns with low s/Φ_L of the longitudinal bars and heavy steel stirrup confinement (non slender bars) under cyclic loading showed a clear upgraded mechanical behavior. Their response was superior compared to columns with slender bars, or to plain concrete columns subjected to cyclic loading. A lower bound ratio of MCR=0.153 corresponded to a clearly adequate mechanical response. A practically negligible contribution of compressed slender bars to the total axial load carried by the column come up, especially when the external confinement is low. Results of cyclically loaded specimens varied a lot. Columns with slender and non slender bars had no significant variation of the axial strain at failure. Though, higher strains were recorded in columns with non slender bars. Results of cyclically loaded specimens also varied a lot.

Considering a bearing load approach, the criterion of adequate confinement led to a lower bound value of MCR = 0.184 (or 0.153 per ACI 440). It corresponded to a softening behavior (degradation of load <15%) for columns containing slender bars. For non slender bars columns of the category displayed a hardening behavior, independently of the mode of loading. The strengthening requirements were

higher if a clear hardening behavior was desired and a significant strain ductility upgrade, around the upper limit value of 10‰ of ACI recommendations. Near that performance was the response of specimens having MCR=0.256.

Similar were the results from the experimental investigation by Rousakis et al. 2012b concerning rectangular reinforced concrete columns with GFRP jackets. Even a light external strengthening of deficient reinforced concrete columns of rectangular section (side ratio equal to 1.66) with GFRP confinement could provide a significant enhancement of their stress-strain response. Strengthening with 4 layers of GFRP sheets that corresponded to f_{le}/f_{co} = 0.173 (calculated according to ACI approach), led to a stabilized post-peak stress-strain behaviour with bearing load higher than $0.8f_{cc}$ and failure strains higher than 1%, irrespectively of the bars slenderness and quality.

For half of the previous FRP strengthening (f_{le}/f_{co} = 0.086) the behaviour of the columns was clearly degrading at post-peak load region. Initiation of stabilization of load could be recognised in cases of close stirrups, yet it occurred at load lower than $0.8f_{cc}$. However the upgrade of failure strains was not negligible even for this very low strengthening. It ranged around 0.8% axial strain. In above cases, columns with more slender and lower quality bars present further degrading overall stress-strain behaviour (Figure 1).

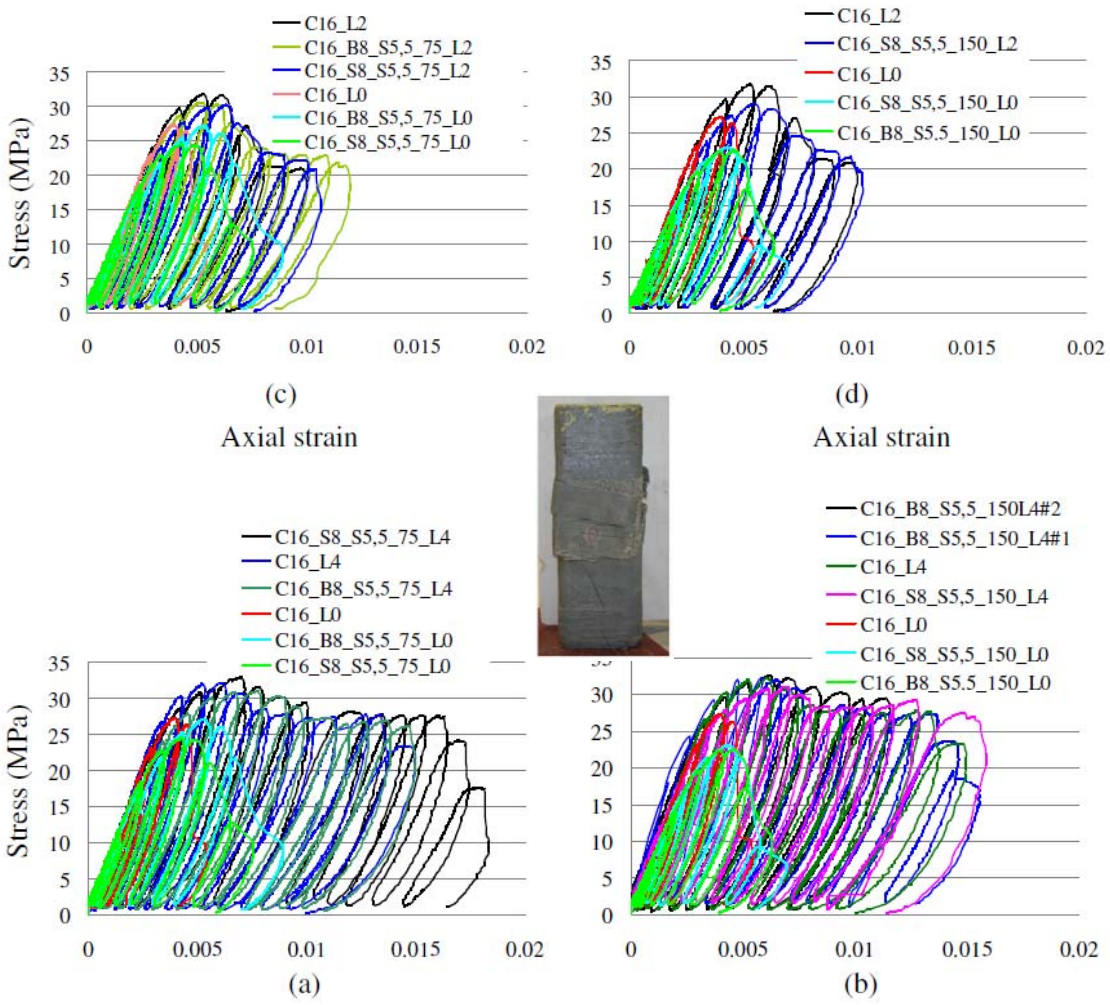

Figure 1: Stress-strain curves of FRP confined plain and reinforced concrete specimens compared against unwrapped specimens (adapted from Rousakis et al. 2012b).

Conclusions and Points for Discussions

The research investigates the lower adequate confinement levels for reinforced concrete columns subjected to monotonic or cyclic compression. The effect of slender bars was also examined. It is concluded that a lower adequate FRP confinement limit f_{le}/f_{co} around 0.175 per ACI 440 could provide reinforced concrete columns with a stable post-peak behaviour with acceptable load drop (<20%) and ultimate axial strains around 1%. The same value could be the limit for the use of strength prediction models of FRP confined columns with slender bars, yet considering their contribution negligible.

Similar are the findings from other experimental campaigns in real scale columns. Yet, the experiments in square or even more in rectangular reinforced concrete columns with slender bars are very limited. The qualitative criteria for adequate behaviour of FRP confined RC columns should be reviewed. Targeted experiments and analyses should address the effects of slender bars, of the shape of the section and other significant parameters.

Key references

Rousakis T.C., Rakitzis T.D., Karabinis A.I. (2012a). Design - Oriented Strength Model for FRP Confined Concrete Members. *ASCE Composites for Construction,* 2012, 16(6), 615–625.

Rousakis T.C., Karabinis A.I. (2012). Adequately FRP confined reinforced concrete columns under axial compressive monotonic or cyclic loading. RILEM Materials and Structures, Springer Netherlands, 2012;45(7) 957-975.

Rousakis T., Tsakiris S., Karabinis A. (2012b). Adequate FRP Confinement of Rectangular Reinforced Concrete Columns Suffering from Premature Bars' Buckling. In: Monti J. (ed.) The 6th International Conference on FRP Composites in Civil Engineering – CICE 2012. Rome 13 - 15 of June 2012. http://www.iifc-hq.org/publications/proceedings-iifc-official-conferences/cice-2012-rome-italy-13-15-june-2012/

Effective Lateral Strain of FRP Confined Concrete – Load Originated Failure Criterion

T.C. Rousakis[1], A.I. Karabinis[2]

Introduction

Most empirical models on FRP confined concrete consider a constant confinement effectiveness coefficient k1 and an effective lateral strain at failure εje of the FRP jacket being lower than the one taken out from direct tension tests on cured FRP sheets. Average constant reduction factors are assumed for the tensile deformability of the jacket with respect to the material of the FRP. Design recommendations for strengthening with FRPs may follow more conservative approaches ending up with a global reduction factor for FRP jackets around 0.55 of deformability under direct tension ε_{ju}. Different specific ultimate strain limits for different FRP materials may be taken into account in Eurocode 8 part 3 for seismic retrofit, for the satisfaction of target curvature ductility requirements.

The numerous available experimental data on uniformly FRP confined concrete allow for a revisiting of the reliability of the assumptions of constant values for k_1 and ε_{je} and of data required by different empirical modeling approaches. As shown in Rousakis et al. 2012 (and also reported in several studies) the experimental value of k_1 is not constant even for specimens with the same normalized confinement pressure, while it may vary with the mechanical properties of concrete and confinement. Moreover k_1 varies throughout the loading of each specimen (Rousakis et al. 2008). However, several reliable models use a constant value of k_1 usually between 2 and 4.5 depending on their experimental database reference. The same study gathers the collective experimental data and remarks from different researches. It is concluded that the effective strain at failure of FRP jacket (ε_{je}) also varies and is usually lower than that of jacket's flat coupons under direct tension. As reported before, this may be due to the compression of the jacket through its bond with the directly compressed concrete as well as due to the stress concentrations because of the development of cracks in concrete. Also the small curvature of the FRP jacket or corner curvatures may cause premature failures. Finally, the quality of execution may lead to lower failure strains. The anchorage arrangement of sheet layers alters the deformability of FRP leading to a marked stress variation. The increase in the number of layers mitigates influences of stress concentrations. On the other hand, it magnifies the effect of features related to the poor implementation of the FRP sheets (such as waving of fibers). Further, the modulus of Elasticity of the fibers (E_f) and in particular the axial tensile rigidity of the jacket in relation to the axial compressive rigidity of concrete seem to affect the deformability of FRP. In high strength concretes with light confinement a softening behavior reveals followed by a premature failure of the jacket (Rousakis et al. 2008). Also, several analyses suggest that even the knowledge of experimentally measured values of the FRP tensile strain at failure does not always lead to more reliable prediction of confined concrete strength enhancement. To the best knowledge of the authors, no reliable correlation of the effective strain at failure with key features of the mechanical problem has emerged so far and a rational approach on ε_{je} is still an open issue.

This contribution presents an alternative reliable and simple approach to predict the FRP confined concrete strength. It is based on the dependence of the strength prediction to the more reliable experimental measurements of the mechanical properties of the confining means (Young's modulus and

[1] Democritus University of Thrace, Xanthi, Greece, trousak@civil.duth.gr
[2] Democritus University of Thrace, Xanthi, Greece, karabin@civil.duth.gr

thickness) and bypasses variables of FRP confinement that are not yet fully determined. The problem of FRP confined concrete is solved with fewer unknowns and a rational failure criterion comes out that interrelates varying k_1 and ε_{je}.

Strength model

As concluded in previous studies of the authors, the product of ε_{je} times k_1 presents a strong linear interrelation with the modulus of elasticity E_f. Thus, following an alternative approach, the approximate estimation of ε_{je} or k_1 in predicting the strength with a Richart et al. model (which is based on simple mechanics) can be avoided. The alternative model is calibrated only with load experimental measurements, thus eliminating errors caused by potential differences in sheet wrapping arrangement, in material testing and strain measurements strategy (axial and lateral) followed by different researchers. A significant feature of the model which expresses indirectly the varying ε_{je} and k_1 is that it can capture the varying strength enhancement observed experimentally in all the range of normalized confining pressures (Rousakis et al. 2012). In Figure 1 it can be seen that the strength predictions of the model seem more rational than the very efficient Campione & Miraglia 2003 (Richart et al. type) model when compared with the experimental ones.

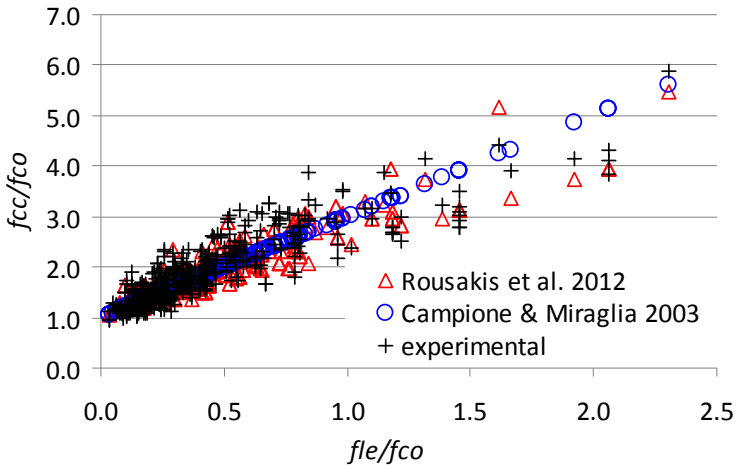

Figure 1: Variability of strength enhancement with normalized confinement pressure. Experimental results and modeling of strength enhancement according to Campione & Miraglia 2003 and Rousakis et al. 2012 models over all data (471 specimens)

The presented model has the following simple expression:

$$f_{cc}/f_{co} = 1+ k_1(f_{le}/f_{co}) = 1+ k_1(0.5\ \rho_f\ E_f\ \varepsilon_{je}/f_{co}) = 1+ (\rho_f\ E_f/f_{co})(\ 0.5\ k_1\ \varepsilon_{je}),\quad \text{that is}$$

$$f_{cc}/f_{co} = 1+ (\rho_f E_f/f_{co})(\alpha\ E_f\ 10^{-6}\ /\ E_{f\mu}\ +\ \beta) \qquad (1)$$

with $\rho_f = 4t_f / d$ and $E_{f\mu} = 10$ MPa (for units' compliance). For FRP sheet wraps α= -0.336 and β= 0.0223. For FRP tube encased concrete α= -0.2300 and β= 0.0195. The model suggests that concrete strength increase depends strongly (among other minor parameters) on the normalized axial rigidity of the confining means ($\rho_f E_f / f_{co}$). The lateral strain at failure of concrete equals the effective strain at failure of an elastic reinforcement (ε_{je}). This strain strongly depends (among other minor parameters) on the modulus of elasticity of its reinforcing fibers (E_f) and on the confinement effectiveness coefficient (k_1). Two sets of parameters α & β are proposed to account for the difference in effectiveness met in the two different confining cases through FRP wrapping or FRP tubes.

Failure criterion

The alternative solution of the FRP confined concrete strength problem considers fewer unknowns. In fact, no tensile tests on FRP coupons or estimation of the ultimate lateral pressure or effective lateral strain at failure of the FRP jacket is necessary. Confinement stiffness and the modulus of elasticity of the different material fibers control the ultimate lateral pressure of the jacket (if a triaxial state of stress

approach is followed). This conclusion allows for the expression of a simple and rigorous failure criterion.

FRP confined cylindrical concrete members are subjected to fairly uniform transverse confinement. These stresses can be calculated through an iterative procedure accounting for the FRP confinement modulus E_l and the transverse expansion of the concrete core. Continuous strain compatibility is assumed between concrete and FRP. Failure in cases of adequate FRP confinement occurs when lateral strain of concrete (lateral strain of concrete is considered equal to its radial strain) equals the circumferential strain at failure (or effective strain ε_{je}) of the FRP jacket. Equation (1) can be rewritten to provide the lateral strain at failure ε_{je} for a given confinement effectiveness ratio $k_1 = (f_{cu}-f_{co})/f_l$ and modulus of elasticity of fibres when the bearing stress behaviour of FRP confined concrete is ever-increasing:

$$0.5\, k_1 \varepsilon_{je} = (\alpha\, E_f\, 10^{-6} / E_{f\mu} + \beta) \quad \text{and finally} \quad \varepsilon_{je} = (\alpha\, E_f\, 10^{-6} / E_{f\mu} + \beta) / (0.5(f_{cui}-f_{co})/f_{li}) \qquad (2)$$

According to above approach, the aforementioned significant variables affecting the deformational behaviour of jacket such as curvature of section, thickness of jacket, resin type, compressive modulus of concrete etc are taken into account indirectly through k_1. Also, above effects are considered fixed for each type of fibre according to their E-modulus. The axial and lateral stresses f_{cui} and f_{li} respectively, generated by any reliable analytical model at each step, could be inserted in the empirical relation (2) together with the E-modulus of the fibres, so as to produce the corresponding stress - effective strain curve. The intersection of the stress-lateral strain curve generated by the analytical model and the lateral strain at failure curve generated by the empirical relation (2) for the member under compression, provides the effective lateral strain. Relation (2) has been derived by experimental results of strength only. Consequently, it is expected to be as accurate as the corresponding expression for concrete strength prediction (Rousakis et al. 2012). The performance of relation (2) is presented in Figure 2.

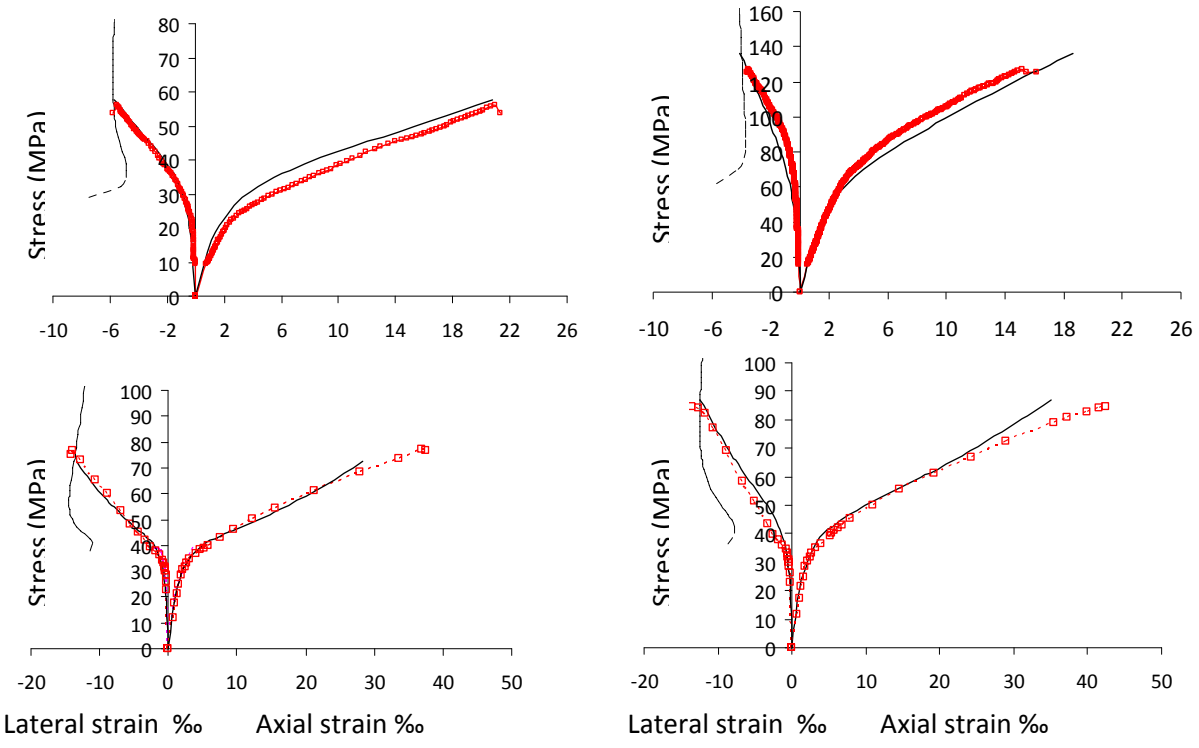

Figure 2: Comparison of experimental σ-ε curves against analytical predictions of Rousakis et al. 2008 model, applying the failure criterion of equation (2). Comparisons for CFRP wrapped concrete specimens 20L2-2t (a) and 60L5-2t (b) and for GFRP tube encased concrete specimens of 10 layers (c) and 14 layers (d).

The prediction of the effective lateral strain is accurate enough.

Conclusions and Points for Discussions

The research presents a rigorous failure criterion for FRP confined concrete. The failure criterion is load-originated and thus is expected to be more accurate than others. It can be used with any reliable analytical model that provides the whole stress-axial and lateral strain curves of FRP confined concrete and thus the values of varying k_1. Then, only the manufacturers' data for E-modulus of FRP fibers are required for the generation of a potential lateral strain failure curve for varying k_1 throughout loading. The intersection of the curve with the stress-lateral strain curve of the analytical model provides the effective lateral strain at failure of the FRP jacket (ε_{je}). This strain varies with the concrete strength, the layers of confinement or the modulus of elasticity of the fibers, in accordance with experimental evidence. The presented failure criterion could improve the predictive performance of analytical models. In addition, it could be further developed to address other significant parameters that affect the effective lateral strain at failure of FRP jackets. Databases of experimental results should include ε_{je}. in order to favour elaborations.

Key references

Rousakis T.C., Karabinis A.I., Kiousis P.D., Tepfers R. (2008). Analytical modelling of Plastic Behaviour of Uniformly FRP Confined Concrete Members. *Elsevier, Journal of Composites Part B: Engineering,* Volume 39, Issues 7-8, October-December 2008, Pages 1104-1113.

Rousakis T.C., Rakitzis T.D., Karabinis A.I. (2012). Design - Oriented Strength Model for FRP Confined Concrete Members. *ASCE Composites for Construction,* 2012, 16(6), 615–625.

Use of composite ropes in confinement of reinforced concrete members

T.C. Rousakis[1]

Introduction

Use of unbonded, non-impregnated fibers to confine concrete members may be an efficient technique to enhance both compressive strength and ultimate strain of concrete members. Triantafillou and Papanicolaou (2005), Triantafillou et al. 2006, in their study comparing FRP and TRM confinement, have also included spirally applied unbonded carbon fiber textile strips with end anchorages (resin impregnated). The strips were applied on a plain concrete column with square section and low corner radius of 15 mm. The efficiency of the method was similar to that of TRM technique in terms of strength and strain ductility for 4 layers. For lower confinement of 2 layers, the ultimate strain of confined columns was inferior. The results were remarkable considering the inherent brittleness of carbon fibers. Shimomura and Phong (2007) used rope reinforcements made of aramid or of vinylon fibers. In this study, real scale reinforced concrete columns have been wrapped externally with fiber rope reinforcements and presented upgraded shear resistance for higher horizontal top displacement under cyclic loading. Furthermore, aramid fiber ropes have been used as spiral internal shear reinforcement in real scale reinforced concrete beams.

The recent study by Rousakis 2014 has focused on the use of composite fiber ropes as external reinforcement to confine plain concrete cylinders. The technique is least time-consuming and 'green' application as the rope is applied by hand, is non-impregnated, unbonded and anchored mechanically. Polypropylene fiber ropes (PPFR) and vinylon fiber ropes (VFR) have been used that are nontoxic and recyclable. The FRs were practically insensitive to concrete cracking and local damage and could be used to retrofit already cracked concrete cylinders without prior crack treatment. PPFRs presented no fracture for concrete axial compressive strain as high as 10%. After the termination of the tests they could be removed and reused. Adequate PPFR confinement of columns led to ever-increasing compressive bearing stresses.

Hybrid confining scheme

PPFRs have been applied as external wraps in already glass FRP confined cylinders (Rousakis 2013). In the proposed hybrid confining scheme, external PPFRs presented no fracture even after the fracture of the FRP and they could be reused**.** Adequate PPFR confinement could resist the fracture of the FRP jacket and presented an acceptable temporary load drop. Then, further upgrade of the bearing load capacity of the columns followed. External FR wrapping technique is highly energy dissipative retrofit that could further contribute to the resisting mechanisms of FRP strengthened concrete members in cases of seismic overloads.

Effects of carbon nanotube enriched resins

The abovementioned hybrid scheme was further upgraded with the use of Multi-Walled Carbon Nanotubes (MWCNTs, Figure 1) in order to enrich the epoxy resin used for the impregnation of the glass sheet (Rousakis et al. 2014). Impregnating resin S2WV was reinforced in lab with only 0.125 wt% MWCNTs using mechanical mixing and mild sonication. Then, the resin was applied several days after mixing, by adding the catalyst in-situ and following the ordinary procedure for two-component

[1] Democritus University of Thrace, Xanthi, Greece, trousak@civil.duth.gr

impregnating epoxy resins. The pot-life and the workability of the enriched resin presented no difference. Thus, the use of MWCNT enriched resin in strengthening applications is practicable. MWCNT enriched resin dogbone specimens prepared in lab conditions, presented around 10% lower maximum tensile stress than the original S2WV resin. On the other hand, they showed a plastic-like behaviour and the strain at failure reached 11.5%. In the same study, the mechanical properties of MWCNT enriched resins of lower viscosity were significantly upgraded both in terms of ultimate stress and strain. The MWCNT enrichment of resins may provide significant upgrade of the performance of cured FRPs at elevated temperature as well as they may enable for the strain registration of the structural member by presenting piezoresistivity. Apart from above-mentioned advantages, the hybrid glass FRP – PPFR scheme with nanoenriched resin S2WV_0.125% presented 7.5% higher maximum stress at higher axial strain. Also, the temporary load loss after glass jacket fracture was lower and exhibited earlier load regaining (27% lower axial strain at load regaining).

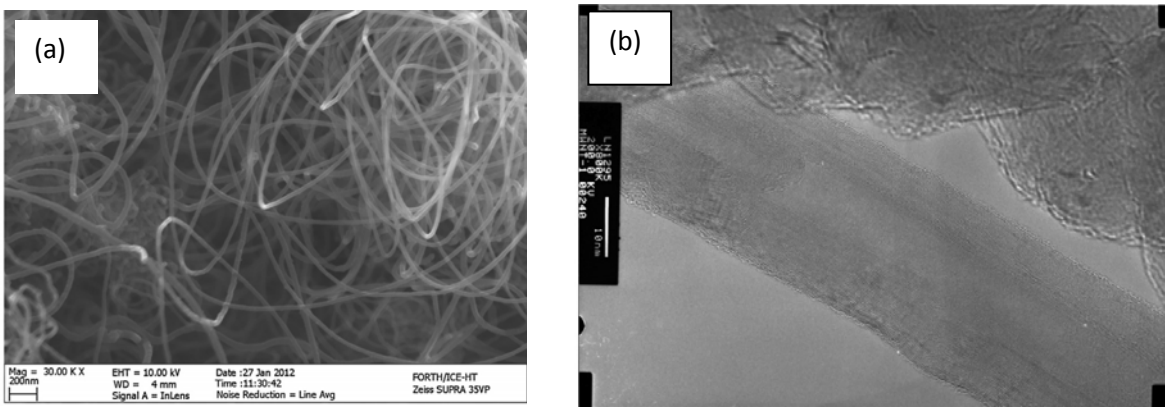

Figure 1: Scanning Electron Microscopy image of the MWCNTs (a). Transmission Electron Microscopy image of the nanotube (b) (adapted from Rousakis et al. 2014)

Effects of strengthening with composite rope on square reinforced concrete columns

Elastic fiber ropes of ultra-high extension capacity made of polypropylene (PPFRs) have been used to confine reinforced concrete columns of square section with very low corner radius and slender steel bars (Rousakis and Tourtouras 2014). They were applied by hand as passive (loose) confinement or as active confinement, through pretension of the rope. PPFR showed a very high stress redistribution capacity and preserved full contact with the dilating and variably damaged concrete core throughout loading (Figure 2a). PPFR could confine adequately square concrete sections with around 10 mm corner radius and slender longitudinal bars, without fracture of the rope, for concrete axial strains higher than 5% (Figure 2b). The reinforced concrete column with four layers of external PPFR wrapping achieved 40% higher load than the one without strengthening. The temporary load drop was negligible and the post-peak behaviour was stable, reaching 5.8% axial strain of concrete. Pretension of the PPFR wrapping could lead to enhanced stress-strain behaviour of the columns, with lower quantity of external strengthening material than in the case of non-pretensioned PPFR wrapping.

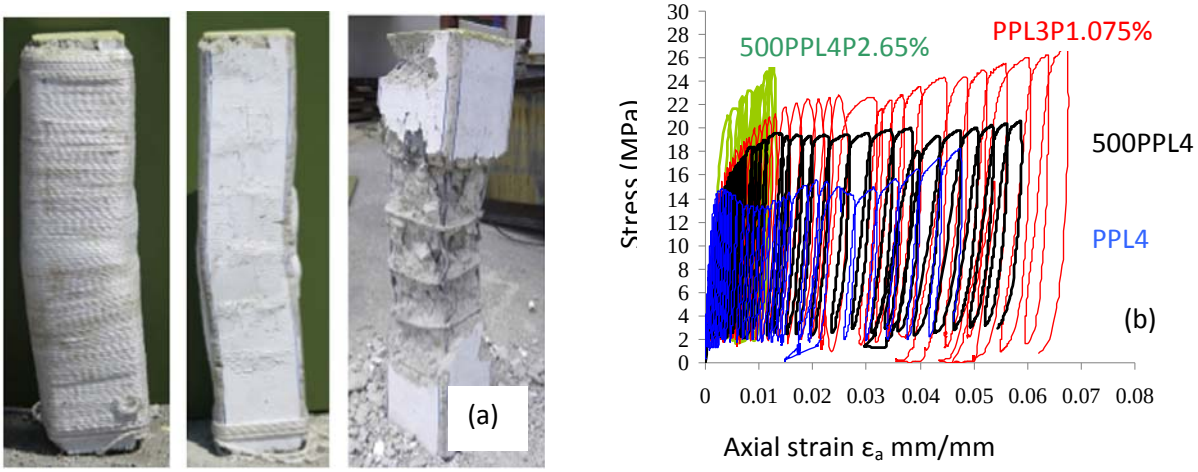

Figure 2: Reinforced concrete column 500PPL4 after cyclic compression loading (a). Comparative diagram of stress – axial strain behaviour of columns (b) with passive and active PPFR confinement (adapted from Rousakis et al. 2014)

Conclusions and Points for Discussions

Non-impregnated, unbonded composite ropes of high extension capacity may be applied as stand-alone or in hybrid FRP-FR confining schemes to improve axial load capacity and especially strain ductility of concrete elements under cyclic compression. They may strengthen efficiently reinforced concrete columns of square section with very low corner radius and with slender bars. Adequate active confinement may extend remarkably the linear behaviour of square columns with slender bars. MWCNT enrichment of impregnating resins may raise the temperature resistance of FRP systems and enable for strain recording. Preliminary analytical elaborations suggest that expressions valid for FRPs could be used as a basis for an adequate confining lateral rigidity approach to design strengthening. The efficiency of strengthening with composite ropes in square columns in terms of strain appears to be higher than the corresponding of FRPs. Seismic retrofit could benefit a lot from the unique redistribution characteristics of the technique. More experiments and analytical investigations are necessary to fully utilize the potential of the emerging techniques and nanomaterials as well as the unique properties of other fibers such as basalt, aramid etc.

Key references

Rousakis T. (2014). Elastic Fiber Ropes of Ultrahigh-Extension Capacity in Strengthening of Concrete Through Confinement. J. Mater. Civ. Eng., 26(1), 34–44.

Rousakis T. (2013). Hybrid Confinement of Concrete by FRP Sheets and Fiber Ropes Under Cyclic Axial Compressive Loading. ASCE, J. Compos. Constr., 17(5), 732–743.

Rousakis T.C., Kouravelou K.B., Karachalios T.K. (2014). Effects of Carbon Nanotube Enrichment of Epoxy Resins on Hybrid FRP - FR Confinement of Concrete. Elsevier, Journal of Composites Part B: Engineering. Volume 57, February 2014, Pages 210-218.

Rousakis T.C., Tourtouras I.S. (2014). RC Columns of Square Section – Passive and Active Confinement with Composite Ropes. Elsevier, Journal of Composites Part B: Engineering. Volume 58, March 2014, pages 573-581.

The effectiveness of FRP-jacketing when applied to pre-damaged RC columns

G.E. Thermou[1], S.P. Tastani[2], S.J. Pantazopoulou[3]

Introduction

Review of previous experiments on brittle R.C. columns through FRP jacketing illustrates that the efficiency of FRP jacketing in strengthening applications is superior to that which is observed when jacketing is used as a repair means. Actually, performance of the repair appears to be related to the state of damage along the anchorage or lap splice of primary reinforcement sustained in the initial phase and whether these defects have been corrected or not, by additional measures such as concrete replacement in cases of cracked cover or by epoxy injections along the damaged anchorages, prior to FRP jacketing (Thermou and Pantazopoulou 2009). Surprisingly, this type of repair proves more effective in elements that have failed in a brittle manner rather than in cases that have undergone extensive yielding; the reason for that is that brittle failure along the member length occurs before the anchorage of the reinforcement has sustained excessive yield penetration, which cannot be avoided in ductile member behaviour (Thermou et al. 2011, Tastani et al. 2012, 2013). In order to trace the reasons why previously damaged R.C. members (such as columns) jacketed with FRP do not always perform as efficiently as in cases where jacketing was applied prior to damage accumulation, it is necessary to focus into the basic differences regarding the jacketing function in these two conditions. Emphasis should be placed on the effects of previous damage on the inelastic strain capacity of reinforcement which often depends on its anchorage conditions beyond the jacketed length.

Observed behaviour of repaired and strengthened RC columns

Figure 1 depicts images from typical modes of failure reported in tests on reinforced concrete members with FRP jacketing either with or without prior damage. A common example, particularly with old-type columns with brittle details, is the case where initial damage was perpetrated by shear failure. These are cases which, after FRP jacketing with or without replacement of cracked concrete, present an altered mode of failure upon reloading, which is marked by flexural ductility and relatively full hysteresis loops with little pinching. The appearance of damage of the retrofitted specimens is marked by the formation of a single major flexural crack at the column interface with the footing (Thermou and Pantazopoulou 2009), and concrete compaction due to the development of very large compressive strains in the compression zone of the encased element. On the other hand, there are examples where FRP-jacketing repair followed an initial phase of post-yielding flexural response; the force-displacement hysteresis loops of such repaired columns is marked by bar sliding in the anchorage, limited post-repair inelastic energy dissipation, as illustrated by severe pinching in the load displacement envelopes. Another important characteristic for their identification from the large inventory of tests is the relatively low initial stiffness and drift at yielding well in excess of the benchmark value of 0.5%.

Strain development capacity of a previously damaged anchorage

An important reference case in the proposed methodology is that where yielding has penetrated deep enough into the anchorage, that the remaining bonded length $L_{b,min}$ barely suffices to support the bar force (Fig. 2; here the depth of yield penetration is, $\ell_r=L_b-L_{b,min}$). In that extreme situation, the remaining bonded length must mobilize the bond strength of the material ($f_b=f_{b,max}$), so that: $L_{b,min}=D_b(f_{s,y}/f_{b,max})/4$. Since in this extreme condition of maximum possible yield penetration bond stress over $L_{b,min}$ is constant

[1] Aristotle University of Thessaloniki, Greece, gthermou@civil.auth.gr
[2] Demokritus University of Thrace, Greece, stastani@civil.duth.gr
[3] University of Cyprus, Cyprus, pantazopoulou.stavroula@ucy.ac.cy

and equal to the strength, it follows from equilibrium that bar stresses attenuate linearly over that segment (since $f_b(x)=df_s(x)/dx$).

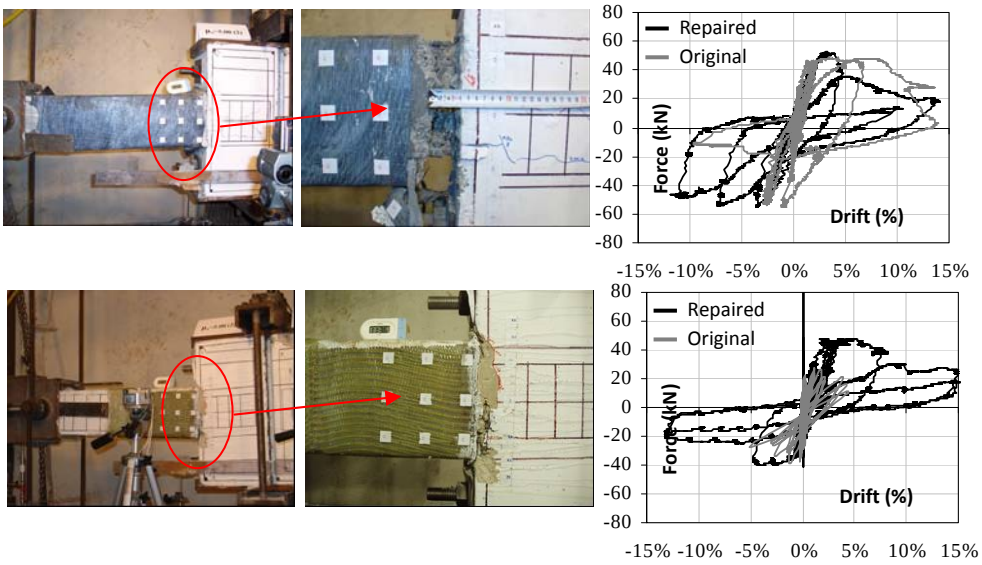

Figure 1: Modes of failure reported in tests of R.C. members retrofitted by FRP jacketing (Thermou et al. 2009).

It is may be shown that the plastic strain, $\varepsilon_{s,plastic}$, that occurs in the tension reinforcement (strain range developed beyond bar yielding) is linearly related to the inelastic drift experienced by the member:

$$\varepsilon_{s,plastic} = \left(\varepsilon_{s,t}^{T} - \varepsilon_{s,y}\right) \approx \left[\theta_u - \theta_y\right] \cdot \frac{d-c}{\ell_p + 0.5 \cdot \ell_r} = \theta_{pl} \cdot \frac{d-c}{\ell_p + 0.5 \cdot \ell_r} \quad (1)$$

According to Eq. (1) the larger the length of yield penetration (ℓ_r), the larger the fraction of the total rotation θ_u that is owing to elastic strains (θ_y), and the smaller the fraction that remains for inelastic rotation (θ_{pl}). So although the total value of the rotation capacity may be high (i.e. in the order of 4-6%), in the presence of significant yield penetration response may be unacceptable owing to the very high compliance (flexibility) of the member to lateral displacement without toughness.

Therefore, if during the initial loading phase the imposed rotations have exceeded the yield limit, the tension strain will have experienced a commensurate plastic strain. Furthermore, there is a limiting $\varepsilon_{s,plastic}$ value that may be sustained by the anchorage before pullout failure. To evaluate this limit, the minimum required anchorage length required to sustain the bar yielding force is estimated from $L_{b,min}=\alpha(D_b/4)\cdot(f_{s,y}/f_b)$, where D_b is the bar diameter and f_b is the bond strength, and α=0.7 if hooks are present, α=1 for straight anchorages. Thus, assuming that yield penetration may extend over the residual length (L_b-$L_{b,min}$), it follows that:

$$\varepsilon_{s,plastic}^{max} = \frac{L_b - L_{b,min}}{L_{b,min}} \cdot \varepsilon_{s,y} \quad (2)$$

Note that after the preloading phase (i.e., when the initial damage is inflicted), if the imposed drift has exceeded even once the yielding limit, then upon unloading the tension reinforcement has residual plastic strains at the critical section, their magnitude given by Eq. (1). But of far greater significance is that the residual strain capacity of the bar, which is available for inelastic response during the post-repair service-life of the member, is the difference of $\Delta\varepsilon_{s,plastic}=\varepsilon_{s,plastic}^{max}-\varepsilon_{s,plastic}$. Therefore, in the new phase of loading (after retrofit), the peak inelastic drift that may be imposed on the specimen before deterioration due to anchorage failure is only:

$$\Delta\theta_{pl} = \Delta\varepsilon_{s,plastic}\frac{\ell_p + 0.5\cdot\ell_r^{max}}{d-c} \quad (3)$$

Equation (3) already identifies the fundamental difference in FRP-jacketing of pre-damaged columns as compared to columns in pristine condition – for columns that have experienced excessive yielding prior to jacketing, the plastic rotation capacity after jacketing is limited by the dependable residual strain range of tension reinforcement, which depends on the extent of damage that has been sustained in the anchorage – i.e. over a part of the structure that lies outside the repaired region.

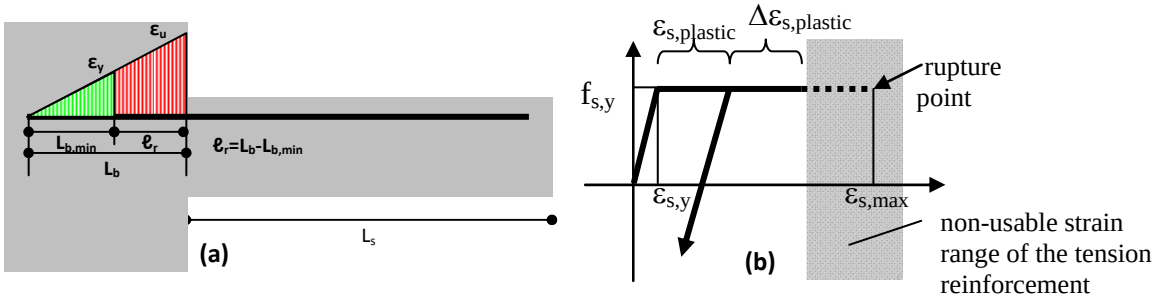

Figure 2: (a) Distribution of bar strains along the bar anchorage; (b) Stress-strain diagram of the tension reinforcement.

Strength condition for development of inelastic response

Necessary condition for the development of inelasticity during the first stage of loading of the member (prior to repair) is the occurrence of flexural yielding. Thus, the use of the above equations is feasible provided that occurrence of premature modes of failure before yielding in flexure is precluded. Similar are the implications of an inadequate anchorage or lap splice – i.e. conditions of the primary reinforcement which cannot support the development of flexural yielding prior to anchorage or lap-splice failure. Thus, in these cases of premature failure in the pre-repair loading phase, it may be said that the entire inelastic strain range that the anchorage could develop, is available for the post repair phase of loading: $\Delta\varepsilon_{s,plastic}=\varepsilon_{s,plastic}^{max}$ (Fig. 2b). The prime conclusion of the preceding analysis is the following:

(i) If detailing of the member in the initial phase of loading is adequate to support flexural yielding, and the applied load history enters into the inelastic range of response, then, in the post-repair condition (after jacketing with FRP wrapping in the critical regions) the member will have a reduced rotation capacity as limited by Eq. (3) despite the repair. The only way to enhance the rotation capacity of the jacketed member would be by elimination of the implications of yield penetration (length over which bond is deteriorated and cannot support bar development); this can be achieved by epoxy injection inside the anchorages before proceeding to the application of the intervention method (i.e., wrapping the member with composite fabrics). This measure will enhance the rotation capacity of the jacketed member and lead to a different strength hierarchy. The objective is not to remove the plastic strain of the reinforcement, but rather, to reduce future demand for localized strain in that plasticized section. If the anchorage is healed, rotation capacity of the jacketed member will be owing to deformations occurring along its length. Otherwise, it will be owing to slip from the already damaged anchorage. Hence, epoxy injection inside the anchorages should be established as a requirement necessarily accompanying the repair in field applications.

(ii) If the member is detailed so poorly that premature failure by shear, cover separation, cracking along short or unconfined lap splices occurs prior to flexural yielding, then after the repair, the full range of dependable plastic strain development capacity is available by the longitudinal bar anchorage, and thus, after jacketing with FRP wraps a ductile behavior may be safely anticipated to the extent allowed by the available anchorage length.

Determining whether yielding by flexure will precede or not the other modes of failure requires a dependable estimation of member strengths (in terms of the shear force carried by the member) in the pre-repair phase (in the first phase of loading). Here the state of stress referred to, is induced during earthquake response (lateral sway of the structure), so that shear force is constant over the member length, with a zero moment value near the member's midheight.

Conclusions and Points for Discussions

Through consistent review of the reported experimental evidence from tests on columns which were repaired with FRP jacketing after having sustained extensive earthquake induced damage, the effectiveness of this repair option as compared to strengthening is re-evaluated by exploring the mechanics of the strengthened and repaired members under lateral displacement (relative drift). The main conclusions drawn and points of discussion are:

- Kinematic relationships based on the mechanics of bond and development capacity of reinforcement are necessary to describe the strain development capacity of the repaired columns. Design guidelines that will cover this category of repairs are necessary.
- The damage sustained in the anchorage and lap splice zones of such structural elements reduces the post-repair ductility and inelastic deformation capacity of the affected member even after jacketing.
- Concrete cover replacement in lap splices and epoxy injections in anchorages are proposed as necessary measures accompanying the repair through FRP jacketing of seismically damaged structural members, in order to secure the development capacity of longitudinal reinforcement, which is pre-requisite for inelastic flexural rotation capacity of the columns after repair through FRP jacketing.
- There are limited test data on the behaviour of FRP jacketed pre-damaged members. More tests are necessary as to enhance the already existing database (Thermou et al. 2011) and facilitate the derivation of design expressions for this type of intervention (i.e. FRP jacketing of pre-damaged RC columns).

Key references

Thermou, G. E., and Pantazopoulou, S. J. (2009). Fiber reinforced polymer retrofitting of substandard RC prismatic members. *Journal of Composites for Construction*, ASCE, 13(6), 535-546.

Thermou, G. E., Tastani, S. P. and Pantazopoulou, S. J. (2011). The effect of previous damage on the effectiveness of FRP-jacketing for seismic repairs of RC structural members. *SP 275, Fiber Reinforced Polymer Reinforcement for concrete structures, American Concrete Institute*.

Tastani, S. P., Thermou, G. E., and Pantazopoulou, S. J. (2012). Yield penetration in bar anchorages and the effect on rotation capacity. Befestigungstechnik, Bewehrungstechnik und . . . II, Rolf Eligehausen zum 70, Geburtstag, Fuchs, Werner, Hofmann, Jan (Hg.), 449-470, (ISBN 978-3-8382-0397-3).

Tastani, S. P., Thermou, G. E. and Pantazopoulou, S. J. (2012). Deformation analysis of reinforced concrete columns after repair with FRP jacketing. Proc., 15th World Conference on Earthquake Engineering, Lisbon, Portugal, Paper No. 3164.

CONFINEMENT OF RC COLUMNS WITH TRM JACKETS

Dionysios BOURNAS [1] Thanasis TRIANTAFILLOU [2]

[1] Faculty of Engineering, The University of Nottingham, UK
[2] Department of Civil Engineering, University of Patras, Greece

INTRODUCTION

The upgrading of existing reinforced concrete (RC) structures through jacketing of columns has become a very popular technique in an increasingly large number of rehabilitation projects, both seismic and non-seismic. The use of fiber-reinforced polymers (FRP) has gained considerable popularity among all jacketing techniques, due to the favorable properties offered by these materials, namely high strength to weight ratio, corrosion resistance, ease and speed of application, and minimal change of geometry. Despite all these advantages, the FRP retrofitting technique has a few drawbacks, e.g. poor behavior at high temperatures; high costs; inapplicability on wet surfaces or at low temperatures; and difficulty to conduct post-earthquake assessment behind FRP jackets; these are mainly attributed to the organic epoxy resins used to bind the fibers. An interesting alternative to FRP materials are the so-called Textile-Reinforced Mortars (TRM) [1,3]. These new materials are made of textiles, that is fabric meshes made of long woven, knitted or even unwoven fiber rovings in at least two directions, impregnated with inorganic binders, such as cement-based mortars. In this State-of-the-art report the authors are summarizing recent experimental investigations on the use of TRM jackets as a means of confining poorly detailed old-type RC columns with deformed rebars, which suffer from limited deformation capacity under seismic loads due to either buckling of the longitudinal bars [4] or bond failure at lap splice regions [5].

EXPERIMENTAL PROGRAMME

A total of 9 large-scale RC column specimens with the same geometry were constructed and tested under cyclic uniaxial flexure with constant axial load (Fig. 1a). Three specimens were constructed with continuous longitudinal reinforcement (Series L0_...). One specimen was tested without retrofitting, as control (L0_C), the second one was retrofitted with a double-layered CFRP jacket (specimen L0_R2),and the third one was retrofitted with an equal (to its FRP counterpart) stiffness and strength carbon fiber TRM jacket comprising four layers (specimen L0_M4). The effectiveness of TRM versus FRP jackets, applied at the ends of old-type RC columns for specimens constructed with lap splicing of longitudinal reinforcement above the column base, was evaluated for two different lap lengths, which were selected equal to 20 and 40 bar diameters. Columns with the shorter lap lengths (Series L20d_...) were designed as follows: One specimen was tested without retrofitting as control (L20d_C), the second one was retrofitted with a double-layered CFRP jacket (specimen L20d_R2) and the third one was retrofitted with an equal (to its FRP counterpart) stiffness and strength carbon fiber TRM jacket comprising four layers (specimen L20d_M4). Columns with longer lap lengths (Series L40d_...) were given the notation L40d_C, L40d_R2 and L40d_M4. A photograph of the application method of textile combined with mortar binder to provide column jacketing is shown in Fig. 1c.

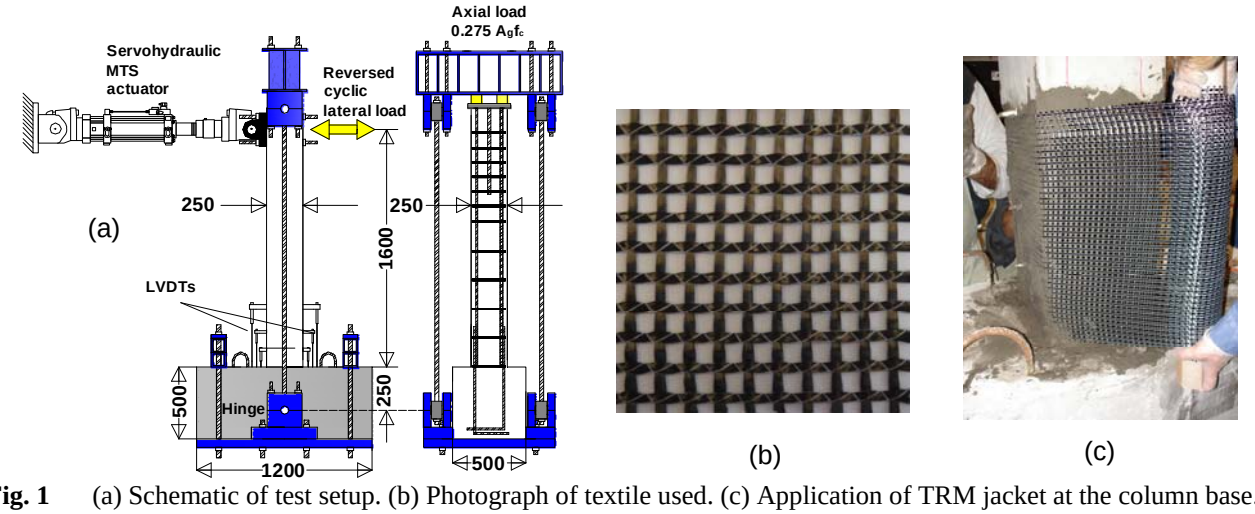

Fig. 1 (a) Schematic of test setup. (b) Photograph of textile used. (c) Application of TRM jacket at the column base.

TEST RESULTS AND DISCUSSION

The response of all columns tested is given in Fig. 2 in the form of load-drift ratio loops. The performance and failure mode of all tested specimens was controlled by flexure. The failure mode of the unretrofitted specimen with continuous longitudinal bars was controlled by bar buckling above the column base. The drift ratio at failure sustained by the unretrofitted column at failure was 3.43%. The behavior and failure mode of retrofitted columns (L0_R2, L0_M4) was not controlled by longitudinal bar buckling. Overall, the behavior of the TRM jacketed specimen was quite different from and far better than that of the FRP confined and unretrofitted specimens. Member deformation capacity increased by a factor of 1.5, and 2.3 for specimens L0_R2 and L0_M4, respectively, in comparison with the control specimen, corresponding to drift ratios at failure equal to 5.15% and 7.81%; this indicates a higher effectiveness of TRM versus FRP jackets, by about 50%.

Longitudinal and horizontal splitting cracks were developed along the splice length of lapped bars for both unretrofitted specimens L20d_C and L40d_C, which sustained drift rations of 3.59% and 3.28%, respectively. TRM and FRP jacketed columns, with either short or long lap length, responded far better than their unretrofitted counterparts both in terms of strength and deformation capacity at failure. Specimens L20d_R2 and L20d_M4 (with short lap lengths) sustained reversed deformation cycles up to 6.3% drift before failing due to pull-out bond failure of the spliced. Columns with longer lap splices (L40d_R2 and L40d_M4) behaved in an identical manner until the end of the test at a drift ratio of 7.81%, resulting in an increase of the members' deformation capacity by a factor of more than 2.5. Peak resistance was practically the same as in the unretrofitted column, indicating that a lap splice length of 40 diameters is adequate for the development of the columns' full strength.

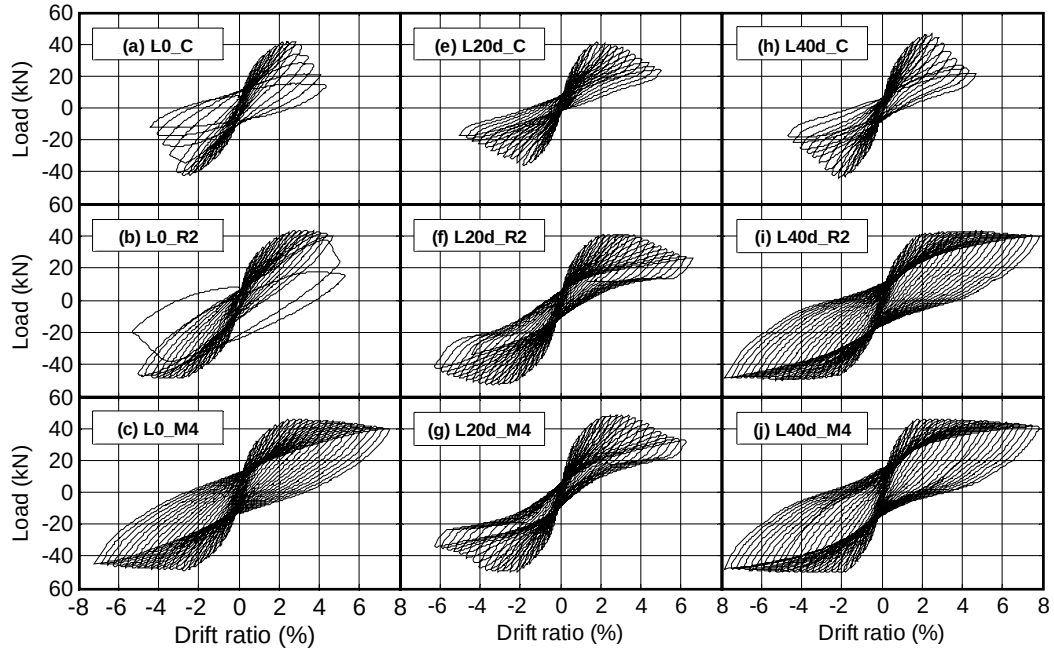

Fig. 2 Load versus drift ratio curves for specimens tested.

CONCLUSIONS

The tests on full-scale columns under cyclic uniaxial flexure show that TRM jackets are quite effective as a means of increasing the cyclic deformation capacity and the energy dissipation of old-type RC columns with poor detailing, by delaying bar buckling or by preventing splitting bond failures at columns with inadequate lap splices. Compared with equal stiffness and strength FRP, TRM jacketing has practically the same effectiveness. Despite their relatively limited number, the available test results [1-5] indicate that TRM jacketing is an extremely promising solution for the confinement of poorly detailed RC columns in seismic regions.

REFERENCES

[1] Triantafillou, T.C., Papanicolaou, C.G., Zissimopoulos, P. and Laourdekis, A., "Concrete Confinement with Textile-Reinforced Mortar Jackets", *ACI Structural Journal*, 103, 1, 2006, pp 28-37.

[2] Bournas, D. A., Lontou, P. V., Papanicolaou, C. G. and Triantafillou, T. C., "Textile-Reinforced Mortar (TRM) versus FRP Confinement in Reinforced Concrete Columns", *ACI Structural Journal*, 104, 6, 2007, pp. 740-748.

[3] Bournas, D. A., Triantafillou, T. C., Zygouris, K., and Stavropoulos, F. (2009). “Textile-reinforced mortar (TRM) versus FRP jacketing in seismic retrofitting of RC columns with continuous or lap-spliced deformed bars.” J. Compos. Constr., 13(5), 360–371.

[4] Bournas, D.A., and Triantafillou, T.C., (2011), "Bar Buckling in RC Columns Confined with Composite Materials", ASCE Journal of Composites for Construction, 15(3), 393-403.

[5] Bournas, D.A., and Triantafillou, T.C., (2011), "Bond Strength of Lap Spliced Bars in Concrete Confined with Composite Materials", ASCE Journal of Composites for Construction, 15(2), 156-167.

Bars buckling prevention by means of FRP confinement

G.P. Lignola[1], A. Prota[2]

Introduction

Premature failure modes due to buckling of compressed bars close to beam-column joints or in other locations where steel bars are highly stressed could reduce the seismic capacity of existing reinforced concrete structures.

Buckling failure mode is a premature failure mode related to the instability of compressed slender reinforcing steel bars. The main parameter governing this phenomenon has been recognized as the stirrups spacing over bar diameter ratio (Cosenza and Prota 2006); hence recent building codes prescribe strict limitations to the ratio between the stirrups spacing and the diameter of reinforcing steel bars.

Internal transverse steel reinforcements (e.g. stirrups) carry out the function of cage, shear strengthening, confinement and then they are the main internal devices that avoid the longitudinal steel bars buckling, but in most of all existing Reinforced Concrete (RC) structures the amount and the spacing between steel stirrups are inadequate. In hollow cross sections, as can be found in bridge piers, buckling is the main reason of premature failure (Lignola et al. 2009 and 2012).

A previous experimental program by Cosenza and Prota (2006) investigated the longitudinal steel bars behaviour under axial load. The results of those tests can be used to study the buckling mode of longitudinal bars between two consecutive layers of transverse reinforcement. The tests highlighted that the compressive behaviour of the bars (and then the buckling mode) depends on the L/D ratio: where L is the spacing between two consecutive stirrups and D is the longitudinal bars diameter. In particular varying this ratio the buckling can be elastic or inelastic.

Considering the restraint needed to avoid buckling over a critical length involving several stirrups of a longitudinal bar in the strain-hardening range of axial compression, Priestley et al. (1996) provided the volumetric ratio, ρ_s, of the transverse confining steel, according to:

$$\rho_s = \frac{0.45 n f_s^2}{E_r E_h} \tag{1}$$

where n and f_s are, respectively, the number of longitudinal bars and their expected longitudinal stress, E_h is the transverse reinforcement elastic modulus. E_r is the reduced modulus of the longitudinal reinforcement at f_s, equal to:

$$E_r = \frac{4 E E_t}{\left(\sqrt{E} + \sqrt{E_t}\right)^2} \tag{2}$$

where E is the longitudinal reinforcement elastic modulus and E_t is the tangent modulus from f_s to f_u, the ultimate stress. Eqn. (2) is usually suggested for the scope, however, strictly speaking, it is related to bars with rectangular cross section and not for circular cross sections. However, on safe side, lowest

[1] University of Naples "Federico II", Italy, glignola@unina.it
[2] University of Naples "Federico II", Italy, aprota@unina.it

possible values for E_r should be used and circular bars provide higher values (Papia et al. 1988, Giamundo et al. 2012), hence Eqn. (2) us in safe side for real circular bars.

FRP wrapping – available guidelines

In existing structures, retrofitting of deficient members, not presenting the minimum transverse reinforcement ratio (e.g. given by Eqn. 1), may be needed by means of external strengthening, e.g. FRP wrapping. To design a retrofit intervention the main parameter needed is the FRP thickness, t_f, required to prevent the buckling.

The equations suggested by the Italian CNR DT200 R1 guidelines (2013) to evaluate the FRP thickness needed to prevent the internal bars buckling failure are practically derived by extending the Eqn. (1) for the stirrups in the case of circular cross section, proposed by Priestley et al. (1996) to the FRP case. In fact, considering a circular cross section, the volumetric ratio, ρ_s, of the transverse confining steel, can be transformed into an equivalent volumetric ratio of the FRP wrapping, $\rho_s = \rho_{frp} = 4\, t_f/d$. In this case d is the diameter of circular cross sections and $E_h = E_f$ is the FRP elastic modulus. Hence, the minimum required reinforcement thickness is given by:

$$t_f = \mu \frac{n f_s^2}{E_r E_f} d \qquad (3)$$

Italian CNR guidelines (2013) extends the value $\mu = 0.45/4$, derived from Priestley et al. (1996) for circular cross sections, pragmatically to any non-circular cross section, where d is the maximum side dimension of the cross section.

Giamundo et al. (2012) proposed a refined analytical model providing different values for μ in the case of circular and rectangular cross sections, separating, in the latter, the case of corner and central bars, involving membrane and flexural regime of FRP wrapping. According to the novel model, the unique value $\mu = 0.45/4$ is not always safe in those different conditions.

FRP wrapping – novel analytical approach

Giamundo et al. (2012, 2013, 2014) developed an analytical approach to study the buckling of longitudinal bars. They proposed to evaluate the effects of FRP wrapping modelled as elastic springs used to restrain laterally the bar buckling (Figure 1). Equations derived from solid mechanics were the basis of the proposed model, accounting for the longitudinal bar as an Euler beam restrained by elastic springs along its length. These formulations account also for inelastic buckling by means of reduced modulus theory. Previous studies evidenced the sensitivity of the predictions to steel mechanical parameters.

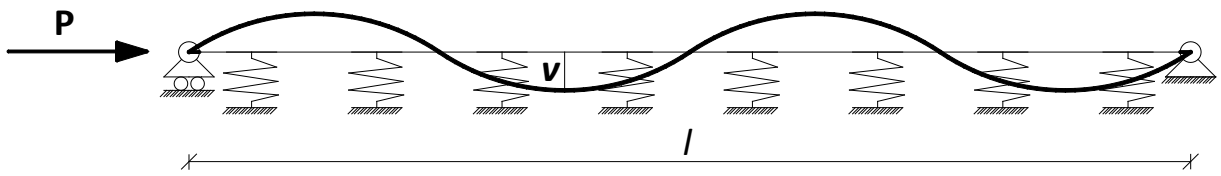

Figure 1: Euler buckling of a hinged beam with transverse springs (n_w=4)

The classical Euler instability problem, accounting for elastic springs of stiffness k, requires the solution of the following differential problem, providing the solution in terms of critical load P_{cr}:

$$E_r I v^{IV} + P v^{II} = -kv \quad \rightarrow \quad P_{cr} = \frac{\pi^2 E_r I}{L^2}\left(n_w{}^2 + \frac{kL^4}{E_r I \pi^4 n_w^2} \right) \tag{4}$$

In Eqn. (4 right) n_w = 1,2,3,… is the number of inflection waves and I is the moment of inertia. Figure 2 shows the Euler's curve and the critical load, P_{cr}, relationships varying the length, L, (for n_w = 1,2,3) whose minimum is obtained for each n_w by:

$$P_{cr} = 2\sqrt{kE_r I} \tag{5}$$

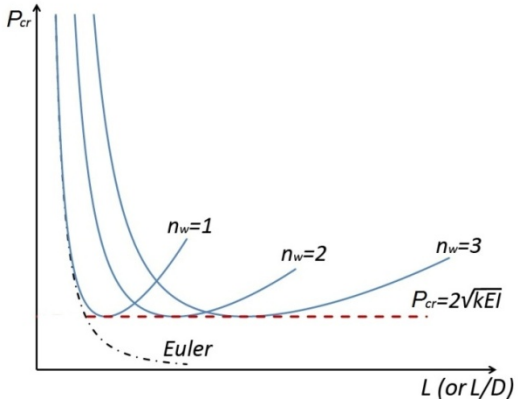

Figure 2: Critical load as a function of L (or L/D): minimum safe value

The critical load value achieved by Eqn. (5), is the minimum, and it is independent on beam length, L. This value is the safest value to be used in design phase. However when L/D spacing is small enough to avoid bar buckling (i.e. Euler curve in Figure 2 is higher than P_{cr}), FRP wrapping provides no benefits.

A more general form of Eqn. (5) showing longitudinal steel stress (corresponding to critical load), f_s, is:

$$f_s = \sqrt{\frac{E_r}{n\pi} k} \tag{6}$$

In reality Eqn. (6) is recursive because E_r is an implicit function of f_s. The equations for k in the different cases reported in Table 1 (where h is the minimum side dimension of the rectangular cross section and ε_f is the FRP strain) allows to design the FRP wrapping required to prevent longitudinal bars buckling.

The appropriate lateral stiffness is evaluated according to the following structural layouts where the bar represents a transverse load for the FRP jacket in different configurations.

Effect of different cross section shapes

For columns with different cross section shapes, the FRP wrapping assumes different stiffness (i.e. different values for spring stiffness k). Therefore it is needed to assess the equivalent spring stiffness in the proposed analytical model, depending on the cross section shape.

Table 1 reports the different equivalent spring stiffness k depending on cross section shape and also on bar position and FRP regime.

Table 1: Lateral stiffness of FRP wrapping

Cross section shape	Bar position	Regime	k
Circular	Every	Membrane	$\frac{4\pi E_f t_f}{d}$
Rectangular (d>h)	Corner	Membrane	$\frac{2E_f t_f}{d}$
	Central	Flexural	$\frac{16E_f t_f^3}{4ht_f^2 + d^3}$
	Central	Membrane	$\frac{2E_f t_f}{d}\frac{2\varepsilon_f}{1+\frac{\varepsilon_f}{d/h}}$

In circular cross section the FRP wrap is uniformly stretched in the circumferential direction, hence it is in a membrane regime. Conversely in rectangular (or square) cross sections the FRP is in membrane regime if the bar is in a corner position (Figure 3), while if a bar is along a side (central position, Figure 4) both regimes are activated, however the increase of FRP thickness required to avoid buckling of a central bar is much higher than the thickness required to avoid buckling of a corner bar, even looking at the membrane regime. In fact, in membrane regime the FRP stiffness is higher than in flexural regime.

Impact on available guidelines

According to the proposed model, the unique value $\mu = 0.45/4$ used in Eqn. (3) is not safe in these different conditions; it is suggested a value of $\mu = 0.25$ for circular cross sections and $\mu = \pi/2$ for corner bars in rectangular cross sections. In the case of central bars, the required thickness is ten to hundred times higher than the thickness required for corner bars, depending on the FRP allowable strain in the wrap (Giamundo et al. 2013). However a further high impact is given by the variability of reduced modulus E_r (Giamundo et al. 2014).

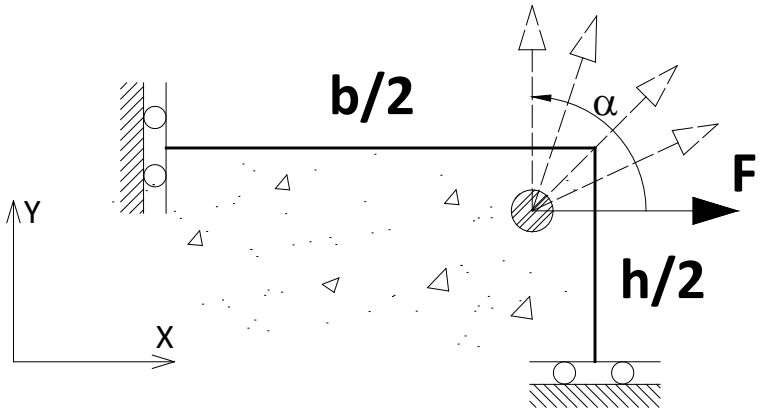

Figure 3: Basic structural scheme of FRP spring stiffness: corner bar

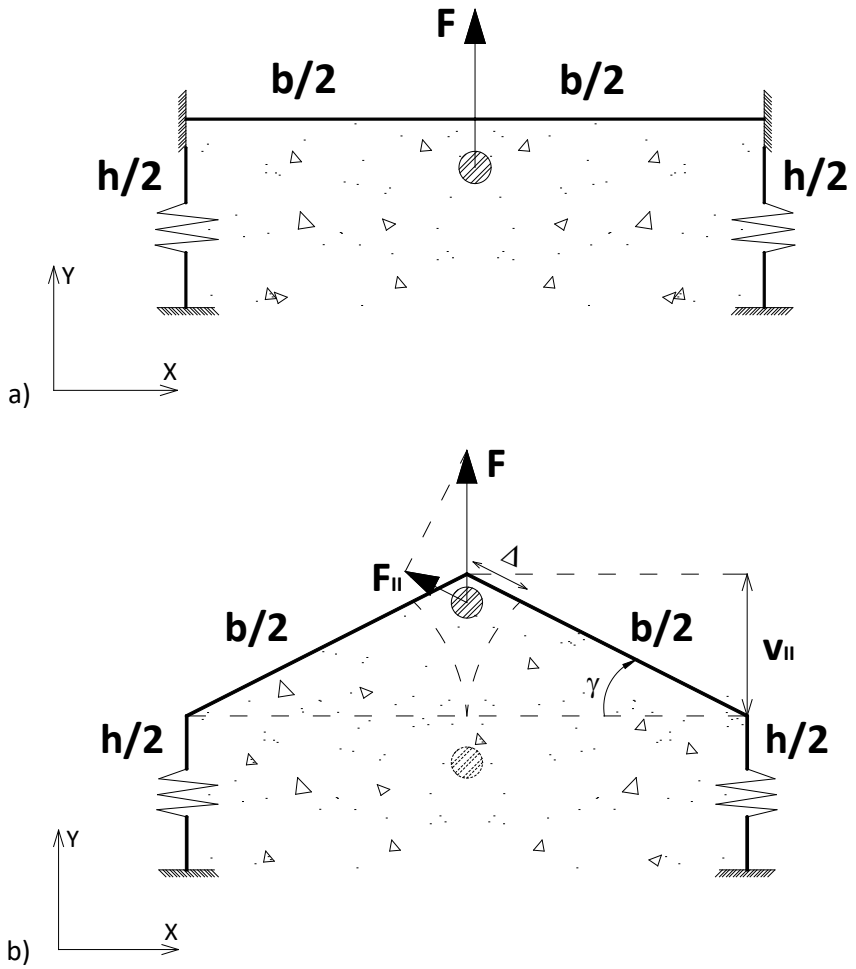

Figure 4: Basic structural scheme of FRP spring stiffness: central bar (flexural and membrane regime)

Conclusions and Points for Discussions

Reduced modulus plays a crucial role in the evaluation of FRP wrapping efficiency in restraining bars buckling and this jeopardizes the simple use of Eqn. (6) by practitioners. For this reason a design chart is provided in Figure 5 relating directly the expected longitudinal steel stress (corresponding to critical load), f_s, to the lateral stiffness k/n provided by FRP. The design charts cover almost all the typical FRP lateral stiffness k/n and steel behaviours (according to Ramberg & Osgood 1943 steel constitutive behaviour) in terms of different hardening ratios, f_u/f_y, ranging between 1.05 and 1.25 and yielding strengths, f_y, ranging between 450 MPa and 650 MPa.

- An analytical approach to study the buckling of longitudinal bars was proposed. Equations derived from solid mechanics were the basis of the proposed model, accounting for longitudinal bars as Euler beams restrained by elastic springs along their length. These formulations account also for inelastic buckling, by means of reduced modulus theory.
- Beside analytical refined formulations, a design chart, oriented to practitioners, was proposed. It is also analytically derived. These formulations have shown that the effect of FRP wrapping is negligible for L/D ratios less than about 6.5 for both circular and rectangular cross sections. For rectangular cross sections the FRP is almost unable to prevent the central bar buckling, mainly because of reduced thickness of FRP wraps (hence because of reduced flexural stiffness). Conversely FRP is effective for corner bars in noncircular sections and always in circular sections.

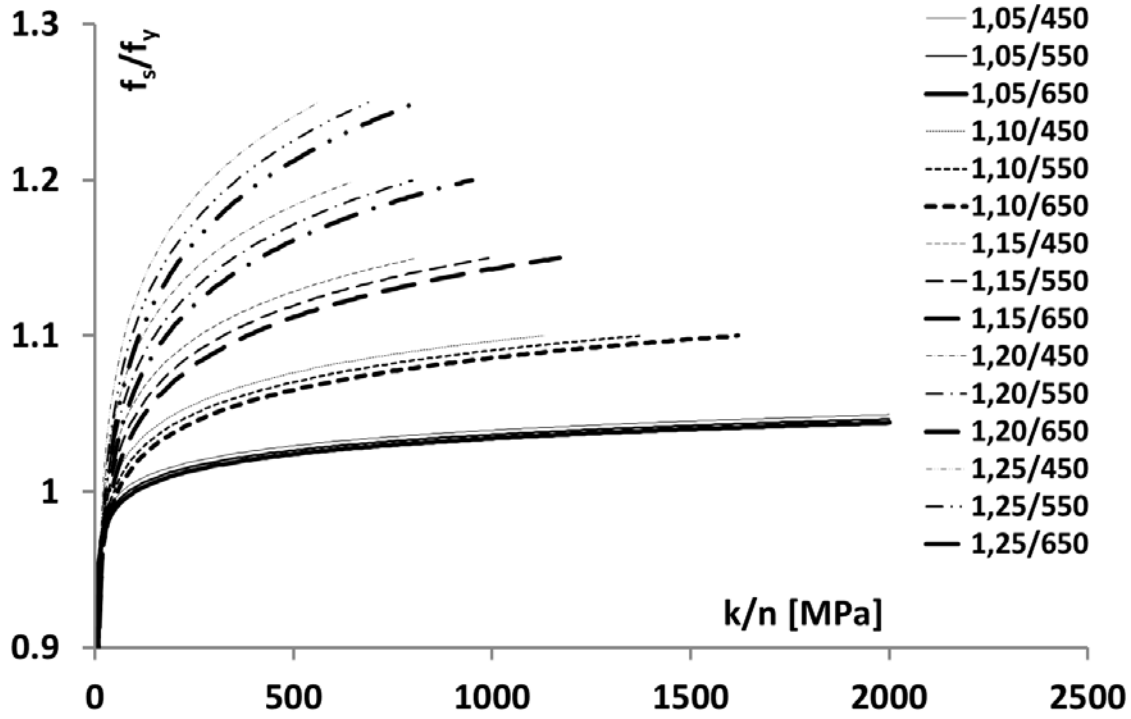

Figure 5: Normalized critical stress (Ramberg-Osgood steel Model) for different f_u/f_y ratios and f_y

Key references

CNR-DT 200 R1 (2013). Guide for the Design and Construction of Externally Bonded FRP Systems for Strengthening Existing Structures Guidelines, Rome, Italy

Cosenza E. and Prota A. (2006) Experimental behavior and numerical modeling of smooth steel bars under compression. Journal of Earthquake Engineering, 10(3):313-329.

Giamundo V., Lignola G.P., Prota A and Manfredi G (2014) Analytical evaluation of FRP wrapping effectiveness in restraining reinforcement bars buckling. Journal of Structural Engineering, 140(7). 04014043:1-12

Giamundo V., Lignola G.P., Prota A. and Manfredi G. (2012) Restraining bars buckling by means of FRP wrapping: an analytical approach. In proceedings "15th World Conference on Earthquake Engineering". Lisbon, Portugal

Giamundo V., Lignola G.P., Prota A. and Manfredi G. (2013) Effectiveness of FRP wrapping on internal reinforcement buckling for non-circular concrete members. 11th International Symposium on Fiber Reinforced Polymer Reinforcement for Concrete Structures FRPRCS11 2013, Guimarães, Portugal

Lignola G.P., Prota A., Manfredi G. and Cosenza E. (2009) Non linear modeling of RC hollow piers confined with CFRP. ELSEVIER Composite Structures. 88(1):56-64.

Lignola G.P., Prota A., Manfredi G. and Cosenza E. (2012) Multiscale Non linear analysis of RC hollow piers wrapped with CFRP under shear-type load. Construction & Building Materials, 35:947-959.

Papia M., Russo G., Zingone G. (1988) Instability of longitudinalbars in R.C. columns. Journal of Structural Engineering ASCE. 114(2):445–461.

Priestley, M.J.N., Seible, F. and Calvi, G.M. (1996) Retrofit Design, in Seismic Design and Retrofit of Bridges, John Wiley & Sons, Inc., Hoboken, NJ, USA.

Ramberg, W., Osgood W.R. (1943). Description of stress-strain curves by three parameters. Technical Note No. 902, National Advisory Committee For Aeronautics, Washington DC.

Effects of pointwise variability of confinement in noncircular cross sections

G.P. Lignola[1], A. Prota[2]

Introduction

Several researchers have demonstrated that circular concrete columns have a huge increment in strength and ductility when wrapped with FRP. Square and rectangular shapes were found to have less increment in strength and ductility than their circular counterparts, however typical cross sections of concrete columns are not circular, but square or rectangular (Lignola et al. 2005, 2014a; De Luca et al. 2011). The non circular shape presents non uniform confining pressure, hence the confinement stress, f_l, is not easily computed for such cross sections, to be inserted in confinement equations.

The seminal models studied at the beginning of last century were built on Coulomb plasticity criterion (e.g. Richart et al. 1928), so they originated from solid mechanics (Figure 1). Coulomb plasticity criterion was easily implemented in circular cross sections because it accounts for a linear relationship between lateral uniform confining pressure $f_l(=\sigma_3)$ and confined concrete strength $f_{cc}(=\sigma_1)$ (Eqn. 1) needing the evaluation of the k_1 constant, where f_{co} is the unconfined concrete strength (σ_1 with $\sigma_3=0$).

$$f_{cc} = c + \sigma_3 \cdot \tan^2\left(45° + \frac{\phi}{2}\right) = f_{co} + k_1 \cdot f_l \qquad (1)$$

The aim of any simple model, practice oriented, is to provide a reliable value of such parameter, f_l, primarily being easily estimated.

Based on a detailed analysis of the stress state, a simplified closed form solution is proposed to account for the non-uniform confined concrete behaviour in non-axisymmetric sections. The non-uniform confining stress field in such cross-sections is incorporated explicitly in the model evaluating the integral mean value of the pointwise variable stress field over the cross-section. The key aspect of the proposed methodology is the evaluation of the effective equivalent pressure to be inserted in a triaxial confinement model (like as the one in Eqn. 1), to account for the peculiarities of square and rectangular cross-sections. This approach has been extended to masonry confinement, too (Lignola et al. 2014b). Hence the first step is to estimate the pointwise variable stress state over the cross-section.

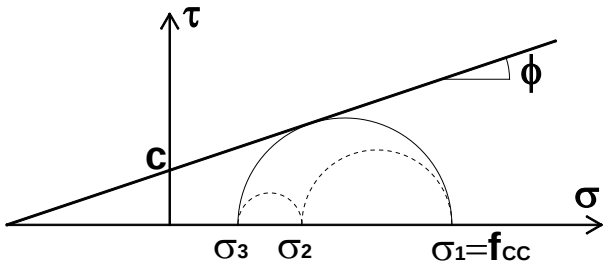

Figure 1: Confined concrete strength in Mohr–Coulomb failure envelope, non uniform confinement

Pointwise variable stress state over the cross-section

The passive confinement on axially loaded concrete members is due to the transverse dilation of concrete and the presence of a confining device which opposes this expansion and determines for concrete a triaxial state of stress variable point by point in a noncircular section.

[1] University of Naples "Federico II", Italy, glignola@unina.it
[2] University of Naples "Federico II", Italy, aprota@unina.it

The confining stress field inside the cross-section, ensuring equilibrium and compatibility, is given by the following equations (Braga et al. 2006):

$$\sigma_x = A\left(x^2 - y^2\right) - Bl^2 \tag{2}$$

$$\sigma_y = A\left(y^2 - x^2\right) - Bl^2 \tag{3}$$

$$\tau_{xy} = -2Axy \tag{4}$$

The constants A and B have been determined (refer to Lignola et al. 2009a for symbol explanation) by guaranteeing the compatibility of the confining device and concrete both orthogonally and parallel to the wrapping (the sum of displacements of concrete - expansion due to the axial load and contraction due to the inward confining pressure - is equal to the wrap expansion due to the same pressure, but in the outward direction).

$$A = \frac{21E_cE_ft_f}{25E_cL^3 + 12E_ft_fL^2\left(2\nu_c + 5\right)} \cdot \varepsilon_l \tag{5}$$

$$B = \frac{18E_cE_ft_f}{25E_cL^3 + 12E_ft_fL^2\left(2\nu_c + 5\right)} \cdot \varepsilon_l \tag{6}$$

the confining pressures (Eqns. 2-4) become a function of axial strain ε_c, in concrete. The key aspect of the model is the different contribution of confining stress field not equal in the two transverse directions x and y. For brevity, herein is shown the case of square cross sections only (Figure 2).

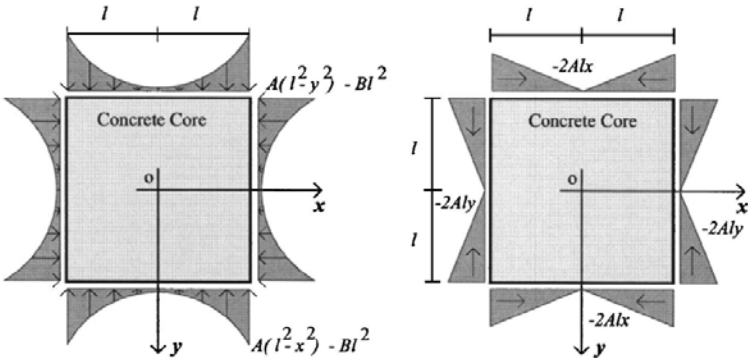

Figure 2: Stress variable point by point in a square section (stress state at boundaries only is shown)

Potential and limits of point wise evaluation

The evaluation of different contributions of confining stresses not uniform and variable in the two transverse directions allows to develop a refined model accounting for the meshing of the cross section and point wise evaluation (Lignola et al. 2008, 2009b). A similar approach was used for rectangular cross sections (Lignola et al. 2010), but not discussed herein. However it turns easily into a major disadvantage if a simplified model is expected. To gain the accuracy of the pointwise variability, but ensuring the simplicity of a practitioner oriented model, an equivalent confining pressure should be evaluated.

Furthermore the knowledge of exact lateral stress state at each longitudinal bar location, for instance, allows to evaluate accurately the bond behaviour of lap spliced bars. Nowadays the design of FRP wrapping to improve bond at insufficient lap length regions in old existing structures, is based on average confinement level of cross sections. Some improvements of design provisions for FRP wrapping at lap splice locations have been proposed recently thanks to the knowledge of pointwise stresses. Not

only the general lower efficiency of confinement in noncircular cross section has been taken into account, but also the confinement pointwise variability. Therefore, in the novel model (Giamundo et al. 2012, 2016), bars with different location in a noncircular cross section performs differently in terms of lap splice behaviour, while in all other previous models the performance is assumed to be uniform in the cross section, hence it is potentially conservative in some situations and unsafe in others.

Integral mean value of the pointwise variable stress field over the cross-section

Recalling the Coulomb plasticity criterion, the failure envelope can be associated to the minimum confining pressure (Figure 1), being the failure (outermost) circle independent on σ_2.

This is the main idea allowing to evaluate the equivalent confining pressure. Hence, the strength of concrete is related only to minimum confining pressure in each point (minimum principal stress, $\sigma_3=f_{l,min}$ according to Eqn. 7), and integrated over the cross-section.

$$f_{l,\min} = \sigma_3 = \frac{\sigma_x + \sigma_y}{2} - \sqrt{\frac{\left(\sigma_x - \sigma_y\right)^2}{4} + \tau_{xy}{}^2} \tag{7}$$

The axial stresses are integrated over cross-section and divided by the total area A to provide directly the average confined concrete strength, $f_{cc,sq}$ (see Eqn. 8). In this way an average lateral pressure (term in brackets in Eqn. 8) is evaluated, which can be assumed as the equivalent confining pressure to be inserted in the confinement model to obtain directly, and without any meshing, the confined concrete strength in square sections.

$$\begin{aligned} f_{cc,sq} &= \frac{\int_{Cross-Section} \left(f_{cc}\right) dA}{\int_{Cross-Section} dA} = \frac{\int_{Cross-Section} \left(f_{co} + k_1 f_l\right) dA}{\int_{Cross-Section} dA} = \\ &= f_{co} + k_1 \cdot \left(\frac{\int_{Cross-Section} \left(f_{l,\min}\right) dA}{\int_{Cross-Section} dA} \right) = f_{co} + k_1 \cdot f_{l,sq} \end{aligned} \tag{8}$$

and the closed form solution for equivalent confining pressure provided by the integral (8), is given by

$$f_{l,sq} = \frac{4E_c E_f t_f}{25E_c l + 12E_f t_f \left(5 + 2\nu_c\right)} \varepsilon_l \tag{9}$$

where symbols are: l the half length of a side of the square cross-section, E_f and t_f the Young modulus and total thickness of the wrap respectively, ε_l the strain in the wrap. The nonlinear mechanical properties of concrete are (secant) Young modulus E_c and dilation ratio ν_c at failure.

Both the nonlinear mechanical properties of concrete should be evaluated iteratively, however this makes the model not enough straightforward for practitioners. For this reason the discussion continues to account, in a simplified manner, for rectangular cross sections too and discussing an approximation for the nonlinear part of the equations.

Simplifications to account for rectangular cross sections and concrete nonlinearities

Formally the same approach has been adopted in Lignola et al. 2010, however to provide a direct, practical tool, oriented to the profession, a simplified confinement model for rectangular cross-sections has been developed. The basic idea is that the behaviour of a rectangular cross-section is assumed as in

between the behaviour of two square cross-sections having the sides equal to the longest and shortest sides of the rectangular cross-section. According to this, the equivalent confining pressure for rectangular cross section is:

$$f_{l,rect} = \left(\frac{2}{\frac{25l_x}{t_f E_f} + \frac{NL}{E_{co}}} + \frac{2}{\frac{25l_y}{t_f E_f} + \frac{NL}{E_{co}}} \right) \varepsilon_l \qquad (10)$$

where NL is the nondimensional factor accounting for the nonlinear mechanical properties of concrete (secant elastic modulus at ultimate, E_c, is expressed as a fraction of initial elastic Young modulus, E_{co}), and it makes the model not easily applicable, requiring an iterative approach. For this reason, the impact of the nondimensional factor NL can be evaluated by means of a wide sensitivity analysis (Lignola et al. 2016) based on a database of about fifty experimental tests on rectangular (plain) concrete columns wrapped with glass and carbon FRP, and with enough data reported in relevant papers. The database includes a wide stock of combinations in terms of column dimensions, concrete classes, thickness and capacity of FRP wraps.

The term NL/E_{co} is always negligible (i.e. at least one or two orders of magnitude lower, but usually more) compared to $25l/(t_f E_f)$. In Eqn. 10, NL=0 can be assumed and introducing a mechanical reinforcement ratio, ω_i (where i stands for dimension along x or y), as:

$$\omega_i = \frac{E_f \varepsilon_l t_f}{f_{co} l_i} \qquad (11)$$

hence the final simplified confinement equation for rectangular cross section, Eqn. 10, becomes:

$$\frac{f_{cc,rect}}{f_{co}} = 1 + k_1 \frac{f_{l,rect}}{f_{co}} = 1 + \frac{2k_1}{25}\left(\omega_x + \omega_y\right) \qquad (12)$$

Confinement model validation

An overview of the predictability of the proposed simplified model is provided in Figure 3a on the well-known format of the 45° line.

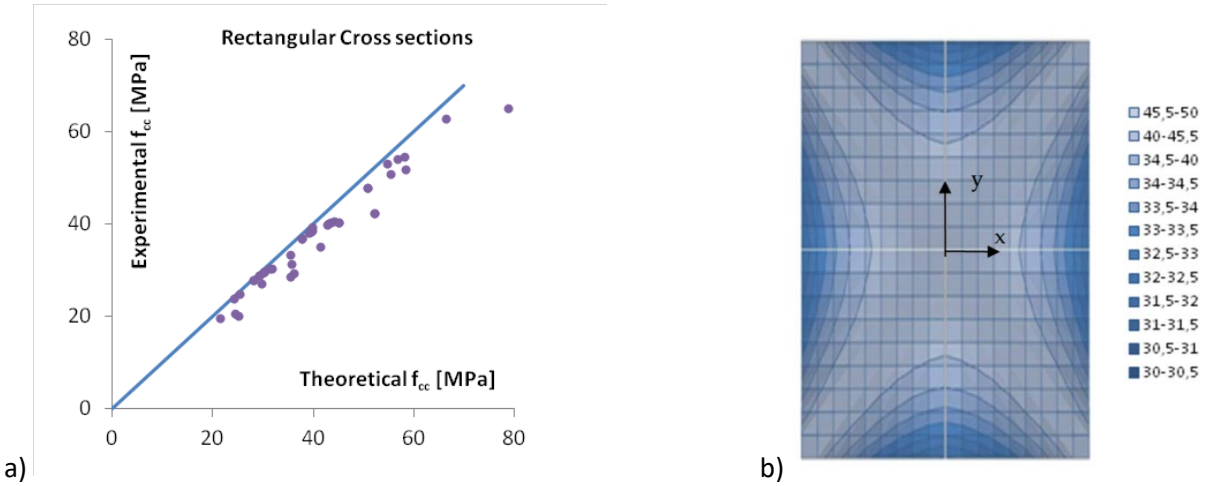

Figure 3: a) Validation of proposed model on experimental database; b) pointwise variability over cross section of confined concrete strengths, f_{cc}

It is noted that the model is generally not conservative, however the predictability is quite high (point cloud aligns along 45° line) and the definition of partial safety factors, for design purposes, requires a further step (i.e. a statistical regression based calibration, like as in Lignola et al. 2014c, to account for all sources of uncertainties, apart the model equation) out of the scope of present work.

Conclusions and Points for Discussions

- To effectively model the confinement of non circular members it is required a mechanically based approach. The pointwise great variability of stresses and the nonlinear mechanical behaviour of confined material (i.e. concrete) makes the modelling very complex and requiring at least iterative evaluations and probably a computational support.
- To provide a simplified closed form solution to determine directly the ultimate confined concrete strength (even by hand calculation), starting from a detailed description of the confining stress field (Figure 3b), a series of sequential simplifications were provided.
- Based on the accuracy of the expected result, a practitioner could stop at every "simplification" step, but the last step provides a very simple equation yet providing satisfactory results. The most simple equation is analogous to those provided by "conventional" models (empirically, best fitting, based), however the derivation is quite different, more rigorous for square cross sections, more approximated for rectangular cross sections, yet effective.

Key references

Braga F, Gigliotti R and Laterza M (2006) "Analytical Stress-strain relationship for concrete confined by steel stirrups and/or FRP jackets". J. Struct. Eng., 132(9), 1402–1416.

De Luca A, Nardone F, Matta F, Nanni A, Lignola GP and Prota A (2011) "Structural Evaluation of Full-Scale FRP-Confined Reinforced Concrete Columns" J. Compos. for Construction 15(1), 112-123.

Giamundo V., Lignola G.P., Fabbrocino F., Prota A. and Manfredi G. (2016) "Influence of FRP wrapping on reinforcement performances at lap splice regions in RC columns". Composites: Part B, DOI: 10.1016/j.compositesb.2016.10.069

Giamundo V., Lignola G.P., Prota A. and Manfredi G. (2012) "Friction Increase of Spliced Bars due to FRP Wrapping". In proceedings "6th International Conference on Fiber Reinforced Polymer (FRP) Composites in Civil Engineering (CICE 2012)". Rome, Italy

Lignola GP, Angiuli R, Prota A and Aiello MA (2014b) "FRP Confinement of masonry: analytical modeling". Materials and Structures. 47(12), 2101-2115.

Lignola GP, Jalayer F, Nardone F, Prota A and Manfredi G (2014c) "Probabilistic design equations for the shear capacity of RC members with FRP internal shear reinforcement". Composites: Part B, 67, 199-208.

Lignola GP, Prota A and Manfredi G (2014a) "Simplified Modeling of Rectangular Concrete Cross-Sections Confined by External FRP Wrapping" Polymers 6(4), 1187-1206.

Lignola GP, Prota A and Manfredi G (2016) "Simplified modeling of concrete confinement". In proceedings "Fourth International Conference on Sustainable Construction Materials and Technologies (SCMT4)", Las Vegas, USA: 1045-1054.

Lignola GP, Prota A, Manfredi G and Cosenza E (2005) "Confinement of RC Hollow Columns using CFRP laminates". In proceedings "Third International Conference on Composites in Construction CCC 2005". Lyon, France

Lignola GP, Prota A, Manfredi G and Cosenza E (2008) "Unified Theory For Confinement of RC Solid and Hollow Circular Columns". Composites: Part B, 39(7-8):1151-1160.

Lignola GP, Prota A, Manfredi G and Cosenza E (2009a) “Analysis of FRP Confinement On Prismatic RC Columns”. Proceedings of 9th International Symposium on Fiber Reinforced Polymer Reinforcement for Concrete Structures FRPRCS9 2009. Sydney, Australia, #129.

Lignola GP, Prota A, Manfredi G and Cosenza E (2009b) “Analysis of Reinforced Concrete Hollow Square Piers Behavior: Benefits Of FRP Confinement”. International Journal of Advanced Structural Engineering, 1(1): 17-34.

Lignola GP, Prota A, Manfredi G and Cosenza E (2010) “Non linear refined modeling of FRP Confinement on Prismatic RC Columns”. In proceedings “14th European Conference on Earthquake Engineering”. Ohrid, Republic of Macedonia.

Richart FE, Brandtzaeg A and Brown RL (1928) “A Study of the Failure of Concrete Under Combined Compressive Stresses” Univ. of Illinois Engineering Experimental Station, Champaign, Ill, Bulletin 185.

Some remarks on confinement effects and potential guidelines implications

G.P. Lignola[1], A. Prota[2]

Introduction

Existing analytical models for predicting the stress–strain behaviour of FRP-confined concrete are mostly derived for cylindrical plain concrete columns. It is commonly assumed that FRP fails when hoop strain in the jacket reaches its ultimate tensile strain determined according to flat coupon tests. However in most cases this FRP ultimate tensile strain is not reached at the rupture of the FRP jacket. This jeopardized most of the validations of older proposed models and opened the floor to empirical formulations. Square- and rectangular-section columns were found to experience less increase in strength and ductility than their circular counterparts, particularly in some cases where very slender walls formed the reinforced concrete members. Even if more refined approaches has been proposed recently (e.g. Lignola et al 2009a), usually design codes and guidelines follow simplified approaches, mainly based on empirical formulations, experimentally based on regression analyses.

In this paper, some remarks are provided on critical points in confinement applications, potentially having an impact on next generation design guidelines.

Ultimate FRP strain in confinement applications

The existing models available for confined concrete assessment both in terms of ultimate capacity and of stress-strain relationships rely on an assumed value of the ultimate FRP strain and the average absolute error of all models showed a remarkable decrease when the confining device effective strain is inserted in the equations. In particular, confinement models based on regression analyses are very sensitive to the value adopted for the ultimate FRP strain. In fact, FRP ultimate tensile strain determined experimentally according to flat coupon tests is usually not reached at the rupture of the FRP jacket in confined concrete columns compression tests.

Reasons for this have been provided by many authors (a summary is in Lignola et al 2008a). Firstly this phenomenon may be attributed to the scatter in the FRP tensile strength and in the strain measurement. The characterization of tensile properties of FRP is actually influenced by the testing procedure, thus standard test protocols are needed.

When concrete is internally cracked and further loaded it experiences non-homogeneous deformations thus leading to local stress concentrations in the FRP jacket. This effect is likely more evident in large diameter columns. Moreover the presence of voids, protrusions and misalignments of fibers in the FRP can reduce the capacity of the composite material.

If shear is not transferred across the interface between the jacket and the concrete, then the strain in the jacket would be uniform around the perimeter of the cross section. But, if a degree of bond between the jacket and underlying concrete allows jacket stresses to be transferred into the concrete, then the average strain in the jacket is altered. Moreover if the jacket crosses a splitting crack, there would be a strain concentration. Unless the measurement is made exactly at the strain concentration, obviously the measured jacket strains at rupture are lower than the real capacity. Furthermore, at a given confining pressure, the FRP hoop strains are inversely proportional to the thickness of the jacket, rising in the overlapping zone.

Several other factors may lead to a “premature” failure of the FRP likely as an uneven tension during lay-up, the temperature, creep, and shrinkage incompatibility between concrete and FRP jacket, the

[1] University of Naples “Federico II”, Italy, glignola@unina.it
[2] University of Naples “Federico II”, Italy, aprota@unina.it

cumulative probability of weaknesses in the FRP material, since jackets are much larger than tensile coupons.

The transfer of longitudinal, axial load through bond with concrete and the radius of curvature in FRP jackets on cylinders leads to a multiaxial stress state in the FRP and these phenomena are likely to produce an average FRP hoop rupture strain in the confined cylinders that is much lower than the one experimentally measured with flat coupon tests.

In any cases the pressure provided by FRP to confine concrete can be assumed not related to the value of FRP strain at its localized failure, but to an average strain in the wrapping, usually smaller than the former, as well as of the flat coupon capacity.

FRP confinement efficiency factor

The ratio between the average FRP hoop strain at rupture in the confined cylinders and the experimentally measured strain with flat coupon tests is termed "efficiency factor", β. If the effective lateral confining pressure is inserted in a confinement model whatever is the material of the confining device, the scattering between theoretical and experimental results can be drastically reduced and a single expression can be formulated to predict benefits provided by confinement, e.g. for concrete, independently from the materials used as confinement device. It is highlighted that also more refined iterative confinement models may need a stop criterion given by the effective failure of the FRP jacket.

A theoretical model has been proposed in Lignola et al (2008a) suggesting an upper bound of the efficiency factor β (upper bound because it neglects stress localization and premature failures) to account for jacket curvature, yielding to a closed form solution, accounting for anisotropy:

$$\beta = \frac{\left(1-\upsilon_{TL}\upsilon_{LT}+\upsilon_{TL}\upsilon_{LT}\frac{t}{R}+\upsilon_{LT}\frac{t}{R}\right)}{\sqrt{1+\left(\frac{f_\theta}{f_r}\frac{t}{R}\right)^2+\left(\frac{f_\theta}{f_z}\right)^2\left(\upsilon_{TL}-\upsilon_{TL}\cdot\frac{t}{R}\right)^2+\frac{f_\theta}{f_r}\frac{t}{R}-\left(\upsilon_{TL}-\upsilon_{TL}\frac{t}{R}\right)\frac{f_\theta}{f_z}+\left(\upsilon_{TL}-\upsilon_{TL}\frac{t}{R}\right)\frac{t}{R}\frac{f_\theta^2}{f_r\cdot f_z}}} \quad (1)$$

where $v_{TL}=v_{LT}\cdot E_T/E_L$ is the Poisson's ratio and E_L and E_T are the transverse and longitudinal elastic moduli, respectively. The longitudinal (circumferential) and transverse (vertical or radial) strengths of the FRP are f_θ and $f_r \approx f_z$, respectively. The sensitivity of the involved parameters has been discussed in Lignola et al (2009b), where it was shown that the main parameter driving the coefficient β is the FRP composite relative strength (f_θ/f_r) and GFRP presents the highest dependence on the analyzed parameters (see in Figure 1 an example related to average FRP properties). Obviously the proposed model is valid also for noncircular cross sections looking at the rounded corners (and the radius of rounding is assumed as the radius to be inserted in the equations).

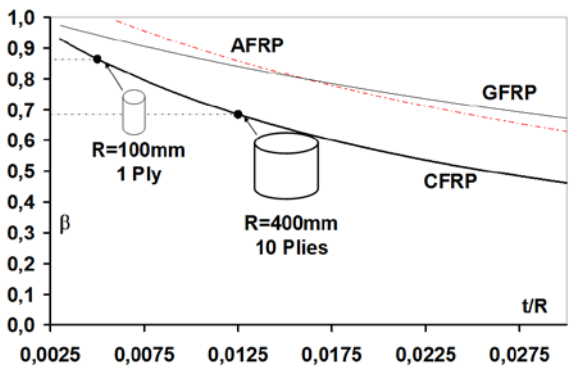

Figure 1: Efficiency factor variation accounting for jacket curvature (example, average FRP properties)

To better limit the range of variability of the effective FRP strain in confinement, a second model was proposed (Zinno et al. 2009, 2010) to analyze the effect of the stress concentrations at the free edge of the FRP jacket (Figure 2). Interlaminar stresses can cause premature failure of the FRP wrapping due to separation or delamination, thus limiting the confinement capacity of the FRP wrapping. This second model provides directly the effective FRP strain depending on the maximum interlaminar shear, τ_{max}, or on the normal tensile interlaminar peel stress, σ_{nmax}, capacity:

$$\varepsilon_{FRP} = \min\left\{\frac{e^{2\gamma L}-1}{e^{2\gamma L}+1}\tau_{\max};\frac{\sigma_{n\max}}{t_a\gamma}\right\}\cdot\frac{1+n}{Etn\gamma} \qquad (2)$$

where the parameters are described in details in the original paper and their typical values are provided.

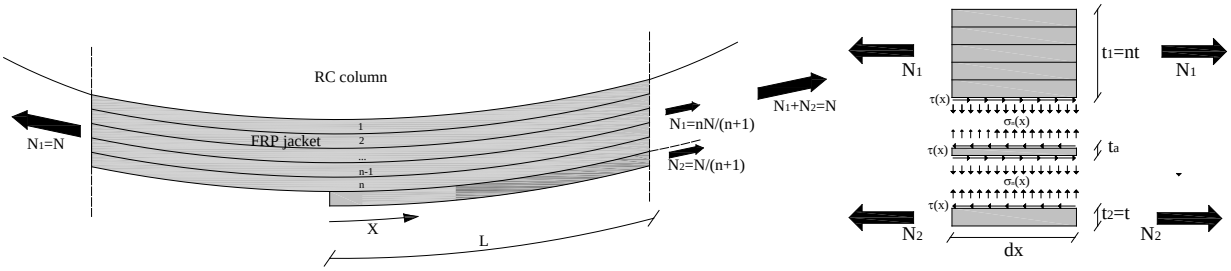

Figure 2: Effect of the stress concentrations at the free edge of the FRP jacket: Interlaminar stresses

Confinement of slender wall members

Slender walls can be found in reinforced concrete members both with hollow cross sections and with rectangular cross sections characterized by high side aspect ratios.

Hollow piers are peculiar of bridge constructions to maximize structural efficiency of the strength-mass and stiffness-mass ratios (Figure 3a). In particularly large members each wall composing the hollow cross-section resists the external actions, rather than as a whole hollow cross section (as shown by preliminary Finite Element analyses conducted in Lignola et al 2009c). In wall-like cross sections the arch-shaped paths of the confining stresses rapidly changes in a straight distributed confinement stress field moving away from the corners (Figure 3b).

The results of the previous works (Lignola et al 2005, 2009d) suggest that a reliable numerical procedure to predict hollow cross section behaviour under combination of flexure/shear and compression should include appropriate models for compressed bars buckling, concrete cover spalling and, of course, confined concrete behaviour. In fact nowadays the common practice (adapting concrete confinement models for circular concrete columns to effectively confined area in noncircular sections with further reduction coefficients) is rather good to assess strength enhancements. Conversely it fails to predict the post-peak behaviour of the existing wall members thus resulting in inaccurate ductility predictions if compressed bars buckling and concrete cover spalling are neglected. In these cases confinement models may be successfully used to predict essentially the strength of the column if the evaluation is limited to the occurrence of buckling of the compressed steel reinforcement bars.

Usually in such cases confinement does not change the actual failure mode (steel reinforcement compressive bars buckling and concrete cover spalling), but it is able to delay bars buckling (Giamundo et al. 2012, 2014) and to let compressive concrete strains attaining larger values, thus resulting in higher load carrying capacity of the member and in significant ductility enhancement. The strength increase in confined concrete due to FRP wrapping turns into load carrying capacity increases mainly in the elements loaded with small eccentricity (it is clear that close to pure bending load the effect of concrete strength enhancement is not relevant because failure moves to tension side and, at lower levels of axial

load, i.e. at higher eccentricities, also the influence of reinforcement buckling on the element behaviour is less significant).

A confinement model, recently proposed, is based on solid mechanics and able to predict the fundamentals of the behaviour of solid and hollow circular (Lignola et al 2008b, 2009d) and solid square (Lignola et al 2014) members confined with FRP. The model traces the evolution of stresses and strains in the concrete and in the confinement jacket and it allows to evaluate, at each load step, the multiaxial state of stress, and eventually the failure, of the concrete or the external reinforcement: e.g. following models on effective FRP strain at failure. The lateral-to-axial strain relationship provides the essential linkage between the response of the concrete column and the response of the FRP jacket in a passive-confinement model. A typical outcome of such an approach is shown in Figure 3a, where the effect of inner, R_i, to outer, R_o, radii ratios is remarked.

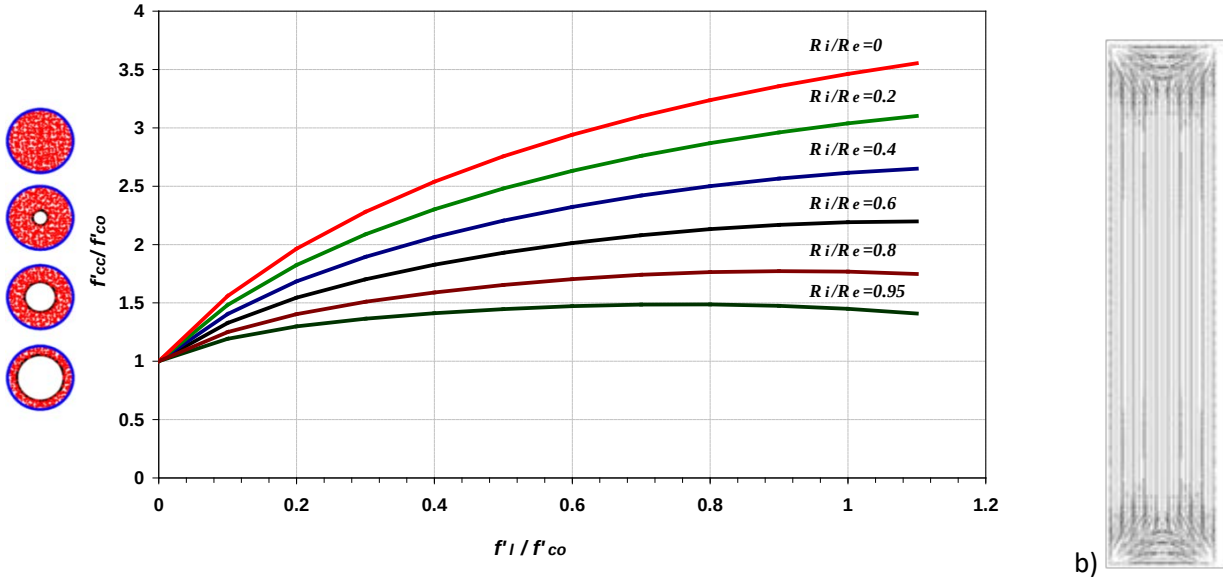

a) b)

Figure 3: Effect of the slenderness in: a) hollow cross section; b) slender wall-like cross sections

An experimental program conducted on wall-like columns (Prota et al. 2006) confirmed that significant strength increases can be achieved by FRP wrapping: the number of plies does not play a major role on the axial strength while it gives improvements in terms of axial ductility. The failure of these walls determines the bulging of the FRP laminates occurring at fiber strains far below the guaranteed ultimate values.

Again, even though a refined nonlinear confinement model was provided for the analysis of RC columns (e.g. Lignola et al 2009a, 2014, 2016), to provide a direct, practical tool, oriented to the profession, it was provided also a simplified confinement model for slender rectangular cross-section, for which the arch-shaped path of the confining stresses was seen to rapidly change in a straight distributed confinement stress field moving away from the corner (Lignola et al 2009c). This alternative simplified approach, that gives rather accurate results despite the heavily reduced computational effort (no iterations are needed) considers the confining stress field only parallel to the longer side of the cross-section, thus neglecting the confinement in the shorter direction. The confining pressure f'_l can be assumed, based on free body diagram equilibrium, equal to $2tE_f\varepsilon_{FRP}/h$ where h is the height of the cross section and is assumed to be smaller than the base b.

After a regression analysis of the ultimate concrete strength surface equation, the following equation is proposed:

$$\frac{f_{cc}}{f'_c} = 1 + 1.42\frac{f'_l}{f'_c} - 1.40\left(\frac{f'_l}{f'_c}\right)^2 + 0.30\left(\frac{f'_l}{f'_c}\right)^3 \quad (3)$$

where $f'_l/f'_c<1.3$.

Equation (3) can be also used to evaluate the stress-strain relationship for confined concrete in slender walls according to the procedure proposed by Spoelstra and Monti (1999), relying on an iterative procedure through which the stress-strain curve crosses a family of stress-strain curves at constant confinement pressure, where at each point the confinement pressure is equal to that induced by the FRP jacket subjected to the corresponding lateral expansion.

Conclusions and Points for Discussions

- FRP Wrapping usually is able to increase slightly the strength of beam and slender column members and mainly their ductility, nevertheless in a capacity design it is essential to check that brittle mechanisms (i.e. shear failure) are prevented by ductile ones also accounting for over strength. For this reason, even if underestimating the FRP strain seems on safe side for confinement applications, there are some situations where it is desirable to know with greater precision the over strength of members (e.g. due to seismic capacity design approaches).
- According to proposed models for FRP confinement efficiency factor, there is a research need to collect and publish in future confinement experimental works also those FRP mechanical properties. It seems important to standardize the calibration process of confinement models by using efficiency factor β, because the average absolute error of confinement models shows a remarkable decrease when effective strain is considered.
- Usually in slender wall members, confinement does not change the actual failure mode (steel reinforcement compressive bars buckling and concrete cover spalling), but it is able to delay these brittle mechanisms thus allowing compressed concrete strains attaining larger values (moderate load carrying capacity increment and significant ductility enhancement).
- Capacity in terms of strength only, can be evaluated by means of a simplified analysis provided extreme fiber compression strains are relatively low (in the order that compressed reinforcement strain should be lower than buckling strain depending on stirrups spacing – i.e. according to Cosenza and Prota 2006). In this way it can be taken into account the effect of concrete cover spalling and compressed reinforcement buckling. For piers carrying mainly axial loads it may be questionable to use the post peak part of the stress strain diagram in design, as the descending part is associated with large deformations and stability problems.
- Adequate transverse reinforcement is a crucial issue in structural walls. Ductility performances require that concrete is well confined and compressed reinforcement buckling is avoided. Bars' buckling determines a strength reduction but an FRP retrofit intervention can be designed.

Key references

Cosenza E. and Prota A. (2006) "Experimental behavior and numerical modeling of smooth steel bars under compression". Journal of Earthquake Engineering, 10(3):313-329.

Giamundo V., Lignola GP, Prota A and Manfredi G (2012) "Restraining bars buckling by means of FRP wrapping: an analytical approach". In proceedings "15th World Conference on Earthquake Engineering". Lisbon, Portugal. Paper #4320

Giamundo V., Lignola GP, Prota A and Manfredi G (2014) "Analytical evaluation of FRP wrapping effectiveness in restraining reinforcement bars buckling". Journal of Structural Engineering, 140(7). 04014043:1-12

Lignola G.P., Prota A., Manfredi G. and Cosenza E. (2008a) “Effective strain in FRP jackets on circular RC columns”, Proc. 4th International Conference on FRP Composites in Civil Engineering (CICE2008), Zurich, Switzerland, Paper 2.A.5

Lignola G.P., Prota A., Manfredi G. and Cosenza E. (2008b) “Unified Theory For Confinement of RC Solid and Hollow Circular Columns”. ELSEVIER Composites part B, 39:7-8,1151-1160.

Lignola G.P., Prota A., Manfredi G. and Cosenza E. (2009a) “Analysis Of FRP Confinement On Prismatic RC Columns”. Proc. 9th International Symposium on Fiber Reinforced Polymer Reinforcement for Concrete Structures FRPRCS9 2009. Sydney, Australia.

Lignola G.P., Prota A., Manfredi G. and Cosenza E. (2009b) “Evaluation Of Effective Ultimate Strain Of FRP Confinement Jackets Applied On Circular RC Columns”. Proc. 9th International Symposium on Fiber Reinforced Polymer Reinforcement for Concrete Structures FRPRCS9 2009. Sydney, Australia.

Lignola G.P., Prota A., Manfredi G. and Cosenza E. (2009c) ”Non linear modeling of RC hollow piers confined with CFRP.” ELSEVIER Composites Structures, vol. 88, Issue 1, pp. 56-64.

Lignola GP, Prota A and Manfredi G (2014) “Simplified Modeling of Rectangular Concrete Cross-Sections Confined by External FRP Wrapping” Polymers 6(4), 1187-1206.

Lignola GP, Prota A and Manfredi G (2016) “Simplified modeling of concrete confinement”. In proceedings “Fourth International Conference on Sustainable Construction Materials and Technologies (SCMT4)”, Las Vegas, USA: 1045-1054.

Lignola GP, Prota A, Manfredi G and Cosenza E (2005) “Confinement of RC Hollow Columns using CFRP laminates”. In proceedings “Third International Conference on Composites in Construction CCC 2005”. Lyon, France

Lignola GP, Prota A, Manfredi G and Cosenza E (2009d) “Analysis of Reinforced Concrete Hollow Square Piers Behavior: Benefits Of FRP Confinement”. International Journal of Advanced Structural Engineering, 1(1): 17-34.

Prota A., Manfredi G. and Cosenza E. (2006) “Ultimate behaviour of axially loaded RC wall-like columns confined with GFRP”. Composites: part B, vol. 37, pp. 670-678.

Spoelstra M.R. and Monti G. (1999) “FRP-confined concrete model.” ASCE Journal of Composites for Construction, 3(3):143-150.

Zinno A., Lignola G.P., Prota A., Manfredi G. and Cosenza E. (2009) “Effect of stress localization at free edge for FRP wrapping in RC confinement applications”. Proc. 15th International Conference on Composite Structures (ICCS 15). Porto, Portugal.

Zinno A., Lignola G.P., Prota A., Manfredi G. and Cosenza E. (2010) “Influence of free edge stress concentration on effectiveness of FRP confinement”. ELSEVIER Composites: Part B, Vol.41, No. 7, 2010:523-532.

3.5 Strengthening of Beam-Column Joints

Experimental tests on FRP strengthened joints and design procedure

C. Del Vecchio[1], M. Di Ludovico[2], A. Prota[3], G. Manfredi[4]

[1,2,3,4] *Department of Structures for Engineering and Architecture, University of Naples "Federico II", ITALY.*

Abstract

The high vulnerability of existing Reinforced Concrete (RC) structural systems is often related to brittle failures of critical members. Field surveys and relevant scientific studies showed that unconfined and poorly detailed beam-column joints were not able to resist moderate-to-large seismic events. The effectiveness of composite materials, such as fiber reinforced polymer (FRP) systems, has been demonstrated by experimental tests on joint subassemblies and entire structural systems. This, along with the simplicity of installation, has strongly promoted the use of the composite material for seismic retrofit of RC structures. Nevertheless, a detailed description of the mechanical behaviour and deboning phenomena characterizing the FRP strengthening system of the joint panel is still lacking. This is due to large number of parameters involved and to the lack of local measurements. In recent years, several experimental tests have been carried out on corner RC beam-column joints focussing on the local behaviour of the FRP strengthening system. The analysis of the local measurements and the effort in collecting the available experimental tests in a comprehensive database resulted in a simple and reliable mechanical model suitable for application in the design practice. A new formulation for the effective FRP strain is proposed to overcome the limitation of the FRP strain to 0.4% as conventionally assumed in available guidelines.

Introduction

The high vulnerability of existing Reinforced Concrete (RC) structural systems is often related to brittle failure of unconfined and poorly detailed beam-column joints as evidenced by post-earthquake field surveys (Del Vecchio et al. 2014; Frascadore et al. 2015). Number of experimental tests and analytical studies demonstrated the effectiveness of FRP systems to improve the strength and deformation capacity of beam-column subassemblies (Antonopoulos and Triantafillou 2003; Prota et al. 2004; Di Ludovico et al. 2008; Frascadore et al. 2015). This background along with FRP properties like light weight, durability and advantages in the installation procedure (Balsamo et al. 2012) strongly promoted the use of composite materials in the aftermath of major recent earthquakes (Di Ludovico et al. 2016a; Di Ludovico et al. 2016b). Although the effectiveness of FRP systems for the strengthening of beam-column joints has been investigated, few studies have specifically focussed on the mechanical behaviour of the joint panel FRP strengthening and on the FRP effective strain at failure. Here a brief summary of the experimental tests performed by Del Vecchio et al. (2014) is reported. Furthermore, the design formulation proposed by Del Vecchio et al. (2015), suitable for application in the design practice, is illustrated. Such an approach is based on a new formulation for the effective FRP strain that overcomes the limitation of the FRP strain to 0.4% as conventionally assumed in available guidelines.

Experimental tests on FRP strengthened joints

Concrete mechanical properties were designed to simulate existing RC constructions. Two joints (T_C1 and T_FL1) had a poor concrete compressive strength (f_{cm}<15 MPa) and four others (T_C2, T_C3, T_FS1, T_FS2) a concrete compressive strength ranging between 15-20 MPa (Table 1). Out of a total number of

[1] Department of Structures for Engineering and Architecture, University of Napoli Federico II, Italy, ciro.delvecchio@unina.it
[2] Department of Structures for Engineering and Architecture, University of Napoli Federico II, Italy, diludovi@unina.it
[3] Department of Structures for Engineering and Architecture, University of Napoli Federico II, Italy, aprota@unina.it
[4] Department of Structures for Engineering and Architecture, University of Napoli Federico II, Italy, gamanfre@unina.it

seven beam-column joint subassemblies, three specimens were tested in the as-built configuration, named T_C1, T_C2 and T_C3. Although characterized by different concrete compressive strength, the as-built specimens (T_C1, T_C2 and T_C3) showed a similar joint panel crack pattern and failure mode (see Figure 1a). Observed joint panel failure was characterized, in each case, by large deep diagonal cracks and concrete "wedge" spalling-off. The hysteretic loop typical of the as-built specimen is reported in Figure 2a. Details about the tested specimens and experimental results are reported in Table 1.

Table 1: Test matrix and experimental results (Del Vecchio et al. 2014)

Spec.	f_{cm}	$t_{f,eq}$	Load sign	$V_{c,MAX}$	ΔV_c	Drift ($V_{c,MAX}$)	Failure Mode	E_{tot} (Drift=3.3%)	ΔE_{tot}	ε_{FRP} (max)
[-]	[MPa]	[%]	[-]	[kN]	[%]	[%]	[-]	[kN*mm]	[%]	[%]
T_C1	12.6	-	+	33.2	-	1.1	JS	7406	-	-
			-	27.6	-	1.3				
T_C2	16.4	-	+	42.6	-	1.3	JS	n.a.[a]	-	-
			-	34.4	-	1.3				
T_C3	16.3	-	+	43.8	-	1.3	JS	10237	-	-
			-	36.9	-	1.3				
T_FL1	13.5	0.053 (scheme 1)	+	38.8	17.0[b]	1.3	FD /JS	8596	16.1[b]	0.72
			-	33.1	19.8[b]	1.3				
T_FS1	17.7	0.053 (scheme 2a)	+	56.1	29.9[c]	2.4	CH /FD		19.4[c]	0.10
			-	45.2	26.6[c]	2.4				
T_FS2	16.4	0.106 (scheme 2b)	+	65.3	51.2[c]	2.3	CH /FC	13460	31.5[c]	0.67
			-	50.1	40.6[c]	1.3				
T_RFL1	16.4	0.053 (scheme 1)	+	45.4	6.4[c]	2.4	FD /JS	10190	-	0.45
			-	35.0	1.7[c]	2.4				

Note: JS = joint shear; CH = column flexural hinging; FD = FRP debonding; FF = tensile failure of FRP fibers.
[a] This test was stopped at a drift of 2.39%; [b] Computed for T_C1; [c] Computed for the average T_C2 and T_C3.

Three specimens (T_FL1, T_FS1, T_FS2) were strengthened to investigate the benefits provided by different FRP layouts (see Figure 1b). One more tests (T_RFL1) was carried out on a pre-damaged joint (T_C2) tested and then retrofitted with FRP after crack filling. The FRP strengthening strategy aimed to avoid joint brittle failure (T_FL1) and increase the subassembly dissipation capacity (T_FS1, and T_FS2).

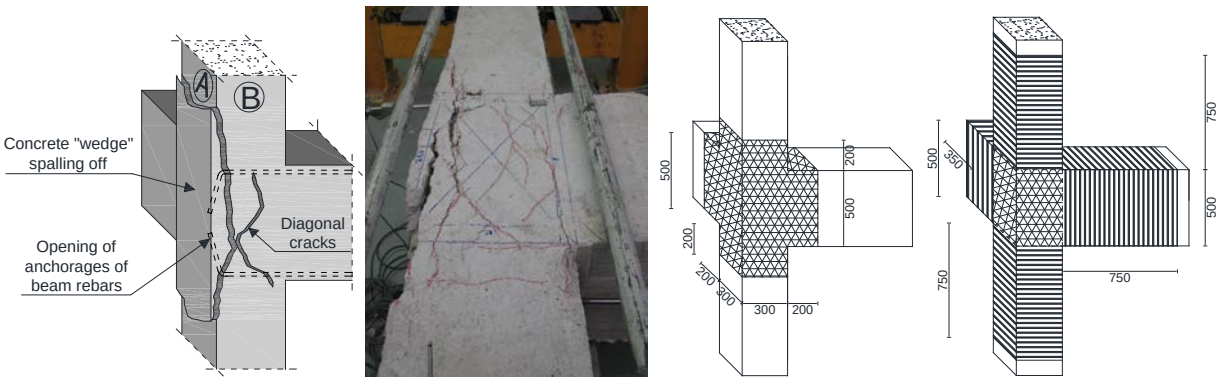

(a) (b)

Figure 1: (a) As-built joint crack pattern, (b) FRP strengthening layouts (dimensions in mm) (Del Vecchio et al. 2014).

The FRP-strengthened specimens showed a significant strength enhancement compared to as-built joints: about 18%, 28% and 46% on average for T_FL1, T_FS1, T_FS2, respectively (Table 1). A significant increase in the energy dissipation (until 31.5% for T_FS2) was also observed. Although the same joint panel strengthening system was adopted on T_FL1 and T_FS1, a different mechanical behavior was observed on such specimens. Indeed, the poor quality concrete of T_FL1 led to premature intermediate debonding which greatly reduced the potential benefits provided by the CFRP joint panel reinforcing system.

Concrete crushing detected at the column-joint interface on T_FL1 demonstrated the need to confine the column ends in order to increase plastic hinge ductility.
Although the strengthening scheme adopted in T_FS1 (see Figure 2b) provided a significant strength increase with respect to the as-built specimens, it was unable to provide significant ductility increase. This was due to the premature FRP debonding immediately after the column yielding.

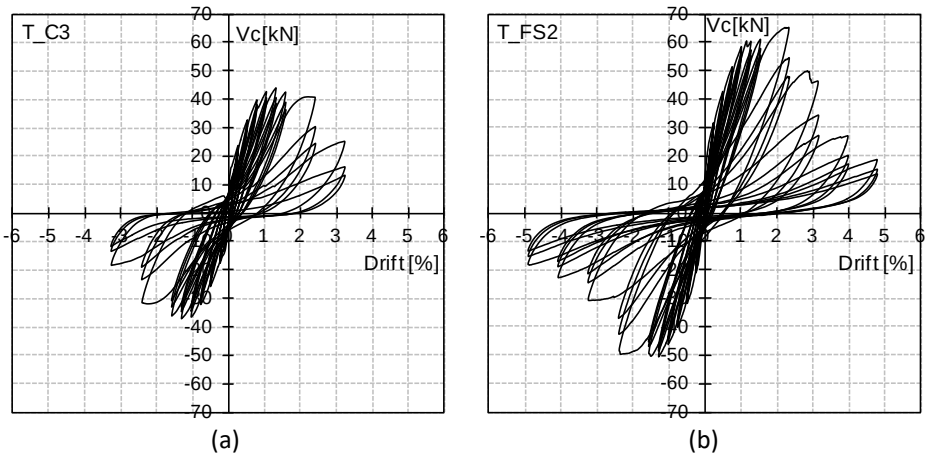

Figure 2: Cyclic hysteresis loop of tested specimens: (a) as-built T_C3 joint, (b) FRP strengthened T_FS2 joint (Del Vecchio et al. 2014).

The use of two CFRP plies to increase joint panel shear capacity, combined with a stronger anchorage solution (T_FS2), prevented joint shear failure before column end yielding. The joint panel deformations were reduced, thus leading to plastic hinge development on the top column (see Table 1). However, due to quadriaxial CFRP failure the ductility reserves of the confined column were not fully exploited. The hysteretic loop of T_FS2 specimen is reported in Figure 2b. A direct comparison between as-built and FRP strengthened joints in terms of skeleton curves is reported in Figure 3a.

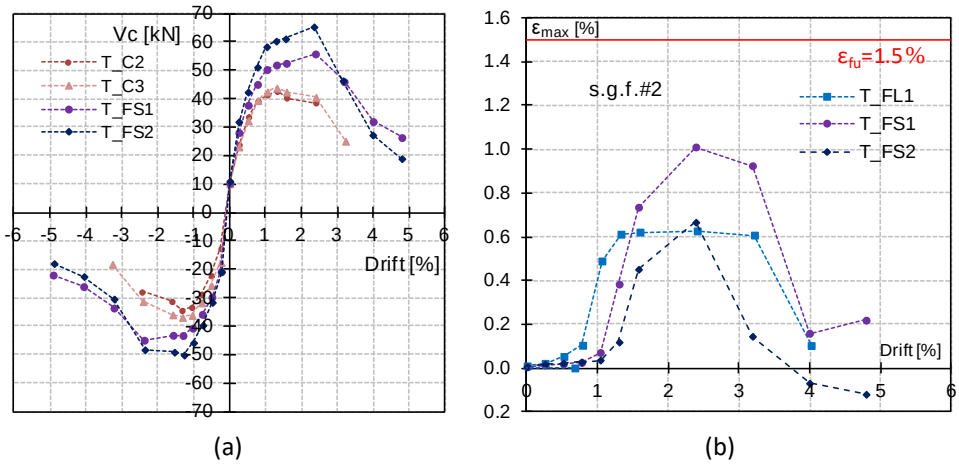

Figure 3: (a) Comparisons of experimental skeleton curves, (b) Joint panel FRP strains (Del Vecchio et al. 2014).

A summary of the maximum recorded FRP strain on the joint panel strengthening system is reported in Table 1. The strains recorded in direction of fibers inclined 45° on the beam axis are depicted in Figure 3b. The recorded strain were significantly higher than 0.4% which is commonly assumed as a maximum value in current guidelines.

Analytical model and design approach

The difficulties in interpreting the mechanical behavior of FRP reinforcement, externally bonded on RC joint panels, are strongly related to the uncertainties of the effective FRP strain. Therefore, the international guidelines and codes on the design of FRP retrofit systems currently do not provide specific

formulations to account for the FRP contribution to the shear strength of beam-column joints. Based on recent experimental observations, a new capacity model to compute the FRP contribution to the shear strength of poorly detailed beam-column joints has been formulated by Del Vecchio et al. (2015). The simple theoretical approach and the use of experimental determined formulations make this model suitable for practitioners involved in the seismic retrofit of existing buildings designed with obsolete code provisions. The proposed model and the model validation is briefly summarized herein.

It allows to determine the required jacket thickness with fibres oriented in multiple directions (multi-axial fabrics with fibres at 0°, 90°, ±45°). This approach is based on the use of the principal tensile stress derived combining the joint shear stress $v_{jh} = V_{jh}/b_c h_c$ and the axial stress $f_a = N/b_c h_c$, N is the axial load acting on the top column. The horizontal shear force acting in the joint, V_{jh}, is derived from equilibrium considerations by using as a target value the yielding moment of framing members (in compliance with a capacity design approach). The principal tensile stress to be used for determining the required FRP amount (FRP area, A_f) is computed from:

$$p_{t,f} = -\frac{f_a}{2} + \sqrt{\left(\frac{f_a}{2}\right)^2 + v_{jh}^2} - k\sqrt{f_{cm}} \quad (1)$$

where: k is a numerical coefficient representing the original joint shear capacity and it is equal to 0.30 for beam–column joints with deformed bars and 0.20 for beam–column joints with smooth bars; f_{cm} is the mean compressive strength of concrete.

In order to calculate the unknown t_f, two parameters should be calculated: the required FRP area, A_f, and the effective FRP strain, ε_{fe}. Thus, in order to simplify the calculation of the equivalent FRP area, $A_{f,eq}$, several equations have been developed for the most common applications.

Uniaxial fabric with fibers in the direction of beam axis (0°) or column axis (90°):

$$\begin{cases} A_{f,eq} = n_l \cdot n_s \cdot t_f \cdot h_b \cdot sin\theta & \text{for } \beta = 0° \\ A_{f,eq} = n_l \cdot n_s \cdot t_f \cdot h_c \cdot cos\theta & \text{for } \beta = 90° \end{cases} \quad (2)$$

Bidirectional fabric with fibers in the direction of beam and column axes (0, 90°):

$$A_{f,eq} = n_l \cdot n_s \cdot t_f \cdot h_c \cdot cos\theta \cdot \left(1 + tan^2\theta\right) \quad (3)$$

Quadriaxial fabric with any fibers in the direction of beam (0°) and column (90°) axes and ±45°:

$$A_{f,eq} = n_l \cdot n_s \cdot t_f \cdot h_c \cdot cos\theta \cdot \left(1 + tan\theta + 2tan^2\theta\right) \quad (4)$$

where β is the inclination of fibres with respect to the beam axis, n_l is the number FRP layers, n_s is the number of joint panel sides strengthened in shear with FRP (1 or 2 sides), and θ is the inclination of concrete compressive strut with respect to the beam axis, $\theta = arctan(h_b/h_c)$.

A power-type expression is used as a best fit to the experimental data, see black line in Figure 4a. Including the two numerical coefficients adopted to account for the influence of the mechanical anchorages and initial damage, the final expression for the FRP effective strain is showed in Eq. (5).

$$\varepsilon_{f,e} = 31.6 \cdot C_{I.D.} \cdot C_{M.A.} \cdot \left(\frac{f_c^{2/3}}{A_{f,eq} \cdot E_f}\right)^{0.6} \quad (5)$$

with $C_{I.D.}$ = 1.0 in case of undamaged joint panel or 0.8 if the FRP strengthening system is applied on a cracked joint panel (otherwise 1). The coefficient $C_{M.A.}$ = 1.0 in the case that the FRP fibers are extended on the adjacent beams or columns without mechanical anchorages or 1.5 if the joint panel FRP strengthening is mechanically anchored at the ends.

The predicted joint shear strength, using the aforementioned approach, show a good match with the experimental data (see Figure 4b).

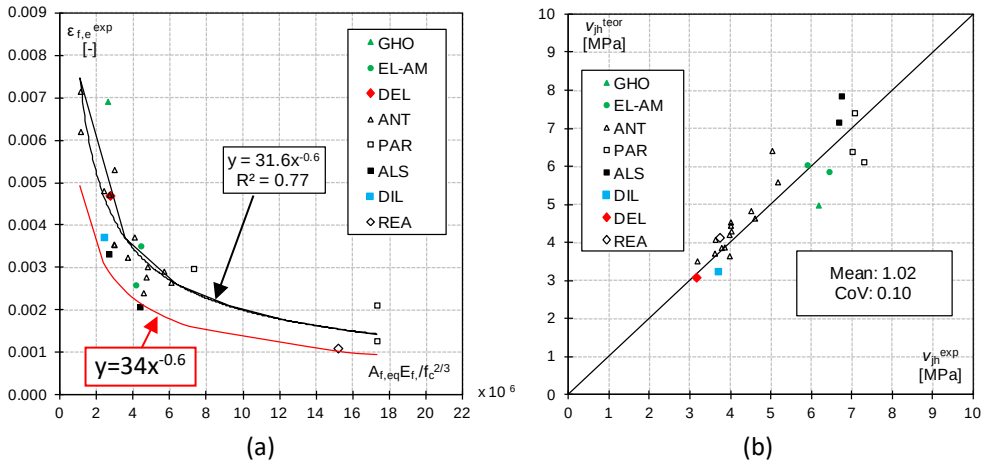

Figure 4: (a) Effective FRP strains in terms of $A_{f,eq}E_f/f_c^{2/3}$(black line is the best fit of data, red line is the desing equation), (b) Comparison of predictions and experimental results in terms of joint panel shear stress (Del Vecchio et al. 2015).

In order to make the model suitable for application in practice, a design formulation for the FRP strain ε_{fd} has been calibrated considering an adequate level of safety according to the Eurocode approach EC0 1990-2002 Annex D (2002). The design FRP strain ε_{fd} is defined according to the Eq. (6) (red line in Figure 4a) and cannot exceed the ultimate FRP strain ε_{fu}:

$$\varepsilon_{fd} = 34\left(\frac{f_{cm}^{2/3}}{A_f E_f}\right)^{0.6} \quad (6)$$

When the FRP strengthening is applied on a repaired substrate, $0.8\varepsilon_{fd}$ should be used.

Based on the demand given in Eq. (1), the FRP thickness t_f (n_l plies of FRP reinforcement) may be estimated from Eq. (7):

$$p_{t,f} = \frac{A_f E_f \varepsilon_{fd}}{b_c(h_c/\sin\theta)} \quad (7)$$

Conclusive remarks

Experimental tests on FRP-strengthened specimens showed the effectiveness of the proposed strengthening solutions for seismic retrofit of poorly detailed RC beam-column joints. In particular, they showed that:

- a suitable amount of joint panel FRP fibers combined with an effective anchoring system significantly reduced the joint panel shear deformation leading to remarkable strength enhancement. This led to a subassembly seismic capacity improvement and to an energy dissipation increase associated with a more favorable ductile failure mode;
- the use of a proper FRP joint panel anchorage solution (i.e. U-shaped uniaxial sheet wrapped also around the beam top side) was a sound solution to avoid FRP end full debonding. However, intermediate debonding may occur in the joint panel FRP strengthening;
- in order to account for debonding phenomena characterizing the joint panel behavior a proper formulation is needed. The limit of 0.4 % suggested in available guidelines as design maximum strain for FRP retrofit of a beam-column joint needs to be better investigated and properly calibrated. Indeed, the maximum strain recorded on FRP was in each case larger than 0.4 % with a maximum value of 1.0 %
- Experimental observations and effective strains recorded on the joint panel allowed to develop a simple and reliable analytical model. The proposed model allows practitioners involved in the

seismic strengthening of existing structures to easily and reliably quantify the amount of FRP reinforcement needed to avoid the brittle shear failure of corner joints.

- Because of the complex stress field acting in the joint panel, a new formulation for the effective FRP strain, that accounts of the debonding phenomena, has been calibrated on experimental tests. The proposed formulation matches well the experimental records in terms of average effective strain. The proposed expression allows to overcome the limitation of the FRP strain to 0.4% as conventionally assumed in available guidelines.

Key references

Antonopoulos, C. P., and T. C. Triantafillou. 2003. Experimental investigation of FRP-strengthened RC beam-column joints. *Journal of Composites for Construction* 7: 39–49. doi:10.1061/(ASCE)1090-0268(2003)7:1(39).

Balsamo, A., M. Di Ludovico, G. P. Lignola, A. Prota, G. Manfredi, and E. Cosenza. 2012. Composites for structural strengthening. In *Wiley Encyclopedia of Composites, Second Edition*, ed. L. Nicolais and A. Borzacchiello. John Wiley & Sons, Inc. doi:10.1002/9781118097298.

European Commitee for Standardization. 2002. *EN1990:2002 Eurocode — Basis of structural design*. Vol. 3. Brussels.

Frascadore, R., M. Di Ludovico, A. Prota, G. M. Verderame, G. Manfredi, M. Dolce, and E. Cosenza. 2015. Local strengthening of RC structures as a strategy for seismic risk mitigation at regional scale. *Earthquake Spectra* 31: 1083–1102. doi:http://dx.doi.org/10.1193/122912EQS361M.

Di Ludovico, M., G. Manfredi, E. Mola, P. Negro, and A. Prota. 2008. Seismic behavior of a full-scale RC structure retrofitted using GFRP laminates. *Journal of Structural Engineering* 134: 810–821. doi:ASCE, ISSN 0733-9445/2008/5-810-821.

Di Ludovico, M., A. Prota, C. Moroni, G. Manfredi, and M. Dolce. 2016a. Reconstruction process of damaged residential buildings outside the historical centres after L'Aquila earthquake - part I: "light damage" reconstruction. *Bulletin of Earthquake Engineering* online pub. doi:10.1007/s10518-016-9877-8.

Di Ludovico, M., A. Prota, C. Moroni, G. Manfredi, and M. Dolce. 2016b. Reconstruction process of damaged residential buildings outside the historical centres after L'Aquila earthquake - part II: "heavy damage" reconstruction. *Bulletin of Earthquake Engineering* online pub. doi:10.1007/s10518-016-9979-3.

Prota, A., A. Nanni, G. Manfredi, and E. Cosenza. 2004. Selective upgrade of underdesigned Reinforced Concrete beam-column joints using carbon Fiber-Reinforced Polymers. *ACI Structural Journal* 5: 699–707.

Del Vecchio, C., M. Di Ludovico, A. Balsamo, A. Prota, G. Manfredi, and M. Dolce. 2014. Experimental investigation of exterior RC beam-column joints retrofitted with FRP systems. *ASCE Journal of Composites for Constructions* 18: 1–13. doi:ASCE, ISSN 1090-0268/04014002(13)/$25.00.

Del Vecchio, C., M. Di Ludovico, A. Prota, and G. Manfredi. 2015. Analytical model and design approach for FRP strengthening of non-conforming RC corner beam-column joints. *Engineering Structures* 87: 8–20. doi:10.1016/j.engstruct.2015.01.013.

3.6 Prestressing Solutions

EXPERIMENTAL EVALUATION OF CONCRETE BEAMS PRESTRESSED BY COMPOSITES

Miroslav Cerny

Klokner Institute, Czech Technical University in Prague, Solinova 7, 166 08 Praha 6
cerny@klok.cvut.cz, cerny@hppro.klok.cvut.cz

The results of statical tests of concrete beams in bending, strenghtened by prestressed carbon strips are presented. C-strip has been located on bottom of the beam and prestressed by 30 kN and 50 kN force. The tests have been focused on analysis of failure mechanisms of RC beams and comparison of loading capacity prestressed and nonprestressed RC beams strengthened by adhesive bonded C-strips.

Tested RC beams.

- 6 beams 140 x 215 x 1600 mm (4 beams strengthended by C-strips 50 / 1.2 mm)
- concrete C 30/35
- steel reinforcement 2x R8 at bottom and 2x R6 at top of the beam

Fig.1 Beam Testing at Instron testing machine

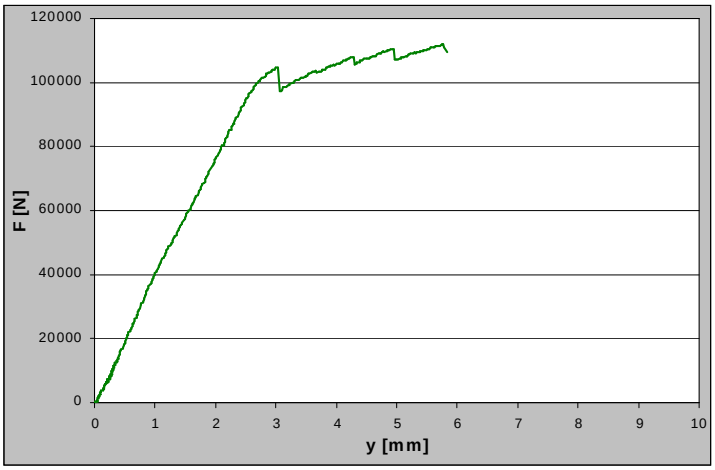

Fig. 2 Load- deformation diagram of the beam prestressed by 50 kN

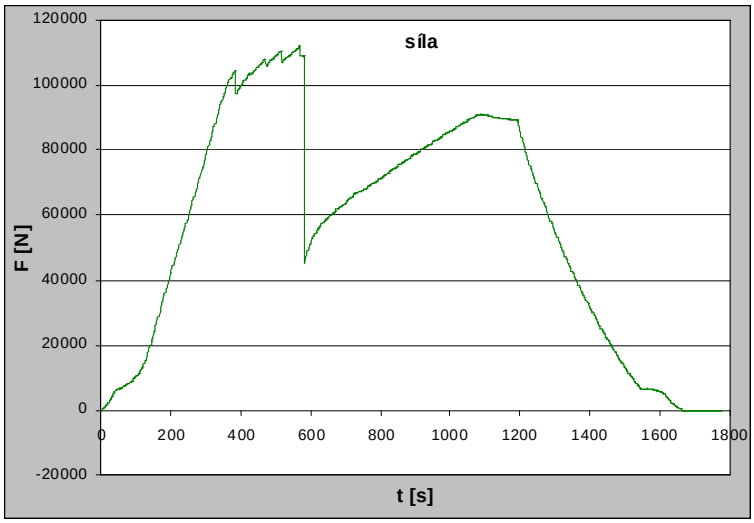

Fig.3 Diagram of vertical force vs time, loading by constant vertical displacement

Table 1 Results of statical tests

Beam	P_r [kN]	P_y [kN]	P_{max} [kN]	w_r [mm]	w_{max}[mm]	w_{40} [kN]
Original	15	40	45	2.5	7	2.3
Strip Adh.	20	-	65	3,5	8	2
Prestr.30kN	80	-	100	3.5	7	1
Prestr.50kN	102	-	110	3	3	1

Conclusions

Two types of prestressed beams strengthened by C-strips Sika 512 (50 x 1,2 mm) with two levels of prestress (force in prestressed C-strip 30 kN and 50 kN) have been tested. Loading capacity of beams prestressed by 30 kN and 50 kN have increased by 120 % and 140 % respectively compared with original and by 50 % compared with adhesive bonded strip strengthening. Vertical deflection at the same loading level (40 kN) has decreased up to 50 % (see Table 1).

References

Cerny, M: Czech Guidelines for Strengthening of Concrete Bridges by Composites and Testing, Third International Conference on FRP Composites in Civil Engineering (CICE 2006), Proceedings, ISBN 0-615-13586-2, December 13-15 2006, Miami, Florida, USA

Cerny M.: A New Method for Evaluation Systems for Prestressing of CFRP Plates, First Asia- Pacific Conference on FRP in Structures „APFIS 2007“, 12.-14.12.2007, Hong Kong, ISBN 978-962-8014-14-9

Structural performance of post-tensioned punching shear strengthening systems of flat slabs

Robert Koppitz[1], Thomas Keller[2]

Introduction

A new strengthening concept was recently developed, introducing a new application for Carbon FRP composites as a post-tensioned punching strengthening system for existing flat slabs. Post-tensioning significantly improves the system efficiency due to the partial unloading of the slab. In predrilled and precut openings, unbonded non-laminated CFRP straps were installed crosswise around the column, see Fig. 8.

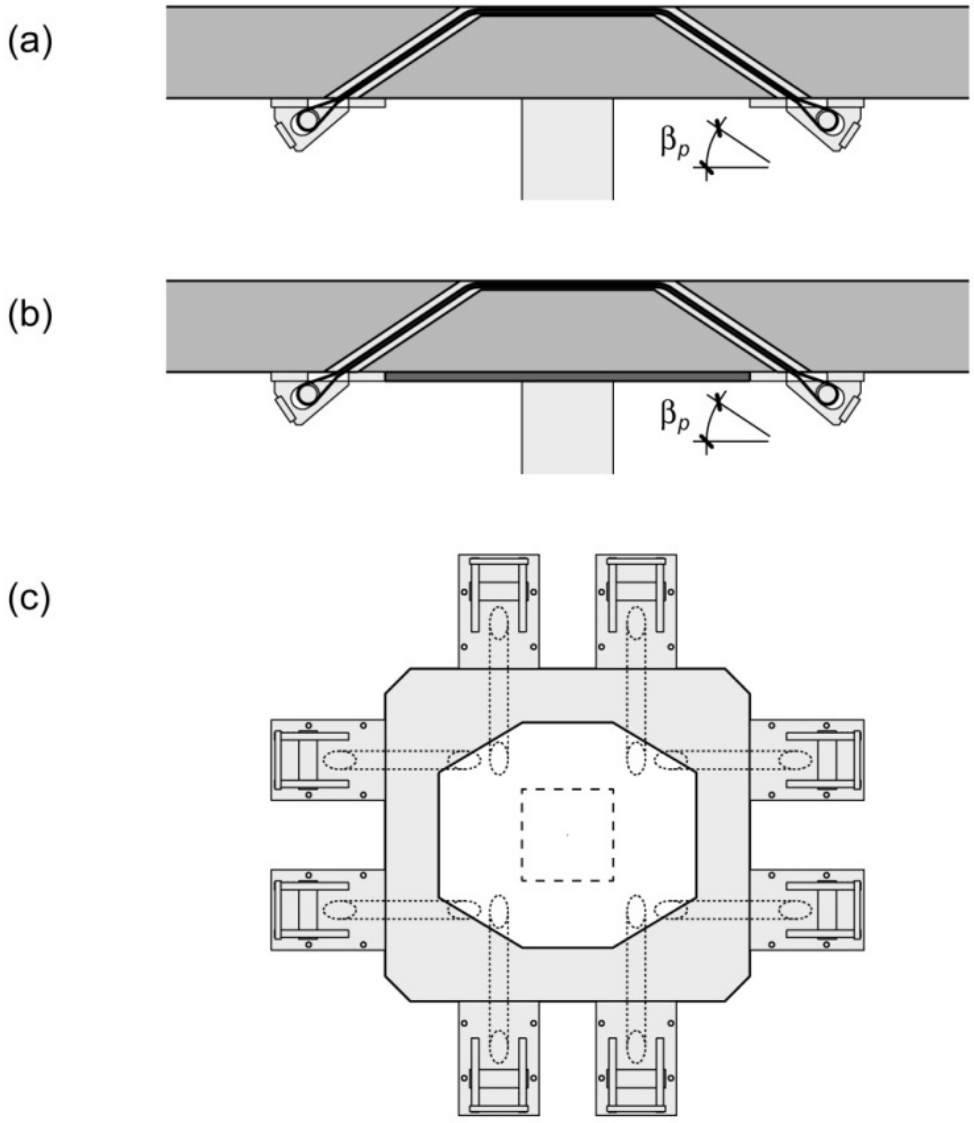

Figure 8. Punching shear strengthening concept with prestressed CFRP straps. (a) Adhesive bonding of anchors with epoxy resin; (b) and (c) steel compression frame as anchor support.

[1] Ecole Polytechnique Fédérale de Lausanne, Switzerland, robert.koppitz@epfl.ch
[2] Ecole Polytechnique Fédérale de Lausanne, Switzerland, thomas.keller@epfl.ch

Experimental Program

The presented punching shear concept was part of a larger experimental campaign for new strengthening methods of totally 19 full-scale punching tests. Square slabs with side lengths of 3.2 m and slab thicknesses of 0.18 to 0.32 m were tested. The specimens were supported in the center by a square steel plate with a side length of 0.25 m; the load was applied at a radius of 1.50 m, Fig. 9. All specimens had an orthogonal flexural reinforcement layout with a reinforcement ratio of approximately 1.5%.

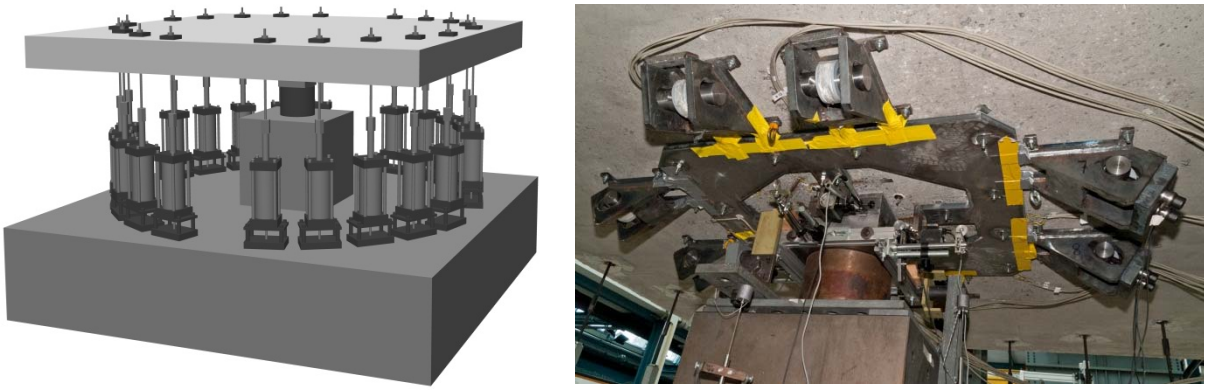

Figure 9. Visualization of experimental setup (left), bottom view with steel frame and anchors (right)

Strap post-tensioning of at least 15% of its tensile strength led to a more ductile slab response although the CFRP materials were brittle. The ultimate load of the unreinforced slabs could be increased by 67-114% via a redistribution of forces from the concrete to the strap system, Fig. 10. The punching shear resistance of the both strengthening systems – the former with adhesively bonded anchors and the new system with steel frame – was similar. The lowest relative increase was observed for the thickest slab.

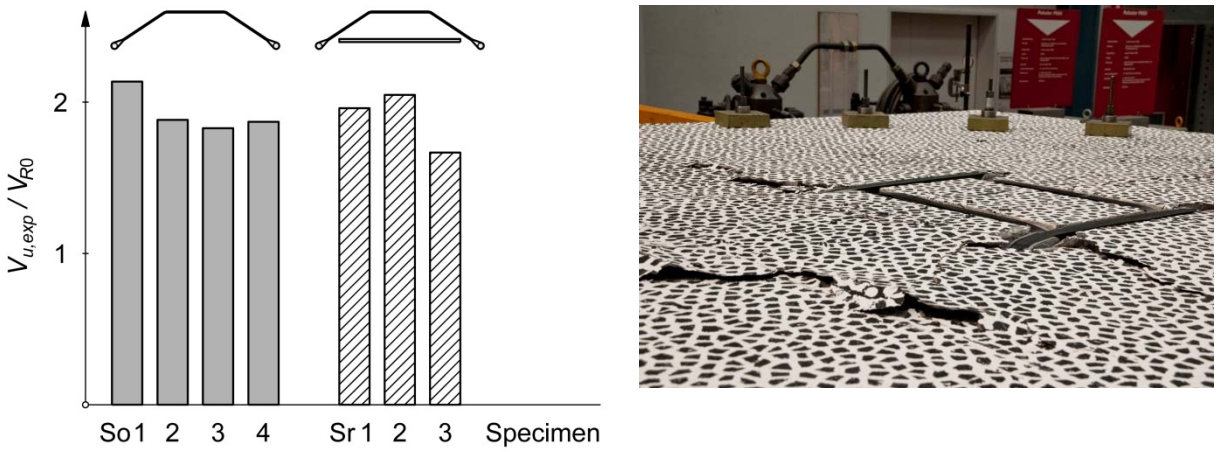

Figure 10. Summary of obtained failure loads Vu,exp, normalized with punching resistance of unreinforced slab VR0 (left), photo of the upper slab surface after failure (right)

3.7 Behaviour at Elevated Temperatures

Behaviour of FRP rehabilitation systems at elevated temperatures

Antonio Bilotta [1], Emidio Nigro [2]

Fiber reinforced polymers (FRP) are composite materials successfully applied to repair and/or strengthen RC structures. For external strengthening of reinforced concrete (RC) structures, the FRP plates are easily bonded on concrete using adhesive, like epoxy resins, which ensure the transfer of forces between concrete and FRP. However, degradation of mechanical properties of composites (strength, stiffness and bond) due to high temperature (Dai et al., 2013; Nigro et al. 2012), moisture absorption (Jia et. al, 2005) and cycling loads (Nigro et al., 2011c; Dai et al., 2005) is a key aspect for a durable efficiency of composite materials.

As concerns the high temperature, a critical condition occurs when the glass transition temperature, Tg, of the polymer matrix is achieved, due to the softening of the resin, which reduces the capacity of stress transfer between the fibers. The precise definition of the value Tg is still under discussion in the scientific community, because the progressive nature of the softening process makes it difficult to identify a precise temperature limit. Nevertheless, the safety check often is conservatively performed, in the temperature domain, with reference to the value of Tg properly reduced (ACI 440.2R-08, 2008).

FRPs which polymerize in ordinary conditions, typical of in situ applications, are characterized by very low Tg (between 45°C and 80°C for normal and heat resistant resins, respectively). For preformed FRPs, used as internal reinforcement, is easily possible to obtain reinforcements with Tg above 100°C. Curing processes carried out at temperatures and pressures different from ordinary ones, allow to further increase the Tg.

Although overcoming the Tg implies a reduction in strength of the reinforcement, the drastic degradation of the resistance is reached at temperatures close to melting of the resin (temperature of crystallization, Tc > Tg) or even higher. The reduction of stiffness, instead, depends on the type of fiber reinforcement and it is generally negligible compared to the reduction of resistance. Therefore, the real capacity of the concrete members reinforced with FRP reinforcement, at high temperatures, can be considerably high (Nigro et al. 2011a, 2001b, 2013a).

By contrast, the softening of the resin which begins when the Tg is achieved, involves a drastic reduction of the adhesion properties (Foster and Bisby, 2008). Hence, the efficiency of the strengthening system for existing structures, which mainly depends on the effectiveness of the bond between FRP and concrete, is strongly affected by the temperature. Some experimental tests (Deuring, 1994) showed similar problem when conventional steel strengthening are used without mechanical anchoring. The comparison between steel and FRP strengthening systems showed that FRP, in particular sheets, without protection behave better than steel plates because of the lower heat conductivity and their smaller weight. Clearly, FRP externally strengthened RC beams or slabs need the protection with additional insulation in order to avoid the debonding between FRP sheets or laminates and concrete support. Consequently, some researches were devoted to study the performances of FRP strengthened elements protected by different insulation systems in order to individuate the minimum requirements to obtain satisfactory performances in fire (Bisby et al, 2005). Obviously, if the FRP strengthening is not directly heated by fire or other sources of heat, the performances may be better. Hence, FRPs can be successfully used to strengthen bridges, where fire is not a primary action to be considered during design (Bisby et al 2005). Nevertheless, should be noted that bituminous paving casting on a bridge deck can easily lead to high temperature (e.g. 200°C).

In Nigro et al 2013b, the thermo-mechanical behavior of RC bridge decks strengthened with externally bonded FRP plates is investigated, by considering two possible environmental conditions leading to

[1] DIST – Department of Structures for Engineering and Architecture, University of Naples Federico II, Italy
antonio.bilotta@unina.it
[2] DIST – Department of Structures for Engineering and Architecture, University of Naples Federico II, Italy
emidio.nigro@unina.it

thermal states different from the normal ones: (a) fire exposure over the bridge deck due to an accident involving camions; (b) bituminous paving casting on a bridge deck at temperature.

Indeed, the temperature at the FRP-to-concrete interface can overcome the glass transition temperature, Tg, due to either an accidental action, namely fire, or a maintenance activity, namely the bituminous paving cast.

The relationships suggested by Italian (CNR-DT 200/2004 and CNR-DT 200R1/2013) and American codes (ACI 440.2R-08, 2008), to evaluate the limit strain for FRP debonding at normal temperature, were modified to take into account the effect of high temperature on the debonding of FRP. Then, thermo-mechanical analyses were performed by varying, the thicknesses of the slab and the protection layer to assess their influence on the thermal field in the structural member. Furthermore, normal resin (NR) with Tg = 45°C and heat-resistant resin (HR) with Tg = 80°C were considered. The results are discussed in terms of both temperatures and safety checks carried out for ultimate and serviceability limit states (ULS and SLS).

The ULS checks are always satisfied, mainly because the flexural capacity provided by FRP can be neglected during fire or maintenance activity. By contrast, the SLS checks performed to assess damages of the FRP strengthening system during these events, show that constructive details and type of resin play a key role.

Palmieri et al. 2013, investigated the behavior of FRP strengthening systems under fire exposure, on six full-scale near-surface mounted (NSM) FRP-reinforced concrete beams exposed to 1 h of fire. All the specimens were preloaded to the service load of the strengthened member. Tests results indicated that, if appropriately insulated, the NSM FRP-strengthened beams can achieve a satisfactory fire endurance of 1 h as per fire resistance test specifications. Moreover, this paper also presents a study on the residual performance of fire-tested beams. Results of this study suggest that if the insulation system is able to maintain the adhesive temperature at relatively low value ($t_{adhesive} \leq 1.6$ Tg for the beam configuration in this test program), the FRP concrete bond degradation under fire is limited, and the FRP-strengthened beam can retain a large part (up to 92% in this test program) of its original strength.

Further experimental results were showed in Palmieri et al 2012. The reinforced concrete beams were strengthened in flexure with NSM FRP bars and insulated with different insulation systems. The specimens were subsequently exposed to a standard fire while subjected to full service load. Tests results on fire indicated that insulated NSM FRP strengthened beams can achieve a fire endurance of at least 2 h. Moreover structural testing to failure at room temperature of the fire testes beams has shown that well insulated members are able to retain (part of) their original strengthened flexural capacity.

Key references

ACI 440.2R-08 (2008). Guide for the Design and Construction of Externally Bonded FRP Systems for Strengthening Concrete Structures. ACI440.2R-08 American Concrete Institute, Farmington Hills, MI, 2008, 76 pp.

Bisby L.A., Green M.F., Kodur V.K.R. “Response to fire of concrete structures that incorporate FRP”, Prog. Struct. Engng. Mater., 7:136-149, 2005.

CNR-DT 200/2004, “Instructions for Design, Execution and Control of Strengthening Interventions by Means of Fibre- Reinforced Composites”, Italian National Research Council, 2004.

CNR-DT 200 R1/2013 Instructions for Design, Execution and Control of Strengthening Interventions by Means of Fibre-Reinforced Composites (in Italian)”, Italian National Research Council, 2013.

Dai J.G., Sato Y., Ueda T., Sato Y. (2005). Static and Fatigue Bond Characteristics of Interfaces between CFRP Sheets and Frost Damage Experienced Concrete. Proceedings of FRPRCS-7, ACI-SP-230-86, pp.1515-1530.

Dai J.G., Gao W.Y., Teng J.G., (2013) Bond-Slip Model for FRP Laminates Externally Bonded to Concrete at Elevated Temperature, Journal of Composites for Construction, Vol. 17, No. 2, April 1, 2013. © ASCE, ISSN 1090- 0268/2013/2-217-228

Deuring M. (1994). Brandversuche an Nachtraglich Verstarkten Tragern aus Beton, "Research Report EMPA No. 148'795", Dubendorf, Swiss Federal Laboratories for Materials Testing and Research, 1994.

Foster, S. and Bisby, L. (2008). "Fire Survivability of Externally Bonded FRP Strengthening Systems." J. Compos. Constr., 12(5), 553–561.

Jia J., Boothby T.E., Bakis C.E., Brown T.L. (2005), Durability Evaluation of Glass Fiber Reinforced-Polymer-Concrete Bonded Interfaces, Journal of Composites for Construction, Vol. 9, No. 4, August 1, 2005. ©ASCE, ISSN 1090-0268/2005/4-348–359

Nigro, E., Cefarelli, G., Bilotta, A., Manfredi, G. and Cosenza, E. (2011a). "Fire resistance of concrete slabs reinforced with FRP bars. Part I: experimental investigations on the mechanical behavior". Composites: Part B, 42 (2011), 1739–1750.

Nigro, E., Cefarelli, G., Bilotta, A., Manfredi, G. and Cosenza, E. (2011b). "Fire resistance of concrete slabs reinforced with FRP bars. Part II: experimental results and numerical simulations on the thermal field". Composites: Part B, 42 (2011), 1751–1763.

Nigro E, Di Ludovico M, Bilotta A (2011c). Experimental Investigation of FRP-Concrete Debonding under Cyclic Actions. Journal of Materials in Civil Engineering, vol. 23, p. 360-371, ISSN: 0899-1561, doi: 10.1061/(ASCE)MT.1943-5533.0000173

Nigro, E., Bilotta, A., Cefarelli, G., Manfredi, G. and Cosenza, E. (2012). "Performance under fire situations of concrete members reinforced with FRP rods: bond models and design nomograms". Journal of Composites for Construction. Journal of Composites for Construction, Vol. 16, No. 4, August 1, 2012.

Nigro, E., Cefarelli, G., Bilotta, A., Manfredi, G. and Cosenza, E. (2013a). Adhesion at high temperature of FRP bars straight or bent at the end of concrete slabs. Journal of Structural Fire Engineering, vol. 4, p. 71-86, ISSN: 2040- 2317, doi: 10.1260/2040-2317.4.2.71.

Nigro E., Bilotta A., Del Prete I. (2013b) High temperature effects on flexural performances of RC bridge decks strengthened with EBR-FRP. ACI Italy Chapter. Bergamo 3-4 October 2013

Palmieri, A., Matthys, S., Taerwe, L. (2012) Experimental investigation on fire endurance of insulated concrete beams strengthened with near surface mounted FRP bar reinforcement Composites Part B: Engineering Volume 43, Issue 3, April 2012, Pages 885–895

Palmieri, A., Matthys, S., Taerwe, L. (2013) Fire endurance and residual strength of insulated concrete beams strengthened with near-surface mounted reinforcement Journal of Composites for Construction. Volume 17, Issue 4, 1 August 2013, Pages 454-462

Behavior of FRP laminates at elevated temperatures and freeze–thaw cycling

M. Di Ludovico[1], F. Piscitelli[2,4], A. Prota[1], M. Lavorgna[3,4] G. Mensitieri[2,4],, M. Manfredi[1]

[1,] *Department of Structures for Engineering and Architecture, University of Naples "Federico II", ITALY.*

[2] Department of Materials Engineering (DIMP), University of Naples Federico II, Italy.

[3] Institute of Composite and Biomedical Materials, National Research Council, Portici, Naples, Italy.

[4] Technological District on Polymeric and Composite Materials, Engineering and Structures (IMAST), Portici, Naples, Italy.

Abstract

Although FRPs offer numerous advantages over traditional materials in the field of flexural and/or shear strengthening or for confining reinforcement of structural members, the greatest weakness of FRPs is represented by the limited knowledge on their mechanical properties at elevated temperature and/or freeze-thaw cycling. In order to investigate on such aspect, a series of experimental tension tests on FRP coupons have been carried out in an environmental chamber under controlled temperature and relative humidity conditions. Due to reduced capacity that commercially available resins have to transfer loads over fibres around Tg, several new matrices solutions (neat epoxy and nanocomposites systems, respectively) have been formulated and characterized by dynamic mechanical analysis (DMA). The goal of such re-formulation was to increase both Tg and elastic modulus in the rubber region of the resin in order to improve the mechanical performance of FRP coupons. The effects of freeze thaw cycling has also been investigated on the FRP coupons made by commercially available and re-formulated matrices. The experimental test pointed out that the developed formulations could provide significant improvements on the mechanical properties of FRP laminates subjected to elevated temperatures or to freeze-thaw cycles.

Introduction

Several issues concern the combined use of epoxy resins and carbon or glass reinforcing fibres under elevated temperatures and/or freeze-thaw cycling. Indeed, such conditions could lead to significant reduction in the mechanical properties of the polymer matrix limiting its ability to transfer forces between fibres; thus a localized concentration of stresses on the fibres and consequently a premature failure of the FRP strengthening system could be achieved. The performances at elevated temperatures and/or at freeze-thaw cycling exposure of structural members strengthened by using externally bonded FRP laminates are mainly related to two aspects: the bond behaviour between FRP and the member substrate; the mechanical properties of laminates themselves. The latter aspect has been very limited experimentally investigated; only few tests have been performed to evaluate the residual tension strength of FRP coupons after exposure to elevated temperatures (Foster and Bisby 2005) or freeze-thaw cycling. However, only few studies have been conducted to investigate on the FRP mechanical properties at elevated temperature or after freeze–thaw cycling related to service conditions (i.e. FRP external application exposed to sun in hot regions, cycling exposure in Mediterranean climates), in spite of the

[1] Department of Structures for Engineering and Architecture, University of Napoli Federico II, Italy, diludovi@unina.it; aprota@unina.it; gamanfre@unina.it.
[2] Department of Materials Engineering (DIMP), University of Naples Federico II, Italy, giuseppe.mensitieri@unina.it.
[3]Institute of Composite and Biomedical Materials, National Research Council, Portici, Naples, Italy, marino.lavorgna@imcb.cnr.it
[4] Technological District on Polymeric and Composite Materials, Engineering and Structures (IMAST), Portici, Naples, Italy, Filomena.Piscitelli@imcb.cnr.it.

ACI 400.2R-08 [10] prescription states the service temperature should not exceed the value corresponding to the Tg decreased of 15 °C (i.e. Tg - 15 °C).

Thus, the present paper summarizes the experimental evidences of extensive experimental programs dealing with a series of experimental tension tests on carbon FRP (CFRP) laminates both under controlled temperature and relative humidity conditions or after freeze-thaw cycles exposure (Di Ludovico et al. 2012, Nardone et al. 2012).

Experimental tests

Because of the reduced capacity that commercially available resins have to transfer loads over fibres around glass transition temperature, Tg, two new systems based on epoxy resin were formulated and characterized by dynamic mechanical analysis (DMA). The main goal of the new formulated systems was to increase Tg, the elastic modulus in the rubber region of the resin and to improve their performances under freeze-thaw cycles. Two different approaches were investigated. First a new epoxy system (namely neat epoxy) was formulated and cured at 60°C after an hour at room temperature. Secondly, to improve the mechanical properties of epoxy matrix by curing at room temperature, a nanocomposite system was obtained by direct dispersion of preformed nanodimensioned silica particles to the neat epoxy resin, (Di Ludovico et al. 2012). The main mechanical properties of commercially available matrices and new formulated ones as well as their influence on the mechanical behaviour of FRP coupons under axial load at different temperature values and after exposure to freeze-thaw cycles are herein summarized.
The experimental program consisted of uniaxial tension tests on CFRP laminates. Carbon fibres sheets with a unit weight of 600 g/m^2 (thickness of 0.33mm) were impregnated by using a commercial available epoxy resin or reformulated matrices (neat epoxy and nanocomposite system). Coupons length, L, and width, B, were equal to 360mm and 25mm, respectively (see Figure1 (a)); the matrix saturated fiber sheets were sandwiched at the ends between two steel plates to ensure a uniform, smooth surface. Three series of tests were performed: 1) tests at room temperature and relative humidity; 2) tests at controlled temperature, T=70°C and relative humidity RH =65%; 3) tests on specimens pre-treated by exposure to freeze-thaw cycles.

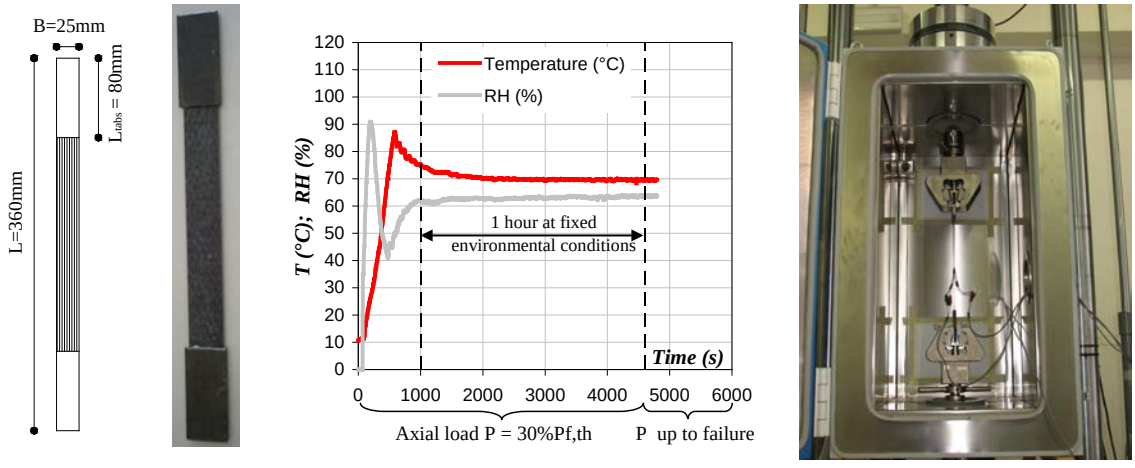

Figure 1: Specimen geometry; Temperature and relative humidity exposure profiles; test setup.

- Room Temperature Tests

Tensile tests were carried out at room temperature and humidity conditions under a servo-hydraulic MTS testing machine under displacement control (0.033 mm/s) according to ASTM D 3039/D 3039M guidelines; the results, processed according to ACI 440.3R provisions, are summarized for each series of specimens in the first three rows of Table 1. Experimental outcomes showed that the new formulated matrices increased the performances of specimens in terms of ultimate strain (13% and 16% for neat epoxy and nanocomposite system, respectively) and tensile strength (10% and 12%, respectively); the modulus of elasticity, mainly related to the fibers type, was not significantly influenced by the matrices

used to impregnate the specimens. In particular, the use of nanocomposite system clearly allowed not only to attain at least the same performances of specimens impregnated with commercial resins but to significantly improve the mechanical properties of the analyzed specimens.

Table 1: Mechanical properties of composites.

Fibers	Matrix	Series	N° of tests	Elastic Modulus, E		Ultimate strain, ε_u		Tensile strength, σ_u	
				Mean	COV	Mean	COV	Mean	COV
				[GPa]	[%]	[%]	[%]	[MPa]	[%]
Carbon (unit weigth (600g/m^2)	Comm. epoxy	Room Temp.&RH	8	220	3.5	1.31	10.2	2890	10.7
	Neat epoxy		9	214	6.1	1.49	12.2	3168	10.0
	Nanocom. system		11	215	10.3	1.52	9.7	3228	6.1
	Comm. epoxy	T=70° RH=65%	4	219	11.9	0.95	14.4	2056	6.1
	Neat epoxy		6	237	2.6	1.36	6.5	3222	5.5
	Nanocom. system		5	242	5.9	1.35	13.0	3245	11.5
	Comm. epoxy	Freeze-Thaw (210 cycles)	6	232	11.8	1.00	12.1	2643	9.3
	Neat epoxy		6	210	9.7	1.47	14.5	3063	8.2
	Nanocom. system		10	225	9.1	1.00	7.3	3167	5.6

- Controlled Temperature T=70°, relative humidity RH=65% tests

To simulate field service conditions of externally bonded FRP laminates, experimental tests on CFRP coupons have been conducted in three steps: 1) coupon pre-load at about 30% of the theoretical coupon failure load, $P_{f,th}$; 2) one hour at controlled conditions in the environmental chamber and constant axial load $P=0.3P_{f,th}$.; 3) uniaxial tension test at controlled conditions in the environmental chamber up to the flat coupon failure (see Figure 1 (b) and (c)).
Experimental outcomes (see Table 1) confirmed that the impregnation of carbon fibres with neat epoxy or nanocomposites system led to significant gains of specimens' mechanical performances with respect to those impregnated with a commercial epoxy: ultimate strains increase equal to 44% and 42%, respectively; tensile strength increase of about 57% and 58%, respectively.
Moreover, it is worth nothing that elevated temperature exposure implied a strong degradation of mechanical properties of coupons impregnated with a commercial epoxy (a decrease of about 27% for both ultimate strain and tensile strength was recorded with respect to specimens tested at room temperature) as opposed to the almost unchanged performances of specimens with new formulated matrices. Such effect could be clearly related to the increased Tg values of new formulated matrices that allowed to uniformly transfer loads to fibres during the tests preventing localized concentration of stresses and thus premature FRP laminate failure. In the case of neat epoxy impregnated coupons, tensile strength gain at T=70°C with respect to tests performed at room temperature could be explained as a post-curing effect of epoxy matrix.

- Tests after exposure at freeze-thaw cycles

Tensile tests were carried out at room temperature and humidity conditions on CFRP specimens after exposure to 80 and 210 freeze-thaw cycles. Each freeze-thaw cycle duration was one day; cycle details are reported in Figure 2. Experimental results (see Table 1) in terms of modulus of elasticity, ultimate strain and tensile strength after 210 freeze-thaw cycles confirmed the trends recorded on the previous series of tests: new formulated matrices impregnation improved the ultimate axial strain and strength of CFRP laminates.

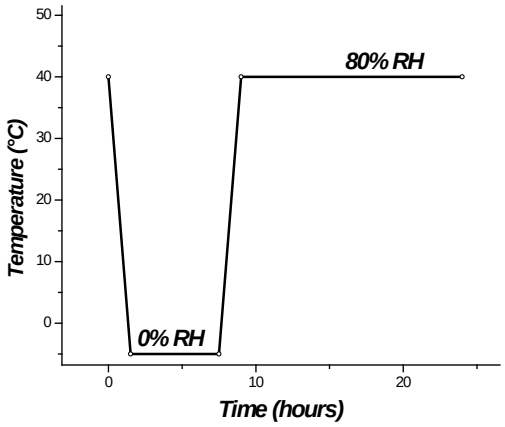

Figure 2: Freeze-thaw cycle.

Conclusions

The experimental results point out that the developed formulations of epoxy resins provide a significant increase of ultimate strength and strain of CFRP coupons both at room and elevated temperatures with respect to commercial systems, without significant change of the elastic modulus. The mechanical performances were also improved after exposure to 210 freeze-thaw cycles. Experimental outcomes strongly confirmed that the use of matrices characterized by higher values of Tg and elastic modulus in the rubber region with respect to those traditionally available on the market, could allow to overcome one of the main limit of FRP laminates related to their poor performances under elevated temperatures.

Key references

Foster S.K., Bisby LA.: “High temperature residual properties of externally bonded FRP systems for concrete” Proc. of FRPRCS7 International symposium, American Concrete Institute; 2005, pp. 1235-1252.

American Concrete Institute (ACI) Committee 440. Guide for the design and construction of externally bonded FRP systems strengthening concrete structures. ACI 440.2R-08. Farmington Hills, MI: ACI; 2008

Di Ludovico M., Piscitelli F., Prota A., Lavorgna M., Mensitieri G., Manfredi G., (2012) "Improved Mechanical Properties of CFRP Laminates at Elevated Temperatures and Freeze-Thaw Cycling", Construction and Building Materials, Vol. 31, June 2012, pp. 273-283, (ISSN 0950-0618), Elsevier. doi:10.1016/j.conbuildmat.2011.12.105.

Nardone F., Di Ludovico M., De Caso y Basalo F., Prota A., Nanni A., (2012), "Tensile Behavior of Epoxy Based FRP Composites under Extreme Service Conditions" , Composites Part B, Vol. 43, Issue 3, April 2012, pp. 1468-1474, Elsevier. doi:10.1016/j.compositesb.2011.08.042.European Commitee for Standardization. 2002. *EN1990:2002 Eurocode — Basis of structural design*. Vol. 3. Brussels.

ASTM D 3039/D 3039M, “Standard Test Method for Tensile Properties of Polymer Matrix Composite Materials”, Apr 10, 2000.

ACI Committee 440, “Guide Test Methods for Fiber-Reinforced Polymers (FRPs) for Reinforcing or Strengthening Concrete Structures”, ACI440.3R-04 American Concrete Institute, Farmington Hills, MI, 2004, 40 pp.

3.8 Composite Reinforcement and Design Guidelines

Fibre Reinforced Polymer Reinforcement Enters MC2010

Thanasis Triantafillou
Professor, Dept. of Civil Engineering
University of Patras
Patras, Greece

Stijn Matthys
Professor, Magnel Laboratory for Concrete Research University of Ghent, Belgium

Abstract

Most applications of fibre-reinforced polymers (FRP) deal with externally bonded reinforcement as a means to repair and strengthen damaged reinforced concrete (RC) structures or to retrofit RC structures in seismic regions. As internal reinforcement, FRP rebars or (more rarely) prestressing elements, are used in special projects, combining material strength and durability characteristics. Over the last years several national and international design guidelines have become available, specifically for the design and application of FRP strengthened or reinforced concrete structures. These efforts demonstrate clearly the interest in FRP as a novel reinforcing material for concrete construction. Hence, the time was there to introduce FRP reinforcement also in the new Model Code 2010 (MC2010). Main contributions to MC2010 relate to chapters 5.5 "Non-metallic reinforcement" and 6.2 "Bond of non-metallic reinforcement". The material presented in these two chapters is further elaborated next.

Introduction

Most applications of fibre-reinforced polymers (FRP) deal with externally bonded reinforcement as a means to repair and strengthen damaged structures, to retrofit structures in seismic regions, to protect and strengthen historical buildings, to modify the concept or use of a structure, to increase structural safety, or to meet serviceability criteria. Offering high strength, light weight and excellent durability characteristics, in combination with ease of application, FRP bonding has become a technique of increased popularity in the field of structural upgrading. Commercial applications started increasing since the early 90s and are mainly based on carbon or glass fibre reinforced polymer (CFRP or GFRP) elements [1]. Examples of strengthening with FRP are given in Fig. 1. The application consists of bonding the FRP to the roughened concrete surface at ambient conditions by means of a structural adhesive (generally epoxy). Other developments involve the use of prestressed externally bonded reinforcement [2], near surface mounted reinforcement, in which the FRP is bonded into grooves in the concrete [3], and the use of textile reinforced mortar (TRM) overlays [4].


(a)
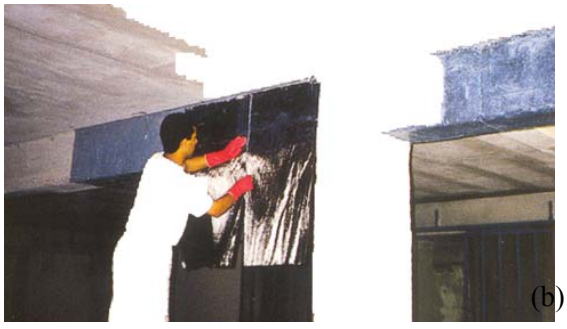
(b)

Fig. 1 (a) Flexural strengthening of a slab, (b) shear strengthening of a beam.

As internal reinforcement, rebars or (more rarely) prestressing elements, often GFRP or CFRP, respectively, are used, combining material strength and durability characteristics. The application of GFRP rebars is mainly relevant in specific areas and is not to be seen as a general alternative to steel rebars. These areas are structural parts subjected to environments leading to severe durability issues, building parts which need to be electromagnetically neutral (e.g. hospitals with magnetic resonance imaging equipment) and particular elements such as the "soft-eye" (portion of a deep foundation slurry wall where a tunnel boring machine is launched). An example of internal FRP reinforcement is given in Fig. 2.

Fig. 2 Bridge deck reinforcement with GFRP.

Over the last years several national and international design guidelines have become available, specifically for the design and application of FRP strengthened or reinforced concrete structures, among which [5, 6]. These efforts demonstrate clearly the interest in FRP as a novel reinforcing material for concrete construction and rehabilitation. Hence, the time was there to introduce FRP reinforcement also in the new Model Code 2010 (MC2010) [7]. Main contributions to MC2010 relate to chapters 5.5 "Non-metallic reinforcement" and 6.2 "Bond of non-metallic reinforcement". The material presented in these two chapters is further elaborated in this contribution.

FRP as reinforcement

General

Non-metallic reinforcing elements consist of a high number of continuous, directionalized, organic or inorganic fibres (e.g. carbon, glass, aramid, basalt, PBO), typically embedded in a polymeric matrix. Both the terms "non-metallic reinforcement" and "FRP (fibre reinforced polymer) reinforcement" are used for this reinforcement type.

FRP reinforcement is available in various forms. For new structures bars, tendons and grids are used to reinforce and prestress concrete elements. In the repair sector, these elements are used to strengthen existing structures by means of external post-tensioning and near surface mounted reinforcement. Strips, laminates, sheets or fabrics are used for externally bonded reinforcement (EBR) strengthening. Grids, fabrics and textiles may also be used in combination with shotcrete or mortar overlays.

The geometrical, mechanical and technological properties of FRP reinforcement basically depend on fibre and resin type and properties, constituent volume fractions, production parameters, shape and surface texture. In general FRPs are characterized by high axial strength, high ratio of axial-to-transverse strength, limited ultimate strain, low weight, excellent chemical resistance and non-

susceptibility to a wide range of aggressive media, electromagnetic neutrality, excellent fatigue characteristics (depending on fibre type), and limited ratio of long-term to short-term static strength for some fibre types. Non-metallic reinforcement shall comply with national or international product standards that specify their geometrical, mechanical and technological properties. For instance, ISO 10406, specifies test methods applicable to FRP reinforcement for concrete applications [8, 9].

Quality control and designation

The fabrication of non-metallic reinforcement shall be subject to a factory production control by the manufacturer, and a continuous external control by an independent qualified body, including certification and regular audits.

The designation of non-metallic reinforcing elements normally includes the relevant product standard, the fibre and matrix materials, the nominal dimensions (e.g. diameter, width, thickness) and the characteristic tensile strength, modulus of elasticity and ultimate strain in the direction of the fibres. MC2010 specifies that each product shall be clearly identifiable with respect to this designation.

Geometrical properties

Non-metallic reinforcing elements may be pre-cured, wet lay-up or pre-impregnated (prepreg). The configuration is further characterized by the type of fibre(s) and matrix, fibre orientation(s) and constituent fractions. Constituent material fractions can either be given by mass (weight) or by volume. Pre-cured systems are manufactured in various shapes, generally by pultrusion. Wet lay-up systems are manufactured with fibres lying in one (typically) or more directions and impregnated with the matrix at the job site. Prepreg systems are manufactured with unidirectional or multidirectional fibre sheets or fabrics pre-impregnated at the manufacturing plant with partially polymerized resin. They may be bonded externally to concrete members with or without the use of additional resin.

The size of non-metallic reinforcing elements is defined by a nominal diameter for circular bars or by the nominal cross-section dimensions for other products (e.g. thickness, width). The definition of the nominal cross-section is for pre-cured forms typically based on the global nominal dimensions (diameter, thickness, width). Alternatively or for wet lay-up/prepreg forms, an equivalent dry fibre cross-section may be used (referring to the continuous fibres as principal stress bearing component). The latter is obtained as the ratio of the fibre mass per length and the fibre density. For FRP with multiple fibre directions, where a different amount of fibres per unit length is applied in different fibre directions, the definition of the nominal dry fibre cross-section always relates to the specified fibre direction, and more than one nominal cross-section (or nominal thickness) may be given depending on the fibre direction. As design verifications are based on equilibrium of forces, the definition of the nominal cross-section (used in a consistent way) does not influence the outcome of the design. However, if data sheets of FRP products are compared, the possible difference in definition of the nominal cross-section should be taken into account.

The surface of non-metallic reinforcement may be plain or deformed. Surface characteristics include the characteristics of the ribs or indentations or other surface deformations (e.g. sand-coating) by means of which bond with the concrete is achieved.

Mechanical properties

The mechanical properties are defined on the basis of standard tests. For quality control purposes and design calculations, the mechanical properties of a product are referred to the nominal cross-sectional area.

FRP materials and products are typically used as *tension* elements. The tensile stress-strain response is quasi linear elastic for most FRP. The slope of the stress-strain diagram gives the modulus of elasticity and is typically defined as a secant modulus, following product standards [8, 9]. Indicative stress-strain diagrams for CFRP (carbon FRP), GFRP (glass FRP) and AFRP (aramid FRP) are given in Fig. 3. The characteristic values of the tensile strength (f_f) and the ultimate strain (ε_{fu}) are respectively denoted f_{fk} and ε_{fuk}. For serviceability limit state verifications a linear stress-strain response $\sigma_f = E_f \ \varepsilon_f$ is considered, referring to the mean value of the secant modulus of elasticity E_f. For ultimate limit state verification, the design stress-strain curve is idealised by means of a linear response up to f_{fk} and ε_{fuk}. The slope of this design stress-strain curve refers to a modulus f_{fk}/ε_{fuk}.

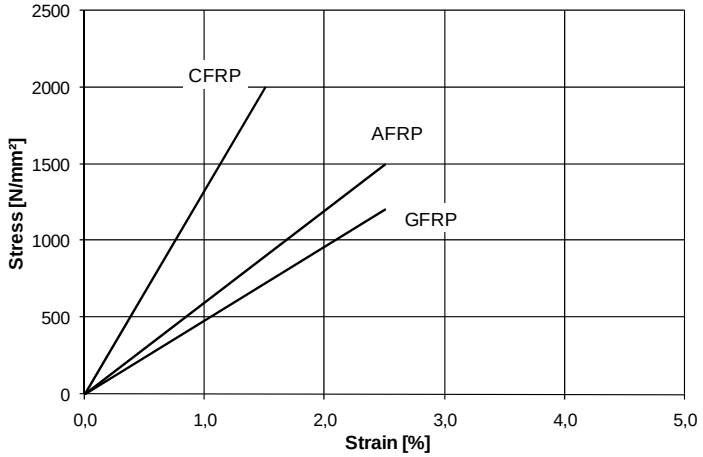

Fig. 3 Stress-strain diagrams of FRP reinforcement in the principal fibre direction.

The material factor γ_f for FRP reinforcement is taken 1.25 and 1.0 for the persistent/transient and accidental design situations, respectively. Sometimes the application of non-metallic reinforcement is designed for durability. This can be considered explicitly in the design by considering the relative resistance of generic FRP types to aggressive environments and the desired service life of the structure. These allow to consider adapted values for the material factor and allowable stress level, as outlined in [5, 6].

The *compressive* or transverse *shear* properties for a particular reinforcing element, if needed for a particular application, should be given by the manufacturer, who should also provide a description of the test method used to determine the properties. Given the generally limited compressive modulus of elasticity and the risk of micro-buckling or kinking of the fibres within the matrix material, non-metallic reinforcement is generally not used to resist high compressive stresses.

If a non-metallic reinforcing element is subjected to *fatigue* loading, growth of internal or surface flaws may occur, resulting in a reduced mechanical strength compared to the short-term static

strength. High modulus fibre composites have superior fatigue resistance. Cyclic tension fatigue strength of unidirectional CFRP and AFRP exceeds that of prestressing steel, while that of GFRP is lower. The fatigue strength of CFRP is higher than for AFRP. Indicative values are given in Table 1.

Table 1 Fatigue strength of reinforcement after $2x10^6$ cycles.

	σ_{max}/f_{tk} (a) [-]	$\Delta\sigma$ (b) [MPa]
Prestressing steel	~ 0.60	~ 200
E-glass/polyester (rod)	~ 0.50	~ 60
E-glass/epoxy (rod)	~ 0.50	~ 75
Aramid/vinylester (rod)	~ 0.60	~ 235
Carbon/vinylester (rod)	~ 0.60	> 350
Carbon/epoxy (strand)	~ 0.60	~ 310

(a) Applied maximum stress as a function of the characteristic tensile strength of the reinforcement.
(b) Stress range yielding fatigue failure at $2x10^6$ cycles.

FRP reinforcement combines elastic fibres, which have excellent resistance to *creep*, with a viscoelastic polymer matrix, which may show significant creep deformations. As FRP tensile members normally have a high degree of fibre orientation, large fibre volume fractions and a high ratio of fibre over matrix stiffness, the tensile force shared by the matrix is extremely low, so that FRP creep deformations are negligible.

The permissible stress level against *stress rupture* depends on the fibre/resin system, the alignment of the fibres and the fibre volume fraction. Stress rupture is adversely influenced by the environmental conditions. Generally, CFRP can withstand stress levels up to at least 80 % of its short term strength, while considerably lower stress levels apply for AFRP (about 50 % on a 50 years basis) and GFRP (about 30 % on a 50 years basis).

Relaxation of GFRP, CFRP and AFRP prestressing elements after 50 years of loading can be estimated as 4-14%, 2-10% and 11-25%, respectively. These values depend on the stress level and environmental influence. Prestressing loss due to relaxation of FRP is compensated by a lower prestressing loss due to concrete shrinkage and creep (given the high ratio of the modulus of elasticity of FRP to that of concrete).

Although fibres exhibit relatively high thermal stability, polymer resins are strongly affected by *temperature*. As a result, the material and bond properties of FRP are influenced by temperature and decrease significantly when reaching the glass transition temperature T_g. The glass transition temperature T_g is of particular importance, as it reflects the change of molecular mobility of polymer materials. For factory processed FRP elements, the matrix generally has a T_g in the range of 130-140 °C. The T_g of cold-cured (ambient-cured) adhesives/saturating resins may be lower (typically in the range of about 50-80 °C for epoxy). In the event of fire, sufficient concrete cover should be available so that the glass transition temperature is only reached after the required time span. For external reinforcement systems, fire protection systems may be required [10].

Technological properties

Key technological properties of interest are: the bond characteristics of FRP reinforcement and their relationship to the surface characteristics; the requirements concerning bendability (thermoset resin based FRP elements are not bendable in situ, whereas thermoplastic resin based FRP elements are bendable given proper application procedures); product-specific values for the coefficient of thermal expansion in the longitudinal as well as in the transverse direction; and the excellent chemical resistance and non-susceptibility of FRP to a wide range of aggressive media.

Bond of FRP reinforcement

Bond of FRP reinforcement is the term used to denote the interaction and transfer of force between FRP reinforcement and concrete. At the serviceability limit state, bond influences width and spacing of cracks, tension stiffening and curvature. At the ultimate limit state, bond is responsible for strength at end anchorages or at intermediate regions (the latter in the case of externally bonded reinforcement).

The bond behaviour of FRP reinforcement to concrete depends mainly on the reinforcement geometry, application type (e.g. internal or externally bonded) and surface characteristics. It is different from that of conventional steel reinforcement, given for example that: the modulus of elasticity of FRP is generally lower than that of steel, especially in the transverse direction; the shear stiffness of FRP is significantly lower than that of steel; the surface deformations relate to the resin matrix, which has lower shear strength than steel. It is generally possible to obtain bond strengths for non-metallic reinforcement of similar or greater magnitude than for steel reinforcement.

Bond and anchorage of internal FRP reinforcement (rebars)

Bond of plain (smooth) bars is governed by the adhesion between the bar surface and the concrete, provided that the interlaminar shear strength between the fibres is higher. The bond strength of plain bars is generally low and splitting bond forces can be neglected. Their use is limited as they need to be combined with other anchoring devices such as bends and transverse bars. Bond of deformed (surface treated) bars is often governed by the shear strength of the deformations (provided that the interlaminar shear strength between the fibres is higher). In this case, influence of concrete strength is limited compared to bond of steel bars. For high strength deformations, concrete shear failure similar to deformed steel bars is more predominant. The bond strength of deformed FRP bars is similar or superior to that of steel bars. Splitting bond forces can govern in case insufficient confinement by the surrounding concrete is provided. Depending on the surface texture, splitting tendency of FRP bars is lower or higher compared to deformed steel bars. Analytical modelling of bond splitting is provided in [6].

The bond stress-slip relationship (for the case of monotonic loading) for deformed steel rebars is applicable for FRP reinforcement, provided that the use of model parameters is calibrated on the basis of experimental results. Generally, a bond stress-slip relationship with an ascending and descending branch is assumed, as shown in Fig. 4a [6].

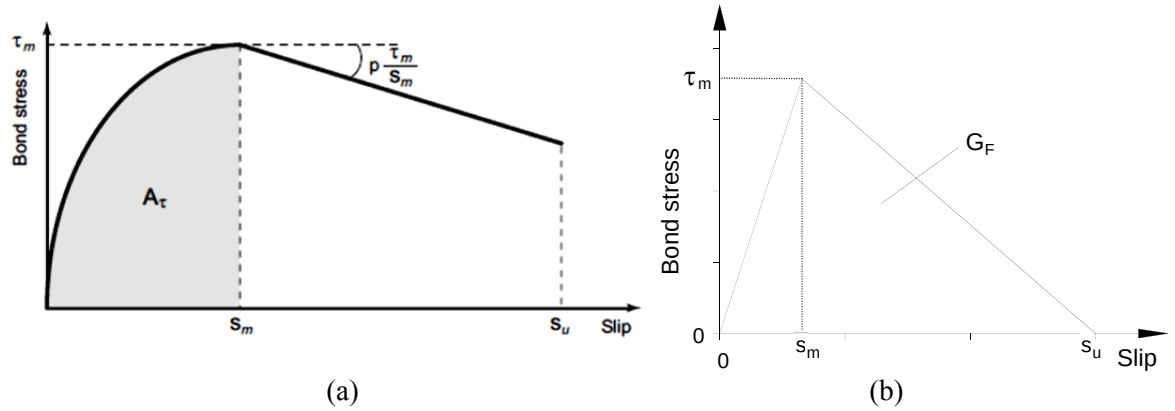

Fig. 4 Bond stress-slip relationship for (a) internal and (b) external FRP reinforcement.

Bond and anchorage of externally bonded FRP reinforcement

General

In the case of externally (or near surface) bonded reinforcement the bond behaviour relates to the glued joint between the external FRP reinforcement and the concrete. As part of any flexural or shear strengthening design, the evaluation of the maximum force that may be transferred from the concrete to the external reinforcement, as well as the evaluation of shear and normal stresses at the concrete-FRP interface is required. The former is necessary when designing at the ultimate limit state; the latter when designing at the serviceability limit state.

The constitutive bond model for externally bonded FRP reinforcement is assumed bilinear (Fig. 4b). This model has been proposed by various authors, among which [11], and is also discussed in [5]. The model parameters basically relate to the fracture energy G_F of the glued joint connection between the external reinforcement and the concrete and have to be calibrated on the basis of experimental results.

Debonding of the FRP can be predicted by considering the different bond failure modes which can occur, as outlined next.

Bond-critical failure modes

Depending on the starting point of the debonding process, the bond-critical failure modes in flexural and shear strengthening with FRP can be classified into two main categories: “end debonding” or “intermediate crack debonding”.

If insufficient anchorage capacity is provided interfacial end debonding occurs as shown in Fig. 5a. A specific form of end debonding is concrete cover separation or concrete rip-off, see Fig. 5b. The latter failure mode is obtained when a shear crack at the end of the FRP reinforcement propagates into a debonding mode at the level of the internal reinforcement.

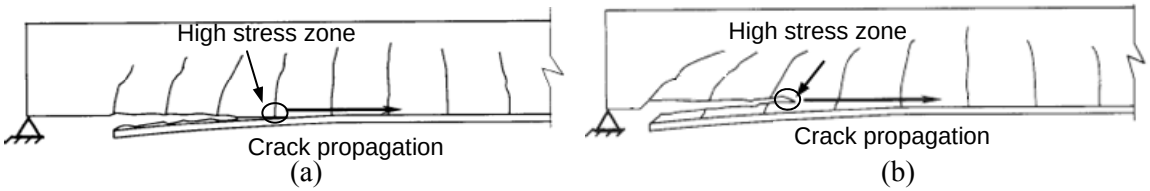

Fig. 5 End debonding: (a) anchorage failure and (b) concrete rip-off failure.

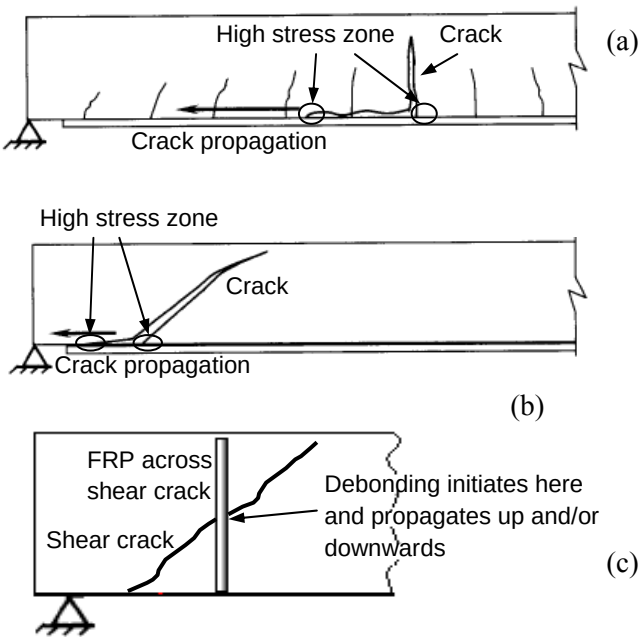

Fig. 6 Initiation of debonding at (a) intermediate flexural crack in flexural strengthening, (b) inclined crack in flexural strengthening and (c) shear crack in shear strengthening.

Debonding of FRP can also be caused by bridging of intermediate cracks, as illustrated in Fig. 6a,b, for the case of flexural strengthening, and Fig. 6c, for the case of shear strengthening.

Maximum bonded length

With reference to a typical bond test, as represented in Fig. 7, the ultimate value of the force transferred to the FRP system prior to debonding depends on the length, ℓ_b, of the (uncracked) bonded area. The maximum bonded length, $\ell_{b,max}$, is defined as the length that, if exceeded, no

further increase in the force transferred between the concrete and the FRP would be possible.

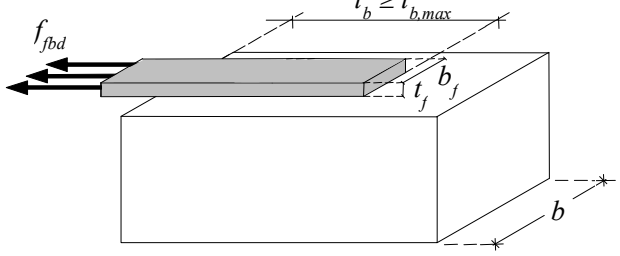

Fig. 7 Bond test configuration.

The maximum bonded length may be estimated as

$$\ell_{b,\max} = \sqrt{\frac{E_f t_f}{k_{bl} f_{ctm}}} \quad \text{(units: mm, MPa)} \tag{1}$$

where E_f is modulus of elasticity in the stress direction of the FRP, t_f is the thickness of the FRP, f_{ctm} is the mean tensile strength of the concrete substrate and k_{bl} is the bond length calibration factor obtained from test results (in the order of 2).

Strength for end debonding – anchorage failure

The mean and the design ultimate bond strengths, that is the maximum tensile stress in the FRP limited by bond to concrete in a single (uncracked) anchorage zone, are estimated as

$$f_{fbm} = k_m k_b \beta_\ell \sqrt{\frac{2E_f}{t_f} f_{cm}{}^{2/3}} \quad \text{(units: mm, MPa)} \tag{2a}$$

$$f_{fbd} = \frac{k_k}{\gamma_{f,b}} k_b \beta_\ell \sqrt{\frac{2E_f}{t_f} f_{cm}{}^{2/3}} \quad \text{(units: mm, MPa)} \tag{2b}$$

where f_{cm} is the mean cylinder compressive strength of concrete, $\gamma_{f,b}$ is the FRP partial safety factor for debonding (equal to 1.5) and β_ℓ is the length factor, defined as:

$$\beta_\ell = \frac{\ell_b}{\ell_{b,\max}} \cdot \left(2 - \frac{\ell_b}{\ell_{b,\max}}\right) \quad \text{if} \quad \ell_b \le \ell_{b,max}, \ \beta_\ell = 1 \text{ otherwise} \tag{3}$$

On the basis of calibration with experimental results, for epoxy bonded CFRP systems k_m = 0.25 and, under the hypothesis of normal distribution of the bond strength, the 5% percentile can be calculated assuming k_k = 0.17.

Strength for end debonding – concrete rip-off

This debonding mode can be avoided by providing shear strengthening (transverse wrapping) at the end of the FRP. The design of the shear strengthening aims at extending the existing shear links up to the level of the FRP.

Strength for intermediate debonding

According to a simplified procedure, the design ultimate bond strength for intermediate debonding is obtained by multiplying f_{fbm} and f_{fbd} by a factor k_c. If specific experimental data are not available, k_c may be taken equal to 2.0 and 1.5, for the mean and the design ultimate bond strength, respectively. Alternative and more detailed approaches to prevent the debonding failure at intermediate cracks can be adopted, based on the envelope line of tensile stress and on the force transfer between the concrete and the FRP.

Interfacial stresses for the serviceability limit state

It is assumed that bond interface crack initiation will not occur under service load, provided proper detailing and limitation of deflections and crack widths has been carried out. Bond stresses (shear and normal) at serviceability limit state can be calculated on the basis of linear elastic analysis.

Mechanical anchorages for externally bonded FRP reinforcement

Debonding at the ends of the FRP can be avoided, or an enhancement of the debonding load can be achieved, using anchorage systems. Various solutions are available and can be designed for the specific case, employing the fibres themselves with suitable configurations, e.g. transverse wrapping (Fig. 8a), spike anchors (Fig. 8b) or additional devices such as bolts or plates.

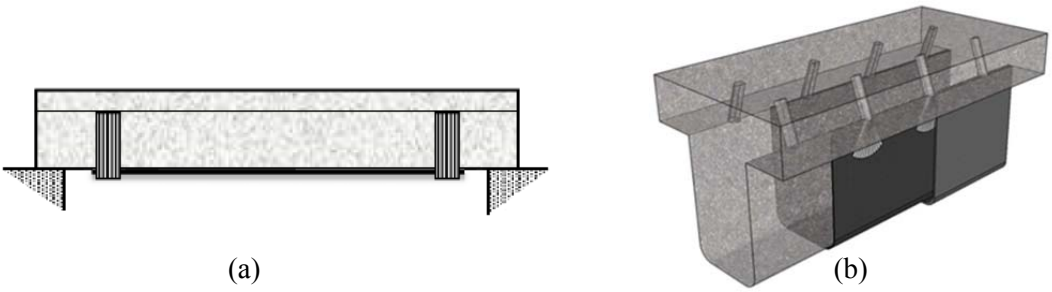

(a) (b)

Fig. 8 (a) End anchorage using transverse wrapping and (b) spike anchors.

The ultimate value of the force transferred to the FRP system prior to debonding depends on the efficiency of the anchorage system. In the presence of mechanical anchorage, the design anchorage strength f_{fad} may be taken equal to:

$$f_{fad} = k_a f_{fd} \tag{4}$$

where f_{fd} is the design tensile strength of the FRP, equal to the characteristic tensile strength f_{fk} divided by the safety factor γ_f, and k_a is the effectiveness coefficient of the specific anchorage system ($k_a \leq 1$), provided on the basis of experimental results.

Conclusions

The use of non-metallic or so-called FRP reinforcement in concrete construction and upgrading is gradually more and more widely accepted. This durable, light weight, high strength reinforcement has demonstrated its value in practical applications worldwide. Thorough research and material development achievements linked to engineering practice stimulated this process, as well as the development of national and international design guidelines, among which the work of fib Task Group 9.3 “FRP reinforcement for concrete structures”. With the further introduction of FRP reinforcement in MC2010 the authors believe a logical and necessary step is made for the further acceptance and more wide spread use of FRP reinforcement for strengthening and reinforcing concrete structures.

References

1. *Taerwe, L.* and Matthys, S.: FRP for Concrete Construction: Activities In Europe, ACI Concrete International, 1999, 21(10), 33-36.
2. *Triantafillou*, T. C., Deskovic, N. and Deuring, M.: Strengthening of concrete structures with prestressed fiber reinforced plastic sheets. ACI Structural Journal, 1992, 89(3), 235-244.
3. *Blaschko, M.* and *Zilch, K.*: Rehabilitation of concrete structures with CFRP strips glued into slits. Proceedings of the 12th International Conference on Composite Materials, Paris, 1999.

4. *Triantafillou, T. C.*, Papanicolaou, C. G., Zisimopoulos, P. and Laourdekis, T.: Concrete confinement with textile reinforced mortar (TRM) jackets. ACI Structural Journal, 2006, 103(1), 28-37.
5. *fib*: Externally bonded FRP reinforcement for RC structures, fib Bulletin 14, 2001, Lausanne.
6. *fib*: FRP reinforcement in RC structures. fib Bulletin 40, 2007, Lausanne.
7. *fib*: Model Code 2010, Final draft, fib Bulletins 65 and 66, 2012, Lausanne.
8. *ISO 10406-1*: Fibre-reinforced polymer (FRP) reinforcement of concrete - Test methods - Part 1: FRP bars and grids, 2008.
9. *ISO 10406-2*: Fibre-reinforced polymer (FRP) reinforcement of concrete - Test methods - Part 2: FRP sheets, 2008.
10. *Palmieri, A.*, Matthys, S. and Taerwe, L.: Fire endurance and residual strength of insulated concrete beams strengthened with near surface mounted reinforcement. Journal of Composites for Construction, published online Ocotber 2012 (DOI:10.1061/(ASCE)CC.1943-5614.0000338).
11. *Holzenkämpfer, P.*: Ingenieurmodelle des verbundes geklebter bewehrung für betonbauteile. Dissertation, TU Braunschweig, 1994 (In German).

Flowcharts for EBR design according to fib bulletin 14

A. Serbescu[1], M. Guadagnini[2] and K. Pilakoutas[3]

Introduction

The following set of flowcharts summarizes the steps of a typical design process for strengthening RC beams with FRP materials, according to fib bulletin 14 (2001). Any FRP strengthening design should start by estimating the capacity of the existing RC beam and assessing the FRP strengthening feasibility (Flowchart 1). Depending on the strengthening target, the design can be governed by either ultimate (Flowchart 2) or serviceability limit state (Flowchart 3).

Initial Assessment

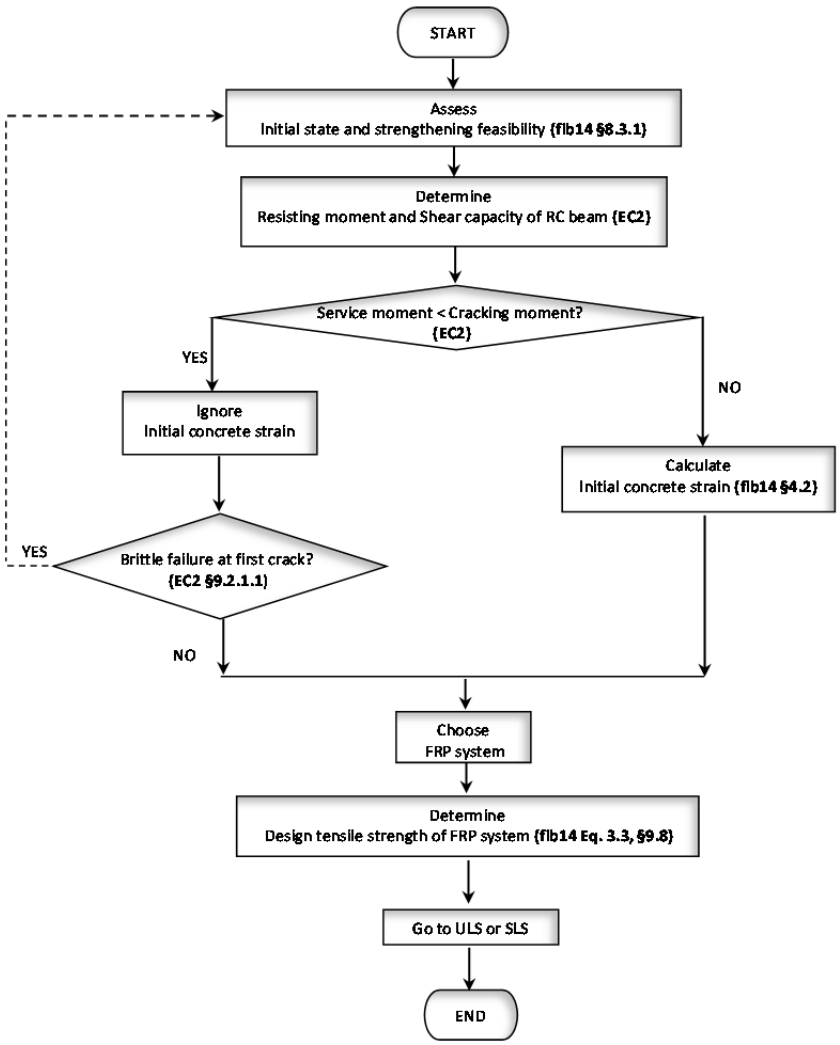

Figure 1: Initial state

[1] The University of Sheffield, UK, a.serbescu@sheffield.ac.uk
[2] The University of Sheffield, UK, m.guadagnini@sheffield.ac.uk
[3] The University of Sheffield, UK, k.pilakoutas@sheffield.ac.uk

Ultimate Limit State

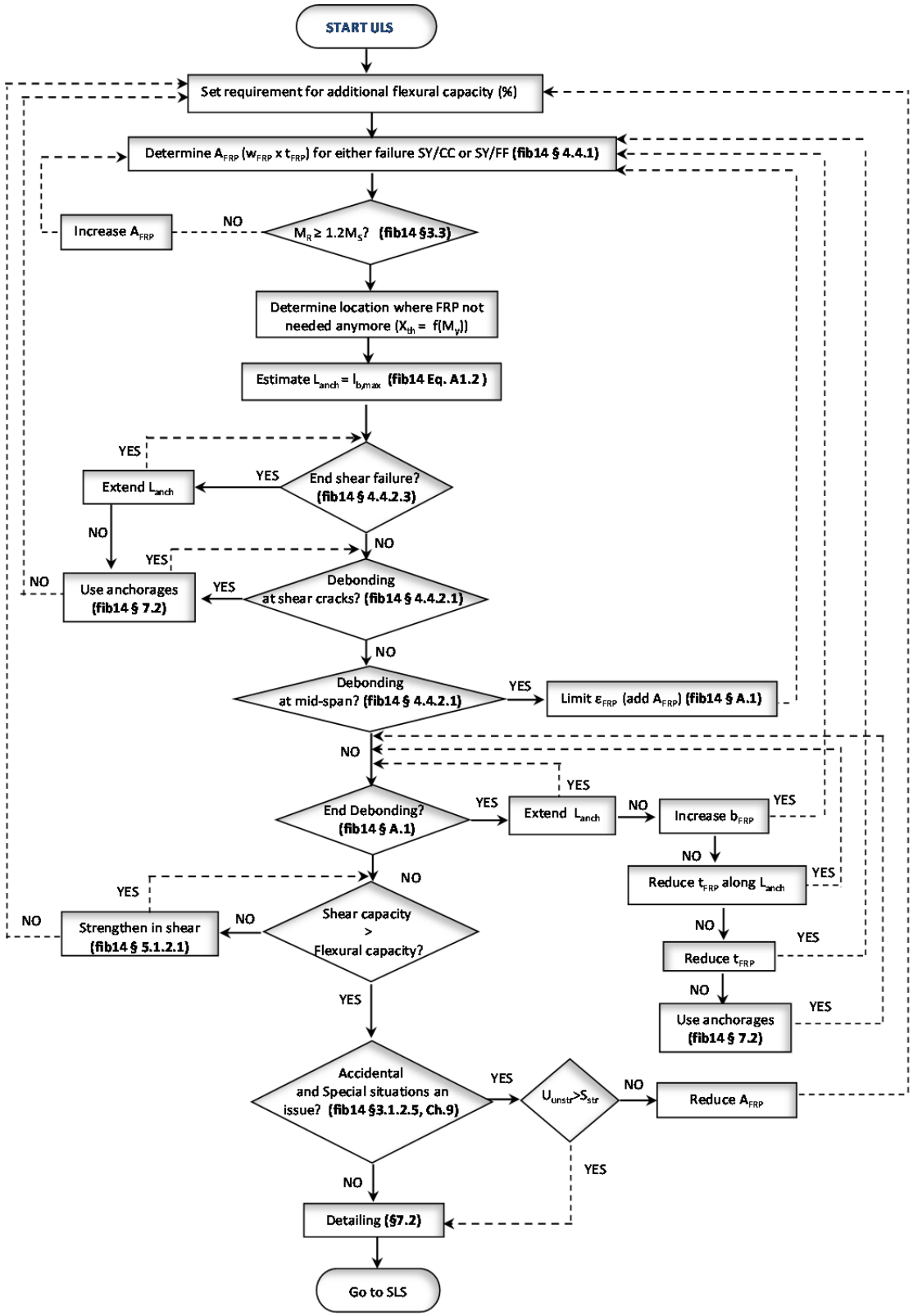

Figure 2: Ultimate Limit State

Serviceability Limit State

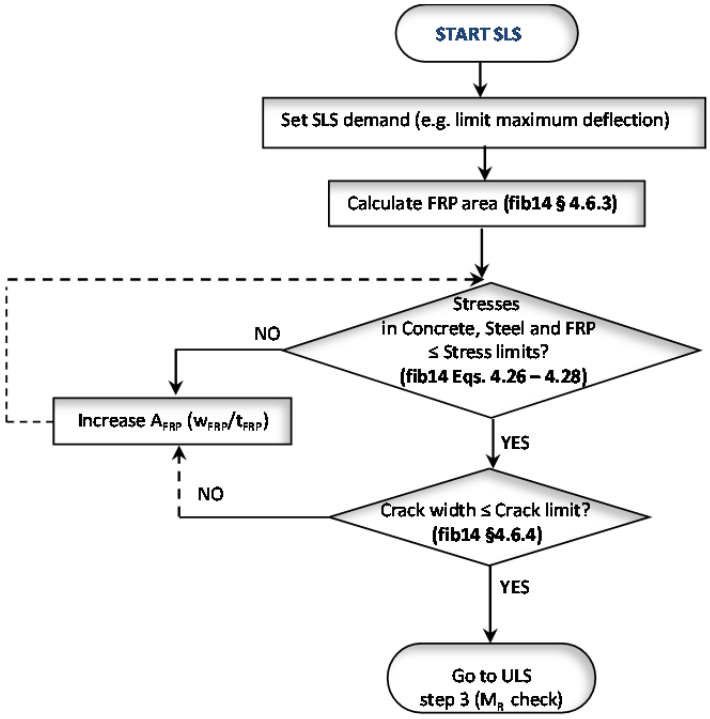

Figure 3: Serviceability Limit State

Conclusions and Points for Discussions

- While designing for one limit state, it is required to check that all criteria are still satisfied at the other one. For instance, the amount of FRP needed for SLS (e.g. to control deflection or crack width) is significantly high and could affect the ductility performance. Similarly, providing an amount of FRP sufficient to meet ULS requirements does not necessarily satisfy SLS criteria.
- Other design strategies can also be adopted such as: starting the design by imposing a maximum strain on the FRP to avoid mid-span debonding or starting the design with identifying the location of $N_{fa,max}$ (Eq. A1-1)
- Bond interface cracking at SLS (section 4.6.5) may be of concern if no extra anchorage is provided or crack width limitation is not met.

Key references

fib bulletin 14 (2001). Externally bonded FRP reinforcement for RC structures, International Federation for Structural Concrete - Technical report, Lausanne.

Italian design code provisions - CNR DT200/R1: end/intermediate debonding of EBR

Antonio Bilotta[1], Francesca Ceroni[2] & Emidio Nigro[3]
[1]DIST – Department of Structures for Engineering and Architecture, University of Naples Federico II, Italy
antonio.bilotta@unina.it
[2]DING - Structural Engineering, University of Sannio, Italy
ceroni@unisannio.it
[3]DIST – Department of Structures for Engineering and Architecture, University of Naples Federico II, Italy
emidio.nigro@unina.it

Externally bonded (EB) Fiber-Reinforced-polymer (FRP) sheets and laminates are widely employed for enhancing the bending capacity of reinforced concrete (RC) beams (Teng et al. 2001). Although alternative systems are possibly available to connect the FRP strip to concrete members (Napoli et al., 2010; Bilotta et al., 2011), external bonding is still the most common technique. However, the adhesion between FRP and concrete substrate is an issue of concern and generally controls the ultimate capacity of RC beams. Particularly, intermediate debonding phenomenon which begins from a flexural or flexural-shear crack away from the ends of the FRP reinforcement (intermediate crack) throughout the FRP-concrete interface is one of the most common and peculiar failure modes observed in RC beams externally strengthened in bending by bonded FRP. On the other hand, the possible premature failure due to debonding can occur also at the end of the reinforcement (end debonding) before the intermediate debonding in case of absence of specific end anchoring systems. According to well-established mechanical models, end-debonding is basically due to the high interface shear stresses developing in the neighborhood of the FRP cut-off section as a result of the abrupt change in the transverse section of the strengthened beam (fib bulletin 14, 2001; ACI 440.2 R-08, 2008).

By contrast, a higher level of uncertainty still overshadows the mechanical understanding of intermediate debonding due to the complex interaction of several phenomena, such as cracking in concrete (spacing and inclination of cracks), amount of internal longitudinal and transversal steel reinforcement, steel yielding in longitudinal rebars, interface adhesion properties, loading pattern, and so on (Arduini and Nanni, 1997). As a result of this partial understanding, different alternative analytical approaches were proposed within the scientific literature and adopted by the most common codes of standards for performing the required safety checks (fib bulletin 14, 2001; ACI 440.2 R-08, 2008; JSCE, 2001; CNR DT 200/R1, 2012). A possible classification of those approaches based on the nature of the procedures utilized for checking the strengthened beam against intermediate debonding is proposed in (Faella et al, 2004;).

Italian design code provisions were recently updated based on several experimental tests. In particular, the results of flexural tests on beams and slabs and of bond tests on concrete specimens externally bonded with FRP plate and sheets were used to calibrate two bond strength models, based on the same fracture energy approach, for intermediate debonding and end-debonding, respectively.

Specific fracture energy – Plate end debonding

In the following, reference is made to the general scheme of shear bond test drawn in Figure 1. Moreover, the fracture energy is called Γ_F according to CNR-DT200/R1 (2012)

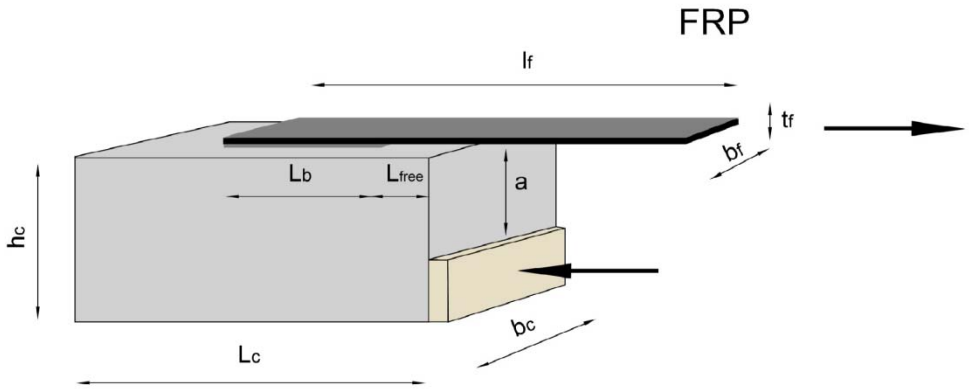

Figure 1 - General scheme of an asymmetrical push-pull bond test.

The maximum tensile force, F_{max}, at debonding in an FRP external reinforcement characterized by an infinite bonded length can be calculated as:

$$F_{\max} = b_f \int_0^{\infty} \tau_b(x)\, dx, \qquad (1)$$

being $\tau_b(x)$ the bond shear stress distribution along the concrete-FRP interface and b_f the width of the FRP reinforcement.

Moreover, the fracture energy corresponding to a generic bond shear stress-slip law, $\tau_b(s)$, can be expressed as:

$$\Gamma_F = \int_0^{\infty} \tau_b(s)\, ds \qquad [F/L] \qquad (2)$$

This expression has the meaning of an energy [F L] for unit surface [L^2].

Under the hypothesis that the concrete member has a stiffness much larger than the reinforcement F_{max} can be written as follows:

$$F_{\max} = b_f \cdot \sqrt{2 \cdot E_f \cdot t_f \cdot \Gamma_F} \qquad (3)$$

where t_f, b_f, E_f are the thickness, the width, and the Young modulus of the FRP reinforcement.

The fracture energy, Γ_F, depends on both the strength properties of adherents, concrete and adhesive, and the characteristics of the concrete surface. If the FRP reinforcement is correctly applied, the debonding occurs in the concrete and the specific fracture energy of the interface law can be written in a form similar to that used for the shear fracture (mode I). Therefore, the fracture energy can be expressed as a function of the concrete shear strength: $\Gamma_f(\tau_{b,\max})$, where $\tau_{b,max}$ depends on both tensile, f_{ct}, and compressive, f_c, concrete strength. Actually, bond stresses orthogonal to the reinforcement are always present along the FRP reinforcement, as experimentally evidenced by the visual inspection of the debonded surface configuration (Mazzotti et al., 2008)

The general Eq. (3) for debonding load can be particularized by introducing the dependence of the fracture energy on the bond shear strength. Indeed, the bond shear strength depends on the concrete strength and can be related to the Mohr's circle representing the stress condition in the concrete at failure. Thus, different formulations for shear strength can be considered varying the dependence on the concrete strength.

If a Coulomb's failure criterion is adopted, the term $\sqrt{f_{cm} \cdot f_{ctm}}$ is 2 times the cohesion associated to the Mohr's circle of an interface concrete element subjected to both shear and normal stresses.

Hence the following relationship for the fracture energy can be assumed:

$$\Gamma_f = k_G \cdot k_b \cdot \sqrt{f_{cm} \cdot f_{ctm}} \qquad (4)$$

where

- f_{cm} and f_{tcm} are the mean value of the cylindrical compressive strength and the tensile strength of the concrete respectively,
- k_b is the shape factor expressed as:

$$k_b = \sqrt{\frac{2 - b_f / b}{1 + b_f / b}} \geq 1 \qquad with \qquad \frac{b_f}{b} \geq 0.25 \qquad (5)$$

- b_f is the width of the laminate and b is the width of the concrete member
- the coefficient k_G shall be experimentally adjusted.

The value of such coefficient has been computed over a large population of experimental results available in the literature. Moreover preformed (plates) and cured in-situ (sheets) FRP systems have been distinguished in order to better exploit the performances of the two systems. Totally, 216 data of bond tests for sheets and 68 for plates have been collected (Bilotta et al., 2011).

For specimens strengthened with FRP sheets the main parameters vary in the following ranges: concrete width b_c = 100-500 mm, width of FRP reinforcement b_f = 25-100 mm, b_f/b_c = 0.17–1, thickness of FRP reinforcement t_f = 0.083-0.507 mm, bonded length of FRP reinforcement L_b = 75-500 mm, number of layers of FRP reinforcement n = 1-3, Young's modulus of FRP reinforcement E_f = 82-390 GPa, mean compressive strength of concrete f_{cm} = 17-62 MPa, and mean tensile strength of concrete f_{ctm} = 1.3-4.3 MPa.

Analogously, for specimens strengthened with FRP plates the main parameters vary in the following ranges: b_c = 150-230 mm, b_f = 25-100 mm, b_f/b_c = 0.11–0.63, t_f = 1.0-1.6 mm, n = 1, L_b = 150-400 mm, E_f = 108-400 GPa, f_{cm} = 15-53 MPa, and f_{ctm} = 1.10-3.8 MPa.

The calibrating procedure was based on a detailed and consistent statistical analysis according to the 'design by testing' procedure suggested in the Eurocode 0 (EN1990, 2002 – Annex D). Different corrective factors allow different percentiles values of k_G to be attained. The assessment of the percentiles has been carried out taking into account also the variance of the materials (concrete and FRP materials).

The statistical analysis of the experimental results has provided an average value of K_G equal to 0.063mm and a 5th percentile equal to 0.023mm for plates and an average value equal to 0.077mm and a 5th percentile equal to 0.037mm for sheets.

Using the mean values Eq. (4) gives the mean value of the energy fracture Γ_{Fm}. When the characteristic values are used in Eq. (4), the characteristic value, Γ_{Fk} , of the fracture energy is obtained.

Through Eqns 3 and 4 the plate end debonding stress can be calculated as

$$f_{fdd} = \frac{1}{\gamma_{fd}} \sqrt{\frac{2 \cdot E_f \cdot \Gamma_{Fd}}{t_f}} \qquad (6)$$

being

- $\gamma_{f,d}$ a safety factor on gluing application uncertainness (it shall be assumed equal to 1.2 or 1.5 for controlled or not controlled gluing application)
- $\Gamma_{Fd} = \Gamma_{Fk}/FC$ where FC is a confidence factor (in the range of 1.00-1.35) based on the level of knowledge achieved on the existing material properties and typically used for the assessment and retrofitting of buildings (European Code - UNI EN 1998-3).

In Figure 2, the experimental values of strain, $\varepsilon_{fdd} = f_{fdd}/E_f$, in the FRP reinforcement at debonding for the selected tests of the collected database are plotted together with the mean and characteristics curves easily calculated through Eqns (3) and (4) for the different values of k_G (for further details see section **Error! Reference source not found.**).

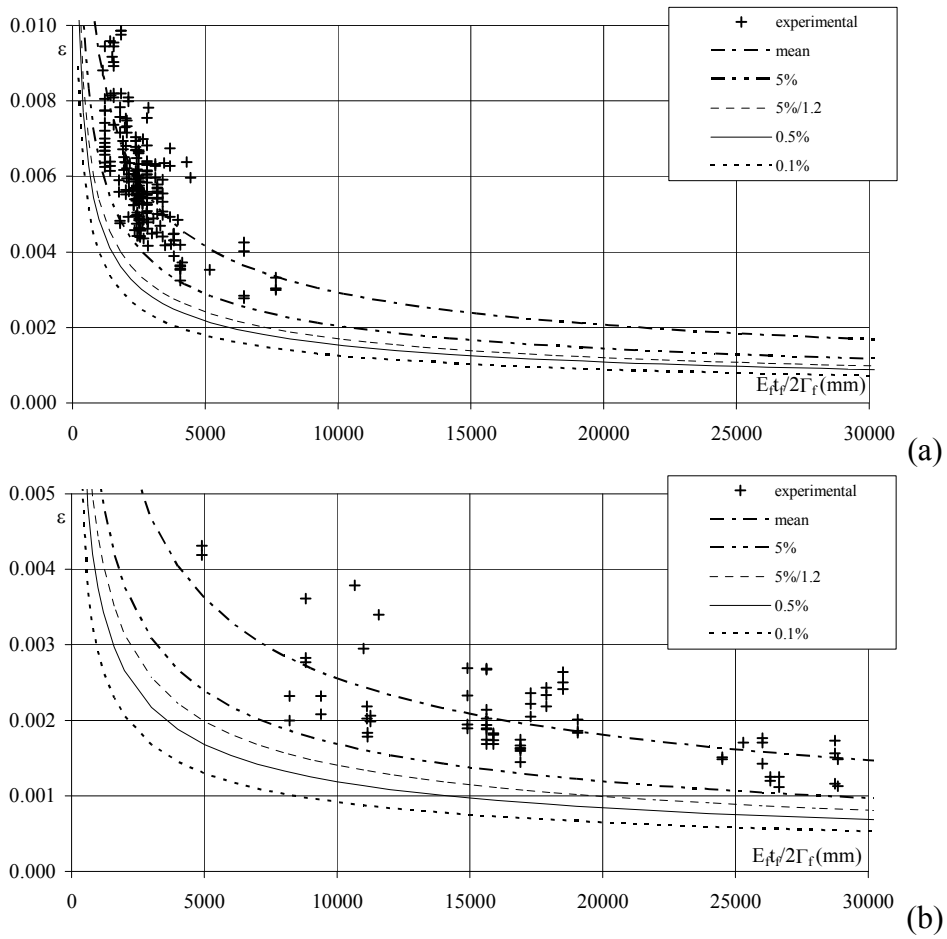

Figure 2 - Experimental strain at failure vs. theoretical results:
a) cured in situ systems (216 data); b) preformed systems (68 data).

Simplified method for IC debonding

Unless a more detailed analysis can be carried out basing on the envelope line of tensile stress (Oller et al., 2009a,b; Finckh and Zilch 2011) or on the force transfer between the concrete and external FRP reinforcement (fib bulletin 14, 2001), a simplified method is suggested in CNR DT200/2012. Such method is based on the definition of a maximum value for the axial strain ε_{fd} which can be developed in the FRP laminate before of the occurrence of intermediate debonding failure.

A wide database was assembled by collecting data of 214 experimental tests on FRP-strengthened RC beams (Bilotta et al., 2013); For specimens strengthened with FRP systems cured in situ (fabrics), the relevant geometric and mechanical parameters range in the following intervals: concrete width bc = 75-960 mm, FRP width bf = 30-480 mm, bf/bc = 0.17-1.0, FRP thickness tf = 0.11-2.55 mm, Young modulus of FRP Ef = 21-390 GPa, mean compressive strength of concrete fcm = 21-61 MPa, mean tensile strength of concrete fctm = 2.3-4.3 MPa.

For specimens strengthened with precured FRP systems (laminates), the key parameters vary in the following ranges: concrete width bc = 180-800 mm, FRP width bf = 25-280 mm, bf/bc = 0.13-1.0, FRP thickness t_f = 1.0-6.0 mm, Young modulus of FRP Ef = 190-220 GPa, mean compressive strength of concrete f_{cm} = 12.6-53.4 MPa, mean tensile strength of concrete fctm = 1.62-4.25 MPa.

A total number of 214 experimental results were collected (164 FRP cured in situ systems and 50 FRP preformed system).

The maximum strain can be evaluated as

$$\varepsilon_{fdd,2} = \frac{f_{fdd,2}}{E_f}\sqrt{\frac{2\cdot\frac{k_{G,2}\cdot k_b}{FC}\cdot\sqrt{f_{cm}\cdot f_{ctm}}}{E_f\cdot t_f}} \qquad (7)$$

This relationship is similar to that proposed for the plate end debonding and the coefficient k_{G2} has been experimentally adjusted in order to give average and design provisions basing on the collected database of 214 data. The calibrating procedure was based on a detailed and consistent statistical analysis according to the 'design by testing' procedure suggested in the Eurocode 0 (EN1990, 2002 – Annex D). Different corrective factors allow different percentiles values of $k_{G,2}$ to be attained. The assessment of the percentiles has been carried out taking into account the variance of the materials.

The statistical analysis of the experimental results has provided an average value of $k_{G,2}$ equal to 0.32 mm and a 5th-percentile equal to 0.10mm. No difference was done into assess $k_{G,2}$ for plates and sheets since the values resulted very similar.

References

ACI Committee 440.2 R-08 (2008): Guide for the Design and Construction of Externally Bonded FRP Systems for Strengthening Concrete Structures.

Arduini, M., Nanni, A., "Behavior of Precracked RC Beams Strengthened with Carbon FRP Sheets," Journal of Composites for Construction, 1, 2, 1997, pp. 63-70.

Bilotta A., Ceroni F., Nigro E., Pecce M. (2011b). Design by testing of debonding load in RC element strengthened with EBR FRP materials, 10th International Symposium on Fiber Reinforced Polymer Reinforcement for Reinforced Concrete Structures, April 2-4, 2011, Tampa, Florida, USA.

Bilotta A., C. Faella, E. Martinelli, E. Nigro (2013). Design by testing procedure for intermediate debonding in EBR FRP strengthened RC beams. ENGINEERING STRUCTURES, vol. 46, p. 147-154, ISSN: 0141-0296, doi:10.1016/j.engstruct.2012.06.031

Bilotta A., Ceroni F., Di Ludovico M., Nigro E., Pecce M., Manfredi G. (2011). Bond Efficiency of EBR and NSM FRP Systems for Strengthening Concrete Members, Journal of Composites for Construction, Vol. 15, Issue 5, Pages: 757-772, DOI: 10.1061/(ASCE)CC.1943-5614.0000204.

CNR DT 200/R1 (2012): Instructions for Design, Execution and Control of Strengthening Interventions by Means of Fibre-Reinforced Composites (in Italian), Italian National Research Council.

Faella C., Martinelli E., Nigro E., Debonding in FRP-strengthened RC beams: comparison between code provisions, Proceedings of the Second International Conference on FRP Composites in Civil Engineering, Paper 074; Adelaide (Australia), 8-10 December 2004

Ferracuti B., Martinelli E., Nigro E., Savoia M., Fracture Energy and Design Rules against FRP-Concrete Debonding, Proc. of 8th FRPRCS Conference, 16-18 July 2007, Patras (GR);

fib-CEB-FIP - Task Group 9.3 (2001), Externally Bonded FRP Reinforcement for RC Structures, Technical Report Bulletin 14,

Finckh, W.; Zilch, K.; Ellinger, M.: Evaluating the bond stress relationship of externally bonded CFRP-strips at the intermediate crack element. In: M. Motavalli, B. Havranek und E. Saqan (Hg.): Proceedings of SMAR 2011, the 1st Middle East Conference on Smart Monitoring, Assessment and Rehabilitation of Civil Structures. 8 - 10 February 2011, Dubai, 2011

JSCE (2001): Recommendations for upgrading of concrete structures with use of continuous fiber sheets, Concrete Engineering Series 41.

Napoli A., Matta F., Martinelli E., Nanni A., Realfonzo R. (2010). Modelling and verification of response of RC slabs strengthened in flexure with mechanically fastened FRP laminates, Magazine of Concrete Research, 62(8): 593-605.

Oller E. Cobo D., Marí A.R. (2009b). Design Proposal to Avoid Peeling Failure in FRP-Srengthened Reinforced Concrete Beams, Journal of Composites for Construction, Vol. 13, No. 5, pp. 384-393.

Teng J.G., Chen J.F., Smith S.T., Lam L., FRP-strengthened RC structures. Chichester, West Sussex, UK: John Wiley and Sons, 2002. p. 245.

Comparison of the existing guidelines to evaluate the intermediate crack debonding in externally bonded FRP reinforcement

E. Oller[1], A. Marí[2]

Introduction

Externally bonded (EB) fiber reinforced polymer (FRP) laminates have been already proved as an effective strengthening technique, specially in flexure and confinement, with applications worldwide. However, as observed in many experimental programs, flexural strengthening by EB FRP reinforcement is often limited by the laminate debonding before the appearance of a classical mode of failure (concrete in compression or FRP rupture). This laminate debonding usually occurs in the concrete, since it is the weakest material of the interphase concrete-adhesive-laminate. The debonding mechanism initiates along the span due to the existence of intermediate cracks (IC debonding) or at the plate end (PE debonding).

The existing guidelines include some formulations to avoid this type of premature failures when designing the EBR.

Bending test database of reinforced concrete (RC) beams externally strengthened by fiber reinforced polymer (FRP) laminates

In order to evaluate the reliability of different formulations related to the premature laminate debonding, a database of 626 RC beams FRP-strengthened and tested in flexure has been assembled. From the database, 403 beams have been selected since they were well-documented and they were reported to fail due to laminate debonding. Beams included in the database have a rectangular cross-section, are externally strengthened by FRP wet lay-up or pultruded laminates, which are not anchored along its length, and were tested in a simply supported configuration.

In relation to the debonding initiation area of the selected beams, in 273 out of the 403 tests, laminate debonding was reported to be initiated near the load application point (Intermediate crack (IC) debonding). In the remaining tests, failure was initiated at the laminate end (Plate end (PE) debonding) and propagated or not along the concrete cover, a shear crack was observed at the laminate end, or no details about the debonding failure were reported.

Comparative analysis of existing formulations to prevent intermediate crack (IC) debonding

In this section a comparative analysis of the different existing formulations to prevent intermediate crack (IC) debonding included in the existing guidelines is performed. The existing formulations are based on limiting neither:

- the maximum laminate strain (CNR-DT200/2004, 2004; ACI 440.2R-08, 2008; Simplified strain analysis of DAfStb, 2013);

- the maximum laminate tensile stress (CNR-DT 200/2004, 2004; JSCE, 2001-Wu and Niu, 2000); or the laminate tensile stress increment between two adjacent cracks (Fib Bulletin 14, 2001-Niedermeier, 2000; JSCE, 2001-Wu and Niu, 2000; DAfStb 2013 (simplified and detailed analysis));

- the shear stress (Fib Bulletin 14, 2001-Matthys, 2000; TR-55, 2012).

[1] Universitat Politècnica de Catalunya, Spain, antonio.mari@upc.edu
[2] Universitat Politècnica de Catalunya, Spain, eva.oller@upc.edu

In the application of the formulations, mean values instead of characteristic values of the material properties are used and the safety coefficients are assumed to be equal to 1.0.

Statistical results from the application of the different models to the database

Table 1 summarizes the statistical parameters related to the comparative analysis of the existing formulations previously mentioned to avoid IC debonding. These parameters are: minimum (column 4), mean (column 5), maximum (column 6), median (column 7), standard deviation (column 8), coefficient of variation (COV) (column 9) of the ratio between the experimental value and theoretical prediction described in column 2 for each model.

If the mean value of the experimental and theoretical ratio is higher than 1.0, the theoretical model is conservative and underestimates the resisting capacity of the strengthened section. The best model should have the mean ratio close to 1.0 and a low coefficient of variation. The mean is used as a measure of the conservative bias of the procedure. The coefficient of variation is a relative measure of accuracy and sample variability. The more homogeneous the sample, the smaller the coefficient of variation.

Table 1: Statistical results for the models for IC debonding included in the existing guidelines.

Model	Ratio	#	Min	Mean	Max	Med	St. Dev.	COV
Fib Bulletin 14 (2001) - Niedermeier (2000)	$\Delta\sigma_{exp}/\Delta\sigma_{th}$	273	0.16	6.38	34.74	5.41	4.59	0.72
Fib Bulletin 14 (2001) - Matthys (2000)	τ_{exp}/τ_{th}	273	0.03	0.65	3.96	0.56	0.45	0.68
JSCE (2001) – Wu and Niu (2000) (1)	σ_{exp}/σ_{th}	273	0.30	1.54	3.34	1.52	0.52	0.34
JSCE (2001) – Wu and Niu (2000) (2)	$\Delta\sigma_{exp}/\Delta\sigma_{th}$	273	0.06	1.04	3.27	1.00	0.48	0.47
CNR-DT200/2004 (2004)	σ_{exp}/σ_{th}	273	0.24	1.06	2.30	1.03	0.37	0.35
ACI-440.2R-08 (2008)	$\varepsilon_{exp}/\varepsilon_{th}$	273	0.24	1.18	8.42	1.09	0.69	0.58
TR-55 (2012)	τ_{exp}/τ_{th}	273	0.02	0.81	1.92	0.81	0.27	0.33
DAfStb (2013) simplified strain	$\varepsilon_{exp}/\varepsilon_{th}$	273	0.51	2.51	6.48	2.20	1.18	0.47
DAfStb (2013) simplified detailed analysis	$\Delta\sigma_{exp}/\Delta\sigma_{th}$	273	0.07	1.48	6.52	1.29	0.86	0.58
DAfStb (2013) detailed analysis	$\Delta\sigma_{exp}/\Delta\sigma_{th}$	273	0.07	1.28	5.05	1.12	0.75	0.59

In relation to the performance of existing guidelines, the Italian CNR-DT200/2004 shows a mean value of 1.06 close to 1.00 and the lowest coefficient of variation (0.35), followed by the JSCE with a similar mean value of 1.04 and a slightly higher coefficient of variation of 0.48. The statistical behaviour of the ACI-440.2R-01 (2008) is similar to the detailed analysis of the german DAfStb (2013) with slightly more conservative mean values (1.28 for the DAfStb and 1.18 for the ACI) and a similar coefficient of variation (0.53 for the DAfStb and 0.58 for the ACI). The TR-55 (2012) gives the lowest coefficient of variation, but its mean value is below 1.0, because it has around 10% of test with a shear stress ratio lower than 0.5 that reduce significantly the mean value. Finally, the Fib Bulletin 14 (2001) performed statistically worse

than other guidelines. On one hand, the approach of Niedermeier (2001) seems conservative and in some cases the approach based on Matthys (2000) gives unsafe values for the shear stresses. However, in this last approach, the mean value is 1.00 and the coefficient of variation is 0.68 by applying a safety factor to the concrete of 1.5.

The DAfStb guideline gives three approaches: a simplified limit for the laminate strain and a detailed and simplified analysis based on the envelope of tensile stresses. The simplified analysis of IC debonding DAfStb gives a similar coefficient of variation (0.58) and a more conservative mean value (1.48 for the simplified and 1.28 for the detailed analysis). The simplified limit for the laminate strain is more conservative than the analysis based on the envelope of tensile stresses, giving a mean value of 2.51.

It should be noted that, in this study, the german DAfStb has been applied to the whole database, even it was developed only for CFRP strips. However, the statistical results obtained when the database was only applied to CFRP strips are similar to those obtained for the general database.

Figure 1 represents the experimental to the theoretical values for the studied parameter for each existing guideline.

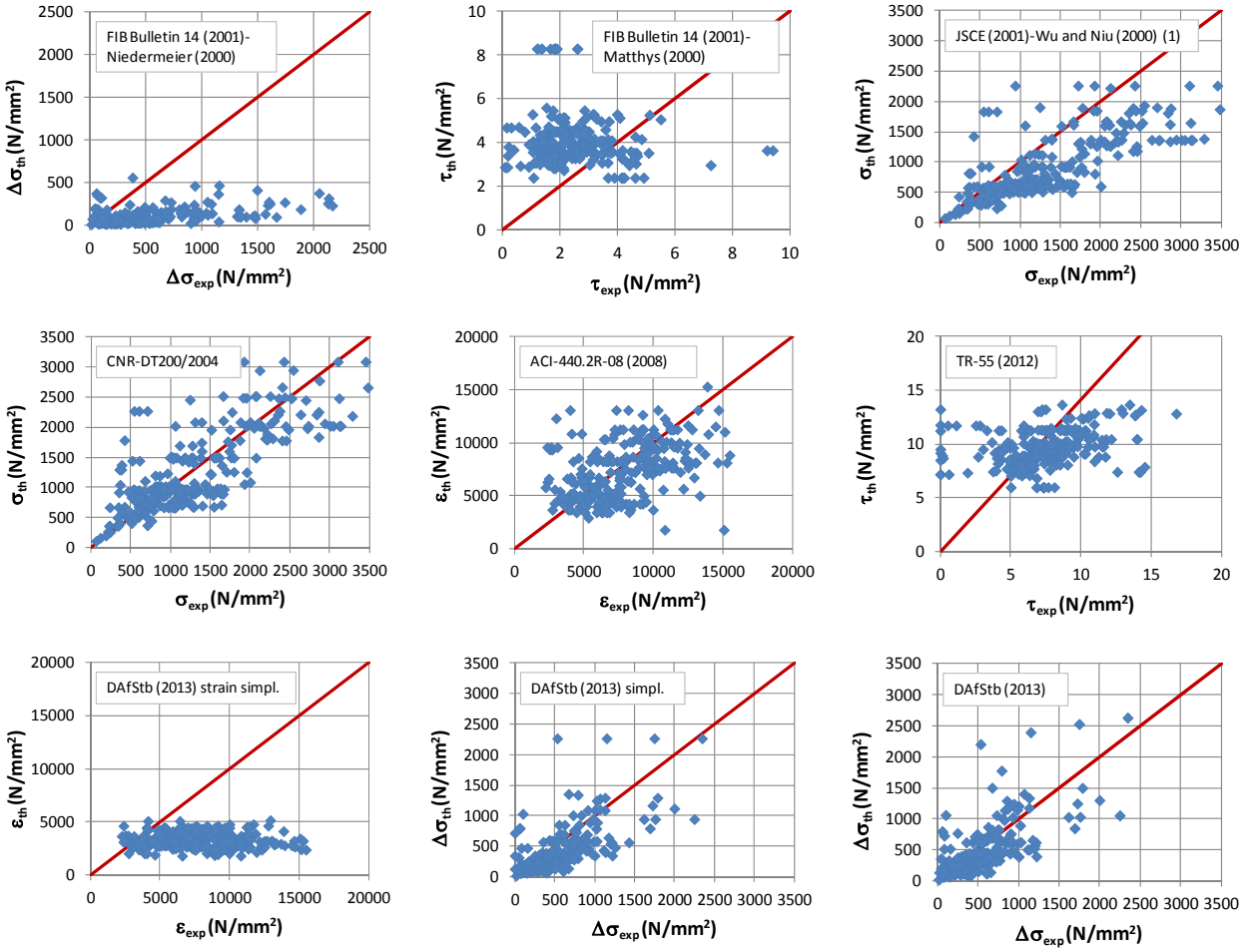

Figure 1: Experimental to predicted parameters for some if the existing guidelines.

Conclusions and Points for Discussions

A database of bending tests has been assembled from the existing experimental research to evaluate the reliability of the different models included in the existing guidelines to prevent intermediate crack (IC) debonding in externally bonded strengthened structures.

The statistical performance of the different models is analysed in terms of a safe mean and median and a low coefficient of variation. The Italian CNR-DT200/2004 shows a mean value of 1.06 close to 1.00 and the lowest coefficient of variation (0.35), followed by the JSCE with a similar mean value of 1.04 and a slightly higher coefficient of variation of 0.48. Most of the remaining models are more conservative.

Key references

American Concrete Institute (ACI) ACI Committee 440 (2008). Guide for the design and construction of externally bonded FRP systems for strengthening concrete structures, ACI 440.2R-08.

CNR (National Research Council) Advisory Committee on technical recommendations for construction (2004). Guide for the Design and Construction of Externally Bonded FRP Systems for Strengthening Existing Structures, CNR-DT200/2004, Rome.

Concrete Society. (2012). Design guidance for strengthening concrete structures using fibre composite materials, TR-55.

Federation Internationale du Beton, Task Group 9.3 FRP Reinforcement for Concrete Structures. Externally bonded FRP reinforcement for RC structures (2001). Technical report on the design and use of externally bonded fibre reinforced polymer reinforcement (FRP EBR) for reinforced concrete structures, Fib Bulletin 14.

German Committee for Reinforced Concrete (2013). DAfStb Heft 595 Erläuterungen und Beispiele zur DAfStb-Richtlinie Verstärken von Betonbauteilen mit geklebter Bewehrung.

Japan Society of Civil Engineers (2001). Recommendations for upgrading of concrete structures with use of continuous fiber sheets. JSCE Concrete Engineering Series, Vol. 41.

Matthys S. (2000). Structural behaviour and design of concrete members strengthened with externally bonded FRP reinforcement, PhD thesis, Faculty of Engineering, Department of Structural Engineering, Ghent University, Ghent, Belgium.

Niedermeier, R. (2000). Envelope line of tensile forces while using externally bonded reinforcement. PhD thesis, TU Münich, Munchen, Germany.

Wu, Z. and Niu, H. D. (2000) Study on debonding failure load of RC beams strengthened with FRP sheets. *Journal of Structural Engineering A*, Vol. 46 (A), pp. 1431-1441.

Wu, Z. S. and Niu H. D. (2007) Prediction of crack-induced debonding failure in R/C structures flexurally strengthened with externally bonded FRP composites. JSCE, *Journal of materials. Concrete structures and Pavements*, Vol. 63 nº 4, pp. 620-639.

Comparison of the existing guidelines to evaluate the FRP contribution in shear strengthened beams

E. Oller[1], A. Marí[2], I. Rodríguez[3]

Introduction

Nowadays, there is a lack of worldwide consensus on the evaluation of the shear strength contribution of the externally bonded FRP reinforcement, in elements strengthened in shear through this technique. One of the main reasons might be the complexity of the resisting mechanisms, not only for the shear strengthening system but also for reinforced concrete. In addition, there is evidence of significant differences between the experimental results and theoretical predictions given by the existing guidelines.

The correct evaluation of the FRP shear strength will allow us to design efficient strengthening solutions which ensure that the structure is capable to satisfy the existing requirements with the minimum cost of the intervention.

The existing guidelines provide formulations to evaluate the shear strength contribution of the FRP laminates which are similar to the contribution of the internal transverse steel reinforcement to the shear strength (Eq. (1)).

$$V_f = \frac{A_f}{s_f} \cdot z_f \cdot f_f \cdot \left(\cot\theta + \cot\alpha\right) \cdot \sin\alpha \qquad (1)$$

The main difference with the transverse internal steel formulations is that the FRP reinforcement does not yield at failure. The definition of the stress at the FRP is the main difference between the existing guidelines, f_f. In this paper, a comparative analysis of the existing formulations to evaluate the FRP contribution is performed.

Shear test database of reinforced concrete (RC) beams externally strengthened by bonding (EB) fiber reinforced polymer (FRP) laminates in shear

To evaluate the reliability of different formulations to evaluate the contribution of EB FRP reinforcement to the shear strength, a database of 536 RC beams FRP-strengthened and tested in shear has been assembled. Selected beams were well-documented, had a rectangular (432) or a T-section (104) cross-section, were externally strengthened in a wrapped (270), U-shaped (118) or side configuration (148) with FRP wet lay-up or pultruded laminates in a continuous or discontinuous manner.

Comparative analysis of existing formulations to evaluate the shear strength contribution of the EB FRP

In this section a comparative analysis of the different existing formulations for the FRP shear strength contribution included in the existing guidelines is performed. These formulations are:

- Fib Bulletin 14 (2001) (developed for fully wrapped or properly anchored CFRP or AFRP, and side U-shaped CFRP, continuous or discontinuous).

[1] Universitat Politècnica de Catalunya, Spain, antonio.mari@upc.edu
[2] Universitat Politècnica de Catalunya, Spain, eva.oller@upc.edu
[3] Universitat Politècnica de Catalunya, Spain, ismael.rodriguez.g@estudiant.upc.edu

- CNR-DT200/2004 (2004) (developed for fully wrapped, U-shaped or side-bonded laminates, continuous or discontinuous).
- ACI 440.2R-08 (2008) (developed for fully wrapped, U-shaped or side-bonded laminates, discontinuous)
- TR-55 (2012) (developed for fully wrapped, U-shaped or side-bonded laminates, continuous or discontinuous).
- DAfStb (2013) (developed for fully wrapped, U-shaped laminates anchored in the compression zone, continuous or discontinuous, do not consider an inclined FRP laminate).

In the application of the formulations, mean values instead of characteristic values of the material properties are used and the safety coefficients are assumed to be equal to 1.0. In addition, it is assumed a strut inclination angle θ of 45^{o} for all the formulations.

Statistical results from the application of the different models to the database

Table 1 and 2 summarize the statistical parameters related to the comparative analysis of the existing formulations previously mentioned to evaluate the FRP contribution to the shear strength in rectangular and T RC beams, respectively. These parameters are: minimum (column 4), mean (column 5), maximum (column 6), median (column 7), standard deviation (column 8), coefficient of variation (COV) (column 9) of the ratio between the experimental value and theoretical prediction of the FRP contribution to the shear strength, V_f. The experimental value, $V_{f,exp}$, is calculated as the difference between the ultimate shear force of the strengthened beam and the ultimate shear force of the unstrengthened beam. Those tests with negative experimental values for the FRP contribution were not considered in this analysis.

If the mean value of the experimental and theoretical ratio, $V_{f,exp}/V_{f,th}$ is higher than 1.0, the theoretical model is conservative and underestimates the resisting capacity of the strengthened section. The best model should have the mean ratio close to 1.0 and a low coefficient of variation. The mean is used as a measure of the conservative bias of the procedure. The coefficient of variation is a relative measure of accuracy and sample variability. The more homogeneous the sample, the smaller the coefficient of variation.

As observed the number of tests analysed for each formulation is different since some of them are not developed for certain cases (i.e. Fib bulletin 14 does not consider side bonded).

In relation to the performance of existing guidelines, all the formulations show a significant dispersion with coefficients of variation higher than 0.70. For rectangular sections, the ACI-440.2R-08 gives the mean value closest to 1.04, and the FIB Bulletin 14 (2001) is the more conservative formulation with a mean value of 4.92. For T-sections, the german DAfStb and the Italian CNR-DT200/2004 gives the mean value close to 1.0.

Table 3, 4 and 5 show the same statistical results for rectangular sections, regarding the FRP configuration. When analysing the results for the different FRP configurations, the Italian CNR-DT200/2004 and the ACI-440.2R-08 show the best performance for wrapped and U-shaped configurations, respectively. The TR-55 gives also good results for the U-shaped configuration. For side bonded configurations, almost all the formulations give an unsafe mean value, below 1.0.

This analysis regarding the FRP configuration has not been performed for T-sections, since only 3 of them were fully wrapped and the remaining 91 were strengthened in a U-shaped configuration.

Table 1: Statistical results for the models for V_{FRP} included in the existing guidelines for rectangular RC beams.

Model	#	Min	Mean	Max	Med	St. Dev.	COV
Fib Bulletin 14 (2001)	257	0.09	4.92	17.06	4.40	3.75	0.76
CNR-DT200/2004 (2004)	421	0.03	1.96	52.94	0.94	4.53	2.31
ACI-440.2R-08 (2008)	211	0.03	1.04	5.03	0.87	0.86	0.83
TR-55 (2012)	421	0.02	1.30	14.04	0.77	1.84	1.41
DAfStb (2013)	282	0.05	1.60	10.99	1.20	1.54	0.96

Table 2: Statistical results for the models for V_{FRP} included in the existing guidelines for T-RC beams.

Model	#	Min	Mean	Max	Med	St. Dev.	COV
Fib Bulletin 14 (2001)	77	0.19	4.48	14.83	3.52	3.11	0.70
CNR-DT200/2004 (2004)	94	0.02	0.97	40.72	0.44	4.16	4.28
ACI-440.2R-08 (2008)	31	0.13	1.28	5.17	0.85	1.20	0.94
TR-55 (2012)	94	0.03	1.74	22.61	0.84	3.57	2.06
DAfStb (2013)	38	0.15	1.04	3.51	0.84	0.74	0.71

Table 3: Statistical results for the models for V_{FRP} included in the existing guidelines for rectangular RC beams strengthened in a wrapped configuration.

Model	#	Min	Mean	Max	Med	St. Dev.	COV
Fib Bulletin 14 (2001)	106	0.09	2.74	15.91	1.60	3.34	1.22
CNR-DT200/2004 (2004)	118	0.07	1.31	4.55	1.18	0.90	0.68
ACI-440.2R-08 (2008)	60	0.07	1.65	5.03	1.73	1.08	0.65
TR-55 (2012)	118	0.09	2.77	14.04	1.85	2.88	1.04
DAfStb (2013)	118	0.08	2.48	10.99	1.94	1.99	0.80

Table 4: Statistical results for the models for V_{FRP} included in the existing guidelines for rectangular RC beams strengthened in a U-shaped configuration.

Model	#	Min	Mean	Max	Med	St. Dev.	COV
Fib Bulletin 14 (2001)	153	0.32	6.46	17.06	6.13	3.22	0.50
CNR-DT200/2004 (2004)	165	0.03	0.80	2.16	0.72	0.44	0.55
ACI-440.2R-08 (2008)	89	0.10	1.04	2.75	1.00	0.58	0.55
TR-55 (2012)	165	0.03	0.93	2.55	0.82	0.57	0.61
DAfStb (2013)	96	0.10	1.13	2.70	1.12	0.55	0.48

Table 5: Statistical results for the models for V_{FRP} included in the existing guidelines for rectangular RC beams strengthened in a sided configuration.

Model	#	Min	Mean	Max	Med	St. Dev.	COV
Fib Bulletin 14 (2001)	-	-	-	-	-	-	-
CNR-DT200/2004 (2004)	140	0.09	3.86	52.94	1.29	7.44	1.93
ACI-440.2R-08 (2008)	62	0.03	0.45	2.00	0.24	0.49	1.09
TR-55 (2012)	140	0.02	0.50	2.19	0.34	0.41	0.82
DAfStb (2013)	68	0.05	0.74	2.59	0.62	0.45	0.61

Conclusions and Points for Discussions

A database of beams externally strengthened in shear by FRP laminates tests has been assembled from the existing experimental research to evaluate the reliability of the different models included in the existing guidelines to evaluate the contribution of the FRP to the shear strength.

The statistical performance of the different models is analysed in terms of a safe mean and median and a low coefficient of variation. In general, a huge dispersion is observed for all models.

Key references

American Concrete Institute (ACI) ACI Committee 440 (2008). Guide for the design and construction of externally bonded FRP systems for strengthening concrete structures, ACI 440.2R-08.

CNR (National Research Council) Advisory Committee on technical recommendations for construction (2004). Guide for the Design and Construction of Externally Bonded FRP Systems for Strengthening Existing Structures, CNR-DT200/2004, Rome.

Concrete Society. (2012). Design guidance for strengthening concrete structures using fibre composite materials, TR-55.

Federation Internationale du Beton, Task Group 9.3 FRP Reinforcement for Concrete Structures. Externally bonded FRP reinforcement for RC structures (2001). Technical report on the design and use of externally bonded fibre reinforced polymer reinforcement (FRP EBR) for reinforced concrete structures, Fib Bulletin 14.

German Committee for Reinforced Concrete (2013). DAfStb Heft 595 Erläuterungen und Beispiele zur DAfStb-Richtlinie Verstärken von Betonbauteilen mit geklebter Bewehrung.

3.9 Databases and Modelling

Calibration of design formulas based on experimental tests

Antonio Bilotta[1], Francesca Ceroni[2] & Emidio Nigro[3]

[1]DIST – Department of Structures for Engineering and Architecture, University of Naples Federico II, Italy

antonio.bilotta@unina.it

[2]DING - Structural Engineering, University of Sannio, Italy

ceroni@unisannio.it

[3]DIST – Department of Structures for Engineering and Architecture, University of Naples Federico II, Italy

emidio.nigro@unina.it

Although the assessment of models for bond strength for concrete elements externally strengthened with FRP materials (both NSM and EBR systems) has been widely dealt with by various researchers, the definition of safety factors to calculate design values is still an open item. Thus, in this section a general procedure to calibrate design formulas based on experimental results of different types of tests (i.e. bond shear tests, bending tests for assess flexural or shear strength of beams and slabs) is showed (Monti et al., 2009). The procedure was developed in according to the 'design by testing' procedure suggested in the European codes (EN1990). The procedure is not devoted to introduce new strength models, but to refine the existing strength models suggested in literature and codes based on a consistent statistical analysis of a continuously increasing amount of experimental results. Indeed, the procedure allows different corrective factors to be assessed, in order to predict both mean and characteristic values of the investigated bond strength according to a Limit State design approach.

With reference to a general bond model, (e.g. for EBR-FRP strengthening systems or NSM ones), the resistance model can be expressed as:

$$P_{th} = b \cdot g_t\left(\underline{X}\right) \tag{1}$$

where $g_t\left(\underline{X}\right)$ is the theoretical resistance model, function of the vector $\underline{X}$ containing all the geometrical and mechanical parameter included in the model (e.g. for EBR systems $\underline{X} = \left\{E_f, t_f, b_f, k_b, f_{cm}, f_{ctm}\right\}$)

The strength model is fine-tuned by the least-square coefficient, *b*, which minimizes the difference between each theoretical and experimental value of the database. Usually, this can be simply carried out considering the regression line of the graph $\varepsilon_{th,i}$ vs. $\varepsilon_{exp,i}$. The slope of this line provides the least-square coefficient, *b*.

After the definition of the strength model (Monti et al., 2009) and in order to correct the model error, a random variable δ should be defined as the ratio of the experimental value to the theoretical one.

The variable δ is related to the maximum strain in the FRP reinforcement at failure, as follows:

$$\delta_i = \frac{\varepsilon_{\max,\exp,i}}{\varepsilon_{\max,th,i}} \tag{2}$$

Thus, the mean provision for the maximum strain can be assumed as:

$$\varepsilon_{\max,th,m} = \overline{\delta} \cdot \varepsilon_{\max,th} \tag{3}$$

In the Eq. (3) the model error is represented by $\overline{\delta}$, that is the mean value of the variable δ_i.

In the State Limit approach, any strength is assumed as a random variable and, in general, the 5% percentile (usually named 'characteristic value') of its frequency distribution is used for design purposes. A very suitable distribution is the Gaussian one, but the check of the normality hypothesis of the random variable should be required to use it. In order to check the normality assumption of

the variable δ, the curve of cumulative frequency of δ can be compared with the theoretical Gaussian distribution having the same mean and standard deviation for the considered set of data. An example of acceptable agreement between the experimental and the theoretical distribution is showed in Figure 1. Also statistical tests, such as Kolmogorov-Smirnov, are suitable to check the normality hypothesis. When the normality hypothesis is rejected, the theoretical lognormal distribution can be assumed in order to achieve a better fitting of the experimental results (Ceroni and Pecce, 2012).

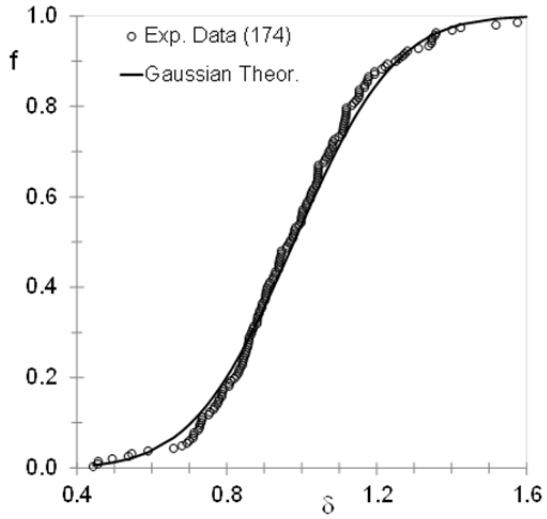

Figure 1 - Experimental vs. theoretical cumulative frequency curves of variable δ.

Thus, if the maximum strain is assumed as a random variable having a Gaussian distribution the 5% percentile of the maximum strain can be calculated as:

$$\varepsilon_{\max,th,5\%} = \varepsilon_{\max,th,m} - 1.64 \cdot \left[Var\left(\varepsilon_{\max,th,m}\right)\right]^{0.5} \quad (4)$$

where the variance of $\varepsilon_{max,th,m}$ can be expressed as function of the variance of the mechanical parameters influencing the bond model and of the variable δ (Monti et al., 2009; EN1990 – Annex D).

For example, if the mechanical parameter is only E_f, the variance of $\varepsilon_{max,th,m}$ can be expressed as follows:

$$Var\left(\varepsilon_{\max,th,m}\right) = C_{E_f}^2 \cdot Var\left(E_f\right) + C_{\delta}^2 \cdot Var\left(\delta\right) \quad (5)$$

Indeed, the geometrical properties can be considered as deterministic values fixed in the design and not random variables. Mechanical properties are generally characterized by Gaussian distributions. If necessary, the variance, i.e. the Coefficient of Variation (*CoV*), of material mechanical properties can be assessed according to literature information (Bilotta et al 2011).

References

Bilotta A., Di Ludovico M., Nigro E. (2011). FRP-to-Concrete Interface Debonding: Experimental Calibration of a Capacity Model. COMPOSITES. PART B, ENGINEERING, vol. 42, p. 1539-1553, ISSN: 1359-8368

Ceroni F., Pecce M. (2012). Statistical analysis of debonding load in concrete elements externally strengthened with CFRP materials, Advances in Structural Engineering Vol. 15 No. 1, pp. 155-168.

European Committee for Standardization. (2002) EN 1990 - Eurocode - Basic of Structural Design. 2002.

Monti G., Alessandri S., Santini S. (2009). Design by Testing: A Procedure for the Statistical Determination of Capacity Models, Journal of Construction and Building Materials, Special Issue on FRP Composites, Vol. 23, pp. 1487-1494, Elsevier.

Published Tests on Concrete Confined with FRP Jackets

I. Balafas, Instructor, Dept. Civil & Env. Eng., University of Cyprus, Cyprus, ibalafas@ucy.ac.cy
S.P. Tastani, Lecturer, Civil Eng. Dept., Democritus Univ. of Thrace, Greece, stastani@civil.duth.gr
S.J. Pantazopoulou, Dept. Civil & Env. Eng., University of Cyprus, Cyprus, pantazopoulou.stavroula@ucy.ac.cy

Description

A unified database is assembled by merging several individual databases found in the literature (listed in the References). Criteria for inclusion of any given test is the requirement that lateral strains have been measured on the FRP jacket and reported during the test, at least up to the onset of failure. This strain measure is required so that lateral confining pressures, responsible for the strength and deformation capacity enhancement, may be estimated and considered explicitly in the exercise of calibration of the analytical models.

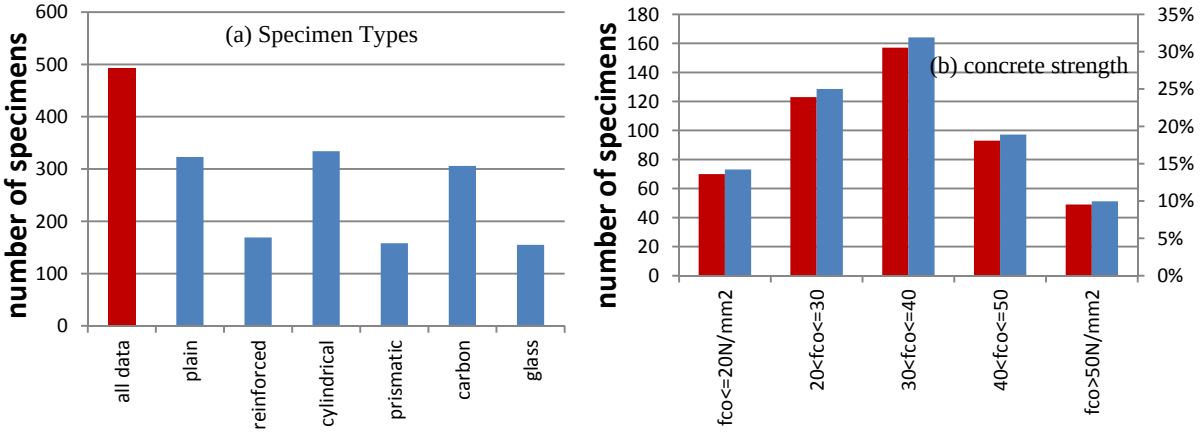

Figure (a) and (b): (a): The distribution of available tests in the database. (b) Concrete strength of specimens. The axis to the right represents the percentage over the total available number, of each specimen category.

Figure (a) outlines the range of parameters included in the available database of tests. Data are classified based on the shape of the specimen cross-section and the presence or not, of internal reinforcement. Numbers of reported samples decrease when going from plain to reinforced, or from specimens with circular to rectangular cross sections. Reinforced specimens are intended to model columns with brittle details, which are the most likely candidates for jacketing in real retrofit applications. About two in three of the specimens studied in either group have a circular encased cross section, whereas the remaining specimens have orthogonal cross sections. For this reason the available specimens are further subdivided in four subsets: (a) specimens with a circular cross-section and without steel reinforcement, (b) specimen with a circular cross-section and steel reinforcement, (c) specimens with a rectangular cross-section, without steel reinforcement, and (d) specimens with a rectangular cross-section and embedded steel reinforcement. In this database, the experimental values of peak stress, ultimate stress, ultimate axial strain, and axial strain corresponding to peak stress are included for each specimen together with the geometrical characteristics of the specimen and mechanical properties of the materials (concrete, steel and FRP).

More than 1000 specimens are available in the literature under the first category (plain concrete, subsets (a) and (b)), but the number of specimens that report lateral strain records is only around 500. Unreinforced specimens are used to study the confinement effectiveness on strength and strain capacity of plain concrete: reported specimen failures in these cases are owing to one of the following causes: (i) debonding of the jacket, (ii) rupture at the corners due to stress concentration (in orthogonal cross

sections), (iii) exhausting the strain capacity of the jacket due to dilation of the encased concrete material.

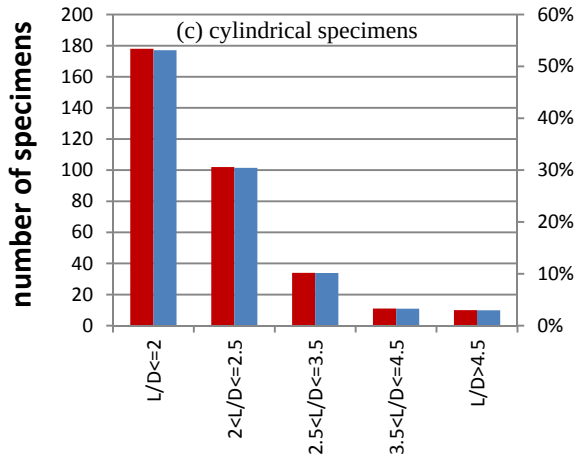

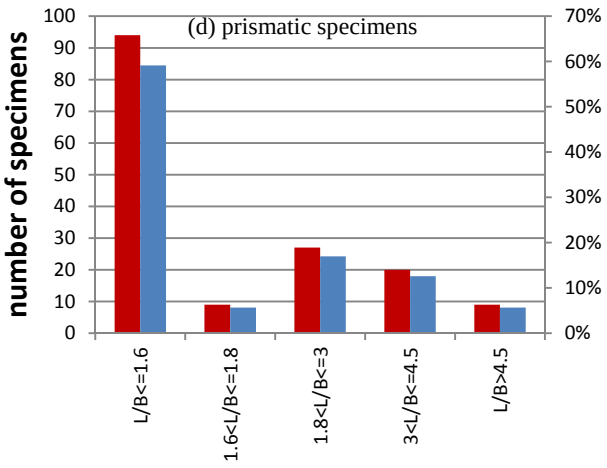

Figures (c) and (d): Aspect ratio (height to diameter/side) of available cylindrical and prismatic specimens.

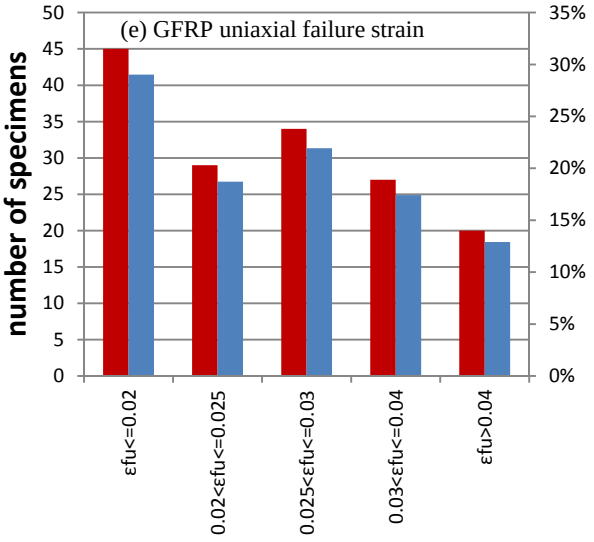

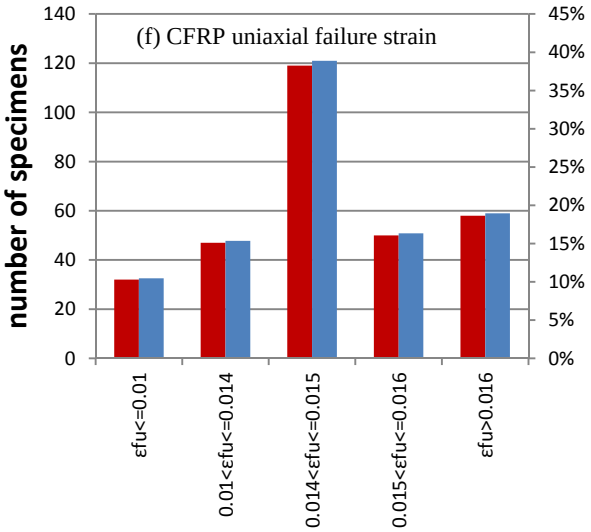

Figures (e) and (f): Coupon failure strain (ε_{fu}) for GFRP and CFRP jackets.

The response of FRP encased, plain concrete typically follows a bilinear stress – strain law, where the stiffness of the ascending branch primarily depends on the properties of concrete, whereas the slope of the hardening branch is determined by the stiffness of the jacket. Parameters of study in this database are, the jacketing material type, the number of jacket layers, the fiber orientation in the wrap (measured by the angle of placement of the wrap weave relative to the direction of axial compression), the layout of the jacket sheets (continuous or strips), the strength of encased concrete, f_{co}, and the radius of chamfer used in the corners.

A total of 150 specimens are FRP-jacketed reinforced-concrete columns (subsets (c) and (d)). In terms of scale, several are simple cylinders and prisms reinforced with embedded longitudinal and transverse reinforcement, having an aspect ratio (height to cross section height) around 2 (specimen height is usually around 300-400mm whereas a typical cross sectional dimension is in the range of 150 – 200 mm; in most cases, dimensions of specimens are prescribed by limitations in the testing equipment). A number of specimens are full scale columns with height to section aspect ratio well above 2, and much larger dimensions and embedded reinforcement sizes than the common example.

Figures (i) and (j) give the ratios of confined to unconfined concrete strengths, further normalized by the

lateral confining pressure at peak load, $(f_{cc}/f_{co})/\sigma_{lat}$ –this variable illustrates the strength ratio increase achieved, for each MPa of lateral confining pressure – for example a value of the ratio equal to 0.3 means that 1 MPa pressure will achieve 30% confined strength increase.
Similarly, Figures (k) and (l) report the ratio of confined to unconfined concrete strain at peak stress, normalized by the lateral pressure, $(\varepsilon_{cc}/\varepsilon_{co})/\sigma_{lat.}$ The variable illustrates the strain capacity increase for each MPa of lateral pressure.

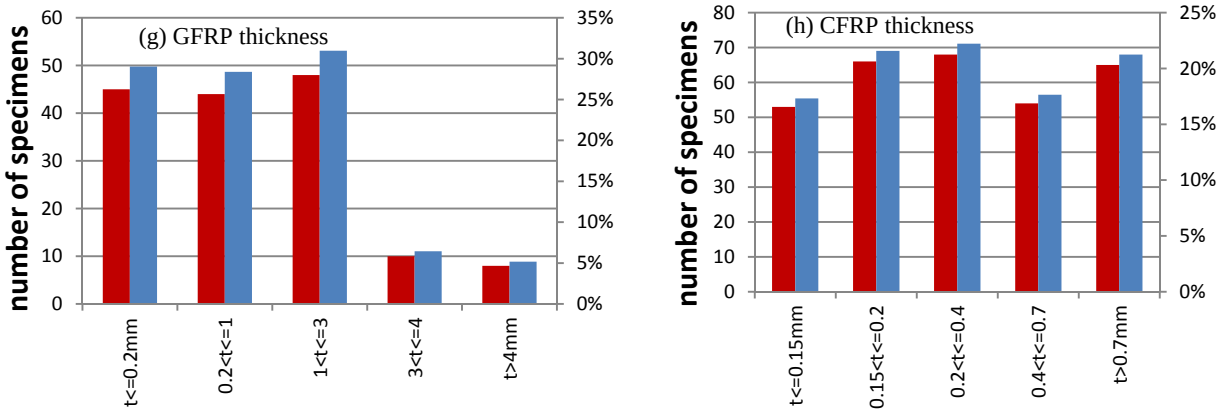

Figures (g) and (h): GFRP and CFRP jacket thickness over the total number of tests.

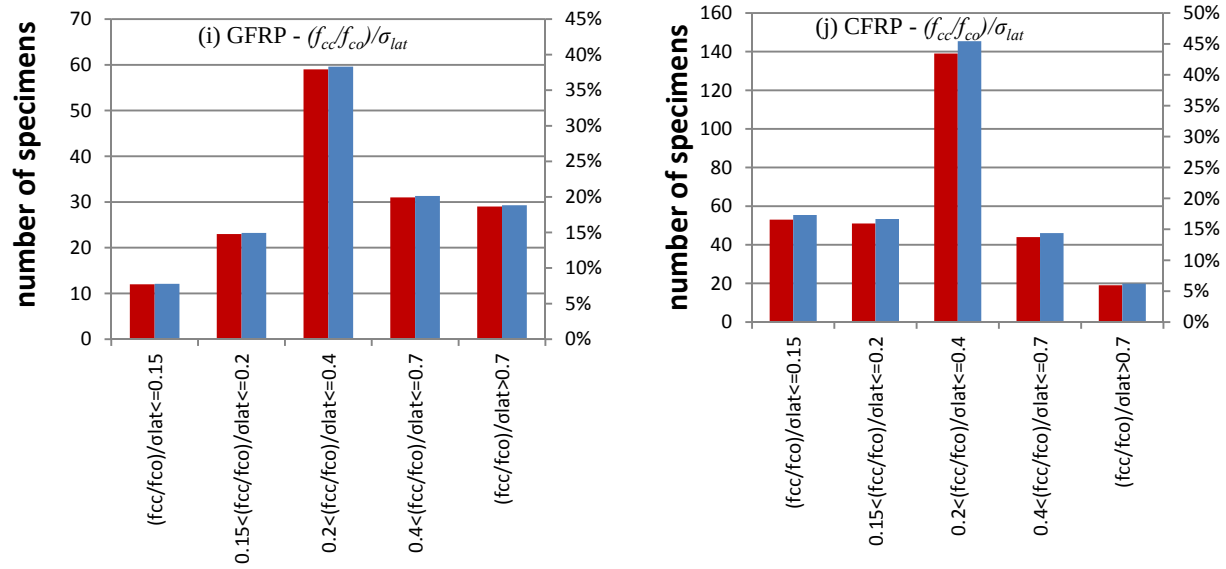

Figures (i) and (j): Ratio of confined to unconfined concrete strength, normalized to lateral confining pressure at peak response, $(f_{cc}/f_{co})/\sigma_{lat,}$ for GFRP and CFRP jackets respectively.

Finally, Figures (m) and (n) show the confinement efficiency based on tests (k_e = ratio of FRP jacket average strain / strain capacity measured from coupon tests) for glass and carbon fiber wraps.

Database extension and usage

The intention is to extend the database so that most of the published data are included. Available experimental literature comprises a diverse collection of specimen subgroups originating from different investigations published in the literature. Typically, each investigation considers a relatively small number of specimens (up to 20 on average), so parametric influences determined through these studies only account for a small range of combinations of values for the important parameters. To obtain a spherical assessment of analytical models through calibration with the test results, the boundaries posed by the individual experimental studies need to be overcome by a collective consideration of all the available data into a single extended database.

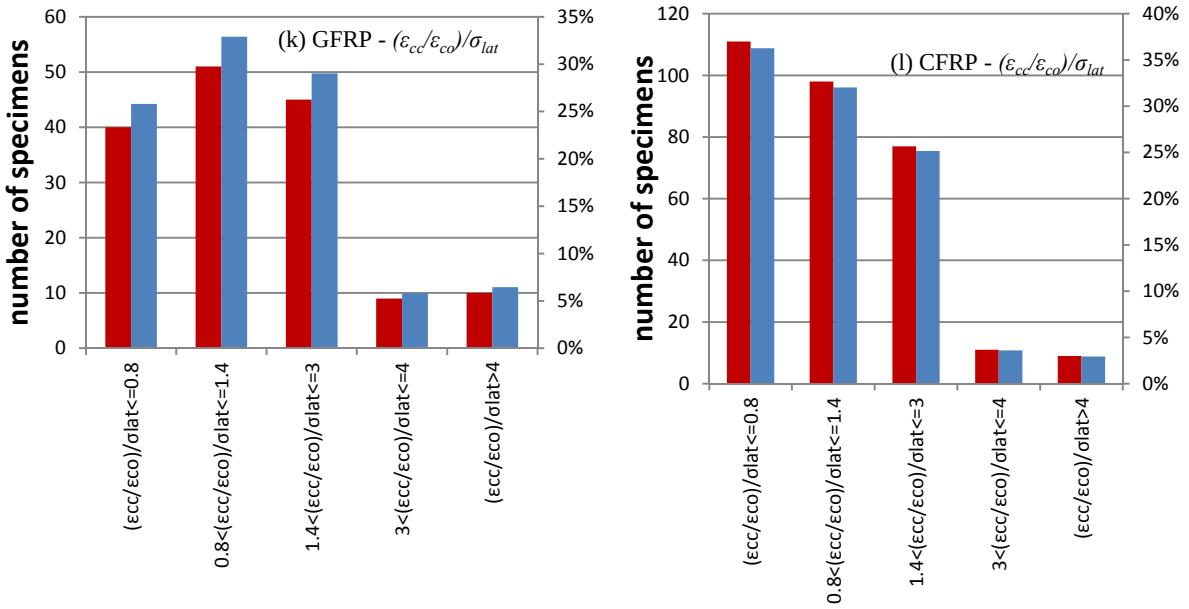

Figures (k) and (l): Ratio of confined to unconfined concrete strain at peak stress, normalized to lateral confining pressure at peak response, $(\varepsilon_{cc}/\varepsilon_{co})/\sigma_{lat}$, for GFRP and CFRP jackets respectively.

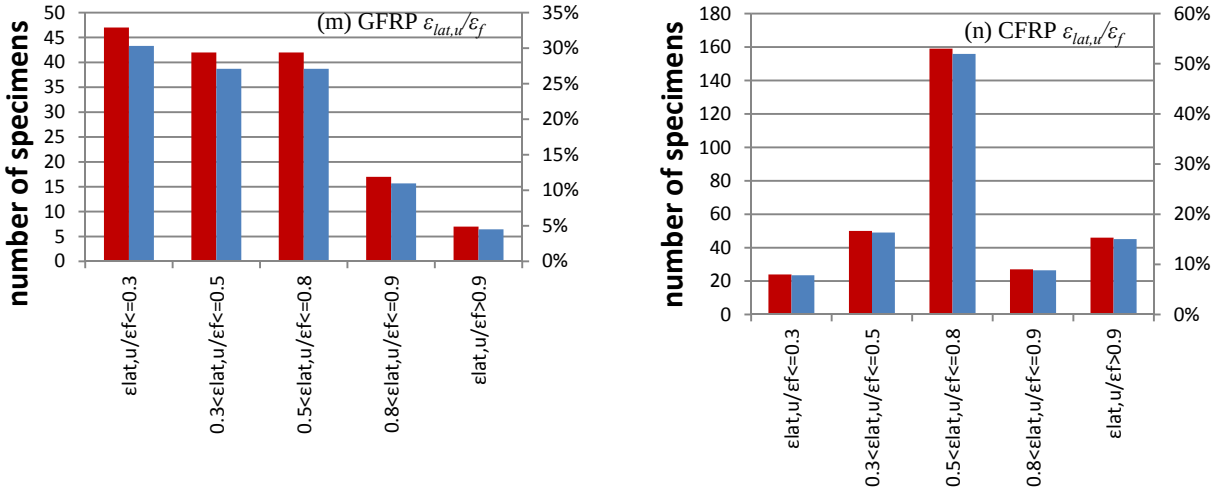

Figures (m) and (n): Confinement efficiency based on tests (k_e = ratio of FRP jacket average strain / strain capacity measured from coupon tests) for glass and carbon fiber wraps.

References – Plain Concrete

Ahmad SH, Khaloo AR, Irshaid A. (1991). "Behavior of concrete spirally confined by fiberglass filaments". Mag Concrete Res, 43(156):143–148.

Aire C, Gettu R, Casas JR. (2001). Study of the compressive behaviour of concrete confined by fiber reinforced composites. In: Proc. of the international conference ''composites in constructions''. Lisse (NL): Balkema Publishers, p. 239–243.

Almusallam TH. (2007). "Behavior of normal and high-strength concrete cylinders confined with E-glass/epoxy composite laminates." Composites: Part B, 38: 629–639.

Arduini M, Di Tommaso A, Manfroni O, Ferrari S, Romagnolo M. (1999). Il Confinamento Passivo di Elementi Compressi in Calcestruzzo con Fogli di Materiale Composito. Industria Italiana del Cemento;1:836–41 [in Italian].

Berthet JF, Ferrier E, Hamelin P. (2005). "Compressive behavior of concrete externally confined by composite jackets. Part A: experimental study." Constr Build Mater, 19:223–32.

Bortolotti L, Lai S, Carta S, Cireddu D. (1999). Comportamento a Carico Assiale di Conglomerati ad Alta Resistenza Confinati con Tessuto di Fibra di Carbonio. In: Proc. of Atti delle Giornate AICAP Conf., vol. 1. Turin, November,. p. 5–14 [in Italian].

Bullo S. (2003). Experimental study of the effects of the ultimate strain of fiber reinforced plastic jackets on the behavior of confined concrete. In: Proc. of the international conference ‘‘composites in construction’’. Cosenza; Italy, p. 465–470.

Campione G, Miraglia N. (2003). “Strength and strain capacities of concrete compression members reinforced with FRP.” Cement Concrete Compos, 25:31–41.

Carey S, Harries KA. (2005). “Axial behavior and modeling of confined small-, medium-, and large-scale circular sections with carbon fiber-reinforced polymer jackets.” ACI Struct J, 102(4):596–604.

Ciupala MA, Pilakoutas K, Mortazavi AA. (2007). Effectiveness of FRP composites in confined concrete. In: Proc. of FRPRCS-8 int. symposium. Patras, Greece; July, p. 1–10.

Cui C. (2009). Behaviour of normal and high strength concrete confined with fibre reinforced polymers (FRP). MSc Thesis, University of Toronto. p. 1–376.

De Lorenzis L, Micelli F, La Tegola A. (2002) Influence of specimen size and resin type on the behavior of FRP confined concrete cylinders. In: Proc. of the 1st int. conf. ‘‘advanced polymer composites for structural applications in construction’’. London (UK): Thomas Telford; p. 231–9.

Demers M, Neale KW. (1994). Strengthening of concrete columns with unidirectional composite sheets. In: Proc. of the 4th int conf on short and medium bridges. Montreal. p. 895–905.

Faella C, Realfonzo R, Salerno N. (2005). R/C elements confined by FRP. In: ACI special publication. Spring Convention, New York; April.

Faella C, Realfonzo R, Salerno N. (2004). Sulla resistenza e deformazione di elementi in c.a. confinati con tessuti in FRP. In: Proc. of the XI national congress ‘‘L’ingegneria sismica in Italia’’. Genova; January [in Italian].

Harmon TG, Slattery KT. (1992). Advanced composite confinement of concrete. In: Proc. of the 1st int. conf. on advanced composite materials in bridges and structures. Sherbrooke, Québec; October. p. 29–306.

Harries KA, Carey SA. (2002). “Shape and gap effects on the behavior of variably confined concrete”. Cement Concrete Res. 33:881–90.

Harries KA, Kharel G. (2003). “Experimental investigation of the behavior of variably confined concrete”. Cement Concrete Res. 33:873–80.

Howie I, Karbhari VM. (1994). Effect of materials architecture on strengthening efficiency of composite wraps for deteriorating columns in the north-east. In: Basham KD, editor. Proc. of the 3rd mater. eng. conf., infrastructure: new materials and methods of repair. Material engineering division. ASCE. p. 199–206.

Ilki A., Peker O., Karamuk E., Demir C., Kumbasar N., (2008). “FRP retrofit of low and medium strength circular and rectangular reinforced concrete columns”, ASCE Journal of Materials in Civil Engineering, 20(2): 169-188.

Jiang T, Teng JG. (2007). “Analysis-oriented stress–strain models for FRP-confined concrete.” Eng Struct. 29:2968–2986.

Karabinis AI, Rousakis TC. (2001). Carbon FRP confined concrete elements under axial load. In: Proc. of the 3rd int conf ‘‘FRP composites in civil engineering’’, CICE 2001. Hong Kong; December.

Karbhari VM, Gao Y. (1997). “Composite jacketed concrete under uniaxial compression-verification of simple design equations.” J Mater Civil Eng. 9(4):185–93.

Kono S, Inazumi M, Kaku T. (1998). Evaluation of confining effects of CFRP sheets on reinforced concrete members. In: Proc. of ICCI ’98 conf. Tucson, Ariz. p. 343–55.

Lam L, Teng JG. (2004). “Ultimate condition of fiber reinforced polymer-confined concrete.” J Compos Constr, 8(6): 539–48.

Lam L, Teng JG, Cheung CH, Xiao Y. (2006). “FRP-confined concrete under cyclic axial compression.” Cement Concrete Compos, 28(10): 948–58.

Li G. (2006). “Experimental study of FRP confined concrete cylinders.” Eng Struct, 28:1001–8.

Lin C, Li Y. (2003). “An effective peak stress formula for concrete confined with carbon fibre reinforced plastics.” Can J Civil Eng, 30: 882–9.

Lin HJ, Liao CI. (2004). “Compressive strength of reinforced concrete column confined by composite material.” Compos Struct, 65: 239–50.

Mandal S, Hoskin A, Fam A. (2005). “Influence of concrete strength on confinement effectiveness of fiber-reinforced polymer circular jackets.” ACI Struct J. 102(3): 383–92.

Mastrapa J.C., (1997). The effect of construction bond on confinement with FRP composites. MSc thesis. University of Central Florida, Orlando, Florida.

Matthys S, Taerwe L, Audenaert K. (1999). Tests on axially loaded concrete columns confined by fiber reinforced polymer sheet wrapping. In: Proc. of the fourth int. symposium on fiber reinforced polymer reinforcement for reinforced concrete structures, ACI SP-188, Michigan, USA. p. 217– 29.

Micelli F, Myers JJ, Murthy S. (2001). Effect of environmental cycles on concrete cylinders confined with FRP. In: Proc. of the int. conf. ‘‘composites in constructions’’. Lisse, NL, Balkema Publishers. p. 317–22.

Miyauchi K, Nishbayashi S, Inoue S., (1997). Estimation of strengthening effects with carbon fiber sheet for concrete column. In: Proc. of FRPRCS-3 int. symposium. Japan Concrete Institute, Sapporo, Japan; October. p. 217–24.

Modarelli R, Micelli F, Manni O., (2005). FRP-confinement of hollow concrete cylinders and prisms. In: Proc. of FRPRCS-7 int. symposium. Kansas City, USA; November. p. 1–18.

Nanni A, Bradford NM., (1995). "FRP jacketed concrete under uniaxial compression." Constr Build Mater, 9(2):115–24.

Pessiki S, Harries KA, Kestner JT, Sause R, Ricles JM, (2001). "Axial behavior of reinforced concrete columns confined with FRP jackets." J Compos Constr, 5(4):237–45.

Pessiki S., Harries K., Kestner J., Sause R., Ricles J., (2001). "Axial behavior of RC columns confined with FRP jackets", ASCE Journal of Composites for Construction, 5(4): 237-245.

Picher F, Rochette P, Labossiére P. (1996). Confinement of concrete cylinders with CFRP. In: Proc. of ICCI '96 conf. Tucson, Arizona; January. p. 829–41.

Purba BK, Mufti AA. (1999). "Investigation of the behavior of circular concrete columns reinforced with carbon fiber reinforced polymer (CFRP) jackets." Can J Civil Eng, 26:590–6.

Richart F., Brandtzaeg A., Brown R., (1928). "Study of failure of concrete under combined compressive stresses", Bull. No. 185, Eng. Experiment Station Univ. of Illinois, Urbana, III.

Rochette P, Labossière P. (2000). "Axial testing of rectangular column models confined with composites." J Compos Constr, 4(3):129–36.

Rousakis T, You C, De Lorenzis L, Tamuz˘s V, Tepfers R. (2003). Concrete cylinders confined by carbon FRP sheets subjected to monotonic and cyclic axial compressive load. In: Tan KH, editor. Proc. of FRPRCS-6 int. symposium, Singapore; July. p. 571–80.

Rousakis T. (2001). Experimental investigation of concrete cylinders confined by carbon FRP sheets, under monotonic and cyclic axial compressive load. Research report, Chalmers University of Technology, Göteborg, Sweden.

Rousakis T.C., Karabinis A.I. (2012). "Adequately FRP confined reinforced concrete columns under axial compressive monotonic or cyclic loading." Materials and Structures, 45:957–975.

Rousakis T.C., Karabinis A.I., Kiousis P.D. (2007). "FRP-confined concrete members: Axial compression experiments and plasticity modeling." Engineering Structures 29: 1343–1353.

Shahawy M, Mirmiran A, Beitelamann T. (2000). "Tests and modelling of carbon- wrapped concrete columns." Composites: Part B, 31:471–80.

Shehata IAEM, Carneiro LAV, Shehata LCD. (2007). Strength of confined short concrete columns. In: Proc. of FRPRCS-8 int. symposium. Patras, Greece; July. p. 1– 10.

Silva MAG, Rodrigues CC. (2006). "Size and relative stiffness effects on compressive failure of concrete columns wrapped with glass FRP." J Mater Civil Eng, 18(3):334–42.

Tastani S., Pantazopoulou S.J., (2008). "Detailing procedures for seismic rehabilitation of RC members with fiber reinforced polymers", Engineering Structures, 30(2): 450-461.

Teng JG, Yu T, Wong YL, Dong SL. (2007). "Hybrid FRP–concrete–steel tubular columns: concept and behaviour." Constr Build Mater, 21(4): 846–54.

Thériault M, Neale KW M, Claude S. (2004). "Fiber reinforced polymer-confined circular concrete columns: investigation of size and slenderness effects." J Compos Constr, 8(4): 323–31.

Toutanji HA. (1999). "Stress–strain characteristics of concrete columns externally confined with advanced fiber composite sheets." ACI Mater J., 96(3): 397–404.

Wang LM, Wu YF. (2008). "Effect of corner radius on the performance of CFRP-confined square concrete columns: test". Eng Struct, 30: 493–505.

Wang Z., Wanga D., Smith S.T. and Lu D. (2012). "Experimental testing and analytical modeling of CFRP-confined large circular RC columns subjected to cyclic axial compression." Engineering Structures 40: 64–74.

Watanabe K, Nakamura H, Honda T, Toyoshima M, Iso M, Fujimaki T, et al. (1997). Confinement effect of FRP sheet on strength and ductility of concrete cylinders under uniaxial compression. In: Proc. of FRPRCS-3 int. symposium, vol. 1, Sapporo, Japan. p. 233–40.

Wu G, Wu ZS, Lu ZT, Ando YB. (2006). "Experimental study on concrete cylinders confined with various FRP under uniaxial compression." ACI Special Publ, SP-238-23: 381–94.

Xiao Y, Wu H. (2000). "Compressive behavior of concrete confined by carbon fiber composite jackets." J Mater Civil Eng, 12(2): 139–46.

Yan Z, Pantelides CP, Reavely LD. (2006). "Fiber-reinforced polymer jacketed and shape-modified compression members. I: experimental behavior." ACI Struct J, 103(6):885–93.

Zhang S, Ye L, Mai YW. (2000). "A study on polymer composites strengthening system for concrete columns." Appl Compos Mater, 7(2–3): 125–38.

References – Reinforced Concrete

De Diego A., Artega A., Recurero A., Lopez-Hombrados C., “Strengthening of square RC columns using FRPs”, FIB 2nd International Congress, CD ROM Proc., Naples, Italy.

Ilki A., Peker O., Karamuk E., Demir C., Kumbasar N., (2008). “FRP retrofit of low and medium strength circular and rectangular reinforced concrete columns”, ASCE Journal of Materials in Civil Engineering, 20(2): 169-188.

Karabinis A.I., Rousakis T.C., (2006). “FRP confining effects on steel reinforced concrete square sections subjected to axial load”, FIB 2nd International Congress, CD ROM Proc., Naples, Italy.

Matthys S., Toutanji H., Audenaert K., Taerwe L., (2005). “Axial load behavior of large-scale columns confined with FRP composites”, ACI Structural Journal, 102(2): 258-267.

Pan J., Xu T., Hu Z., (2007). “Experimental investigation of load carrying capacity of the slender RC columns wrapped with FRP”, Construction and Building Materials, Vol. 21: 1991-1996.

Paula R., Silva M., (2003). “Sharp edge effects on FRP confinement of RC square columns”, University Nova de Lisboa, Portugal. http://www.quakewrap. Com.

Pessiki S, Harries KA, Kestner JT, Sause R, Ricles JM. (2001). Axial behavior of reinforced concrete columns confined with FRP jackets. J Compos Constr. 5(4): 237–45.

Rousakis T.C., Karabinis A.I. (2012). Adequately FRP confined reinforced concrete columns under axial compressive monotonic or cyclic loading. Materials and Structures, 45:957–975.

Tastani S., Pantazopoulou S., Zdoumba D., Plakantaras, V., Akritidis E., (2006). “Limitations of FRP-jacketing in confining old-type RC members in axial compression”, ASCE Journal of Composites for Construction, 10(1): 13-25.

Wang Z., Wanga D., Smith S.T. and Lu D. (2012). Experimental testing and analytical modeling of CFRP-confined large circular RC columns subjected to cyclic axial compression, Engineering Structures 40: 64–74.

Wang, Y., Resprero, N., (2001). “Investigation of concentrically loaded RC columns confined with glass FRP jackets”, ACI Structural Journal, 98(3): 377-385.

Upgraded Experimental Database for FRP Confined Concrete

T.C. Rousakis[1], N. Nistico[2], A.I. Karabinis[3]

Introduction

Current studies concerning statistical elaboration and review of existing experimental results in databases for confined concrete, usually include only the characteristic maximum bearing stress and corresponding strain values as well as the failure values. In cases of confined concrete members failure values may be defined at 20% or 15% drop of maximum load (when the post-peak load behaviour is degrading) or upon fracture of the FRP jacket. Existing international guides and codes provide semi-empirical relations to predict strength and strain at failure. Also, relations for the whole stress - axial strain curve are included. Fewer involve also prediction of the stress – lateral strain behaviour. Several existing recommendations include additional failure criteria related to lateral strain level or axial strain level in order to ensure the integrity of the columns or avoidance of shear failures among else. ACI 440.2R-08 and CNR-DT200 refer to 0.4% lateral strain as a limit value to avoid concrete shear failures. ACI 440.2R-08 also restricts the maximum compressive strain to 1% to prevent excessive cracking and the resulting loss of concrete integrity. Thus, design of FRP confined columns requires the estimation of stress and axial strain values at 0.4% lateral strain limit and stress at 1% axial strain, through reliable models.

The contribution focus on the preliminary results of an advanced experimental database based on the whole stress-strain response curves. The database provides significant data necessary for the extensive assessment of the existing design models. The experimental database contains information on: a) the failure stress and strain values, b) on the stress and strain values at the level of 0.4% lateral strain as well as c) on the stress at the level of 1% axial strain.

Axial strain prediction is poor for most of the existing models according to several assessment studies. Thus, the elaboration concerned the performance of strength models recommended by existing guidelines when compared against gathered experimental values. It investigated the ability of the strength models proposed by existing codes to predict stress at failure assuming that the effective lateral stress is known (use of experimental lateral strain). Then all models were assessed with respect to their predictions for the stress at 0.4% lateral strain and at 1% axial strain by using the corresponding experimental lateral strain at the 1% axial strain level. All strength predictions were compared against experimental values.

The elaboration suggests that the upgraded database based on whole stress-strain curves is necessary to ensure reliable design for confinement for different limit states. More details on the upgraded database can be found in Rousakis et al. 2012.

Confinement models in existing guidelines

The elaboration included the semi-empirical simple design relations proposed by different guides and codes for strength predictions: *fib* bulletin 14 model, the CNR DT200/2004 model, the ACI 440.2R-08 model and the Greek Retrofit Code (GRECO) model. The empirical model by Realfonzo & Napoli was also included in the elaboration as it involved a statistical elaboration of most recent experimental data.

Upgraded experimental database on uniform confinement

The database contained a total of 116 experimental results from the following 11 studies that provided the whole stress - axial and lateral strain curves: Nanni & Bradford 1995, Picher et al 1996, Hosotani et

[1] Democritus University of Thrace, Xanthi, Greece, trousak@civil.duth.gr
[2] Sapienza Università di Roma, Italy, nicola.nistico@uniroma1.it
[3] Democritus University of Thrace, Xanthi, Greece, karabin@civil.duth.gr

al 1997, Mirmiran & Shahawy 1997, Saafi et al 1999, Rousakis 2001, Karabinis & Rousakis 2002, Rousakis 2005, Berthet et al 2005, Valdmanis et al 2007 and Almusallam 2007. They covered carbon and glass FRP wraps and tubes. The elastic modulus of the jackets ranged between 27 GPa and 415 GPa. The specimens had plain concrete strength from 25.2 MPa to 171 MPa. The data were grouped in three different categories (Rousakis et al. 2012) as some of the specimens did not reach the 0.01 axial strain or the 0.004 lateral strain level. Twenty specimens had failure values below 0.01 axial strain and 0.004 lateral strain.

Predictive performance of existing models

The database compared the accuracy of the above-mentioned five strength models against the experimental strengths. The analytical predictions were generated using the experimental values of the ultimate lateral strain, of the 0.4% lateral strain and of the lateral strain corresponding to 1% axial strain.

The accuracy of the models was assessed by the parameter A of the equation of the trend line (y=Ax) and the correlation coefficient R^2 of the comparative diagrams. Accurate models exhibit A and R^2 close to 1. The most accurate predictions of ultimate concrete strength assuming the experimental lateral strain at failure, were provided by the Realfonzo & Napoli (A=0.986, R^2 = 0.83) and the ACI model (A=1.025, R^2 = 0.85). The correlation coefficient R^2 was close to the one achieved when relating the concrete strength enhancement and the normalized lateral pressure assuming the experimental ultimate lateral strain. The model of the Greek retrofit code underestimated tests (A=1.077, R^2 = 0.85) while the CNR model overestimated experiments (A=0.958, R^2 = 0.85). The *fib* model significantly underestimated experiments (A=1.168, R^2 = 0.82).

At 0.4% lateral strain the performance of the strength models was worse than for ultimate FRP strain. Realfonzo & Napoli model again provided a fair accurate underestimated overall prediction (A=1.044, R^2 = 0.83). The GRECO model (A=1.066, R^2 = 0.77) and ACI model (A=1.073, R^2 = 0.83) further underestimated tests while CNR model (A=0.942, R^2 = 0.8) overestimated experiments.

The predicted strength at 1% axial strain presented even lower correlation and lower accuracy with respect to the experimental values (Figure 1). The best predictions were given by Realfonzo & Napoli (A=1.043, R^2 = 0.76), ACI (A=1.074, R^2 = 0.76) and GRECO (A=1.082, R^2 = 0.76) models. CNR presented a

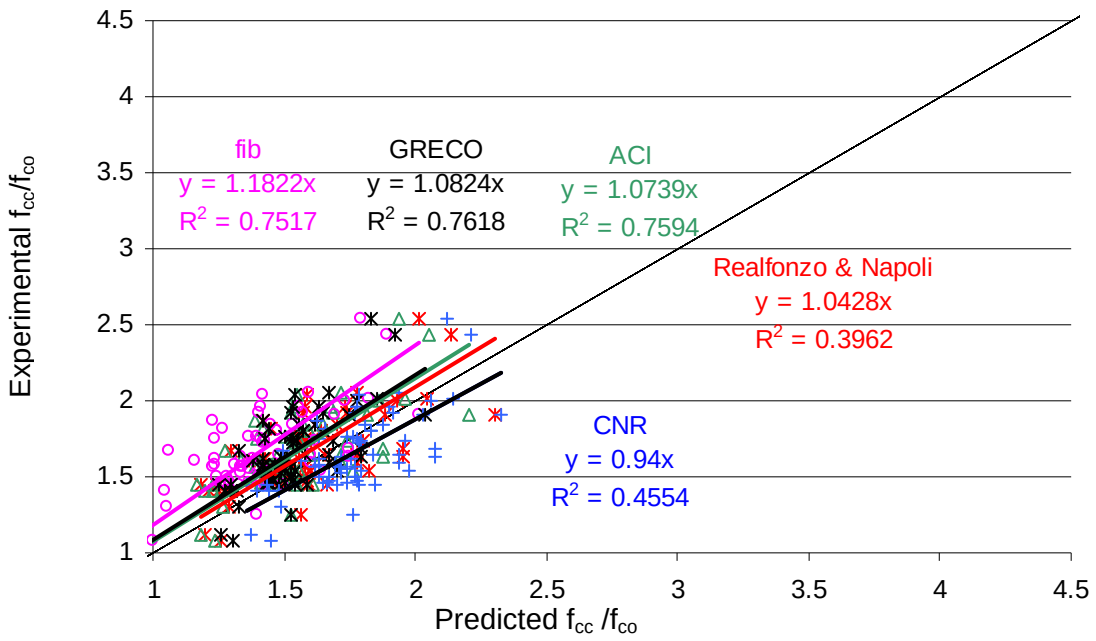

Figure 1: Predicted normalized strength of confined concrete with different existing models versus experiments

poor correlation (A=0.94, R^2 = 0.46). *fib* model deviated significantly from experimental strength values (A=1.182, R^2 = 0.75).

Conclusions and Points for Discussions

The research investigated the viability of the use of the codes' empirical models in predicting the strength of confined concrete at intermediate strain levels. It seems that most of the existing empirical strength models could also provide concrete stress at 0.4% lateral strain level with reasonable accuracy.

The correlation of the experimental concrete strengths versus the experimental lateral pressure exerted by the FRP confinement for the prediction of the strength at 1% axial strain, was very low. As expected, the strength prediction of all models at 1% axial strain presented low correlation, even if the experimental lateral strains corresponding to above level of axial strain were known. Reliable analysis – oriented models provided by the codes should be used in order to estimate the concrete strength at 1% axial strain. The presented upgraded database coming out of full stress-strain curves should be further developed, as it is necessary in order to ensure reliable design for confinement for different limit states.

Key references

Rousakis T., Nistico N., Karabinis A. (2012). Upgraded Experimental Database of Uniformly FRP Confined Concrete Columns for Assessment of Existing Recommendations. *In: Monti J. (ed.) The 6th International Conference on FRP Composites in Civil Engineering – CICE 2012.* Rome 13 - 15 of June 2012. http://www.iifc-hq.org/publications/proceedings-iifc-official-conferences/cice-2012-rome-italy-13-15-june-2012/

Numerical Model of FRP Strengthened Reinforced Concrete in Plane Stress State

V. Vitanov[1]

Introduction

The increased experimental research in the field of structural strengthening using FRP initiated attempts to simulate the behaviour of reinforced concrete strengthened with FRP composites using the finite element method. The majority of the numerical models of FRP strengthened RC members use element overlaying, where one-, two- or even three dimensional elements (solid or layered) that represent the FRP material are placed over the concrete elements, either with (Khomwan & Foster 2004; Wong & Vecchio 2003) or without (Kheyroddin & Naderpour 2008) interface elements which are used to model the adhesive material or the bond between the FRP and the concrete.

An attempt to formulate a material model which will simplify the modeling of FRP strengthened reinforced concrete members (Vitanov 2012b) is presented here. The material model is implemented into ANSYS and tested using experimental data available in the literature.

Model Formulation

The material model presented here is based on the inelastic model for biaxial loading of reinforced concrete of Darwin and Pecknold (1974) which was formulated to be used for structures that can be considered to be in the plane stress state (shear walls, beams, slabs, shear panels, shells, reactor containment vessels) in conjunction with the finite element method. The concrete in this model is treated as incrementally linear, elastic material, which means that during each load increment the material is assumed to behave elastically. Furthermore, it is also considered to exhibit stress-induced orthotropic material behaviour – the material is treated as isotropic before and orthotropic after a crack occurs. The model adopts the fixed and ”smeared crack” approach when modeling the cracking behavior of the concrete. In order to keep track of the material degradation, the concept of “equivalent uniaxial strain” is used. It allows derivation of the actual biaxial stress-strain curves from uniaxial curves. A simple, bilinear model with strain hardening is adopted for the stress-strain behaviour of the steel. The reinforcing steel is considered to be distributed, or “smeared”, throughout the concrete.

The added “third component”, the FRP strengthening, is accounted for in the same fashion as the reinforcing steel. The material is treated as distributed, or “smeared” throughout the concrete. Its material behaviour is assumed to be elastic-brittle, having abrupt failure after reaching its maximal strength. It is also capable of transmitting only tension stresses.

After defining the constitutive matrices of the constituent materials, the constitutive matrix of the composite material in the global coordinates is obtained by their summation:

$$\boldsymbol{D}' = \boldsymbol{D}'_C + \sum_{i=1}^{n} \boldsymbol{D}'_{S,i} + \sum_{i=1}^{m} \boldsymbol{D}'_{F,i} \qquad (1)$$

where D', D'_{C}, $\mathrm{D}'_{\mathrm{S,i}}$ and $\mathrm{D}'_{\mathrm{F,i}}$ are the constitutive matrices if the composite material, concrete, steel and FRP in global coordinates, respectively, n is the number of different reinforcing steels and m is the number of different FRPs used for strengthening.

Verification

The material model described in the previous section was implemented into ANSYS (Vitanov 2012a) in order to check its correctness and usability by comparing the results from the numerical analyses with the available experimental data from the literature.

[1] Civil Engineering Faculty, Ss. Cyril and Methodius University, R.Macedonia, v.vitanov@gf.ukim.edu.mk

Monotonic Loading

Wong (2001) has tested three large-scale beams. They were also numerically modelled by Wong & Vecchio (2003). The beams have just tension reinforcement and no shear steel reinforcement was used. Instead, CFRP strips were glued to the side surfaces to act as shear strengthening. The CFRP fabric used for strengthening was composed of graphite fibres oriented in the longitudinal direction and Kevlar 49 weft in the perpendicular direction. The material had tensile strength of 1090 MPa and ultimate strain of 0.011. Strips of this material with a width of 200 mm were bonded on the side surfaces (not wrapped around the beam) at a central distance of 300 mm between each other. The beams were tested under monotonic three-point loading until failure.

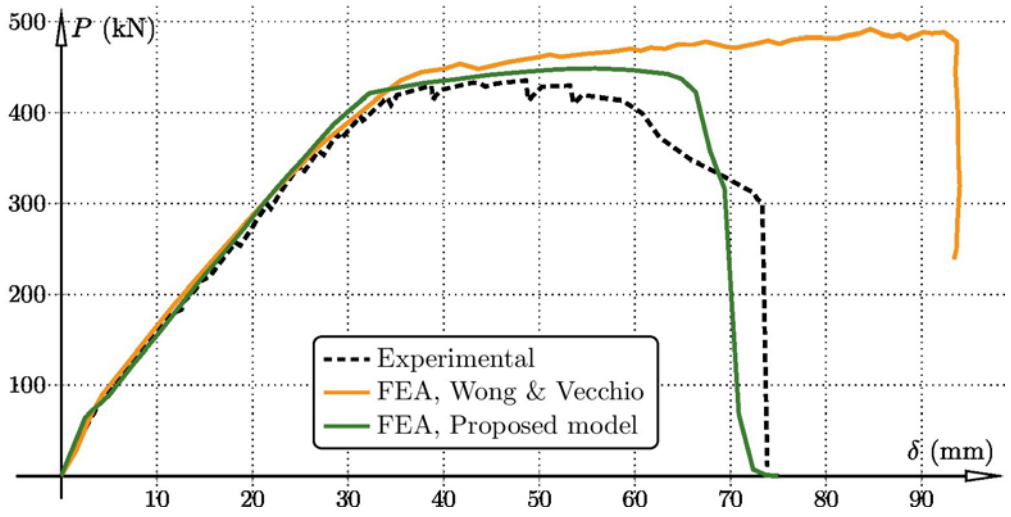

Figure 1: Load versus mid span deflection for the RWOA 3 beam

In the FEM analyses performed by Wong and Vecchio, 2D elements were used to represent the concrete and truss elements were used for the FRP. These had coincident nodes which were connected by contact or link element to simulate the bond between the two materials.

The finite element model used here was build using 4-node quadrilateral Plane182 elements (Vitanov 2013). The resulting load-deflection curves for the longest of the three beams (designated as RWOA 3) are shown in Fig. 1. It can be seen that the obtained results closely follow the experimental curves especially in the deflection range up to the steel yielding point. The failure in the models occurred due to concrete crushing at the top point in the symmetry axes, i.e. the location where the load is applied. The number of performed analyses showed variation in the results in predicting the point of failure which was mostly influenced by the finite element and load step sizes.

Cyclic Loading

Lombard (1999) conducted a testing on reinforced concrete shear wall specimens. Three of the test specimens included a control wall and two strengthened walls. The control wall was tested in its original state which provided a baseline for the evaluation of the repair and strengthening techniques. The two strengthened shear walls were strengthened by applying 0.11 mm carbon fiber sheets to the walls without pre-damage. The first specimen was strengthened with one vertical layer of FRP externally bonded to each face of the wall (Wall 1). The second specimen had one horizontal and two vertical FRP layers on each face of the wall (Wall 2). Both specimens were not loaded until the strengthening was applied.

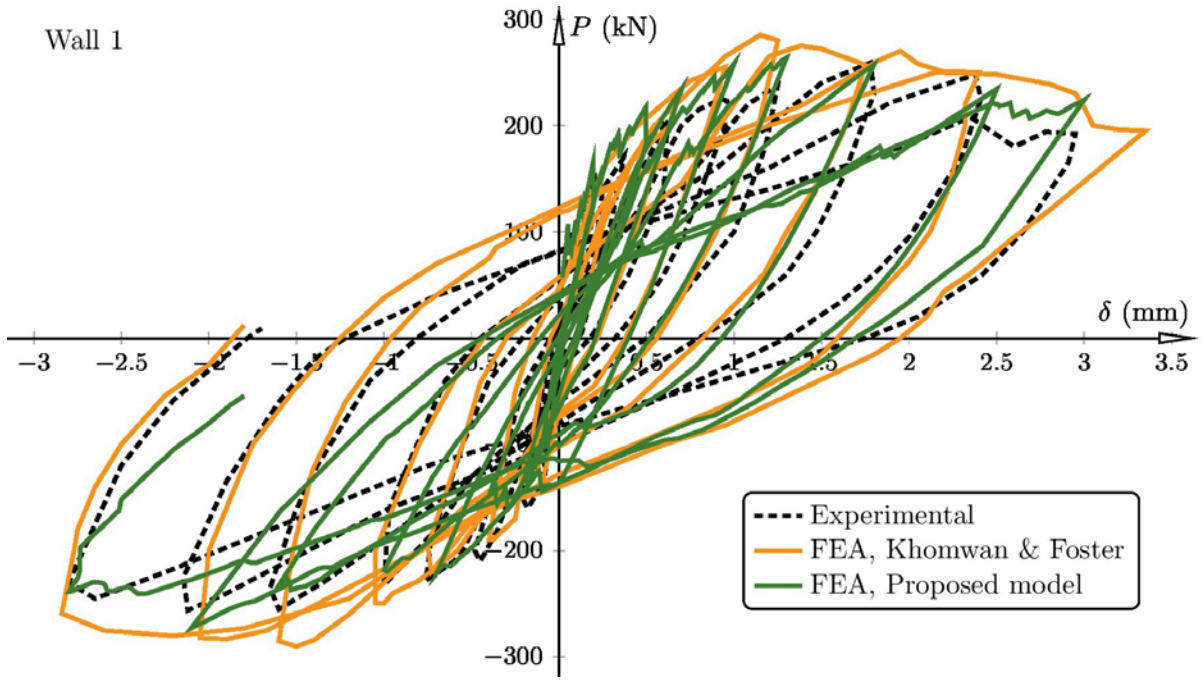

Figure 2: Load-deflection curves for Wall 1

The cyclic load was applied at the middle of the top beam as a series of small displacements. The force and displacement at the same point were taken as results of the performed analyses. These were compared not only with the experimental data, but also with the numerical investigations performed by Khomwan & Foster (2004). Their models were created using 4-node concrete membrane elements with the main steel reinforcement modelled as 1D bar overlay elements. The stirrups in the 'columns' were modeled as smeared through concrete elements. The FRP elements were overlaid over the concrete elements. The connection between them was established via 2D interface elements. The top and bottom beam were also modelled as linear- elastic.

The resulting load-deflection curves for the RC wall strengthened with a single layer of FRP on both sides (designated as Wall 1) are shown in Fig.2. To measure how the numerical results compare to the experimental data the energy dissipated at each cycle (which corresponds to the area of the hysteretic loop) was calculated. The average difference between the measured and the calculated energy dissipation results for this specimen was about 13%.

Conclusions and Points for Discussions

The presented model for reinforced concrete strengthened with FRP gives a good match with experimental results for monotonic biaxial loading. It also compared well with the experimental data from cycled load tests on FRP strengthened RC members in plane stress matching the stress-strain behaviour and the energy loss per cycle rather well.

The results of the numerical analyses show that good match with the structural behaviour is obtained by combining the individual constitutive properties of the concrete, the steel and the FRP using the "smearing" approach to obtain the constitutive model of the "composite" material. This approach enables very simple FEM structural modeling eliminating the need to dedicate separate elements for each of the material components reducing the size and the complexity of the model.

The performed analyses also indicate that in certain cases the model shows higher sensibility to the input parameters (material properties, element type, shape and size or load-step size). This can be expected to a certain degree considering the highly nonlinear nature of the problem and the complex behavior of this composite material especially in cyclic loading conditions or high compression states when failure occurs due to concrete crushing. On the other hand, part of the model result sensibility can

be attributed to the exclusion of some other present nonlinear effects like bond-slip, tension stiffening or reinforcement dowel action. Therefore, the final set of input parameters which would ensure stable solution should be determined by performing several preliminary analyses on the FEM model.

The presented model provides simple modeling of a complex, highly nonlinear material subjected to biaxial monotonic or cycling loading conditions. It is shown that the model is capable of simulating the behaviour of RC members in plane stress which are strengthened with FRP where the strengthening material can be applied in several layers at different orientations and in diverse configurations (continuous over the member surface or just in certain parts) and location (sides or top/soffit).

Key references

Kheyroddin, A. & Naderpour, H., 2008. Nonlinear Finite Element Analysis of Composite RC Shear Walls. *Iranian Journal of Science & Technology, Transaction B, Engineering*, 32(B2), pp.79–89.

Khomwan, N. & Foster, S.J., 2004. Finite Element Modelling of FRP Strengthened Beams and Walls., (UNICIV Report R-432).

Lombard, J., 1999. *Seismic Strengthening and Repair of Reinforced Concrete Shear Walls Using Externally Bonded Carbon Fibre Tow Sheets*. MSc thesis, Carleton University

Vitanov, V., 2012a. Implementation of Inelastic Model of Reinforced Concrete under Biaxial Monotonic Loading into ANSYS. In *2nd International Scientific Meeting: State and Trends of Civil Engineering*. Tuzla, pp. 373–380.

Vitanov, V., 2013. Numerical Model for Biaxial Loading of Reinforced Concrete Strengthened with FRP. In *Second Conference on Smart Monitoring, Assessment and Rehabilitation of Civil Structures, SMAR 2013*. Istanbul TR, p. 153.

Vitanov, V., 2012b. *Numerical Model of FRP Strengthened Reinforced Concrete*. Ph.D Thesis, Civil Enginnering Faculy, Ss. Cyril and Methodius University

Wong, R.S.Y., 2001. *Towards Modelling of Reinforced Concrete Members with Externally-bonded Fibre Reinforced Polymer (FRP) Composites*. MSc thesis, University of Toronto

Wong, R.S.Y. & Vecchio, F.J., 2003. Towards Modeling of Reinforced Concrete Members with Externally Bonded Fiber-Reinforced Polymer Composites. *ACI Structural Journal*, 100(1), pp.47–55.

3.10 Strengthening of Masonry Structures

Seismic Retrofitting of Cultural Heritage with Textile Reinforced Mortar

G. de Felice[1], S. De Santis[2], F. Roscini[3]

Introduction

The performance of cultural heritage building under seismic action is one of the challenging research topic due to the necessity to withstand safety conditions while fulfilling preservation criteria. In some cases, traditional techniques, that ensure the accomplishment of preservation criteria and also provide the adequate durability, are not sufficient for ensuring a sufficient seismic safety. For instance, recent earthquakes in Italy have shown the high seismic vulnerability of thin in-folio brick masonry vaults. Due to their slenderness, these vaults are particularly vulnerable against unsymmetrical service loads, relative horizontal displacement of the abutments and seismic actions. Therefore, in numerous existing structures in seismic-prone regions, the vaults need retrofitting to ensure an adequate safety level according to current standard codes. To this purpose, externally bonded reinforcements with composite materials have proven to be particularly advantageous [1-3] since they provide high mechanical performances with minimum thickness and mass increase.

In the last two decades, most research activities and field applications have made use of composites with polymeric matrix (Fibre Reinforced Polymers, FRPs). Nevertheless, a new generation of composites has been recently proposed that consist of high strength fabrics (made out of steel, carbon, basalt, glass, PBO or natural open meshes) embedded into inorganic (mortar) matrices. Mortar-based reinforcements are named Textile Reinforced Mortars (TRM) or Fabric Reinforced Cementitious Matrix (FRCM) when comprising carbon, glass, basalt, or PBO fabrics, arranged in the form of open meshes, or Steel Reinforced Grout (SRG) when making use of steel textiles. The use of mortar in place of resin ensures the fulfilment of the principles of conservation and restoration, such as respect of authenticity of materials and structural behaviour, minimum intervention, reversibility, substitutability and removability, and compatibility with original substrates and decorative settings. For all these reasons, mortar-based composites appear particularly promising for applications to masonry structures and cultural heritage. However, inorganic matrices may entail lower bond strength than epoxy resins and require proper installation and curing conditions to ensure the bond with the substrate. In the last decade, increasing research efforts have been devoted to the study of TRMs, fostering a fast technological and industrial development. At the same time, several applications have been realized for safeguarding cultural heritage against earthquakes. The TRM-to brick/masonry bond behaviour has been investigated by a number of studies [4-6] that provided fundamental information on bond strength and failure modes, and highlighted the role played by the mechanical properties of the matrix, the layout of the textile, and the roughness of the surface of the substrate. Nevertheless, a better knowledge still needs to be gained, espe-cially on some issues (such as durability, design criteria, installation details, etc.) and, apart from the US document ACI 549.4R-13, no specific guidelines have been developed yet.

In the present paper, the application of mortar-based composites for strengthening brick masonry vaults in the rehabilitation works realized in Italy after 2009 L'Aquila and 2012 Emilia earthquakes is presented and the performances of these system are discussed. The strengthening design for masonry vaults would require that a deeper knowledge is gained on the actual bond behaviour of the composites on a curved substrate and on the key variables that affect it, since in the presence of a curvature, except few recent works [7], the reinforcement-to-substrate bond behaviour has not been sufficiently investigated. To this end, an experimental investigation carried out on the application of TRM systems to the extrados of brick masonry vaults is presented. The tests are devoted to get a deeper knowledge

[1] Roma Tre University, Department of Engineering, Rome, Italy, gianmarco.defelice@uniroma3.it
[2] Roma Tre University, Department of Engineering, Rome, Italy, stefano.desantis@uniroma3.it
[3] Roma Tre University, Department of Engineering, Rome, Italy, francesca.roscini@uniroma3.it

on effectiveness of the reinforcement when applied to a convex substrate. The tests have been carried out both in the laboratory and in the field, allowing for investigating the actual performance of the reinforcement and the resulting increase in load carrying capacity of the vault.

Strengthening of masonry vaults

Among the different mortar based composite systems that are available in the market, in the present case, a unidirectional fabric consisting in very thin cords of Ultra High Tensile Strength Steel (UHTSS) embedded into a lime-based mortar are used for retrofitting of the vaults. Steel textile have about 3200 N/mm^2 tensile strength and 185kN/mm^2 Young's modulus. They were applied with a lime based mortar having 15 N/mm^2 compressive strength and 22kN/mm^2 Young's modulus. With respect to the fabrics with other fibre materials, steel textiles are stiffer and stronger than glass and basalt and thicker than carbon, aramid and PBO, are isotropic (which provides better toughness), more durable in alkaline environment, and need lower cost and energy for production. Figure 1 shows the installation process of the Steel TRM on the extrados of the vault. Given the one-directional properties of the steel wires that constitute the reinforcement, the application is carried out in two subsequent phases in the orthogonal directions, according to the double curvature of the vault. The width and the spacing between the strips are designed to provide the requested increase in strength as well as to prevent any local fall of bricks during seismic events. The steel wires are directly inserted into drilled holes at the abutments and injected as to provide a further restraint. Accordingly, if for any reason the bond between the reinforcement and the extrados of the vault deteriorates, the end connections would still allow the reinforcement to contribute as unbonded tendons. The presence of the steel fabric at the extrados of the vault is able to prevent the opening of cracks, thus inhibiting the four hinges collapse mechanism that would take place in unreinforced vaults. Additionally, the retrofitting of the vault with this technique succeeds in preserving decorative settings at the intrados with no changes in the thickness nor increase in the mass of the structure.

Figure 1. Phases of strengthening brick masonry vaults at the extrados: a) preparation of the extrados of the vault after the removal of the filling; b) application of a primer for enhancing the bond between the extrados of the vault and the inorganic matrix; c) application of the Ultra High Tensile Stress Steel strips; d) end connections at the abutments; e) application of the covering layer of mortar matrix and of a second transversal set of strips; g) construction of brickwork spandrel walls for the backing and filling with granular material.

Laboratory tests on masonry vaults retrofitted with textile reinforced mortar

The tests carried out in the laboratory were designed to simulate as closely as possible the effective behaviour of the vault, including the contribution of the buttresses and of the filling materials. As it is well known, both these contributions are crucial in the stress transfer and cannot be neglected in the analysis. Since the activity is currently underway, only some preliminary results are presented in this note, which however are sufficient to show the effectiveness of the strengthening system. As a preliminary activity, several double lap bond tests were carried out aiming at evaluating the bond properties between the composite system and the brick masonry substrate in the presence of curvature (Figure 2). These tests provided the failure mechanisms and the increase in bond strength related to the convex curvature, allowing to design the strengthening of the vault. The experimental setup was designed to simulate the worst loading conditions that bring the vault up to failure due to the activation of a four hinges mechanism. The load was applied over the filling at about one third of the span by means of an hydraulic actuator. Tests were run under displacement control to follow the whole load displacement post-peak response up to failure. Only two tests on the vaults have been carried out to date, consisting of two sections of the vaults, with 2800 mm span, 55 mm thickness and 500 mm depth. The first specimen was representative of the actual conditions of the vault before retrofitting, while the second specimen was retrofitted by applying the reinforcement to the extrados, consisting in UHTSS with 8 cord/inch, with 150 mm with, having an overall cross section of 25.2mm^2. The applied load was directly provided by the loading cell of the actuator, while the displacement filed of the vault and of the filling during the test was recorded by means of nonconventional contactless measurement methods, such as the Digital Image Correlation. Strain gauges were also glued to the reinforcement textile to record the stress and estimate the load carried by the steel cords. The tests (Figure 3) results can be summarized as follow: the presence of the SRG reinforcement led to an increase of the load carrying capacity of the vault of 280% (from 5.7 kN to 15.4 kN). In the unreinforced specimen, a four hinge mechanism activated, while the SRG strips bonded prevented the development of the cracks at the extrados. Failure occurred by a combination of crushing in the masonry and shear sliding between the bricks under the load application point. The SRG strips detached from the substrates in some portions (detachment occurred at the textile-to-matrix interface).

Figure 2. Bond failure between TRM and brick masonry for planar and curved substrates.

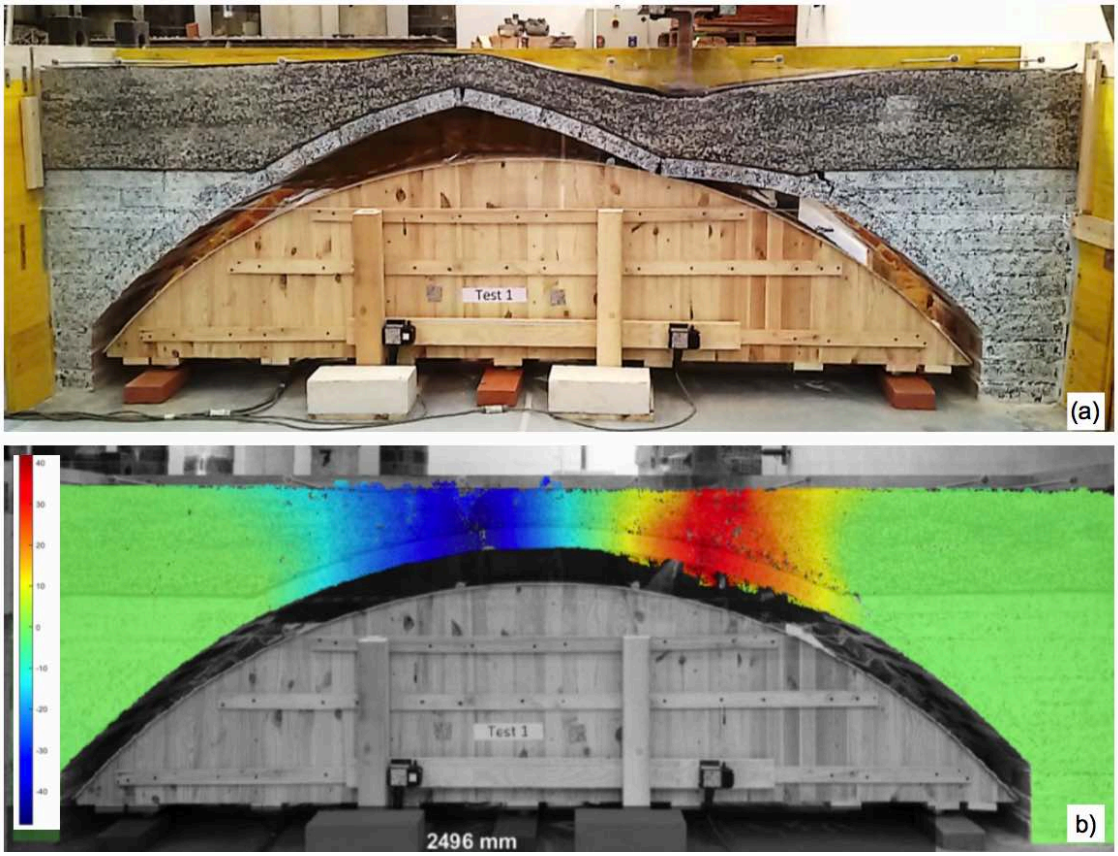

Figure 3. Laboratory tests on real-scale in-folio vaults retrofitted with Textile Reinforced Mortar: a) collapse configuration and b) analysis of the displacement field with Digital Image Correlation.

On-site tests on masonry vaults

Tests were carried out in an historic building in the city centre of L'Aquila, Italy, badly damaged by a strong earthquake in 2009, and currently undergoing important reconstruction and retrofitting works. Testing setup (Figure 5) was designed to simulate the loading conditions that the reinforcement would experience if a crack develops at the extrados of the vault, due to the activation of a mechanism, in order to investigate the reaction that SRG is able to provide up to debonding. The textile was bonded to half of the vault and subjected to tensile loading at the crown. A 1 m long portion of textile was left unbonded and gripped to apply a horizontal (tangent to the vault) load. Two steel plates were used to clamp the textile. A ∅16 threaded steel bar was welded to the lower plate that transferred the load applied by means of a hollow hydraulic actuator, that contrasted with steel beams connected to the side walls. The oil pressure in the actuator was provided by a hydraulic pump and measured by a manostat, allowing for deriving the applied load. The relative displacement between reinforcement textile and substrate at the loaded end (slip) was measured by two linear displacement transducers. Finally, two 10 mm resistive gauges were glued to the unbonded textile to record strains and derive a further measure of the applied load. Three tests were carried out. The first cracks appeared near the loaded end of the reinforcement (i.e., its first bonded section) on the upper side of the SRG strip, and orthogonal to the load direction. Longitudinal cracks also developed on the side of the SRG strip. The crack pattern progressively evolved during load application, up to the detachment of the reinforcement from the substrate, which occurred progressively starting from the loaded end, and at the end

reached the springing section of the vault and involved the whole SRG tape (Figure 4a). At the springing, the SRG strip was connected to the side wall with mechanical end pivots (SRG connectors placed in inclined drilled holes and injected with grout). Tests were never carried out up to the pull off failure of the connectors. At the end of the test, the entire upper layer of mortar matrix disintegrated and the steel textile detached from the lower layer, which did not debonded from the substrate. The load-slip curves of the tests display a good agreement (Figure 4b), considering the variability of substrate and setup, which is unavoidable in field testing. The response is characterized by three phases associated to progressively reducing stiffness. The first phase is associated to an un-cracked behaviour of the reinforcement. The measured displacements are related to elastic deformations and small settings. The second phase is related to the crack development of the matrix and the activation of the detachment of the reinforcement from the masonry substrate. The transition from the first phase to the second phase can be identified by the occurrence of the first cracks and the increase of the relative displacement between reinforcement and substrate. Up to the end of the second phase, the bond behaviour of the SRG reinforcements applied to the vault is similar to that observed in laboratory tests on small-scale specimens [6]. The third phase is a peculiar characteristic of the behaviour of SRG reinforcements applied to the extrados of masonry vaults, since it is related to the very large bonded area and to the curvature of the substrate. In this third phase, in addition to the cohesive strength, a friction contribution activates. The former (cohesive contribution) is associated to the bonded textile that, once the debonding process has initiated, moves away from the loaded end. The latter (friction contribution) is mobilized on the detached portion of the reinforcement, as a result of the curvature of the vault. Since the SRG is applied to the extrados, when a tensile load is applied to the steel textile, normal compressive stresses arise at the reinforcement-to-substrate interface. As shown by the experimental response curves, the component related to friction grows with the increase of the tensile load in the steel cords and of the area of SRG that has detached from the substrate, and significantly contributes to the overall strength. Table 1 lists the main results for each test, namely the maximum attained load (F_{max}), the corresponding load per unit width ($F_{max,u}$), stress in the textile (σ_{max}), and exploitation ratio of tensile strength (η), the mean strain (ε_m) in the textile, and the slip (s) at peak load.

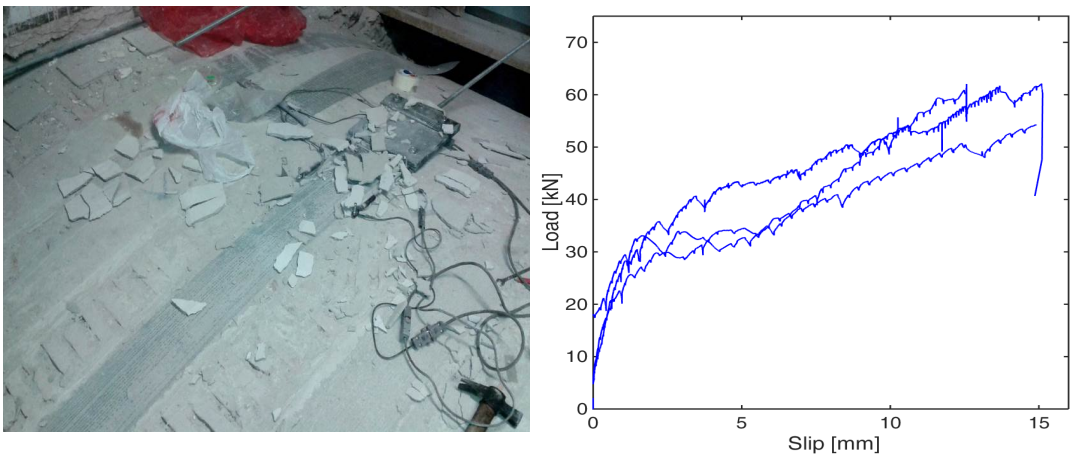

Figure 4. Field tests on extrados strengthening of brick vaults: a) debonding of SRG strips at the end of the test; b) load-slip responses

Table 1. Results of field tests.

Test	F_{max}	$F_{max,u}$	σ_{max}	η	ε_m	s
	kN	kN/m	N/mm^2	-	10^{-3}	mm
1	62.1	414.3	1631.2	56.2%	5.63	15.09
2	54.2	361.6	1423.6	49.1%	4.65	14.88
3	60.9	406.1	1598.9	55.1%	4.91	12.48
Mean	59.1	394.0	1551.2	53.5%	5.06	14.15

Conclusions

Laboratory and field tests were carried out to investigate the effectiveness of mortar-based composite systems for the reinforcement of masonry vaults. Lab tests were performed on full scale brickwork vaults and indicated that the load carrying capacity can be improved by up to about 3 times with steel cords strips applied over the extrados of the vault. In order to reproduce actual field conditions, specimens were provided with buttresses in solid brickwork and filling. Digital image correlation was used to record the displacement of the brick units as well as the strain field in the fill. Field tests provided information on the shear bond strength of SRG strips applied to the extrados of brick masonry vaults: on average, the maximum achieved load was about 60 kN, corresponding to a load per unit width of 350 kN/m, a stress in the textile of $1550N/mm^2$ and an exploitation ratio of the tensile strength of the textile of 53%. The stress attained at failure proves the need of using a textile with particularly high mechanical properties, such as the Ultra High Tensile Strength Steel, for this kind of application. The values of the exploitation ratios are significantly higher (up to 3 times) than those obtained in laboratory tests on plain substrates, indicating the important strength contribution provided by the convex curvature of the extrados surface of the vault. The presence of the end connectors, whose contribution was not mobilized in the tests, could lead to an even higher strength. Failure occurred by detachment at the interface between steel textile and mortar, and not within the substrate as generally occurs with the more traditional FRP reinforcements. Therefore, the result of the test appears basically independent from the mechanical properties of the substrate (strength and stiffness of the masonry of the vault). On the other hand, due to the presence of a friction contribution, the bond strength depends on the curvature of the vault and on the bond length. It is worth highlighting that the performance of the strengthening system strongly depends on the accuracy of the installation, on the preparation of the surface of the substrate (whose roughness should be ensured), and on the curing conditions of the mortars. A larger number of experimental results is needed to develop a deeper understanding of the mechanical behaviour of mortar based composites for the retrofitting of masonry vaults, also considering the lack in the scientific literature of analytical/numerical methods for the reinforcement design and the assessment of the strengthened vault. Nevertheless, the studies carried out so far have indicated that SRG can be an effective and cost efficient solution for the safeguarding of historic masonry structures against earthquakes, and, more in general, for the conservation of architectural heritage.

Acknowledgement

The financial support provided by Kerakoll S.p.a. and the technical participation of Dr. Paolo Casadei are gratefully acknowledged.

Key references

Valluzzi MR, Valdemarca M, Modena C. (2001). Behaviour of brick masonry vaults strengthened with FRP laminates. J Compos Constr; 5(3):163-169.

Foraboschi, P. (2004). Strengthening of masonry arches with fiber-reinforced polymer strips. J Compos Constr 8(3): 191-202.

Borri A, Casadei P, Castori G, Hammond J. (2009). Strengthening of brick masonry arches with externally bonded steel reinforced composites. J Compos Constr; 13(6):468-475.

de Felice G, De Santis S, Garmendia L, Ghiassi B, Larrinaga P, Lourenço PB, Oliveira DV, Paolacci F, Papanicolaou CG. (2014). Mortar-based systems for externally bonded strengthening of masonry. Mater Struct; 47(12):2021-2037.

Razavizadeh A, Ghiassi B, Oliveira DV. (2014). Bond behavior of SRG-strengthened masonry units: Testing and numerical modeling. Constr Build Mater; 64:387-397.

De Santis S, de Felice G. (2015). Steel reinforced grout systems for the strengthening of masonry. Compos Struct;134:533-548.

Malena M, de Felice G. (2014). Debonding of composites on a curved masonry substrate: experimental results and analytical formulation. Compos Struct; 112:194-206.

FRP/SRP and FRPU/SRPU systems as composites-to-masonry strengthening

A. Kwiecień[1], B. Zając[2], F. Ceroni[3], G. de Felice[4], S. De Santis[5], D.V. Oliveira[6], M.R. Valluzzi[7]

Introduction

In the last decade, fast development of composites-to-masonry strengthening system is observed, which are used in practical applications on real structures. In laboratory tests various strengthening systems with aramid, basalt, carbon, glass, polyparaphenylene benzobisoxazole and steel reinforcement fibres were applied on brick and masonry prism substrates. Tested fibres were bonded to the substrates with polymeric and mineral mortars with various bonding length. They were typically tested in single lap shear tests (SLST) or in double lap shear tests (DLST). Many laboratories from Europe were involved in these tests in frame of activities of two RILEM Technical Committees: 223MSC and 250CSM and in frame of the COST Action TU1207. Three Round Robin Tests RILEM campaigns: RRT1, RRT2 and RRT3 on polymeric adhesives were carried out, where FRP/SRP (Fibre/Steel Reinforced Polymers) with epoxy resin adhesives and FRPU/SRPU (Fibre/Steel Reinforced Polyurethanes) with flexible polyurethane adhesives were compared. They were tested in form of wet-lay-up strengthening systems and in form of repair systems (detached composites were bonded again to substrates).

Reduction of stress concentrations and stress redistribution in bond by flexible adhesives

Differences in bond behaviour between stiff and brittle epoxy resin adhesives and highly deformable polyurethane adhesives were primarily observed in pull-off test on bricks [1], which indicated that higher bond strength can be obtained, when less stiff adhesive of higher ultimate deformation is applied. More flexible adhesive allows reducing stress concentrations in brittle substrate and redistributing them to larger bonding area that results in increase of maximum bond strength (Fig. 1a). This phenomenon was also observed in numerical analysis (Fig. 1b) of shear bond tests of masonry elements strengthened with composites [2] and DIC [3], when stiff and flexible adhesives were applied.

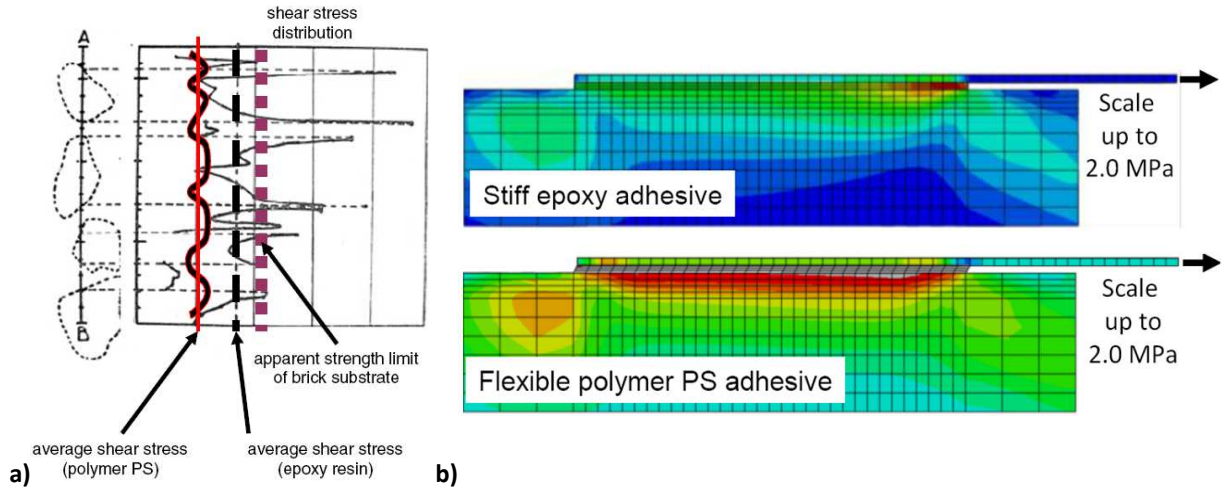

Figure 1: Reduction of stress concentration by flexible polymer (a), comparison of stress distribution in the bond between strengthening fibres and masonry substrate in cases of stiff and flexible adhesives (b) – after [2].

[1] Cracow University of Technology, Poland, akwiecie@pk.edu.pl
[2] Cracow University of Technology, Poland, bozajac@pk.edu.pl
[3] University of Napoli 'Parthenope', Napoli, Italy, francesca.ceroni@uniparthenope.it
[4] University Roma Tre, Rome, Italy, gianmarco.defelice@uniroma3.it
[5] University Roma Tre, Rome, Italy, stefano.desantis@uniroma3.it
[6] University of Minho, Portugal, danvco@civil.uminho.pt
[7] University of Padova, Padova, Italy, valluzzi@dicea.unipd.it

Increase of the ultimate load of composite-to masonry strengthening systems was manifested in two cases. The first one was carried out on repaired shear bond test specimens, where detached FRP/SRP composites bonded to clay bricks (RRT1, [4]) and masonry (RRT2, [5]) substrates with epoxy resin adhesives, were bonded again using highly deformable polyurethane adhesive polymer PS and epoxy resin. They were tested again up to failure in SLST [6-8], (RRT3, [9]). The second one was carried out on new brick specimens, where composite fibres were bonded to brick substrates with polyurethane adhesives, using wet-lay-up method to construct FRPU/SRPU systems. They were tested again up to failure in SLST [10, 11].

Reduction of stress concentrations and stress redistribution in bonds by flexible adhesives results from nonlinear characteristic of polyurethanes, possible to calculate using hyperelastic models [2, 10, 12]. Differences in characteristics of stiff and flexible adhesives used in tests are as follows: the epoxy resins have tensile strength between 30 and 54 MPa, and Young's modulus between 1300 and 4500 MPa, while polyurethane polymer PS has tensile strength 2.87 MPa and Young's modulus 14.8 MPa. The ultimate strains of the tested adhesives are up to 4% and up to 45%, respectively [1, 4]. Possibility of reduction of stress concentrations is advantageous not only for brittle substrates but also for weak natural fibres, vulnerable to notch effect. More effective stress redistribution in an adhesive allows obtained similar high ultimate loads in systems strengthened by weak bamboo fibres as well as in the same systems strengthened by carbon fibres [13]. Moreover, composition of reinforcement from flexible adhesives and fibres manifests very well cyclic resistance and energy dissipation properties, what is required in seismic areas [13-16]. Polyurethane polymer PS adhesive is also easily removable from masonry substrate, what is especially important in application on heritage structures [10, 14-16].

Detached FRP/SRP composites repaired by flexible polyurethane adhesive

To check if repair of detached composites is possible, international laboratory tests on similar masonry specimens strengthened by various composites were done. In the first group, specimens made of weak masonry substrates (brick and prisms made of Italian clay bricks SanMarco Rosso Vivo A6R55W) and strengthened using composites bonded on stiff epoxy resin (bonding length Lb = 160 mm) were tested up to failure in SLST and DLST (RRT1, [4]) at Cracow University of Technology (CUT) – Fig. 2.

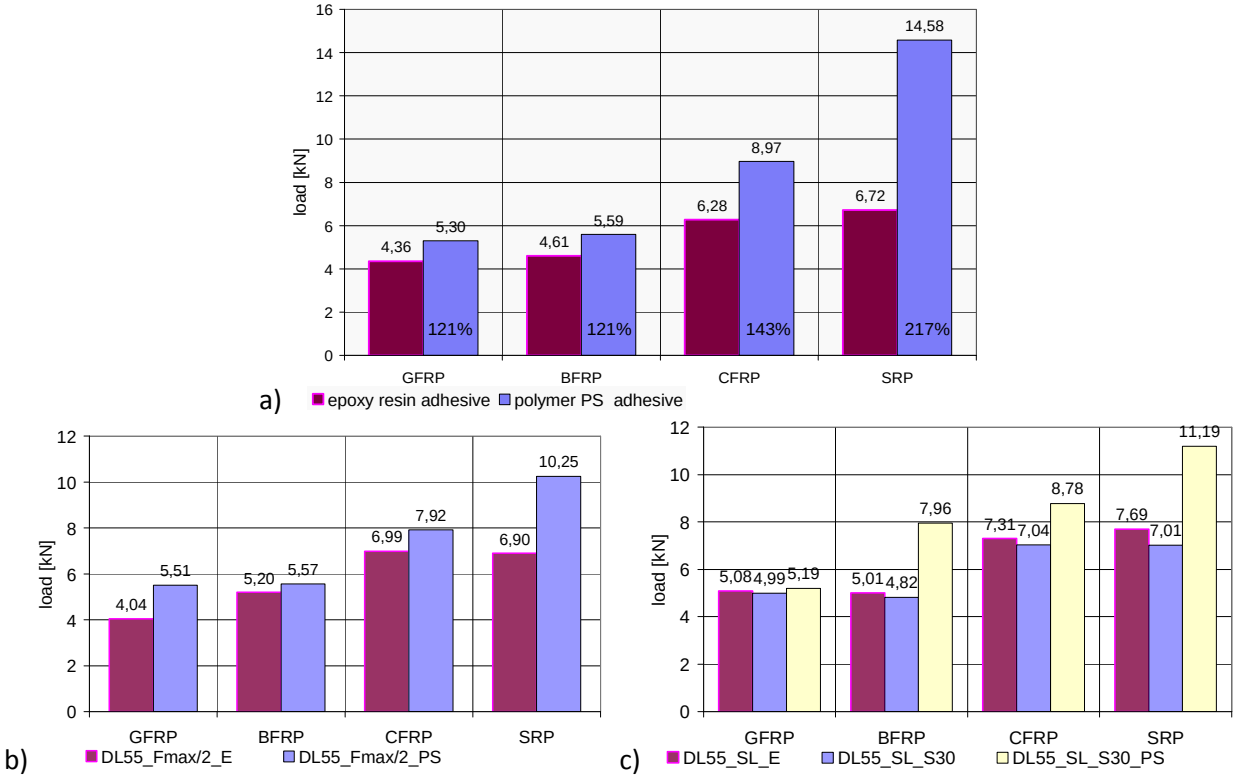

Figure 2: Comparison of mean values of ultimate loads (Lb = 160 mm) obtained before and after repair using only polymer PS adhesive in SLST (a) [2], in DLST (b) and also epoxy S30 adhesive (c) [7].

Composites detached with thin layer of a brick substrate were bonded again as repair using polymer PS adhesive and epoxy resin S30. In all cases of repair using flexible polyurethane polymer PS adhesive, significant increase of ultimate load was observed (Fig. 2) [2, 7]. On the other hand, repair of the weak brick substrate with stiff epoxy resin S30 adhesive was less efficient, because did not received of the level of initial ultimate load (Fig. 2c) [7].

Confirmation of this phenomenon was obtained during international tests RRT2 and RRT3 carried out on brick (Lb = 200 mm) and prism (Lb = 200, 135, 65 mm) specimens (made of the same materials as in the first group) tested up to failure. As previously, composites detached with thin layer of a brick substrate were bonded again as repair using polymer PS adhesive and similarly significant increase of ultimate load was observed (Fig. 3a,b) [9]. Confirmation of better stress redistribution along the bonding length by polyurethane adhesive (RRT3) than epoxy one (RRT2) was also manifested (Fig. 3c).

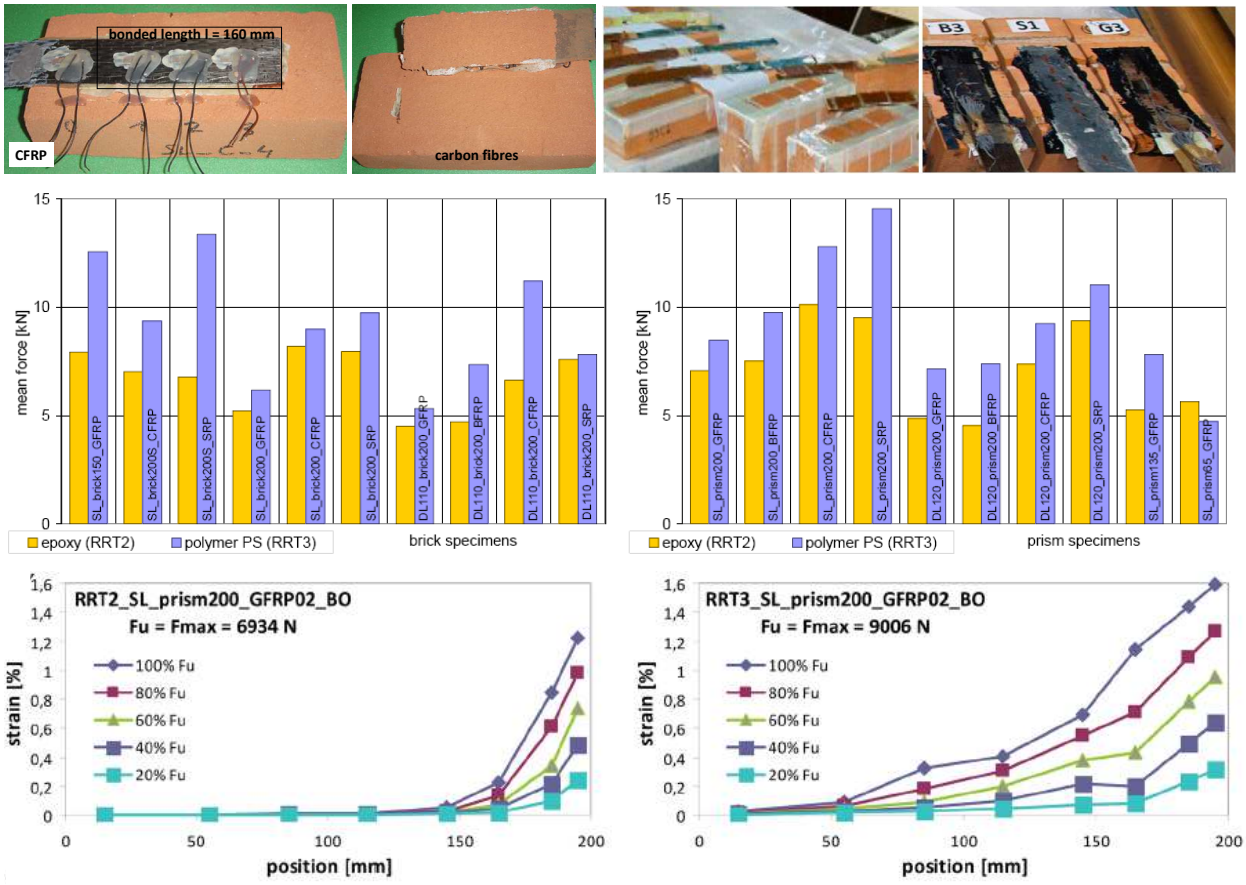

Figure 3: Composites detached after RRT1 and RRT2 and repaired using polyurethane polymer PS during RRT3 (top); comparison of results obtained for brick and prism specimens strengthened with various composites, when epoxy resin (RRT1 and RRT2) and polyurethane repair adhesives (RRT3) were used (middle); strain distribution in the epoxy (RRT2) and polyurethane (RRT3) adhesive (bottom) – after [9].

Comparison of such repair was also tested on stronger Portuguese clay bricks during SLST, using epoxy and polyurethane adhesive. In this case, both repair adhesives manifested significant increase in ultimate load, but epoxy one was more effective than polyurethane [8]. It was in opposite to the results presented in Fig. 2.

Wet-lay-up application of flexible polyurethane as adhesive in FRP/SRP systems

Comparison of wet-lay-up composites-to-brick systems, carried out on weak and strong Italian brick substrates using epoxy resin and polyurethane adhesives, was done in frame of the international cooperation. As in the case o repair, the weak brick systems with polyurethane adhesives manifested higher ultimate load values than the same with epoxy resin adhesives (Fig. 4) [11].

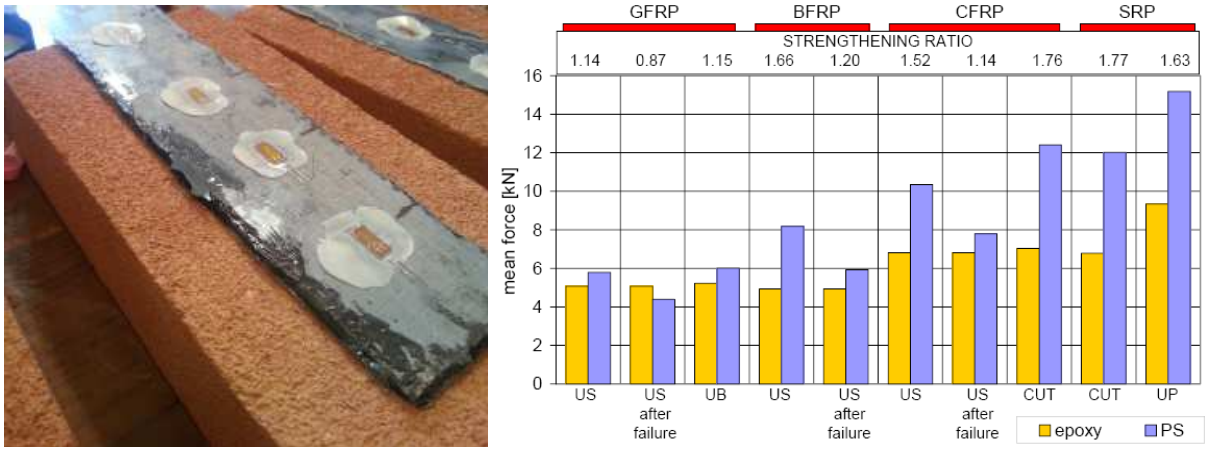

Figure 4: Comparison of results obtained for weak brick specimens strengthened with various composites, when epoxy resin and polyurethane repair adhesives were applied in wet-lay-up method – after [11].

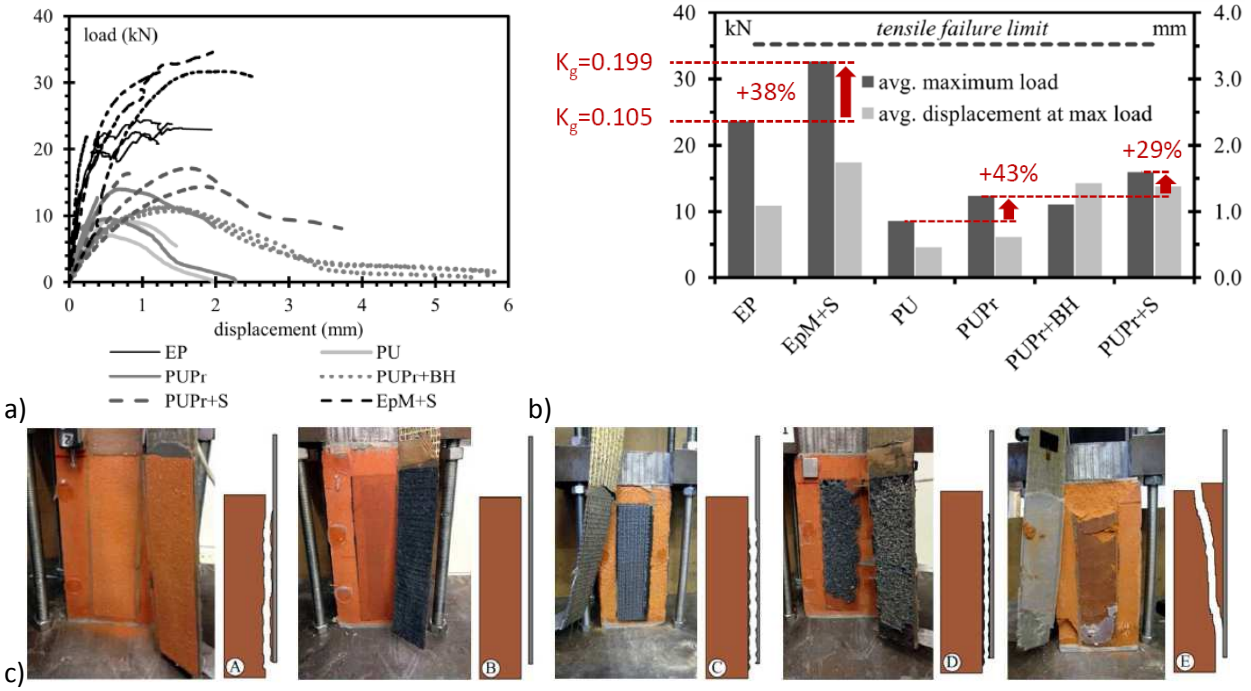

Figure 5: Comparison of results obtained for weak brick specimens strengthened with various composites, when epoxy resin and polyurethane repair adhesives were applied in wet-lay-up method – after [10].

Two papers [8, 10] indicated that strong clay bricks are able carrying higher ultimate loads when epoxy resin is applied as an adhesive than when polyurethane one. Stiffness of epoxy-bonded systems is also higher than polyurethane ones (Fig. 5a,b), but the last one has higher ductility behaviour. Failure modes of specimens with epoxy adhesive manifest rather cohesive failure in the brick substrate, whereas polyurethane adhesive is characterised by cohesive failure in the flexible adhesive (Fig. 5c) [10].

Adhesive flexibility more important than composite reinforcement strength

The similar SLST carried out on the same weak brick and two kinds of composite reinforcement (carbon and bamboo fibres) and two adhesives (epoxy resin and polyurethane) indicated that obtaining of high ultimate strength of composite-to-brick systems is dependent on adhesive flexibility, and not on composite fibres strength. Very weak bamboo composite (BBFRP) was able to transfer the same ultimate load level as high strength carbon one (CFRP), when flexible polyurethane PS was applied (Fig. 6b-d) [13, 14], and was significantly higher than CFRP on epoxy (Fig. 6a). Flexible adhesive characterises good cyclic resistance and energy dissipation and is removable from a substrate (Fig. 6e) [10, 13-16].

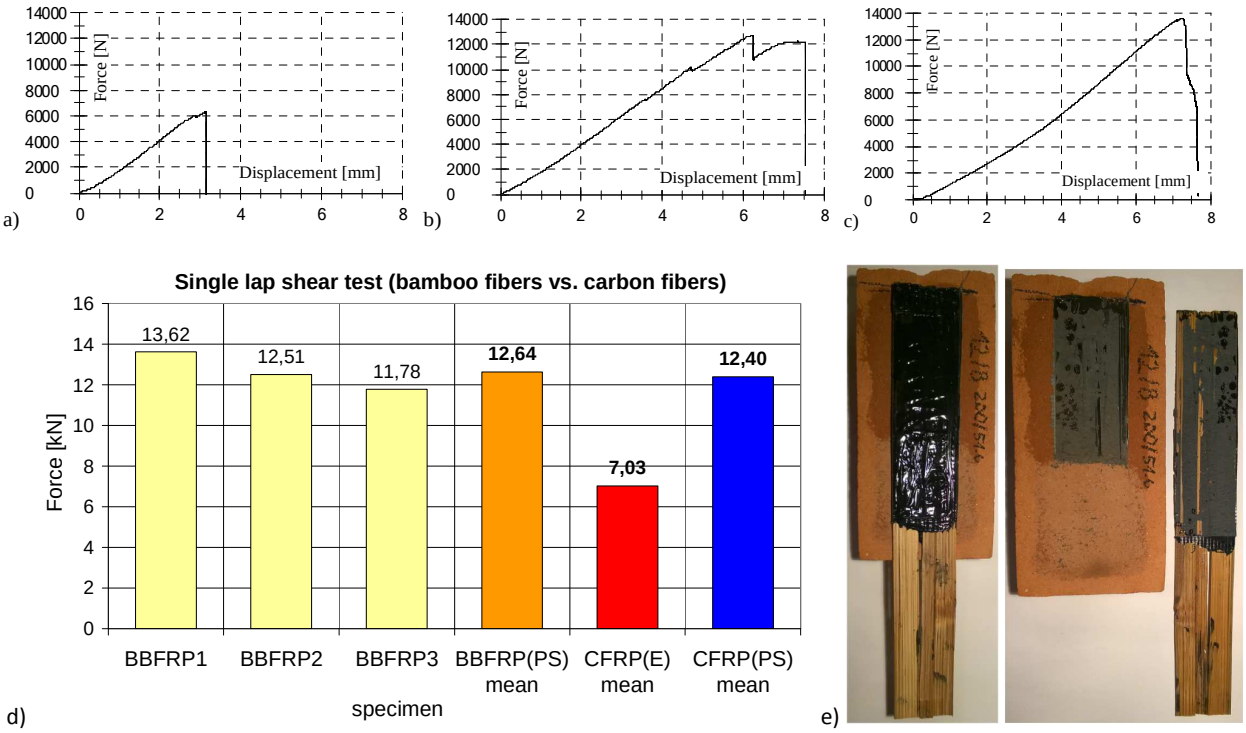

Figure 6: Load-slip characteristics of STST on: CFRP with epoxy (a), CFRP with polyurethane (b), bamboo fibres with polyurethane (c); comparison of mean ultimate loads (d) and removability of polyurethane from brick (e).

Conclusions

Comparison of FRP/SRP systems (epoxy resin adhesive) with FRPU/SRPU systems (polyurethane adhesive) confirmed that flexible adhesives are more advantageous in composite-to-brick strengthening systems tan epoxy resin ones, if weak masonry substrate is taken into consideration. On the contrary, epoxy resin adhesives allow obtain higher ultimate loads in shear, when strong brick substrates are used. This is valid for wet-lay-up systems, as well as for repairs.

Key references

1. Kwiecień A.: Stiff and flexible adhesives bonding CFRP to masonry substrates - investigated in pull-off test and Single-Lap test. Archives of Civil and Mechanical Engineering 12 (2) 2012, Elsevier, ISSN 1644-9665, pp. 228–239.
2. Kwiecień A.: Shear bond of composites-to-brick applied with highly deformable, in relation to resin epoxy, interface materials. Materials and Structures (2014) 47:2005-2020, DOI 10.1617/s11527-014-0363-y.
3. Tekieli M., De Santis S., de Felice G., Kwiecień A., Roscini F.: Application of Digital Image Correlation to composite reinforcements testing. Composite Structures 160 (2017), pp. 670–688.
4. Valluzzi M.R., Oliveira D., Caratelli A., Castori G., Corradi M., de Felice G., Garbin E., Garcia D., Garmendia L., Grande E., Ianniruberto U., Kwiecień A., Leone M., Lignola G.P., Lourenço P.B., Malena M., Micelli F., Panizza M., Papanicolaou C.G., Prota A., Sacco E., Triantafillou T.C., Viskovic A., Zając B., Zuccarino G., "Round Robin Test for Composite-To-Brick Shear Bond Characterization", Materials and Structures, 45 (2012), ISSN 1359-5997, pp. 1761-1791.
5. de Felice G, Bellini A, Ceroni F, De Santis S, Garbin E, Leone M, Lignola GP, Malena M, Micelli F, Mazzotti C, Panizza M, Valluzzi MR (2015). Experimental characterization of composite-to-brick masonry shear bond. Materials and Structures (July) 2016, Volume 49, Issue 7, pp 2581–2596.

6. Kwiecień A., Zając B., Kuboń P.: Post failure repair of strengthening system made of GFRP, BFRP, CFRP and SRP strips bonded to brick substrate - examined in single-lap tests. In Proc. 6th International Conference on FRP Composites in Civil Engineering CICE'2012, Rome 2012.
7. Kwiecień A., Zając B.: Is it Possible to Repair Detached Composites Effectively after Failure of Masonry Strengthening? Key Engineering Materials, Vol. 624 (2015), Trans Tech Publications, Switzerland, pp. 518-525.
8. Ghiassi B., Xavier J., Oliveira D.V., Kwiecień A., Lourenço P.B., Zając B.: Evaluation of the bond performance in FRP-brick components re-bonded after initial delamination. Composite Structures Vol. 123 (May 2015) pp. 271–281, doi:10.1016/j.compstruct.2014.12.047
9. Kwiecień A., de Felice G., Oliveira D.V., Zając B., Bellini A., Ghiassi B., Lignola G.P., Lourenço P.B., Mazzotti C., Prota A., De Santis S.: Repair of composite-to-masonry bond using flexible matrix. Materials and Structures (July) 2016, Volume 49, Issue 7, pp 2563–2580.
10. Garbin E.; Kwiecień A.; Panizza M.; Zając B.; Nardon F.; Valluzzi M.R.: Testing of bond solutions for UHTS steel strand composites applied to extruded bricks. Proceedings of the 16th International Brick and Block Masonry Conference, Padova, Italy, 26-30 June 2016. Edited by Claudio Modena, F. da Porto, and M. R. Valluzzi. CRC Press 2016. Pages 395–402. Print ISBN: 978-1-138-02999-6. eBook ISBN: 978-1-4987-9592-0.
11. Ceroni F., Bellini A., Garbin E., Kwiecień A., Mazzotti C., Panizza M., Valluzzi M.R.: Load bearing capacity and ductility properties of composites-to-brick dependent on an adhesive type. Structural analysis of historical constructions: anamnesis, diagnosis, therapy, controls. Proceedings of the 10th International Conference on Structural Analysis of Historical Constructions, SAHC 2016, Leuven, Belgium, 13-15 September 2016 / eds. Koen Van Balen, Els Verstrynge. – Leiden : CRC Press/Balkema, 2016, pp. 1061-1068.
12. Kwiecień A., Gams M., Zając B. Numerical modelling of flexible polymers as the adhesive for FRPs. 12th International Symposium on Fiber Reinforced Polymers for Reinforced Concrete Structures (FRPRCS-12) & 5th Asia-Pacific Conference on Fiber Reinforced Polymers in Structures (APFIS-2015) Joint Conference, 14-16 December 2015, Nanjing, China.
13. Kwiecień A., Hebel D.E., Wielopolski M., Javadian A., Heisel F.: Bamboo Fibre Reinforced Polymers as Highly Flexible Reinforcement of Masonry Structures in Seismic Areas. 12th International Symposium on Fiber Reinforced Polymers for Reinforced Concrete Structures (FRPRCS-12) & 5th Asia-Pacific Conference on Fiber Reinforced Polymers in Structures (APFIS-2015) Joint Conference, 14-16 December 2015, Nanjing, China.
14. Kwiecień A.: Strengthening of masonry using natural fibers bonding with highly deformable adhesives. GSTF Journal of Engineering Technology (2015) Vol 3 No 2, pp. 103-114, DOI 10.5176/2251-3701_3.2.134.
15. Jasieńko J., Kwiecień A., Skłodowski M.: New flexible intervention solutions for protection, strengthening and reconstruction of damaged heritage buildings. INTERNATIONAL CONFERENCE ON EARTHQUAKE ENGINEERING AND POST DISASTER RECONSTRUCTION PLANNING (ICEE-PDRP 2016), 24-26 APRIL 2016, BHAKTAPUR, NEPAL Tybet.
16. Kwiecień A., Gams M., Viskovic A., Zając B.: Temporary and removable quick seismic protection of weak masonry structures using highly deformable adhesives. Structural analysis of historical constructions : anamnesis, diagnosis, therapy, controls. Proceedings of the 10th International Conference on Structural Analysis of Historical Constructions, SAHC 2016, Leuven, Belgium, 13-15 September 2016 / eds. Koen Van Balen, Els Verstrynge. – Leiden : CRC Press/Balkema, 2016, pp. 1528-1535.

Differences in strain distribution of stiff mineral and flexible polyurethane adhesives in DIC observation

A. Kwiecień[1], Ł. Hojdys[2], P. Krajewski[3], M. Tekieli[4]

Introduction

Stiff and brittle adhesives as epoxy resin or mineral mortars are applied in composite strengthening systems, bonded to concrete and masonry substrates (also of brittle character). Composite reinforcement textiles made of aramid, basalt, carbon, glass, polyparaphenylene benzobisoxazole, steel or natural fibers are known as FRP/SRP Fibre/Steel Reinforced Polymers when epoxy resins are used, or as FRCM (Fabric Reinforced Cementitious Matrix), TRM (Textile Reinforced Mortar), SRG (Steel Reinforced Grout) when mortar-based composites are used. There are observed in such systems peaks of stress concentration and low effective bonding lengths [1-3], proportional to high stiffness of adhesives [4]. In last few years, application of FRPU/SRPU (Fibre/Steel Reinforced Polyurethanes) with flexible polyurethane adhesives in single lap shear tests (SLST) on masonry substrates were tested in European laboratories [3, 5-7]. They results manifested increase of maximum load, ultimate slip and ultimate work for the composite systems with flexible adhesives, in comparison to the same parameters for the systems with stiff adhesives. Flexibility of an adhesive layer is key issue in an aspect of reduction of stress concentration and stress redistribution, when it is loaded in SLST, and can be observed using Digital Image Correlation (DIC).

Tested setup and results of SLST

There were compared four different composite strengthening systems (Table 1). In all of them, solid clay bricks SanMarco Rosso Vivo A6R55W were used, previously adopted in Round Robin Tests run by the RILEM TCs 223MSC [1, 2] and 250CSM [3, 7], as substrates in form of single bricks or masonry prisms. Material parameter details can be found in [1, 3]. The presented SLST were carried out at Cracow University of Technology using setup presented in Fig. 1a and DIC system with photo camera and CivEng Vision softwere [8] – Fig. 1b.

The specimens (Table 1) were chosen because of different failure modes presented in Fig. 2, to be visualized by DIC with various strain distribution. Load-slip characteristics of the tested specimens are presented in Fig. 3. The specimen A3/3 is the same as R12, but was tested after durability test (immersed in alkaline agent for 3000 hours).

Table 1: Tested specimens and their failure modes

Specimen	Fibre	Adhesive	Substrate	Failure mode
RR-T-B-CTF-1	Basalt	Cement based mortar	Masonry prism	A
RR-T-A-C-M17	Carbon	Lime based mortar	Masonry prism	B/C
R12	Steel	Polyurethane PS	Brick	C
A3/3	Steel	Polyurethane PS	Brick	D

[1] Institute of Structural Mechanics, Cracow University of Technology, Poland, akwiecie@pk.edu.pl
[2] Institute of Building Materials and Structures, Cracow University of Technology, Poland, lhojdys@pk.edu.pl
[3] Institute of Building Materials and Structures, Cracow University of Technology, Poland, pkrajews@pk.edu.pl
[4] Institute for Computational Civil Engineering, Cracow University of Technology, Poland, mtekieli@l5.pk.edu.pl

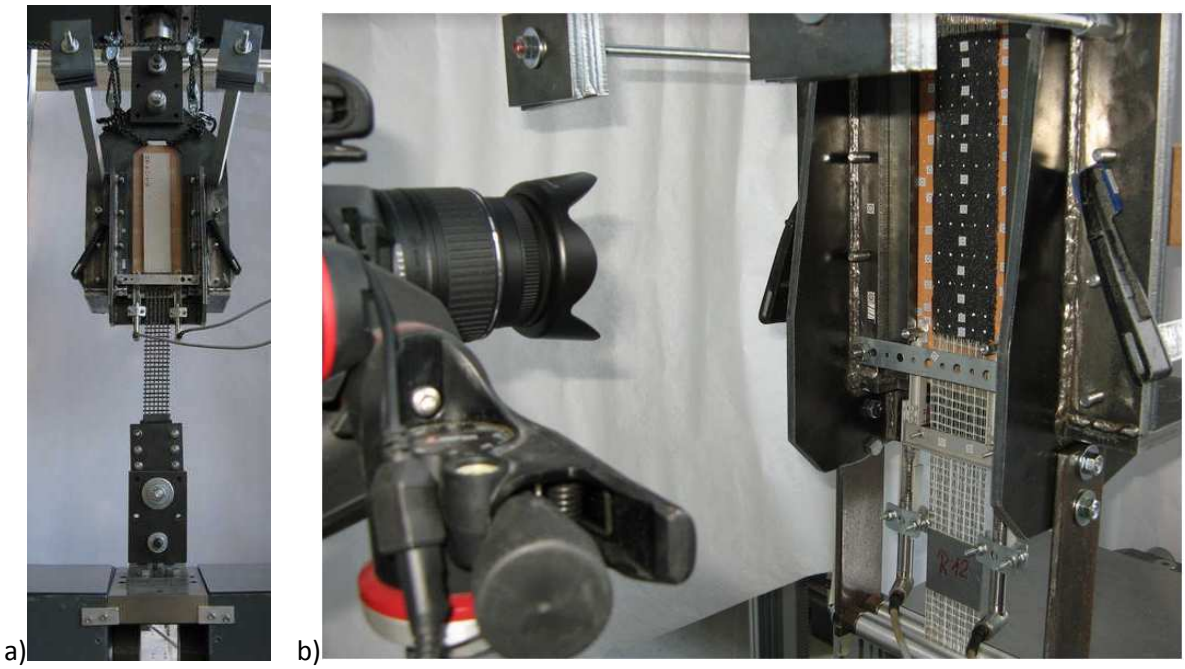

Figure 1: SLST setup (a) and DIC measurement system with markers at the specimen surface (b)

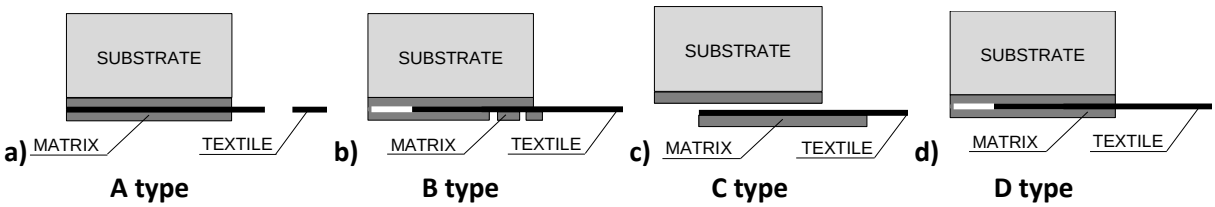

Figure 2: Observed failure modes: A type – tensile rupture of the fibres (out of the bond area), B type – fibres slippage within the matrix with cracking of the outer layer of mortar, C type – debonding at the fibres-to-matrix interface, D type – fibres slippage within the adhesive matrix

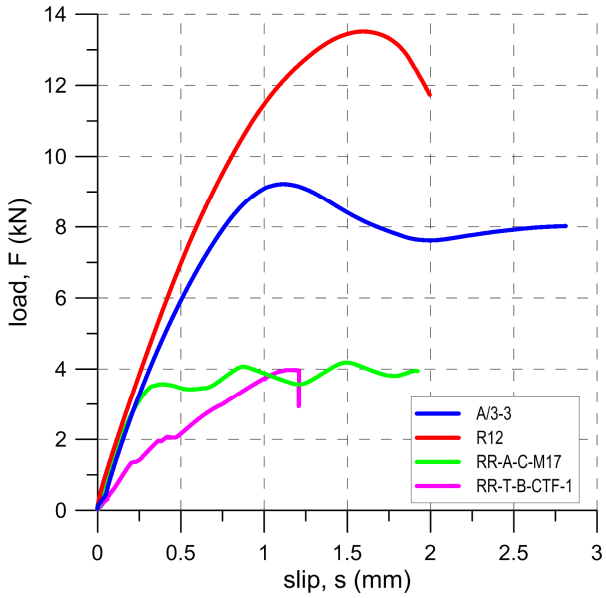

Figure 3: Load-slip characteristics of STST

Characteristic results obtained from load-slip curves presented in Fig. 3 are listed in Table 2. The table includes three groups of results: the maximum force and the corresponding slip with the calculated work at the maximum force, the ultimate slip and the corresponding force with the calculated work at the ultimate slip, and calculated ductility and work ratios.

Table 2: SLST results of the tested specimens

Specimen	Max force (kN)	Max slip (mm)	Max work (kJ)	Ultimate force (kN)	Ultimate slip (mm)	Ultimate work (kJ)	Ductility ratio (f)/(c)	Work ratio (g)/(d)
(a)	(b)	(c)	(d)	(e)	(f)	(g)	(h)	(i)
RR-T-B-CTF-1	3.973	1.149	18.645	2.935	1.208	18.876	1.05	1.01
RR-T-A-C-M17	4.181	1.502	14.047	3.941	1.922	15.208	1.28	1.08
R12	13.514	1.594	41.246	11.734	1.995	44.046	1.25	1.07
A3/3	9.218	1.122	23.319	8.020	2.812	35.843	2.506	1.54

SLST results presented in Table 2 indicate that flexible polyurethane adhesives (even after durability tests) allow obtained 2-3 times higher maximum and ultimate loads, as well as 2-3 times higher maximum and ultimate work, and more ductile behaviour and than mineral adhesives. This phenomenon is caused by ability of flexible polyurethanes of high deformability to redistribute shear stress to the whole bonding area and to reduce stress concentrations in brittle substrates, responsible for cracks initiation. Reduction and redistribution of stress in substrate allow increasing bond strength in composite reinforcement systems in the case of wet-lay-up application and repair bonding [3, 5, 7, 9-11].

Visualization of bond behaviour made of stiff and flexible adhesives

DIC used during SLST of the tested specimens allowed comparing strain distribution observed at the matrix surface, reflecting the work of the composite-to-substrate interface. Four cases of strain distribution, characteristic for failure type shown in Fig. 2, are presented in Fig. 4-7.

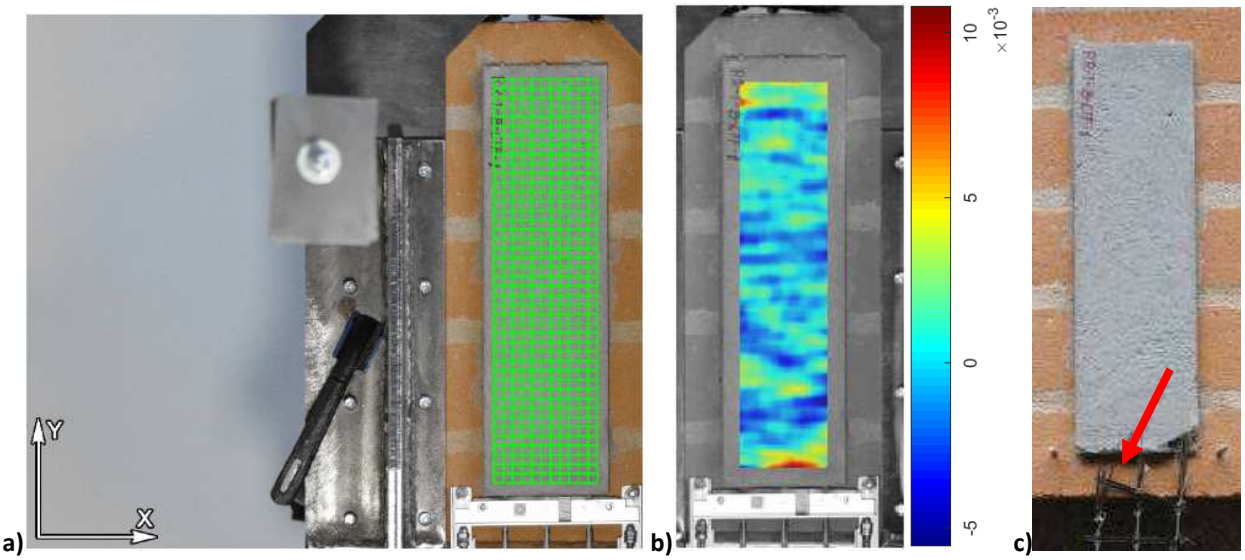

Figure 4: Basalt fibres embedded in cement base mortar (RR-T-B-CTF-1): grid of markers with coordinate system (a), map of strain by DIC with [%] scale (b), fibre rupture (A type failure) (c)

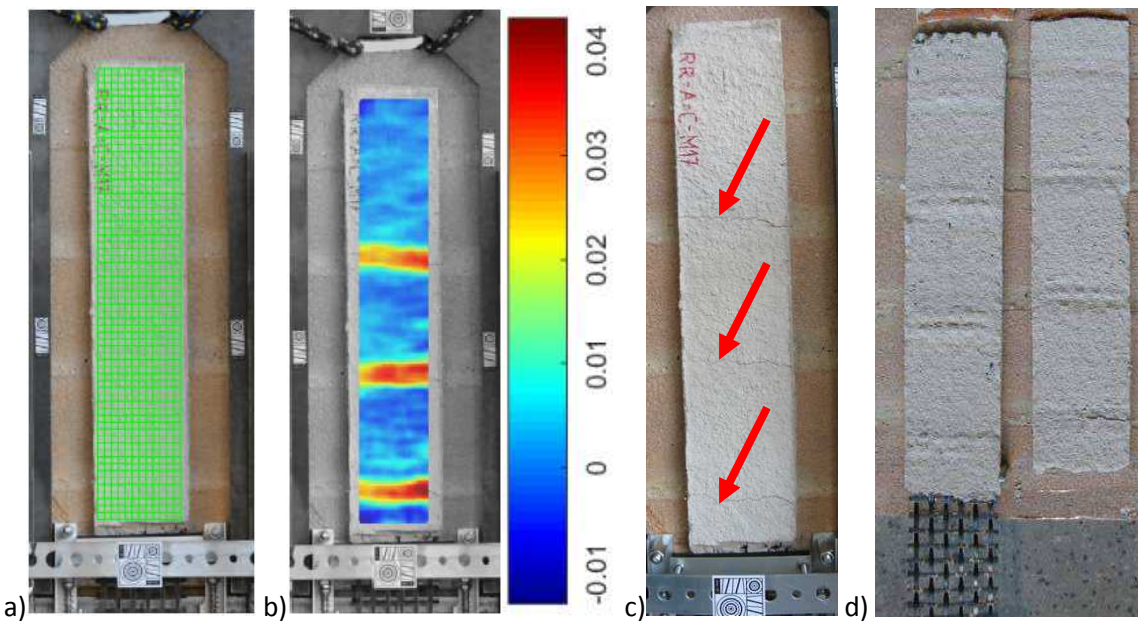

Figure 5: Carbon fibres embedded in lime base mortar (RR-T-A-C-M17): grid of markers (a), map of strain by DIC with [%] scale (b), visualization of cracks location (c), composite detachment initiated by cracks (B/C type failure) (d)

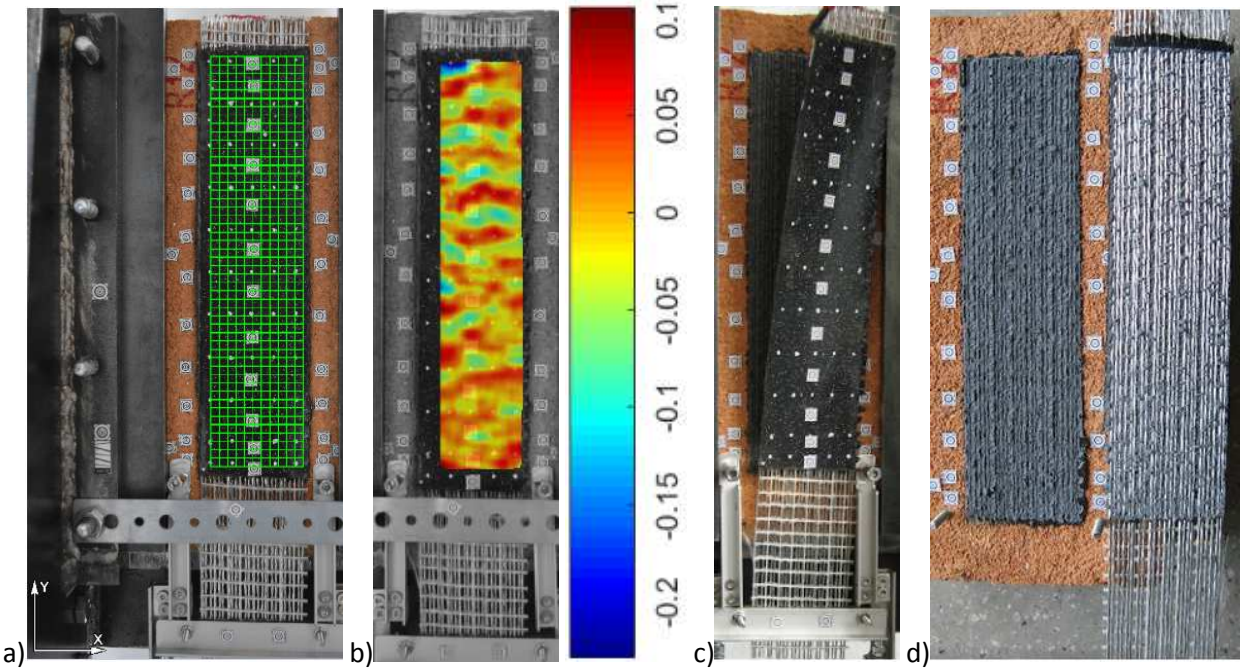

Figure 6: Steel fibres embedded in polyurethane PS matrix without ageing in alkaline agent (R12): grid of markers with coordinate system (a), map of strain by DIC with [%] scale (b), visualization of composite detachment at the composite-adhesive interface (c), adhesive failure (C type failure) (d)

In the first case (Fig.4), basalt fibres embedded in stiff and strong cement based mortar underwent rupture just at the matrix boundary at the loaded end. DIC clearly showed a relatively low peak of strain concentration occurrence in the place of failure, when the rest of the bond did not work. Stiff mortar did not allow for stress redistribution, causing a notch effect. Stress concentration in yarns and uneven stress distribution between them caused rupture of single fibres in a yarn at the interface with matrix and activated telescopic effect in local fibres slippage.

In the second case (Fig. 5), carbon fibres embedded in less stiff and weak lime based mortar were able to activate larger bonding area to work. The matrix transferred shear stress from loaded fibres to the

masonry substrate, up to the moment when the matrix strength was overcame in the place of weak substrate (mortar joint), resulting in the first crack occurrence at the loaded end, detachment of the first part of matrix and small load drop (Fig. 3). Interlocking effect between the matrix and the mortar joint caused small load increase up to the next brittle failure with the second crack and larger detached area. The same behaviour was observed with the third crack, and finally failure occurred when the fourth crack was activated.

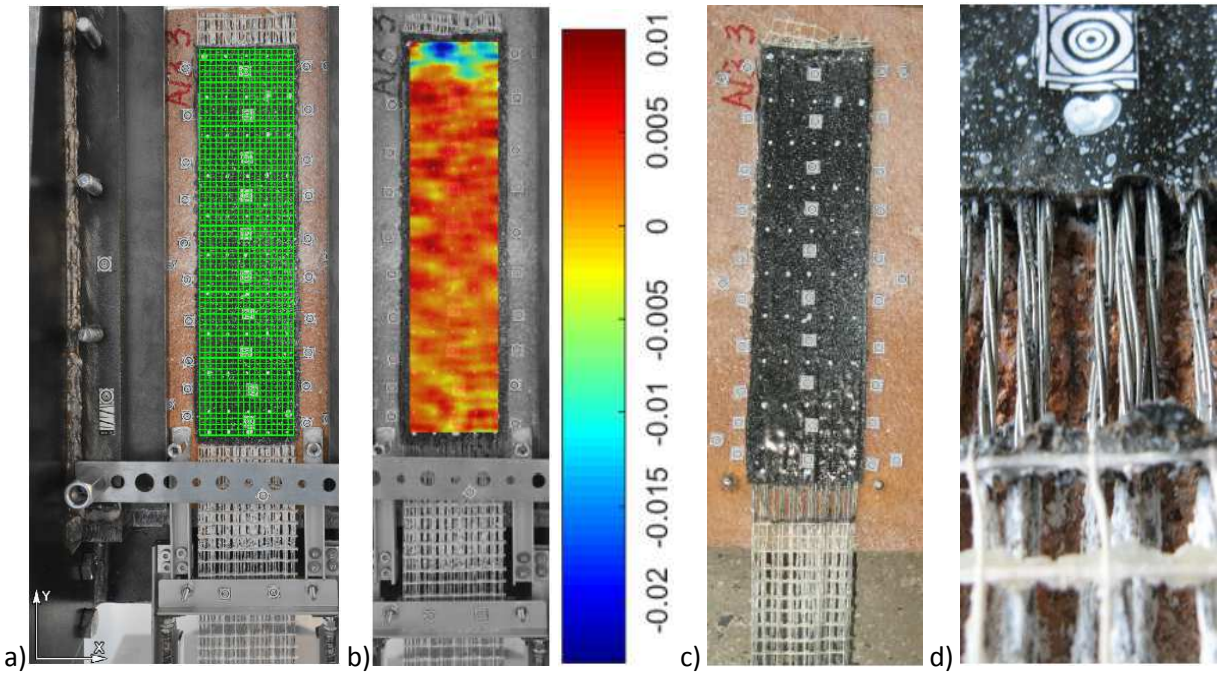

Figure 7: Steel fibres embedded in polyurethane PS matrix tested after ageing in alkaline agent (A3/3): grid of markers with coordinate system (a), map of strain by DIC with [%] scale (b), visualization of steel fibres slippage within the adhesive matrix (D type failure) (c), (d)

Completely different behaviour was observed for steel fibres embedded in flexible and highly deformable polyurethane PS matrix (Fig. 6). Low stiffness matrix allowed for redistributing of the shear stress along the whole bonding area, what resulted in significant load increase (Fig. 3) and in the work amount increase (Table 2). Redistribution caused reduction of stress concentration peaks (observed in stiff matrices) and thus bond ability to transfer higher loads. Final failure occurred at the interface between steel fibres and flexible matrix at relatively high level of strain observed at the whole surface of the strengthened area.

Similar specimen, as presented in Fig. 6, underwent ageing by immersing in alkaline agent for 3000 hours. In this process, the agent were able to penetrate the steel fibres weave by capillarity starting at the uncovered ends, initiating their corrosion inside the polyurethane matrix. Weakened by corrosion adhesive between steel fibres and the matrix resulted in drop of the maximum load, but also in increase of ductile behaviour (Fig. 3). Final failure in form of fibres slippage within the matrix was accompanied by the more or less even strains observed at the whole surface of the strengthened area (Fig. 7).

Conclusions

Composite strengthening systems are effective tools using for improving of structural strength in civil engineering . Typically, stiff adhesives of high strength are used, which generates stress concentrations responsible for failure mechanism. The use of more flexible adhesives allows reducing peaks of stress concentrations by redistributing them along the whole bonding area, what results in higher loads carried by the composite strengthening systems.

DIC started to be popular in the research analysis, because is able to visualise strain distributions at the whole investigated area. In the presented analysis, DIC showed and confirmed that shear load increase

in composite strengthening systems with flexible adhesives is caused by more even stress distribution along the bonding length than in stiff and brittle mineral adhesives. The DIC visualisation also proofed that the effective bonding length of the presented flexible adhesive is longer than the applied in the tested setup (250-260 mm). This aspect, mentioned previously in [5], will be investigated in the future.

Key references

1. Valluzzi M.R., Oliveira D., Caratelli A., Castori G., Corradi M., de Felice G., Garbin E., Garcia D., Garmendia L., Grande E., Ianniruberto U., Kwiecień A., Leone M., Lignola G.P., Lourenço P.B., Malena M., Micelli F., Panizza M., Papanicolaou C.G., Prota A., Sacco E., Triantafillou T.C., Viskovic A., Zając B., Zuccarino G., "Round Robin Test for Composite-To-Brick Shear Bond Characterization", Materials and Structures, 45 (2012), ISSN 1359-5997, pp. 1761-1791.
2. Kwiecień A.: Stiff and flexible adhesives bonding CFRP to masonry substrates - investigated in pull-off test and Single-Lap test. Archives of Civil and Mechanical Engineering 12 (2) 2012, Elsevier, ISSN 1644-9665, pp. 228–239.
3. Kwiecień A., De Felice G., Oliveira D.V., Zając B., Bellini A., Ghiassi B., Lignola G.P., Lourenço P.B., Mazzotti C., Prota A., De Santis S.: Repair of composite-to-masonry bond using flexible matrix. Materials and Structures (July) 2016, Volume 49, Issue 7, pp 2563–2580
4. Nemes O., Lachaud F., Mojtabi A., Contribution to the study of cylindrical adhesive joining. *Int. Journal of Adhesion & Adhesives*, 26 (2006), 474-480.
5. Ghiassi B., Xavier J., Oliveira D.V., Kwiecień A., Lourenço P.B., Zając B.: Evaluation of the bond performance in FRP-brick components re-bonded after initial delamination. Composite Structures Vol. 123 (May 2015) pp. 271–281, doi:10.1016/j.compstruct.2014.12.047
6. Garbin E.; Kwiecień A.; Panizza M.; Zając B.; Nardon F.; Valluzzi M.R.: Testing of bond solutions for UHTS steel strand composites applied to extruded bricks. Proceedings of the 16th International Brick and Block Masonry Conference, Padova, Italy, 26-30 June 2016. Edited by Claudio Modena, F. da Porto, and M. R. Valluzzi. CRC Press 2016. Pages 395–402. Print ISBN: 978-1-138-02999-6. eBook ISBN: 978-1-4987-9592-0.
7. Ceroni F., Bellini A., Garbin E., Kwiecień A., Mazzotti C., Panizza M., Valluzzi M.R.: Load bearing capacity and ductility properties of composites-to-brick dependent on an adhesive type. Structural analysis of historical constructions : anamnesis, diagnosis, therapy, controls. Proceedings of the 10th International Conference on Structural Analysis of Historical Constructions, SAHC 2016, Leuven, Belgium, 13-15 September 2016 / eds. Koen Van Balen, Els Verstrynge. – Leiden : CRC Press/Balkema, 2016, pp. 1061-1068.
8. Tekieli M., De Santis S., de Felice G., Kwiecień A., Roscini F.: Application of Digital Image Correlation to composite reinforcements testing. Composite Structures 2016. Composite Structures Available online 22 October 2016. http://dx.doi.org/10.1016/j.compstruct.2016.10.096. (In Press)
9. Kwiecień A.: Highly deformable polymers for repair and strengthening of cracked masonry structures. GSTF International Journal of Engineering Technology (JET) Vol.2 No.1, May 2013, ISSN 2251-3701, pp.182-196.
10. Kwiecień A., Zając B.: Is it Possible to Repair Detached Composites Effectively after Failure of Masonry Strengthening? Key Engineering Materials, Vol. 624 (2015), Trans Tech Publications, Switzerland, pp. 518-525.
11. Kwiecień A.: Strengthening of masonry using natural fibers bonding with highly deformable adhesives. GSTF Journal of Engineering Technology (2015) Vol 3 No 2, pp. 103-114, DOI 10.5176/2251-3701_3.2.134.

An Innovative Structural and Energy Retrofitting System for Masonry Walls using Textile Reinforced Mortars Combined with Thermal Insulation: Mechanical and Fire Behaviour

T. Triantafillou[1], K. Karlos[2], K. Kefalou[3], E. Argyropoulou[4]

Introduction

Masonry walls have been proven to be prone to failure during high or moderate intensity earthquakes or high wind pressure, hence they represent a significant hazard to life safety. Moreover, structural decay due to ageing or cumulative seismic-induced damage poses a direct threat to the preservation and safeguarding of masonry structures that comprise an important part of many countries' cultural heritage. Thereby, there is an urgent need for upgrading existing masonry structures, both in seismic areas, where structures designed according to old seismic codes have to meet upgraded performance levels demanded by current seismic design standards, and in non-seismic areas, e.g. due to change of usage and/or the introduction of more stringent design requirements.

Numerous techniques have been developed aiming at increasing the strength and/or deformation capacity of masonry walls, including the use of metallic or polymer-based grid reinforced surface coatings, shotcrete overlays, internal or external prestressing with steel ties, externally bonded or near-surface mounted fibre reinforced polymers (FRP) and textile reinforced mortar (TRM) jacketing. TRM-based solutions for masonry structures are becoming increasingly promising, as they combine the favourable properties offered by FRP systems (e.g. high strength and stiffness to weight ratio, high deformation capacity, corrosion resistance, ease and speed of application and minimal change in the geometry) while addressing most of the problems associated with the use of organic resins, namely: poor behaviour at elevated temperatures, incompatibility with substrates, combustibility, high costs of epoxies, lack of breathability, potential hazards for the workers, difficulty to conduct post-earthquake assessment behind FRP jackets, reversibility requirements etc.

In addition to structural (including seismic) retrofitting, given the high energy consumption associated to old buildings and their significant environmental impact, there is a strong need for effective solutions for the building envelope energy retrofitting. Towards this goal, a wide range of solutions has been proposed, with external and internal insulations becoming increasingly popular, due to high energy savings, the quick and easy application and the low cost.

Textile reinforced mortar (TRM) jacketing has minimal, if any, thermal insulation capacity, while external or internal insulation has no load bearing capacity. In this study the authors propose, for the first time, the combination of textile reinforced mortar (TRM) jacketing with thermal insulation into a single system, which will provide both structural (including seismic) and energy retrofitting. In this new system, illustrated in Fig. 1, the TRM is combined with the insulating material as a single unit, which may be either in the form of a prefabricated board or

[1] University of Patras, Greece, ttriant@upatras.gr
[2] University of Patras, Greece, karloskyriakos@gmail.com
[3] University of Patras, Greece, kalliopi.kefalou@gmail.com
[4] University of Patras, Greece, Eirini.argyr@gmail.com

constructed in situ. Depending on the loading, the aesthetics and the constructability requirements, the system may be placed either on both sides of existing masonry walls (preferably, if subjected to out-of-plane cyclic loading) or on one side. The TRM may be placed outside the insulating material, inside, that is between the insulation and the masonry wall, or on both faces (outside and inside) of the insulation. All the above are investigated experimentally in the present study for the case of masonry walls subjected to out-of-plane cyclic loading. The study includes fire testing of some of the masonry walls prior to mechanical testing. The details of the work are published in Triantafillou et al. (2006).

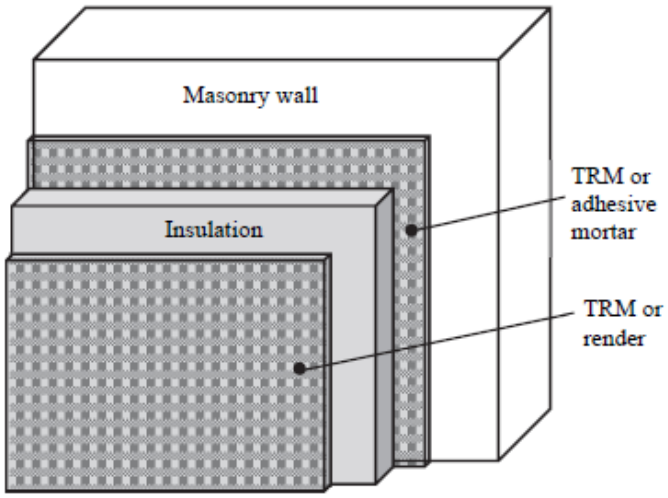

Figure 1: Schematic view of proposed structural and energy retrofitting system on one side of the masonry wall

Experimental Program

The investigation was carried out on two series of medium-scale, single-wythe, fired clay brick wallettes comprising running bond courses. The masonry wall in all specimens measured (approximately) 1500 mm in height, 400 mm in width and 85 mm in thickness. The specimens were subjected to cyclic out-of-plane bending, such that the plane of failure would form perpendicular to the bed joints (e.g. as in typical vertically supported walls loaded out-of-plane). Series A specimens were insulated using expanded polystyrene with a density equal to 29 kg/m^3 and a thermal conductivity coefficient equal to λ_p = 0.029 W/mK. Series B specimens were insulated using a fire-resistant insulation material made of foamed cement with a density equal to 115 kg/m^3 and a thermal conductivity coefficient equal to λ_c = 0.045 W/mK; specimens in this series were subjected to fire testing prior to mechanical testing.

Whereas all specimens received the same amount of structural retrofitting (four layers of textile), the investigation considered the following key parameters: cement-based versus polymer-based (not fire-resistant) insulating material; one sided versus two sided insulation; one sided versus two sided TRM jacketing; placement of the TRM jackets outside the insulation, between the insulation and the masonry or both outside the insulation and between the insulation and the masonry; thickness of the fire-resistant insulating material; and the displacement amplitude of the loading cycles.

All specimens were constructed using ridge-faced, 6-hole, horizontally perforated clay bricks, supplied by a local manufacturer, and a general-purpose masonry cement mortar. One specimen was used as control (M), without TRM or insulation (Fig. 2a). Series A included six different designs: (i) specimens 2M2 and 2M2s retrofitted on both sides with TRM containing

two layers of textile and no insulation (Fig. 2b); (ii) specimens 2iMi2 and 2iMi2s retrofitted on both sides with TRM containing two layers of textile and one layer of insulating material on both sides, between the TRM and the masonry (Fig. 2c); (iii) specimens 1i1M1i1 and 1i1M1i1s retrofitted on both sides with TRM containing one layer of textile, one layer of insulating material and a second TRM jacket with one layer of textile, such that the TRM forms the faces of a sandwich system with the insulation as the core material (Fig. 2d); (iv) specimens 2ii2M and 2ii2Ms retrofitted on one side with a sandwich system comprising TRM faces with two layers of textile and a core with two layers of insulation material (Fig. 2e); (v) specimens 2iiM2 and 2iiM2s with two layers of insulation material on one side and TRM jackets with two layers of textile on the outside (Fig. 2f); and (vi) specimen 2iMi2_na as in (ii) above (Fig. 2c), but with retrofitting materials "non-anchored" (hence the letters "na" at the end of the specimens' notation), i.e. not extending all the way to the end of the walls, so that they were not clamped between the end supports and the masonry. All specimens in Series A, except the ones in design (vi), that is the one with "non-anchored" retrofitting, were tested in pairs, corresponding to two different displacement amplitudes (1 mm and 2 mm) of the loading cycles.

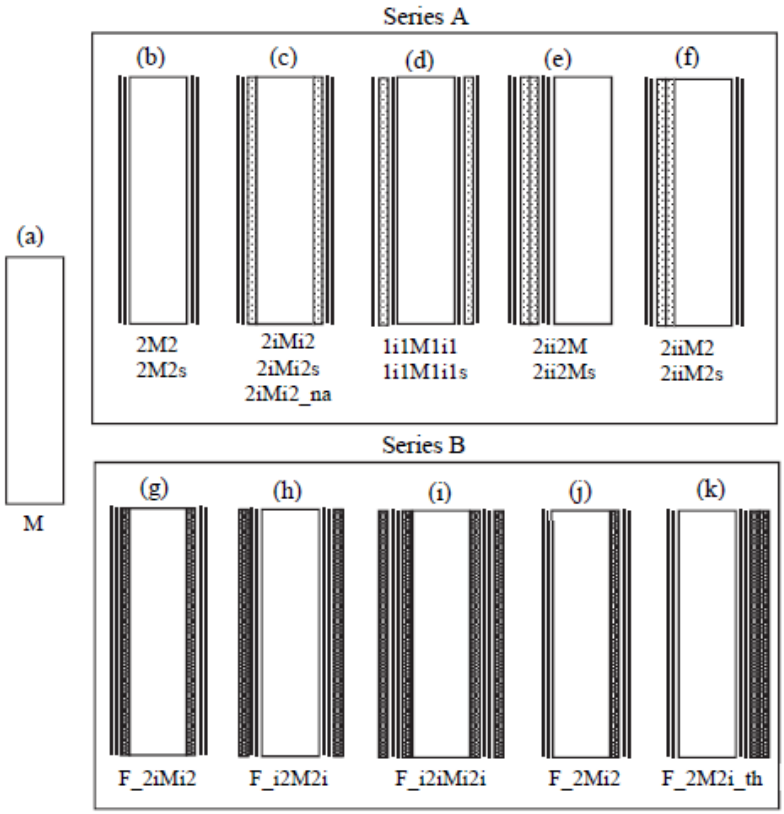

Figure 2: (a) Control specimen; (b)-(f) Series A specimens; and (g)-(k) Series B specimens

Series B included five different designs, subjected to fire testing prior to mechanical testing: (i) one specimen (F_2iMi2) retrofitted on both sides with TRM containing two layers of textile and one layer of fire-resistant insulating material on both sides, between the TRM and the masonry (Fig. 2g); (ii) one specimen (F_i2M2i) retrofitted on both sides with TRM containing two layers of textile and one layer of fire-resistant insulating material on both sides, outside the TRM (Fig. 2h); (iii) one specimen (F_i2iMi2i) retrofitted on both sides with two layers of fire resistant insulating material and TRM containing two layers of textile between the two insulating layers (Fig. 2i); (iv) one specimen (F_2Mi2) with one layer of fire-resistant insulating material on one

side (interior) and TRM jackets with two layers of textile on the outside (Fig. 2j); and (v) one specimen (F_2M2i_th) retrofitted on both sides with TRM containing two layers of textile and one thicker layer (hence the letters "th" at the end of the specimens' notation) of fire-resistant insulating material on one side (interior) (Fig. 2k).

For the specimens receiving externally bonded strengthening, a commercial textile with equal quantity of polymer-coated glass fibre rovings in two orthogonal directions was used. Each fibre roving was 3 mm wide and the clear spacing between rovings was 7 mm. The weight of the textile was 300 g/m^2 and the nominal thickness of each layer (based on the equivalent smeared distribution of fibres) was 0.06 mm. The guaranteed tensile strength of the glass fibres (as well as of the textile, when the nominal thickness is used) in each direction, as taken from data sheets of the producer, was equal to 1400 MPa. The elastic modulus of glass fibres was 74 GPa. All other details on masonry, mortars, application methods etc. are given in Triantafillou et al. (2016).

All strengthened specimens were subjected to cyclic out-of-plane loading using a stiff steel frame. The walls were laid horizontal (with the bonded surfaces facing upwards and downwards) and were loaded in three-point bending (Fig. 3a) at a span of 1.30 m. Two pairs of steel hinges were placed at each support (along the specimens' width, at top and bottom) and a third one was placed at mid-span (that is along the load application line).

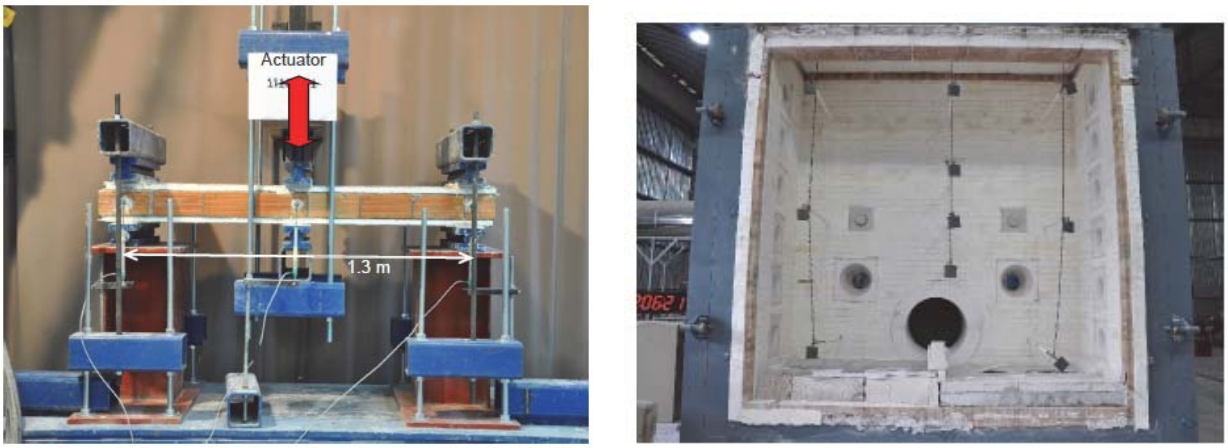

Figure 3: (a) Experimental setup for mechanical testing; (b) furnace used for fire testing

All specimens in Series B were subjected to one-sided fire testing for 90 minutes inside a 3x3x1.2 m furnace (Fig. 3b) according to EN 1363-1. While the mean temperature in the furnace reached 1006 ^{o}C, temperatures in the TRM on the exposed (to fire) face of each wall were measured through the use of thermocouples as follows: 870 ^{o}C in specimens F_2iMi2 and F_2Mi2, 340 ^{o}C in specimens F_i2M2i and F_i2iMi2i, and 90 ^{o}C in specimen F_2M2i_th.

Fire resulted in full or partial damage of the TRM on the exposed face of each wall, depending on the protection provided by the insulating material. In specimens F_2iMi2 and F_2Mi2, with the insulation between the TRM and the masonry, the TRM was fully destroyed. In specimens F_i2M2i and F_i2iMi2i, with a 20 mm thick fire insulation material on top of the TRM, the insulating material developed cracks and the TRM was partially damaged. Finally, in specimen F_2M2i_th, with the 70 mm thick insulating material, damage in the TRM was minimal, if any.

Following fire testing, the specimens were left to cool; a couple of days later they were subjected to mechanical testing.

Results and Discussion

The results are briefly discussed next on the basis of the load versus out-of-plane displacement response. Peak load values in the push and pull directions, P_{max}^{+} and P_{max}^{-}, mid-span displacements at failure, δ_u^{+} and δ_u^{-} (defined as the point of the load versus mid-span displacement envelope curve where either sudden load reduction was detected or a 20% reduction in load was noted in specimens with gradual post-peak load reduction), cumulative energy dissipation capacity and observed failure modes and stiffness properties for all specimens are discussed in Triantafillou et al. (2016).

Series A – Mechanical testing only

The control specimen (M) of Series A failed under monotonic loading at a maximum load of 3.42 kN, following the formation of a single crack at the brick – head joint interfaces closest to the loading line (mid-span). Visual inspection revealed that the crack caused fracture of two bricks and propagated stepwise through one of the bed joints (in the longitudinal direction). All other (retrofitted) specimens failed at higher loads (see Table 1), as described next.

The load versus mid-span displacement hysteresis loops for all retrofitted specimens in Series A are given in Fig. 4. Specimens 2M2 and 2M2s failed due to gradual tensile rupture of the TRM jacket both in the push and in the pull direction (Fig. 4a, b), following the formation of a single crack at mid-span of the masonry wall. Specimens 2iMi2 and 2iMi2s (Fig. 4c, d) failed in a similar way, except for specimen 2iMi2 in the push direction, which failed due to debonding at the interface between the masonry and the insulation. In these specimens the middle crack propagated from the masonry wall through the insulation and then caused sudden rupture of the fibres. Failure in specimen 2iMi2_na (Fig. 4e) was due to debonding, which was caused by the less favourable anchorage conditions of the retrofitting system; this fact highlights the importance of anchorage. Specimens 1i1M1i1 and 1i1M1i1s (Fig. 4f, g) failed due to rupture of the fibres, first in the outer faces, due to the higher lever arm, and then in the inner ones. As expected, specimens 2ii2M and 2ii2Ms (Fig. 4h, i) performed well only in the push direction, because the retrofitting system was one-sided, that is all four layers of the textile were placed on the same (tension) side (Fig. 2e); failure in this direction occurred due to fibre rupture in the outer face. In the pull direction these specimens displayed low strength, as if they were without strengthening, due to the lack of reinforcement in the tension zone. Finally, in specimens 2iiM2 and 2iiM2s (Fig. 4j, k) failure was due to rupture of the fibres in the push direction and due to debonding at the interface between the two insulation layers and between the masonry and the first insulation layer in the pull direction.

Overall, it is concluded that the new retrofitting system is extremely effective. In terms of strength and deformation capacity, the combined use of textile reinforcement with insulation material is better than the use of TRM alone. TRM jacketing without insulation (specimen 2M2) increased the strength by approximately 170% [(9.28 kN-3.42 kN)/3.42 kN=1.71], whereas this increase varied from 200% [(10.25-3.42)/3.42=1.99] to 340% [(15.14-3.42)/3.42=3.43] when the (double sided) textile reinforcement was combined with insulation layers, due to the increased lever arm of the tension reinforcement. The respective numbers for specimens type “s” (small displacement amplitude increment) are 135% [(8.06-3.42)/3.42 = 1.36], 190% [(10.01-3.42)/3.42 = 1.93] and 285% [(13.18-3.42)/3.42 = 2.85]. As, expected, jackets with

unfavourable bond conditions (specimen 2iMi2_na) were less effective; they increased the strength by at least 200%, whereas the strength increase in specimen 2iMi2, with favourable bond conditions, was at least 235% [(11.47-3.42)/3.42=2.35].

In terms of deformation capacity, as expressed by the mid-span displacement at failure, TRM jacketing combined with insulation was always much more effective than the TRM system alone, by up to approximately 140-145%.

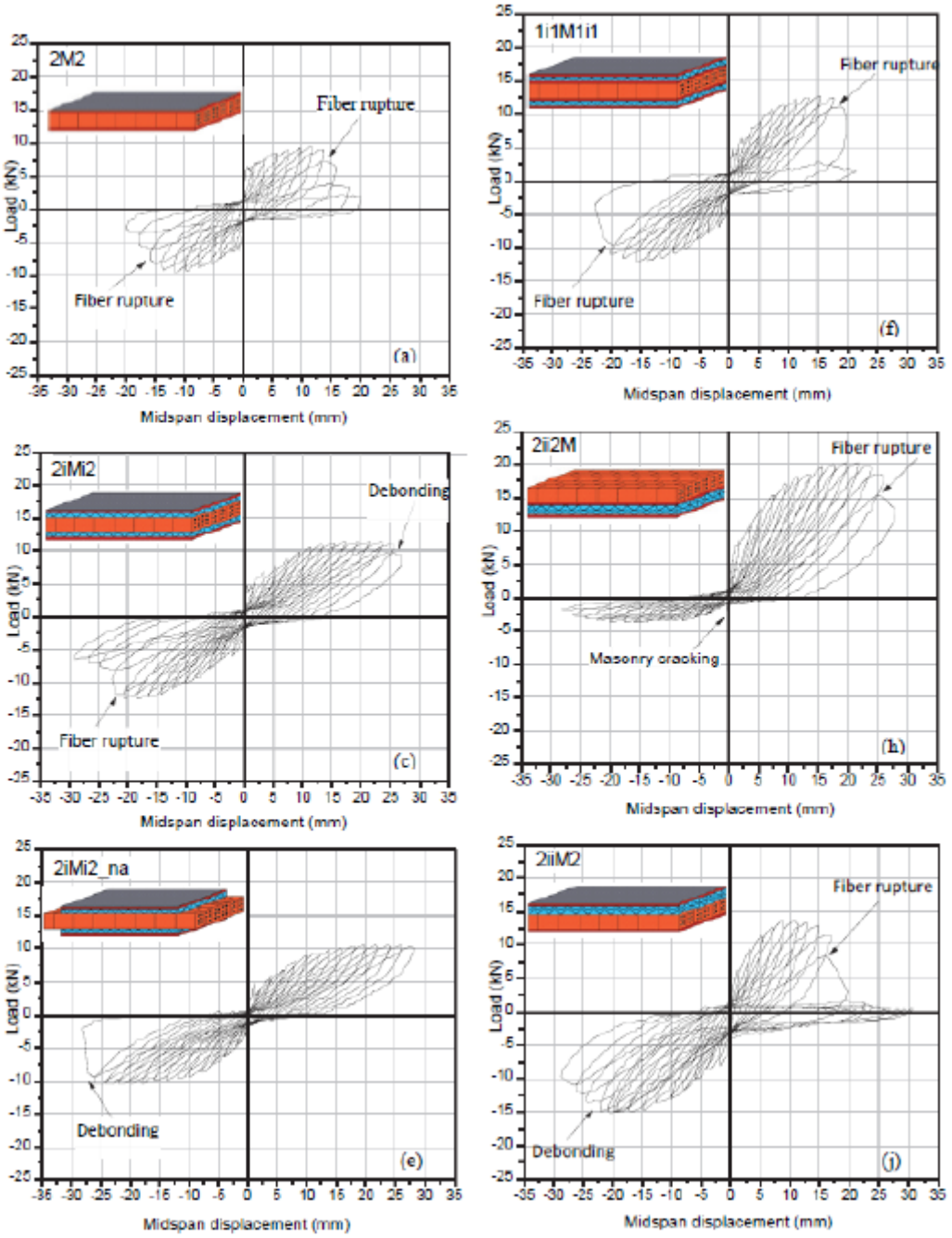

Figure 4: Load versus mid-span displacement hysteresis loops for some specimens in Series A

Series B – Mechanical testing after fire testing

The load versus mid-span displacement hysteresis loops for all retrofitted specimens in Series B are given in Fig. 5. Specimen F_2iMi2 displayed poor behaviour in the pull direction, because the TRM jacket mobilized in tension in this direction had already failed during fire testing. Failure in this direction occurred due to masonry (flexural) cracking. In the push direction

failure was due to debonding at the interface between the masonry and the insulation. Specimen F_i2M2i failed due to tensile rupture of the TRM jacket both in the push and in the pull direction, following the formation of a single crack at mid-span of the wall. Partial damage of the TRM jacket on the fire-exposed face of the wall resulted in reduced capacity when this jacket was subjected to tension, that is in the pull direction. Failure in specimen F_i2iMi2i in the push direction was due to debonding at the interface between the insulating material and the masonry. In the push direction the capacity of the specimen was reduced substantially, due to damage of the TRM (subjected to tension in this direction) during fire testing. Finally, specimen F_2M2i_th failed due to tensile rupture of the TRM jacket at high loads both in the push and in the pull direction, following the formation of a single crack at mid-span.

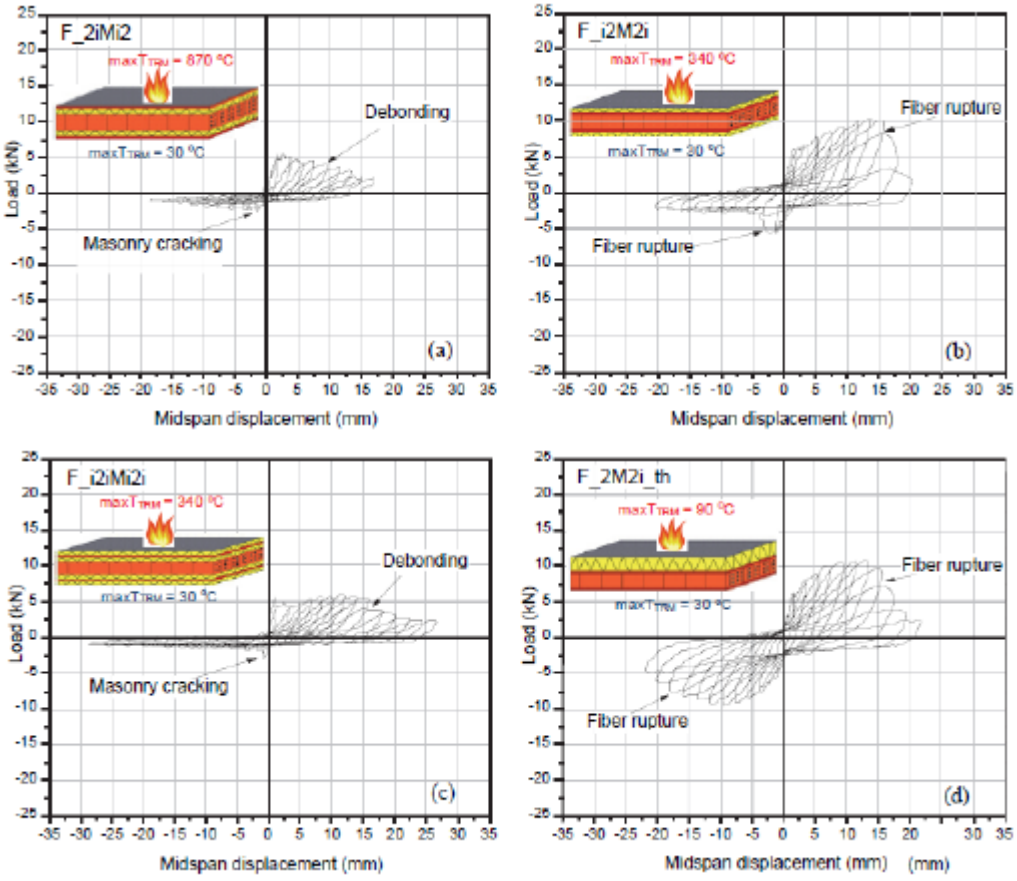

Figure 5: Load versus mid-span displacement hysteresis loops for specimens in Series B

Overall, it is concluded that if the TRM is protected by a fire-resistant insulating material of proper thickness, the new retrofitting system is extremely effective after the event of fire. The effectiveness depends on the thickness of the insulation: 70 mm of a cement-based insulating material provided full protection (specimen F_2M2_th), whereas 20 mm of the same material was 40% [(9.52-5.62)/9.52=0.41] less effective, as concluded by comparing the response of specimens F_2M2I_th and F_i2M2i. On the other hand, the lack of fire insulation outside the TRM (specimens F_2iMi2, F_2Mi2) yields poor behaviour. In terms of deformation capacity, as expressed by the mid-span displacement at failure, TRM jacketing combined with proper fire insulation (specimen F_2iMi2) was slightly more effective than the TRM system alone (specimen 2M2), by approximately 13-15%.

Conclusions

The present study presents an innovative system for both structural (including seismic) and energy retrofitting of masonry walls, involving the combination of textile reinforced mortar (TRM) and thermal insulating materials. The system was tested on brick masonry wallettes subjected to out-of-plane cyclic bending. Some of the wallettes were subjected to fire testing prior to mechanical testing, to assess the effectiveness of the new system under realistic fire conditions.

Overall, it is concluded that the new retrofitting system not only improves the thermal performance of masonry walls but also is extremely effective as a means of structural retrofitting. In terms of strength and deformation capacity of walls not subjected to fire, the combined use of textile reinforcement with insulation material is better than the use of TRM alone. In case of masonry walls subjected to fire prior to mechanical loading, the new system is quite effective provided that the TRM is placed under the fire-resistant insulating material. In this case, the effectiveness of the retrofitting increases with the thickness of the fire insulation.

From the results obtained in this study the authors believe that TRM jacketing may be combined effectively with thermal insulation, which can be fire-resistant too. The proposed system provided an extremely promising solution for combined structural and energy retrofitting of masonry subjected to out-of-plane bending. Further investigation is currently under way to enhance the experimental database and to optimize the proposed solution through analytical and numerical modelling.

References

EN 1363-1 (1999). Fire resistance tests – Part 1: General requirements, European Committee for Standardization, Brussels.

Triantafillou, T, Karlos, K., Kefalou, K and Argyropoulou, E (2016). An Innovative Structural and Energy Retrofitting System for URM Walls using Textile Reinforced Mortars Combined with Thermal Insulation: Mechanical and Fire Behavior. *Construction and Building Materials*, accepted for publication.

3.11

Strengthening of Timber Structures

FRP reinforcement and production of duo laminated timber beams

Basterra, L.A.[1]; Acuña, L.; Casado, M.; López, G.; Morillas, L.; Balmori, J.A.

1 Introduction

Reinforcing timber structures in service with Fiber Reinforced Polymers (FRP) materials is a well-known technique, extensively developed in the literature [1]. However, direct applications of FRP to commercial wood products for new structures [2] is limited to few cases such as FiRP® Reinforced Glulam Technology. Based on previous work [3,4,5], this research focuses on the improvement and enhancement of fast-growing, low-cost, low-strength timber, through the incorporation of internal FRP reinforcements.

For this purpose, we produced and tested reinforced duo laminated beams, with timber from species such as poplar (*Populus x euroamericana I-214*) and maritime pine (*Pinus pinaster Ait.*), which are currently only designated for non-structural purposes in Spain. In addition, a series of non-reinforced duo beams were produced to serve as a control group. We studied how to increase the stiffness of the beams and to homogenize their mechanical performance, by applying different types of FRP reinforcements, adhesives, and ratios of reinforcement, at relative competitive costs.

Laminated duo beams are used, as they represent the most basic system of industrialization. The GFRP reinforcement is introduced into the glue line, protected from fire action [6] and atmospheric agents. This also allows for different widths of reinforcement, without any visual impact (Fig. 1).

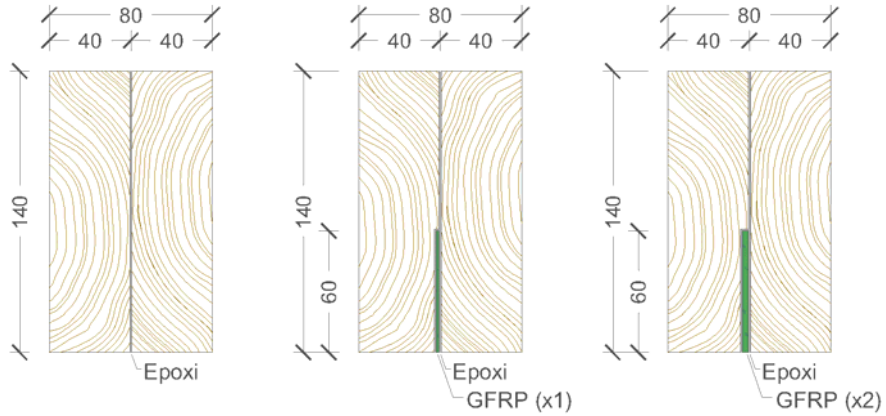

a) Unreinforced beam (control). b) Reinforced beam (simple). c) Reinforced beam (double).

Fig. 1. Variants of tested beams.

2 Materials and methods

2.1 Type of timber

The wood used in the manufacture of test specimens belongs to the species *Populus x euroamericana I-214* and *Pinus pinaster Ait.*, which basic characteristics are shown in Table 1.

[1] *Research group of Timber Structures and Wood Technology of the University of Valladolid (Spain).*
Email: maderas@uva.es URL: http://www3.uva.es/maderas/

Table 1. Cross section and mechanical properties of the timber.

Type of timber	Cross section *(mm)*	Young´s Modulus *(GPa)*	Ultimate stress *(MPa)*
Populus x euroamericana I-214	(40+40) x 140	7.83 (10.18)[a]	36.02 (25.51)[a]
Pinus pinaster Ait	(40+40) x 140	11.01 (14.77)[a]	54.75 (25.41)[a]

[a] COV% is given in parenthesis

2.2 Selection and characterization of FRP fibers

The first phase of the research focused on the testing and characterization of various high modulus fiber fabrics available. Tensile tests were performed, according to ASTM D2256-02 [7], to obtain the elasticity moduli of each material, and a comparison was drawn between their mechanical performance and their cost. Among the analyzed fibers, 3 types were chosen: FIDFLAX UNI 300 HS 50, FIDGLASS UNI 300 HT 73 and SIKAWRAP-203 C / 45. A series of reinforced beams were made and subjected to four-point flexural tests, according to EN-408: 2011 [11]. The results obtained from this testing showed the improvements produced by different reinforcements [8]. A partial conclusion from this first phase is that the best mechanical / price improvement ratio is achieved with fiberglass reinforcements.

2.3 Selection and characterization of adhesives

Preliminary tests with different types of epoxy resin were carried out to verify the bond between these wood species and FRP. The following EPX adhesives were tested according to UNE-EN 56543: 1988 [9]: Spabond 340LV; Sikadur 30; Sikadur 330; Sikadur 31CF; Mapei Mapewood Primer 100; Mapei Mapewood Gel 120; Mapei Paste 140. Eventually, the Sikadur 30 epoxy resin was selected to be the most compatible with the GFRP reinforcements and wood species used.

2.4 Production and testing of GFRP strips

The vacuum infusion process was used to drive unsaturated isophthalic polyester resin into the laminate, reinforced with 1200 g/m^2 and 2400 g/m^2 uniaxial E-glass fibers. Some specimens were tested in tension (Fig. 2) until failure (Fig. 3), according to ISO 527-5: 2010 [10], to obtain their modulus of elasticity and ultimate tensile strength (Table 2).

Fig. 2. GFRP tension test according to ISO 527-5.

Fig. 3. GFRP strip failure analysis

Table 2. Cross section and mechanical properties of the reinforcement.

Type of composite	Cross section *(mm)*	Young´s Modulus *(GPa)*	Ultimate stress *(MPa)*	Resin type
GFRP 1200 g/m^2	2.1 x 15	21.6	455	thermosetting
GFRP 2400 g/m^2	3.4 x 15	26.8	570	thermosetting

3 Results and discussion

3.1 MDF beams testing (scale 1:25)

In order to reduce the variability due to the heterogeneity of wood, and to accurately study the effects of GFRP reinforcement, we tested 60 duo beams (19 + 19) x 60 x 1200 mm, made of medium density fiberboard "FINSA MDF FIBRALAC" and different GFRP ratios. The tests were performed according to UNE-EN 408: 2011 [11], and showed elastic stiffness and ultimate loads up to 1.5 kN. The differences between the results obtained in the 3 groups are significant, with improvements in the elastic moduli (MOE) of 26% and 38% in comparison to the unreinforced section (Fig. 4).

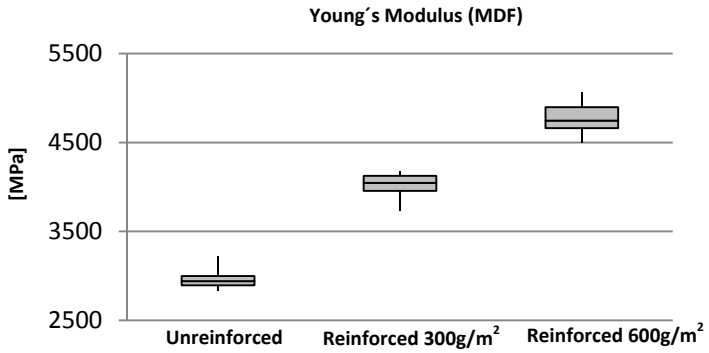

Fig. 4. Box and Whisker plot of Young´s Modulus of MDF beams.

3.2 *Populus x euramericana* and *P. pinaster* beams testing (scale 1:2)

The following groups of duo beams were made:

Table 3. Duo beams tested

Group	Wood species	Specimens	Reinforcement
1	*P. pinaster*	30	Unreinforced
2		30	GFRP 1200 g/m^2
3		30	GFRP 2400 g/m^2
4	*Populus x euramericana*	30	Unreinforced
5		30	GFRP 1200 g/m^2
6		30	GFRP 2400 g/m^2

Beams were tested in bending, according to UNE-EN 408: 2011 (Fig. 5), and the effects of GFRP reinforcements in the MOE, ultimate strength (MOR) and improvement in the dispersion of results were measured and analyzed. The failure modes of each beam were also observed.

Fig. 5. Four point bending test, according to UNE-EN 408 standard.

The results of these tests are shown in Fig. 6, showing an important improvement in reinforced *Populus* beams. In contrast, *P. pinaster* beams showed no significant improvements.

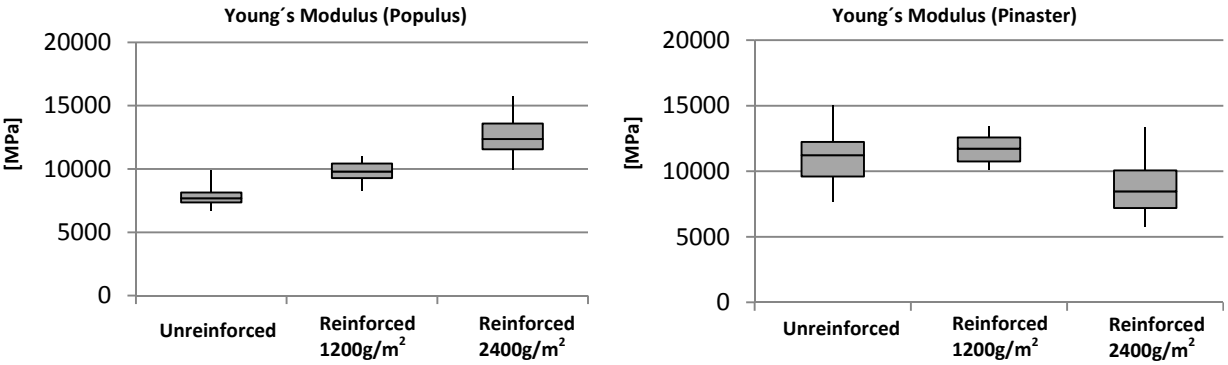

a) Populus beams Young´s Modulus results. b) Pinaster beams Young´s Modulus results.

Fig. 6. Box and Whisker plot of Young´s Modulus for populus and pinaster beams.

3.3 Creep testing

In order to study the long-term behavior of the reinforced duo beams, in relation to unreinforced ones, a long-term test has been set up, according to UNE-EN 380: 1998 [12], with a total load of 10 kN, which represents approximately 20% of ultimate load of the beams (Fig. 7). The ambient conditions of the laboratory remain nominally constant, 20 ± 2ºC; 65 ± 5% humidity in air, corresponding to a hygroscopic balance of 12% HR in the wood. Constant monitoring is now carried out using LVDTs and strain gauges to measure the history of deformations in the beams throughout the testing time.

Fig. 7. Creep testing.

4 Conclusions

• The best performance/cost ratio found in this research corresponds to rigid fiberglass reinforcement.
• The most compatible adhesive for the GFRP reinforcements and the wood species tested is the Sikadur-30 epoxy resin.
• Duo control tests with DMF board beams, show that the incorporation of GFRP reinforcements can increase their mechanical performance by 26-38%.
• The incorporation of GFRP reinforcements decreases the variability in the mechanical properties of the beams, reducing the effects of wood defects and irregularities, and increasing the characteristic values (5% percentile).

- *Populus* reinforced duos beams with GFRP significantly improve their mechanical properties.
- Reinforced duos of *P. pinaster* with GFRP do not reach the expected improvements.

5 Acknowledgments

This project received funding from the Ministry of Science and Innovation of the Government of Spain, through the sub-program Fundamental Research Projects Not Oriented, 2013–2015 (BIA2012-31233). The authors would also like to thank SIKA for their collaboration in this project.

6 References

[1] C.E. Bakis, L.C. Bank, V.L. Brown, E. Cosenza, J.L. Davalos, J.J. Lesko, A. Machida, S.H. Rizkalla, T.C. Triantafillou, Fiber-Reinforced polymer composites for construction - State of the art review. J. Compos. Constr. 6:2(73) (2002) 73–87.

[2] A. Parvez, The reinforcement of timber for structural applications and repair. PhD thesis, Dpt. Mech Eng. University of Bath, 2004.

[3] F.H. Theakston, A feasibility study for strengthening timber beams with fiberglass, Can. Agric. Eng. January (1965) 17–19.

[4] W.M. Bulleit, Reinforcement of wood: A review, Wood Fiber Sci. 16 (3) (1984) 391–397.

[5] K.U. Schober, A.M. Harte, R. Kliger, R. Jockwer, Q. Xu, J.-F. Chen, FRP reinforcement of timber structures, Constr. Build. Mater. 97 (2015) 106–118.

[6] Z.A. Martin, D.A. Tingley, Fire resistance of FRP reinforced glulam beams, in: Proc. World Conf. Timber Eng., Whistler, Canada, 2000.

[7] ASTM D2256-02 'Standard Test Method for Tensile Properties of Yarns by the Single-Strand Method'.

[8] L.A. Basterra Otero, L. Acuña, G. Casado, G. López, A. Bueno. Strength testing of Poplar duo beams, *Populus x euramericana* (Dode) Guinier cv. I-214, with fiber reinforcement. Constr. Build. Mater. 36 (2012) 90–96.

[9] UNE-EN 56543:1988 Physical and mechanical properties of wood. Determination of shear stress.

[10] ISO 527-5:2010 Plastics - Determination of tensile properties - Part 5: Test conditions for unidirectional fiber-reinforced plastic composites.

[11] UNE-EN 408:2011 Timber structures - Structural timber and glued laminated timber - Determination of some physical and mechanical properties.

[12] UNE-EN 380:1998 Timber structures. Test methods – General principles for static load testing.

3.12 Case studies

Shear and Flexural Upgrading of RC Beams Using CFRP Sheets and Laminates

Erkan AKPINAR[1], Onur ERTAS[2], Ozlem IMREN[3], Sevket OZDEN[4]

Introduction

Upgrading the deficient reinforced concrete (RC) buildings in Turkey is a critical issue for the public safety. The deficiency may be either due to the aging and corrosion or due to the lack of on-site quality control and mis-interpretation of the blue-prints. Such buildings need to be strengthened especially before being hit by a catastrophic earthquake. The intervention methods for the strengthening applications supposed to be rapid, easily applicable and cost effective in terms of not only application budget but also the occupancy interruption expenditures. Strengthening of the existing buildings by using the fiber reinforced polymer (FRP) applications is one of the most effective strengthening techniques among the other intervention choices. Ease of application, relatively short time duration for the installation, limited time elapse for occupancy/operation delay, and the adaptability to almost all cases can be listed as superior advantages of FRP strengthening techniques.

In this paper, the FRP strengthening application at a RC public building, even during its construction period in 2014 in Kayseri, Turkey, is presented. The city is located in 3rd grade seismic zone according to Turkish Seismic Code 2007 (TSC 2007) of which seismic zone classification is similar to Eurocode. The building has a U-shaped plan (*Fig.1*) and was composed of a ground floor (h=4.0m) and four storeys above with h=3.2m. The diaphragm system was two-way solid slab with beams in the building. Typical column and peripheral beam dimensions were 500x500mm and 300x600mm, respectively. The inner beams were 300x450mm in dimensions.

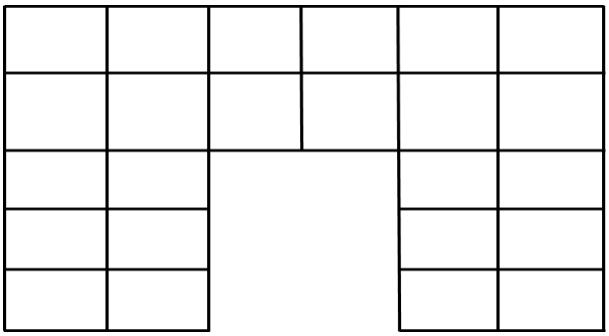

Figure 1: Plan of the strengthened building

The construction steps for that specific building were first to cast the columns at a specific height, and to cast the beams and the slabs afterwards. During the construction process, due to the lack of skilled onsite quality control engineers, all columns were cast at a height only 450mm shorter than the specified floor height, in order to preserve a space for the beams and the slabs. Unfortunately, the peripheral beams were 600mm in height and the flexural reinforcement for the positive moment was mis-placed resulting a reduction of 150mm in the useful depth of the beams. Moreover, the reinforcement for the negative moment at the beam ends was also less than the design specified values. In some other locations, especially for long span beams, the positive span moment and shear capacities were below the design values. In short, there were a wide spread of deficiencies in flexural moment capacity (either or both the positive and the negative sides) and shear capacities in beams of the building. The problem was concentrated on the second floor and identified well after the completion of the floors above. Strengthening of the beams was the only alternative against demolishing and reconstruction. The constructor preferred strengthening to reduce its overall budget and the owner accepted the strengthening designs offered for that specific problem.

[1] KOCAELI UNIVERSITY Department of Civil Engineering, Kocaeli Turkey, akpinarerkan@yahoo.com
[2] ACIBADEM RESTORASYON Architecture & Engineering Ltd. Co., Istanbul Turkey, ertas@acibademrestorasyon.com
[3] ACIBADEM RESTORASYON Architecture & Engineering Ltd. Co., Istanbul Turkey, imren @acibademrestorasyon.com
[4] OKAN UNIVERSITY Department of Civil Engineering, Istanbul Turkey, sevketozden@yahoo.com

The Challenges

The building to be strengthened would be used for public services and it was needed to be operational as soon as possible. Since the structural problem was related to member deficiencies and there was no need to enhance the lateral load capacity, in addition to time constraint, FRP strengthening technique was considered the best way for the intervention.

The shortage of moment capacity was not only in positive moment region but also in the negative sides of the beam supports. As it is a well-known matter about the negative moment capacity enhancement for beams, continuity of the reinforcement in beam to/through column is still a standing problem especially for the FRP strengthening. Therefore, a solution scheme for the continuity of the reinforcement should have to be adapted at the top face of the beams near the joints. Beside the moment capacity enhancement, shear strength upgrading was another issue for the beams in the building. The evaluation proses have shown that spread shear reinforcement needed along the beams. Obtaining the proper shear behaviour, it was aimed to have closed loops for the FRP wrapping instead of using U-shaped or end-anchored applications. Since the beams and slabs connected monolithically and cutting or slitting the edges excessively for the FRP wrapping would have given damage to the load flow and rigidity of the system, it was decided to just drill holes and supply the FRP continuity through the CFRP anchors bonded on the CFRP sheets.

The Solution

After the completion of the assessment and the analysis phases, the first thing on the field was the member surface preparation and the corner rounding at a 3 cm diameter. Some pictures related to the preparation process are shown in *Fig.2*. There exist certain amounts of unevenness on several beams. Prior the FRP application, such surfaces repaired with high quality cement based grout of which compressive strength is higher than 20 MPa after 1 day of pouring and tensile strength is 2 MPa after 28 days after pouring (*Fig.3 a*). The holes near the edges of the beams for shear strengthening were drilled and pressurise air was used for the cleaning (*Fig. 3 b and 3 c*). The epoxy based primer was rolled on to the concrete surfaces before the FRP application for the surface saturation (*Fig.3 d*). CFRP plates and sheets were used as FRP material for the strengthening application. The properties of CFRP materials are given in *Table 1*.

(a) (b)

Figure 2: Concrete surface preparation and corner rounding proses

There was positive and negative moment capacity deficiencies in beams, therefore, both the lower side at the mid-span and the upper side-regions near the joints of the beams were strengthened where needed. For the positive moment strengthening of the beams, CFRP plates were applied until and 150mm beyond the contra flexure points supplying an anchorage length (*Fig.4 e, 4 f*). On the other hand, for the negative moment strengthening of the beams, it was more complicated than the previous one since the continuity of the introduced CFRP material was crucial at the beam to column joint region for proper improvement. By doing so, CFRP plates ends at the joint region were bonded to a custom

made L-shaped steel anchorage pre-placed to the interrelated corner of the beam to column joint (*Fig.4*). Initially, after the surface preparation, holes were drilled on the column ends and anchorage steel bars were placed by using a high strength epoxy based grout (bond strength is higher than 3 MPa). The next step after the curing of the epoxy based grout, L-shaped steel anchorage apparatus bonded to CFRP plates were fastened to the bars, CFRP plates also glued to the concrete surface at the same time. CFRP wraps passing over this region which were applied originally for the shear reinforcement following the flexural strengthening, were clamped the L-shaped anchorage and supplied a secure supplementary measure for the application. It was calculated and designed that the weakest point of this negative moment intervention was the anchorage bars embedded into the columns. It was aimed that any possible failure for the assemblage would be occurred by yielding of the anchored bars to result in a limited ductility.

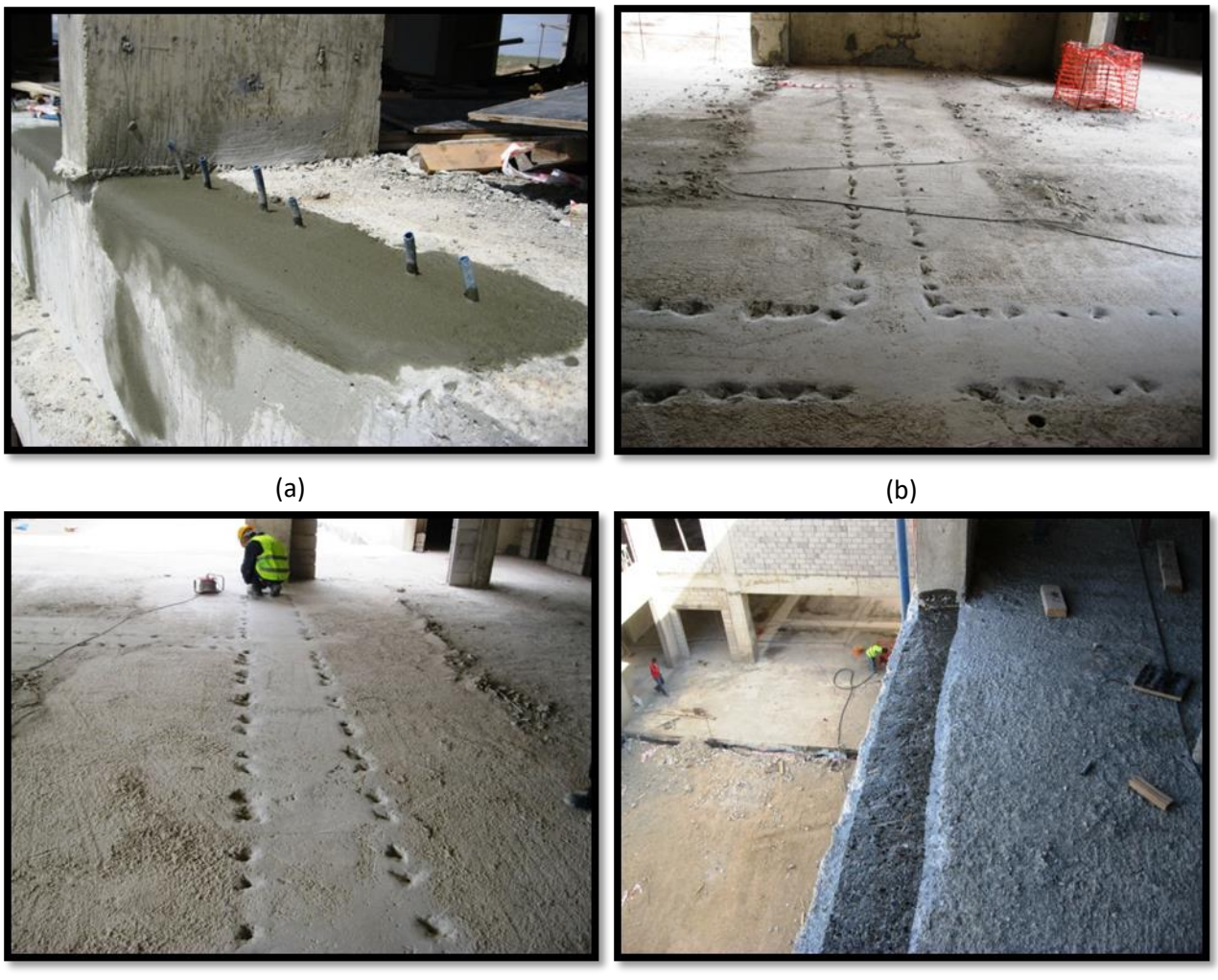

(a) (b)

(c) (d)

Figure 3: Repairing the unevenness on the surface and drilling holes

Table 1. Properties of used CFRP materials

	Carbon Fiber Sheet	Carbon Fiber Laminate
Modulus of Elasticity (MPa)	230,000	165,000
Tensile Strength (MPa)	4,900	2,500
Thickness (mm)	0.166	1.2
Width (mm)	500	50
Elongation at Break (%)	-	1.5
Total Fabric Weight (gr/m^2)	300	-

Figure 4: Flexural strengthening of beams a, b, c, d negative moment strengthening application, e, f positive moment strengthening application (f is also represents the shear strengthening application)

After the completion of the flexural strengthening, shear strengthening was carried out. Since the spread shear strengthening needed along the beams, it was decided to use full wrapping using CFRP sheets instead of using U-shaped or end-anchored application. On the other hand, it was obvious that the cutting or slitting the beam to slab edges excessively for the fully wrapping were harmful for the global behaviour and also time consuming effort. For overcoming this constraint, it was decided to drill

holes with a constant space along the beam to slab edges and supplied the CFRP sheets continuity through them. Accordingly, after the flexural strengthening phase completed, CFRP wraps were applied at each ends of the material were passed through the pre-drilled holes. The props of the CFRP sheets coming out through the holes were spliced 200 mm for obtaining sufficient anchorage. Further step, before the epoxy was not totally cured, was sand blasted by hand to roughen the surface of the beams for good bonding for the following plaster application.

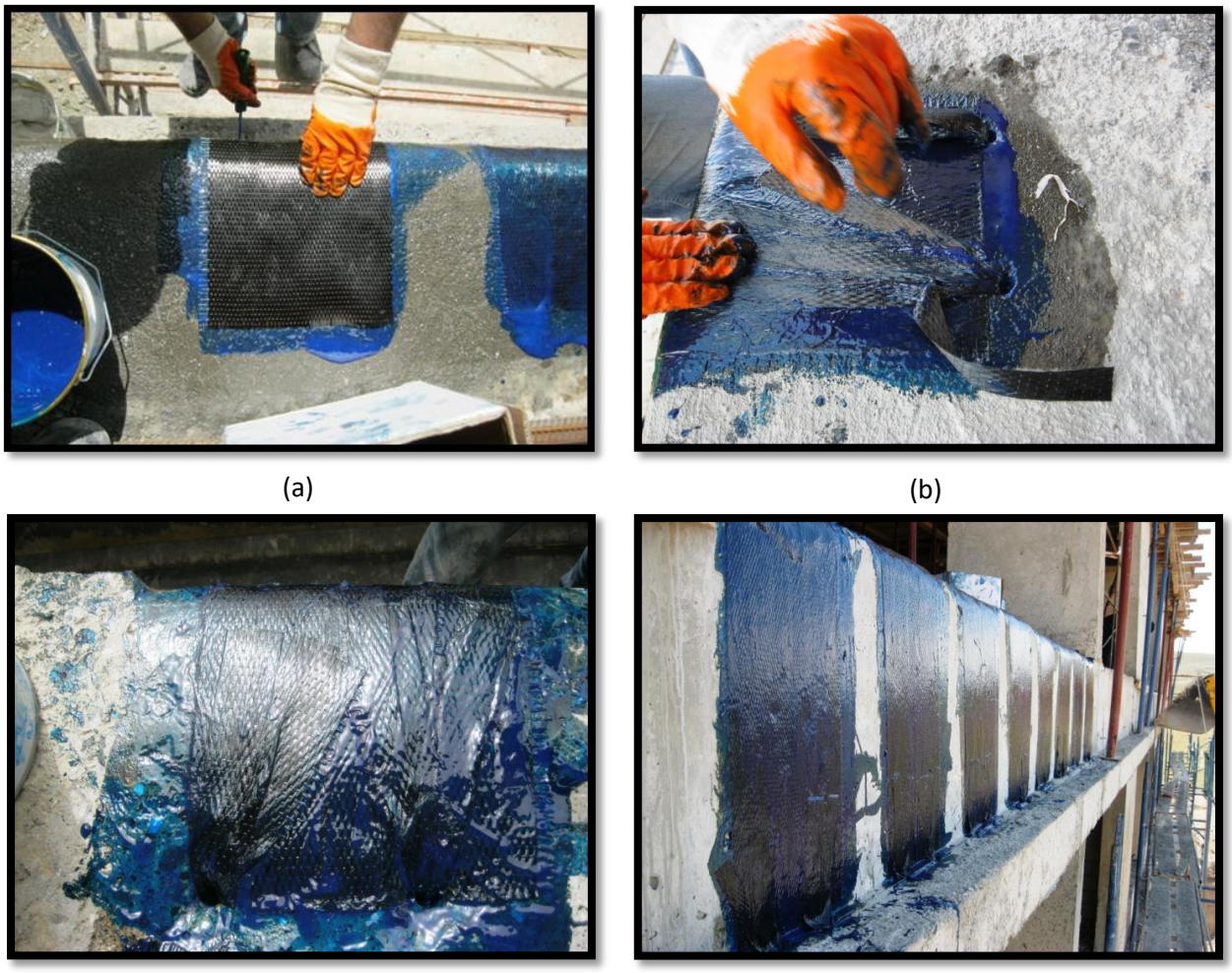

(a) (b)

(c) (d)

Figure 5: Shear strengthening of beams and fan type lap splice of FRP ends

Project details

City, Country	Kayseri, Turkey
Owner	Public Affairs
Contractor	Privately owned company
Designer	Sevket Ozden
Completion Date	October 2014
Images	Courtesy of ACIBADEM Restorasyon Ltd.Sti.

Key references

Turkish Seismic Code 2007 (TSC 2007)

BASF Material Property Data Sheets

Column Strengthening at Commercial Ground Floor

Erkan AKPINAR[1], Ozlem IMREN[2], Onur ERTAS[3], Sevket OZDEN[4]

Introduction

The speed of increase in the number of reinforced concrete buildings within the overall building stock experienced its first peak in the early 1980's in Istanbul, Turkiye. This rapid development was basically due to the high demand of the people migrating from small villages or cities to Istanbul because of the social and economic developments. The high construction speed and the lack of enough number of qualified personnel in private and municipal bodies resulted in buildings without proper engineering services. The building contractors were rarely engineers. Usually an "experienced" worker, mainly a "formwork master", was taking the whole responsibility to apply the design project on the field, or even re-shape the building during the construction according to the demands of the building owners. At the same time the inflationary rate of 1980's was causing the prices for the construction goods and services to increase overnight. Therefore, the pressure of keeping the final budget as predicted and the errors made by the "masters" resulted in low quality buildings with smaller frame sections and definitely lesser reinforcement ratios than designed, hence resulting a building stock very sensitive to the earthquakes.

The residential building which is the topic of this case study was constructed in the very beginning of 1980's. The structural blue-prints were not available at all. The basement of the building was serving as a parking area while two restaurants were occupying the ground floor. There were three floors above for residential purposes. The location of the building is very popular and the real-estate prices are well above the city average.

Many municipal regulations related to the footprint area and the mandatory distances between the building facade and the road, similarly the neighbouring buildings, changed since 1980's. Currently, in some districts in Istanbul, the buildings can use less footprint area within the registered land as compared to the 1980's. Therefore the building owners do not prefer to reconstruct their buildings. At the same time, the legal written structure of the building ownership in Turkiye usually do not courage a consensus for the structural interventions to the buildings by the owners.

The seismic upgrading of the building was the main target. Fortunately, the two commercial spaces on the ground floor belong to the same person and he was the person who demanded the seismic upgrading of the building structure. During summer 2015 and summer 2016, the two restaurants renewed their interior decoration thoroughly allowing enough time and space for the structural intervention.

The Challenges

The building plan (*Fig.1*) clearly shows the irregularity in the shear wall layout and the irregularity in column dimensions (350x600mm; 350x650mm; 350x750mm; 350x900mm) without a symmetry. The field observations revealed that the columns experienced severe corrosion (*Fig.2, Fig.3, Fig.4*). In the shear walls and in corner columns the tie bars were simply discontinuous due to local and severe corrosion. The corner columns were not only underwent severe corrosion but also some indications of vertical load carrying deficiencies observed during the site investigation.

As a start for the intervention, all the column plasters and the cover concrete was chipped out (Fig.2; *Fig.4; Fig.5*) and longitudinal bars and tie bars were covered with an epoxy layer in order to stop or delay the corrosion (*Fig.5*). A high strength mortar was used to restore the original cross-sectional

[1] KOCAELI UNIVERSITY Department of Civil Engineering, Kocaeli Turkey, akpinarerkan@yahoo.com
[2] ACIBADEM RESTORASYON Architecture & Engineering Ltd. Co., Istanbul Turkey, imren@acibademrestorasyon.com
[3] ACIBADEM RESTORASYON Architecture & Engineering Ltd. Co., Istanbul Turkey, ertas@acibademrestorasyon.com
[4] OKAN UNIVERSITY Department of Civil Engineering, Istanbul Turkey, sevketozden@yahoo.com

dimensions (*Fig.6*). It should be noted that the first layer of high strength mortar was applied onto the member surface while the corrosion repair epoxy layer was still wet. By doing so, the bond between the mortar layer and the epoxy coated surfaces were satisfied.

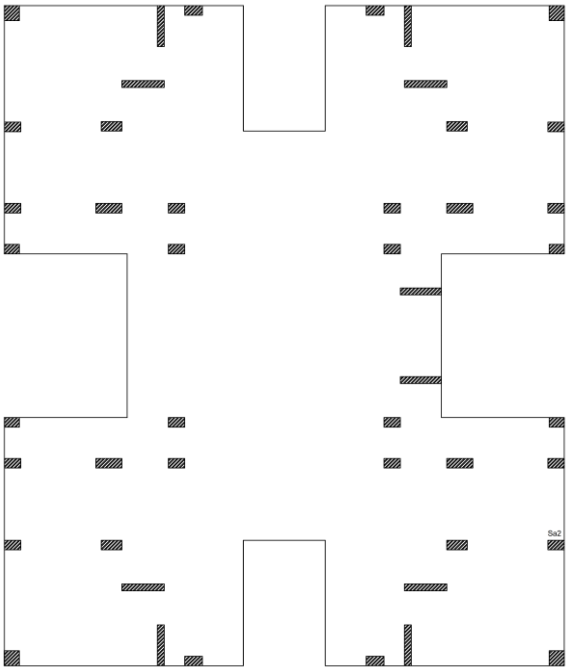

Fig.1 - Column Locations on the Ground Floor

Fig.2 - Corrosion Damage on Columns

Fig.3 – Cracks on Corner Column

Fig.4 – Cleaning on Corner Column

Fig.5 – Corrosion Repair on Shear Walls

Fig.6 – Restoring the Original Cross-Section

Fig.7 – CFRP Application on Shear Walls

Fig.8 – CFRP Application on Corner Columns

Fig.9 – Sand Cover for Better Plastering

Fig.10 – Plastering Against Fire

The member surface texture was smooth and the corners were rounded to 35mm after the application of the high strength mortar layer. The workmanship for this plaster layer should be high quality in order to be able to bond the CFRP layer to the columns. Producer specified amount of primer was applied onto the member surfaces for a better bonding of the CFRP layers with impregnation epoxy. Furthermore the amount of impregnating epoxy was in good agreement with the producer specified values (*Fig.7; Fig.8*).

Once the CFRP layer was bonded to the surface of the column, satisfying that the impregnation epoxy was still wet, a layer of sand was blasted by hand to roughen the surface (*Fig.9*) for further bonding of the fire protection layer (*Fig.10*). Finally fire protection layer was plastered and the intervention was stopped.

The above procedure for the intervention with carbon fiber seems easy to apply, however a stringent field investigation and a very detailed capacity calculations are to be accompanied.

Since there was no chance to intervene the overall building but the ground floor, a capacity check was made for the ground floor columns and any possibility of shear failure was discarded by wrapping the columns and shear walls with carbon fiber. Turkish Seismic Code of 2007 (TSC 2007) was used for all the calculations. However, the vertical cracks on the column surface and the flaking type of concrete failures observed when the cover concrete was chipped out on the corner columns reminded the possibility of failure under compressive forces. Although the axial load level on the corner columns was below the balance point, there might be a local defect in concrete that causes such flaking under compression.

The 600x600mm columns with a corner radius of 35mm, were confined by 300gr/m^2 CFRP by 6 layers. The lateral confining pressure was calculated as 1.9 MPa, resulting a confined concrete compressive strength of 14.6 MPa. The confined concrete strength which is approximately 46% higher than the existing in-situ value, was considered to be acceptable for the upgrading of the ground floor columns.

The reinforcement layout of the columns (Table.1), flexural capacities under vertical service loads (Table.2) and the shear strength after CFRP application (Table.3) are summarised in the following tables. It should be noted that the design shear values are calculated with the assumption that the hinging will take place on both end of the columns. In other words, the design shear force is calculated from capacity moments. However, for the 600x600mmm corner columns, the number of layers was not calculated by the shear demand, but by the confinement demand for strength enhancement.

Table 1 – Dimensions and Reinforcement Layout

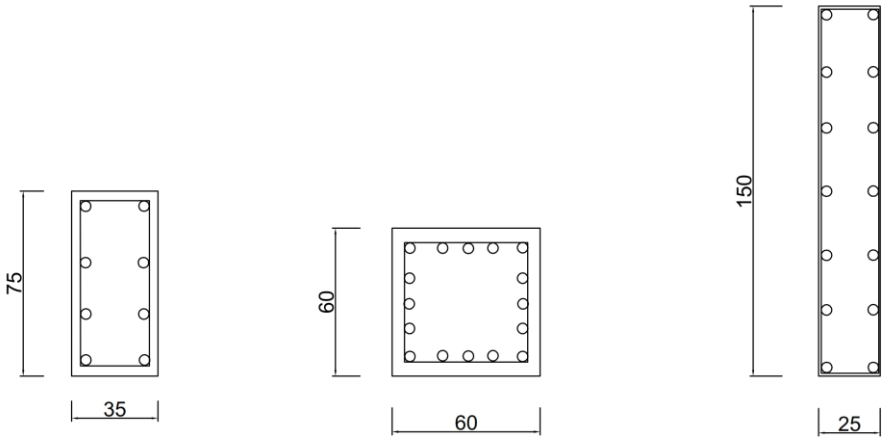

Inner Columns:	Corner Columns:	Shear Walls:
350x750 mm	600x600 mm	250x1500 mm
8 bars D=18mm (ρ_L=0.008)	16 bars D=18mm (ρ_L=0.011)	14 bars D=14mm (ρ_L=0.006)
Tie bars : D=8mm, s=25cm	Tie bars : D=8mm, s=25cm	Tie bars : D=8mm, s=25cm
f_{yk}= f_{ywk}= 220MPa	f_{yk}= f_{ywk}= 220MPa	f_{yk}= f_{ywk}= 220MPa
(diameter of tie bars reduced to 4mm due to corrosion)	(rupture in some tie bars due to corrosion)	(rupture in some tie bars due to corrosion)

Table 2 – Column Flexural Capacities

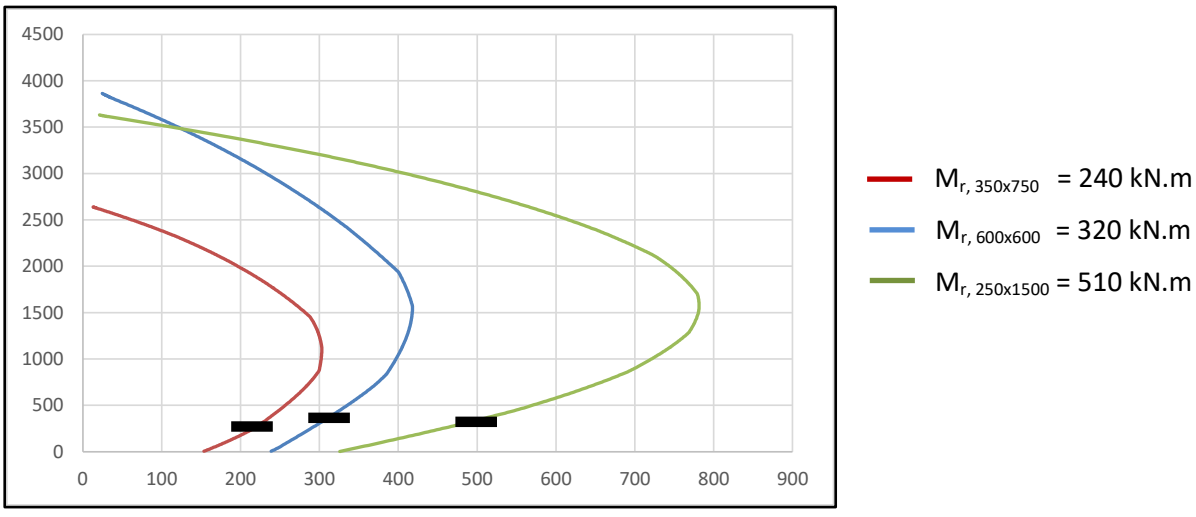

Table 3 – Shear Capacities of Columns

b	h	f_{cm} (*)	D_{tiebar}	V_c	V_s	V_r	V_{max} (**)	M_r	h_{column}	V_d (***)	$\Delta V=V_F$	n_{CFRP}	$V_{f,R}$	$V_r+V_{f,R}$	$V_d / (V_r+V_{f,R})$
(mm)	*(mm)*	*(MPa)*	*(mm)*	*(N)*	*(N)*	*(kN)*	*(kN)*	*(kN.m)*	*(m)*	*(m)*	*(kN)*	*(Layers)*	*(kN)*	*(kN)*	
600	600	10	0	258,991	0	207	509	320	1.5	427	219	3	475	682	0.63
350	750	10	4	188,847	9,883	161	375	240	2.7	178	17	1	198	359	0.50
250	1500	10	0	269,782	0	216	549	510	2.7	378	162	2	792	1,008	0.37

(*) : Existing Concrete Compressive Strength
(**) : Diagonal Shear Compression Failure Capacity
(***) : Design Shear Strength when Column Hinges
NOTE : The cabon fiber is unidirectional, 300gr/m2, Ef=200,000 Mpa.; Turkish Earthquake Code is used for Design

The Solution

There were two problems with building. One was the corrosion and the loss of shear capacity of the columns due to the loss in tie-bars, the second was the vertical cracking and flaking type of concrete failure on the corner columns. The ground floor of the building was used by two restaurants, and the upper floors were not even naming an overall structural intervention against a possible seismic event in the region. And these were the basic constraint for the strengthening interventions.

The intervention methodology must be simple, quick and must not violate the continuity of the commercial areas. The use of reinforced concrete jacketing or steel bracing was not even on the table while the intervention types were discussed with the owner and with the business holders of the two restaurants. In this project, all the benefits of use of carbon fiber were named and satisfied.

The columns and shear walls were wrapped with CFRP against shear, while the corner columns were wrapped for confinement. It should be noted that the column dimensions after this intervention was not altered.

The weakest point for the carbon fiber applications was the epoxy against fire. A final layer of fire proof plaster was applied for all the CFRP wrapped columns.

Authors believe that the composites will have a wider market-space in Turkiye in the future, especially for commercial, educational and health buildings where the space can not be sacrificed for any upgrading of the structure.

Project details

City, Country	Yesilkoy, Istanbul TURKIYE
Owner	Seven owners in total
Contractor	ACIBADEM Restorasyon Ltd.Sti.
Designer	Sevket Ozden
Completion Date	June 2016
Images	Courtesy of ACIBADEM Restorasyon Ltd.Sti.

Key references

Turkish Seismic Code 2007 (TSC 2007)

BASF Material Property Data Sheets

WG4

Whole-life-costing and life cycle assessments

Economic Study on the Usage of FRPs with Concrete in Bridges

I. Balafas, Instructor, Dept. Civil & Env. Eng., University of Cyprus, Cyprus, ibalafas@ucy.ac.cy
C.J. Burgoyne Reader, Dept. of Eng., University of Cambridge, UK, cjb@eng.cam.ac.uk

Introduction

Steel corrosion in concrete bridges is currently the biggest threat to their durability. Globally, vast governmental budgets are spent so that bridge stocks remain in an acceptable condition. To solve the growing problem FRP materials have been proposed as an alternative concrete reinforcement. Even though extensive research has taken place in the last 30 years, their use has been limited to prototype structures. The construction industry hesitates to invest in these materials due to their high initial cost.

Initial cost optimization

A design method is developed which can optimise the use of FRPs in concrete in reinforced and prestressed applications. The structure is solved for design limits under working and ultimate loads, and the results are plotted on a section depth versus bar area diagram (Figure 1) (Balafas et al 2012). A feasible zone is then formed and the optimum solution found by applying well established non-linear optimisation algorithms. The structure is optimized in terms of flexural as well as shear reinforcement. The method can be applied for any reinforcing material. The use of the method revealed that reinforced applications with FRPs are normally governed by deflection and FRP-snapping design constraints. The prestressed applications on the other hand are governed by tensile stress in the concrete at the working load and FRP snapping constraints. The optimum steel initial costs are cheaper than FRPs solutions. Using FRPs as shear reinforcements in the form of stirrups is not effective and novel forms, which use the FRP properties more efficiently, need to be found.

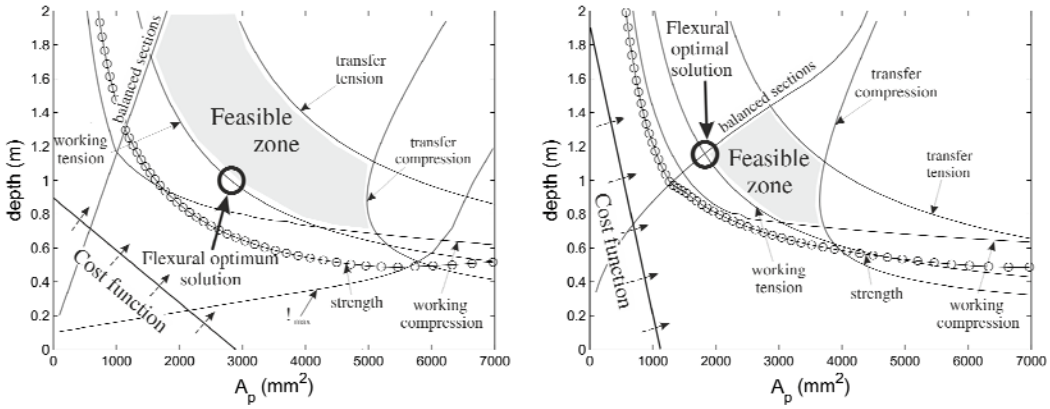

Figure 1: Optimal solution of prestressed beam with: (a) steel, and (b) AFRP tendon

Life cycle cost determination

Life-cycle costs for the structure are also determined. The bridge lifetime is assumed to consist of two time periods. The corrosion-initiation period which is the time at which steel starts to corrode, due to its exposure to de-icing salts, and the time-to-cover-cracking period during which active corrosion takes place, with the rust products causing excessive pressure on the cover which finally spalls. Models are developed to determine those time periods. In the time-to-corrosion-initiation model chlorides penetrate by diffusion and convection. Chloride binding are also included. Coupling of humidity and temperature are assumed. The environment is modelled and introduced into the problem through the boundary

conditions. The problem ends up as a system of differential equations and finite difference methods were employed for their solution (Balafas 2003).

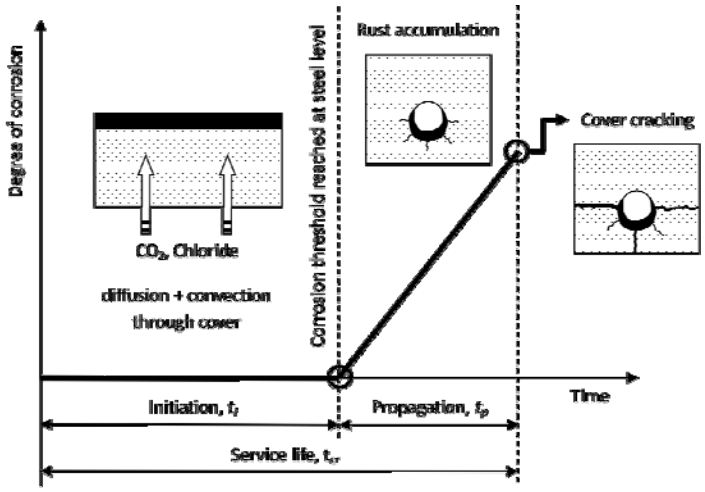

Figure 2: Structural service lifetime: corrosion initiation and propagation

In the time-to-cover-cracking model the active corrosion and rust production are described as a function of the environmental conditions. Some of the rust volume fills the concrete pores around the bars, and the rest caused pressure on the cover. A ring model is used to idealize the structure. When the rust products pressure is excessive the cracks grow outwards from the bar and eventually reach the surface. The model shows that the corrosion-initiation period is short for high annual average humidity and wide temperature fluctuation between winter and summer (Balafas et al 2010). On the other hand time-to-cover-cracking is short for average annual humidity and high temperatures during the year.

When the bridge is under repair and lane closure conditions take place, user delay costs arise. Delay costs consist of queue-delay, speed-delay, vehicle-operating and accident costs. A model is developed to evaluate these and theories from transportation engineering are used. It is found that user delay costs do not depend on the road size and can be very high for all road types.

The results in general show that the life-cycle costs and in particular user delay costs can be enormous. Repair costs are normally multiple times lower than the user delay costs. Thus if a bridge is to be repaired the speed rather than the material cost is of economic importance. The user delay costs can be so high that even if they occur at a relatively long time from bridge construction, they can justify the much higher initial costs of a FRP reinforced bridge (Balafas 2003).

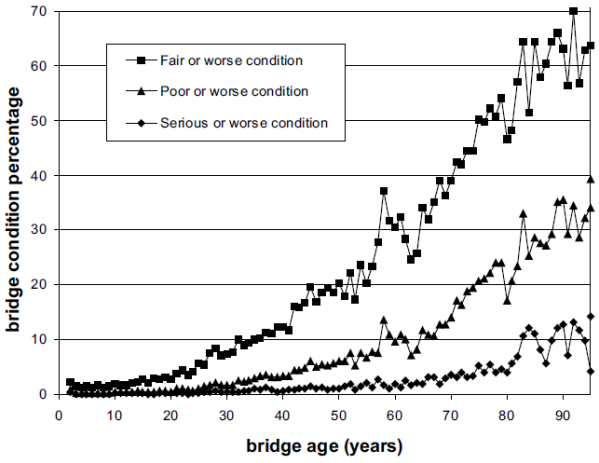

Figure 3: Condition versus age evolution on the USA-bridge-stock.

Finally a study on available USA bridge stock condition data is performed (Figure 3). Theories on predicting product lifetime are applied to the data to predict the condition of the stock in the future. A model is developed to predict future bridge stock conditions and the results show that a considerable number of bridges have to be repaired in the future and the net present value of those repairs reach very high values. Important decisions have to be made now to face up to the problem.

References

Balafas, I., Fibre-Reinforced-Polymers Versus Steel in Concrete Bridges: Structural Design and Economic Viability, PhD Thesis, University of Cambridge, 2003.

Balafas, I. and Burgoyne, C. J. Economic design of beams with FRP rebar or prestress, Magazine of Concrete Research, Vol. 64, No.10, 885-898, 2012.

Balafas, I. and Burgoyne, C. J. Environmental effects on cover cracking due to corrosion, Cement and Concrete Research, Vol. 40, Issue 9, 1429-1440, 2010.

Life-Cycle Environmental Assessment of Strengthening Options for RC Columns

C. Menna[1], D. Asprone[1], A. Prota[1]

[1] *Department of Structures for Engineering and Architecture, University of Naples Federico II, ITALY.*

Abstract

The advantages of strengthening techniques employing fibre reinforced polymers (FRPs) in terms of structural performance have been widely demonstrated in the literature. However, very few studies have investigated their environmental performance and any related potential benefits. The present work aims to investigate the environmental footprint of three different retrofit options applied to reinforced concrete (RC) columns: *i)* carbon fibre wrapping, *ii)* steel wire wrapping, and *iii)* steel jacketing. The corresponding environmental performance is analysed using a life-cycle assessment (LCA) approach. The main hypothesis of the study is that the different retrofit options are designed to guarantee the same structural performance in terms of the shear strength of a retrofitted RC column. The LCA analysis is conducted from "cradle to grave", and includes the following phases: the extraction and processing of raw materials, manufacturing, the preparation of the substrate, and the installation of the external reinforcement. The analysis revealed some important insights concerning the material that has the most impact and makes a comparison of their environmental effects. This preliminary assessment can be extended to drive the decision-making process for structural retrofits, identifying the most suitable option for the construction industry given the goal of sustainability.

Introduction

The renovation and rehabilitation of existing structures are becoming a key contributor to construction activities. In 2010, the global spend on maintenance and repair works was estimated to be about 85% of the construction sector's total expenditure (Mourad and Shannag, 2010). Generally, most of this rehabilitation work consists of repairing old, deteriorated structures and/or structures damaged by natural hazardous events. For reinforced concrete (RC) structures, the deterioration phenomena mainly depend on physical aging, chemical aging (e.g. corrosion), and overloads induced by harmful experiences (e.g. earthquake, fire), all of which lead to a reduction in the service life of an RC structure.

In order to avoid the high costs of replacing a structure and also guarantee a given structural performance for an existing RC building, several strengthening techniques have been developed in recent decades, including external bonding steel, continuous fibre-reinforced composite laminates, jacketing, and carbon/steel/basalt/glass fabric wrapping. Significant research work has been conducted on the use of fibre reinforced polymers (FRPs) (Bakis, Bank et al. 2002; Nanni 2003; Teng et al. 2003; El Maaddawy and Soudki 2008; Yaqub and Bailey 2011). However, other than the advantages offered by the strengthening techniques referred to above in terms of structural performance and rapid installation, the environmental performance/benefits of these approaches still need to be fully investigated. Indeed, very few studies have been conducted that assess the sustainability performances of these retrofit solutions (Pimenta and Pinho 2011).

[1] Department of Structures for Engineering and Architecture, University of Napoli Federico II, Italy, costantino.menna@unina.it; d.asprone@unina.it; aprota@unina.it.

In this context, the present study aims to investigate the environmental footprint related to the application of three retrofit techniques applied to RC columns: carbon fabric wrapping (CFW), steel fabric wrapping (SFW) and steel jacketing (SJ). The main objective is to analyse and compare the environmental performances of all the above retrofit options (which are designed to guarantee the same structural performance) in order to identify the solution that has the lowest environmental impact.

Methods

The environmental impact of CFW, SFW, and SJ when applied to an RC column is assessed in a life-cycle assessment (LCA) comparative framework (ISO:14040 2006). The main hypothesis of the study is that the different strengthening solutions are designed to achieve the same structural performance in terms of the shear strength of the retrofitted RC column. The LCA framework covers the period from "cradle to grave" and includes the following phases: the extraction and processing of raw materials, manufacturing, the preparation of the substrate, and the installation of the reinforcement. The other life-cycle phases such as use, maintenance, end of life, and transportation are not included in the analysis. The details of each strengthening technique are described as follows:

- *Carbon and steel fabric wrapping*: these strengthening techniques involve adding (in the form of wrapping) a layer of composite material to an existing RC column.
- *Steel jacketing*: SJ includes the use of longitudinal and transverse reinforcement around existing columns. Longitudinal L-shaped steel ties are placed on opposite corners (over the entire length of the column). This type of strengthening improves the axial and shear strength of the column.

The functional unit chosen for the analysis is defined as "*the application of different strengthening techniques on 1 m of an RC column with a given cross-section in order to achieve an increase in shear strength of 30 kN*". In particular, the considered cross-section is 30 x 30 cm^2 in terms of its dimensions and has 4 ϕ 12 mm as its longitudinal reinforcement. The length of 1 m was also chosen as the reference length of the column for applying the reinforcement. The increased shear strength was calculated according to the national structural codes and FRP guidelines (NTC 2008; CNR 2004).

The design shear strength resulting from the application of the different strengthening options (V_{Rd}) was calculated according to Equation 1 for the CFW and SFW cases (CNR 2004). Equation 2 (NTC 2008; Circolare n.617 2009) was used to calculate the increase in the shear strength due to the SJ reinforcement.

$$V_{Rd\,CWF/SWF} = \frac{1}{\gamma_{Rd}} \cdot 0{,}9 \cdot d \cdot f_{fed} \cdot 2 \cdot t_f \cdot (cotg\beta + cotg\theta) \cdot \frac{w_f}{\rho_f} \qquad (1)$$

where

γ_{Rd} is the safety factor equal to 1.2 according to (CNR 2004).

d is the effective depth of the column cross-section, 280 mm.

f_{fed} is the design strength of the reinforcement (Table 2; CNR 2004).

t_f is the thickness of the dry fabric (Table 2).

β is the inclination angle of the fibers with respect to the column axis; its value is 90° (Figure 1a).

θ is the inclination angle of the concrete strut, chosen as 45° (Figure 1a).

w_f and ρ_f are the width and distance of the fibers, respectively; w_f/p_f is equal to 1 in the case of the reinforced sheet (Figure 1a).

$$V_{Rd\,SJ} = 0.9 \cdot d * \frac{A_{sw}}{s} \cdot 0{,}5 \cdot f_{ywd} \cdot (cotg\alpha + cotg\theta) \cdot sen\alpha \qquad (2)$$

where

d is the effective depth of the column cross-section, 280 mm (Figure 1b).

A_{sw} is the area of transverse steel reinforcement (Table 3).

s is the distance between two transverse reinforcements; its value is 50 mm (Figure 1b).

f_{ywd} is the design strength of the transverse reinforcement (Table 3).

θ is the inclination angle of the concrete strut, chosen as 45° (Figure 1b).

α is the inclination angle of the transverse reinforcement with respect to the column axis; its value is 90° (Figure 1b).

The values of V_{Rd}, calculated for each reinforcement technique, are reported in Table 1. Table 2 shows the technical data of the CFW and SFW used for the V_{Rd} calculation. In the case of the SFW, two layers of external reinforcement are needed to guarantee the final shear strength increment. Table 3 reports the dimensions of the transverse and longitudinal reinforcement used in the V_{Rd} calculation.

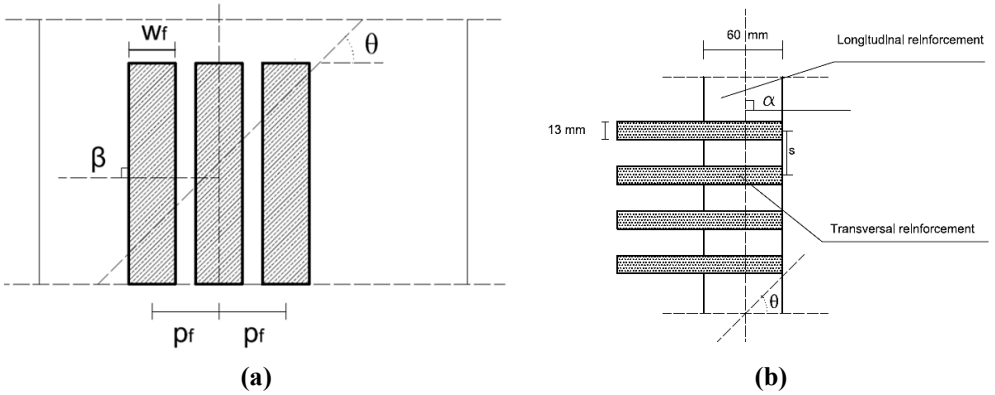

Figure 1- (a) CWF/SWF and (b) SJ reinforcing details.

Table 1- VRd, increase in shear strength

	CFW	***SFW***	***SJ***
V_{Rd} (kN)	33.2	34.8	31.4

Table 2: Technical data for the CFW and SFW (Mapei S.P.A.)

	Unit	***CFW***	***SFW***
Type of fiber		*High-strength carbon fiber*	*High-strength steel fiber*
Weight	g/m^2	300	2100
Density	kg/m^3	1800	7850
Equivalent thickness of dry fabric (t_f)	mm	0.166	0.36
Tensile modulus of elasticity	MPa	230000	210000
Elongation at breakage	%	2	2.6
Design strength of reinf. fibers (f_{fed})	MPa	475	123

**In the case of the SFW, two layers of external reinforcement are needed to guarantee the final shear strength increment.*

Table 3: Reinforcement dimension of SJ

	Unit	***Transverse reinforcement***	***Longitudinal reinforcement***
b	(mm)	13	60
t_j	(mm)	0.9	6)
A_{sw}	(mm)	11.7	360
Design strength of (f_{ywd})	MPa	532	275

For all the strengthening techniques, the following life-cycle phases were considered:

- *Material production*: this phase includes the raw material extraction and the manufacturing process of the materials used in each retrofit technique.
- *Application phase*: this consists of
  1) The preparation phase (of the substrate that has to be reinforced):
     - The external surface of the RC column is thoroughly flushed with clean water to remove as much dirt, debris, and contaminants as possible.
     - The damaged or deteriorated concrete is removed.
     - The reinforcement bars are treated with anti-corrosive proper products in order to reduce the steel oxidation.
     - Where needed, a concrete layer is added to the external surface of the RC column.
  2) Installation phase:
     - A layer of primer is applied to the RC column surface.
     - The external reinforcement is applied to the RC column.

Both primary and secondary data were utilized for the life-cycle inventory analysis. Primary data were used to model steel material manufacturing (e.g. transverse and longitudinal reinforcement) and steel/carbon wrap fabric production. In particular, technical information reported in the datasheets of (Mapei S.P.A.) and in the (ReLuis 2011) guidelines were used to model CFW and SFW production, while the technical data contained in (Gruppo AFV Beltrame) and in the (ReLuis 2011) guidelines was used to model steel material manufacturing for the SJ technique.
The secondary data were directly retrieved from the product databases available in the Simapro 7.3 LCA software package (Simapro), namely the Ecoinvent (Hedemann and König 2007) and IDEMAT (IDEMAT2001 2001) databases.

Impact Assessment

In the present study, the IMPACT 2002+ methodology (Jolliet, Margni et al. 2003) was adopted to calculate and quantify the environmental impact of the three strengthening techniques in the reference scenario. The LCA results are discussed in terms of damage (damage categories) and characterization assessments (mid-point categories). Figure 2 shows the LCA comparison of the investigated strengthening techniques. As can be seen, the SJ technique has the highest environmental impact in almost all the damage and mid-point categories. In particular, in the human health, ecosystem quality, and climate change damage categories, CFW and SFW have an environmental impact that is between 20-80% lower than that of the SJ solution. The CFW technique has the highest impact in the resource damage category, whereas the SFW option is characterized by the lowest environmental impact. In detail, the SJ solution is responsible for the highest environmental burden in terms of the material production phase. A contribution analysis (ISO:14040 2006) was conducted to evaluate which material/process influences the environmental results of the SJ solution. In this way, it was possible to determine which substance and/or process played a significant role in the LCA results. This analysis, which was conducted for each damage category, reveals that reinforcement production (steel material manufacturing) influences the environmental impact of the SJ solution as follows:

- Human health category: the LCA result is influenced by the steel materials produced in electric and basic oxygen furnaces ("steel, converter, unalloyed" and "steel, electric, un- and low-alloyed"); this process emits a large amount of dioxins and sulfur dioxide.

- Ecosystem quality: the LCA results are influenced by the production of steel materials and, in particular, by steel materials produced in basic oxygen furnaces ("steel, converter, unalloyed") that emit a large amount of aluminium and zinc emissions into the air and water.
- Climate change: the steel materials produced in basic oxygen furnaces ("steel, converter, unalloyed") influence the LCA results in this end-point category; these materials emit a large amount of CO_2 emissions into the atmosphere.
- Resources: in order to produce steel ("steel, converter, unalloyed"), several non-renewable raw materials such as uranium, coal, oil, and natural gas are used.

Finally, CFW has the highest environmental impact in the resources category, as shown in Figure 2. This result is influenced by epoxy resin and carbon fibre production. The environmental impact of epoxy resin (used as impregnating resin) and carbon fibres accounts for 70% of the total burden in the material production phase, whereas the epoxy resin (used as primer) accounts for 26% of the total environmental impact in the installation phase.

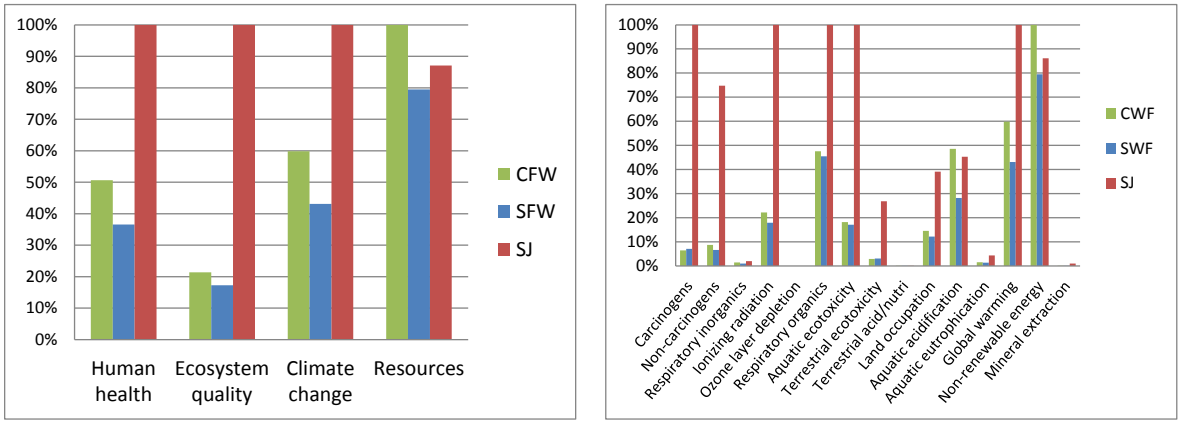

(a) **(b)**

Figure 2-LCA comparison; (a) Damage assessment; (b) Characterization categories

Conclusions

The present study assessed the environmental impact of different strengthening techniques applied to RC columns. Three techniques were examined using an LCA approach: carbon and steel fabric wrapping and steel jacketing. All of them were designed to achieve the same structural performance in terms of shear strength for a retrofitted RC column. The first objective of this research was to use a life-cycle perspective to evaluate the relative environmental impact of each alternative. In particular, the LCA results on the CFW solution revealed that the material production (carbon fabric manufacturing) and application phases (application of primer to the external surface of the RC column) made the same environmental contribution. In the SFW solution, the LCA results were mainly influenced by the application phase (two-component resin used as primer), while in the SJ solution, the major environmental impact was related to the material production phase. In particular, the steel material manufacturing accounted for 90% of the total environmental burden. When the strengthening solutions were compared, the results reveal that the SJ technique has the most impact in almost all the damage and impact categories, which is mainly due to the refining and melting process for steel (material

production phase). The CFW solution had the highest impact in the resources category, which was mainly due to the epoxy resin used as an impregnating system and the carbon fiber production.

Key references

Bakis, C., L. Bank, et al. (2002). "Fiber-Reinforced Polymer Composites for Construction—State-of-the-Art Review." Journal of Composites for Construction 6(2): 73-87.

Circolaren.617 (2009). "Istruzioni per l'applicazione delle 'Nuove norme tecniche per le costruzioni di cui al decreto ministeriale 14 gennaio 2008"

CNR - National Research Council (2004). Guide for the design and construction of external bonded FRP systems for strengthening existing structures. CNR-DT200/2004.

Ecoindicator 99 "http://www.pre.nl/contact.htm;"

El Maaddawy, T. and K. Soudki (2008). "Strengthening of reinforced concrete slabs with mechanically-anchored unbonded FRP system." Construction and Building Materials 22(4): 444-455.

Gruppo AFV Beltrame " http://www.beltrame.it/"

Hedemann, J. and U. König (2007). Technical Documentation of the Ecoinvent Database. Final Report Ecoinvent Data v2.0 No. 4, Swiss Centre for Life Cycle Inventories, Dübendorf, CH.

IDEMAT2001 (2001). "The Netherlands: Faculty of Industrial Design Engineering of Delft University of Technology."

ISO:14040 (2006). Environmental management- life cycle assessment-principles and framework, ISO - International Organization for Standardization.

Jolliet, O., M. Margni, et al. (2003). " IMPACT 2002+: A New Life Cycle Impact Assessment Methodology." International Journal of Life Cycle Assessment 8(6): 324 – 330.

Mapei S.P.A. " http://www.mapei.com/."

Mourad, SM., Shannag, MJ., (2012) "Repair and strengthening of reinforced square columns using ferrocement jackets". Cement & Concrete Composites, 34, pp. 288-294.

Nanni, A. (2003). "North American design guidelines for concrete reinforcement and strengthening using FRP: principles, applications and unresolved issues" Construction and Building Materials 17: 439-446.

NTC (2008). "NTC, Norme Tecniche per le Costruzioni (2008), D.M 14 gennaio 2008."

Pimenta, S. and S. T. Pinho (2011). "Recycling carbon fibre reinforced polymers for structural applications: Technology review and market outlook." Waste Management 31(2): 378-392.

ReLuis (2011). "(Rete dei Laboratori Universitari di Ingegneria Sismica), linee guida per riparazione e rafforzamento di elementi strutturali, tamponature e partizioni, www.reluis.it/doc/pdf/Linee_guida1.pdf."

Simapro http://www.pre-sustainability.com/, Prè consultant.

Teng, J., J. Chen, et al. (2003). "Behaviour and strength of FRP-strengthened RC structures: a state-of-the-art review." Structures & Buildings 156(1): 51-62.

Yaqub, M. and C. G. Bailey (2011). "Repair of fire damaged circular reinforced concrete columns with FRP composites." Construction and Building Materials 25(1): 359-370.

Advanced Composites in the COST Countries: Research and Development

HEIA-FR/HES-SO, activities at iTEC

Prof. Dr. Daia Zwicky[1]

Introduction

The Institute of Construction and Environmental Technologies (iTEC) of the School of Engineering and Architecture Fribourg (HEIA-FR) is active in research on structural applications of FRP composites since almost 20 years, initially guided by Prof. em. René Suter and since 10 years by the author.

Several R&D projects explore different possibilities of FRP applications in new structural elements and strengthening of existing, of which a selection is presented hereafter. Structural applications of fibre-reinforced cementitious matrix (FRCM), other uses of FRP products as well as full FRP girder elements are also ongoing at iTEC but not further reported here; information on these researches can be found in Zwicky (2013), Michels et al. (2014), Fridez (2015), Zwicky and Bärtschi (2016), Zwicky and Mabboux (2014), Mabboux and Zwicky (2012), and Macchi (2016).

Strengthening of concrete slabs

First research projects at iTEC (Suter and Héritier 1999) focused on the experimental comparison of the performances of externally bond steel and CFRP plates for strengthening concrete slab strips of 6 m simple span and 0.85 m width, internally reinforced with steel reinforcing bars Ø12/150 longitudinally and Ø8/150 transversally, Figure 1.

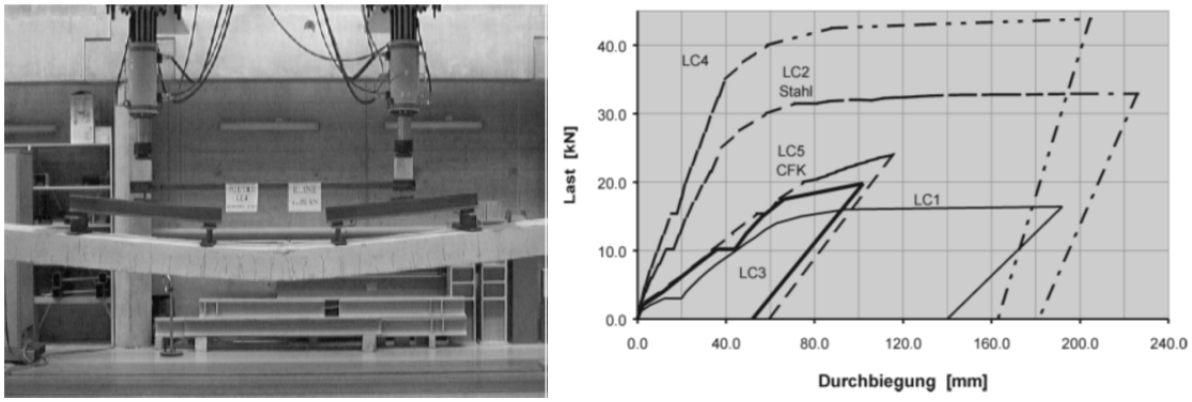

Figure 1: Load tests up to failure on concrete slab strips, passively strengthened with steel and CFRP plates (left) and experimental deflection vs load response (right), from Suter and Jungo (2001)

It could be concluded that steel plates considerably improve Serviceability Limit State (SLS), thanks to their sectional stiffness (Figure 1), while this effect could not be observed for the much thinner CFRP plates, Table 1, with an elastic modulus of 170 GPa and a tensile strength of 3090 MPa. At Ultimate Limit State (ULS), the steel strengthened concrete slabs behaved very ductile while the CFRP strengthened slabs failed by brittle bond rupture of the strengthening plates, induced by vertical relative displacements at shear cracks. This early study also contributed to the strain limitation for FRP strengthening plates at ULS to 8‰, as currently (still) prescribed in an associated Swiss code (SIA 166 2004), and to the conclusion that prestressing the CFRP plates would considerably increase their

[1] University of Applied Sciences Western Switzerland (HES-SO), School of Engineering and Architecture Fribourg (HEIA-FR), Institute of Construction and Environmental Technologies (iTEC), Switzerland, daia.zwicky@hefr.ch

effectiveness in strengthening. The effect of prestressing was investigated in a second experimental study, analogously to the first.

Table 1: Test parameters for concrete slab strips strengthened with externally bonded steel and CFRP plates

Test specimen	LC1	LC2	LC3	LC4	LC5	LP1	LP2	LP3	LP4
Bonded plates (2x)	--	5·100	1.2·50	6·140	1.2·80	1.2·50	1.2·80	1.2·50	1.2·80
Plate material	--	S235	CFRP	S235	CFRP	CFRP			
Prestressing strain	--	0‰				4‰		6‰	

Figure 2 shows the experimentally identified effects of prestressing CFRP bonded plates in the flexural response of strengthened concrete slab strips (Suter and Jungo 2001). It becomes evident that prestressing has a positive effect on behaviour of a strengthened concrete slab, in terms of stiffness at SLS as well as strength and ductility at ULS, as also becomes clear from the attainable ultimate strains in the CFRP plates. These results also confirm the suitability of limiting (additional) plate strains to approx. 8‰ (SIA166 2004). Further experimental investigations concerned the performance evaluation of a mechanical anchorage system for the prestressed CFRP plates, allowing prestressing strains of up to 10‰ if required. However, a prestressing limit strain of 6‰ to 8‰ is recommended by the authors, as difficulties in practical execution increase more than proportional with increasing prestressing strain.

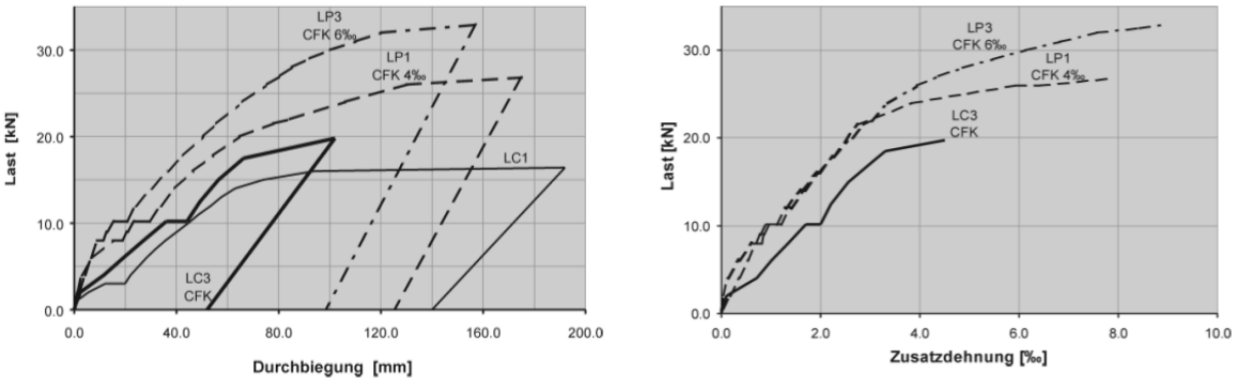

Figure 2: Experimental deflection vs load response of CFRP strengthened concrete slab strips, with and without prestressing (left) and additional strain in CFRP plate vs load (right), from Suter and Jungo (2001)

Confinement of concrete columns

Synthetic fibre sheets

A further research project on application of FRP in structural strengthening investigated confinement of concrete columns with aramid, carbon and glass fibre sheets against vehicle impact (Suter and Conus 2005). Large experimental test series on square and circular columns showed that aramid is best suited as sheet material for strengthening, being clearly superior to carbon fibre sheets. Glass fibre sheets did not prove effective, due to their low elastic modulus.

Bending tests, performed on 5.2 m long column elements strengthened with a varying number of longitudinal and transverse aramid sheets (Table 2), showed impressive increases in flexural resistance of up to 260% and in ultimate deformation of up to 175%, Figure 3 (left). All columns were internally reinforced with 8Ø20 reinforcing bars longitudinally and Ø8/300 hoops transversally.

Further tests on short column elements with 2.4 m span showed that shear resistance and deformation ductility is even more increased by this strengthening method, Figure 3 (right), up to approx. 350% of an unstrengthened column.

Table 2: Test parameters for bending tests on long columns strengthened with aramid fibre sheets AK-60

Test specimen	PK1	PK2	PK3	PK4
Longitudinal layers	--	2	3	4
Transverse layers	--	2		

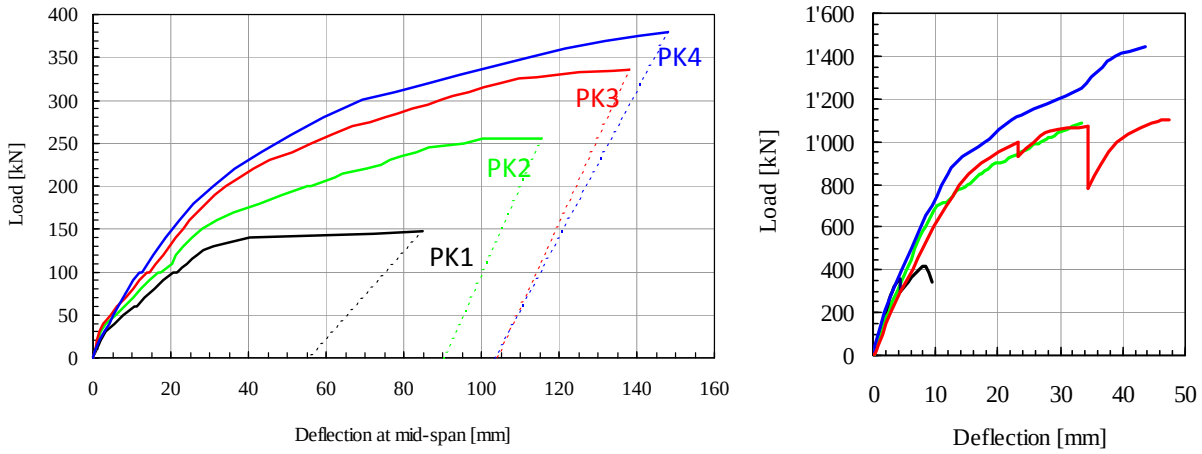

Figure 3: Experimental deflection vs load response of aramid sheet strengthened concrete columns in bending (left) and in shear (right), from Suter et al. (2001)

A last test series in compression on column elements of 1.8 m length of type PK1 and PK2 showed that the resistance increase is limited to some 25%, due the geometrical form of square cross-sections. Circular columns are much more efficiently reinforced with fibre sheets (Suter and Pinzelli 2001).

Natural fibre sheets

A recent study project (Moix and Sturny 2013) investigated the performance of flax fibre sheets for the confinement of concrete cylinders in compression. The applied flax fibre sheets have a tensile strength of 650 MPa and show a slightly non-linear behaviour that can be approximated with to linear regimes, with an initial elastic modulus of 49.2 GPa up to 35% of tensile strength and a second modulus of 35.2 GPa up to tensile strength (Chopard and Zwicky 2014). The equivalent sheet thickness is only 0.21 mm.

Test results on cylinder specimens Ø150 mm and 300 mm height, Figure 4, being strengthened with 2, 4 and 6 loops of flax fibre sheets show that strength increases up to 60% are attained, compared to an unstrengthened specimen. Deformation capacity of confined specimens is even more importantly improved, up to a factor of 5. Being inferior to 3% per specimen type, test result variability is also very low. The results in Figure 4 further show that it should also be possible to reach a very ductile behaviour of a compressed concrete member without considerably increasing its ultimate strength, that is, probably with 3 loops of flax fibre sheet confinement in the present case.

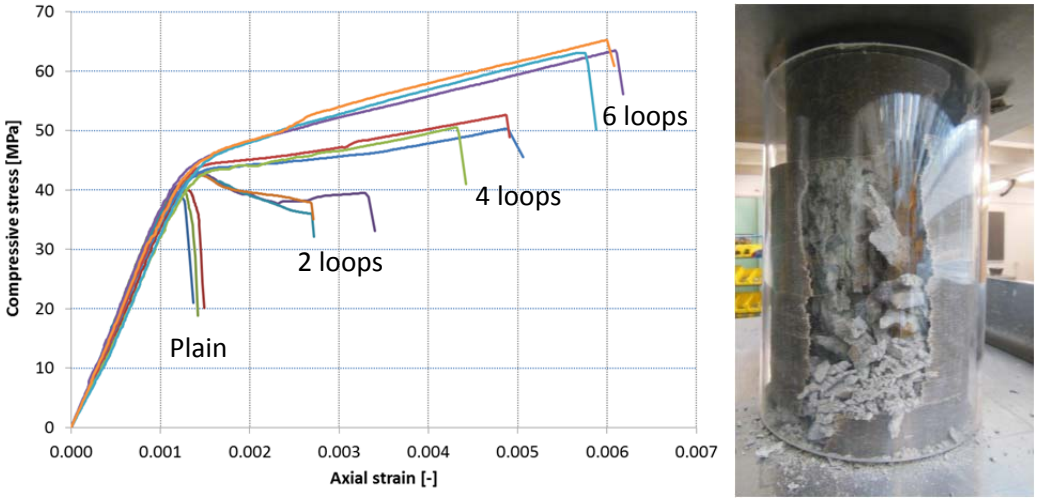

Figure 4: Experimental response of axial strain vs stress of confined concrete cylinders, strengthened with 0, 2, 4 or 6 loops of flax fibre sheets, and specimen state after failure, according to Moix and Sturny (2013)

Comparative calculations according to theoretical approaches (fib 14 2001), Figure 5, using few estimated parameters (elastic modulus, compressive strength and associated strain) show that the general tendencies of the experimental behaviour can be reproduced very well.

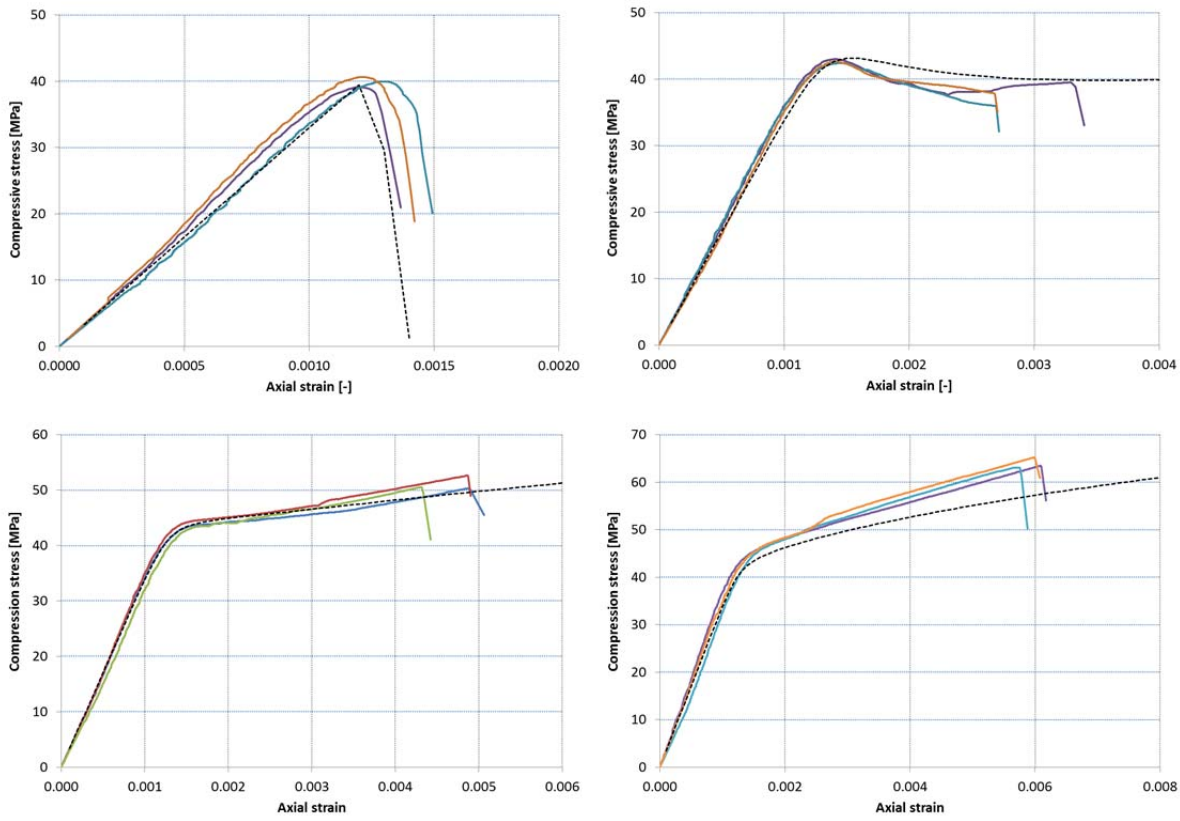

Figure 5: Comparison of experimental and analytical results for axial strain vs stress of unconfined and flax fibre sheet confined concrete cylinders

Strengthening of masonry walls

Several studies explored the possibility of applying externally bonded CFRP sheets for seismic strengthening of shear walls made of artificial stone masonry. The effects of different arrangements of CFRP sheet strengthening, applied on one wall side only, on the structural response of brick masonry walls of 1.4 m height, 1.8 m length and 0.15 m thickness was analysed experimentally in static-cyclic shear tests (Bischof and Suter 2014, Bischof et al. 2014), using vertical sheets at the edges only as well as vertical sheets in combination with diagonal CFRP sheets (at 45° and 60°). It was found that ultimate shear strength can be increased by up to 70% while deformation capacity remains more or less the same (increase ≤ 10%). Failure was always attained in compression in the brick masonry.

Mechanical anchorage of CFRP sheets to concrete slabs (usually available at bottom and top of masonry walls) was investigated in further experimental, analytical and numerical study, targeting the anchorage for exterior and interior walls. For bond anchorage of the CFRRP sheets on steel profiles, it could be found that the sheets can be exploited up to 40% to 50% of the theoretical tensile strength, independently of the available bond length between 40 mm and 85 mm. If bonded to concrete and including mechanical fastening (exterior wall anchorage), this level of exploitation was more or less confirmed for light CFRP sheets (200 g/m^2) while it could not be found for heavy CFRP sheets (400 g/m^2) where only 30% of the theoretical tensile strength was reached. If the sheets are anchored to a concrete slab by L-shaped steel profiles (interior wall anchorage), it was found that the geometrical properties of the anchorage profile play a major role. With the applied steel profiles, exploitation of the theoretical tensile strength of the CFRP sheets was limited to a general average of about 20%. It could thus be concluded that construction details play a major role for the mechanical anchorage of CFRP sheets. More details can be found in Bischof and Suter (2014) and Bischof et al. (2014).

Improvement of timber beams

Prestressing of timber beams with NSM CFRP lamellas (Zwicky 2009)

Timber beams are often statically determinate, due to erection procedures and to their sensitivity to imposed deflections, also in relation to their (assumed) elastic behaviour. Deflection criteria for SLS often govern the design of such flexural elements, while their resistance at ULS can rarely be exploited. As timber, as a natural material, exhibits large scatter in flexural resistance and bending stiffness, design values are defined accordingly at low but (supposedly) conservative levels. Some improvement in SLS performance of timber beams can be achieved by using glued laminated timber (glulam) sections instead of cut timber sections. The structural stiffness, however, is usually still too low to achieve that ULS verifications govern the structural design.

This lack of SLS stiffness gave the idea for a new type of composite element: glulam of lowest quality timber is reinforced with prestressed near-surface mounted CFRP plates. In a preliminary, mainly experimental study, conducted to the benefit of a Swiss SME, the feasibility of structural elements made of low quality glulam beams, reinforced with NSM prestressed CFRP plates, should be checked. Foci were on potential increases in bending stiffness and resistance with regard to different prestressing force levels, and the anchorage behaviour of the prestressed plates at the beam ends. Full-scale 6-point bending tests on single-span glulam-CFRP beams with a span of 5 m, Figure 6 (left), were carried out on seven specimens; a non-strengthened glulam specimen served as a reference beam. Two specimens each were prestressed with CFRP laminate forces of 80, 100 and 120 kN, respectively.

Figure 6 (right) shows the cross-section of the beams. The CFRP laminate is near-surface mounted (NSM) in a slot of 4…5 mm width; the cut is 5 mm deeper than the laminate, in order to "hide" it in the section. The applied CFRP plate has a cross-section of 1.4·50 mm^2, an average elastic modulus of 165 GPa and a tensile strength of 2'800 MPa.

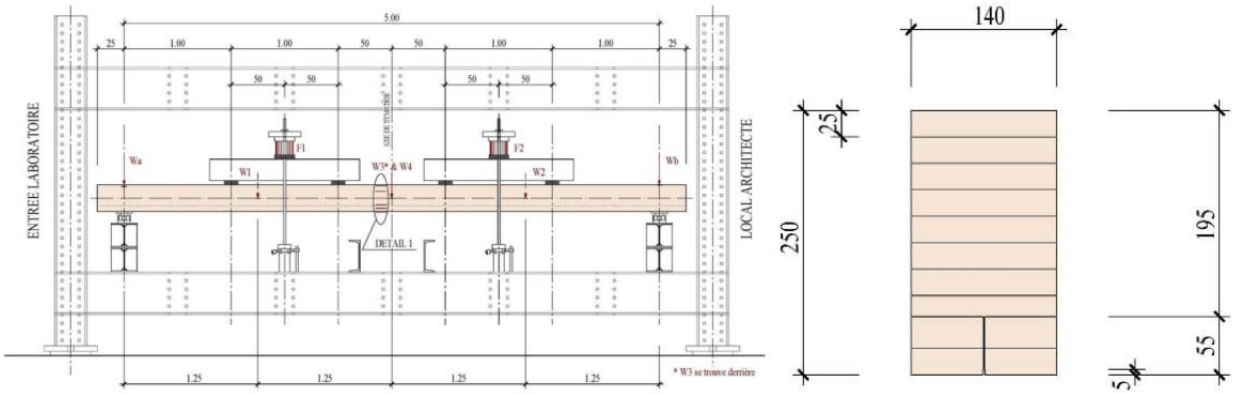

Figure 6: Full-scale 6-point bending tests on glulam beams with NSM prestressed CFRP plate (left) and cross-sections of the glulam beam (right), from Zwicky (2009)

The anchorage of the prestressed CFRP plate at beam ends was analysed visually before and after the load tests. Figure 7 shows the laminate anchorage zones for the different prestressing levels. Only one of the girders with 80 kN prestressing showed significant deformations of the anchorage before loading. For one of the beams with 120 kN prestressing force, the anchorage zone was loaded additionally at failure, Figure 7 (far right). The girders with prestressing forces lower than 120 kN showed no sign of additional loading after the tests. All pictures in Figure 7 show that local cracks, due to the prestressing force transfer, occur as delamination along the annual growth rings of the timber lamellas. Such cracks are primarily an SLS design concern (appearance); failure test results show that the anchorage of the laminate is still fully functional at ULS. This is probably also due to the fact that the NSM laminates are applied at the lower beam face, where the anchorage is laterally compressed by the bearing stress. It could be concluded that the prestressing force should not be released in one stage, but gradually as it is also recommended for concrete structures. From the present results, it can be seen that the anchorage force level must be below 80 kN for the present glulam quality.

Figure 7: Anchorage of the CFRP laminate at the beam's end – prestressing force of 80 kN, 100 kN, 120 kN prior to load test and 120 kN after load test (from left to right), from Zwicky (2009)

The CFRP laminate anchorage was examined analytically by applying the preliminary Swiss Code SIA 166 (2004) for externally bonded reinforcement, even though that it explicitly excludes its application to timber structures; however, the goal was to determine the order of magnitude of anchorage resistance. Applying the resistance model to the test beams leads to a force of approx. 108 kN that could maximally can be anchored, while the associated anchorage length amounts to approx. 260 mm. This is qualitatively confirmed by the test results; a prestressing force of 80 kN could be anchored more or less properly, while the other test girders showed more or less heavy signs of delamination. Still, due to the

arrangement of the annual growth rings in the timber lamellas and the spatial orientation of the timber grains, the prestressing force could still be (partially) anchored.

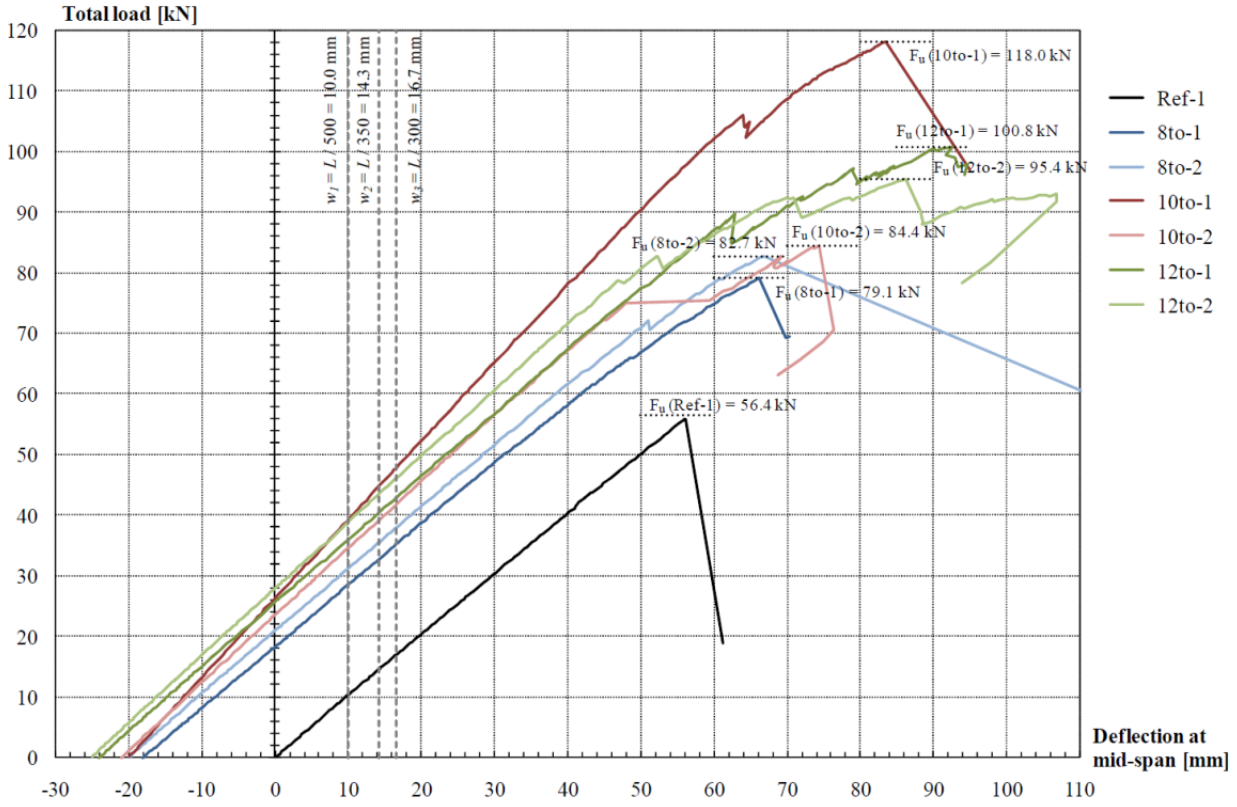

Figure 8: Mid-span deflection vs applied load response of glulam beams with NSM prestressed CFRP plate, from Zwicky (2009)

Figure 8 shows that admissible SLS load levels can be considerably increased if prestressing is applied to glulam beams. In general, the SLS load level of the CFRP-glulam composite beams is increased with increasing prestressing force, up to 200…380% of the non-strengthened reference. The load increase is reduced with decreasing deflection limit, as the major part of deflection reduction is a result of the initial counter-sag due to the eccentrically arranged NSM prestressing. Applying prestressed CFRP plates is thus particularly effective, if a flexural element has to be designed for severe deflection limits, and a higher prestressing force generally increases the load level for the deflection criterion under consideration. If the applicable loads due to counter-sag from prestressing are eliminated from the comparison, the relative SLS load increases remain below 8%, confirming that the major part of load increase is associated to counter-sag. Beam 10to-1 evidently is an exception from this conclusion; this beam already displayed a much stiffer behaviour during the test, Figure 8, probably attributed to a considerably higher Young's modulus of the glulam section. The other composite beams are still slightly stiffer than the reference beam, showing the favourable influence of the approx. 15 times stiffer CFRP plate on the glulam beam behaviour, also confirmed analytically (Zwicky 2009).

Since bending failure of timber beams usually occurs on the tension face, a higher prestressing force increases the ultimate loads. The failure loads for a specific prestressing level are surprisingly close to each other (except for beam 10to-1). Hence, application of a CFRP laminate – from industrial production, thus with a low scatter of its mechanical properties – corresponds to an indirect

improvement of the scatter in glulam properties. In all tests, at least the two lowermost lamellas failed; with 120 kN prestressing, even three lamellas ruptured at ultimate load.

The compression force from prestressing allows higher strains in the decisive glulam lamellas at the tension face; these strains lead to higher curvatures and thus to higher deflections until failure. Furthermore, the stiffer CFRP laminate attracts the stresses in the cross-section and unloads the timber, allowing additional strains in the surrounding glulam lamellas until failure in flexural tension. Still, as expected from the application of glulam and CFRP in a composite element, all beams showed only small plastic deformations until failure. Nevertheless, plastic deformations and failure loads increase with increasing prestressing force.

Prestressing glulam sections with CFRP laminates and considering the composite action of the two materials can considerably increase serviceability and ultimate limit state loads. Moreover, the scatter of these characteristics is significantly reduced. However, SLS loads are still governing the design of the composite CFRP-glulam beam, since all values are higher than an estimated global safety factor, see Zwicky (2009). The governing of ULS design hoped for, could thus not be achieved for statically determinate timber structures.

Flexural reinforcement with flax fibre sheets

Under tension, timber generally shows a linear-elastic behaviour up to brittle fracture, being further attained by flaws, such as knots, and fibre misalignments. In compression, it usually exhibits a high plastic deformation capacity. This phenomenon is intuitively understood by thinking of timber as relatively short, aligned fibres; when loaded in tension, the fibres tend to separate from each other in a brittle fracture. If the same fibres are compressed, they rather displace relatively towards each other, allowing substantial displacements and hence a more ductile behaviour, also explaining why the ultimate load of timber beams in bending is usually attained by rupture at the tension face. Thus, strengthening the tension face of timber beams would allow a better exploitation of their load-bearing capacity and the potential plastic deformation capacity in compression.

Flax fibre sheets are considered appropriate as reinforcement of the flexural tension face of timber beams, as their softness allows reinforced beams to be sawn and planed without damaging the usually available cutting tools as well as their sustainability as a renewable resource. The impact of flax fibre sheet reinforcement of glulam beams was investigated in a preliminary analytical and experimental study on full-scale specimens (Chopard 2013).

Three 5.40m-long glulam timber beams with a characteristic bending strength of 24 MPa were submitted to a 6-point bending test: one unreinforced beam (“ref”), one reinforced with two layers of flax fiber sheets (“+2”) and one reinforced with four layers of flax fibre sheets (“+4”). The reinforcement was inserted during glulam fabrication; flax fiber sheets of average thickness t = 0.21 mm per layer were laid on top of the bottom lamella before the glued boards were pressed in the usual fabrication process. Figure 9 (left) shows the reinforcement of the +4 beam. The reinforcement sheets were placed above the bottom timber lamella (and not under it) for fire protection and aesthetics.

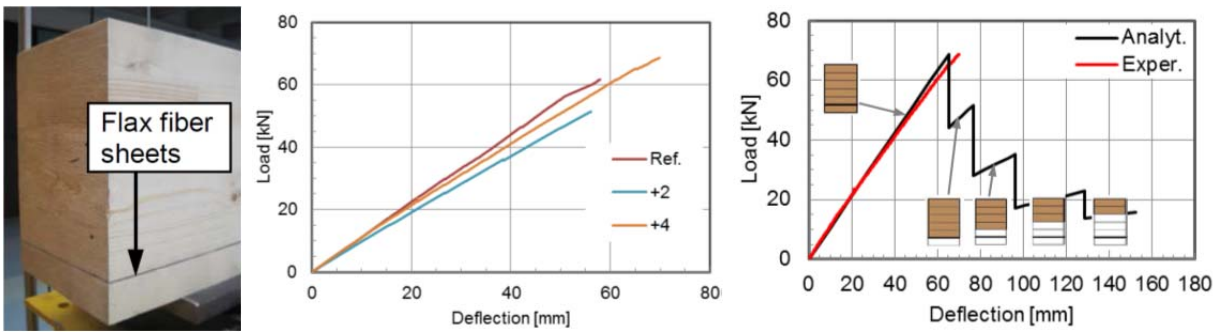

Figure 9: Glulam beam specimen "+4" with flax fibre sheet (left), experimental mid-span deflection vs applied load response of all specimens, and comparison to analytical results, from Chopard and Zwicky (2014)

Figure 9 (middle) shows the global behaviour of all test specimens, with overall disappointing results. All specimens exhibited a practically linear-elastic behaviour up to rupture at the tension face of the beam. Both reinforced beams proved less rigid than the reference. The +4 beam showed a slightly higher rupture load than the reference beam. The +2 specimen was of a particularly poor glulam quality; its results were inferior to those of the reference specimen, both in terms of bending stiffness and bending strength.

Analytical re-calculations (Chopard and Zwicky 2014) showed that the cross-sectional behaviour can be reproduced only satisfactorily, while the deflection behaviour is excellently reproduced. The elastic energy liberated at rupture of the outermost timber lamella cut the flax fibre sheets, preventing the tests to go on with a reduced cross-section, as established analytically, Figure 9 (right).

The calibrated analytical model was further used to explore other improvement options by providing flax fibre reinforcement, such as obtaining the nominal structural performance of a superior glulam quality, or providing minimum flax fibre sheet reinforcement such that, after rupture of the outermost timber lamella, the same flexural resistance can be attained again. These analytical considerations showed that a substantial thickness of flax fibre composite is needed, i.e. several millimetres and not only the nominal 0.84 mm of flax fibre sheets as used in beam specimen +4. This is due to flax fibre sheets not being rigid enough in relation to its tensile strength, in order to be considerably exploited: at rupture of the timber lamella, the tensile stress in the reinforcement is less than 20% of its tensile strength.

Conclusions and Points for Discussions

- CFRP and concrete: at Ultimate Limit State (ULS), CFRP strengthened slabs failed by brittle bond rupture of the strengthening plates, induced by vertical relative displacements at shear cracks. The early study reported contributed considerably to the strain limitation in FRP strengthening plates at ULS to 8‰, as still prescribed in an associated Swiss code (SIA 166 2004), and to the conclusion that prestressing the CFRP plates would considerably increase their effectiveness. Prestressing strain should be limited to 6‰ to 8‰, as difficulties in practical execution increase more than proportional with increasing prestressing strain.
- FRP confinement: the results exposed here also show that confinement of compressed concrete members can also be attained with natural fibre sheets, and that existing analytical approaches for synthetic fibre sheets can be applied. Open questions primarily concern failure criteria to be considered for abandoning the theoretical analysis.
- CFRP and masonry: CFRP sheets are an efficient means for strengthening masonry walls but rely heavily on the mechanical anchorage of the sheets to the adjacent concrete slabs. Further

experimental, analytical and numerical research should target the bonding behaviour of CFRP sheet to metal profiles.

- CFRP and timber: NSM prestressed CFRP laminates could allow an indirect upgrade of low glulam quality, since the absolute level of stress and its reliability is increased; this approach should be verified with more tests and corresponding theoretical analysis. The latter should consider the elasto-plastic behaviour of timber in compression. In order to allow the correct design of the plate anchorage at ULS, a resistance model for NSM externally bonded reinforcement laminates should be developed, potentially similar to SIA 166 (2004), i.e. considering the shear resistance of the surrounding timber lamellas (or the tensile resistance perpendicular to the grains) and specific fracture energy of the interface. Procedures and tools for releasing the prestressing force gradually should be developed. Since the necessary prestressing forces are lower than the ones investigated here, it could also be possible to apply GFRP instead of CFRP, decreasing cost.
- Flax FRP and timber: the ultimate strain of flax fibres being approx. five times higher than that of timber in tension, they are not the ideal materials to be associated. Pre-tensioning the flax fibre sheets is another improvement possibility but associated tools and procedures still have to be developed. The use of natural FRP, in combination with other materials subject to high strain localization at an early stage loading (e.g. cracking of masonry, reinforced concrete) may also allow a better exploitation of their mechanical properties, as the reinforcement is already activated as cracking develops and not only at failure.

References

Zwicky D. (2013). Concrete Slab Strengthening with CFRP Textile Reinforced Shotcrete. In: *Assessment, Upgrading and Refurbishment of Infrastructures*, Proceedings of the IABSE Symposium, Rotterdam, May 2013.

Michels J., Zwicky D., Scherer J., Harmanci Y.E. and Motavalli M. (2014). Structural Strengthening of Concrete with Fiber Reinforced Cementitious Matrix (FRCM) at Ambient and Elevated Temperature – Recent Investigations in Switzerland. *Advances in Structural Engineering.* 17(2):1785-1799.

Fridez A. (2015). *Ancrage des treillis en fibres de carbone dans le béton projeté*. Master thesis, School of Engineering and Architecture Fribourg, University of Applied Sciences Western Switzerland.

Zwicky D. and Bärtschi H.-R. (2016). Development of extremely thin prefabricated concrete façade elements. In: *Challenges in Design and Construction of an Innovative and Sustainable Built Environment*, Proceedings of the 19th IABSE Congress, Stockholm, Sept. 2016.

Macchi N. (2016). *Structural Behavior and design of shear panels made of glass fiber reinforced polymers (GFRP shear panels).* Master thesis, School of Engineering and Architecture Fribourg, University of Applied Sciences Western Switzerland.

Zwicky D. and Mabboux J. (2014). Post-Buckling Shear Resistance of Composite Panels. In: *Composites in Civil Engineering*, Proceedings of the 7th International Conference on FRP Composites in Civil Engineering, Vancouver BC, Aug. 2014.

Mabboux J. and Zwicky D. (2012). Post-Buckling Shear Resistance of Riveted Composite Panels, In: *Composites in Civil Engineering*, Proceedings of the 6th International Conference on FRP Composites in Civil Engineering, Rome, June 2012.

Suter R. and Héritier C. (1999). Renforcement de structures au moyen de lamelles collées en acier et en composite CFK (Structural strengthening with externally bonded steel and CFRP lamellas, in French). *Chantiers.* Nr. 2.

SIA 166 (2004). *Klebebewehrungen* (Externally bonded reinforcement, in German). Swiss Society of Engineers and Architects, Zurich.

Suter R. and Jungo D. (2001). Vorgespannte CFK-Lamellen für die Verstärkung von Bauwerken (Prestressed CFRP lamellas for structural strengthening, in German). *Beton- und Stahlbetonbau.* 96(5):350-358.

Suter R., Conus F., Pinzelli R. and Chang K. (2001). Reinforcement of Bridge Piers with FRP Sheets to Resist Vehicle Impact. In: *Composites in Civil Engineering*, Proceedings of the 1st International Conference on FRP Composites in Civil Engineering, Hong Kong, Dec. 2001.

Suter R. and Conus F. (2005). *Renforcement de pile de ponts contre l'impact de véhicules lourds – essais sur des colonnes en béton renforcées par des tissus en aramide* (Strengthening of bridge piers to resist vehicle impact – tests on large concrete columns strengthened by aramid sheets, in French). Federal Department of the Environment, Transport, Energy and Communications DETEC, Federal Roads Authority FEDRO, report nr. 590.

Suter R. and Pinzelli R. (2001). Confinement of Concrete Columns with FRP sheets. In: *Non-metallic Reinforcement for Concrete Structures*, Proceedings of FRPRCS-5, Cambridge, June 2001.

Moix J. and Sturny, C. (2013). *Application des matériaux composites en fibres végétales dans le domaine du genie civil* (Application of vegetable fibre composites in civil engineering). 2nd year Bachelor study project, School of Engineering and Architecture Fribourg, University of Applied Sciences Western Switzerland.

Chopard L. and Zwicky D. (2014). Bending Behavior of Glulam Beams Reinforced with Flax Fiber Sheets. In: *Composites in Civil Engineering*, Proceedings of the 7th International Conference on FRP Composites in Civil Engineering, Vancouver BC, Aug. 2014.

fib 14 (2001). *Externally bonded FRP reinforcement for RC structures*. Bulletin 14:60-84.

Bischof P., Suter R., Chatzi E. and Lestuzzi P. (2014). On the Use of CFRP Sheets for the Seismic Retrofitting of Masonry Walls and the Influence of Mechanical Anchorage. *Polymers.* 6:1972-1998.

Bischof P. and Suter R. (2014). Retrofitting Masonry Walls with Carbon Mesh. *Polymers.* 6:280-299.

Zwicky D. (2009). Improving the Performance of Timber Beams with Prestressed Laminates. In: *Sustainable Infrastructure – Environment Friendly, Safe and Resource Efficient*, Proceedings of the IABSE Symposium, Bangkok, Sept. 2009.

Chopard, L. (2013). *Etude expérimentale sur le comportement structural des poutres en BLC renforcées par des tissus en fibres naturelles* (Experimental study on the structural behaviour of glulam beams reinforced with natural fibre sheets). 3rd year Bachelor study project, School of Engineering and Architecture Fribourg, University of Applied Sciences Western Switzerland.

COST Action TU 1207

Strengthening of civil structures with FRP - State-the-art of research in Switzerland

In Switzerland, the following Institutes had worked and/or are working in the field. They are part of the Swiss Network.

Empa (Duebendorf near Zurich)

- Structural Engineering Research Laboratory (Prof. M. Motavalli, Dr. C. Czaderski)
- Mechanical Systems Engineering Research Laboratory (Dr. G. Terrasi)

EPFL Lausanne

- CCLab, Composite Construction Lab (Prof. T. Keller, Dr. A.Vassilopoulos)
- ICOM, Steel Structures Lab (Dr. C. Louter)

ETH Zurich (Prof. T.Vogel)

University of Applied Sciences, Rapperswil (HSR) (Prof. A. Kenel)

University of applied sciences (UAS) Fribourg (Prof. D. Zwicky, Prof. R. Suter)

Furthermore, the following companies are part of the Swiss Network:

- Sika
- S&P
- FiReP

Activities of Empa, Structural Engineering Research Laboratory

Professor Dr. Masoud Motavalli, Dr. Christoph Czaderski, Dr. Julien Michels

Pioneering work at Empa

Ibach bridge in Switzerland, first application of CFRP strips on a civil structure in 1991

Reinforce concrete beam strengthenend with a steel plate glued with an expoxy. Long-term test since 1970.

Prestressed CFRP strips for strengthening of concrete → gradient anchorage

Prestressed CFRP strips for strengthening of steel

Prestressed CFRP strips for strengthening of timber

Lectures at ETH Zurich

Activities of Empa, Mechanical Systems Engineering Research Laboratory

Dr. Giovanni Terrasi

Prefabricated thin-walled HPC structural elements prestressed with pultruded carbon tendons (collaboration with company SACAC from Switzerland)

Lectures at ETH Zurich

EPFL, Activities of CCLab and collaborating institutes

Professor Thomas Keller, Dr. Anastasios P. Vassilopoulos

Development of a prestressed and permanent soil-/ rock anchor made of non-corrosive carbon fiber composite materials. Swiss Innovation Promotion Agency CTI (2012-2015).

The objective of the proposed project is to develop a prestressed and permanent soil-/ rock anchor made of non-corrosive carbon fiber composite materials (CFRP), see Fig.1. Work in the past one and half years was mainly focused on two aspects: 1) compression test on grouting materials, including cement grout and epoxy grout. The objective is to find a suitable grouting material for the CFRP ground anchor. 2) pull out test on anchor model using only one loop. The objective is to develop an anchor with capacity of at least 300kN using only one loop.

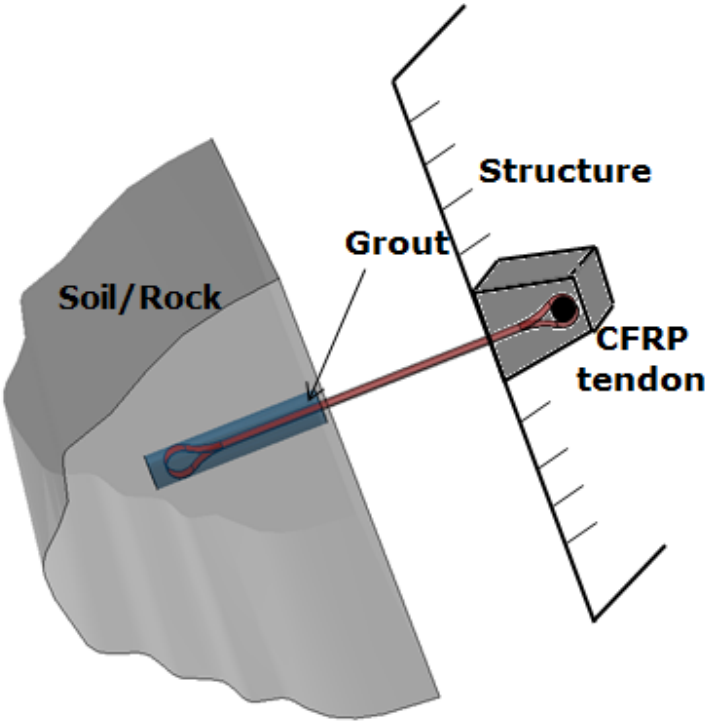

Figure 1. Schematic representation of the develop CFRP tendon

Compression tests

Totally 18 specimens made of cement grout and 3 specimens made of epoxy grout were investigated to obtain the complete compression stress-strain curves. Test setups are shown in Fig.2. During the experiments on the cement grout, the influence of different factors on stress-strain behavior of grout were investigated, including different loading control methods , loading rates, friction-reducing methods.

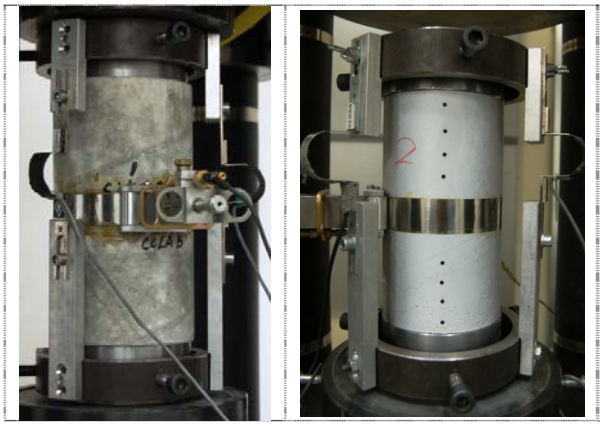

Fig. 2 Test setups for the cement (left) and the epoxy (right) grout

Pullout test on anchor model

Test set-up and layout of instrumentation are shown in Fig. 3 based on the compression test, cement grout sikagrout 212 was chosen as the grouting material for this anchor specimen. The objective of this test is to obtain an anchor with at least 300kN of capacity using only one loop.

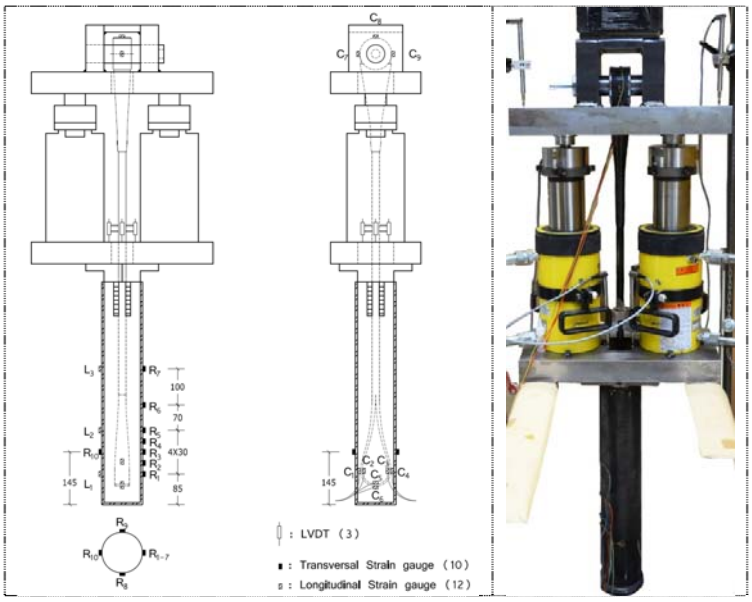

Fig. 3 Experimental setups and instrumentation lay-out

Future work

- More pull out test on anchor models using different grouting material (epoxy grout) and confinement material (CFRP ring).
- Develop a CFRP ground anchor with capacity of 1000kN.
- Develop an economical installation method.
- Verify the structural safety and serviceability.

Development of a high-performance thermally-insulating load-transfer element made of fiber-reinforced polymers for concrete structures. Swiss Innovation Promotion Agency CTI (2012-2015).

A new concept of a structural element for the balcony connections of concrete structures is introduced, see Fig. 4. The structural elements and the thin insulation layer (d=50mm), as well, are assembled in a PVC box, making the installation procedure easy on the construction site.

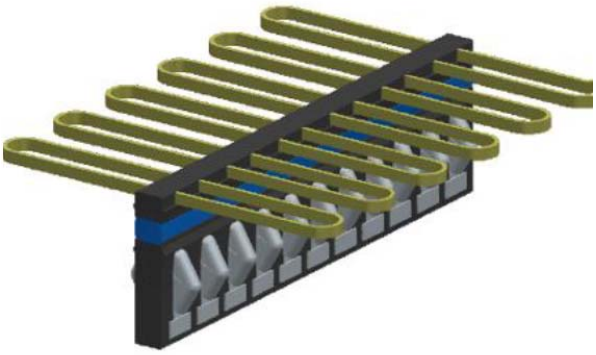

Figure 4. The new FRP thermal bridge concept.

Analyzing the cantilever beam of the balcony's connection by a strut-and-tie model, under a vertical load on the cantilever the tensile forces that are created are taken by an AFRP loop. The equivalent compression forces are transferred by a rectangular pultruded element. The shear forces, transferred by the diagonals of the truss analogy, are undertaken by a GFRP hexagonal sandwich element, in form of compressive forces, Fig. 5.

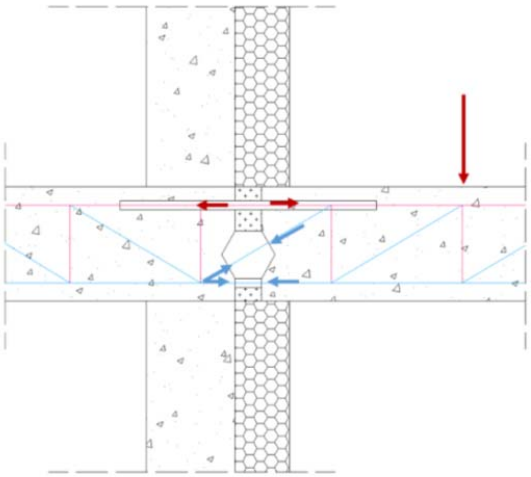

Figure 5. Structural model of the FRP thermal break

Experimental investigation

The behavior of the new thermal bridge structural elements has been experimentally investigated (see Fig. 6). The GFRP hexagonal sandwich element was loaded under compressive loads, while the AFRP loop was loaded under tension simulating the tensile forces this element should transfer supporting the cantilever structure.

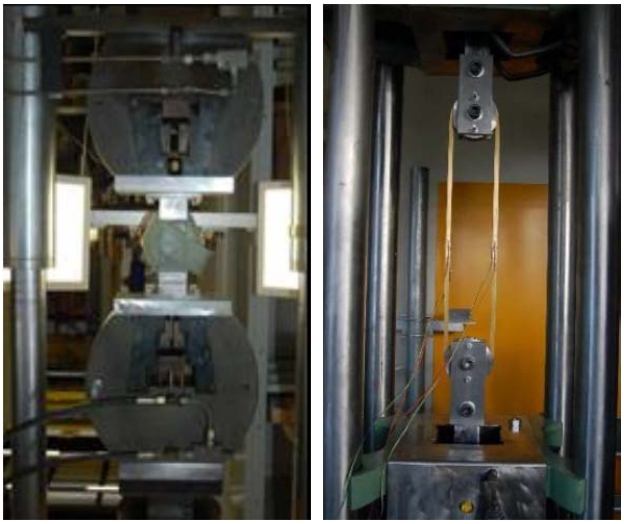

Figure 6. Experimental set-up for compression (left) tension (right) of the new thermal bridge components

Numerical simulations

For the evaluation of the thermal performance, thermal simulations were carried out for the balcony thermal bridge under steady state conditions. The multiphysics software FLUENT was used and the simulations were performed according the standard ISO 10211:2007. Demanding wall thermal transmittance was chosen, U=0.1W/m^{2}K, for the numerical analyses following the concept of the MINERGIE standard. Fig. 7 shows the thermal bridge model and the temperature distribution of the thermal bridge with the new thermal break. It is obvious that in the internal side of the thermal bridge, the temperature is uniform and there is no condensation risk.

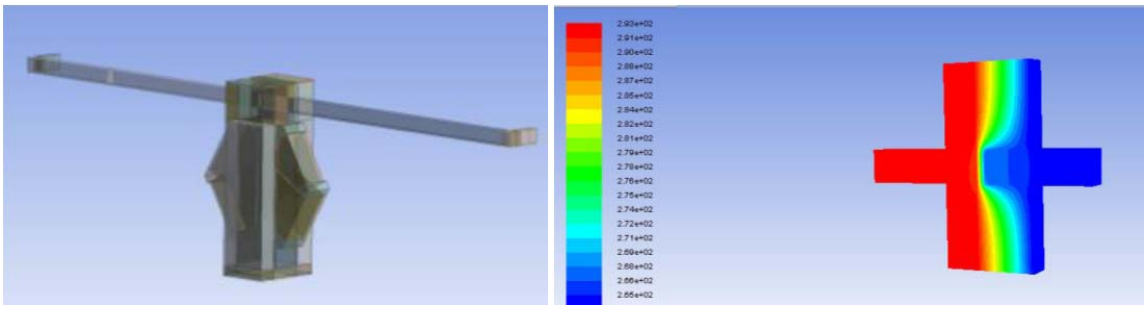

Figure 7. New thermal bridge model and temperature distribution numerical results

Structural performance of post-tensioned punching shear strengthening systems of flat slabs. Swiss Innovation Promotion Agency CTI (2010-2014) – Collaboration with the Institute for Civil and Environmental Engineering (IBU) at Rapperswil University of Applied Sciences (HSR), Switzerland.

A new strengthening concept was recently developed, introducing a new application for Carbon FRP composites as a post-tensioned punching strengthening system for existing flat slabs. Post-tensioning significantly improves the system efficiency due to the partial unloading of the slab. In predrilled and precut openings, unbonded non-laminated CFRP straps were installed crosswise around the column, see Fig. 8.

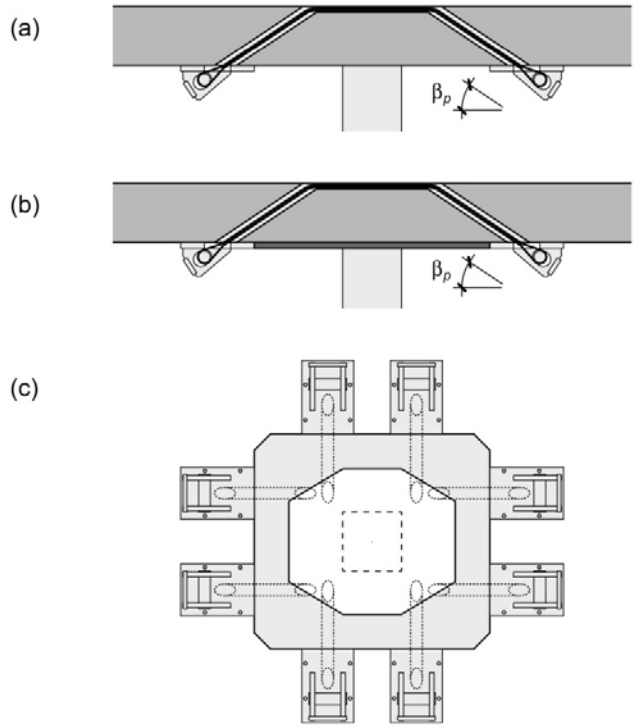

Figure 8. Punching shear strengthening concept with prestressed CFRP straps. (a) Adhesive bonding of anchors with epoxy resin; (b) and (c) steel compression frame as anchor support.

The main objective of the research project is the investigation of the structural performance of the presented strengthening concept. The effect of the two anchoring methods on the slab behavior has to be analyzed. The system performance has to be verified with full-scale laboratory experiments. A comprehensive theoretical model has to be developed which is able to reproduce the operating mode of the strengthening concept, considering the local prestressing around the column. The validity of the model has to be proved with the results of the experimental campaign. This forms the basis for a simplified design model.

Experimental investigation

The presented punching shear concept was part of a larger experimental campaign for new strengthening methods of totally 19 full-scale punching tests. Square slabs with side lengths of 3.2 m and slab thicknesses of 0.18 to 0.32 m were tested. The specimens were supported in the center by a square

steel plate with a side length of 0.25 m; the load was applied at a radius of 1.50 m, Fig. 9. All specimens had an orthogonal flexural reinforcement layout with a reinforcement ratio of approximately 1.5%.

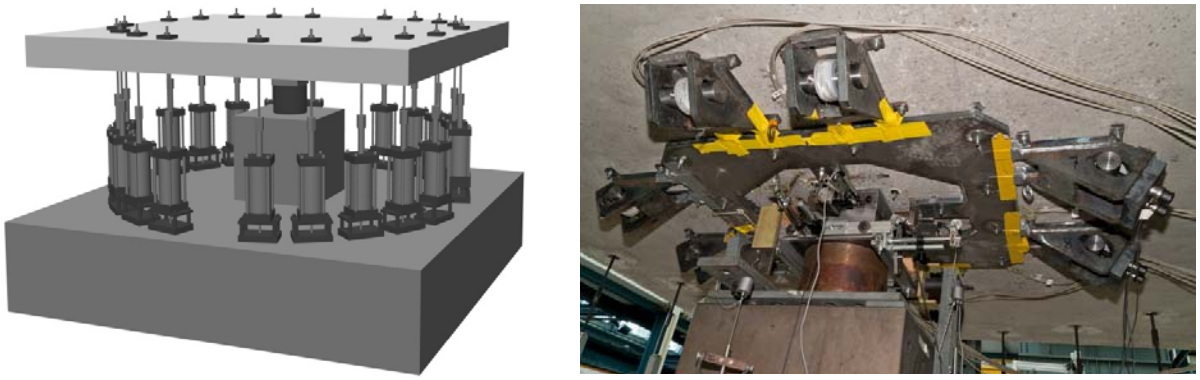

Figure 9. Visualization of experimental setup (left), bottom view with steel frame and anchors (right)

Strap post-tensioning of at least 15% of its tensile strength led to a more ductile slab response although the CFRP materials were brittle. The ultimate load of the unreinforced slabs could be increased by 67-114% via a redistribution of forces from the concrete to the strap system, Fig. 10. The punching shear resistance of the both strengthening systems – the former with adhesively bonded anchors and the new system with steel frame – was similar. The lowest relative increase was observed for the thickest slab.

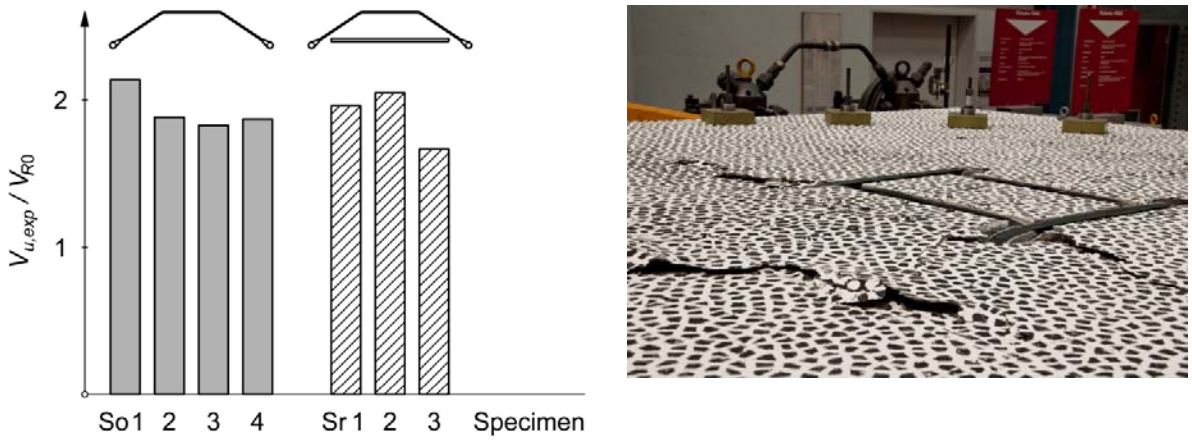

Figure 10. Summary of obtained failure loads Vu,exp, normalized with punching resistance of unreinforced slab VR0 (left), photo of the upper slab surface after failure (right)

Finished and on-going projects on the use of structural adhesives for bridge engineering

In bridge engineering, cold-curing epoxy adhesives have already been used for more than 50 years, although only in specific applications. Advances have been made in the bonding of structural and semi-structural elements of bridges, such as bearings, expansion joints, concrete deck slabs to steel girders in composite bridges and joining of precast concrete segments, as a substitute for or in combination with conventional joining methods.

An extensive investigation on this subject has been performed by CCLab between 2007 and 2011 in the frame of a research project funded by the Federal Road and Bridges Authority (FEDRO) of Switzerland. The project entitled “Thermophysical and thermomechanical behavior of

cold-curing structural adhesives in bridge construction” has been completed in 2011, see PhD Thesis, No. 5244.

A new project has been funded by FEDRO in order to investigate the durability of epoxy based structural adhesives in used in bridge engineering. The project, entitled “Durability and fatigue life of cold-curing structural adhesives in bridge construction” has been initiated on July 2013, and its main objective is the quantification of the long term effect of physical and chemical ageing parameters on the physical and mechanical properties of cold-curing epoxy based structural adhesives.

EPFL, Activities of ICOM

Dr. Christian Louter

Composite structural glass beams

The structural glass research group at the ICOM Steel Structures Laboratory at the EPFL Ecole polytechnique fédérale de Lausanne, focuses on the use of glass as a load-bearing material in building structures, and is guided by Dr. Christian Louter. One of the concepts currently under investigation by the research group are composite structural glass beams in which a steel, GFRP or CFRP reinforcement is incorporated. The main purpose of this reinforcement is to provide residual load-carrying capacity in the event of glass breakage. Several composite glass beam configurations are developed and investigated. Furthermore, several bonding techniques to connect the reinforcement to the glass are studied. In this respect, also the durability of adhesives is investigated and the effects of parameters such as temperature, humidity and load-duration on the structural performance of the composite glass beams are investigated.

More information is available at http://icom.epfl.ch/glass

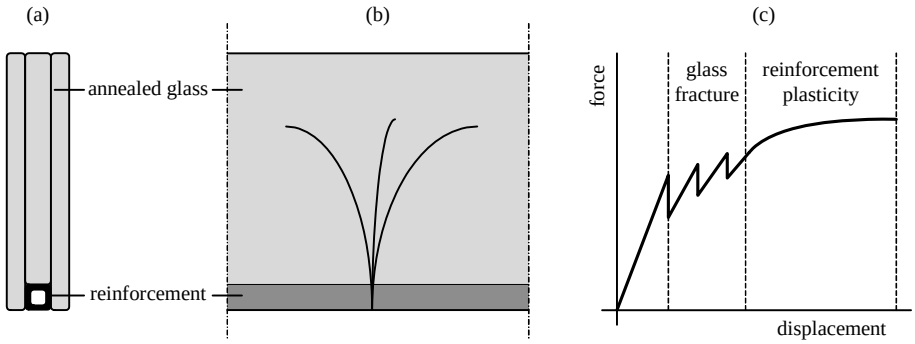

Figure 1. Schematic representation of the functioning of the composite glass beam concept (a) cross-section of the composite glass beam; (b) side-view of a cracked composite glass beam; (c) force-displacement diagram of composite glass beam loaded in displacement controlled bending (Louter, 2011)

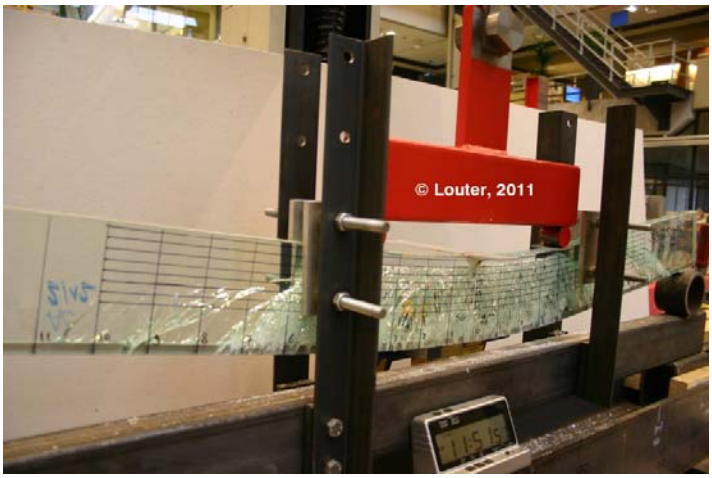

Figure 2: Composite glass beam with steel reinforcement during bending test, demonstrating a significant residual load-carrying capacity. (Louter, 2011)

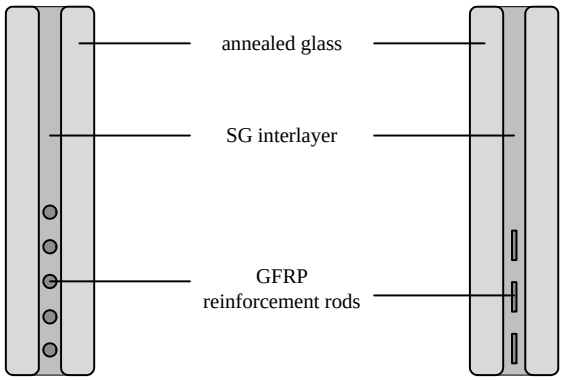

Figure 3: Schematic representation of the concept of composite glass beams with GFRP (Glass Fiber Reinforced Polymer) reinforcement rods embedded in the interlayer. (Louter, 2011)

Figure 4: Composite glass beam with GFRP reinforcement during bending test. (Louter, 2011)

Activities of University of applied sciences (UAS) Fribourg

Prof. D. Zwicky (Prof. R. Suter)

Seismic resistance and strengthening of masonry with FRP

Textile CFRP reinforced shotcrete (ARMO mesh) for bending and seismic

Externally bonded FRP

Confinement

NSMR strengthening of timber with prestressed CFRP

Bending behavior of glulam beams reinforced with flax fiber sheets text

Shear resistance of composite panels

Strengthening of Concrete Structures using CFRP Composites - State of Research at Empa, Switzerland Contribution

Christoph Czaderski[1], Julien Michels[2], Juan Manuel Gallego[3]

Introduction

Carbon Fiber Reinforced Polymer (CFRP) strips are, due to their high tensile strength $f_{t,u}$ > 2,000 MPa, their resistance against corrosion and their easy handling on site (ρ≅1.6 g/cm3), an efficient technique for retrofitting existing reinforced concrete structures [1]. Generally, the CFRP strips are bonded to the concrete surfaces with an epoxy adhesive. Thanks to the pioneering work of Professor Urs Meier and his team from Empa, the first application of CFRP strips on a bridge was performed 25 years ago in Switzerland in 1991 [2].
By prestressing the strips, the excellent mechanical performances can be further utilized. An adequate anchorage is necessary in order to avoid a premature debonding failure. Currently several mechanical systems are available on the market, generally requiring the installation of permanent dowels and anchor plates resulting in a less appealing appearance. As a countermeasure, the gradient anchorage was introduced at Empa [3]. The idea is to eventually obtain a purely concrete-adhesive-strip connection without any remaining mechanical devices. The advantages of this method are enhanced durability, improved aesthetics and a lower construction height. Text taken from [4].

Prestressed externally bonded reinforcement

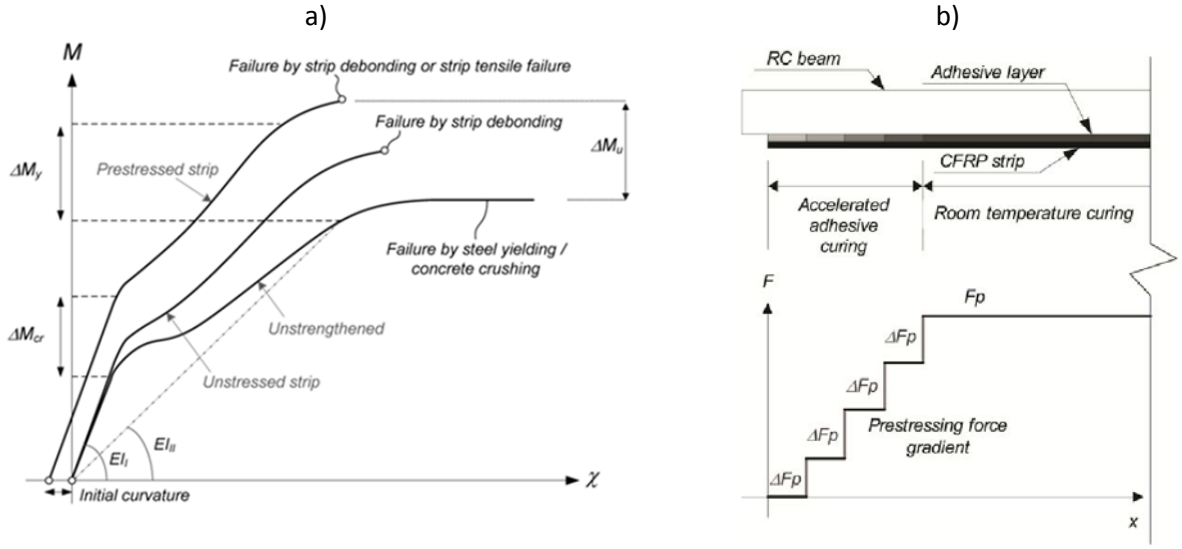

Figure 1: a) Different moment-curvature behaviour of unstrengthened, strengthened with unstressed strip and strengthened with prestressed strip (taken from [5]), b) schematic sketch of gradient anchorage (taken from [6]).

Several investigations have documented the structural advantages of prestressed FRP reinforcement in retrofitting. A first positive aspect is the possibility to actively act against dead loads and thus reduce the existing deflections and cracks in the structure. With a sufficient amount of initial prestrain in the laminate, the cracking load is considerably increased compared to a reference (unstrengthened) beam (Figure 1a)). The same is valid for the load at which the inner steel reinforcement begins to yield. The ultimate load carrying capacity is also generally enhanced. However, a decrease of ductility, resulting in

[1] Empa, Swiss Federal Laboratories for Materials Science and Technology, Switzerland, christoph.czaderski@empa.ch
[2] Empa, Swiss Federal Laboratories for Materials Science and Technology, Switzerland, julien.michels@empa.ch
[3] Empa, Swiss Federal Laboratories for Materials Science and Technology, Switzerland, juan.gallegomartin@empa.ch

a lower deflection when reaching the ultimate load, can be observed when an initial prestress is applied to the laminate. While a structure that is retrofitted with an unstressed strip always exhibits debonding failure at the peak load, tensile failure of the external reinforcement can be obtained if the initial prestrain is sufficiently high. Text taken from [7].

Development of gradient anchorage method

The method is based on the possibility of considerably reducing the necessary curing time of the epoxy adhesive by applying high temperature. The gradient anchorage method is characterized by a segment wise adhesive heating and subsequent gradual prestress force decrease symmetrically at both strip ends [8]. If the initial prestrain of the strip is too high, the risk of debonding failure is imminent if the total force is released in one step. With the present technique, the total prestress force is distributed over several segments, resulting in a reduced bond shear stress in the end region. A schematic representation of the force gradient is given in Figure 1b. In the framework of a CTI-funded project, the gradient anchorage method including the feasible equipment was developed, see [8-11] for more details and experimental work.

Investigation of Bond Behaviour of unstressed and prestressed EBR

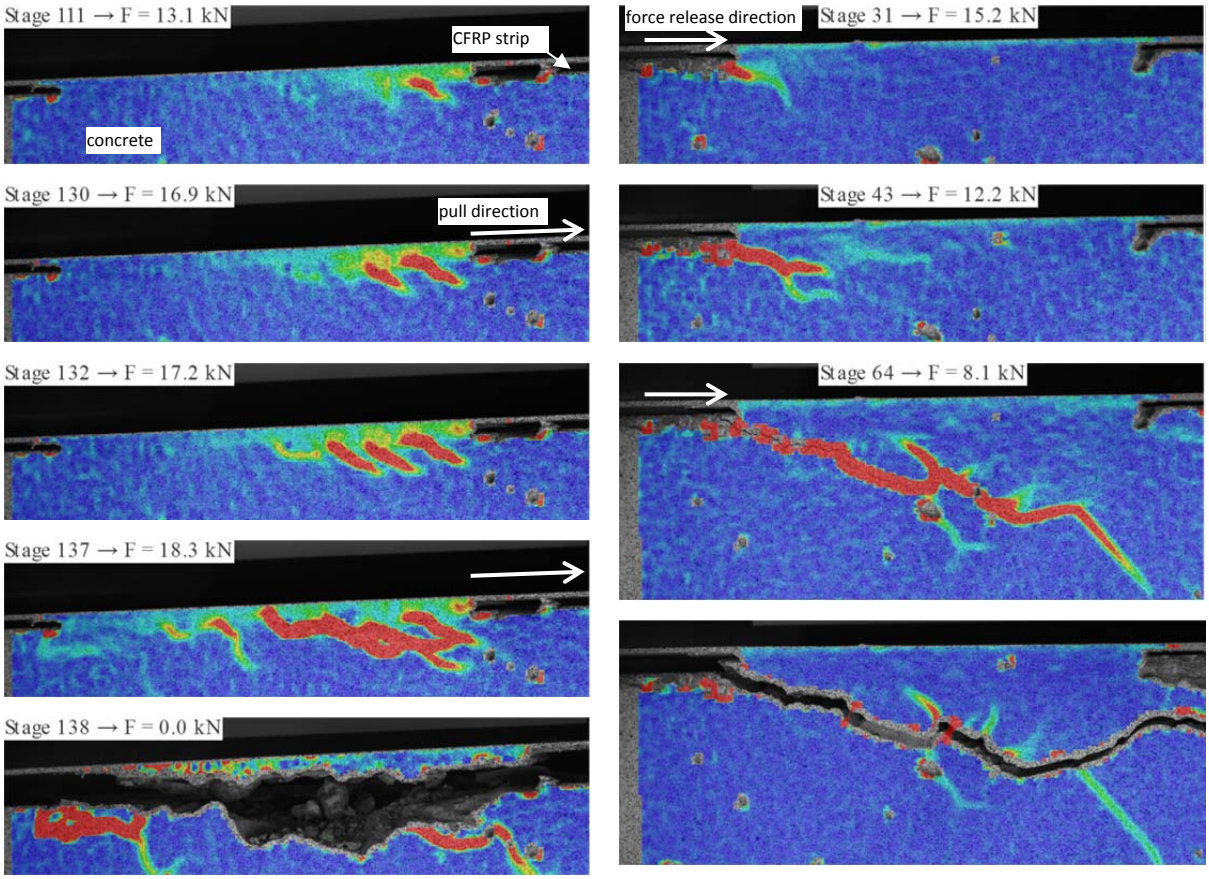

Figure 2: CFRP strips glued on the surface of a concrete surface. Image correlation measurements from the side, which show the cracks under the strip in the concrete: Left: failure mechanism of a lap-shear test, pulling direction is to the right hand side. Right: failure mechanism of a prestress force release test, the prestress force was released from the left side. (taken from [12]).

In the framework of a PhD project, the bond behaviour and bond mechanism of unstressed and prestressed externally bonded CFRP strips were investigated. The cracking behaviour and development in the concrete under the CFRP strips during loading was studied by image correlation measurements, Figure 2, [13] and [14]. Furthermore, beam tests were performed in order to verify the small scale tests,

[15]. Currently, long-term durability investigations on residual anchorage resistances of gradient anchorages are performed in the framework of a doctoral study at Empa/ETH Zurich.

Large-scale bridge girder strengthening

The gradient anchorage method was applied on large-scale bridge girders in the laboratory and tested up to failure. Figure 3 displays one of the 17 meter long bridge girders in the Empa laboratory, which were taken from a bridge in the south part of Switzerland. The load-displacement diagram from the failure tests is also given Figure 3, showing the significant increase in the load-carrying capacity of the girder strengthened with prestressed compared to the strengthening with unstressed CFRP strips.

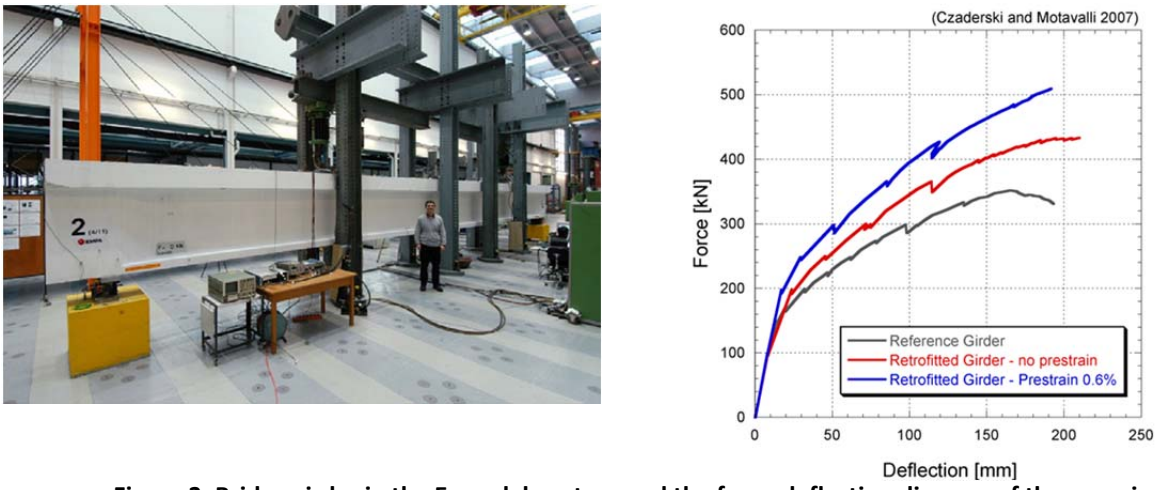

Figure 3: Bridge girder in the Empa laboratory and the force-deflection diagram of the experiments by Czaderski et al. [5] and [16] to show the feasibility of the gradient anchorage method.

Figure 4 presents the investigation on two 18.4 meter long bridge girders, which were performed in the framework of the TULCOEMPA project. In this project, in collaboration with the Technical University of Lodz, Poland, two bridge girders of the road bridge Szczercowska Wieś in Poland were copied and newly manufactured at Empa and tested, one girder not strengthened and one strengthened. Afterwards, the girders of the real bridge in Poland were retrofitted with prestressed CFRP strips anchored with the gradient anchorage, see [17, 18] for more details.

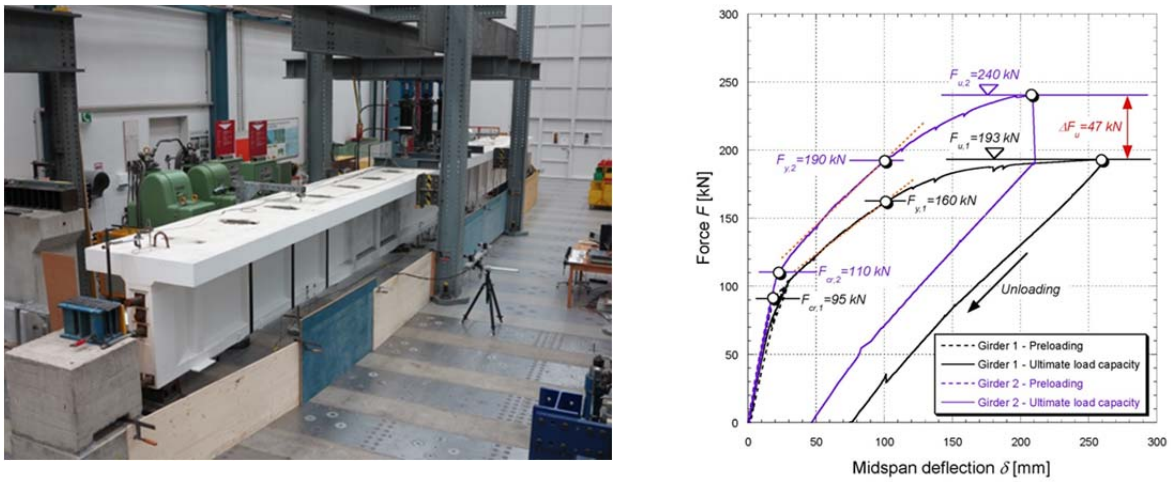

Figure 4: Bridge girder in the Empa laboratory and the force-deflection diagram of the experimental program by Michels et al. [17].

Long-term behaviour of EBR

In 1970, Empa performed an investigation on strengthening of reinforced concrete by applying steel plates to the concrete surface with epoxy resin. Beside static tests and a fatigue test, also a long-term

test on a beam in the laboratory which was heavily loaded with a sustained load (Figure 5a)) was started. The test is still running as visible in Figure 5a).

A bridge over the river Rhine (Figure 5b)) was strengthened with unstressed CFRP strips in 1996, [19]. Since then, in order to study the long-term behaviour, Empa performed in more or less regular intervals measurements on the strips, see [20] and [21].

From both projects, not any deterioration of the epoxy and CFRP strips could be observed.

Figure 5: Left: long-term test at Empa since 1970, the reinforced concrete beam was strengthened with a steel plate by using an epoxy adhesive. Right: Rhine bridge between Switzerland and Austria, which was strengthened with unstressed CFRP strips in the year 1996.

Prestressed confinement

Janke et al. [22] found that prestressing the confinement reinforcement significantly affects the residual strength of columns after an overload. To estimate the residual strength, the concentric load on the confined cylinders was increased only up to a predefined overload above the unconfined load capacity (Figure 6a). The confinement reinforcement was then removed and the residual capacity was determined in another compression test (Figure 6b) up to failure.

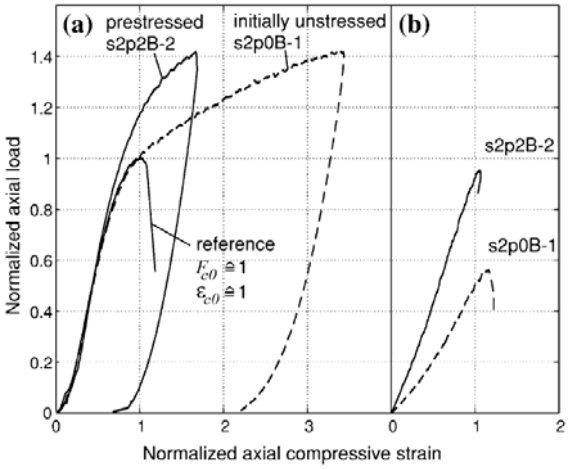

Figure 6: (a) Load cycle to 140 % of unconfined compressive strength with confinement, (b) failure test after removal of confinement (taken from [5]).

In the experiments the axial compressive strain and plastic deformation of the unstressed specimens was significantly higher than that of the prestressed confinement in response to the same overload (Figure 6a). In the example shown in Figure 6a the axial compressive strain of the initially unstressed confined specimen and the prestressed confined specimen were 3.5 times and 1.7 times higher than that of the unconfined reference specimen at peak load, respectively. The residual strength was 56 and 95 %, respectively. Therefore, prestressing the confinement reinforcement significantly reduces damage

to the confined concrete under overloads compared to unstressed confinement reinforcement, which was demonstrated by a higher residual capacity (Figure 6b) and lower axial strain (Figure 6a). The latter could be beneficial to serviceability limit states (lower displacements), while the former significantly improves the safety of construction under special circumstances (for example a fire which could cause a failure of the confinement). Text taken from [5].

Long-term behaviour of unstressed and prestressed EBR at elevated temperature

A possible further application of externally bonded CFRP strips are box-girder bridges with their cantilevers in transverse direction (Figure 7 and [23]). Such an installation rises the following two questions: 1) how does the CFRP/epoxy/concrete system behave during and after the warm asphalt application, and 2) how does the system behave on the long-term?

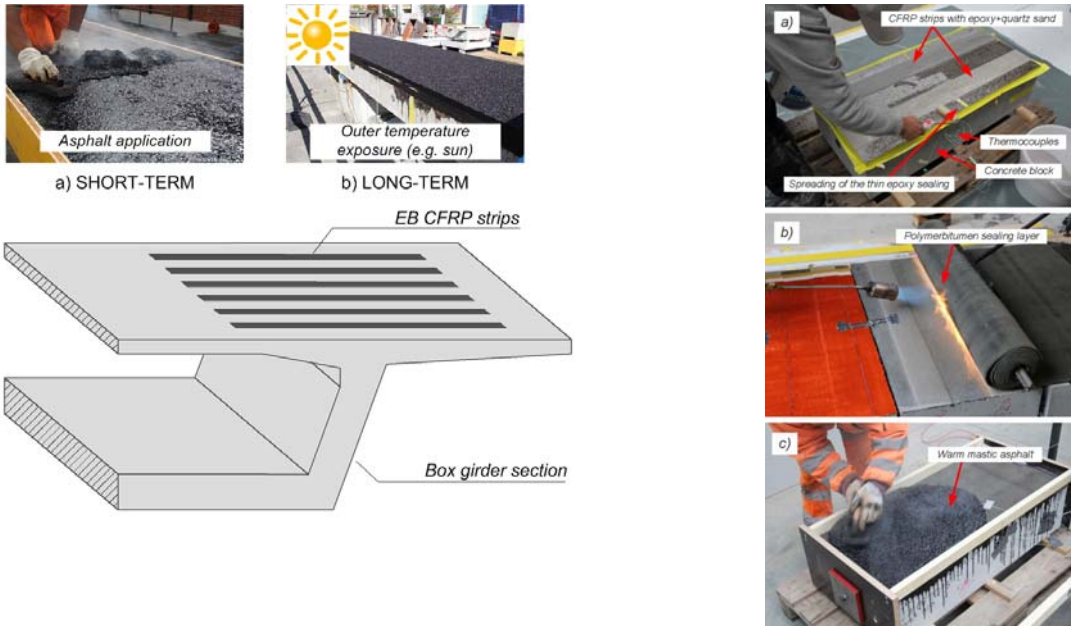

Figure 7: Left: CFRP strip strengthening in transverse direction in a RC box-girder bridge and elevated temperature scenarios. Right: typical road build-up for bridges in Switzerland. Taken from [23].

Experiments regarding the temperature evolution in an epoxy adhesive layer for an EB CFRP strengthening system were performed at Empa according to the typical road build-up for bridges in the canton of Zurich (Switzerland). The construction process comprises mainly in three steps: a) sealing layer (epoxy mixture) extended directly on the concrete substrate, b) PBD (German acronym for polymer-bitumen water proofing membrane), and c) warm mastic asphalt (approximately 230°C in the transportation truck), see Figure 7 right. Steps b) and c) induce elevated temperatures in the epoxy resin layer below the CFRP strips. Whilst being almost negligible for the PBD installation, during the application of the warm mastic asphalt layer the epoxy temperature climbs to almost 80°C followed by a plateau-like evolution and a slow cooling process. Ambient temperature is reached again after several hours. The residual bond strength of the CFRP/epoxy/concrete system after the warm mastic asphalt exposure was investigated through small- and large-scale tests.

If the CFRP strip is unstressed, no problems regarding a softer epoxy due to exceeding the glass transition temperature should arise. Post-curing due to the asphalt scenario is even beneficial for the bond between the different components [24]. In spite of the good behaviour of these unstressed strips, different results have been observed when prestressed strips anchored with the gradient anchorage method were tested. The temperature stability of prestressed strips in small scale tests was studied during the simulation of the asphalt scenario, showing a slight decrease of the initial prestress force after reach the initial room temperature [25]. However, on a large-scale slab tests, one of the two prestressed strips did not survive the simulation of the asphalt scenario, what means that an isolation would be necessary for such an application.

Large-scale slabs with real mastic asphalt layers extended on the top surface and subjected to sustained loads were installed in order to evaluate the long-term behaviour due to environmental exposure, showing so far a good behaviour of these elements. Furthermore, fatigue tests performed at elevated temperature in similar elements were carried out without seeing any fatigue failure of the longitudinal steel bars, neither significant fatigue degradation of the strip/epoxy/concrete joints.

Acknowledgement

The authors express their gratitude to the Swiss innovation promotion agency for their support in the framework of the project CTI No. 10493.2 PFIW-IW. The financial contribution of the Swiss Road Authorities (FEDRO/ASTRA) within the framework of the projects AGB 2001/485 and AGB 2012/001 is also very much appreciated. Furthermore, the support of the Marie Curie Initial Training Network Endure (MC-ITN-2013-607851) for the scholarship of the third author is esteemed. Thanks go also to the industrial partner S&P Clever Reinforcement AG (Switzerland) for their partnership during the CTI project and Sika for providing of material.

References

1. Meier, U., *Strengthening of structures using carbon fibre epoxy composites.* Construction and Building Materials, 1995. **9**(6): p. 341-351.
2. Meier, U. and M. Deuring, *The application of fiber composites in bridge repair - a world premiere at the gates of Lucerne.* Strasse und Verkehr, 1991. **77**(9): p. 534-535.
3. Meier, U. and I. Stöcklin, *A Novel Carbon Fiber Reinforced Polymer (CFRP) System for Post-Strengthening*, in *International Conference on Concrete Repair, Rehabilitation and Retrofitting (ICCRRR), November 21-23, 2005*. 2005: Cape Town, South Africa. p. 477-479.
4. Michels, J., C. Czaderski, and M. Motavalli, *Gradient anchorage for prestressed CFRP strips bonded to concrete*, in *Structural Concrete in Switzerland*. 2014, fib-CH, Swiss national group of the international federation for structural concrete: The forth fib-Congress, February 10 to 14, 2014, Mumbai, India. p. 35-39.
5. Michels, J., J. Barros, I. Costa, J. Sena-Cruz, C. Czaderski, G. Giacomin, R. Kotynia, J. Lees, C. Pellegrino, and E. Zile, *Prestressed FRP Systems*, in *Design Procedures for the Use of Composites in Strengthening of Reinforced Concrete Structures*, C. Pellegrino and J. Sena-Cruz, Editors. 2016, Springer. p. 263-301.
6. Michels, J., C. Czaderski, R. El-Hacha, and M. Motavalli, *Partially Cured Epoxy Adhesive for Anchoring Prestressed CFRP Strips on Concrete*, in *APFIS 2012, The Third Asia-Pacific Conference on FRP in Structures*. 2012: Hokkaido University, Japan, February 2-4, 2012. p. 8.
7. Motavalli, M., C. Czaderski, and K. Pfyl-Lang, *Prestressed CFRP for strengthening of reinforced concrete structures - recent developments at Empa Switzerland.* Journal of Composites for Construction, ASCE, 2011. **15**(2): p. 194-205.
8. Michels, J., J. Sena-Cruz, C. Czaderski, and M. Motavalli, *Structural strengthening with prestressed CFRP strips with gradient anchorage.* Journal of Composites for Construction, ASCE, 2013. **17**(5): p. 651-661.
9. Czaderski, C., E. Martinelli, J. Michels, and M. Motavalli, *Effect of curing conditions on strength development in an epoxy resin for structural strengthening.* Composites Part B: engineering, 2012. **43**(2): p. 398-410.
10. Michels, J., C. Czaderski, R. El-Hacha, R. Brönnimann, and M. Motavalli, *Temporary bond strength of partly cured epoxy adhesive for anchoring prestressed CFRP strips on concrete.* Composite structures, 2012. **94**(9): p. 2667-2676.
11. Michels, J., E. Martinelli, C. Czaderski, and M. Motavalli, *Prestressed CFRP Strips with Gradient Anchorage for Structural Concrete Retrofitting: Experiments and Numerical Modeling.* Polymers, 2014. **6**(1): p. 114-131.
12. Michels, J., E. Zile, C. Czaderski, and M. Motavalli, *Debonding failure mechanisms in prestressed CFRP/epoxy/concrete connections.* Engineering Fracture Mechanics, 2014. **132**: p. 16-37.

13. Czaderski, C., K. Soudki, and M. Motavalli, *Front and Side View Image Correlation Measurements on FRP to Concrete Pull-Off Bond Tests.* Journal of Composites for Construction, ASCE, 2010. **14**(4): p. 451-463.
14. Czaderski, C., *PhD Thesis No. 20504: Strengthening of reinforced concrete members by prestressed, externally bonded reinforcement with gradient anchorage*. Institute of Structural Engineering. 2012: ETH Zurich. DOI: http://dx.doi.org/10.3929/ethz-a-007569614.
15. Harmanci, Y.E., J. Michels, and C. Czaderski, *Calculation Technique for Externally Unbonded CFRP Strips in Structural Concrete Retrofitting.* ASCE Journal of Engineering Mechanics, J. Eng. Mech. 04016026, http://dx.doi.org/10.1061/(ASCE)EM.1943-7889.0001014, 2016
16. Czaderski, C. and M. Motavalli, *40-Year-old full-scale concrete bridge girder strengthened with prestressed CFRP plates anchored using gradient method.* Composites Part B: Engineering, 2007. **38**(7-8): p. 878-886.
17. Michels, J., M. Staśkiewicz, C. Czaderski, R. Kotynia, Y. Harmanci, and M. Motavalli, *Prestressed CFRP Strips for Concrete Bridge Girder Retrofitting: Application and Static Loading Test.* ASCE Journal of Bridge Engineering, 2016. **21**(5): p. 04016003.
18. Kotynia, R., M. Staskiewicz, J. Michels, C. Czaderski, and M. Motavalli. *Pioneering strengthening of bridge girders with pretensioned CFRP laminates in Poland*. in *SMAR 2015, Antalya, Turkey, 7-9 September 2015*. 2015.
19. Walser, R. and W. Steiner, *Strengthening a Bridge with Advanced Materials.* Structural Engineering International, 1997(2): p. 110-112.
20. Czaderski, C. and U. Meier, *Long-Term Behaviour of CFRP Strips for Post-Strengthening*, in *2nd International fib Congress*. 2006: Naples, Italy, June 5-8, 2006. p. 110-112.
21. Meier, U., R. Brönnimann, P. Anderegg, G. Terrasi, M. Motavalli, and C. Czaderski. *Carbon fiber reinforced composites proved to be very successful in construction during a quarter of a century*. in *ECCM17 - 17th European Conference on Composite Materials*. 2016. Munich, Germany, 26-30th June 2016.
22. Janke, L., C. Czaderski, J. Ruth, and M. Motavalli, *Experiments on the residual load-bearing capacity of prestressed confined concrete columns.* Engineering Structures, 2009. **31**(10): p. 2247-2256.
23. Gallego, J.M., C. Czaderski, and J. Michels, *Influence of the asphalt pavement on the short-term static strength and longterm behaviour of RC slabs strengthened with externally bonded CFRP strips.* Engineering Structures, submitted 2016.
24. Michels, J., J.M. Gallego, and C. Czaderski. *Effect of temperature on the bond strength and long-term behavior of EB CFRP strips on concrete in bridge construction*. in *7th International Conference on Advanced Composite Materials in Bridges and Structures*. 2016. Vancouver, British Columbia, Canada, 24 – 26 August 2016.
25. Gallego, J.M., C. Czaderski, and J. Michels, *Prestress force-release tests at elevated temperatures - Gradient anchorage stability for prestressed EB CFRP strips.* Composite Structures, 2016. **137**: p. 159-169.

Strengthening of Steel Structures using CFRP Composites: State of Research at Empa, Switzerland

Elyas Ghafoori [1]

Introduction

CFRP Strengthening of Metallic Structures

Application of carbon fiber-reinforced polymer (CFRP) materials for retrofitting concrete girders has been extensively investigated and used in practice. Many studies demonstrated the beneficial influence of such composite strips for flexural, shear and confinement strengthening of concrete structures. However, strengthening techniques and the accompanying theory for steel structures have not been developed as thoroughly as those for concrete structures (e.g., Ghafoori and Motavalli 2015b, Ghafoori and Motavalli 2015c, Ghafoori and Motavalli 2015a). There are several differences between the behavior of bonded joints in CFRP-strengthened concrete and metallic members, which will be briefly explained in this section.

Key Differences between Strengthening of Steel and Concrete Structures

Failure mode: The main difference between CFRP–steel and CFRP–concrete bonded joints is that in the former, failure will likely occur in the adhesive layer and in the latter failure is expected to occur in the concrete. Therefore, by providing an adequate bond length, the optimal strength of a bond joint is dependent on the fracture energy of the adhesive for the former and the fracture energy of the concrete for the latter. In the FRP-strengthened steel structures, interfacial failure should happen within the adhesive layer in the form of cohesion failure to maximize the effectiveness of FRP strengthening and minimize variations of the interfacial bond capacity as a result of different surface preparations. Furthermore, it has been observed that the inappropriate surface preparation of the steel substrate prior to the bond application will result in an adhesion failure at the steel-to-adhesive interface. Assuming the adhesive as the weakest point of a CFRP-steel bond joint, Ghafoori and Motavalli 2016a have developed a prestressed unbonded reinforcement (PUR) system that can be used as an alternative to the bonded CFRP reinforcement. The developed PUR system functions without using an adhesive layer, hence the performance of system is no longer dependent on the fracture energy of the adhesive. Strengthening using the PUR system is recommended for cases when the surface of the structure, which has to be retrofitted, is not smooth enough to be bonded to CFRP plates, or when there is concern about the effects of high ambient temperatures, moisture, water or fatigue loading on the CFRP-to-metal bond behavior.

Stiffness and deformations: Recent experimental and numerical results studies at Empa (Ghafoori and Motavalli 2015b, Ghafoori and Motavalli 2015c) have shown that pre-stressing the CFRP strips does not increase the stiffness of the retrofitted steel beams. This finding is in contrast to retrofitted concrete beams, in which the cracks are often initiated at even low load levels. In the latter case, pre-stressed laminates can close the existing cracks more efficiently than non-pre-stressed laminates, and thereby, the overall cross-section area of the concrete beam is increased, which results in increased stiffness. For the same reason, pre-stressed laminate can increase the stiffness of the cracked steel members. Therefore, one of the main difference between the behavior of the CFRP bonded concrete and steel beams is that in the former the cracks are initiated at low load levels in the tension face of the concrete beams, and the bonded CFRP laminate tends to close the crack openings. However, in the latter, the steel does not crack even after yielding and the effect of having adhesive between the CFRP laminate

[1] Empa, Swiss Federal Laboratories for Materials Science and Technology, Switzerland, elyas.ghafoori@empa.ch

and steel substrate is limited to transferring the shear stresses from the steel substrate to the CFRP laminate along the connection.

Strengthening Steel Structures using Prestressed Bonded CFRP Composites

Ghafoori and Motavalli 2015c have used bonded non-prestressed normal modulus (NM), high modulus (HM) and ultra-high modulus (UHM) for flexural strengthening of steel beams. It has been shown that UHM CFRP strip are effective in increasing the stiffness of the metallic girders and reducing the deformations. Metallic members have been traditionally strengthened using non-pre-stressed CFRP plates. However, in non-pre-stressed retrofit systems, the dead loads are not transferred to the CFRP plates and only a portion of the live load is transferred to the CFRP plates. As an alternative, by using pre-stressed CFRP plates, a portion of the dead load is transferred to the CFRP plates in addition to the live load (Ghafoori 2013, Ghafoori and Motavalli 2013). It has been shown that prestressed CFRP strips can increase the flexural yield and ultimate load capacity of steel beams substantially. Ghafoori and Motavalli 2015b have shown that prestressed CFRP strips can be used for strengthening of steel beams that are prone to later-torsional buckling (LTB) to increase the LTB strength. Moreover, Ghafoori et al. 2012b studied the performance of notched steel beams retrofitted with CFRP patches under high-cycle fatigue loading regime. The test results for a four-point bending test scheme with a cyclic loading frequency of 4.2 Hz showed that the CFRP patch extended the fatigue life substantially, and in some case, a complete fatigue crack arrest was achieved.

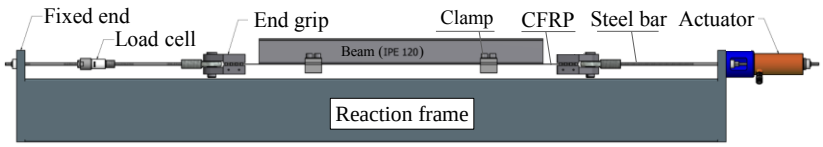

Figure 1. Elements of the pre-stressing set-up, which uses an independent reaction frame to pull the CFRP strip (Ghafoori and Motavalli 2015b).

Strengthening Steel Structures with Prestressed Unbonded CFRP Composites

The majority of the existing research on CFRP strengthening of metallic members has used CFRP material bonded to the steel substrate. As it has been discussed before, the efficiency of the bonded retrofit system is mainly dependent on the behavior of the CFRP-to-steel bond joint. Sophisticated surface preparation is required prior to bonding the CFRP to the steel member to maximize the efficiency of the composite system and reduce the risk of debonding.

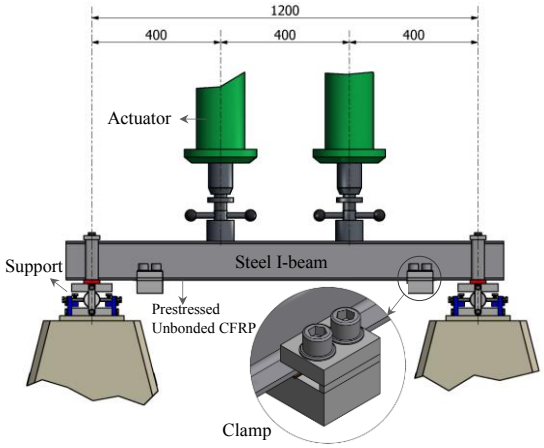

(a)

(b)

Figure 2. a) Test set-up (dimensions in mm), b) elements of the mechanical anchorage system (Ghafoori and Motavalli 2015b).

Many studies have raised concerns about the influence of environmental conditions (e.g., elevated or subzero temperatures, water and moisture and ultraviolet light) and dynamic loads (e.g., fatigue, impacts and earthquakes) on the behavior of the CFRP-to-steel bond joint. Because of these concerns, which are mainly associated with the long-term performance of the CFRP-to-steel bond joints, a pre-stressed un-bonded retrofit (PUR) system has been recently designed and tested at Empa (Ghafoori and Motavalli 2015b, Ghafoori and Motavalli 2015c, Ghafoori and Motavalli 2015a, Fernando et al. 2010). In contrast to the PBR system, the PUR system works without using any bond; instead, it uses a pair of friction clamps to connect the CFRP plates to the steel member. An independent reaction frame to pull the CFRP strips was developed, as shown in Figure 1. The pre-stressed CFRP strip was then attached to the steel beam using mechanical clamps. The force in the actuator was then released and the CFRP strip out of mechanical clamps was cut.

The retrofitted beams was tested in a four-point bending static loading test set-up, as shown in Figure 2.a. Figure 2.b depicts the elements of the mechanical anchorage system. It has been shown that prestressed unbonded and bonded CFRP strip have almost identical effect on the behavior of steel beams. Prestressed unbonded CFRP strips could prevent fatigue crack initiation (Ghafoori et al. 2015b) and propagation (Aljabar et al. 2016, Ghafoori et al. 2012a, Hosseini et al. 2016, Ghafoori and Motavalli 2016b, Aljabar et al.) in steel beams. In summary, the results of the extensive tests have shown that the static and fatigue behavior of steel beams are strongly governed by the prestress level in the CFRP strip, rather than the effect of the adhesive bond. Bonded and unbonded systems have shown relatively similar results, particularly in the linear-elastic domain (Ghafoori 2015).

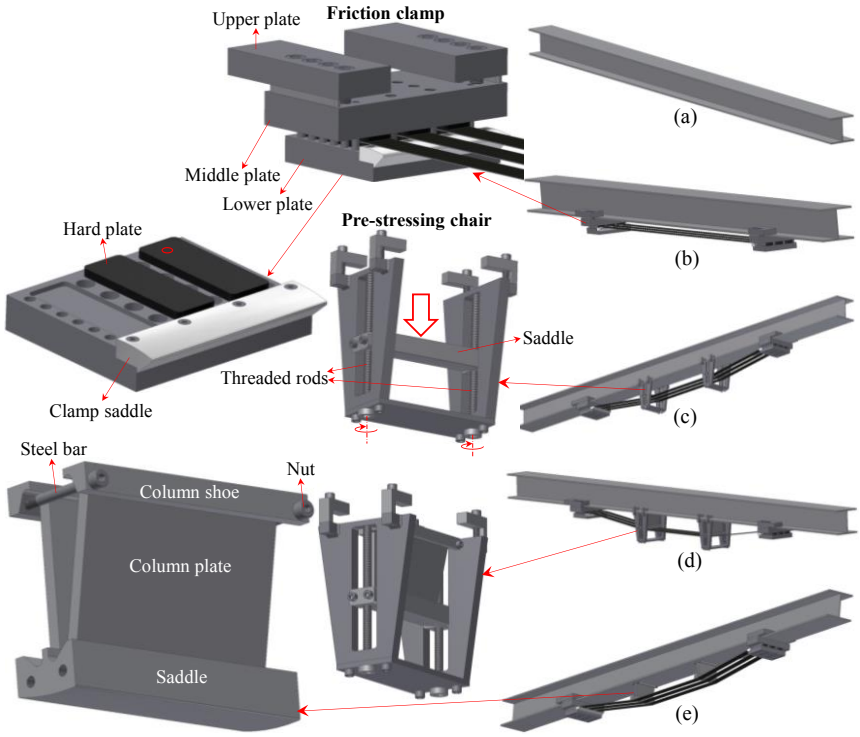

Figure 3. Different elements of the trapezoidal retrofit system: a) initial state of the beam, b) clamps are fixed, and the CFRP plates are placed between the two clamps, c) using pre-stressing chair, the saddle pushes the CFRP plates away from the beam that induces pre-stress in the CFRP plates, d) two plates are positioned between the beam and the saddle, and e) the pre-stress chair is removed (Ghafoori and Motavalli 2015a).

Trapezoidal PUR system: Figure 2.a shows a PUR system with straight CFRP strips. Ghafoori and Motavalli 2015a have recently developed and patented a trapezoidal PUR system for strengthening of a historic metallic railway bridge in Switzerland. A summary of the prestressing procedure is explained as follows. Assume an I-beam as shown in Figure 3.a. First, the mechanical clamps are placed near two ends of the beam, and three parallel CFRP plates are placed and tightened inside the clamps, as shown in Figure 3.b.

Each CFRP plate has dimensions of 50 mm width and 1.2 mm thickness. Each friction clamp is consisted of a lower plate, a middle plate and two upper plates. The middle and the lower plates consist of three hard plates, which provide a uniform stress distribution along the CFRP anchorage length. Each CFRP

plate is anchored between the lower plate and the middle plate and is subjected to compressive force, which is applied by pre-tensioned bolts. The beam flange is also gripped between the middle plate and the upper plates and subjected to the compressive force of pre-tensioned bolts. A pre-stressing chair is used to increase the eccentricity between CFRP plates and steel beam, as shown in Figure 3.c.

The pre-stressing chair consists of a saddle that can move along two vertical threaded bars. The distance between the saddle and the beam can be manually changed by turning the threaded rods using a wrench. Thus, by turning the threaded rods, the saddle pushes the CFRP plates away from the beam, and the CFRP pre-stress is increased. A larger eccentricity between the CFRP plates and the beam corresponds to a larger CFRP pre-stress level. After the desired pre-stress level is achieved, two plates are placed between the CFRP plates and the beam (see Figure 3.d). Each plate is positioned between the saddle and a shoe. The two shoes are connected by two steel bars and four nuts, as shown in Figure 3.e, and then the pre-stressing chair is removed. Figure 3.e shows the final configuration of the strengthened beam. More details can be found in Ghafoori and Motavalli 2015a, Ghafoori et al. 2015a. The system has been then used for fatigue strengthening of a 120-year-old railway metallic bridge in Switzerland (see Figure 4.a). Figure 24.b shows a riveted cross-girder of the bridge after strengthening.

More recently, Kianmofrad et al. 2017 have suggested four different variants of the prestressed PUR systems: trapezoidal PUR (TPUR), triangular PUR (TriPUR), flat PUR (FPUR), and contact PUR (CPUR) systems. The behavior of each system has been examined using numerical, analytical and experimental results. The paper lists the advantage and disadvantage of each retrofit technique.

(a) (b)

Figure 4. (a) Münchenstein railway metallic Bridge (120-year-old) subjected to a passenger train. The bridge consists of 10 panels with the total length of 45.2 m, width of 5 m and height of 6.15 m and built on a 45-deg skew. (b) The cross-girders were retrofitted with pre-stressed un-bonded CFRP strips.

Conclusions

The two main differences between the behavior of CFRP–concrete and CFRP–metal bonded members are concerned with the failure mode and the stiffness of the retrofitted members. These differences resulted in development of different CFRP prestressing concepts for strengthening of concrete and metallic members at Empa, which were briefly explained in this paper. For strengthening of metallic members, laboratory test results showed that adhesive bond does not have much influence on the static and fatigue behavior of retrofitted steel beams, however CFRP prestressing plays an important role. Therefore, in order to minimize the concerns related to effects of high ambient temperatures, moisture, water or fatigue loading on the CFRP-to-metal bond behavior, a prestressed unbonded retrofit system has been recently developed at Empa. Details about fatigue strengthening of a 120-year-old railway metallic bridge in Switzerland using prestressed unbonded CFRP strips were given.

References

Aljabar, N. J., Zhao, X. L., Al-Mahaidi, R., Ghafoori, E., Motavalli, M. & Koay, Y. C. 2017. Fatigue tests on UHM-CFRP strengthened steel plates with central inclined cracks under different damage levels. *Composite Structures,* http://dx.doi.org/10.1016/j.compstruct.2016.10.122.

Aljabar, N. J., Zhao, X. L., Al-Mahaidi, R., Ghafoori, E., Motavalli, M. & Powers, N. 2016. Effect of Crack Orientation on Fatigue Behaviour of CFRP- Strengthened Steel Plates. *Composite Structures,* 152**,** 295-305.

Fernando, D., Schumacher, A., Motavalli, M., Teng, J. G., Yu, T. & Ghafoori, E. 2010. Fatigue strengthening of cracked steel beams with CFRP plates. *ASME International Mechanical Engineering Congress and Exposition, Proceedings (IMECE).*

Ghafoori, E. 2013. Interfacial stresses in beams strengthened with bonded prestressed plates. *Engineering Structures,* 46**,** 508-510.

Ghafoori, E. 2015. Fatigue strengthening of metallic members using un-bonded and bonded CFRP laminates. *PhD Thesis, ETH-Zurich (http://dx.doi.org/10.3929/ethz-a-010453130)*.

Ghafoori, E. & Motavalli, M. 2013. Flexural and interfacial behavior of metallic beams strengthened by prestressed bonded plates. *Composite Structures,* 101**,** 22-34.

Ghafoori, E. & Motavalli, M. 2015a. Innovative CFRP-Prestressing System for Strengthening Metallic Structures. *Journal of Composites for Construction,* 19**,** 04015006.

Ghafoori, E. & Motavalli, M. 2015b. Lateral-torsional buckling of steel I-beams retrofitted by bonded and un-bonded CFRP laminates with different pre-stress levels: experimental and numerical study. *Construction and Building Materials,* 76**,** 194–206.

Ghafoori, E. & Motavalli, M. 2015c. Normal, high and ultra-high modulus CFRP laminates for bonded and un-bonded strengthening of steel beams. *Materials and Design,* 67**,** 232–243.

Ghafoori, E. & Motavalli, M. 2016a. Method for pre-stressing a steel structure, and steel structure pre-stressed using said method. *United States Patent No. 20160145815*.

Ghafoori, E. & Motavalli, M. 2016b. A Retrofit Theory to Prevent Fatigue Crack Initiation in Aging Riveted Bridges Using Carbon Fiber-Reinforced Polymer Materials. *Polymers,* 8**,** 308.

Ghafoori, E., Motavalli, M., Botsis, J., Herwig, A. & Galli, M. 2012a. Fatigue strengthening of damaged metallic beams using prestressed unbonded and bonded CFRP plates. *International Journal of Fatigue,* 44**,** 303-315.

Ghafoori, E., Motavalli, M., Nussbaumer, A., Herwig, A., Prinz, G. & Fontana, M. 2015a. Determination of minimum CFRP pre-stress levels for fatigue crack prevention in retrofitted metallic beams. *Engineering Structures,* 84**,** 29–41.

Ghafoori, E., Motavalli, M., Zhao, X. L., Nussbaumer, A. & Fontana, M. 2015b. Fatigue design criteria for strengthening metallic beams with bonded CFRP plates. *Engineering Structures,* 101**,** 542-557.

Ghafoori, E., Schumacher, A. & Motavalli, M. 2012b. Fatigue behavior of notched steel beams reinforced with bonded CFRP plates: Determination of prestressing level for crack arrest. *Engineering Structures,* 45**,** 270-283.

Hosseini, A., Ghafoori, E., Motavalli, M. & Nussbaumer, A. 2016. Stress Analysis of Unbonded and Bonded prestressed CFRP-Strengthened Steel Plates. *8th International Conference on Fiber Reinforced Polymer (FRP) Composites in Civil Engineering (CICE2016), 14-16 December 2016, Hong Kong, China.*

Kianmofrad, F., Ghafoori, E., Elyasi, M. M., Motavalli, M. & Rahimian, M. 2017. Strengthening of metallic beams with different types of pre-stressed un-bonded retrofit systems. *Composite Structures,* 159**,** 81-95.

Externally bonded FRP for the strengthening of RC structures (EBFRP). State of the art in FRANCE

Emmanuel FERRIER[1], Marc Quiertant[2], S.Chatainier[2], K.Benzarti[2]

[1]Université LYON 1

[2]IFSTTAR, Paris

Introduction

This contribution gives an overview of the main result obtained in France on EBFRP applied on RC structures. Of course, it does not cover all researches done in this field since the 90's in France, but covers the main outline and interesting points. This state of the art is divided into several parts: the academic or institutional research point of view, design issues, field applications and conclusion.

Academic or institutional Research

Research started in the earlier 90's in France on the topic of external bonded FRP. Mainly, the works have focused on the problem of flexural behaviour of beams. Since then, several researchers have investigated this scientific problem at different levels from material, to structure with some interesting developments in the field of bonding issues using specific testing devices [2], FRP durability studies [3-7] but also in the field of reinforced structures.
As regard durability issues, a major hindrance to the acceptance of polymer composites in civil engineering applications is the interactions of these materials with the surrounding environment, manifested by the sensitivity of the polymeric matrix to weathering. An experimental approach of studying the ageing of polymeric matrix composites has been proposed by several authors in France [3-6]. The composite specimens were subjected to specific exposure conditions representative of civil engineering environments. The composite properties were monitored by several characterisation tests. In ref [5]., the ageing behaviour of model concrete-composite interfaces was investigated and the influence several parameters was evaluated using the pull-off and single-shear tests. It was found that hygrothermal ageing causes a progressive and significant decrease in the pull-off strength of the bonded interfaces for CFS and CFRP strengthened specimens prepared from non carbonated concrete slabs. Moreover, the failure mode evolves from a substrate failure towards a mixed or interfacial failure [5].

NSM strengthening [8, 9], shear strengthening [10] and flexural behaviour [11] have been investigated on beam or slab with the original study of punching behaviour [12]. The experimental work reported in references [8,9] confirms the ability of the NSM technique to increase the load-bearing capacity of RC beams. A lot of parameters may influence the efficiency of this technique, as for example the cross-section of NSM bars, the steel re-bar cross-section, the concrete cross-section, the strength of both concrete and filling material. Some investigation has been carried out on aged RC structures damaged by corrosion process and then strengthened by NSM; this is an original study not common in literature review.
As regard slabs [12], the simplified model set up with the calculus process satisfies the fixed requirement of modelling the behaviour of slab in reinforced (and strengthened) concrete in the load phase. It makes it possible to model the mid-span displacements, strain and stress of the different materials at any point of the slab.
Columns behavior [13, 14] has also been investigated to consider the effect of compression behavior and flexural loading. Depending on the CFRP strengthening system (type of material and bonding process), significant increases in deformability and strength can be achieved for columns under combined flexural-compressive loading. The maximum strength enhancement was characterized by a

ratio of 1.30. Deformation capacity and ductility improvement was more outstanding than the gains in strength. It was demonstrated that externally confined column could undergo large deformation without rupture. This characteristic is important considering that an over-compressed structures could adapt to abnormal loads and before full redundancy, redistribute bending moments to other elements.

More recently some interesting development has been done on seismic retrofitting of RC structures such as columns or shear wall. On this topic, studies has confirmed some well know results : the FRP axial stiffness value influences the ductility of columns through the dispersion of cracks which is itself the result of energy dissipation. Indeed, the increase of ductility is the main objective in seismic strengthening. A decrease in rigidity is obtained with a judicious combination of mechanical properties of the composite (modulus of elasticity) and its geometrical configuration (width and spacing of the FRP bands, reinforcement ratio etc.) [15]. A specific work has been done on FRP anchorage systems [16]. The main objective of this study was to examine new techniques for strengthening column-beam or wall-foundation joints and for avoiding sliding failure at these critical points. For this purpose, four innovative types of FRP reinforcement were investigated. The experimental results provided evidence indicating their effectiveness, as they were successful in (a) limiting FRP debonding failure, (b) improving the overall load capacity by facilitating load transfer at the joint and (c) enhancing ductility.

Finally, on-site durability studies have been conducted by Ifsttar, and quality control of the bonded concrete/composite interface has been successfully applied using Non-Destructive Evaluation techniques such as Shearography and Infrared Thermography [17]. Results demonstrated that shearography associated to a depressure loading makes it possible to determine not only locations and areas of defects but also enables to assess the quality of adhesion. Moreover, thermography offers a simple method with real-time and full-field imaging capabilities that makes it possible to inspect repaired structures in a qualitative way (detection of the bonding defects).

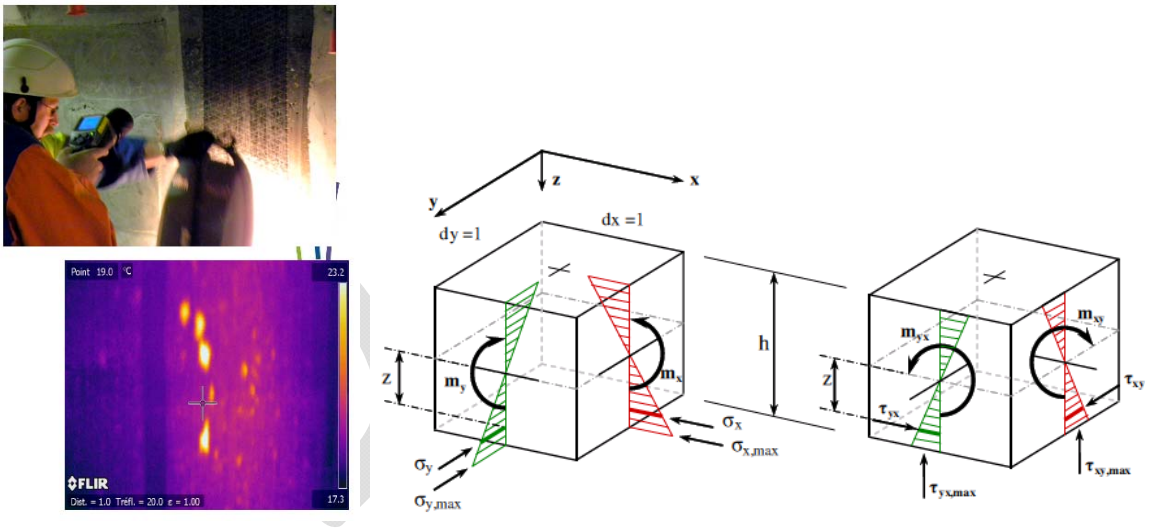

Figure 1 : quality control of bonding [17] and mechanical study of a slab [12]

Design recommendation and active working group

Based on researches conducted in France in the field of EBFRP, and on a literature survey at the internal level, a working group from the Fench Association of Civil Engineering (AFGC, [1]) was launched in 1998, and published its first recommendations in 2003. Material characterization, bonding measurement and flexural behaviour have been fixed first. Then,, a compression model and punching failure have been added in a second edition. The working group still continues to improve the document, and has introduced the Eurocode philosophy in the last version (2011). This document is only available in French but an English translation is scheduled for 2015.

In 2012, a specialised working group on “paraseismic strengthening” has been opened under the supervision of AFGC, and specific recommendations will published in 2015.

Main field applications

Beams are the main RC structures concerned by EBFRP strengthening, in order to increase their shear or flexural behaviour. Columns may also be concerned by confinement. Building, bridges, industrial structures and dams can also be strengthened. Usually, the problem at the origin of the strengthening is a need for an increased loading capacity or a modification of the structure (examples in Figure 2). In facts, there are other multiple applications: repair of structures damaged by accident or aging, strengthening of structures that change of function (track added on a motorway bridge, floor that must sustained heavier load than expected due to new machine, change in the structure of a building...). In addition, the development of seismic regulations, management or explosion hazards, also opens perspectives for composites strengthening systems.

(a) Beams of Parking strengthened by EBFRP (b) Bridge strengthened by EBFRP

Figure 2 : Examples of field applications

Conclusions and Points for Discussion

Based on this state of the art, EBFRP still need research for full application in the field of construction. The following points can be considered as crucial issues:

- Temperature behaviour for serviceability issue need to be fixed
- Anchorage details should be more deeply studied
- Fire issue specially due to Eurocode
- Seismic behaviour and design need improvement at a design stage
- Alternative cement based EBFRP systems can be studied [18]

Key references

[1] AFGC, Recommandations provisoires pour le renforcement des structures en béton armé par matériaux composites, 2011

[2] Sylvain Chataigner, Jean-Francois Caron, Karim Benzarti, Marc Quiertant, Christophe Aubagnac, Use of a single lap shear test to characterize composite-to-concrete or composite-to-steel bonded interfaces, Construction and Building Materials, Volume 25, Issue 2, February 2011, Pages 468-478

[3] Karim Benzarti, Francesco Freddi, Michel Frémond, A damage model to predict the durability of bonded assemblies. Part I: Debonding behavior of FRP strengthened concrete structures, Construction and Building Materials, Volume 25, Issue 2, February 2011, Pages 547-555

[4] E. Ferrier, M. Quiertant, K. Benzarti, P. Hamelin, Influence of the properties of externally bonded CFRP on the shear behavior of concrete/composite adhesive joints, Composites Part B: Engineering, Volume 41, Issue 5, July 2010, Pages 354-362

[5] Karim Benzarti, Sylvain Chataigner, Marc Quiertant, Céline Marty, Christophe Aubagnac, Accelerated ageing behaviour of the adhesive bond between concrete specimens and CFRP overlays, Construction and Building Materials, Volume 25, Issue 2, February 2011, Pages 523-538

[6] S. Marouani, L. Curtil, P. Hamelin, Ageing of carbon/epoxy and carbon/vinylester composites used in the reinforcement and/or the repair of civil engineering structures, Composites Part B: Engineering, Volume 43, Issue 4, June 2012, Pages 2020-2030

[7] E. Ferrier, L. Michel, B. Jurkiewiez, P. Hamelin, Creep behavior of adhesives used for external FRP strengthening of RC structures, Construction and Building Materials, Volume 25, Issue 2, February 2011, Pages 461-467

[8] Firas Al-Mahmoud, Arnaud Castel, Raoul François, Christian Tourneur, Anchorage and tension-stiffening effect between near-surface-mounted CFRP rods and concrete, Cement and Concrete Composites, Volume 33, Issue 2, February 2011, Pages 346-352

[9] Firas Al-Mahmoud, Arnaud Castel, Raoul François, Christian Tourneur, RC beams strengthened with NSM CFRP rods and modeling of peeling-off failure, Composite Structures, Volume 92, Issue 8, July 2010, Pages 1920-1930

[10] C Diagana, A Li, B Gedalia, Y Delmas, Shear strengthening effectiveness with CFF strips, Engineering Structures, Volume 25, Issue 4, March 2003, Pages 507-516

[11] N. Attari, S. Amziane, M. Chemrouk, Flexural strengthening of concrete beams using CFRP, GFRP and hybrid FRP sheets, Construction and Building Materials, Volume 37, December 2012, Pages 746-757

[12] L. Michel, E. Ferrier, A. Agbossou, P. Hamelin, Flexural stiffness modelling of RC slab strengthened by externally bonded FRP, Composites Part B: Engineering, Volume 40, Issue 8, December 2009, Pages 758-765

[13] Marc Quiertant, Jean-Luc Clement, Behavior of RC columns strengthened with different CFRP systems under eccentric loading, Construction and Building Materials, Volume 25, Issue 2, February 2011, Pages 452-460

[14] J.F. Berthet, E. Ferrier, P. Hamelin, Compressive behavior of concrete externally confined by composite jackets. Part A: experimental study, Construction and Building Materials, Volume 19, Issue 3, April 2005, Pages 223-232

[15] G. Promis, E. Ferrier, P. Hamelin, Effect of external FRP retrofitting on reinforced concrete short columns for seismic strengthening, Composite Structures, Volume 88, Issue 3, May 2009, Pages 367-379

[16] Samiullah Qazi, Laurent Michel, Emmanuel Ferrier, Experimental investigation of CFRP anchorage systems used for strengthening RC joints, Composite Structures, Volume 99, May 2013, Pages 453-461

[17] Frédéric Taillade, Marc Quiertant, Karim Benzarti, Christophe Aubagnac, Shearography and pulsed stimulated infrared thermography applied to a nondestructive evaluation of FRP strengthening systems bonded on concrete structures, Construction and Building Materials, Volume 25, Issue 2, February 2011, Pages 568-574

[18] Amir Si-Larbi, Amen Agbossou, Emmanuel Ferrier, Laurent Michel, Strengthening RC beams with composite fiber cement plate reinforced by prestressed FRP rods: Experimental and numerical analysis Composite Structures, Volume 94, Issue 3, February 2012, Pages 830-838

http://www.tu1207.eu